

**DESIGN OF ROBUST PSS AND FACTS-BASED
CONTROLLERS FOR STABILITY
ENHANCEMENT OF POWER SYSTEMS**

BY

ALI TALEB AL-AWAMI

A Thesis Presented to the
DEANSHIP OF GRADUATE STUDIES

KING FAHD UNIVERSITY OF PETROLEUM & MINERALS

DHAHRAN, SAUDI ARABIA

In Partial Fulfillment of the
Requirements for the Degree of

MASTER OF SCIENCE

In

ELECTRICAL ENGINEERING

May 2004

UMI Number: 1420922

INFORMATION TO USERS

The quality of this reproduction is dependent upon the quality of the copy submitted. Broken or indistinct print, colored or poor quality illustrations and photographs, print bleed-through, substandard margins, and improper alignment can adversely affect reproduction.

In the unlikely event that the author did not send a complete manuscript and there are missing pages, these will be noted. Also, if unauthorized copyright material had to be removed, a note will indicate the deletion.

UMI[®]

UMI Microform 1420922

Copyright 2004 by ProQuest Information and Learning Company.

All rights reserved. This microform edition is protected against unauthorized copying under Title 17, United States Code.

ProQuest Information and Learning Company
300 North Zeeb Road
P.O. Box 1346
Ann Arbor, MI 48106-1346

KING FAHD UNIVERSITY OF PETROLUEM & MINERALS

DHAHRAN 31261, SAUDI ARABIA

DEANSHIP OF GRADUATE STUDIES

This thesis, written by

ALI TALEB AL-AWAMI

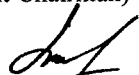
under the direction of his Thesis Advisors and approved by his Thesis Committee, has been presented to and accepted by the Dean of Graduate Studies, in partial fulfillment of the requirements for the degree of

MASTER OF SCIENCE IN ELECTRICAL ENGINEERING

Thesis Committee



Dr. Jamil Bakhshwain
(Department Chairman)



Dr. Osama Jannadi
(Dean of Graduate Studies)

12-6-2004
Date



Dr. Youssef Abdel-Magid (Chairman)



Dr. Mohammed Abido (Co-chairman)



Dr. Samir Al-Baiyat (Member)



Dr. Jamil Bakhshwain (Member)



Dr. Ibrahim El-Amin (Member)

Dedicated to
My Beloved Parents
and
My Sincere Wife

ACKNOWLEDGEMENTS

In the name of Allah, the most Merciful, the most Gracious. All praise is due to Allah; we praise Him, seek His help, and ask for His forgiveness. I am thankful to Allah, who supplied me with the courage, the guidance, and the love to complete this research. Also, I cannot forget the ideal man of the world and most respectable personality for whom Allah created the whole universe, Prophet Mohammed (Peace Be Upon Him).

I would like to acknowledge all those who helped me to complete this thesis. Acknowledgement is due to King Fahd University of Petroleum & Minerals for providing support to carry out this work

I am indebted to my thesis advisors, Dr. Youssef Abdel-Magid and Dr. Mohamed A. Abido. I am grateful to their constant encouragement and invaluable instructions and suggestions that helped me in accomplishing this work successfully. They continuously kept an eye on the progress of this work and their programming experience was of great benefit to me. I would like to express my deep appreciation to them.

Many thanks are due to my thesis committee members, Dr. Samir Al-Baiyat, Dr. Jamil Bakhshwain, and Dr. Ibrahim El-Amin for their involvement and the time they spared to review this thesis.

Some of my friends had direct participation in this study. I assigned them some table formatting tasks to perform and they showed great interest in helping me. To name, those are Fouad Al-Musaher, Abu Ali Al-Maqabi, and my youngest brother Ahmed Al-Awami. I am proud to have such fellows who deserve my high appreciation.

Special thanks go to my friend Hani Al-Sheikh for his moral support. I am also bound to my fellows Bader Al-Musaher, Mohammad Al-Howar and Ali Al-Mahoozi for their interest in following up my progress.

During the course of this thesis, my brothers, sisters, and family members looked closely at my progress and kept encouraging me towards success. Batool, Muneer, Shaker, Tahani, Muhsen, Mohammad, and Amin, you all deserve my warm thanks.

My grandmother Amna, may her souls rest in peace, was constantly praying for my family and me. I am always grateful to her and still remember her prayers.

My sincere and profound gratitude are due to my mother and father. I cannot forget their kind care and their interest in my success. Their prayers and moral support will always boost my progress.

Specially and most sincerely, I would like to pay my warmest tribute to my beloved wife whose patient love and strong emotional support made my life pleasant even in the hardest times. Ayat, you are making my life more meaningful.

2	FACTS DEVICES	25
2.1	Introduction	25
2.1.1	Thyristor-Controlled Phase Shifters (TCPS)	25
2.1.2	Thyristor-Controlled Series Capacitor (TCSC)	26
2.1.3	Static VAR Compensator (SVC)	27
2.1.4	Unified Power Flow Controller (UPFC)	27
2.2	Power Flow Modulation Using Facts Devices	29
2.2.1	Thyristor-Controlled Phase Shifters (TCPS)	29
2.2.2	Thyristor-Controlled Series Capacitor (TCSC)	30
2.2.3	Static VAR Compensator (SVC)	31
2.2.4	Unified Power Flow Controller (UPFC)	32
3	POWER SYSTEM MODEL	34
3.1	Single-Machine Infinite-Bus System with G1 FACTS Devices	34
3.1.1	SMIB System Nonlinear Model	34
3.1.1.1	Generator Model	34
3.1.1.2	Excitation system and PSS	35
3.1.1.3	FACTS-based stabilizers	36
3.1.2	SMIB System Linearized Model	38
3.2	Single-Machine Infinite-Bus System with UPFC	43
3.2.1	SMIB System Nonlinear Model	43
3.2.2	SMIB System Linearized Model	47
3.3	Multimachine Power System	51
3.3.1	Multimachine Power System Nonlinear Model	51

3.3.2	Multimachine System Linearized Model	52
3.3.3	Multimachine Power System Nonlinear Model with SVCs	56
3.3.4	Multimachine System Linearized Model with SVCs	57
4	PARTICLE SWARM OPTIMIZER	63
4.1	Steps of the PSO Algorithm	66
5	PROBLEM FORMULATION	68
5.1	System Models and Stabilizer Structures	68
5.2	Objective Functions	71
5.3	Optimization Problem	71
6	PROPOSED APPROACH	73
6.1	Controllability Measure	73
6.2	Damping Torque Coefficient Analysis	74
6.3	Implementation	75
7	OPTIMIZATION RESULTS: FIRST GENERATION FACTS DEVICES	78
7.1	Electromechanical Mode Controllability Measure	78
7.2	Optimization Results for PSS, SVC, TCSC, and TCPS	81
7.2.1	Single-Point Tuning	81
7.2.1.1	Individual Design with J_1	82
7.2.1.2	Individual Design with J_2	92
7.2.1.3	Coordinated Design with J_2	102
7.2.2	Multiple-Point Tuning	114
7.2.2.1	Individual Design with J_1	115
7.2.2.2	Individual Design with J_2	125

7.2.2.3	Coordinated Design with J_1	135
8	OPTIMIZATION RESULTS: UNIFIED POWER FLOW CONTROLLER	147
8.1	Electromechanical Mode Controllability Measure	147
8.2	Optimization Results for PSS and the UPFC-Based Stabilizers	150
8.2.1	Single-Point Tuning	150
8.2.1.1	Individual Design with J_1	150
8.2.1.2	Individual Design with J_2	161
8.2.1.3	Coordinated Design with J_1	171
8.2.2	Multiple-Point Tuning	184
8.2.2.1	Individual Design with J_1	184
8.2.2.2	Individual Design with J_2	195
8.2.2.3	Coordinated Design with J_2	205
9	ROBUST COORDINATED DESIGN OF PSS AND SVC FOR MULTIMATINE POWER SYSTEM	218
9.1	Electromechanical Mode Controllability Measure	219
9.2	Optimization Results for PSS and SVC-based Stabilizers	221
9.2.1	Single-Point Tuning	222
9.2.1.1	Individual Design with J_1	222
9.2.1.2	Coordinated PSS3-SVC7 Design with J_1	236
9.2.1.3	Coordinated SVC7-SVC9 Design with J_1	243
9.2.2	Multiple-Point Tuning	249
9.2.2.1	Individual Design with J_1	250

9.2.2.2	Coordinated PSS3-SVC7 Design with J_1	264
9.2.2.3	Coordinated SVC7-SVC9 Design with J_1	271
10	CONCLUSIONS AND FUTURE WORK	278
10.1	Conclusions	278
10.2	Future Work	279
	APPENDICES	281
	NOMENCLATURE	283
	BIBLIOGRAPHY	286
	Vita	300

LIST OF TABLES

Table	Table Title	Page
7.1	Optimal parameter settings with J_1 , single-point tuning, individual design	82
7.2	System eigenvalues of nominal loading conditions with J_1 settings, single-point tuning, individual design	83
7.3	System eigenvalues of light loading conditions with J_1 settings, single-point tuning, individual design	83
7.4	System eigenvalues of heavy loading conditions with J_1 settings, single-point tuning, individual design	83
7.5	System eigenvalues of leading Pf loading conditions with J_1 settings, single-point tuning, individual design	84
7.6	Optimal parameter settings with J_2 , single-point tuning, individual design	92
7.7	System eigenvalues of nominal loading conditions with J_2 settings, single-point tuning, individual design	93
7.8	System eigenvalues of light loading conditions with J_2 settings, single-point tuning, individual design	93
7.9	System eigenvalues of heavy loading conditions with J_2 settings, single-point tuning, individual design	93
7.10	System eigenvalues of leading Pf loading conditions with J_2 settings, single-point tuning, individual design	94
7.11	Optimal parameter settings with J_2 , single-point tuning, coordinated design	103
7.12	System eigenvalues of nominal loading conditions with J_2 settings, single-point tuning, coordinated design	103
7.13	System eigenvalues of light loading conditions with J_2 settings, single-point tuning, coordinated design	103
7.14	System eigenvalues of heavy loading conditions with J_2 settings, single-point tuning, coordinated design	104
7.15	System eigenvalues of leading Pf loading conditions with J_2 settings, single-point tuning, coordinated design	104
7.16	Loading conditions and parameter uncertainties considered in the design stage	114
7.17	Open-loop eigenvalues associated with the EM modes of all the 16 points considered in the robust design process	114
7.18	Damping ratios of the open-loop eigenvalues associated with the EM modes of all the points considered in the robust design process	115
7.19	Optimal parameter settings with J_1 , multiple-point tuning, individual design	115
7.20	System eigenvalues of nominal loading conditions with J_1 settings, multiple-point tuning, individual design	116

7.21	System eigenvalues of light loading conditions with J_1 settings, multiple-point tuning, individual design	116
7.22	System eigenvalues of heavy loading conditions with J_1 settings, multiple-point tuning, individual design	116
7.23	System eigenvalues of leading Pf loading conditions with J_1 settings, multiple-point tuning, individual design	117
7.24	Optimal parameter settings with J_2 , multiple-point tuning, individual design	125
7.25	System eigenvalues of nominal loading conditions with J_2 settings, multiple-point tuning, individual design	126
7.26	System eigenvalues of light loading conditions with J_2 settings, multiple-point tuning, individual design	126
7.27	System eigenvalues of heavy loading conditions with J_2 settings, multiple-point tuning, individual design	126
7.28	System eigenvalues of leading Pf loading conditions with J_2 settings, multiple-point tuning, individual design	127
7.29	Optimal parameter settings with J_1 , multiple-point tuning, coordinated design	135
7.30	System eigenvalues of nominal loading conditions with J_1 settings, multiple-point tuning, coordinated design	136
7.31	System eigenvalues of light loading conditions with J_1 settings, multiple-point tuning, coordinated design	136
7.32	System eigenvalues of heavy loading conditions with J_1 settings, multiple-point tuning, coordinated design	137
7.33	System eigenvalues of leading Pf loading conditions with J_1 settings, multiple-point tuning, coordinated design	137
8.1	Optimal parameter settings with J_1 , single-point tuning, individual design	151
8.2	System eigenvalues of nominal loading conditions with J_1 settings, single-point tuning, individual design	152
8.3	System eigenvalues of light loading conditions with J_1 settings, single-point tuning, individual design	152
8.4	System eigenvalues of heavy loading conditions with J_1 settings, single-point tuning, individual design	153
8.5	System eigenvalues of leading Pf loading conditions with J_1 settings, single-point tuning, individual design	153
8.6	Optimal parameter settings with J_2 , single-point tuning, individual design	161
8.7	System eigenvalues of nominal loading conditions with J_1 settings, single-point tuning, individual design	162
8.8	System eigenvalues of light loading conditions with J_1 settings, single-point tuning, individual design	162
8.9	System eigenvalues of heavy loading conditions with J_1 settings, single-point tuning, individual design	163
8.10	System eigenvalues of leading Pf loading conditions with J_1 settings, single-point tuning, individual design	163
8.11	Optimal parameter settings with J_1 , single-point tuning, coordinated design	171
8.12	System eigenvalues of nominal loading conditions with J_1 settings, single-	

	point tuning, coordinated design	172
8.13	System eigenvalues of light loading conditions with J_1 settings, single-point tuning, coordinated design	172
8.14	System eigenvalues of heavy loading conditions with J_1 settings, single-point tuning, coordinated design	173
8.15	System eigenvalues of leading Pf loading conditions with J_1 settings, single-point tuning, coordinated design	173
8.16	Loading conditions and parameter uncertainties considered in the design stage	185
8.17	Open-loop eigenvalues associated with the EM modes of all the 16 points considered in the robust design process	185
8.18	Damping ratios of the open-loop eigenvalues associated with the EM modes of all the points considered in the robust design process	185
8.19	Optimal parameter settings with J_1 , multiple-point tuning, individual design	185
8.20	System eigenvalues of nominal loading conditions with J_1 settings, multiple-point tuning, individual design	186
8.21	System eigenvalues of light loading conditions with J_1 settings, multiple-point tuning, individual design	186
8.22	System eigenvalues of heavy loading conditions with J_1 settings, multiple-point tuning, individual design	187
8.23	System eigenvalues of leading Pf loading conditions with J_1 settings, multiple-point tuning, individual design	187
8.24	Optimal parameter settings with J_2 , multiple-point tuning, individual design	195
8.25	System eigenvalues of nominal loading conditions with J_2 settings, multiple-point tuning, individual design	196
8.26	System eigenvalues of light loading conditions with J_2 settings, multiple-point tuning, individual design	196
8.27	System eigenvalues of heavy loading conditions with J_2 settings, multiple-point tuning, individual design	197
8.28	System eigenvalues of leading Pf loading conditions with J_2 settings, multiple-point tuning, individual design	197
8.29	Optimal parameter settings with J_2 , multiple-point tuning, coordinated design	205
8.30	System eigenvalues of nominal loading conditions with J_2 settings, multiple-point tuning, coordinated design	206
8.31	System eigenvalues of light loading conditions with J_2 settings, multiple-point tuning, coordinated design	206
8.32	System eigenvalues of heavy loading conditions with J_2 settings, multiple-point tuning, coordinated design	207
8.33	System eigenvalues of leading Pf loading conditions with J_2 settings, multiple-point tuning, coordinated design	207
9.1	Generator operating conditions	221
9.2	System loading conditions	221
9.3	Optimal parameter settings with J_1 , single-point tuning, individual design	223
9.4	System eigenvalues of Base Case loading conditions with J_1 settings, single-point tuning, individual design	223

9.5	System eigenvalues of Case 1 loading conditions with J_1 settings, single-point tuning, individual design	224
9.6	System eigenvalues of Case 2 loading conditions with J_1 settings, single-point tuning, individual design	224
9.7	System eigenvalues of Case 3 loading conditions with J_1 settings, single-point tuning, individual design	225
9.8	Optimal parameter settings with J_1 , single-point tuning, coordinated PSS3-SVC7 design	237
9.9	System eigenvalues of Base Case loading conditions with J_1 settings, single-point tuning, coordinated PSS3-SVC7 design	237
9.10	System eigenvalues of Case 1 loading conditions with J_1 settings, single-point tuning, coordinated PSS3-SVC7 design	238
9.11	System eigenvalues of Case 2 loading conditions with J_1 settings, single-point tuning, coordinated PSS3-SVC7 design	238
9.12	System eigenvalues of Case 3 loading conditions with J_1 settings, single-point tuning, coordinated PSS3-SVC7 design	239
9.13	Optimal parameter settings with J_1 , single-point tuning, coordinated SVC7-SVC9 design	244
9.14	System eigenvalues of Base Case loading conditions with J_1 settings, single-point tuning, coordinated SVC7-SVC9 design	244
9.15	System eigenvalues of Case 1 loading conditions with J_1 settings, single-point tuning, coordinated SVC7-SVC9 design	245
9.16	System eigenvalues of Case 2 loading conditions with J_1 settings, single-point tuning, coordinated SVC7-SVC9 design	245
9.17	System eigenvalues of Case 3 loading conditions with J_1 settings, single-point tuning, coordinated SVC7-SVC9 design	246
9.18	Open-loop eigenvalues associated with the EM modes of the four operating cases considered in the robust design process	250
9.19	Damping ratios of the open-loop eigenvalues associated with the EM modes of the four operating cases considered in the robust design process	250
9.20	Optimal parameter settings with J_1 , multiple-point tuning, individual design	250
9.21	System eigenvalues of Base Case loading conditions with J_1 settings, multiple-point tuning, individual design	251
9.22	System eigenvalues of Case 1 loading conditions with J_1 settings, multiple-point tuning, individual design	252
9.23	System eigenvalues of Case 2 loading conditions with J_1 settings, multiple-point tuning, individual design	252
9.24	System eigenvalues of Case 3 loading conditions with J_1 settings, multiple-point tuning, individual design	253
9.25	Optimal parameter settings with J_1 , multiple-point tuning, coordinated PSS3-SVC7 design	265
9.26	System eigenvalues of Base Case loading conditions with J_1 settings, multiple-point tuning, coordinated PSS3-SVC7 design	265
9.27	System eigenvalues of Case 1 loading conditions with J_1 settings, multiple-point tuning, coordinated PSS3-SVC7 design	266
9.28	System eigenvalues of Case 2 loading conditions with J_1 settings, multiple-	

	point tuning, coordinated PSS3-SVC7 design	266
9.29	System eigenvalues of Case 3 loading conditions with J_1 settings, multiple-point tuning, coordinated PSS3-SVC7 design	267
9.30	Optimal parameter settings with J_1 , multiple-point tuning, coordinated SVC7-SVC9 design	272
9.31	System eigenvalues of Base Case loading conditions with J_1 settings, multiple-point tuning, coordinated SVC7-SVC9 design	272
9.32	System eigenvalues of Case 1 loading conditions with J_1 settings, multiple-point tuning, coordinated SVC7-SVC9 design	273
9.33	System eigenvalues of Case 2 loading conditions with J_1 settings, multiple-point tuning, coordinated SVC7-SVC9 design	273
9.34	System eigenvalues of Case 3 loading conditions with J_1 settings, multiple-point tuning, coordinated SVC7-SVC9 design	274

LIST OF FIGURES

Figure	Figure Title	Page
2.1	Schematic diagram of TCPS	26
2.2	Schematic diagram of TCSC	26
2.3	Schematic diagram of SVC	27
2.4	Schematic diagram of UPFC	28
2.5	Transmission line without FACTS devices	29
2.6	Transmission line with a TCPS	30
2.7	Transmission line with a TCSC	31
2.8	Transmission line with a SVC	32
2.9	A phasor diagram showing the modulation of real power flow through bus voltage magnitude and phase regulation.	33
3.1	Single machine infinite bus system (SMIB) with G1 FACTS devices	35
3.2	IEEE type-ST1 excitation system with PSS	36
3.3	SVC with lead-lag controller	37
3.4	TCSC with lead-lag controller	37
3.5	TCPS with lead-lag controller	38
3.6	Linearized power system model equipped with a SVC, TCSC, and TCPS	43
3.7	Single machine infinite bus system (SMIB) with a UPFC	46
3.8	UPFC with lead-lag controller	46
3.9	UPFC with lead-lag controller and DC voltage regulator	47
3.10	Linearized power system model equipped with a UPFC	50
3.11	Linearized model of the i th machine in multimachine power system	55
3.12	Linearized model of the i th machine in multimachine power system with a G1 FACTS device	62
4.1	Flow chart of PSO algorithm	67
6.1	Approach implementation plan for a SMIB system with G1 FACTS devices	76
6.2	Approach implementation plan for a SMIB system with a UPFC	76
6.3	Approach implementation plan for a multimachine power system	77
7.1	Minimum singular value with all controllers at $Q = -0.4$ pu	79
7.2	Minimum singular value with all controllers at $Q = 0.0$ pu	80
7.3	Minimum singular value with all controllers at $Q = 0.4$ pu	80
7.4	Damping torque coefficient with the proposed controllers at $Q = -0.4$ pu, J_1 settings, single-point tuning, individual design	85
7.5	Damping torque coefficient with the proposed controllers at $Q = 0.0$ pu, J_1 settings, single-point tuning, individual design	86

7.6	Damping torque coefficient with the proposed controllers at $Q = 0.4$ pu, J_1 settings, single-point tuning, individual design	86
7.7	Rotor angle response for 6-cycle fault with nominal loading, J_1 settings, single-point tuning, individual design	88
7.8	Speed response for 6-cycle fault with nominal loading, J_1 settings, single-point tuning, individual design	88
7.9	Electrical power response for 6-cycle fault with nominal loading, J_1 settings, single-point tuning, individual design	89
7.10	Terminal voltage response for 6-cycle fault with nominal loading, J_1 settings, single-point tuning, individual design	89
7.11	PSS stabilizing signal for 6-cycle fault with nominal loading, J_1 settings, single-point tuning, individual design	90
7.12	B_{svc} response for 6-cycle fault with nominal loading, J_1 settings, single-point tuning, individual design	90
7.13	X_{tcsc} response 6-cycle fault with nominal loading, J_1 settings, single-point tuning, individual design	91
7.14	Φ_{tcps} response 6-cycle fault with nominal loading, J_1 settings, single-point tuning, individual design	91
7.15	Damping torque coefficient with the proposed controllers at $Q = -0.4$ pu, J_2 settings, single-point tuning, individual design	95
7.16	Damping torque coefficient with the proposed controllers at $Q = 0.0$ pu, J_2 settings, single-point tuning, individual design	96
7.17	Damping torque coefficient with the proposed controllers at $Q = 0.4$ pu, J_2 settings, single-point tuning, individual design	96
7.18	Rotor angle response for 6-cycle fault with nominal loading, J_2 settings, single-point tuning, individual design	98
7.19	Speed response for 6-cycle fault with nominal loading, J_2 settings, single-point tuning, individual design	98
7.20	Electrical power response for 6-cycle fault with nominal loading, J_2 settings, single-point tuning, individual design	99
7.21	Terminal voltage response for 6-cycle fault with nominal loading, J_2 settings, single-point tuning, individual design	99
7.22	PSS stabilizing signal for 6-cycle fault with nominal loading, J_2 settings, single-point tuning, individual design	100
7.23	B_{svc} response for 6-cycle fault with nominal loading, J_2 settings, single-point tuning, individual design	100
7.24	X_{tcsc} response 6-cycle fault with nominal loading, J_2 settings, single-point tuning, individual design	101
7.25	Φ_{tcps} response 6-cycle fault with nominal loading, J_2 settings, single-point tuning, individual design	101
7.26	Damping torque coefficient with coordinated PSS & SVC-based stabilizer at $Q = -0.4$ pu, J_2 settings, single-point tuning	105
7.27	Damping torque coefficient with coordinated PSS & SVC-based stabilizer at $Q = 0.0$ pu, J_2 settings, single-point tuning	106
7.28	Damping torque coefficient with coordinated PSS & SVC-based stabilizer at $Q = 0.4$ pu, J_2 settings, single-point tuning	106

7.29	Rotor angle response for 6-cycle fault with nominal loading, J_2 settings, single-point tuning, coordinated design	108
7.30	Speed response for 6-cycle fault with nominal loading, J_2 settings, single-point tuning, coordinated design	108
7.31	Electrical power response for 6-cycle fault with nominal loading, J_2 settings, single-point tuning, coordinated design	109
7.32	Terminal voltage response for 6-cycle fault with nominal loading, J_2 settings, single-point tuning, coordinated design	109
7.33	PSS stabilizing signal for 6-cycle fault with nominal loading, J_2 settings, single-point tuning, coordinated design	110
7.34	B_{svc} response for 6-cycle fault with nominal loading, J_2 settings, single-point tuning, coordinated design	110
7.35	Rotor angle response for 6-cycle fault with light loading, J_2 settings, single-point tuning, coordinated design	111
7.36	Speed response for 6-cycle fault with light loading, J_2 settings, single-point tuning, coordinated design	111
7.37	Electrical power response for 6-cycle fault with light loading, J_2 settings, single-point tuning, coordinated design	112
7.38	Terminal voltage response for 6-cycle fault with light loading, J_2 settings, single-point tuning, coordinated design	112
7.39	PSS stabilizing signal for 6-cycle fault with light loading, J_2 settings, single-point tuning, coordinated design	113
7.40	B_{svc} response for 6-cycle fault with light loading, J_2 settings, single-point tuning, coordinated design	113
7.41	Damping torque coefficient with the proposed controllers at $Q = -0.4$ pu, J_1 settings, multiple-point tuning, individual design	118
7.42	Damping torque coefficient with the proposed controllers at $Q = 0.0$ pu, J_1 settings, multiple-point tuning, individual design	119
7.43	Damping torque coefficient with the proposed controllers at $Q = 0.4$ pu, J_1 settings, multiple-point tuning, individual design	119
7.44	Rotor angle response for 6-cycle fault with nominal loading, J_1 settings, multiple-point tuning, individual design	121
7.45	Speed response for 6-cycle fault with nominal loading, J_1 settings, multiple-point tuning, individual design	121
7.46	Electrical power response for 6-cycle fault with nominal loading, J_1 settings, multiple-point tuning, individual design	122
7.47	Terminal voltage response for 6-cycle fault with nominal loading, J_1 settings, multiple-point tuning, individual design	122
7.48	PSS stabilizing signal for 6-cycle fault with nominal loading, J_1 settings, multiple-point tuning, individual design	123
7.49	B_{svc} response for 6-cycle fault with nominal loading, J_1 settings, multiple-point tuning, individual design	123
7.50	X_{tcsc} response 6-cycle fault with nominal loading, J_1 settings, multiple-point tuning, individual design	124
7.51	Φ_{tcps} response 6-cycle fault with nominal loading, J_1 settings, multiple-point tuning, individual design	124

7.52	Damping torque coefficient with the proposed controllers at $Q = -0.4$ pu, J_2 settings, multiple-point tuning, individual design	128
7.53	Damping torque coefficient with the proposed controllers at $Q = 0.0$ pu, J_2 settings, multiple-point tuning, individual design	129
7.54	Damping torque coefficient with the proposed controllers at $Q = 0.4$ pu, J_2 settings, multiple-point tuning, individual design	129
7.55	Rotor angle response for 6-cycle fault with nominal loading, J_2 settings, multiple-point tuning, individual design	131
7.56	Speed response for 6-cycle fault with nominal loading, J_2 settings, multiple-point tuning, individual design	131
7.57	Electrical power response for 6-cycle fault with nominal loading, J_2 settings, multiple-point tuning, individual design	132
7.58	Terminal voltage response for 6-cycle fault with nominal loading, J_2 settings, multiple-point tuning, individual design	132
7.59	PSS stabilizing signal for 6-cycle fault with nominal loading, J_2 settings, multiple-point tuning, individual design	133
7.60	B_{svc} response for 6-cycle fault with nominal loading, J_2 settings, multiple-point tuning, individual design	133
7.61	X_{tcsc} response 6-cycle fault with nominal loading, J_2 settings, multiple-point tuning, individual design	134
7.62	Φ_{tcps} response 6-cycle fault with nominal loading, J_2 settings, multiple-point tuning, individual design	134
7.63	Damping torque coefficient with coordinated PSS & TCSC-based controller at $Q = -0.4$ pu, J_1 settings, multiple-point tuning	138
7.64	Damping torque coefficient with coordinated PSS & TCSC-based controller at $Q = 0.0$ pu, J_1 settings, multiple-point tuning	139
7.65	Damping torque coefficient with coordinated PSS " TCSC-based controller at $Q = 0.4$ pu, J_1 settings, multiple-point tuning	139
7.66	Rotor angle response for 6-cycle fault with nominal loading, J_1 settings, multiple-point tuning, coordinated design	141
7.67	Speed response for 6-cycle fault with nominal loading, J_1 settings, multiple-point tuning, coordinated design	141
7.68	Electrical power response for 6-cycle fault with nominal loading, J_1 settings, multiple-point tuning, coordinated design	142
7.69	Terminal voltage response for 6-cycle fault with nominal loading, J_1 settings, multiple-point tuning, coordinated design	142
7.70	PSS stabilizing signal for 6-cycle fault with nominal loading, J_1 settings, multiple-point tuning, coordinated design	143
7.71	X_{tcsc} response 6-cycle fault with nominal loading, J_1 settings, multiple-point tuning, coordinated design	143
7.72	Rotor angle response for 6-cycle fault with light loading, J_1 settings, multiple-point tuning, coordinated design	144
7.73	Speed response for 6-cycle fault with light loading, J_1 settings, multiple-point tuning, coordinated design	144
7.74	Electrical power response for 6-cycle fault with light loading, J_1 settings, multiple-point tuning, coordinated design	145

7.75	Terminal voltage response for 6-cycle fault with light loading, J_1 settings, multiple-point tuning, coordinated design	145
7.76	PSS stabilizing signal for 6-cycle fault with light loading, J_1 settings, multiple-point tuning, coordinated design	146
7.77	X_{tcsc} response 6-cycle fault with light loading, J_1 settings, multiple-point tuning, coordinated design	146
8.1	Minimum singular value with all controllers at $Q = -0.4$ pu	148
8.2	Minimum singular value with all controllers at $Q = 0.0$ pu	149
8.3	Minimum singular value with all controllers at $Q = 0.4$ pu	149
8.4	Damping torque coefficient with the proposed controllers at $Q = -0.4$ pu, J_1 settings, single-point tuning, individual design	155
8.5	Damping torque coefficient with the proposed controllers at $Q = 0.0$ pu, J_1 settings, single-point tuning, individual design	155
8.6	Damping torque coefficient with the proposed controllers at $Q = 0.4$ pu, J_1 settings, single-point tuning, individual design	156
8.7	Rotor angle response for 6-cycle fault with nominal loading, J_1 settings, single-point tuning, individual design	157
8.8	Speed response for 6-cycle fault with nominal loading, J_1 settings, single-point tuning, individual design	157
8.9	Electrical power response for 6-cycle fault with nominal loading, J_1 settings, single-point tuning, individual design	158
8.10	Terminal voltage response for 6-cycle fault with nominal loading, J_1 settings, single-point tuning, individual design	158
8.11	DC voltage response for 6-cycle fault with nominal loading, J_1 settings, single-point tuning, individual design	159
8.12	PSS stabilizing signal for 6-cycle fault with nominal loading, J_1 settings, single-point tuning, individual design	159
8.13	δ_E response for 6-cycle fault with nominal loading, J_1 settings, single-point tuning, individual design	160
8.14	m_B response 6-cycle fault with nominal loading, J_1 settings, single-point tuning, individual design	160
8.15	Damping torque coefficient with the proposed stabilizers at $Q = -0.4$ pu, J_2 settings, single-point tuning, individual design	165
8.16	Damping torque coefficient with the proposed stabilizers at $Q = 0.0$ pu, J_2 settings, single-point tuning, individual design	165
8.17	Damping torque coefficient with the proposed stabilizers at $Q = 0.4$ pu, J_2 settings, single-point tuning, individual design	166
8.18	Rotor angle response for 6-cycle fault with nominal loading, J_2 settings, single-point tuning, individual design	167
8.19	Speed response for 6-cycle fault with nominal loading, J_2 settings, single-point tuning, individual design	167
8.20	Electrical power response for 6-cycle fault with nominal loading, J_2 settings, single-point tuning, individual design	168
8.21	Terminal voltage response for 6-cycle fault with nominal loading, J_2 settings, single-point tuning, individual design	168
8.22	DC voltage response for 6-cycle fault with nominal loading, J_2 settings,	

	single-point tuning, individual design	169
8.23	PSS stabilizing signal for 6-cycle fault with nominal loading, J_2 settings, single-point tuning, individual design	169
8.24	δ_E response for 6-cycle fault with nominal loading, J_2 settings, single-point tuning, individual design	170
8.25	m_B response 6-cycle fault with nominal loading, J_2 settings, single-point tuning, individual design	170
8.26	Damping torque coefficient with coordinated PSS & m_B -based controller at $Q = -0.4$ pu, J_1 settings, single-point tuning	174
8.27	Damping torque coefficient with coordinated PSS & m_B -based controller at $Q = 0.0$ pu, J_1 settings, single-point tuning	175
8.28	Damping torque coefficient with coordinated PSS & m_B -based controller at $Q = 0.4$ pu, J_1 settings, single-point tuning	175
8.29	Rotor angle response for 6-cycle fault with nominal loading, J_1 settings, single-point tuning, coordinated design	177
8.30	Speed response for 6-cycle fault with nominal loading, J_1 settings, single-point tuning, coordinated design	177
8.31	Electrical power response for 6-cycle fault with nominal loading, J_1 settings, single-point tuning, coordinated design	178
8.32	Terminal voltage response for 6-cycle fault with nominal loading, J_1 settings, single-point tuning, coordinated design	178
8.33	DC voltage response for 6-cycle fault with nominal loading, J_1 settings, single-point tuning, coordinated design	179
8.34	PSS stabilizing signal for 6-cycle fault with nominal loading, J_1 settings, single-point tuning, coordinated design	179
8.35	m_B response 6-cycle fault with nominal loading, J_1 settings, single-point tuning, coordinated design	180
8.36	Rotor angle response for 6-cycle fault with light loading, J_1 settings, single-point tuning, coordinated design	180
8.37	Speed response for 6-cycle fault with light loading, J_1 settings, single-point tuning, coordinated design	181
8.38	Electrical power response for 6-cycle fault with light loading, J_1 settings, single-point tuning, coordinated design	181
8.39	Terminal voltage response for 6-cycle fault with light loading, J_1 settings, single-point tuning, coordinated design	182
8.40	DC voltage response for 6-cycle fault with light loading, J_1 settings, single-point tuning, coordinated design	182
8.41	PSS stabilizing signal for 6-cycle fault with light loading, J_1 settings, single-point tuning, coordinated design	183
8.42	m_B response 6-cycle fault with light loading, J_1 settings, single-point tuning, coordinated design	183
8.43	Damping torque coefficient with the proposed stabilizers at $Q = -0.4$ pu, J_1 settings, multiple-point tuning, individual design	188
8.44	Damping torque coefficient with the proposed stabilizers at $Q = 0.0$ pu, J_1 settings, multiple-point tuning, individual design	189
8.45	Damping torque coefficient with the proposed stabilizers at $Q = 0.4$ pu, J_1	

	settings, multiple-point tuning, individual design	189
8.46	Rotor angle response for 6-cycle fault with nominal loading, J_1 settings, multiple-point tuning, individual design	191
8.47	Speed response for 6-cycle fault with nominal loading, J_1 settings, multiple-point tuning, individual design	191
8.48	Electrical power response for 6-cycle fault with nominal loading, J_1 settings, multiple-point tuning, individual design	192
8.49	Terminal voltage response for 6-cycle fault with nominal loading, J_1 settings, multiple-point tuning, individual design	192
8.50	DC voltage response for 6-cycle fault with nominal loading, J_1 settings, multiple-point tuning, individual design	193
8.51	PSS stabilizing signal for 6-cycle fault with nominal loading, J_1 settings, multiple-point tuning, individual design	193
8.52	δ_E response for 6-cycle fault with nominal loading, J_1 settings, multiple-point tuning, individual design	194
8.53	m_B response 6-cycle fault with nominal loading, J_1 settings, multiple-point tuning, individual design	194
8.54	Damping torque coefficient with the proposed stabilizers at $Q = -0.4$ pu, J_2 settings, multiple-point tuning, individual design	199
8.55	Damping torque coefficient with the proposed stabilizers at $Q = 0.0$ pu, J_2 settings, multiple-point tuning, individual design	199
8.56	Damping torque coefficient with the proposed stabilizers at $Q = 0.4$ pu, J_2 settings, multiple-point tuning, individual design	200
8.57	Rotor angle response for 6-cycle fault with nominal loading, J_2 settings, multiple-point tuning, individual design	201
8.58	Speed response for 6-cycle fault with nominal loading, J_2 settings, multiple-point tuning, individual design	201
8.59	Electrical power response for 6-cycle fault with nominal loading, J_2 settings, multiple-point tuning, individual design	202
8.60	Terminal voltage response for 6-cycle fault with nominal loading, J_2 settings, multiple-point tuning, individual design	202
8.61	DC voltage response for 6-cycle fault with nominal loading, J_2 settings, multiple-point tuning, individual design	203
8.62	PSS stabilizing signal for 6-cycle fault with nominal loading, J_2 settings, multiple-point tuning, individual design	203
8.63	δ_E response for 6-cycle fault with nominal loading, J_2 settings, multiple-point tuning, individual design	204
8.64	m_B response 6-cycle fault with nominal loading, J_2 settings, multiple-point tuning, individual design	204
8.65	Damping torque coefficient with coordinated δ_E and m_B -based controller at $Q = -0.4$ pu, J_2 settings, multiple-point tuning	208
8.66	Damping torque coefficient with coordinated δ_E and m_B -based controller at $Q = 0.0$ pu, J_2 settings, multiple-point tuning	209
8.67	Damping torque coefficient with coordinated δ_E and m_B -based controller at $Q = 0.4$ pu, J_2 settings, multiple-point tuning	209
8.68	Rotor angle response for 6-cycle fault with nominal loading, J_2 settings,	

	multiple-point tuning, coordinated design	211
8.69	Speed response for 6-cycle fault with nominal loading, J_2 settings, multiple-point tuning, coordinated design	211
8.70	Electrical power response for 6-cycle fault with nominal loading, J_2 settings, multiple-point tuning, coordinated design	212
8.71	Terminal voltage response for 6-cycle fault with nominal loading, J_2 settings, multiple-point tuning, coordinated design	212
8.72	DC voltage response for 6-cycle fault with nominal loading, J_2 settings, multiple-point tuning, coordinated design	213
8.73	δ_E response for 6-cycle fault with nominal loading, J_2 settings, multiple-point tuning, coordinated design	213
8.74	m_B response 6-cycle fault with nominal loading, J_2 settings, multiple-point tuning, coordinated design	214
8.75	Rotor angle response for 6-cycle fault with light loading, J_2 settings, multiple-point tuning, coordinated design	214
8.76	Speed response for 6-cycle fault with light loading, J_2 settings, multiple-point tuning, coordinated design	215
8.77	Electrical power response for 6-cycle fault with light loading, J_2 settings, multiple-point tuning, coordinated design	215
8.78	Terminal voltage response for 6-cycle fault with light loading, J_2 settings, multiple-point tuning, coordinated design	216
8.79	DC voltage response for 6-cycle fault with light loading, J_2 settings, multiple-point tuning, coordinated design	216
8.80	δ_E response for 6-cycle fault with light loading, J_2 settings, multiple-point tuning, coordinated design	217
8.81	m_B response 6-cycle fault with light loading, J_2 settings, multiple-point tuning, coordinated design	217
9.1	Minimum singular values with all controllers with respect to the first EM mode as load increases, $Q_A = 0.55$ pu, $Q_B = 0.35$ pu, and $Q_C = 0.25$ pu	220
9.2	Minimum singular values with all controllers with respect to the second EM mode as load increases, $Q_A = 0.55$ pu, $Q_B = 0.35$ pu, and $Q_C = 0.25$ pu	220
9.3	Rotor angle response for 6-cycle fault with base case, J_1 settings of PSS2, single-point tuning, individual design	226
9.4	Speed response for 6-cycle fault with base case, J_1 settings of PSS2, single-point tuning, individual design	226
9.5	Electrical power response for 6-cycle fault with base case, J_1 settings of PSS2, single-point tuning, individual design	227
9.6	Terminal voltage response for 6-cycle fault with base case, J_1 settings of PSS2, single-point tuning, individual design	227
9.7	PSS stabilizing signal for 6-cycle fault with base case, J_1 settings of PSS2, single-point tuning, individual design	228
9.8	Rotor angle response for 6-cycle fault with base case, J_1 settings of PSS3, single-point tuning, individual design	228
9.9	Speed response for 6-cycle fault with base case, J_1 settings of PSS3, single-point tuning, individual design	229
9.10	Electrical power response for 6-cycle fault with base case, J_1 settings of	

	PSS3, single-point tuning, individual design	229
9.11	Terminal voltage response for 6-cycle fault with base case, J_1 settings of PSS3, single-point tuning, individual design	230
9.12	PSS stabilizing signal for 6-cycle fault with base case, J_1 settings of PSS3, single-point tuning, individual design	230
9.13	Rotor angle response for 6-cycle fault with base case, J_1 settings of SVC7, single-point tuning, individual design	231
9.14	Speed response for 6-cycle fault with base case, J_1 settings of SVC7, single-point tuning, individual design	231
9.15	Electrical power response for 6-cycle fault with base case, J_1 settings of SVC7, single-point tuning, individual design	232
9.16	Terminal voltage response for 6-cycle fault with base case, J_1 settings of SVC7, single-point tuning, individual design	232
9.17	B_{svc} response for 6-cycle fault with base case, J_1 settings of SVC7, single-point tuning, individual design	233
9.18	Rotor angle response for 6-cycle fault with base case, J_1 settings of SVC9, single-point tuning, individual design	233
9.19	Speed response for 6-cycle fault with base case, J_1 settings of SVC9, single-point tuning, individual design	234
9.20	Electrical power response for 6-cycle fault with base case, J_1 settings of SVC9, single-point tuning, individual design	234
9.21	Terminal voltage response for 6-cycle fault with base case, J_1 settings of SVC9, single-point tuning, individual design	235
9.22	B_{svc} response for 6-cycle fault with base case, J_1 settings of SVC9, single-point tuning, individual design	235
9.23	Rotor angle response for 6-cycle fault with base case, J_1 settings, single-point tuning, coordinated PSS3-SVC7 design	240
9.24	Speed response for 6-cycle fault with base case, J_1 settings, single-point tuning, coordinated PSS3-SVC7 design	240
9.25	Electrical power response for 6-cycle fault with base case, J_1 settings, single-point tuning, coordinated PSS3-SVC7 design	241
9.26	Terminal voltage response for 6-cycle fault with base case, J_1 settings, single-point tuning, coordinated PSS3-SVC7 design	241
9.27	PSS stabilizing signal for 6-cycle fault with base case, J_1 settings, single-point tuning, coordinated PSS3-SVC7 design	242
9.28	B_{svc} response for 6-cycle fault with base case, J_1 settings, single-point tuning, coordinated PSS3-SVC7 design	242
9.29	Rotor angle response for 6-cycle fault with base case, J_1 settings, single-point tuning, coordinated SVC7-SVC9 design	247
9.30	Speed response for 6-cycle fault with base case, J_1 settings, single-point tuning, coordinated SVC7-SVC9 design	247
9.31	Electrical power response for 6-cycle fault with base case, J_1 settings, single-point tuning, coordinated SVC7-SVC9 design	248
9.32	Terminal voltage response for 6-cycle fault with base case, J_1 settings, single-point tuning, coordinated SVC7-SVC9 design	248
9.33	B_{svc} response for 6-cycle fault with base case, J_1 settings, single-point	

	tuning, coordinated SVC7-SVC9 design	249
9.34	Rotor angle response for 6-cycle fault with base case, J_1 settings of PSS2, multiple-point tuning, individual design	254
9.35	Speed response for 6-cycle fault with base case, J_1 settings of PSS2, multiple-point tuning, individual design	254
9.36	Electrical power response for 6-cycle fault with base case, J_1 settings of PSS2, multiple-point tuning, individual design	255
9.37	Terminal voltage response for 6-cycle fault with base case, J_1 settings of PSS2, multiple-point tuning, individual design	255
9.38	PSS stabilizing signal for 6-cycle fault with base case, J_1 settings of PSS2, multiple-point tuning, individual design	256
9.39	Rotor angle response for 6-cycle fault with base case, J_1 settings of PSS3, multiple-point tuning, individual design	256
9.40	Speed response for 6-cycle fault with base case, J_1 settings of PSS3, multiple-point tuning, individual design	257
9.41	Electrical power response for 6-cycle fault with base case, J_1 settings of PSS3, multiple-point tuning, individual design	257
9.42	Terminal voltage response for 6-cycle fault with base case, J_1 settings of PSS3, multiple-point tuning, individual design	258
9.43	PSS stabilizing signal for 6-cycle fault with base case, J_1 settings of PSS3, multiple-point tuning, individual design	258
9.44	Rotor angle response for 6-cycle fault with base case, J_1 settings of SVC7, multiple-point tuning, individual design	259
9.45	Speed response for 6-cycle fault with base case, J_1 settings of SVC7, multiple-point tuning, individual design	259
9.46	Electrical power response for 6-cycle fault with base case, J_1 settings of SVC7, multiple-point tuning, individual design	260
9.47	Terminal voltage response for 6-cycle fault with base case, J_1 settings of SVC7, multiple-point tuning, individual design	260
9.48	B_{svc} response for 6-cycle fault with base case, J_1 settings of SVC7, multiple-point tuning, individual design	261
9.49	Rotor angle response for 6-cycle fault with base case, J_1 settings of SVC9, multiple-point tuning, individual design	261
9.50	Speed response for 6-cycle fault with base case, J_1 settings of SVC9, multiple-point tuning, individual design	262
9.51	Electrical power response for 6-cycle fault with base case, J_1 settings of SVC9, multiple-point tuning, individual design	262
9.52	Terminal voltage response for 6-cycle fault with base case, J_1 settings of SVC9, multiple-point tuning, individual design	263
9.53	B_{svc} response for 6-cycle fault with base case, J_1 settings of SVC9, multiple-point tuning, individual design	263
9.54	Rotor angle response for 6-cycle fault with base case, J_1 settings, multiple-point tuning, coordinated PSS3-SVC7 design	268
9.55	Speed response for 6-cycle fault with base case, J_1 settings, multiple-point tuning, coordinated PSS3-SVC7 design	268
9.56	Electrical power response for 6-cycle fault with base case, J_1 settings,	

	multiple-point tuning, coordinated PSS3-SVC7 design	269
9.57	Terminal voltage response for 6-cycle fault with base case, J_1 settings, multiple-point tuning, coordinated PSS3-SVC7 design	269
9.58	PSS stabilizing signal for 6-cycle fault with base case, J_1 settings, multiple-point tuning, coordinated PSS3-SVC7 design	270
9.59	B_{svc} response for 6-cycle fault with base case, J_1 settings, multiple-point tuning, coordinated PSS3-SVC7 design	270
9.60	Rotor angle response for 6-cycle fault with base case, J_1 settings, multiple-point tuning, coordinated SVC7-SVC9 design	275
9.61	Speed response for 6-cycle fault with base case, J_1 settings, multiple-point tuning, coordinated SVC7-SVC9 design	275
9.62	Electrical power response for 6-cycle fault with base case, J_1 settings, multiple-point tuning, coordinated SVC7-SVC9 design	276
9.63	Terminal voltage response for 6-cycle fault with base case, J_1 settings, multiple-point tuning, coordinated SVC7-SVC9 design	276
9.64	B_{svc} response for 6-cycle fault with base case, J_1 settings, multiple-point tuning, coordinated SVC7-SVC9 design	277
C.1	A detailed three-generator nine-bus system	282

THESIS ABSTRACT

Name ALI TALEB AL-AWAMI
Title DESIGN OF ROBUST PSS AND FACTS-BASED CONTROLLERS FOR STABILITY ENHANCEMENT OF POWER SYSTEMS
Degree MASTER OF SCIENCE
Major Field ELECTRICAL ENGINEERING
Date of Degree MAY 2004

The objective of this thesis is to investigate the effectiveness of the coordinated design of power system stabilizers and FACTS-based stabilizers to improve power system transient stability. Three power systems are studied: a single-machine-infinite-bus system with First Generation (G1) FACTS devices, a single-machine infinite-bus system with a UPFC, and a multimachine power system. To estimate the controllability of each stabilizer control signal on the electromechanical modes, singular value decomposition is employed. In each system, the problem of designing all the stabilizers, PSSs and FACTS-based stabilizers, individually is formulated as an optimization problem. Particle swarm optimizer is utilized to search for the optimum stabilizer parameter settings that optimize a given eigenvalue-based objective function. Coordinated design of the different stabilizers is also carried out by finding the best parameter settings for more than one stabilizer at a given operating condition simultaneously. To ensure the robustness of the proposed control schemes, the design procedure is repeated considering a wide range of operating conditions. To assess the effectiveness of the proposed designs, damping torque coefficient analysis, eigenvalue analysis, as well as nonlinear time-domain simulations are carried out.

Keywords: Power system stability, PSS, FACTS, SVC, TCSC, TCPS, UPFC, singular value, damping torque, robust control, particle swarm, optimization.

MASTER OF SCIENCE DEGREE

KING FAHD UNIVERSITY OF PETROLEUM & MINERALS, DHAHRAN

MAY 2004

خلاصة الرسالة

الاسم	علي طالب العوامي
عنوان الرسالة	تصميم قوي الثبات لمضبطات شبكة الطاقة والمضبطات المستندة على الأنظمة المرنة لنقل التيار المتردد بهدف تحسين ثبات شبكة الطاقة الكهربائية
الدرجة	الماجستير في العلوم
التخصص	الهندسة الكهربائية
تاريخ التخرج	مايو 2004 م

الهدف من البحث هو دراسة كفاءة التصميم المترامن لمضبط شبكة الطاقة الكهربائية مع المضبطات المستندة على الأنظمة المرنة لنقل التيار المتردد لغرض تحسين مضاائلة نظام الطاقة. يدرس البحث ثلاثة أنظمة للطاقة: نظام طاقة ماكينة واحدة ذو ناقل لامتناهي مجهز بأجهزة الجيل الأول من الأنظمة المرنة لنقل التيار المتردد، نظام طاقة ماكينة واحدة ذو ناقل لامتناهي مجهز بجهاز التحكم الموحد لتدفق الطاقة، ونظام طاقة متعدد المكاين. لتقدير مدى قدرة هذه المضبطات المختلفة على مضاائلة الشكل الكهروميكانيكي، يتم تطبيق طريقة تحليل القيمة الشاذة. تصاغ مسألة تصميم المضبطات بشكل مسألة الحل الأمثل بحيث تستخدم طريقة سرب الجسيمات للبحث عن أفضل قيم لمكونات كل مضبط على حدة لتحقيق أمثل قيمة لمقياس الأداء باعتبار نقطة تشغيل واحدة. يتم بعد ذلك تصميم أكثر من مضبط بشكل مترامن بنفس الطريقة. من أجل التأكد من أن المضبطات المقترحة ذات ثبات قوي، يعاد تصميمها باعتبار نقاط تشغيل عديدة. للتحقق من كفاءة التصاميم المقترحة، جرى اختبارها عن طريق تحليل معامل عزم المضاائلة، تحليل مضاائلة الشكل الكهروميكانيكي، والمحاكاة الزمنية غير الخطية لإشارات الشبكة.

درجة الماجستير في العلوم

جامعة الملك فهد للبترول والمعادن، الظهران

مايو 2004

CHAPTER 1

INTRODUCTION

Power systems, in their early days, were simple and relatively local. That is, power was generated beside the load centers and, hence, exportation and importation of power through long transmission lines were rare. Moreover, systems interconnection between control areas was not common. Fast control was not available since series and shunt reactive compensators, voltage regulating transformers, and phase shifters were manually operated through mechanical devices. Consequently, those devices were limited to control power system performance during steady-state operation. The only viable solution of transient problems was overdesign of generation and transmission equipment, keeping large stability margins.

Nowadays, power demand has grown rapidly and, therefore, the need for more complex power systems has arisen. On the other hand, expansion in transmission and generation is restricted with the limited availability of resources and the strict environmental constraints. As a result, power systems are today more loaded than before, causing the systems to operate near their transient stability limits. Furthermore, interconnection between distantly located power systems is now a common practice, which gives rise to low frequency oscillations in the range of 0.1-3.0 Hz. If not well

damped, these oscillations may keep growing in magnitude until loss of synchronism results.

Power system stabilizers (PSSs) have been used in the last few decades to serve the purpose of enhancing power system damping of low frequency oscillations. PSSs, which operate on the excitation system of generators, have proved to be efficient in performing their assigned tasks. However, PSSs may adversely affect voltage profile, may result in leading power factor, and may not be able to suppress oscillations resulting from severe disturbances, especially those three-phase faults which may occur at the generator terminals.

FACTS devices have shown very promising results when used to improve power system steady-state performance. Through the modulation of bus voltage, phase shift between buses, and transmission line reactance, static VAR compensators (SVCs), thyristor-controlled phase shifters (TCPSs), and thyristor-controlled series capacitors (TCSCs), respectively, can cause a substantial increase in power transfer limits during steady-state. Because of the extremely fast control action associated with FACTS-device operations, they have been very promising candidates for utilization in power system damping enhancement. It has been observed that utilizing a feedback supplementary control, in addition to the FACTS-device primary control, can considerably improve system damping and can also improve system voltage profile, which is advantageous over PSSs.

However, possible interaction between PSSs and FACTS-based stabilizers may deteriorate much of their contributions to, and may even cause adverse effect on, damping of system oscillations. Therefore, coordinated design between PSSs and FACTS-based

stabilizers is a necessity, both to make use of the advantages of the different stabilizers and to avoid the demerits accompanied with their operations.

1.1 Literature Review

Since the late 1950's, most new generating units were equipped with automatic voltage regulators (AVRs), which control the excitation of the generator's field winding. Electromechanical oscillations of low frequencies, in the range of 0.1-3 Hz, are usually inherent to interconnected power systems due to the application of AVRs [6][161]. Oscillations associated with a single generator or a single plant are called local modes. These modes are usually in the range of 0.7-3.0 Hz. On the other hand, oscillations associated with groups of generators or groups of plants are called inter-area modes, which are in the range of 0.1-0.8 Hz. [8]

1.1.1 Power System Stabilizers

Supplementary excitation control of the low-frequency oscillations is well known as a power system stabilizer (PSS). Since the 1960's, PSSs have been used to add damping to electromechanical oscillations. They act through the generator's excitation system to generate a component of electrical torque, called damping torque, proportional to speed change. Since then, applying PSSs has attracted the attention of researchers. Extensive research has been conducted in such fields as effect of PSS on power system stability, PSS input signals, PSS optimum locations, and PSS tuning techniques.

1.1.1.1 General Concepts and Analytical Investigation of PSS Application

In 1969, de Mello and Concordia [5] introduced an extensive analysis of the phenomenon of synchronous machine stability under small perturbations by studying the single-machine infinite-bus (SMIB) system represented by the linear K1-K6 model. Their work developed insights into effects of excitation systems and requirement of supplementary stabilizing action for such systems based on the concept of damping and synchronizing torques.

Larsen and Swann [6] deeply discussed, in a three-part paper, the general concepts associated with PSSs. In Part I, the concepts of applying and tuning PSSs utilizing speed, frequency, and power input signals have been described. Part II dealt with the performance objectives of PSSs. It was considered that the objective of PSSs is to extend stability limits on power transfer by enhancing damping of system oscillations through excitation control. Larsen and Swann studied PSSs using inputs of power, speed and frequency with respect to tuning concepts and performance capabilities. Part III addressed the major practical considerations associated with applying PSSs. [6]

In 1989, Kundur et al. [7] presented a detailed analytical work to determine the parameters of phase-lead PSSs so as to enhance the steady-state as well as transient stability of both local and inter-area modes. These parameters included the signal washout, stabilizer gain, and stabilizer output limits. They concluded that by proper tuning, the fixed-parameter PSS can satisfy the requirements for a wide range of system conditions and, hence, the need of adaptive PSS is of little incentive. [7]

Two years later, Klein et al. [8] considered a fundamental study of the nature of inter-area mode of oscillations. Klein et al. [9] further investigated the effect of PSSs on inter-

area and local modes in interconnected power systems. They mainly emphasized the effect of PSS location and load location and characteristics.

Recently, Kundur [10] examined the choice of input signals, control design procedure, coordination with other control and protective functions, hardware considerations, and functioning procedures. In his discussion of the characteristics of each input signal, Kundur's conclusions generally agreed with those stated in [6].

1.1.1.2 Identification of Optimum locations of PSSs

A number of papers have addressed the problem of selecting the most suitable locations for PSS installation in multimachine power systems. de Mello et al. [11] made use of eigenvalue analysis techniques to sequentially select the optimum PSS locations. Hsu and Chen [12] have proposed a novel technique to identify the optimum PSS locations by participation factors (PFs). The participation factors can be defined as the sensitivities of the eigenvalues with respect to the diagonal elements of the system matrix A . One of the main advantages of this technique is that the PFs are real quantities whereas the eigenvectors in [11] are complex quantities. One year later, Ostojic [13] has extended the PF technique by introducing new coupling factors between each pair of system machines, making it possible to identify the sites where the application of PSSs ensures maximum improvement of overall system damping characteristics. Martins and Lima [14] presented a way of locating PSSs based on transfer function residues. Based on the transfer function residues method, Yang and Feliachi [15] suggested a method to classify oscillation modes as either local or inter-area.

Klein et al. [9] has investigated the usefulness of the three techniques described above. They concluded that eigenvectors, PFs, and residues can be misleading when the

system has identical or very close eigenvalues. In such cases, the eigenvectors are not unique and lose their physical meaning. Frequency response can be used to distinguish this situation from the resonance phenomenon.

Another method of optimal PSS siting was proposed by Lu et al. [16], which takes into account the effect of the B matrix. Feliachi [17] has developed his method based on a quadratic performance measure, which is a function of the A , B , and C matrices, and the left and right eigenvectors. Another novel technique for selection of PSS locations has been presented by Zhou et al [18,19]. Based on the right and left eigenvectors, the sensitivity of PSS effect (SPE) is defined and used to select the best PSS locations. It is worth noting that this method considers the effect of control, i.e. closed loop effect.

1.1.1.3 PSS Tuning Techniques

The subject of selecting PSS parameters has attracted the attention of many researchers [20-65]. A wide spectrum of PSS tuning approaches has been proposed. These approaches have included pole placement [20-30], damping torque concepts [6,31,32], H_∞ and LQG/LTR [33-35], nonlinear and variable structure [36-38], and the different optimization and artificial intelligence techniques [39-64]. Some of the proposed PSSs are analog and others are digital. Self-tuning PSSs have been proposed along with fixed-parameter PSSs. The conventional and widely used PSS structure is the lead-lag compensator. However, state-feedback and PID controllers have been also suggested.

In 1981, Fleming et al. [20] provided a tuning procedure based on pole placement, enabling the selection of PSS parameters such that prespecified improvements in the damping ratios of the poorly damped modes are realized approximately. Abe and Doi [21] have developed another procedure by combining the frequency response and the pole

placement method. Gooi et al. [22] described an iterative pole placement technique, based on the synchronous and damping torques. The drawback of this technique is the need for truth table and signal flow graph building. This drawback has been avoided in [23] while achieving a similar objective by using linear algebra. Lim and Elangovan [24] have proposed another method based on the complex frequency domain and with a design objective similar to that of [22] and [23]. The method presented in [24] does not need any truth table or signal flow graph construction. Moreover, this method can be used to compute the damping and synchronizing coefficients of any generator and, with slight modifications, the iterative method can also be used to determine only those eigenvalues in the dynamic stability range [24]. An approach based on decentralized model control (DMC) theory has been proposed for the simultaneous selection of PSS parameters in a multimachine power system [25]. Chen and Hsu [26] presented another pole-placement algorithm for the design of decentralized output feedback PSSs suitable for large-scale power systems. Another pole-placement method has been developed by Yu and Li [27]. The method involves pole-zero cancellation, which makes it only effective for one operating point. Chandra et al. [28] has developed a self-tuning control technique that was robust for many operating conditions. Some authors have proposed the use of PID PSSs in placing the poles [29,30].

One of the interesting approaches in PSS parameter selection is based on damping torque concepts, originally developed by Larsen and Swann [6] for the simple single-machine infinite-bus system. Gibbard [31,32] has extended this approach to the more realistic multimachine system.

To overcome the problem of PSSs robustness, H_∞ control design technique, which produces a controller satisfactory for a range of operating conditions, has been proposed. Although H_∞ controllers can guarantee robustness, they have several demerits. Optimal H_∞ controllers are of the same order as the plant. Hence, when H_∞ is applied to a large power system, a good quality reduced model of the system is a necessity. Also, H_∞ controllers achieve their goal by affecting the observability of the open loop poles, and do not affect the damping factor of these poles, which is undesirable in excitation control. In addition, weighting functions need to be selected with care [33,34]. Another approach to overcome the problem of robustness was proposed by some researchers through the utilization of LQG/LTR [35].

Some researchers developed nonlinear and variable structure controllers for the purpose of overcoming the problem of robustness [36-38]. Although the nonlinear stabilizers proposed are fixed-parameter, they are robust since they are independent of the operation conditions of the system.

Since the late 1980's and the early 1990's, the use of optimization techniques in solving the problem of selecting the optimum PSS parameters has been extensively investigated [39-64]. These optimization techniques include gradient-based techniques, linear programming, quadratic programming, and the heuristic methods such as genetic algorithm (GA) [43,45-47], simulated annealing (SA) [48], particle swarm (PSO) [51], Tabu search (TS) [52,53], and evolutionary programming (EP) [54]. In order to be able to use any of the optimization techniques, the problem of selecting the most appropriate PSS parameters need to be formulated as an optimization problem. Therefore, an objective

function to be minimized, or maximized, needs to be defined and equality and inequality constraints should also be determined.

Heuristic optimization techniques have been recently implemented to select the optimum PSS parameters. These population-based algorithms are derivative-free and hence, they can deal with non-differentiable problems. Also, they are more robust in term of the dependence of the final solution to initial guess. Furthermore, there is less opportunity for these algorithms to be trapped in local minima.

Starting from 1997, pioneering work has been accomplished by Abdel-Magid et al. [43-46] to formulate the problem of tuning the PSS parameters into an optimization problem to be solved using GA. The objective function has been selected as to shift all the dominant eigenvalues at different loading conditions and system configurations simultaneously to within a pre-specified region in the s-plane. This region has been defined by a predetermined value of the damping ratio, a predetermined value of the damping factor, or both. The PSS parameter space was defined as inequality constraints. Eigenvalue analysis and nonlinear time-domain simulation results proved the effectiveness of the proposed PSSs to damp out local and inter-area modes over a wide range of loading conditions and system configurations.

Although the application of GA to synthesize the PSS parameters yielded promising results, recent research has identified some deficiencies in GA performance. The deficiency appeared in applying GA to highly epistatic objective functions, in which the parameters to be optimized are much correlated. Also, the mutation and crossover may be time consuming processes and they may cause the new generation to lose advantages obtained in the last generation. As a result, different optimization algorithms, such as

simulated annealing [48], particle swarm [51], tabu search [52,53], and evolutionary programming [54], have been also explored.

To overcome the difficulties associated with the design of robust stabilizers that results in optimal performance with the widely varying operating conditions and system disturbances, adaptive PSSs have been proposed [28,30,55-65]. These adaptive PSS design techniques are based on neural networks [55,56], fuzzy logic [57], neuro-fuzzy technique [58-62], genetic-based fuzzy technique [63,64], and genetic-based rule-based technique [65].

1.1.2 FACTS Devices

Despite the interesting properties provided by PSSs to enhance power system damping, they have adverse effect on system voltage profile, they may result in leading power factor operation, and they may not be able to maintain system stability, especially following a large fault occurring close to the generator terminal [66]. Because of the revolutionary advances in high power electronic device technologies, Flexible AC Transmission Systems (FACTS) devices have been economically proved to be promising candidates for wide application for the purpose of power system stability enhancement.

In 1988, Hingorani [67-71] have initiated the concept of FACTS devices and their application for the following purposes: control of power routing, loading of transmission lines near their steady-state, short-time and dynamic limits, reducing generation reserve margins, and finally, limiting the impact of multiple faults and, hence, containing cascaded outages. This can be performed through the use of thyristor-controlled phase shifters (TCPSs) which control the phase angle, thyristor-controlled series capacitors (TCSCs) which control the line impedance, static VAR compensators(SVCs) which

controls the bus voltage, unified power flow controllers (UPFCs), and other thyristor-controlled devices such as static compensators (STATCOMs), thyristor-controlled dynamic brake, etc. [67-71]

1.1.2.1 Thyristor-Controlled Phase Shifters (TCPS)

Researchers have developed different TCPS schemes in the literature [72-74]. Iravani and Maratukulam [72] described ten different topologies for realization of TCPSs. Iravani et al. [73] have further explored four of those TCPS schemes by applying them in four different systems. Ise et al. [74] compared between two different TCPS schemes.

Compared with other FACTS devices, little attention have been paid to TCPS modeling and control. Based on the equal area criterion, Edris [75] developed a simple control scheme which was conceptualized to extend the capability of the generator to produce sufficient decelerating energy to counterbalance the accelerating energy gained during faults. The TCPS control problem has also been investigated using linear control techniques [73,76]. Iravani et al. [73] developed two control schemes, one for Type-B and Type-C and the other for Type-D and Type-D2. A similar scheme was used in [76] to study the stabilizing effect of TCPSs on inter-area modes of oscillations.

In [77] Abido used simulated annealing (SA) algorithm to determine the optimum settings of TCPS lead-lag controller parameters. The proposed objective function was to maximize the damping ratio of the electromechanical modes. In addition, nonlinear TCPS control schemes have been investigated [78-80].

Because of its difficulties, a little research has been devoted to the problem of modeling of a TCPS applied for a multimachine system [81,82]. The TCPS was modeled in [81] as node power injections whose effects appear as additional bus power injections

at internal buses of the generator. Another mathematical model was reported by Ngan [82] for a Type-B TCPS. The model included the leakage reactance of both the boosting and excitation transformer. The model considered the TCPS as a branch of constant impedance with current injected at its two terminals.

1.1.2.2 Thyristor-Controlled Series Capacitor

A lot of research efforts have been devoted to the control of TCSC. Chen et al. designed a state feedback TCSC controller based on the pole placement technique [83,84]. In addition, they proposed a procedure for determining the optimum location for installing a TCSC in a power system using residue analysis. Also, they developed a technique for coordinated TCSCs. Chen et al. showed that in addition to the better damping effect, the TCSC control causes much less voltage variation at the machine terminal than the PSS control. To overcome the problems associated with the state feedback controller proposed in [83,84], Chen et al. [85] proposed TCSC controllers based on output feedback. A new method based on mode controllability was developed to identify the best TCSC location. Moreover, the analysis of mode observability was used to select the effective output feedback signals local to the TCSC locations. Linear programming has been utilized to find the optimum feedback gains of the coordinated TCSCs.

In [86], a pair of remote voltages was synthesized using the voltages and currents measured at the terminals of a TCSC and the Thevenin impedances. Then, the synthesized angle signal was computed as the difference between the phase angles of the two synthesized voltages. This angle was employed for TCSC controller input. In contrast to [86], de Mello [87] used the rate of change of through power in a TCSC as the feedback signal to the controller. de Mello based his control scheme on the concept of the natural

damping effect of dynamic reactances exhibiting characteristics similar to those in a rotating machine. Recently, Fan and Feliachi [88] identified the most effective signal in damping interarea oscillations for a wide range of operating conditions using transfer function residues.

In 1997, a time optimal control strategy was developed by Chang and Chow [89,90] for the TCSC control for damping interarea modes in interconnected power systems. A performance index of time was minimized to reach the goal of minimum time control.

Robust control approaches have also been explored. Therefore, H_∞ controllers have been proposed [91,92]. A comparison between H_∞ and LQR controllers to improve damping of a multimachine system was established in [91]. It was concluded that H_∞ provided better stability but it needs larger compensation. Line sensitivity coefficients were utilized to obtain the best TCSC sites.

Nonlinear control schemes have been also employed to the design of TCSC controllers. Wang et al. [93] presented a variable structure controller for the TCSC of a SMIB system. Lour and Hsu [94] designed an output feedback VSC utilizing real and reactive power signals, which are local signals. A TCSC controller based on bilinear self-tuning feedback of generator armature current or generator speed measurements has been considered in [95].

Lour and Hsu demonstrated an adaptive TCSC controller based on fuzzy logic control scheme on a SMIB system to improve system damping. The coordination of the proposed FL TCSC controller with a PSS was also investigated [96]. Artificial neural networks are another form of the proposed self-tuning TCSC controllers in the literature [97,98].

Recently, heuristic optimization techniques have been implemented to search for the optimum TCSC based stabilizer parameters for the purpose of enhancing SMIB system stability [99,100]. Abido employed genetic algorithm [99] and simulated annealing [100] to tune a conventional two-stage lead-lag controller for a TCSC.

1.1.2.3 Static VAR Compensator

The primary objective of using static VAR compensators (SVCs) is to control the bus voltage magnitude affected by the ever changing load variations and system operating conditions. It has been found that SVCs can be effective in damping power system oscillations if controlled by a supplementary feedback signal, different from voltage magnitude, is applied. Extensive analysis of the effect of applying SVCs to damp local as well as interarea modes of oscillations has been reported in the literature.

In his analysis of the application of SVCs for stabilizing power systems, Hammad [101] proved that a bus voltage magnitude controlled SVC does not contribute significantly to system damping. A considerable damping effect can be achieved when an SVC is controlled by some auxiliary signals.

Through damping torque analysis, Padiyar and Varma [102] compared the effectiveness of different local signals on enhancing power transfer capability of long transmission lines. Based on the equal-area criterion, Zhou [103] developed a theory to analyze power system damping enhancement by SVC application. It was found that the system $P-\delta$ characteristics can be altered by changing the SVC reactive power output. Zhou proved that system damping can be improved significantly if an SVC is controlled such that its output is proportional to machine speed deviation, which confirmed with Hammad findings. In addition, Zhou agreed with Hammad on the effectiveness of the

SVC discontinuous control. Zhou also proved that the best SVC location for damping oscillations of a one-machine or a two-area system is the electrical center point of the transmission line [103].

Olivera [104] comprehensively studied the effect of SVC control on improving power system damping characteristics through damping and synchronizing torque coefficients. Wang and Swift [105] used a similar approach to that of [104] to investigate the SVC damping control of a SMIB system on the basis of Phillips-Heffron model. It was shown that the SVC damping control provides the power system with negative damping when it operates at a lower load condition than the dead point, the point at which SVC control produces zero damping effect.

Various control schemes have been proposed in the literature for SVC damping control. Lee and Liu [106] applied an eigenstructure assignment technique to design an SVC damping control using a PI controller. Robust control designs, based on H_∞ and structured singular value, have been presented, too. Wang and Tsai [107] designed an H_∞ SVC controller based on a reduced-order system model. Parniani and Iravani [108] developed another optimal robust controller for damping system oscillations using SVC. To avoid pole-zero cancellation accompanying basic H_∞ optimization, a structured singular value design was employed. Unlike H_∞ and structured singular value controllers which do not provide much control over the closed loop pole locations, quantitative feedback theory (QFT) which was adopted by Rao and Sen [109] permits the use of fixed-parameter controller to place all plant poles within a specified region on the s-plane for a wide range of operating conditions. Dash and Sahoo [110] considered the design of a variable structure SVC stabilizer using a sliding mode control technique.

To enhance the robustness of the SVC controllers, different adaptive control schemes have been introduced. Hsu and Cheng [111] made use of the widely used fixed-parameter PI controller, whose parameters were obtained by pole assignment, and extended it by model reference adaptive control (MRAC). Dash et al. [112] designed an SVC stabilizer incorporating both fuzzy logic control with variable structure control strategy. ElSaady et al. [113] used model reference control system with the fuzzy adaptive mechanism to design an SVC stabilizer of a SMIB power system. Chang and Qizhi [114] used Lyapunov functions to design a FLC for implementing bang-bang control on SVCs, aiming to damp system-wide power oscillations for robust performance.

Changaroon et al. [115] proposed a NN control scheme consisting of a neuro-identifier and a neuro-controller which have been developed based on a functional link network (FLN) model. Recently, Hongesombut et al. [116] employed a radial basis function network (RBFN) to design an adaptive SVC stabilizer for a SMIB system.

The approach of converting the problem of tuning an SVC stabilizer into an optimization problem has been also suggested. Lerch and Povh [117] selected to minimize the deviation in tie-line real power flow by means of bang-bang SVC control. Ju et al. [118] highlighted the problem of finding the optimum stabilizer settings for an SVC of the thyristor controlled reactor/thyristor switched capacitor (TCR/TSC) type, which incorporate both continuous and discrete control. GA was applied to minimize the norm of the voltage deviation from the steady state value. Recently, Hasanovic and Feliachi [119] adopted GA to simultaneously tune a multiple power system damping controllers of the conventional lead-lag scheme in different operating conditions to guarantee the robustness of the proposed design.

1.1.2.4 Unified Power Flow Controller

A unified power flow controller (UPFC) is the most promising device in the FACTS concept. It has the ability to adjust the three control parameters, i.e. the bus voltage, transmission line reactance, and phase angle between two buses, either simultaneously or independently. A UPFC performs this through the control of the in-phase voltage, quadrature voltage, and shunt compensation. Till now, not much research has been devoted to the analysis and control of UPFCs.

Makombe and Jenkins [120] experimentally proved that a UPFC can control the three control parameters either individually or in appropriate combinations at its series-connected output while maintaining reactive power support at its shunt-connected input. Through the use of a SMIB system, Limyingcharoen et al. [121] investigated the mechanism of the three control methods of a UPFC in enhancing power system damping. It was shown that a significant reduction in the transient swing can be obtained with any of the three methods by using a simple proportional feedback of machine rotor angle deviation.

High frequency power fluctuations, more than 100 Hz, induced by a UPFC have been investigated in [122].

Several trials have been reported in the literature to model a UPFC for steady-state and transient studies. Under the assumption that the power system is symmetrical and operates under three-phase balanced conditions, Nabavi-Niaki and Iravani [123] developed a steady-state model, a small-signal linearized dynamic model, and a state-space large-signal model of a UPFC. Wang developed two UPFC models [124,125] which have been linearized and incorporated into the Phillips-Heffron model. It was

observed that, unless the UPFC is equipped with a damping controller, the voltage control of the DC link capacitor may interact negatively with PSSs installed in the power system [125]. A power frequency model for the UPFC with its dc link capacitor dynamics included was suggested and a UPFC-network interface was developed in [126]. A current injected UPFC model for improving power system dynamic performance was developed by Meng and So [127]. A UPFC was represented by an equivalent circuit with a shunt current source and a series voltage source. The proposed model features the symmetry property of the Y_{bus} matrix. Schoder et al. [128] developed a UPFC model that can be suited for Power System Toolbox (PST) in MATLAB.

It is generally accepted that the addition of a supplementary controller to the UPFC device can significantly enhance power system damping [126]. Hence, a number of control schemes have been suggested to perform the oscillation damping task. Huang et al. [126] attempted to design a conventional fixed-parameter lead-lag controller for a UPFC installed in the tie-line of a two-area system to damp the interarea mode of oscillation. Mok et al. [129] considered the design of an adaptive fuzzy logic controller for the same purpose. GA was applied to optimize the performance of the FL controller through fine tuning of the scaling factors. Mishra et al. [129] and Schoder et al. [130] developed a Takagi-Sugeno (TS) type FL controller for a UPFC to damp both local and interarea modes of oscillation for a multimachine system. Dash et al. [131] suggested the use of a RBF NN for a UPFC to enhance system damping performance.

Robust control schemes, such as H_∞ [132,133] and singular value analysis [134], have also been explored. A multi-input-multi-output (MIMO) PI controller has been proposed in [135,136]. It has been illustrated that if more than one UPFC controller, such as a

power flow controller, an ac voltage controller, and a dc voltage controller, were designed separately, the dynamic interactions among the various control channels are not considered. Recently, an integrated linear and nonlinear control of a UPFC for stability enhancement of a multimachine system was developed [137].

1.1.3 Coordination between PSS- and FACS-based Controllers

Due to their interesting characteristics, PSS- and FACTS-based controllers may be incorporated simultaneously in the power system to improve its transient performance. However, the dynamic interaction among these controllers needs to be considered in the controller design stage, as one controller may adversely affect the performance of the others.

For a two-area power system, Noroozian and Andersson [138] theoretically demonstrated the effectiveness of the SVC, TCSC and TCPS on damping inter-area oscillation under different loading conditions and load models. It was observed that the damping effect of a TCSC is very robust with respect to load characteristics, that of a SVC are very dependent on load characteristics, and the dependence of load models on damping performance of a TCPS lies in between the two other devices. By means of Hopf Bifurcations (HB), Mithulananthan et al. [139] dealt with the performance and interactions of PSS, SVC and TCSC. Simulation results illustrated that the most effective damping was observed with a PSS.

In 1996, Pourbeik and Gibbard [140] proposed a technique for calculating the damping and synchronizing torque coefficients induced on generators by FACTS controllers in multimachine power systems based on modal analysis, providing an insight into the damping effect of FACTS controllers. Gibbard et al. [141] further investigated

the interactions between and the effectiveness of PSSs and FACTS- based controllers in multimachine systems based on the analysis of both the perturbations in induced torque coefficients and the shifts in rotor modes resulting from increments in stabilizer gains.

Wang and Swift [142,143] developed a novel unified Phillips-Heffron model for a power system equipped with a SVC, a TCSC and a TCPS. Damping torque coefficient analysis has been performed, based on the proposed model, to study the effect of FACTS controllers damping for different loading conditions. Similar conclusions to those presented in [138] were drawn.

A little work has been devoted in the literature to study the coordination control of excitation and FACTS stabilizers. A coordinated optimal controller for the excitation system and a SVC located on the generator bus of a SMIB system was presented in [144]. Rahim and Nassimi [145] presented optimum control strategies for both the SVC and exciter. It was found that for a synchronous generator remotely located from the load center, most of the damping is provided by SVC control.

Nonlinear control theory has been recently employed to design a coordinated excitation and TCPS controller [146], and a coordinated excitation and UPFC controller [147,148] to improve oscillation damping of multimachine systems.

To overcome the drawback of being a centralized scheme, Lee et al. [149] developed an observer-based decentralized optimal control design of a PSS and a TCSC applied to a multimachine system. A similar approach has been utilized by Li et al. [150,151] to design a coordinated optimal controller to implement multiple TCSCs in a multimachine system. A major disadvantage of the proposed schemes in [149-151] is the need of observers.

To ensure the robustness of the control scheme, self-tuning controllers have been proposed. Cheng and Hsu [152] applied a PSS and a SVC to a multimachine system to be able to both provide system damping and regulate system voltage. The PSS employed was a PI fixed-parameter controller tuned per one robust operating condition, while the SVC controller was a PID self-tuning controller tuned using RLS identification method. Coordinated self-tuning fuzzy logic control for switched series capacitor modules and PSS to enhance transient stability of multimachine system was proposed by Hiyama [153].

Based on the unified Phillips-Heffron, Wang presented a method for the coordination of fixed-parameter robust damping PSS and FACTS-based lead-lag controllers in a multimachine system [154].

H_∞ control scheme has also been employed to tune decentralized SVC and TCSC controllers using a model-matching robustness formulation [155]. Moreover Sanchez-Gasca [156] presented a coordinated controller for a TCSC and a TCPS using projective control scheme. So and Yu implemented a similar approach to obtain a coordinated control of a TCSC and a SVC [157]. Pourbeik and Gibbard [158] presented a two-stage method for the simultaneous coordination of PSSs and FACTS-based lead-lag controllers in multimachine power systems by using the concept of induced damping and synchronizing torque coefficients.

Fang and Ngan [159] converted the problem of simultaneously selecting the controller settings of a PSS and a MIMO controller of a UPFC into an optimization problem. The approach was to identify the eigenvalue of the largest real part and then minimize it as a nonlinear optimization problem to be solved by a gradient descent technique. In order to

ensure the robustness of the control system, different operating conditions were simultaneously considered in the parameter optimization process. A similar approach was employed by Ramirez et al. [160] to design a PSS, TCSC and UPFC lead-lag controllers. Lie et al. [161] considered the same approach to find the optimum settings of coordinated PSS, SVC and TCSC lead-lag controllers to enhance multimachine power system transients.

1.2 Thesis Objectives

The objective of this thesis is to investigate the effectiveness of the coordinated design of power system stabilizers and FACTS-base stabilizers to improve power system transient stability. The FACTS devices that are explored are the first generation (G1) FACTS devices, namely the SVC, TCSC, and TCPS, as well as the UPFC. All the simulations are carried out using MATLAB and SIMULINK packages. The procedure that is taken to satisfy the objective is as follows:

- 1) For a SMIB system equipped with a PSS and the three G1 FACTS devices, singular value decomposition (SVD) analysis is employed as a controllability measure of the different control signals on the system electromechanical (EM) mode.
- 2) The problem of designing the PSS and G1 FACTS devices individually is solved via converting it into an optimization problem. Particle swarm optimization (PSO) technique is employed to find the optimum controller parameter settings at a selected operating condition for a given objective function so as to enhance power system damping.

- 3) Eigenvalue analysis and damping torque coefficient analysis are carried out to assess the effectiveness of the proposed controllers on enhancing the EM mode stability.
- 4) Coordinated design of the different stabilizers is carried out by finding the best parameter settings for more than one stabilizer at a given operating condition simultaneously.
- 5) The proposed design is tested by exposing the power system to severe disturbances at different loading levels. At this stage, nonlinear time-domain simulation is performed.
- 6) To ensure the robustness of the stabilizers, steps (2)-(5) are repeated to select the optimum settings of the stabilizers considering a wide range of operating conditions.
- 7) Steps (1)-(6) are repeated to explore the effectiveness of the UPFC and its four control signals on enhancing the damping of the EM mode. The coordination between the PSS and UPFC based on one operating point and multiple operating points is also investigated.
- 8) The proposed technique is extended to the more practical multimachine power system.

1.3 Thesis Organization

This thesis is organized as follows:

Chapter 2 gives a brief introduction of the different FACTS devices and how they modulate power flow. Chapter 3 describes the three models used throughout the simulation process. These models include: a SMIB system model equipped with the G1 FACTS devices, a SMIB system model equipped with a UPFC, and a multimachine power system equipped with SVCs.

The particle swarm optimization technique is addressed in Chapter 4 and the problem formulation is outlined in Chapter 5. The proposed approach to solve the problem is considered in Chapter 6 which gives a description of the singular value decomposition (SVD) technique, damping torque coefficient calculations, and the implementation of the design process.

Chapters 7, 8, and 9 cover the optimization results obtained for the SMIB system with G1 FACTS devices, SMIB system with UPFC, and multimachine power system, respectively.

The thesis is finalized by drawing some conclusions and outlining the work to be carried out in the future.

CHAPTER 2

FACTS DEVICES

2.1 Introduction

2.1.1 Thyristor-Controlled Phase Shifters (TCPS)

The basic function of a TCPS is to control transmission line power flow through the modulation of the phase angle difference between the two sides of the transmission line voltage. The phase shift is accomplished by adding or subtracting a variable voltage component that is in quadrature with the phase voltage of the line. This quadrature voltage component is obtained from a transformer connected between the other two phases. The structure of a TCPS is shown in Figure 2.1.

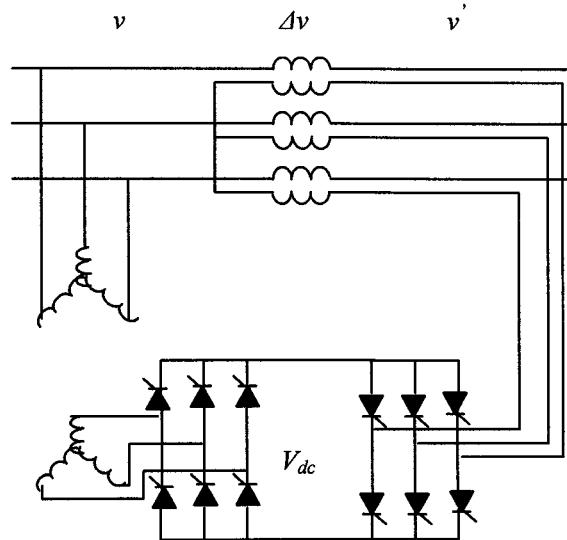


Figure 2.1: Schematic diagram of TCPS

2.1.2 Thyristor-Controlled Series Capacitor (TCSC)

The basic function of a TCSC is to control transmission line power flow through the modulation of the transmission line reactance. This is accomplished by introducing a variable negative impedance, or capacitance, in series with the line's natural positive impedance. The structure of a TCSC is shown in Figure 2.2.

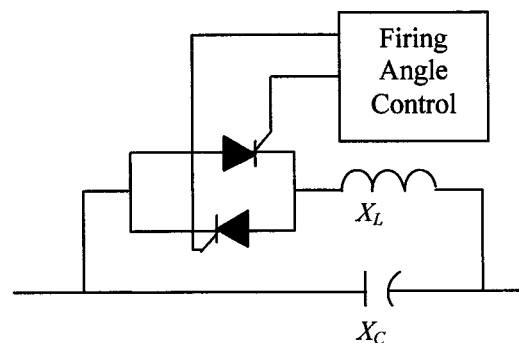


Figure 2.2: Schematic diagram of TCSC

2.1.3 Static VAR Compensator (SVC)

The main function of a SVC, which is a shunt device, is to keep steady-state and dynamic voltages within acceptable limits. It is not intended to modulate line power flow. The SVC uses thyristor valves to rapidly add or remove shunt connected reactors and/or capacitors. The structure of a fixed capacitor/thyristor-controlled reactor (FC/TCR) type SVC is shown in Figure 2.3.

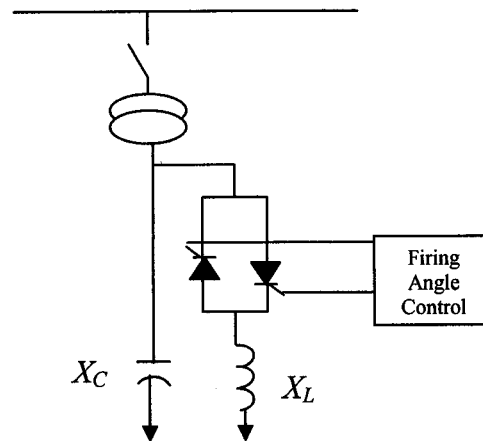


Figure 2.3: Schematic diagram of SVC

2.1.4 Unified Power Flow Controller (UPFC)

A unified power flow controller (UPFC) is the most versatile device in the FACTS concept. It has the ability to adjust the three control parameters, i.e. the bus voltage, transmission line reactance, and phase angle between two buses, either simultaneously or

independently. A UPFC performs this through the control of the in-phase voltage, quadrature voltage, and shunt compensation.

The UPFC consists of a shunt-connected excitation transformer (ET), a series connected boosting transformer (BT), two three-phase GTO based voltage source converters (VSCs), and a common DC link capacitors, see Figure 2.4. The four input control signals to the UPFC are m_E , m_B , δ_E , and δ_B .

The series converter is controlled to inject a voltage, V_{Bt} , in series with the line. The magnitude of V_{Bt} can be varied from 0 to $V_{Bt,max}$ and the angle can be varied independently from 0 to 360° .

The main function of the shunt converter is to supply the real-power demand to the series converter. It also plays the role of regulating the terminal voltage of the interconnected bus by controlling the reactive power supply/demand to that bus.

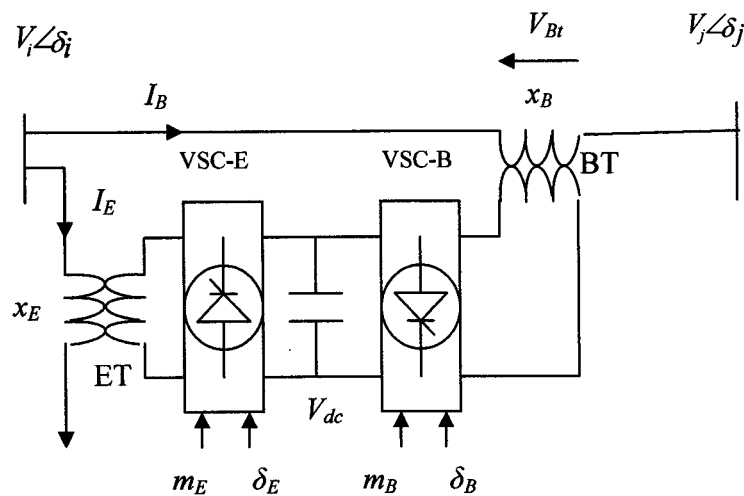


Figure 2.4: Schematic diagram of UPFC

2.2 Power Flow Modulation Using Facts Devices

Ignoring the line resistance, the real power flow in a transmission line of reactance X_{ij} , as shown in Figure 2.5, is given by:

$$P = \frac{V_i V_j}{X_{ij}} \sin(\delta_{ij}) \quad (2.1)$$

where $V_i \angle \delta_i$ and $V_j \angle \delta_j$ are the end bus voltages, and $\delta_{ij} = \delta_i - \delta_j$

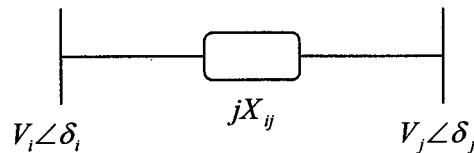


Figure 2.5: Transmission line without FACTS devices

2.2.1 Thyristor-Controlled Phase Shifters (TCPS)

The real power flow through a transmission line equipped with a TCPS, see Figure 2.6, is obtained by:

$$P = \frac{V_i V_j}{X_{ij}} \sin(\delta_{ij} - \Phi) \quad (2.2)$$

where Φ is the phase shift in the voltage phase angle resulting from the TCPS.

Hence, the real power flow through the transmission line can be modulated by controlling the angle Φ .

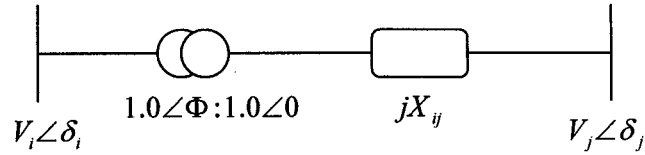


Figure 2.6: Transmission line with a TCPS

2.2.2 Thyristor-Controlled Series Capacitor (TCSC)

The real power flow through a transmission line equipped with a TCSC, Figure 2.7, is obtained by:

$$P = \frac{V_i V_j}{X_{ij}(1-k)} \sin(\delta_{ij}) \quad (2.3)$$

where k represents the TCSC compensation level and is given by

$$k = \frac{X_{CSC}}{X_{ij}} \quad (2.4)$$

The equivalent reactance of the TCSC, X_{CSC} , is given by

$$X_{CSC} = \frac{X_C X_L(\alpha)}{X_C - X_L(\alpha)} \sin(\delta_{ij}) \quad (2.5)$$

and

$$P = \frac{\pi}{2\pi - 2\alpha + \sin(2\alpha)} X_L; \quad \pi/2 \leq \alpha \leq \pi \quad (2.6)$$

where α is the thyristor firing angle.

Hence, the real power flow through the transmission line can be adjusted by controlling the compensation level k .

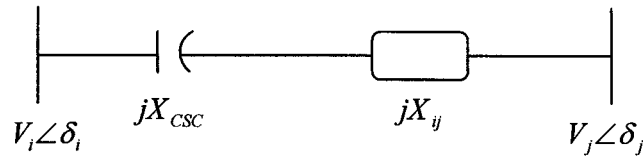


Figure 2.7: Transmission line with a TCSC

2.2.3 Static VAR Compensator (SVC)

The real power flow through a transmission line with a SVC located at the middle of the line, Figure 2.8 is described by:

$$P = 2 \frac{V_i V_m}{X_{ij}} \sin(\delta_{im}) \quad (2.7)$$

where $\delta_{im} = \delta_i - \delta_m$. Since the SVC is located at the electrical midpoint of the line, $\delta_{im} \approx \delta_{ij}/2$ and $V_m \approx V_j$. therefore, the real power can be obtained by:

$$P = 2 \frac{V_i V_j}{X_{ij}} \sin(\delta_{ij}/2) \quad (2.8)$$

The equivalent susceptance of the SVC, B_{SVC} , is given by

$$B_{SVC} = \frac{1}{X_C} - B_L(\alpha) \quad (2.9)$$

and

$$B_L(\alpha) = \frac{2\pi - 2\alpha + \sin(2\alpha)}{\pi X_L}; \quad \pi/2 \leq \alpha \leq \pi \quad (2.10)$$

where α is the thyristor firing angle.

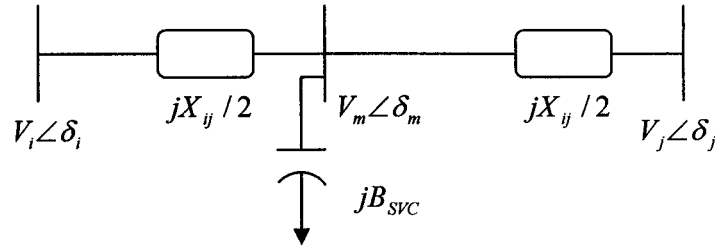


Figure 2.8: Transmission line with a SVC

2.2.4 Unified Power Flow Controller (UPFC)

A UPFC regulates the line real power flow through voltage magnitude and phase regulation. Figure 2.9 shows the different power flow control functions performed by a UPFC. Figure 2.9(a) shows the addition of the general voltage phasor V_{Bt} to the bus voltage V_i . It is worth noticing that the phase of V_{Bt} can range from 0° to 360° . A UPFC can perform voltage regulation via the addition of an in-phase voltage $V_{Bt}=V_0$, see Figure 2.9(b). Voltage regulation and series reactance compensation is carried out through the addition of $V_{Bt}=V_0+V_p$, where V_0 is in phase with the bus voltage V_i and V_p is out-of-phase with the line current by 90° , see Figure 2.9(c). Figure 2.9(d) illustrates the process of phase-shifting. In here, the voltage phasor to be added $V_{Bt}=V_0+V_\phi$, where V_0 is in phase with the bus voltage and V_ϕ shifts the resulting voltage phasor $V_{Bt}+V_0$ by an angle ϕ .

[163]

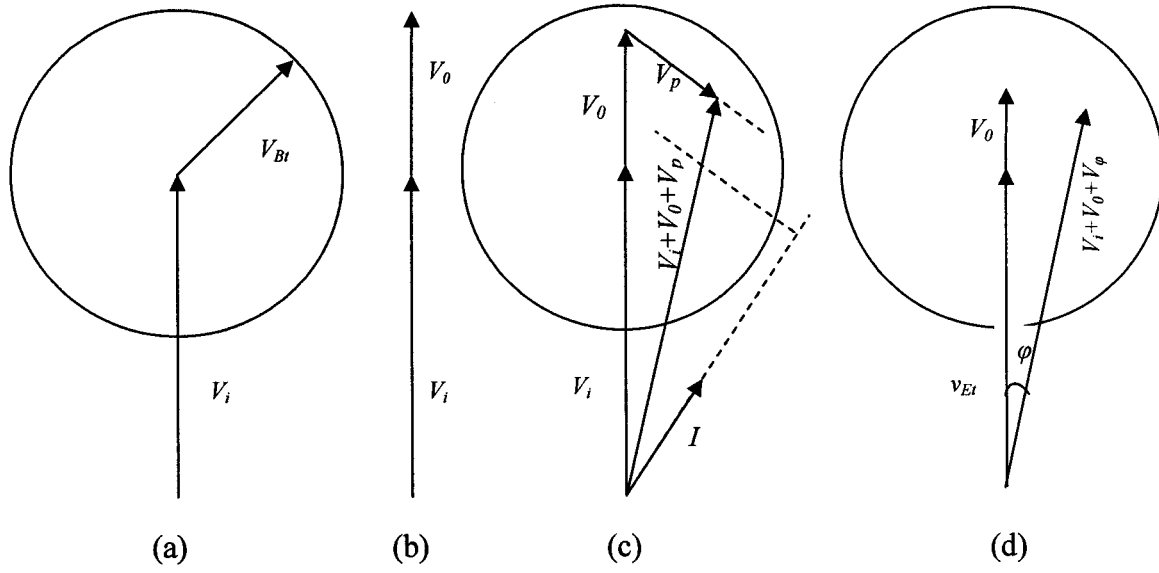


Figure 2.9: A phasor diagram showing the modulation of real power flow through bus voltage magnitude and phase regulation.

CHAPTER 3

POWER SYSTEM MODEL

3.1 Single-Machine Infinite-Bus System with G1 FACTS Devices

A single-machine-infinite-bus (SMIB) system is shown in Figure 3.1. The generator is equipped with a PSS and the FACTS devices included are a SVC, a TCSC and a TCPS. The local load of the generator terminal is a constant impedance load represented by $Y_L = g + jb$, and the impedance of the transmission line is $2Z$ where $Z = R + jX$.

3.1.1 SMIB System Nonlinear Model

3.1.1.1 Generator Model

The generator is represented by the 3rd order model consisting of the swing equation and the generator internal voltage equation. The swing equation can be written as

$$\dot{\delta} = \omega_b(\omega - 1) \quad (3.1)$$

$$\dot{\omega} = (P_m - P_e - D(\omega - 1)) / M \quad (3.2)$$

The internal voltage, E_q' , is given by

$$\dot{E}_q' = (E_{fd} - (x_d - x_d')i_d - E_q') / T_{do}' \quad (3.3)$$

The real power output of the generator is described as

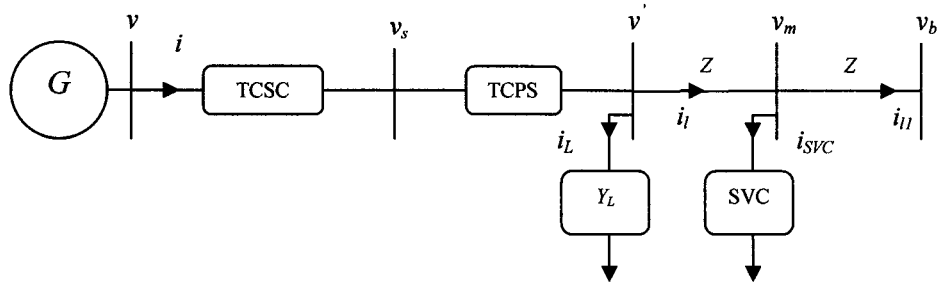


Figure 3.1: Single machine infinite bus system (SMIB) with G1 FACTS devices

$$P_e = v_d i_d + v_q i_q \quad (3.4)$$

3.1.1.2 Excitation system and PSS

The excitation system can be represented by the IEEE type-ST1 system shown in Figure 3.2, and is described by

$$\dot{E}_{fd} = (K_A (V_{ref} - v + u_{PSS}) - E_{fd}) / T_A \quad (3.5)$$

$$v = (v_d^2 + v_q^2)^{1/2} \quad (3.6)$$

$$v_d = x_q i_q \quad (3.7)$$

$$v_q = E'_q - x'_d i_d \quad (3.8)$$

A conventional lead-lag PSS is installed in the feedback loop to generate a supplementary stabilizing signal u_{PSS} , see Figure 3.2. The PSS input is the change in the machine speed.

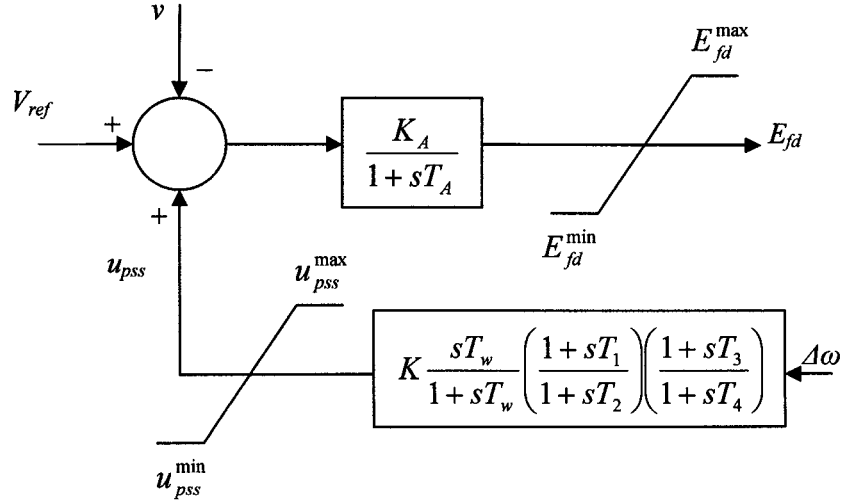


Figure 3.2: IEEE type-ST1 excitation system with PSS

3.1.1.3 FACTS-based stabilizers

Shown in Figure 3.3 is a SVC with a lead-lag supplementary controller. The susceptance of the SVC, B_{SVC} , is given by

$$\dot{B}_{SVC} = (K_s (B_{SVC}^{ref} - u_{SVC}) - B_{SVC}) / T_s \quad (3.9)$$

where B_{SVC}^{ref} is the SVC reference susceptance.

Figure 3.4 shows a TCSC equipped with a lead-lag controller. The TCSC reactance is expressed as

$$\dot{X}_{TCSC} = (K_s (X_{TCSC}^{ref} - u_{TCSC}) - X_{TCSC}) / T_s \quad (3.10)$$

Similarly, Figure 3.5 shows a TCPS equipped with a lead-lag stabilizer. The TCPS phase angle is expressed as

$$\dot{\Phi}_{TCPS} = (K_s (\Phi_{TCPS}^{ref} - u_{TCPS}) - \Phi_{TCPS}) / T_s \quad (3.11)$$

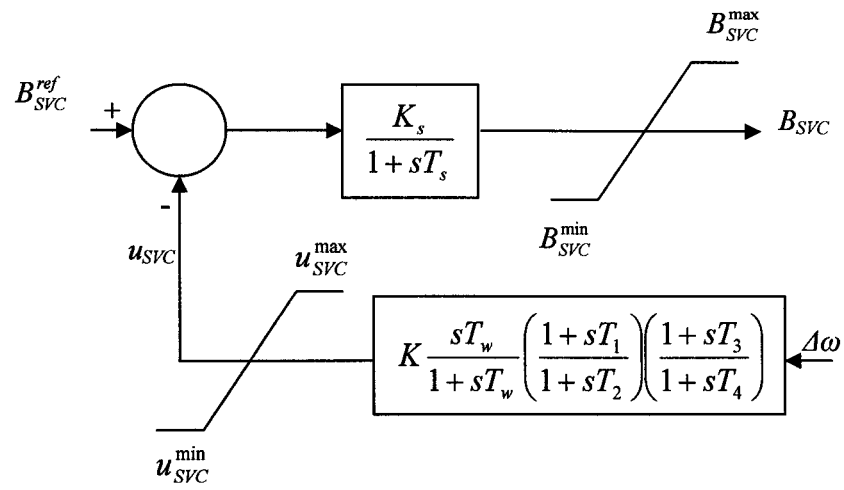


Figure 3.3: SVC with lead-lag controller

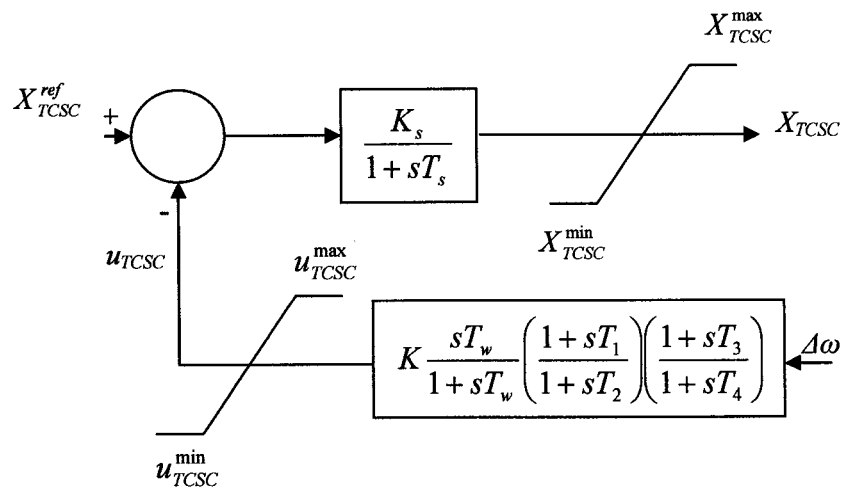


Figure 3.4: TCSC with lead-lag controller

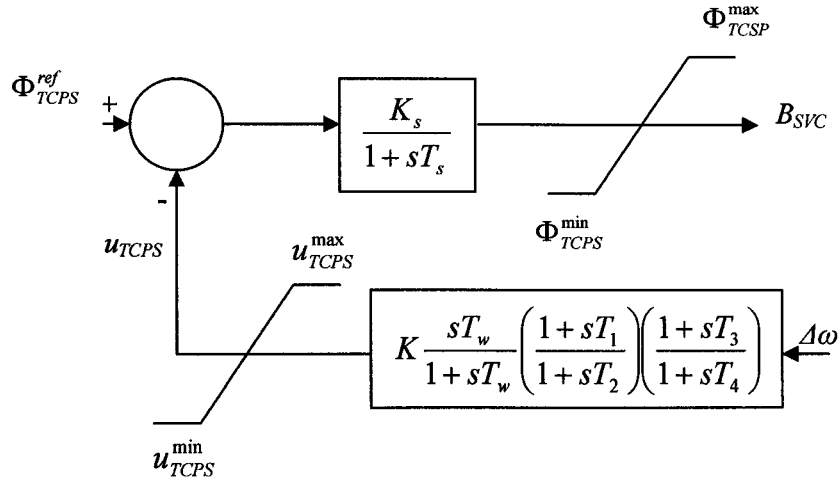


Figure 3.5: TCPS with lead-lag controller

3.1.2 SMIB System Linearized Model

The power system model described in the previous section is nonlinear. For controller design purposes, it is usually more convenient to work with a linear model.

The d and q components of the machine current i and terminal voltage v , see Figure 3.1, can be expressed as:

$$i = i_d + j i_q \quad (3.12)$$

$$v = v_d + j v_q \quad (3.13)$$

The voltage v_s can be expressed as

$$v_s = v - j X_{TCSC} i \quad (3.14)$$

The d and q components of v_s can be written as

$$v_{sd} = x_{qs} i_q \quad (3.15)$$

$$v_{sq} = E_q^i - x_{ds} i_d \quad (3.16)$$

where

$$x_{qs} = x_q + X_{TCSC} \quad (3.17)$$

$$x'_{ds} = x'_d + X_{TCSC} \quad (3.18)$$

The voltage v' can be expressed as

$$v' = \frac{v_s}{k} = \frac{v_s}{k \angle \Phi_{TCPS}} \quad (3.19)$$

The d and q components of v' are

$$v'_d = \frac{1}{k} (v_{sd} \cos \Phi + v_{sq} \sin \Phi) \quad (3.20)$$

$$v'_q = \frac{1}{k} (v_{sq} \cos \Phi - v_{sd} \sin \Phi) \quad (3.21)$$

the load current is

$$i_L = v' Y_L \quad (3.22)$$

where Y_L is defined as

$$Y_L = G + jB \quad (3.23)$$

The current i_L can be decomposed to

$$i_{Ld} = Gv'_d - Bv'_q \quad (3.24)$$

$$i_{Lq} = Gv'_q + Bv'_d \quad (3.25)$$

The line current i_l is written as

$$i_l = i - i_L \quad (3.26)$$

The d and q components of i_l are

$$i_{ld} = i_d - i_{Ld} \quad (3.27)$$

$$i_{lq} = i_q - i_{Lq} \quad (3.28)$$

The midpoint voltage v_m is

$$v_m = v' - i_l Z \quad (3.29)$$

The voltage v_m is decomposed to

$$v_{md} = C_1 v'_d - C_2 v'_q - R i_d + X i_q \quad (3.30)$$

$$v_{mq} = C_2 v'_d + C_1 v'_q - X i_d - R i_q \quad (3.31)$$

where

$$C_1 = 1 + RG - XB \quad (3.32)$$

$$C_2 = RB + XG \quad (3.33)$$

The SVC current is written as

$$i_{SVC} = v_m Y_{SVC} \quad (3.34)$$

The line current i_{l1} is given as

$$i_{l1} = i_l - i_{SVC} \quad (3.35)$$

The infinite bus voltage is

$$v_b = v_m - i_{l1} Z \quad (3.36)$$

The d and q components of v_b are

$$v_{bd} = v_b \sin \delta = v_{md} - R i_{d1} + X i_{q1} \quad (3.37)$$

$$v_{bq} = v_b \cos \delta = v_{mq} - X i_{d1} - R i_{q1} \quad (3.38)$$

Substituting (3.15)-(3.35) into (3.37) and (3.38) and rearranging yields

$$C_3 i_d + C_4 i_q = v_b \sin \delta + C_7 E'_q \quad (3.39)$$

$$C_5 i_d + C_6 i_q = v_b \cos \delta - C_8 E'_q \quad (3.40)$$

Solving (3.39) and (3.40) for i_d and i_q and linearizing gives

$$C_3 \Delta i_d + C_4 \Delta i_q = [v_b \cos \delta \quad C_7 \quad C_9 \quad C_{11} \quad C_{13}] \Delta X_t \quad (3.41)$$

$$C_5 \Delta i_d + C_6 \Delta i_q = [-v_b \sin \delta \quad -C_8 \quad C_{10} \quad C_{12} \quad C_{14}] \Delta X_t \quad (3.42)$$

where

$$\Delta X_t = [\Delta \delta \quad \Delta E'_q \quad \Delta B_{SVC} \quad \Delta X_{TCSC} \quad \Delta \Phi_{TCPS}]^T \quad (3.43)$$

Solving (3.41) and (3.42) for Δi_d and Δi_q results in

$$\Delta i_d = [C_{15} \quad C_{17} \quad C_{19} \quad C_{21} \quad C_{23}] \Delta X_t \quad (3.44)$$

$$\Delta i_q = [C_{16} \quad C_{18} \quad C_{20} \quad C_{22} \quad C_{24}] \Delta X_t \quad (3.45)$$

The constants C_1 - C_{24} are functions of Z , Y_L , x'_d , x_q , i_{d0} , i_{q0} , E'_{q0} , B_{SVC0} , X_{TCSC0} , and Φ_{TCPS0} .

Also, linearizing v_d and v_q yields

$$\Delta v_d = x_q \Delta i_q \quad (3.46)$$

$$\Delta v_q = \Delta E'_q - x'_d \Delta i_d \quad (3.47)$$

Using (3.44)-(3.47) to linearize P_e , E'_q , and v gives

$$\Delta P_e = [K_1 \quad K_2 \quad K_{pB} \quad K_{pX} \quad K_{p\Phi}] \Delta X_t \quad (3.48)$$

$$(K_3 + sT'_{d0}) \Delta E'_q = \Delta E_{fd} - [K_4 \quad 0 \quad K_{qB} \quad K_{qX} \quad K_{q\Phi}] \Delta X_t \quad (3.49)$$

$$\Delta v = [K_5 \quad K_6 \quad K_{vB} \quad K_{vX} \quad K_{v\Phi}] \Delta X_t \quad (3.50)$$

where the constants K_1 - K_6 , K_{pB} , K_{pX} , $K_{p\Phi}$, K_{qB} , K_{qX} , $K_{q\Phi}$, K_{vB} , K_{vX} , and $K_{v\Phi}$ are functions of C_1 - C_{24} .

In matrix form, the linearized power system model can be expressed as

$$\begin{bmatrix} \dot{\Delta\delta} \\ \dot{\Delta\omega} \\ \dot{\Delta E'_q} \\ \dot{\Delta E'_{fd}} \end{bmatrix} = \begin{bmatrix} 0 & 377 & 0 & 0 \\ -\frac{K_1}{M} & -\frac{D}{M} & -\frac{K_2}{M} & 0 \\ -\frac{K_4}{T'_{do}} & 0 & -\frac{K_3}{T'_{do}} & \frac{1}{T'_{do}} \\ -\frac{K_A K_5}{T_A} & 0 & -\frac{K_A K_6}{T_A} & -\frac{1}{T_A} \end{bmatrix} \begin{bmatrix} \Delta\delta \\ \Delta\omega \\ \Delta E'_q \\ \Delta E'_{fd} \end{bmatrix} + \begin{bmatrix} 0 & 0 & 0 & 0 \\ 0 & -\frac{K_{pB}}{M} & -\frac{K_{pX}}{M} & -\frac{K_{p\Phi}}{M} \\ 0 & -\frac{K_{qB}}{T'_{do}} & -\frac{K_{qX}}{T'_{do}} & -\frac{K_{q\Phi}}{T'_{do}} \\ \frac{K_A}{T_A} & -\frac{K_A K_{vB}}{T_A} & -\frac{K_A K_{vX}}{T_A} & -\frac{K_A K_{v\Phi}}{T_A} \end{bmatrix} \begin{bmatrix} u_{PSS} \\ \Delta B_{SVC} \\ \Delta X_{TCSC} \\ \Delta \Phi_{TCPS} \end{bmatrix} \quad (3.51)$$

or

$$\Delta \dot{X} = A\Delta X + B\Delta U \quad (3.51)$$

where

$$\Delta X = [\Delta\delta \quad \Delta\omega \quad \Delta E'_q \quad \Delta E'_{fd}]^T \quad (3.52)$$

$$\Delta U = [u_{PSS} \quad \Delta B_{SVC} \quad \Delta X_{TCSC} \quad \Delta \Phi_{TCPS}]^T \quad (3.53)$$

Figure 3.6 shows a block diagram representing the linearized power system model described by the above equations.

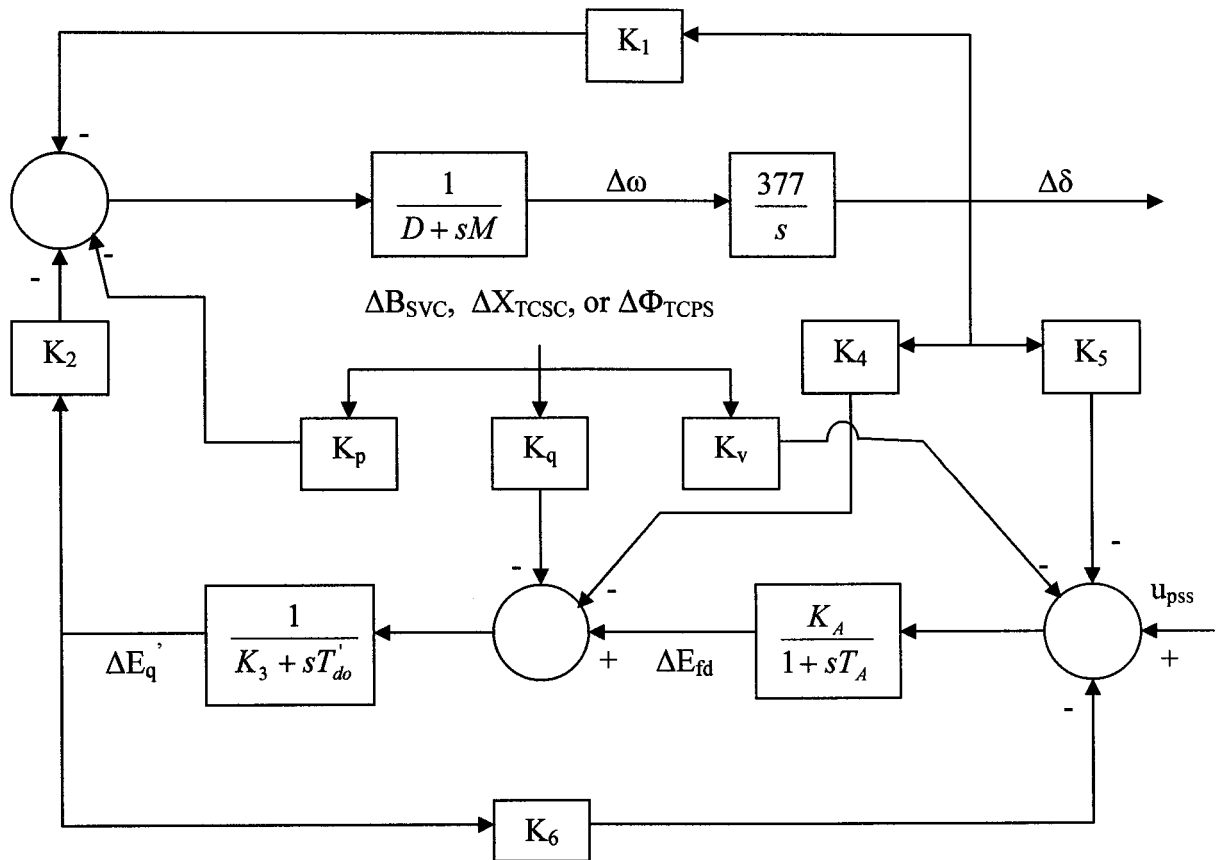


Figure 3.6: Linearized power system model equipped with a SVC, TCSC, and TCPS

3.2 Single-Machine Infinite-Bus System with UPFC

A single machine infinite bus (SMIB) system equipped with a UPFC is shown in Figure 3.7. The generator is equipped with a PSS.

3.2.1 SMIB System Nonlinear Model

By applying Park's transformation and neglecting the resistance and transients of the ET and BT transformers, the UPFC can be modeled as [123-125]:

$$\begin{bmatrix} v_{Etd} \\ v_{Etq} \end{bmatrix} = \begin{bmatrix} 0 & -x_E \\ x_E & 0 \end{bmatrix} \begin{bmatrix} i_{Ed} \\ i_{Eq} \end{bmatrix} + \begin{bmatrix} \frac{m_E \cos \delta_E v_{dc}}{2} \\ \frac{m_E \sin \delta_E v_{dc}}{2} \end{bmatrix} \quad (3.54)$$

$$\begin{bmatrix} v_{Btd} \\ v_{Btq} \end{bmatrix} = \begin{bmatrix} 0 & -x_B \\ x_B & 0 \end{bmatrix} \begin{bmatrix} i_{Bd} \\ i_{Bq} \end{bmatrix} + \begin{bmatrix} \frac{m_B \cos \delta_B v_{dc}}{2} \\ \frac{m_B \sin \delta_B v_{dc}}{2} \end{bmatrix} \quad (3.55)$$

$$\dot{v}_{dc} = \frac{3m_E}{4C_{dc}} [\cos \delta_E \quad \sin \delta_E] \begin{bmatrix} i_{Ed} \\ i_{Eq} \end{bmatrix} + \frac{3m_B}{4C_{dc}} [\cos \delta_B \quad \sin \delta_B] \begin{bmatrix} i_{Bd} \\ i_{Bq} \end{bmatrix} \quad (3.56)$$

The non-linear model of the SMIB system of Figure 3.7 is:

$$\dot{\delta} = \omega_b (\omega - 1) \quad (3.57)$$

$$\dot{\omega} = (P_m - P_e - D(\omega - 1)) / M \quad (3.58)$$

$$\dot{E}'_q = (E_{fd} - (x_d - x'_d)i_d - E'_q) / T'_{do} \quad (3.59)$$

$$\dot{E}'_{fd} = (K_A (V_{ref} - v + u_{PSS}) - E'_{fd}) / T_A \quad (3.60)$$

where P_e , v , v_d , and v_q are represented by (3.4), (3.6)-(3.8), respectively, and

$$i_d = i_{Ed} + i_{Bd} \quad (3.61)$$

$$i_q = i_{Eq} + i_{Bq} \quad (3.62)$$

Also, from Figure 3.7 we have

$$v = jx_{tE}i + v_{Et} \quad (3.63)$$

$$v_{Et} = v_{Bt} + jx_{BV}i_B + v_b \quad (3.64)$$

From (3.63) we have

$$\begin{aligned} v_d + jv_q &= x_q (i_{Eq} + i_{Bq}) + j[E'_q - x'_d (i_{Ed} + i_{Bd})] \\ &= jx_{tE} (i_{Ed} + i_{Bd} + ji_{Eq} + ji_{Bq}) + v_{Etd} + jv_{Etq} \end{aligned} \quad (3.65)$$

$$v_{Etd} + jv_{Etq} = v_{Btd} + jv_{Btq} + jx_{BV}i_{Bd} - x_{BV}i_{Bq} + v_b \sin \delta + jv_b \cos \delta \quad (3.66)$$

From (3.54), (3.55), (3.65), and (3.66) the following can be obtained

$$i_{Ed} = \frac{x_{BB}}{x_{d\Sigma}} E'_q - \frac{m_E \sin \delta_E v_{dc} x_{Bd}}{2x_{d\Sigma}} + \frac{x_{dE}}{x_{d\Sigma}} (v_b \cos \delta + \frac{m_B \sin \delta_B v_{dc}}{2}) \quad (3.67)$$

$$i_{Eq} = \frac{m_E \cos \delta_E v_{dc} x_{Bq}}{2x_{q\Sigma}} - \frac{x_{qE}}{x_{q\Sigma}} (v_b \sin \delta + \frac{m_B \cos \delta_B v_{dc}}{2}) \quad (3.68)$$

$$i_{Bd} = \frac{x_E}{x_{d\Sigma}} E'_q + \frac{m_E \sin \delta_E v_{dc} x_{dE}}{2x_{d\Sigma}} - \frac{x_{dt}}{x_{d\Sigma}} (v_b \cos \delta + \frac{m_B \sin \delta_B v_{dc}}{2}) \quad (3.69)$$

$$i_{Bq} = -\frac{m_E \cos \delta_E v_{dc} x_{qE}}{2x_{q\Sigma}} + \frac{x_{qt}}{x_{q\Sigma}} (v_b \sin \delta + \frac{m_B \cos \delta_B v_{dc}}{2}) \quad (3.70)$$

where

$$x_{q\Sigma} = (x_q + x_{tE} + x_E)(x_B + x_{BV}) + x_E(x_q + x_{tE}) \quad (3.71)$$

$$x_{Bq} = x_B + x_{BV} + x_q + x_{tE} \quad (3.72)$$

$$x_{qt} = x_q + x_{tE} + x_E \quad (3.73)$$

$$x_{qE} = x_q + x_{tE} \quad (3.74)$$

$$x_{d\Sigma} = (x'_d + x_{tE} + x_E)(x_B + x_{BV}) + x_E(x'_d + x_{tE}) \quad (3.75)$$

$$x_{Bd} = x_B + x_{BV} + x'_d + x_{tE} \quad (3.76)$$

$$x_{dt} = x'_d + x_{tE} + x_E \quad (3.77)$$

$$x_{dE} = x'_d + x_{tE} \quad (3.78)$$

$$x_{BB} = x_B + x_{BV} \quad (3.79)$$

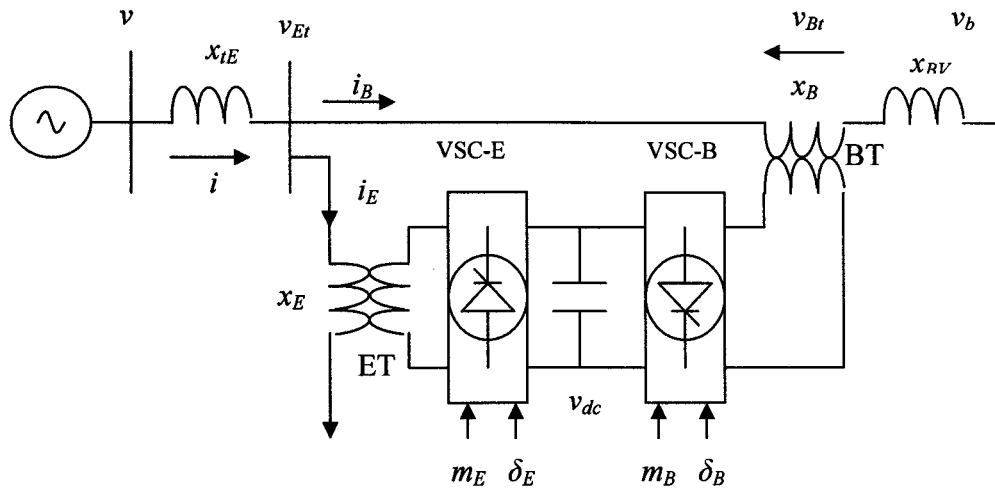


Figure 3.7: Single-machine-infinite-bus system (SMIB) with a UPFC

The conventional lead-lag PSS is installed in the feedback loop to generate a supplementary stabilizing signal u_{pss} , see Figure 3.2.

The UPFC damping controllers are of the structure shown in Figure 3.8, where u can be m_E , δ_E , m_B , or δ_B .

In order to maintain the power balance between the series and shunt converters, a DC voltage regulator must be incorporated. The DC voltage is controlled through modulating the phase angle of the ET voltage, δ_E . Therefore, the δ_E damping controller to be considered is that shown in Figure 3.9, where the DC voltage regulator is a PI-controller.

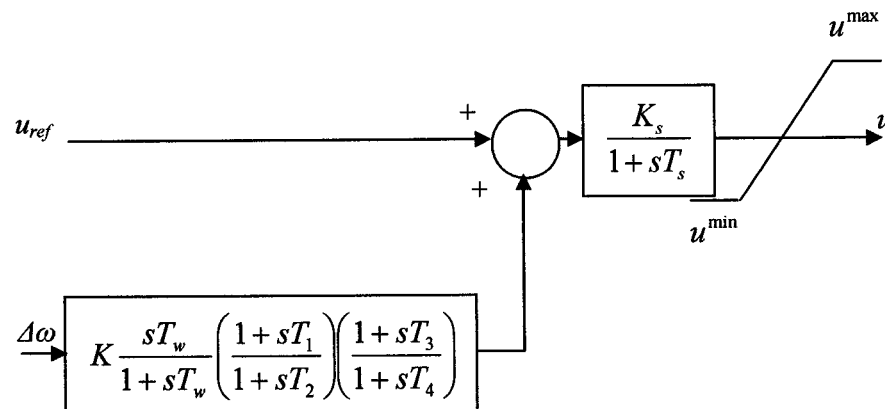


Figure 3.8: UPFC with lead-lag controller

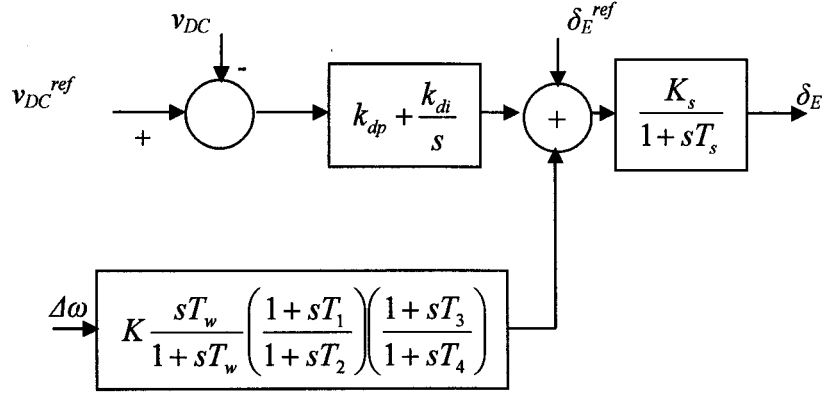


Figure 3.9: UPFC with lead-lag controller and DC voltage regulator

3.2.2 SMIB System Linearized Model

The power system model described in the previous section is nonlinear. For controller design purposes, it is usually more convenient to work with a linear model.

Linearizing (3.67) and (3.69) yield

$$\Delta i_{Ed} = [B_1 \ B_2 \ B_3 \ B_4 \ B_5 \ B_6 \ B_7] \Delta X_u \quad (3.80)$$

$$\Delta i_{Bd} = [B_8 \ B_9 \ B_{10} \ B_{11} \ B_{12} \ B_{13} \ B_{14}] \Delta X_u \quad (3.81)$$

where

$$\Delta X_u = [\Delta \delta \ \Delta E'_q \ \Delta v_{dc} \ \Delta m_E \ \Delta \delta_E \ \Delta m_B \ \Delta \delta_B] \quad (3.82)$$

Hence, the linearized form of (3.61) is

$$\Delta i_d = [B_{15} \ B_{16} \ B_{17} \ B_{18} \ B_{19} \ B_{20} \ B_{21}] \Delta X_u \quad (3.83)$$

Similarly, linearizing (3.68) and (3.70) give

$$\Delta i_{Eq} = [B_{22} \ B_{23} \ B_{24} \ B_{25} \ B_{26} \ B_{27} \ B_{28}] \Delta X_u \quad (3.84)$$

$$\Delta i_{Bq} = [B_{29} \ B_{30} \ B_{31} \ B_{32} \ B_{33} \ B_{34} \ B_{35}] \Delta X_u \quad (3.85)$$

And

$$\Delta i_q = [B_{36} \ B_{37} \ B_{38} \ B_{39} \ B_{40} \ B_{41} \ B_{42}] \Delta X_u \quad (3.86)$$

From (3.7), (3.8), (3.83), and (3.86)

$$\Delta v_d = [B_{43} \quad B_{44} \quad B_{45} \quad B_{46} \quad B_{47} \quad B_{48} \quad B_{49}] \Delta X_u \quad (3.87)$$

$$\Delta v_q = [B_{50} \quad B_{51} \quad B_{52} \quad B_{53} \quad B_{54} \quad B_{55} \quad B_{56}] \Delta X_u \quad (3.88)$$

The constants B_1 - B_{56} are functions of x_{tE} , x_B , x_E , x_{BV} , C_{dc} , x'_d , x_q , i_{d0} , i_{q0} , v_{dc0} , E'_{q0} , m_{E0} , δ_{E0} , m_{B0} , and δ_{B0} .

Using (3.80)-(3.88), P_e , E'_q , v , and v_{dc} can be linearized to

$$\Delta P_e = [K_1 \quad K_2 \quad K_{pd} \quad K_{pe} \quad K_{pde} \quad K_{pb} \quad K_{pdb}] \Delta X_u \quad (3.89)$$

$$\Delta \dot{E}'_q = \frac{1}{T'_{d0}} (\Delta E_{fd} - [K_4 \quad K_3 \quad K_{qd} \quad K_{qe} \quad K_{qde} \quad K_{qb} \quad K_{qdb}] \Delta X_u) \quad (3.90)$$

$$\Delta v = [K_5 \quad K_6 \quad K_{vd} \quad K_{ve} \quad K_{vde} \quad K_{vb} \quad K_{vdb}] \Delta X_u \quad (3.91)$$

$$\Delta \dot{v}_{dc} = [K_7 \quad K_8 \quad -K_9 \quad K_{ce} \quad K_{cde} \quad K_{cb} \quad K_{cdb}] \Delta X_u \quad (3.92)$$

where the constants K_1 - K_9 , K_{pd} , K_{pe} , K_{pde} , K_{pb} , K_{pdb} , K_{qd} , K_{qe} , K_{qde} , K_{qb} , K_{qdb} , K_{vd} , K_{ve} , K_{vde} , K_{vb} , K_{vdb} , K_{ce} , K_{cde} , K_{cb} , and K_{cdb} are functions of B_1 - B_{56} .

In state-space representation, the power system can be modeled as

$$\Delta \dot{X} = A \Delta X + B \Delta U \quad (3.93)$$

where

$$\Delta X = [\Delta \delta \quad \Delta \omega \quad \Delta E'_q \quad \Delta E_{fd} \quad \Delta v_{dc}]^T \quad (3.94)$$

$$\Delta U = [\Delta u_{pss} \quad \Delta m_E \quad \Delta \delta_E \quad \Delta m_b \quad \Delta \delta_b]^T \quad (3.95)$$

$$A = \begin{bmatrix} 0 & \omega_b & 0 & 0 & 0 \\ -\frac{K_1}{M} & -\frac{D}{M} & -\frac{K_2}{M} & 0 & -\frac{K_{pd}}{M} \\ -\frac{K_4}{T'_{do}} & 0 & -\frac{K_3}{T'_{do}} & \frac{1}{T'_{do}} & -\frac{K_{qd}}{T'_{do}} \\ -\frac{K_A K_5}{T_A} & 0 & -\frac{K_A K_6}{T_A} & -\frac{1}{T_A} & -\frac{K_A K_{vd}}{T_A} \\ K_7 & 0 & K_8 & 0 & -K_9 \end{bmatrix} \quad (3.96)$$

$$B = \begin{bmatrix} 0 & 0 & 0 & 0 & 0 \\ 0 & -\frac{K_{pe}}{M} & -\frac{K_{p\delta e}}{M} & -\frac{K_{pb}}{M} & -\frac{K_{p\delta b}}{M} \\ 0 & -\frac{K_{qe}}{T'_{do}} & -\frac{K_{q\delta e}}{T'_{do}} & -\frac{K_{qb}}{T'_{do}} & -\frac{K_{q\delta b}}{T'_{do}} \\ \frac{K_A}{T_A} & -\frac{K_A K_{ve}}{T_A} & -\frac{K_A K_{v\delta e}}{T_A} & -\frac{K_A K_{vb}}{T_A} & -\frac{K_A K_{v\delta b}}{T_A} \\ 0 & K_{ce} & K_{c\delta e} & K_{cb} & K_{c\delta b} \end{bmatrix} \quad (3.97)$$

The linearized dynamic model of the SMIB system with a UPFC is shown in Figure 3.10.

In addition to the PSS input, u_{PSS} , only one UPFC input is considered in this figure.

3.3 Multimachine Power System

In this section, the SMIB system model represented by Figure 3.6 is extended to describe an n -machine m -bus multimachine power system. Due to the interaction between the machines in multimachine system, the K_1 - K_6 are matrices rather than scalars, and the machine parameters, such as K_A and T_A , are vectors.

3.3.1 Multimachine Power System Nonlinear Model

The multimachine nonlinear model can be described by the following set of differential equations, in all that follows $i=1, 2, \dots, n$:

$$\dot{\delta}_i = \omega_b (\omega_i - 1) \quad (3.98)$$

$$\dot{\omega}_i = (P_{mi} - P_{ei} - D_i(\omega_i - 1)) / M_i \quad (3.99)$$

$$\dot{E}'_{qi} = (E_{fdi} - (x_{di} - x'_{di})i_{di} - E'_{qi}) / T'_{doi} \quad (3.100)$$

$$\dot{E}'_{fdi} = (K_{Ai}(V_{refi} - v_i + u_{PSSi}) - E_{fdi}) / T_{Ai} \quad (3.101)$$

where

$$P_{ei} = v_{di}i_{di} + v_{qi}i_{qi} \quad (3.102)$$

$$v_{di} = x_{qi}i_{qi}, \quad v_{qi} = E'_{qi} - x_{di}i_{di} \quad (3.103)$$

$$v_i = (v_{di}^2 + v_{qi}^2)^{1/2} \quad (3.104)$$

Also,

$$I = YV \quad (3.105)$$

where

$$I_i = (i_d + ji_q)e^{j(\delta_i - \frac{\pi}{2})} \quad (3.106)$$

$$V_i = (v_d + jv_q)e^{j(\delta_i - \frac{\pi}{2})} \quad (3.107)$$

$$Y_{ij} = y_{ij}e^{j\beta_{ij}} \quad (3.108)$$

It is worth emphasizing that the capitalized variables I ($n \times 1$), V ($n \times 1$), and Y ($n \times n$) represent complex quantities.

Using (3.105)-(3.108) as well as (3.103) and (3.104), i_{di} and i_{qi} can be expressed as

$$i_{di} = \sum_{j=1}^n y_{ij} [x_{qj} i_{qj} C_{ij} - (E'_{qj} - x'_{dj} i_{dj}) S_{ij}] \quad (3.109)$$

$$i_{qi} = \sum_{j=1}^n y_{ij} [x_{qj} i_{qj} S_{ij} + (E'_{qj} - x'_{dj} i_{dj}) C_{ij}] \quad (3.110)$$

where

$$C_{ij} = \cos(\beta_{ij} + \delta_j - \delta_i) \quad (3.111)$$

$$S_{ij} = \sin(\beta_{ij} + \delta_j - \delta_i) \quad (3.112)$$

3.3.2 Multimachine System Linearized Model

Linearizing (3.109) yields

$$L_d \Delta i_d = P_d \Delta \delta + Q_d \Delta E'_q + M_d \Delta i_q \quad (3.113)$$

where

$$P_{dij} = -y_{ij} [x_{qj} i_{qj} S_{ij} + (E'_{qj} - x'_{dj} i_{dj}) C_{ij}], \quad j \neq i \quad (3.114)$$

$$P_{dii} = -\sum_{\substack{j=1 \\ j \neq i}}^n P_{dij} \quad (3.115)$$

$$Q_{dij} = -y_{ij} S_{ij}, \quad j = 1, 2, \dots, n \quad (3.116)$$

$$M_{dij} = y_{ij}x_{qj}C_{ij}, \quad j = 1, 2, \dots, n \quad (3.117)$$

$$L_{dij} = -y_{ij}x'_{dj}S_{ij}, \quad j \neq i \quad (3.118)$$

$$L_{dii} = 1 - y_{ii}x'_{di}S_{ii} \quad (3.119)$$

Similarly, linearizing (3.110) yields

$$L_q \Delta i_q = P_q \Delta \delta + Q_q \Delta E'_q + M_q \Delta i_d \quad (3.120)$$

where

$$P_{qij} = y_{ij}[x_{qj}i_{qj}C_{ij} - (E'_{qj} - x'_{dj}i_{dj})S_{ij}], \quad j \neq i \quad (3.121)$$

$$P_{qii} = -\sum_{\substack{j=1 \\ j \neq i}}^n P_{qij} \quad (3.122)$$

$$Q_{qij} = y_{ij}C_{ij}, \quad j = 1, 2, \dots, n \quad (3.123)$$

$$M_{qij} = -y_{ij}x'_{dj}C_{ij}, \quad j = 1, 2, \dots, n \quad (3.124)$$

$$L_{qij} = -y_{ij}x_{qj}S_{ij}, \quad j \neq i \quad (3.125)$$

$$L_{qii} = 1 - y_{ii}x_{qi}S_{ii} \quad (3.126)$$

Solving (3.113) and (3.120) simultaneously give

$$\Delta i_d = F_d \Delta \delta + Y_d \Delta E'_q \quad (3.127)$$

$$\Delta i_q = F_q \Delta \delta + Y_q \Delta E'_q \quad (3.128)$$

where

$$F_q = [L_q - M_q L_d^{-1} M_d]^{-1} \cdot [P_q + M_q L_d^{-1} P_d] \quad (3.129)$$

$$Y_q = [L_q - M_q L_d^{-1} M_d]^{-1} \cdot [Q_q + M_q L_d^{-1} Q_d] \quad (3.130)$$

$$F_d = L_d^{-1} [P_d + M_d F_q] \quad (3.131)$$

$$Y_d = L_d^{-1}[Q_d + M_d Y_q] \quad (3.132)$$

Solving (3.102)-(3.104), linearizing, and substituting for Δi_{di} and Δi_{qi} from (3.127) and (3.128) results in

$$\Delta P_e = K_1 \Delta \delta + K_2 \Delta E'_q \quad (3.133)$$

where

$$K_1 = D_t F_d + Q_t F_q \quad (3.134)$$

$$K_2 = I_q + D_t Y_d + Q_t Y_q \quad (3.135)$$

$$K_1 = D_t F_d + Q_t F_q \quad (3.136)$$

Also, linearizing (3.100) and substituting for Δi_{di} and Δi_{qi} from (3.127) and (3.128) yields

$$[I + sT'_{d0} + (x_d - x'_d)Y_d] \Delta E'_q = \Delta E_{fd} - (x_d - x'_d)F_d \Delta \delta \quad (3.137)$$

For the i th machine, it can be written

$$[I + sT'_{d0i} K_{3ii}] \Delta E'_{qi} = K_{3ii} [\Delta E_{fdi} - \sum_{\substack{j=1 \\ j \neq i}}^n \frac{1}{K_{3ij}} \Delta E'_{qj} - \sum_{j=1}^n K_{4ij} \Delta \delta_j] \quad (3.138)$$

where

$$K_{3ij} = [(x_{di} - x'_{di})Y_{dij}]^{-1}, \quad j \neq i \quad (3.139)$$

$$K_{3ii} = [1 + (x_{di} - x'_{di})Y_{dii}]^{-1} \quad (3.140)$$

$$K_{4ij} = (x_{di} - x'_{di})F_{dij}, \quad j \neq i \quad (3.141)$$

$$K_{4ii} = (x_{di} - x'_{di})F_{dii} \quad (3.142)$$

Moreover, linearizing (3.103) and (3.104) and solving for Δv

$$\Delta v = K_5 \Delta \delta + K_6 \Delta E'_q \quad (3.143)$$

where

$$K_5 = D_v x_q F_q - Q_v x_d' F_d \quad (3.144)$$

$$K_6 = D_v x_q Y_q - Q_v x_d' Y_d + Q_v \quad (3.145)$$

$$D_v = v_0^{-1} v_{d0} \quad (3.146)$$

$$Q_v = v_0^{-1} v_{q0} \quad (3.147)$$

It should be noticed that v_0 and v_{d0} are diagonal matrices of the respective initial conditions.

Figure 3.11 shows a block diagram of the i th machine in a multimachine power system.

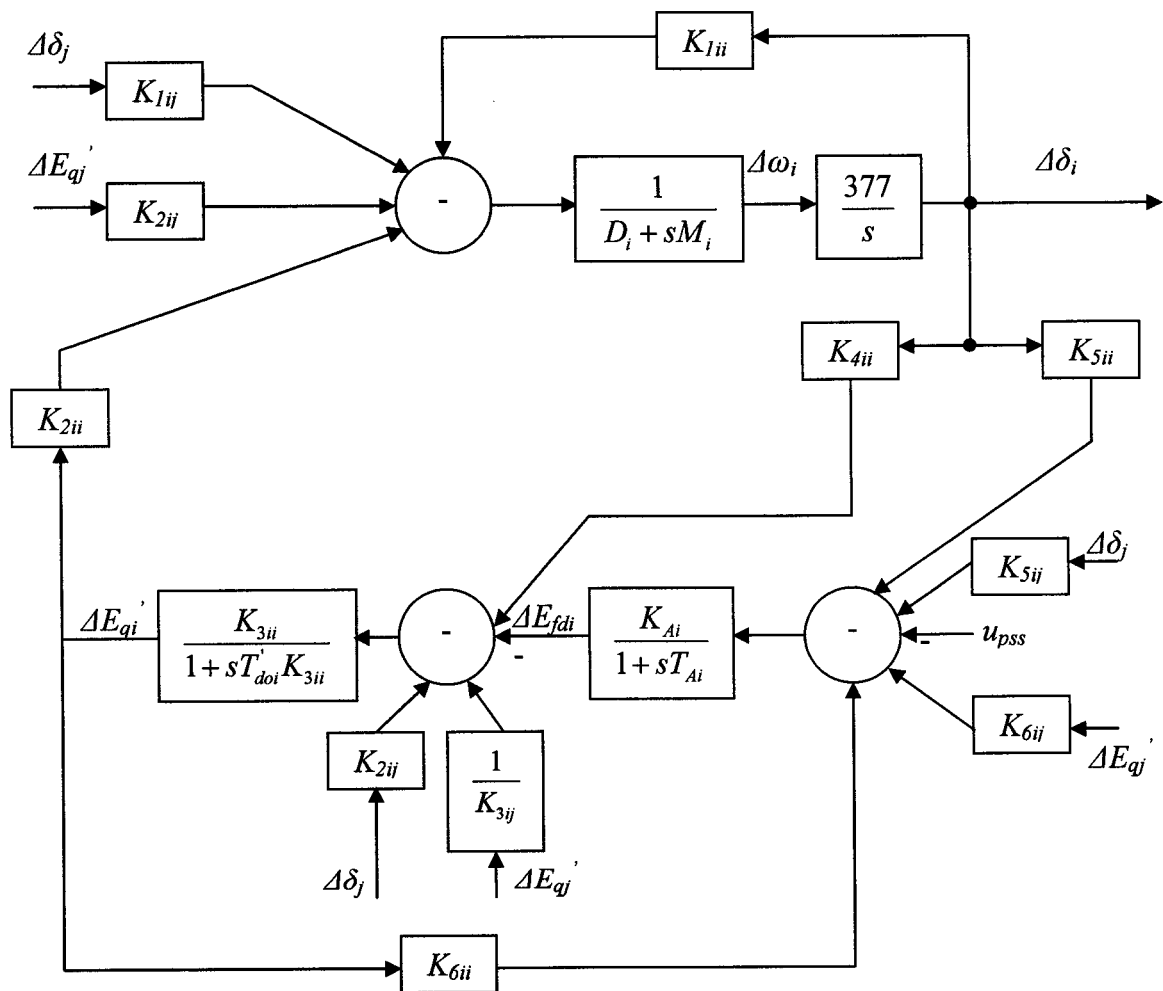


Figure 3.11: Linearized model of the i th machine in multimachine power system

3.3.3 Multimachine Power System Nonlinear Model with SVCs

In the previous multimachine model, the Y -matrix is assumed to be constant. If a FACTS-device is to be added to the system, this assumption is no longer valid. The Y -matrix will be a function of the FACTS device control signal. To incorporate the effects of adding r SVCs into the Y -matrix, for example, the following steps need to be considered:

1. The system $m \times m$ Y -matrix is rearranged as follows

$$Y' = \begin{bmatrix} Y_{nn} & Y_{nr} & Y_{np} \\ Y_{rn} & Y_{rr} & Y_{rp} \\ Y_{pn} & Y_{pr} & Y_{pp} \end{bmatrix} \quad (3.148)$$

where $p = m - (n+r)$, Y_{nn} is an $n \times n$ sub-matrix, Y_{nr} is an $n \times r$ sub-matrix, and so on.

It is worth noticing that all the sub-matrices are constant except Y_{rr} . For example, for $r = 2$,

$$Y_{rr} = \begin{bmatrix} Y_{rr11} - jB_{SVC1} & Y_{rr12} \\ Y_{rr21} & Y_{rr22} - jB_{SVC2} \end{bmatrix} \quad (3.149)$$

2. The resulting Y -matrix is reduced to

$$Y_S = \begin{bmatrix} Y_{NN} & Y_{NR} \\ Y_{RN} & Y_{RR} \end{bmatrix} \quad (3.150)$$

where Y_{NN} is an $n \times n$ sub-matrix, Y_{NR} is an $n \times r$ sub-matrix, and so on. And,

$$Y_{NN} = Y_{nn} - Y_{np} Y_{pp}^{-1} Y_{pn} \quad (3.151)$$

$$Y_{NR} = Y_{nr} - Y_{np} Y_{pp}^{-1} Y_{pr} \quad (3.152)$$

$$Y_{RN} = Y_{rn} - Y_{rp} Y_{pp}^{-1} Y_{pn} \quad (3.152)$$

$$Y_{RR} = Y_{rr} - Y_{rp} Y_{pp}^{-1} Y_{pr} \quad (3.153)$$

Again, all the sub-matrices here are constant except Y_{RR} .

3. Y_S is further reduced to

$$Y = Y_{NN} - Y_{NR}Y_{RR}^{-1}Y_{RN} \quad (3.154)$$

It should be observed that equations (3.98)-(3.113) are still valid except that the Y -matrix is that shown in (3.154).

3.3.4 Multimachine System Linearized Model with SVCs

Without loss of generality, in the derivation it will be assumed that only one SVC is added to the system. If more than one SVC is to be connected, a linear addition of their effect is valid in the linearized model. Hence, Y can be re-written as

$$Y = Y_W - \frac{1}{Y_m - jB_{SVC}} Y_{XY} \quad (3.155)$$

where Y_m is the SVC bus self-admittance

$$Y_W = Y_{NN}, \quad Y_{XY} = Y_{NR}Y_{RN}, \quad \text{and } 1/(Y_m - jB_{SVC}) = Y_{RR}.$$

Define

$$Y_W = y_w e^{j\beta_w}, \quad Y_{XY} = y_{xy} e^{j\beta_{xy}}, \quad R = |Y_m - jB_{SVC}|, \quad \theta = \text{angle}(Y_m - jB_{SVC}), \quad (3.156)$$

$$a_m = \text{Re}(Y_m - jB_{SVC}), \quad \text{and } b_m = \text{Im}(Y_m - jB_{SVC})$$

Consequently, i_{di} and i_{qi} can be expressed as

$$i_{di} = \sum_{j=1}^n y_{wij} [x_{qj} i_{qj} C_{wij} - (E'_{qj} - x'_{dj} i_{dj}) S_{wij}] - \frac{1}{R} \sum_{j=1}^n y_{xyij} [x_{qj} i_{qj} C_{xyij} - (E'_{qj} - x'_{dj} i_{dj}) S_{xyij}] \quad (3.157)$$

$$i_{qi} = \sum_{j=1}^n y_{wij} [x_{qj} i_{qj} S_{wij} + (E'_{qj} - x'_{dj} i_{dj}) C_{wij}] - \frac{1}{R} \sum_{j=1}^n y_{xyij} [x_{qj} i_{qj} S_{xyij} + (E'_{qj} - x'_{dj} i_{dj}) C_{xyij}] \quad (3.158)$$

where

$$C_{wij} = \cos(\beta_{wij} + \delta_j - \delta_i) \quad (3.159)$$

$$S_{wij} = \sin(\beta_{wij} + \delta_j - \delta_i) \quad (3.160)$$

$$C_{xyij} = \cos(\beta_{xyij} + \delta_j - \delta_i - \theta) \quad (3.161)$$

$$S_{xyij} = \sin(\beta_{xyij} + \delta_j - \delta_i - \theta) \quad (3.162)$$

Linearizing (3.157) yields

$$L_d \Delta i_d = P_d \Delta \delta + Q_d \Delta E'_q + M_d \Delta i_q + N_d \Delta B_{SVC} \quad (3.163)$$

where

$$P_{dij} = -y_{wij} [x_{qj} i_{qj} S_{wij} + (E'_{qj} - x'_{dj} i_{dj}) C_{wij}] + \frac{y_{xyij}}{R} [x_{qj} i_{qj} S_{xyij} + (E'_{qj} - x'_{dj} i_{dj}) C_{xyij}], \quad j \neq i \quad (3.164)$$

$$P_{dii} = -\sum_{\substack{j=1 \\ j \neq i}}^n P_{dij} \quad (3.165)$$

$$Q_{dij} = -y_{wij} S_{wij} + \frac{y_{xyij}}{R} S_{xyij}, \quad j = 1, 2, \dots, n \quad (3.166)$$

$$M_{dij} = y_{wij} x_{qj} C_{wij} - \frac{y_{xyij}}{R} x_{qj} C_{xyij}, \quad j = 1, 2, \dots, n \quad (3.167)$$

$$L_{dij} = -y_{wij} x'_{dj} S_{wij} + \frac{y_{xyij}}{R} x'_{dj} S_{xyij}, \quad j \neq i \quad (3.168)$$

$$L_{dii} = 1 - y_{wij} x'_{dj} S_{wij} + \frac{y_{xyij}}{R} x'_{dj} S_{xyij}, \quad j \neq i \quad (3.169)$$

$$N_{di} = -\frac{1}{R^3} [(b_m - B_{SVC}) C_\theta + a_m S_\theta] \sum_{j=1}^n y_{xyij} [x_{qj} i_{qj} C_{ojj} - (E'_{qj} - x'_{dj} i_{dj}) S_{ojj}] \\ + \frac{1}{R^3} [-(b_m - B_{SVC}) S_\theta + a_m C_\theta] \sum_{j=1}^n y_{xyij} [x_{qj} i_{qj} S_{ojj} + (E'_{qj} - x'_{dj} i_{dj}) C_{ojj}] \quad (3.170)$$

$$S_\theta = \sin(\theta), C_\theta = \cos(\theta), S_{ojj} = \sin(\beta_{xyij} + \delta_j - \delta_i), C_{ojj} = \cos(\beta_{xyij} + \delta_j - \delta_i) \quad (3.171)$$

Similarly, linearizing (3.158) yields

$$L_q \Delta i_q = P_q \Delta \delta + Q_q \Delta E'_q + M_q \Delta i_q + N_q \Delta B_{SVC} \quad (3.172)$$

where

$$P_{qij} = y_{wij} [x_{qj} i_{qj} C_{wij} - (E'_{qj} - x'_{dj} i_{dj}) S_{wij}] - \frac{y_{xyij}}{R} [x_{qj} i_{qj} C_{xyij} - (E'_{qj} - x'_{dj} i_{dj}) S_{xyij}], \quad j \neq i \quad (3.173)$$

$$P_{qii} = - \sum_{\substack{j=1 \\ j \neq i}}^n P_{qij} \quad (3.174)$$

$$Q_{qij} = y_{wij} C_{wij} - \frac{y_{xyij}}{R} C_{xyij}, \quad j = 1, 2, \dots, n \quad (3.175)$$

$$M_{qij} = -y_{wij} x'_{dj} C_{wij} + \frac{y_{xyij}}{R} x'_{dj} C_{xyij}, \quad j = 1, 2, \dots, n \quad (3.176)$$

$$L_{qij} = -y_{wij} x_{qj} S_{wij} + \frac{y_{xyij}}{R} x_{qj} S_{xyij}, \quad j \neq i \quad (3.177)$$

$$L_{qii} = 1 - y_{wii} x_{qi} S_{wii} + \frac{y_{xyii}}{R} x_{qi} S_{xyii} \quad (3.178)$$

$$N_{qi} = -\frac{1}{R^3} [-(b_m - B_{SVC}) S_\theta + a_m C_\theta] \sum_{j=1}^n y_{xyij} [x_{qj} i_{qj} C_{ojj} - (E'_{qj} - x'_{dj} i_{dj}) S_{ojj}] \\ - \frac{1}{R^3} [(b_m - B_{SVC}) C_\theta + a_m S_\theta] \sum_{j=1}^n y_{xyij} [x_{qj} i_{qj} S_{ojj} + (E'_{qj} - x'_{dj} i_{dj}) C_{ojj}] \quad (3.179)$$

Solving (3.163) and (3.172) simultaneously give

$$\Delta i_d = F_d \Delta \delta + Y_d \Delta E'_q + U_d \Delta B_{SVC} \quad (3.180)$$

$$\Delta i_q = F_q \Delta \delta + Y_q \Delta E'_q + U_q \Delta B_{SVC} \quad (3.181)$$

where

$$F_q = [L_q - M_q L_d^{-1} M_d]^{-1} \cdot [P_q + M_q L_d^{-1} P_d] \quad (3.182)$$

$$Y_q = [L_q - M_q L_d^{-1} M_d]^{-1} \cdot [Q_q + M_q L_d^{-1} Q_d] \quad (3.183)$$

$$U_q = [L_q - M_q L_d^{-1} M_d]^{-1} \cdot [N_q + M_q L_d^{-1} N_d] \quad (3.184)$$

$$F_d = L_d^{-1} [P_d + M_d F_q] \quad (3.185)$$

$$Y_d = L_d^{-1}[Q_d + M_d Y_q] \quad (3.186)$$

$$U_d = L_d^{-1}[N_d + M_d U_q] \quad (3.187)$$

Solving (3.102)-(3.104), linearizing, and substituting for Δi_{di} and Δi_{qi} from (3.180) and (3.181) results in

$$\Delta P_e = K_1 \Delta \delta + K_2 \Delta E'_q + K_{pB} \Delta B_{SVC} \quad (3.188)$$

where

$$K_1 = D_t F_d + Q_t F_q \quad (3.189)$$

$$K_2 = I_q + D_t Y_d + Q_t Y_q \quad (3.190)$$

$$K_{pBi} = D_{ti} U_{di} + Q_{ti} U_{qi} \quad (3.191)$$

Also, linearizing (3.100) and substituting for Δi_{di} and Δi_{qi} from (3.180) and (3.181) yields

$$[I + sT'_{d0} + (x_d - x'_d)Y_d] \Delta E'_q = \Delta E_{fd} - (x_d - x'_d)F_d \Delta \delta - (x_d - x'_d)U_d \Delta B_{SVC} \quad (3.192)$$

For the i th machine, it can be written

$$[I + sT'_{d0i} K_{3ii}] \Delta E'_{qi} = K_{3ii} [\Delta E_{fdi} - \sum_{\substack{j=1 \\ j \neq i}}^n \frac{1}{K_{3ij}} \Delta E'_{qj} - \sum_{j=1}^n K_{4ij} \Delta \delta_j - K_{qBi} \Delta B_{SVC}] \quad (3.193)$$

where

$$K_{3ij} = [(x_{di} - x'_{di})Y_{dij}]^{-1}, \quad j \neq i \quad (3.194)$$

$$K_{3ii} = [1 + (x_{di} - x'_{di})Y_{dii}]^{-1} \quad (3.195)$$

$$K_{4ij} = (x_{di} - x'_{di})F_{dij}, \quad j \neq i \quad (3.196)$$

$$K_{4ii} = (x_{di} - x'_{di})F_{dii} \quad (3.197)$$

$$K_{qBi} = (x_{di} - x'_{di})U_{di} \quad (3.198)$$

Moreover, linearizing (3.103) and (3.104) and solving for Δv

$$\Delta v = K_5 \Delta \delta + K_6 \Delta E'_q + K_{vB} \Delta B_{SVC} \quad (3.199)$$

where

$$K_5 = D_v x_q F_q - Q_v x'_d F_d \quad (3.200)$$

$$K_6 = D_v x_q Y_q - Q_v x'_d Y_d + Q_v \quad (3.201)$$

$$K_{vB} = D_v x_q U_q - Q_v x'_d U_d \quad (3.202)$$

$$D_v = v_0^{-1} v_{d0} \quad (3.203)$$

$$Q_v = v_0^{-1} v_{q0} \quad (3.204)$$

Figure 3.12 shows a block diagram of the *i*th machine in a multimachine power system equipped with a G1 FACTS device.

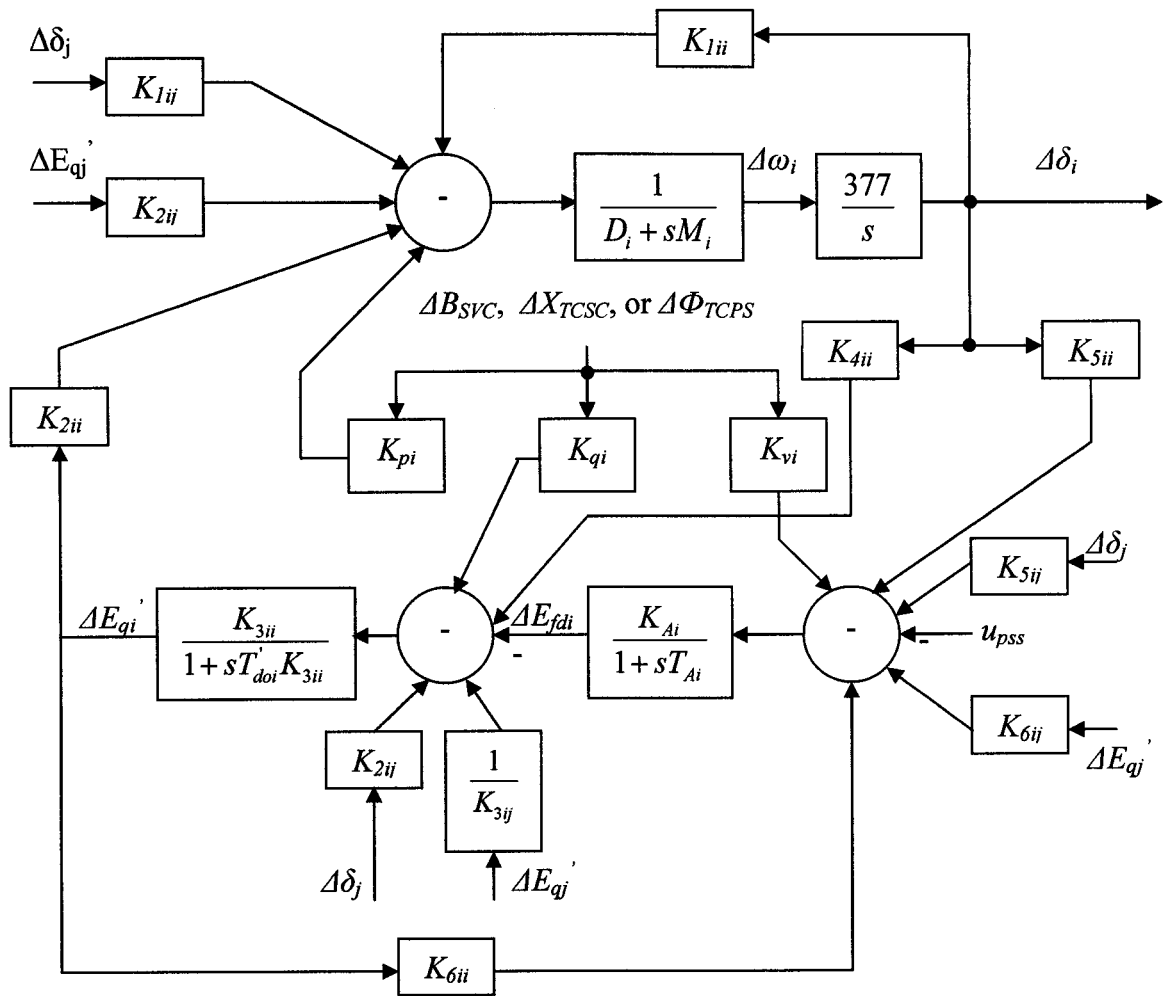


Figure 3.12: Linearized model of the i th machine in multimachine power system with a G1 FACTS device

CHAPTER 4

PARTICLE SWARM OPTIMIZER

A novel population based optimization approach, called Particle Swarm Optimization (PSO) approach, was introduced first in [49]. This new approach features many advantages; it is simple, fast and can be coded in few lines. Also, its storage requirement is minimal.

Moreover, this approach is advantageous over evolutionary algorithms in more than one way. First, PSO has memory. That is, every particle remembers its best solution (local best) as well as the group best solution (global best). Another advantage of PSO is that the initial population of the PSO is maintained, and so there is no need for applying operators to the population, a process which is time- and memory-storage-consuming. In addition, PSO is based on “constructive cooperation” between particles, in contrast with the other artificial algorithms which are based on “the survival of the fittest.”[50]

PSO starts with a population of random solutions. Each particle keeps track of its coordinates in hyperspace which are associated with the fittest solution it has achieved so far. The value of the fitness (*pbest*) is stored. Another best value is also tracked, which is the global best value. The global version of the PSO keeps track of the overall best

value, and its location, obtained thus far by any particle in the population, which is called (*gbest*).

PSO consists of, at each step, changing the velocity of each particle toward its *pbest* and *gbest*. Acceleration is weighted by a random term, with separate random numbers being generated for acceleration toward *pbest* and *gbest*.

Several modifications have been proposed in the literature to improve the PSO algorithm speed and convergence toward the global minimum. One of the most efficient PSO versions uses a time decreasing inertia weight, which leads to a reduction in the number of iterations. The performance of this modified algorithm depends on the method of tuning the inertia weight. The most straightforward way to adjust the inertia weight is to force it to linearly decrease with the number of iterations.

As an alternative to inertia weight technique, constriction factors have been proposed [162]. Constriction-factor-based PSO has been proved to be superior upon inertia-weight-based PSO in terms of the number of iterations to reach the best solution.

PSO starts with a population of random solutions “particles” in a D-dimension space. The i^{th} particle is represented by $X_i=(x_{i1}, x_{i2}, \dots, x_{iD})$. Each particle keeps track of its coordinates in hyperspace which are associated with the fittest solution it has achieved so far. The value of the fitness for particle i (*pbest*) is also stored as $P_i=(p_{i1}, p_{i2}, \dots, p_{iD})$. The global version of the PSO keeps track of the overall best value (*gbest*), and its location, obtained thus far by any particle in the population.

PSO consists of, at each step, changing the velocity of each particle toward its *pbest* and *gbest* according to equation (3.205). The velocity of particle i is represented as $V_i=(v_{i1}, v_{i2}, \dots, v_{iD})$. Acceleration is weighted by a random term, with separate random

numbers being generated for acceleration toward p_{best} and g_{best} . The position of the i^{th} particle is then updated according to equation (3.206).

$$v_{id} = w*v_{id} + c_1*rand()*(p_{id}-x_{id}) + c_2*Rand()*(p_{gd}-x_{id}) \quad (3.205)$$

$$x_{id} = x_{id} + v_{id} \quad (3.206)$$

where, $p_{id} = p_{best}$

and $p_{gd} = g_{best}$

A simplified method of incorporating a constriction factor is represented in equation (3.207), where K is a function of c_1 and c_2 as illustrated by equation (3.208). Eberhart and Shi [162] experimented the performance of PSO using an inertia weight as compared with PSO performance using a constriction factor. They concluded that the best approach is to use a constriction factor while limiting the maximum velocity V_{max} to the dynamic range of the variable X_{max} on each dimension. They showed that this approach provides performance superior to any other published results.

$$v_{id} = K*[v_{id} + c_1*rand()*(p_{id}-x_{id}) + c_2*Rand()*(p_{gd}-x_{id})] \quad (3.207)$$

$$K = kk/|2-\varphi-(\varphi^2-4\varphi)^{0.5}|; \quad kk = 2 \text{ and } \varphi = c_1 + c_2, \varphi > 4 \quad (3.208)$$

4.1 Steps of the PSO Algorithm

Figure 4.1 shows a flow chart of the PSO algorithm. It is described as follows:

Step 1: Define the problem space and set the boundaries, i.e. equality and inequality constraints.

Step 2: Initialize an array of particles with random positions and their associated velocities inside the problem space.

Step 3: Check if the current position is inside the problem space or not. If not, adjust the positions so as to be inside the problem space.

Step 4: Evaluate the fitness value of each particle.

Step 5: Compare the current fitness value with the particles' previous best value ($pbest[]$). If the current fitness value is better, then assign the current fitness value to $pbest[]$ and assign the current coordinates to $pbestx[][d]$ coordinates.

Step 6: Determine the current global minimum among particle's best position.

Step 7: If the current global minimum is better than $gbest$, then assign the current global minimum to $gbest[]$ and assign the current coordinates to $gbestx[][d]$ coordinates.

Step 8: Change the velocities according to (3.205).

Step 9: Move each particle to the new position according to (3.206) and return to **Step 3.**

Step 10: Repeat **Step 3- Step 9** until a stopping criteria is satisfied.

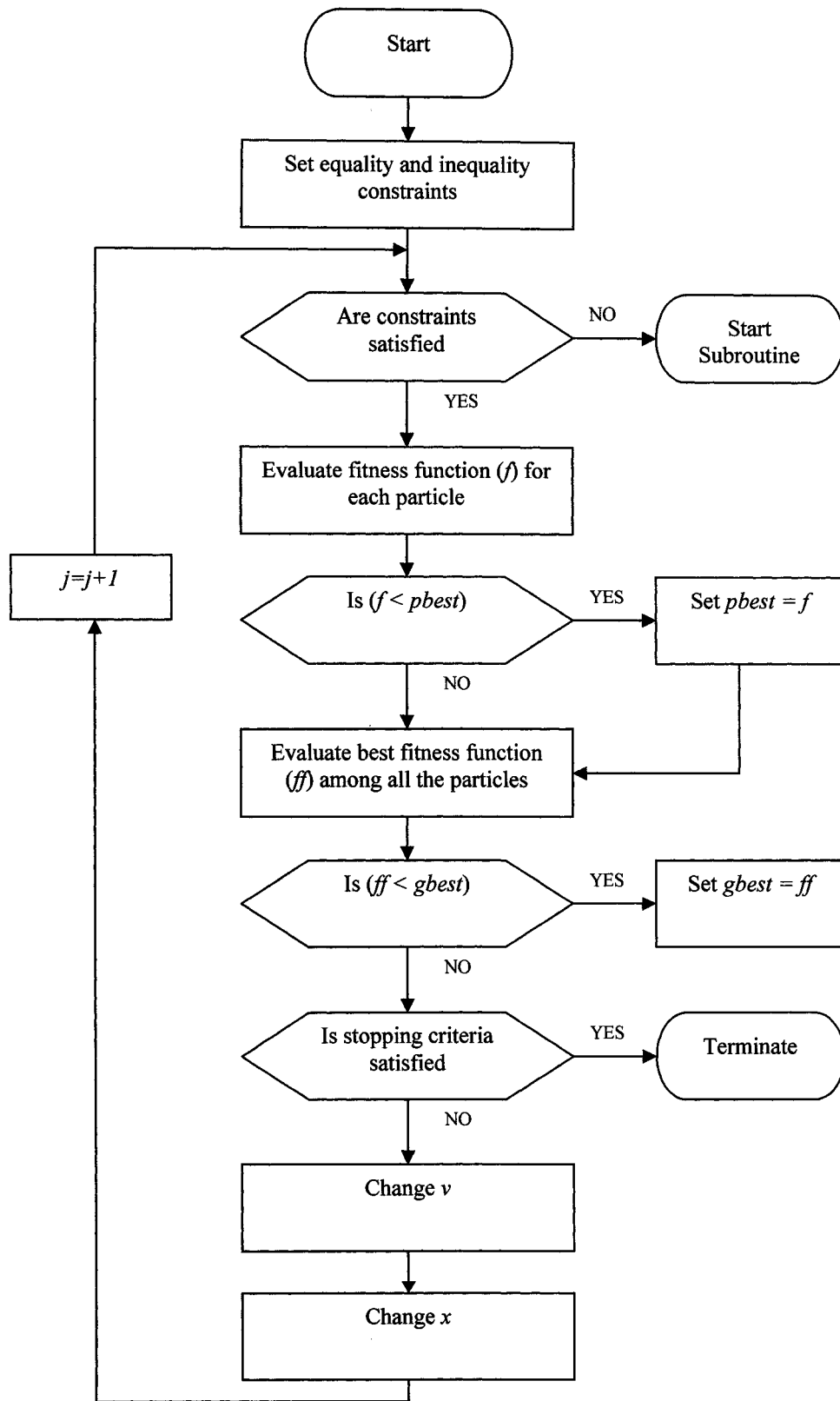


Figure 4.1: Flow chart of PSO algorithm

CHAPTER 5

PROBLEM FORMULATION

5.1 System Models and Stabilizer Structures

In this thesis, the synchronous generator and the exciter are described by the 4th order model outlined in chapter 3, which is widely accepted for analyzing power system dynamics. The model is summarized here as

$$\dot{\delta} = \omega_b(\omega - 1) \quad (5.1)$$

$$\dot{\omega} = (P_m - P_e - D(\omega - 1)) / M \quad (5.2)$$

$$\dot{E}'_q = (E_{fd} - (x_d - x'_d)i_d - E'_q) / T'_{do} \quad (5.3)$$

$$\dot{E}_{fd} = (K_A(V_{ref} - v + u_{PSS}) - E_{fd}) / T_A \quad (5.4)$$

$$v = (v_d^2 + v_q^2)^{1/2} \quad (5.5)$$

$$v_d = x_q i_q$$

$$v_q = E'_q - x'_d i_d$$

$$P_e = v_d i_d + v_q i_q \quad (5.6)$$

In the case of a SMIB system with a UPFC, the UPFC is modeled as

$$\begin{bmatrix} v_{Etd} \\ v_{Etdq} \end{bmatrix} = \begin{bmatrix} 0 & -x_E \\ x_E & 0 \end{bmatrix} \begin{bmatrix} i_{Ed} \\ i_{Eq} \end{bmatrix} + \begin{bmatrix} \frac{m_E \cos \delta_E v_{dc}}{2} \\ \frac{m_E \sin \delta_E v_{dc}}{2} \end{bmatrix} \quad (5.7)$$

$$\begin{bmatrix} v_{Btd} \\ v_{Btdq} \end{bmatrix} = \begin{bmatrix} 0 & -x_B \\ x_B & 0 \end{bmatrix} \begin{bmatrix} i_{Bd} \\ i_{Bq} \end{bmatrix} + \begin{bmatrix} \frac{m_B \cos \delta_B v_{dc}}{2} \\ \frac{m_B \sin \delta_B v_{dc}}{2} \end{bmatrix} \quad (5.8)$$

$$\dot{v}_{dc} = \frac{3m_E}{4C_{dc}} [\cos \delta_E \quad \sin \delta_E] \begin{bmatrix} i_{Ed} \\ i_{Eq} \end{bmatrix} + \frac{3m_B}{4C_{dc}} [\cos \delta_B \quad \sin \delta_B] \begin{bmatrix} i_{Bd} \\ i_{Bq} \end{bmatrix} \quad (5.9)$$

A multimachine power system is modeled as

$$\dot{\delta}_i = \omega_b (\omega_i - 1) \quad (5.10)$$

$$\dot{\omega}_i = (P_{mi} - P_{ei} - D_i (\omega_i - 1)) / M_i \quad (5.11)$$

$$\dot{E}'_{qi} = (E_{fdi} - (x_{di} - x'_{di}) i_{di} - E'_{qi}) / T'_{doi} \quad (5.12)$$

$$\dot{E}'_{fdi} = (K_{Ai} (V_{refi} - v_i + u_{PSSi}) - E'_{fdi}) / T_{Ai} \quad (5.13)$$

where

$$P_{ei} = v_{di} i_{di} + v_{qi} i_{qi} \quad (5.14)$$

$$v_{di} = x_{qi} i_{qi}, \quad v_{qi} = E'_{qi} - x'_{di} i_{di} \quad (5.15)$$

$$v_i = (v_{di}^2 + v_{qi}^2)^{1/2} \quad (5.16)$$

Also,

$$I = YV \quad (5.17)$$

where

$$I_i = (i_d + ji_q)e^{j(\delta_i - \frac{\pi}{2})} \quad (5.18)$$

$$V_i = (v_d + jv_q)e^{j(\delta_i - \frac{\pi}{2})} \quad (5.19)$$

$$Y_{ij} = y_{ij}e^{j\beta_{ij}} \quad (5.20)$$

It is worth emphasizing that if a FACTS device is incorporated in the multimachine system, the Y -matrix is no longer constant; it is a function of the FACTS device control signal.

The PSS and FACTS-based stabilizer will be the very widely used lead-lag controller, whose transfer function is

$$u = K \frac{sT_w}{1 + sT_w} \left(\frac{1 + sT_1}{1 + sT_2} \right) \left(\frac{1 + sT_3}{1 + sT_4} \right) \Delta\omega$$

where

u and $\Delta\omega$ stabilizer output and input

K Stabilizer gain

T_w Washout time constant

$T_1, T_2, T_3,$ and T_4 Stabilizer time constant

In this controller structure, T_w is usually predetermined. The controller parameters to be specified, then, are $K, T_1, T_2, T_3,$ and T_4 .

5.2 Objective Functions

To select the best stabilizer parameters that enhance most the power system transient performance, two eigenvalue-based objective functions are considered:

$$J_1 = \min\{\zeta_i: \zeta_i \text{ is a vector of the damping ratios corresponding to all the complex eigenvalues of the system at the } i\text{th loading condition}\}$$

$$J_2 = \max\{\sigma_i: \sigma_i \text{ is a vector of the damping factors corresponding to all the complex eigenvalues of the system at the } i\text{th loading condition}\}$$

The objective function J_1 identifies the minimum value of the damping ratios among all the system complex modes of all loading conditions considered in the design process. Hence, the goal is to Maximize J_1 to reduce the system response overshoot and enhance the system damping characteristics.

However, the objective function J_2 identifies the maximum value of the damping factors, i.e. the real parts of the eigenvalues, among all the system complex modes of all loading conditions considered in the design process. Hence, the goal is to Minimize J_2 to shift the poorly damped eigenvalues to the left in the s-plane improving the system response settling time and enhancing the system relative stability.

5.3 Optimization Problem

The design problem can be formulated as follows

Optimize J

Subject to

$$K_i^{\min} \leq K_i \leq K_i^{\max}$$

$$T_{1i}^{\min} \leq T_{1i} \leq T_{1i}^{\max}$$

$$T_{2i}^{\min} \leq T_{2i} \leq T_{2i}^{\max}$$

$$T_{3i}^{\min} \leq T_{3i} \leq T_{3i}^{\max}$$

$$T_{4i}^{\min} \leq T_{4i} \leq T_{4i}^{\max}$$

where i is number of stabilizers considered and J can be either J_1 or J_2 .

The proposed approach will employ particle swarm optimizer (PSO) to search for the optimum parameter settings of the given stabilizers.

CHAPTER 6

PROPOSED APPROACH

6.1 Controllability Measure

To measure the controllability of the EM mode by a given input (control signal), the singular value decomposition (SVD) is employed. Mathematically, if G is an $m \times n$ complex matrix, then there exist unitary matrices W and V with dimensions of $m \times m$ and $n \times n$, respectively, such that

$$G = W\Sigma V^B \quad (6.1)$$

where

$$\Sigma = \begin{bmatrix} \Sigma_1 & 0 \\ 0 & 0 \end{bmatrix} \quad (6.2)$$

$$\Sigma_1 = \text{diag}(\sigma_1, \dots, \sigma_r) \quad (6.3)$$

with $\sigma_1 \geq \dots \geq \sigma_r \geq 0$ where $r = \min\{m, n\}$ and $\sigma_1, \dots, \sigma_r$ are the singular values of G .

The minimum singular value σ_r represents the distance of the matrix G from all the matrices with a rank of $r-1$. This property can be used to quantify modal controllability [164,165]. The matrix B can be written as $B=[b_1 \ b_2 \ b_3 \ b_4 \ b_5]$ where b_i is a column vector corresponding to the i th input. The minimum singular value, σ_{min} , of the matrix $[\lambda I - A \ b_i]$ indicates the capability of the i th input to control the mode associated with the eigenvalue

λ . Actually, the higher the σ_{min} , the higher the controllability of this mode by the input considered. As such, the controllability of the EM mode can be examined with all inputs in order to identify the most effective one to control the mode.

6.2 Damping Torque Coefficient Analysis

To assess the effectiveness of the proposed stabilizers, the damping torque coefficient (DTC) is calculated. For a SMIB system, the torque can be decomposed to

$$\Delta T_e(t) = K_{syn} \Delta \delta(t) + K_d \Delta \omega(t) \quad (6.4)$$

where K_{syn} and K_d are the synchronizing and damping torque coefficients, respectively. It is worth mentioning that K_d is a damping measure of the electromechanical mode of oscillations. To calculate K_{syn} and K_d , the error between the actual torque deviation and that obtained by summing both components can be defined as [166]

$$E(t) = \Delta T_e(t) - [K_{syn} \Delta \delta(t) + K_d \Delta \omega(t)] \quad (6.5)$$

Then, K_{syn} and K_d are computed to minimize the sum of the squared errors over the simulation period t_{sim} as

$$\sum^N E^2 = \sum^N [\Delta T_e(t) - (K_{syn} \Delta \delta + K_d \Delta \omega)]^2 \quad (6.6)$$

where $t_{sim} = N \times T_s$, and T_s is the sampling period. Hence, these coefficients should satisfy

$$\frac{\partial}{\partial K_{syn}} \sum^N E^2 = 0 \text{ and } \frac{\partial}{\partial K_d} \sum^N E^2 = 0 \quad (6.7)$$

This results in

$$\sum^N [\Delta T_e \Delta \delta] = K_{syn} \sum^N [\Delta \delta]^2 + K_d \sum^N [\Delta \omega \Delta \delta] \quad (6.8)$$

$$\sum^N [\Delta T_e \Delta \omega] = K_d \sum^N [\Delta \omega]^2 + K_{syn} \sum^N [\Delta \omega \Delta \delta] \quad (6.9)$$

Solving (6.8) and (6.9), K_{syn} and K_d can be calculated.

6.3 Implementation

In SMIB simulation implementation, the proposed objective functions are optimized individually. For each objective function, the optimization is carried out twice: first at one loading condition and then at a wide range of operating conditions. In each case, both individual stabilizer design and coordinated stabilizer design are covered. The implementation plans are shown in Figure 6.1 and Figure 6.2 for a SMIB system with G1 FACTS devices and a SMIB system with a UPFC, respectively.

A similar implementation plan is followed for the multimachine power system, see Figure 6.3. The only exception is that only one objective function is considered there; J_1 .

In all cases, the design process starts with linearizing the system model at each loading condition of the specified range and identifying the complex modes. Then, the objective function is evaluated and PSO is applied to search for the optimal settings of the proposed stabilizer(s) parameters.

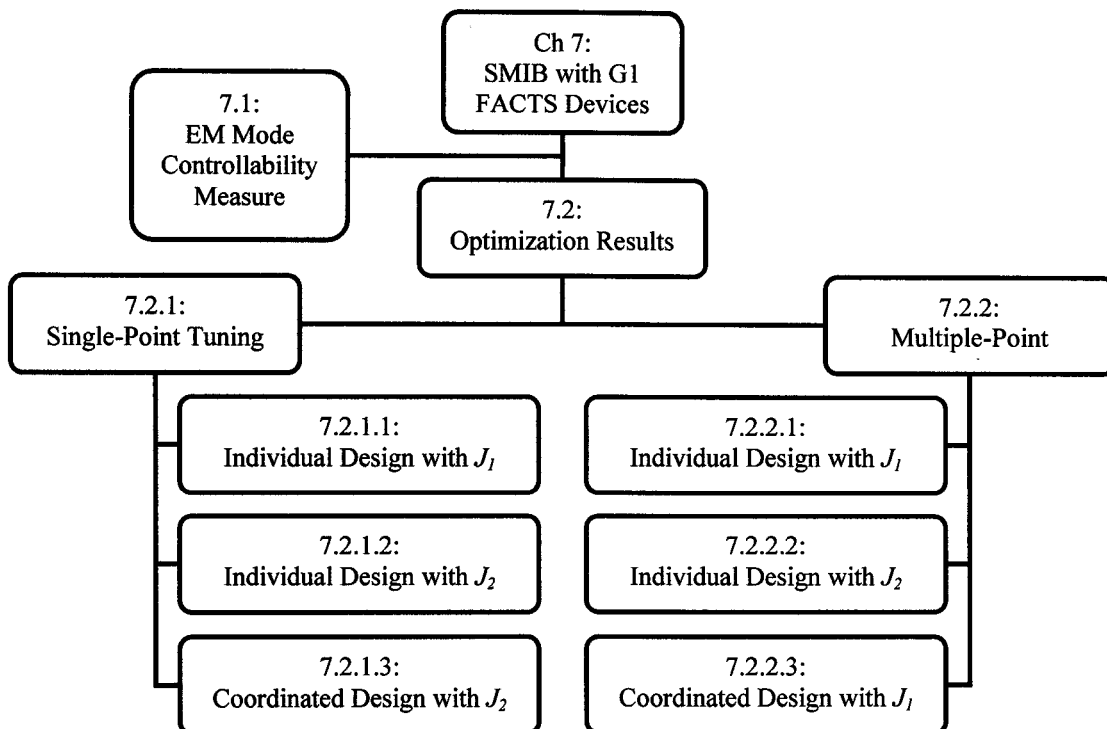


Figure 6.1: Approach implementation plan for a SMIB system with G1 FACTS devices

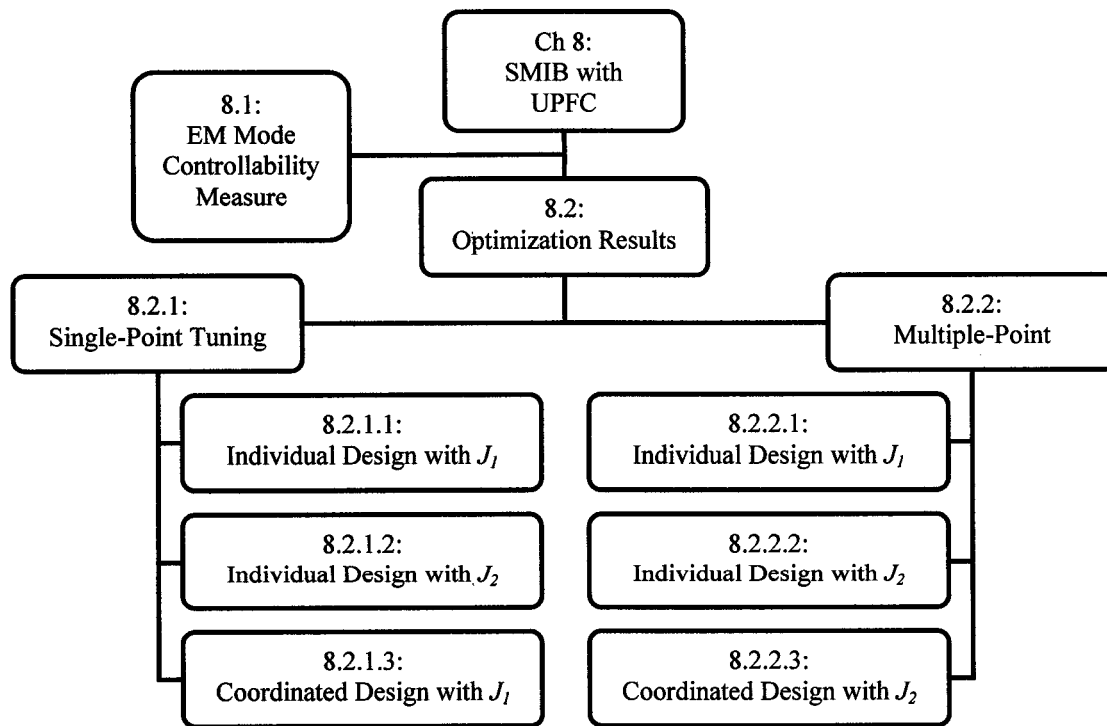


Figure 6.2: Approach implementation plan for a SMIB system with a UPFC

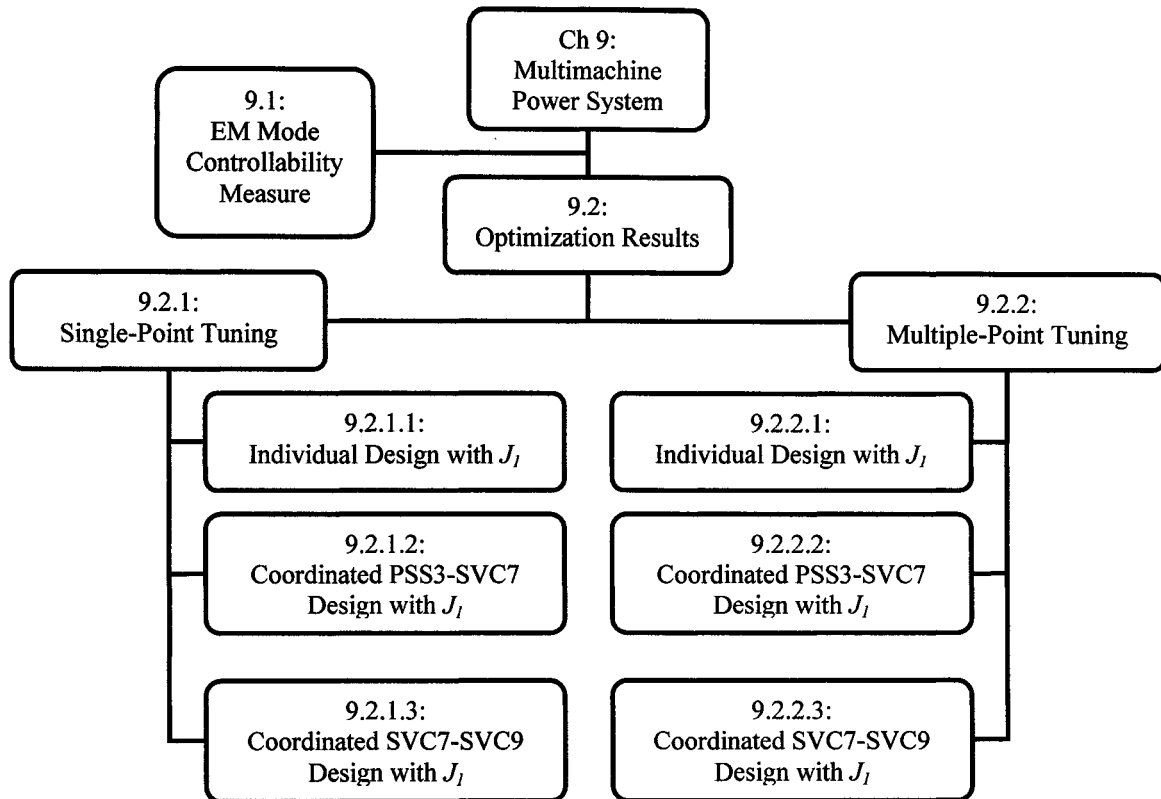


Figure 6.3: Approach implementation plan for a multimachine power system

CHAPTER 7

OPTIMIZATION RESULTS:

FIRST GENERATION FACTS DEVICES

7.1 Electromechanical Mode Controllability Measure

SVD is employed to measure the controllability of the electromechanical (EM) mode from each input signal of PSS, SVC-based stabilizer, TCSC-based stabilizer, and TCPS-based stabilizer. The minimum singular value, σ_{\min} , is estimated over a wide range of operating conditions. For SVD analysis, P_e ranges from 0.05 to 1.4 pu and $Q_e = [-0.4, 0, 0.4]$. At each loading condition, the system model is linearized, the EM mode is identified, and the SVD-based controllability measure is implemented.

For comparison purposes, the minimum singular values for all inputs at $Q_e = -0.4, 0.0$ and 0.4 pu are shown in Figures 7.1-7.3, respectively. From these figures, the following can be noticed:

- The capabilities of the PSS, SVC, and TCSC to control the EM mode are directly proportional to system loading. However, the TCPS capability of controlling the EM mode is less dependent on loading.
- The controllability of TCPS is generally higher than those of the other stabilizers, especially for low and moderate loading.
- At very low loading, PSS, SVC, and TCSC suffer from poor controllability.
- The TCSC enjoys the strongest potential to control the EM mode at high loading conditions.
- The EM mode is least controllable through SVC for the different loading conditions

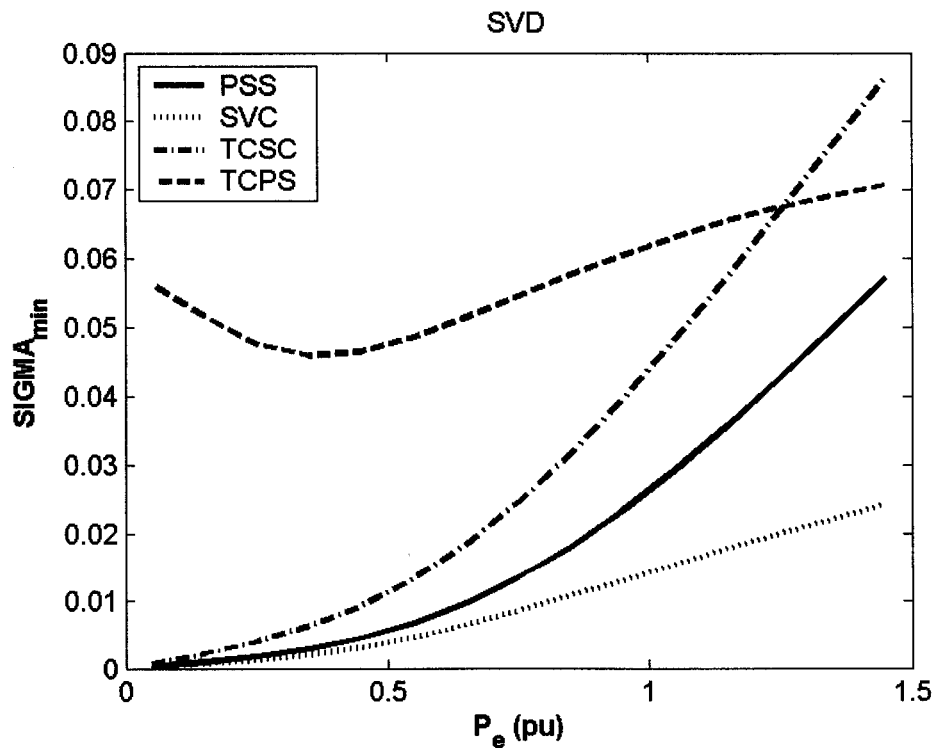


Figure 7.1: Minimum singular value with all controllers at $Q = -0.4$ pu

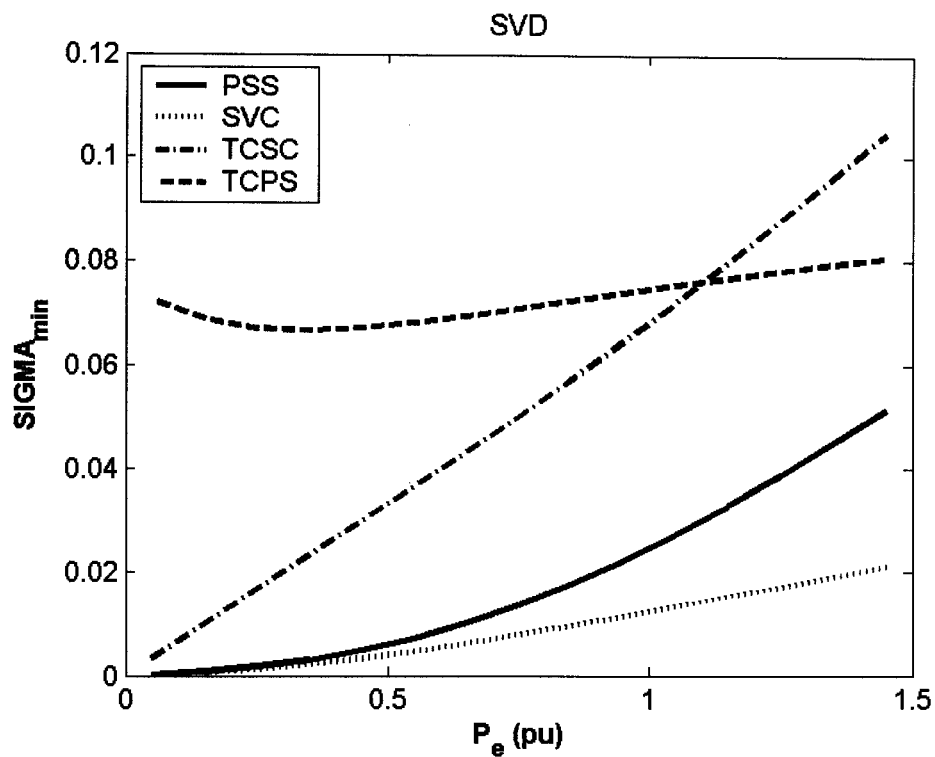


Figure 7.2: Minimum singular value with all controllers at $Q = 0.0$ pu

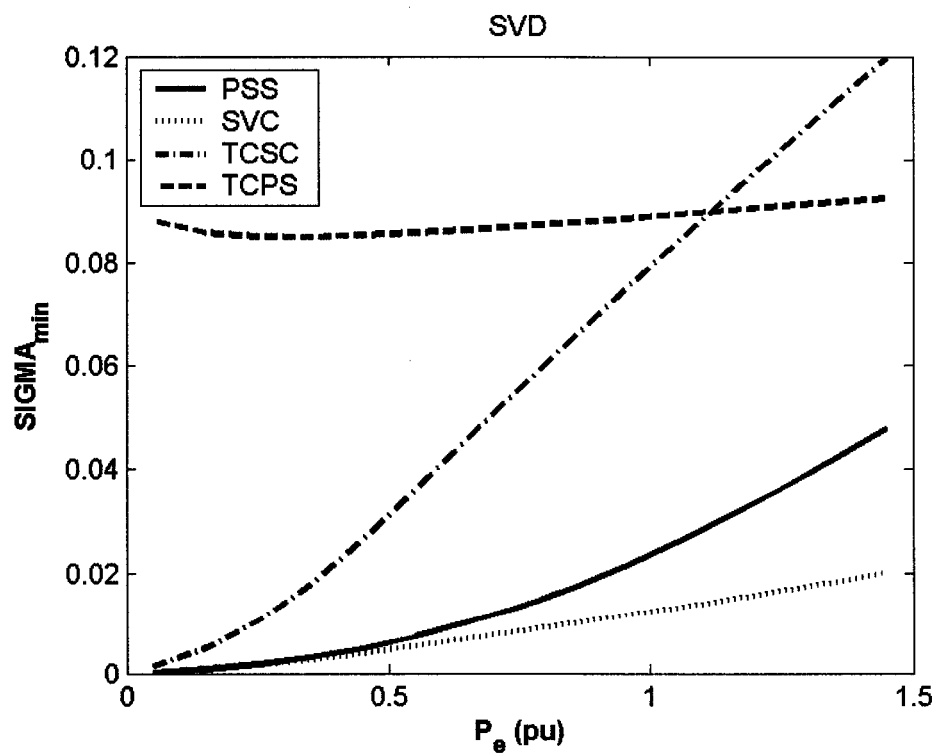


Figure 7.3: Minimum singular value with all controllers at $Q = 0.4$ pu

7.2 Optimization Results for PSS, SVC, TCSC, and TCPS

This chapter presents the optimization results of the two objective functions: J_1 , maximizing the minimum damping ratio, and J_2 , minimizing the maximum damping factor. Both the single-point and multiple-point tuning processes for individual and coordinated designs are considered. The system data is given in Appendix A.

To assess the effectiveness of the proposed controllers, four different loading conditions are considered for eigenvalue analysis. These conditions and disturbances are:

1. Nominal loading (P_e, Q_e)=(1.0,0.015) pu.
2. Light loading (P_e, Q_e)=(0.3,0.015) pu.
3. Heavy loading (P_e, Q_e)=(1.1,0.40) pu.
4. Leading power factor (Pf) loading (P_e, Q_e)=(0.7,-0.3) pu.

Moreover, the nominal and light loading conditions with 6-cycle three-phase fault disturbances are considered for nonlinear time-domain simulations

7.2.1 Single-Point Tuning

In this section, the stabilizers are tuned with only the nominal loading condition, (P_e, Q_e)=(1.0,0.015) pu, taken into account.

7.2.1.1 Individual Design with J_1

The PSS, SVC-, TCSC-, and TCPS-based controllers are designed individually considering the nominal loading condition.

Stabilizer Design: PSO is used to search for the optimum parameter settings of each controller that maximizes the minimum damping ratio of all the system complex eigenvalues. The final settings of the optimized parameters for the proposed stabilizers are given in Table 7.1.

Eigenvalue Analysis: The system eigenvalues without and with the proposed stabilizers at the four operating points, nominal, light, heavy, and leading Pf, are given in Tables 7.2-7.5, respectively. The bold rows of these tables represent the EM mode eigenvalue and its damping ratio. It is evident that the proposed stabilizers greatly improve the system stability. It is also clear that the PSS, SVC and TCSC have relatively poor capabilities to enhance the EM mode damping when the system operates at light loading.

Table 7.1: Optimal parameter settings with J_1 , single-point tuning, individual design

	PSS	SVC	TCSC	TCPS
K	21.686	300.00	10.8202	9.2238
T₁	4.4314	5.0000	4.0061	3.5957
T₂	0.0100	0.9705	0.9165	1.8213
T₃	0.1197	0.0875	3.7632	4.1550
T₄	3.3441	1.0345	2.0083	0.9359

Table 7.2: System eigenvalues of nominal loading conditions with J_1 settings, single-point tuning, individual design

No Control	PSS	SVC	TCSC	TCPS
0.5255±6.5919i, -0.0795	-4.7500± 7.3000i, 0.5500	-4.5975± 5.9522i, 0.6113	-3.4807± 4.1879i, 0.6392	-3.3969± 4.1402i, 0.6343
-10.6940± 5.6612i	-4.9000± 7.5300i	-4.8355± 6.2292i	-9.7437± 11.7263i	-9.7506± 11.8841i
--	-101.02	-20.2238	-13.4470	-1.5399
--	-0.2000	-2.5378	-1.5444	-0.5295
--	-0.3100	-0.7065	-0.4858	-0.2001
--	--	-0.2000	-0.2001	-13.5901

Table 7.3: System eigenvalues of light loading conditions with J_1 settings, single-point tuning, individual design

No Control	PSS	SVC	TCSC	TCPS
0.0382±0.3601i, -0.0060	-1.0300± 6.5700i, 0.1500	-0.6619± 6.2863i, 0.1047	-1.3244± 6.3945i, 0.2028	-8.7181± 9.6344i, 0.6710
-10.2067± 6.3849i	-8.9600± 7.0800i	-9.3694± 6.5559i	-10.2132± 6.4495i	-9.4944± 5.6204i
--	-100.35	-0.2000	-17.1467	-2.5020±
--	-0.2000	-20.0807	-1.2112	0.3295i
--	-0.3000	-1.3892	-0.4930	-0.5254
--	--	-0.8013	-0.2000	-0.2001

Table 7.4: System eigenvalues of heavy loading conditions with J_1 settings, single-point tuning, individual design

No Control	PSS	SVC	TCSC	TCPS
0.6384±6.0839i, -0.1044	-2.7900± 6.3500i, 0.4000	-2.7481± 7.2347i, 0.3551	-1.8058± 1.2019i, 0.8325	-3.5888± 2.2034i, 0.8522
-10.8069± 5.9347i	-6.9000± 8.0900i	-7.6108± 6.1032i	-10.375± 10.781i, 0.6934	-10.059± 12.931i
--	-100.95	-0.9368±	-8.5424±	-11.8832
--	-0.2000	0.3596i	7.0258i	-2.2530
--	-0.3100	-0.2000	-0.4793	-0.5235
--	--	-19.7426	-0.2001	-0.2001

Table 7.5: System eigenvalues of leading Pf loading conditions with J_1 settings, single-point tuning, individual design

No Control	PSS	SVC	TCSC	TCPS
$0.2182 \pm 6.6656i$,	$-4.1400 \pm$	$-1.9464 \pm$	$-1.8884 \pm$	$-3.7864 \pm$
-0.0327	$7.6000i, 0.4800$	$4.5953i, 0.3900$	$5.4270i, 0.3286$	$4.6012i, 0.6354$
$-10.387 \pm$	$-5.5800 \pm$	$-6.4420 \pm$	$-9.5683 \pm$	$-9.3666 \pm$
$5.6970i$	$6.9900i$	$6.9343i$	$10.213i$	$10.299i$
--	-100.89	-20.5568	-17.2876	-13.6501
--	-0.2000	-4.3818	-1.2334	-1.4671
--	-0.3100	-0.6187	-0.4918	-0.5313
--	--	-0.2000	-0.2000	-0.2001

Damping Torque Coefficient Analysis: To quantitatively measure the effectiveness of the proposed PSS, SVC-, TCSC-, and TCPS-based stabilizers in enhancing the system damping characteristics, the damping torque coefficient K_d is calculated. The damping torque coefficient K_d is estimated for each stabilizer over a wide range of loading conditions. Specifically, K_d is calculated for a range of 45 operating points specified by $P_e = [0.05 - 1.45]$ pu in steps of 0.10 pu and $Q_e = [-0.40, 0.00, 0.40]$ pu.

For comparison purposes, K_d for all stabilizers at $Q = -0.4$, $Q = 0.0$, and $Q = 0.4$ pu are shown in Figures 7.4, 7.5, and 7.6, respectively. From these figures, it can be observed that:

- At light and moderate loading, the TCPS-based stabilizer outperforms the other stabilizers while at high loading the TCSC-based stabilizer is the dominant.
- The PSS, SVC, and TCSC suffer from low damping characteristics at light loading.
- Generally, the SVC-based controller is the least effective in damping system oscillations.
- The damping torque coefficient of the TCSC-based stabilizer increases almost linearly with loading level.

- For low and moderate loading, K_d of the TCPS-based stabilizer is almost constant. However, it starts decreasing at very high loading.
- The TCSC and TCPS are more effective at lagging power factor conditions, whereas the PSS is more effective at leading power factor conditions. However, The SVC performance is almost unaffected by power factor characteristics.

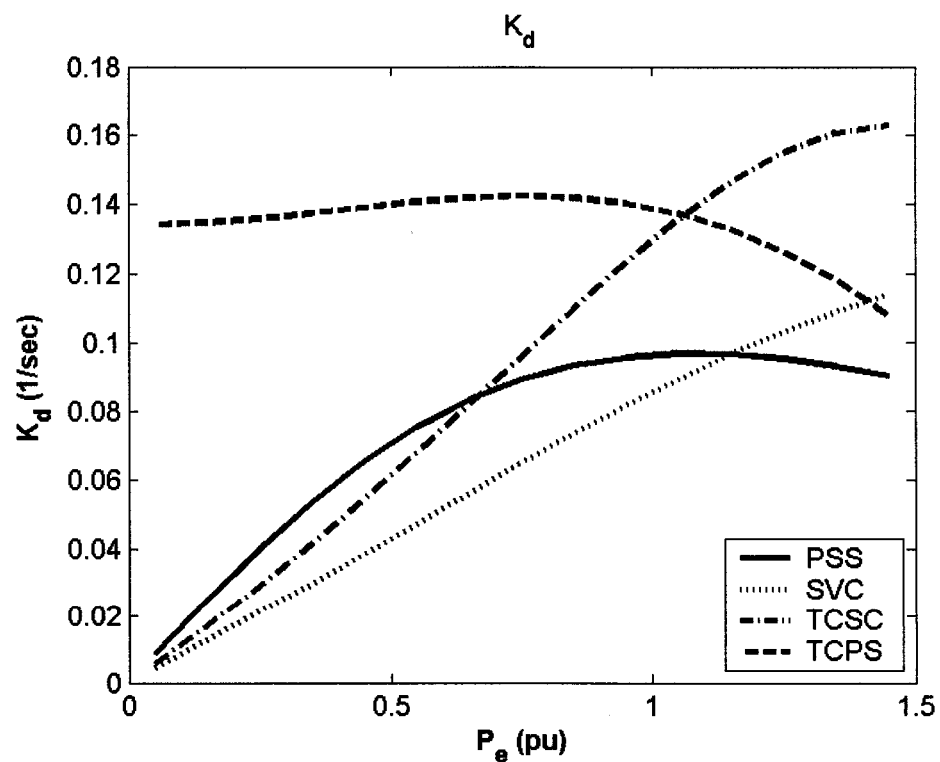


Figure 7.4: Damping torque coefficient with the proposed controllers at $Q = -0.4$ pu, J_1 settings, single-point tuning, individual design

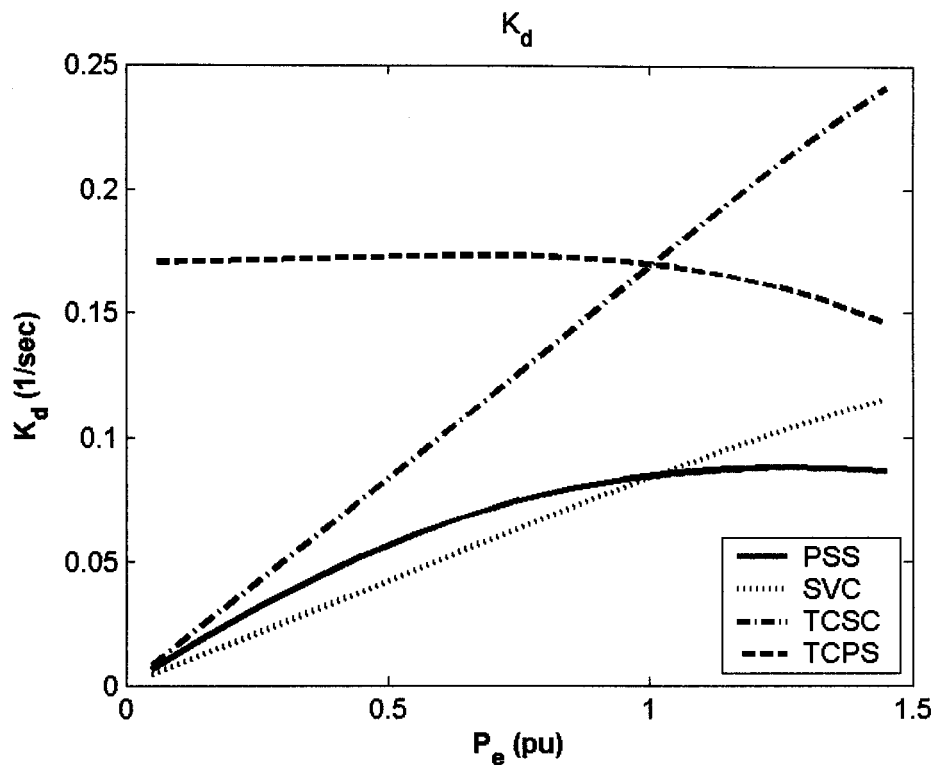


Figure 7.5: Damping torque coefficient with the proposed controllers at $Q = 0.0$ pu, J_1 settings, single-point tuning, individual design

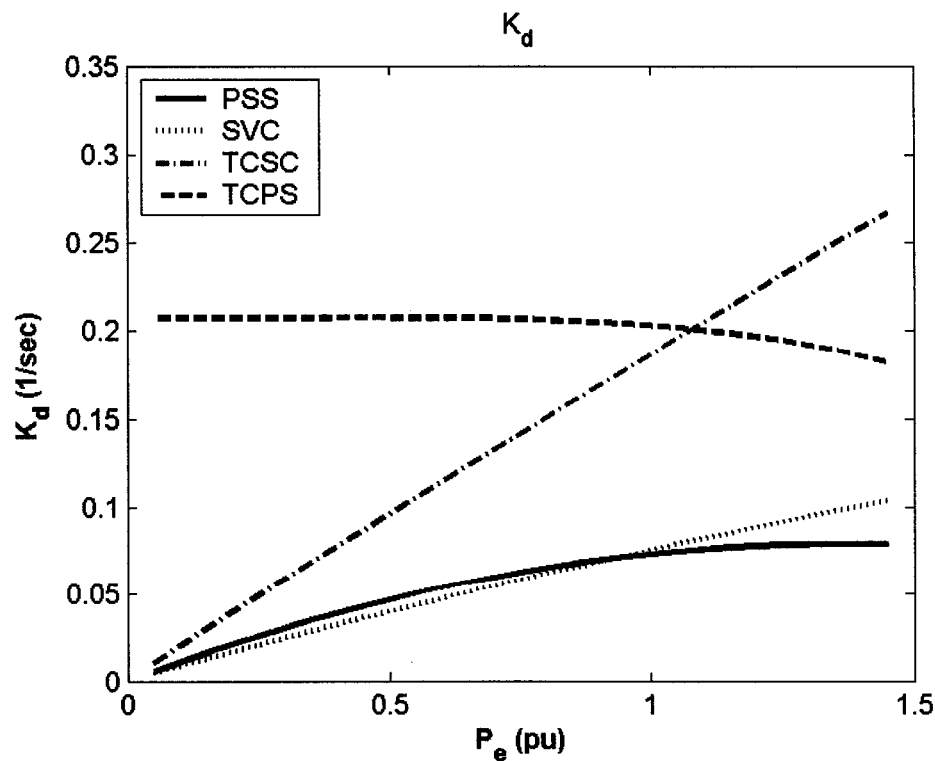


Figure 7.6: Damping torque coefficient with the proposed controllers at $Q = 0.4$ pu, J_1 settings, single-point tuning, individual design

Nonlinear Time-Domain Simulations: Figures 7.7, 7.8, 7.9, and 7.10 show the rotor angle, speed deviation, electrical power, and machine terminal voltage responses, respectively, for a 6-cycle three-phase fault at the nominal loading conditions. It can be readily seen that the TCSC and TCPS performs better than PSS in terms of reduction of overshoot and settling time. This is consistent with the damping torque coefficient analysis results. On the other hand, the damping effort provided by the SVC is not sufficient to keep the system stable. Figures 7.11, 7.12, 7.13, and 7.14 show the control effort provided by the stabilizing signal of PSS, U_{PSS} , the susceptance of SVC, B_{SVC} , the reactance of TCSC, X_{TCSC} , and the angle of TCPS, Φ_{TCPS} , respectively.

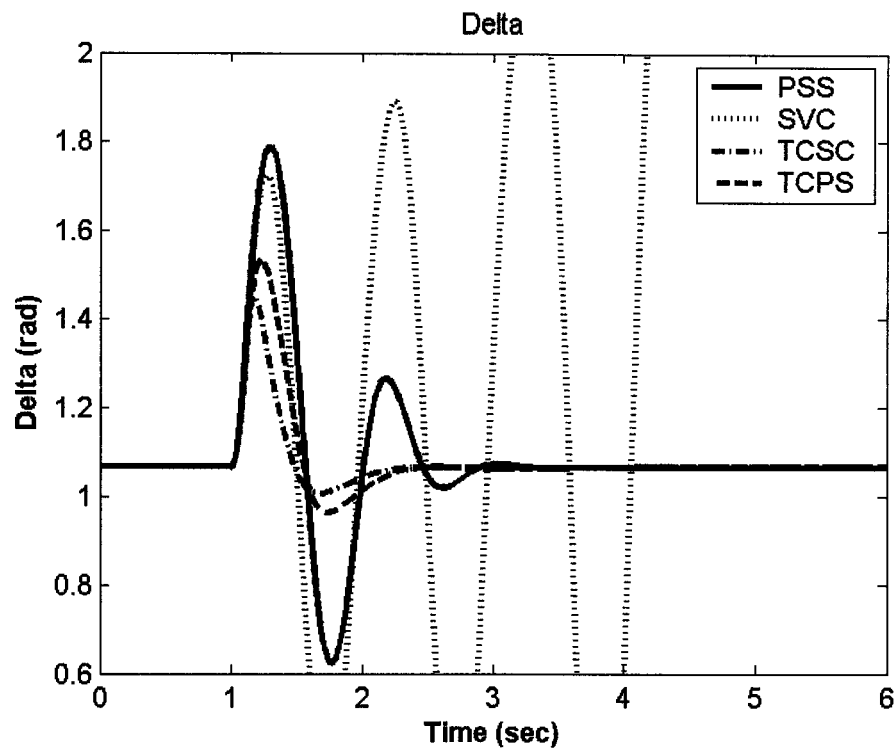


Figure 7.7: Rotor angle response for 6-cycle fault with nominal loading, J_1 settings, single-point tuning, individual design

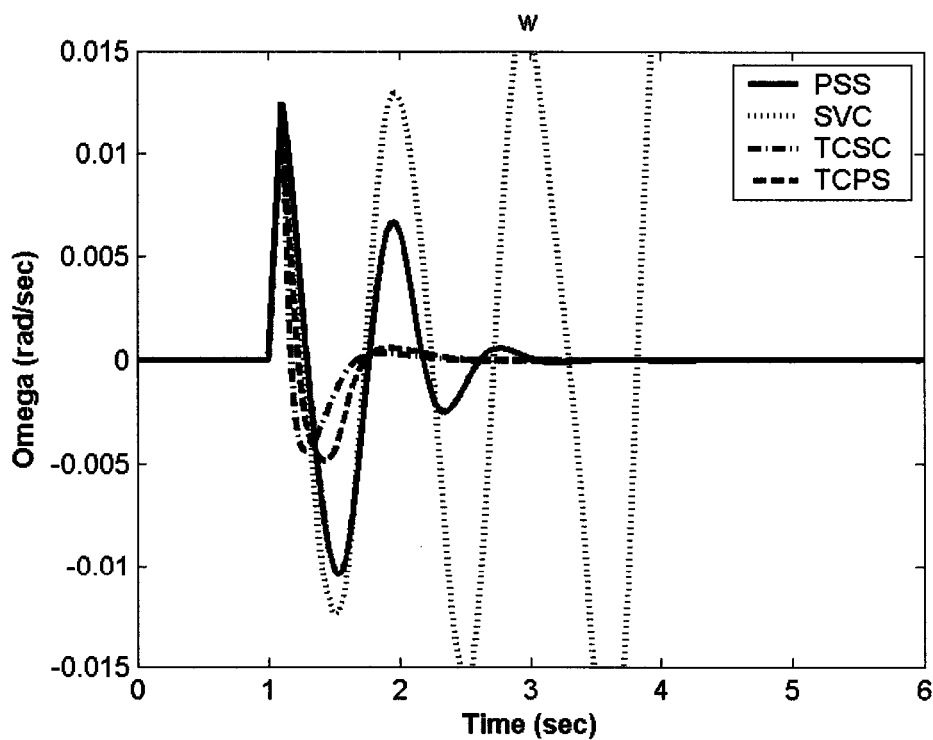


Figure 7.8: Speed response for 6-cycle fault with nominal loading, J_1 settings, single-point tuning, individual design

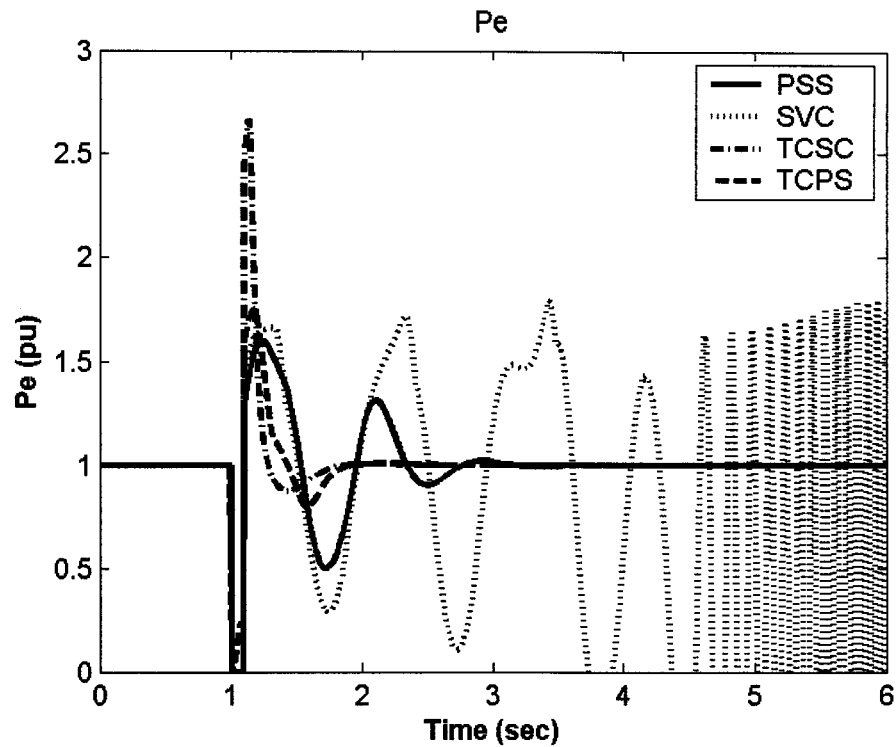


Figure 7.9: Electrical power response for 6-cycle fault with nominal loading, J_1 settings, single-point tuning, individual design

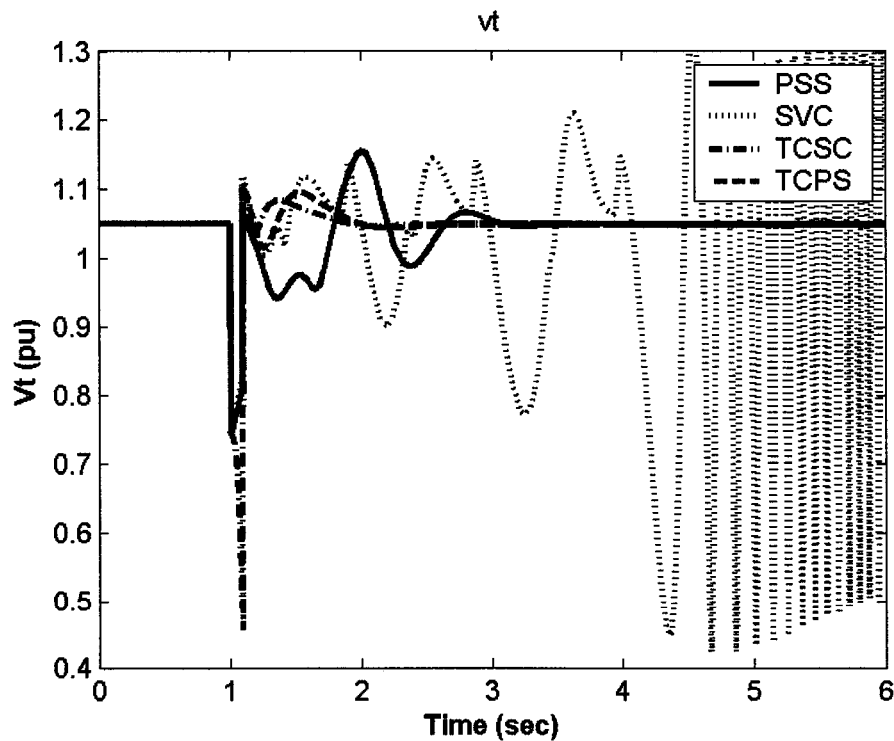


Figure 7.10: Terminal voltage response for 6-cycle fault with nominal loading, J_1 settings, single-point tuning, individual design

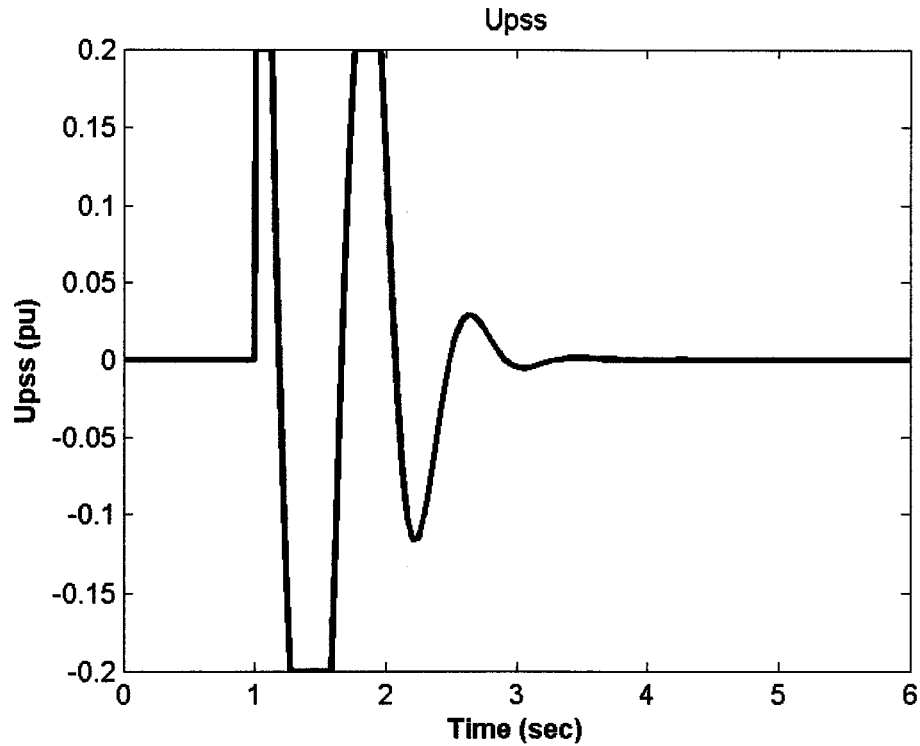


Figure 7.11: PSS stabilizing signal for 6-cycle fault with nominal loading, J_1 settings, single-point tuning, individual design

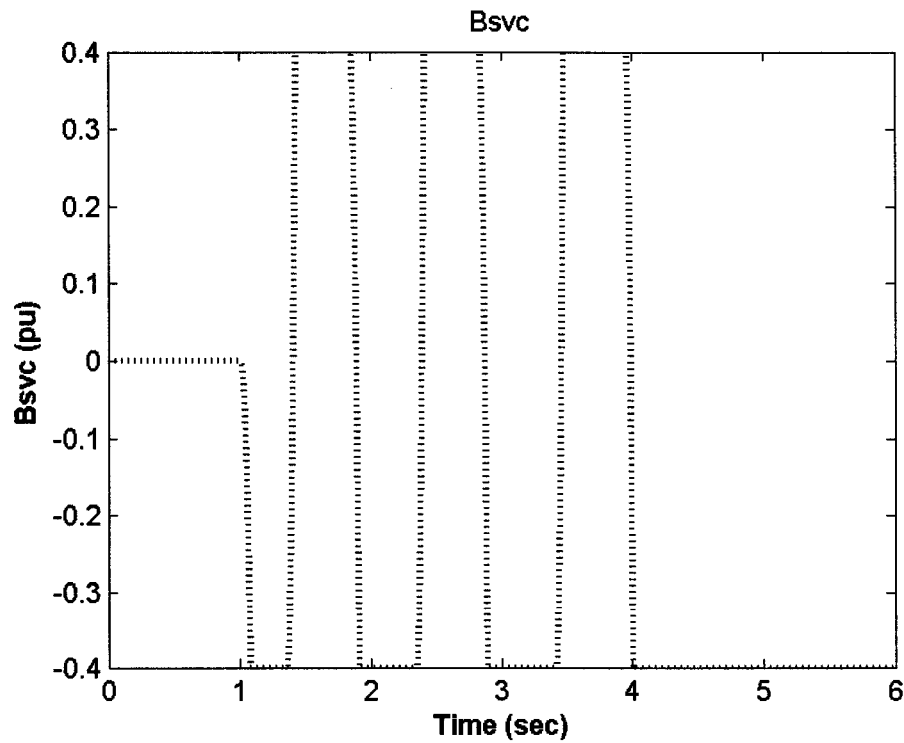


Figure 7.12: B_{svc} response for 6-cycle fault with nominal loading, J_1 settings, single-point tuning, individual design

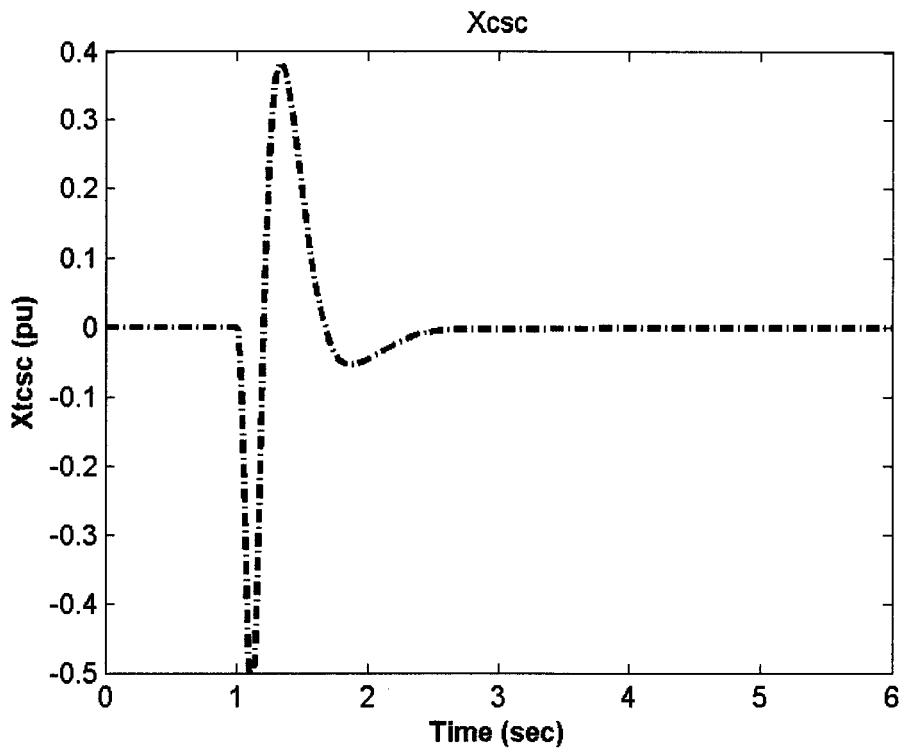


Figure 7.13: X_{tcsc} response 6-cycle fault with nominal loading, J_1 settings, single-point tuning, individual design

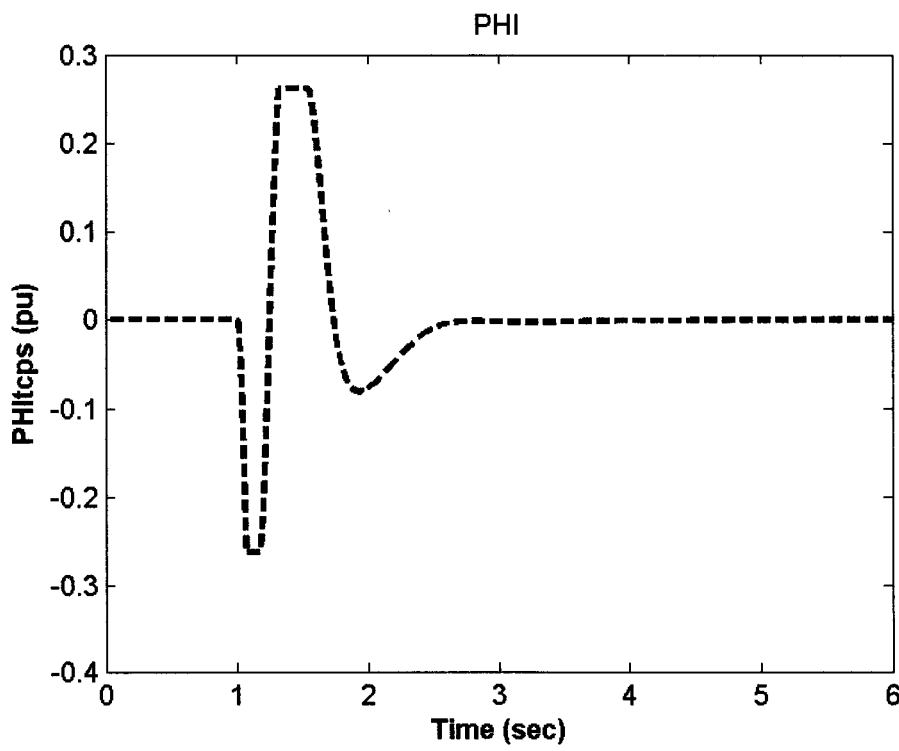


Figure 7.14: Φ_{tcps} response 6-cycle fault with nominal loading, J_1 settings, single-point tuning, individual design

7.2.1.2 Individual Design with J_2

The PSS, SVC-, TCSC-, and TCPS-based controllers are designed individually considering the nominal loading condition.

Stabilizer Design: PSO is used to search for the optimum parameter settings of each controller that minimizes the maximum damping factor of all the system complex eigenvalues. The final settings of the optimized parameters for the proposed stabilizers are given in Table 7.6.

Eigenvalue Analysis: The system eigenvalues without and with the proposed stabilizers at the four loading conditions, nominal, light, heavy, and leading Pf, are given in Tables 7.7-7.10, respectively. The bold rows of these tables represent the EM mode eigenvalues and its damping ratio. It is clear that the proposed stabilizers greatly enhance the system stability. It is also clear that the PSS, SVC and TCSC have relatively poor capabilities to enhance the EM mode damping when the system operates at light loading.

Table 7.6: Optimal parameter settings with J_2 , single-point tuning, individual design

	PSS	SVC	TCSC	TCPS
K	28.0087	300.00	41.0339	50.1000
T₁	0.1204	5.0000	5.0000	5.0000
T₂	2.4795	1.0539	2.1675	2.4879
T₃	2.5447	0.0874	5.0000	5.0000
T₄	0.0100	0.9528	2.2661	2.3756

Table 7.7: System eigenvalues of nominal loading conditions with J_2 settings, single-point tuning, individual design

No Control	PSS	SVC	TCSC	TCPS
0.5255±6.5919i, -0.0795	-4.8800± 7.3600i, 0.5500	-4.7139± 6.0035i, 0.6176	-9.7221± 20.206i, 0.4336	-1.1318± 0.0071i, 1.0000
-10.6940±	-4.7700±	-4.7174±	-0.2000	-9.7406±
5.6612i	7.5100i	6.1699i	-9.4648	21.607i
--	-101.03	-20.223	-9.4285	-9.5423±
--	-0.4000	-2.5441	-1.2783	0.0157i
--	-0.2000	-0.7052	-1.2646	-0.3307
--	--	-0.2000	-0.3594	-0.2000

Table 7.8: System eigenvalues of light loading conditions with J_2 settings, single-point tuning, individual design

No Control	PSS	SVC	TCSC	TCPS
0.0382±0.3601i, -0.0060	-1.0294± 6.5799i, 0.1500	-0.6616± 6.2866i, 0.1047	-4.2239± 6.5313i, 0.5430	-0.8131± 0.4975i, 0.8530
-10.2067±	-8.9600±	-9.3697±	-10.0776±	-9.4945±
6.3849i	7.0800i	6.5542i	6.6947i	19.832i
--	-100.35	-20.080	-11.6512	-10.110±
--	-0.4000	-1.3933	-0.5998	6.0672i
--	-0.2000	-0.7989	-0.3858	-0.3249
--	-20.000	-0.2000	-0.2000	-0.2000

Table 7.9: System eigenvalues of heavy loading conditions with J_2 settings, single-point tuning, individual design

No Control	PSS	SVC	TCSC	TCPS
0.6384±6.0839i, -0.1044	-2.7903± 6.3723i, 0.4000	-2.7446± 7.2369i, 0.3546	-0.6743± 0.6639i, 0.7126	-0.7594± 0.5634i, 0.8031
-10.8069±	-6.9000±	-7.6138±	-9.9286±	-9.9255±
5.9347i	8.1100i	6.0957i	21.193i	23.301i
--	-100.95	-0.9377±	-9.8449±	-9.7340±
--	-0.4000	0.3573i	6.3499i	3.0765i
--	-0.2000	-0.2000	-0.3441	-0.3220
--	--	-19.7432	-0.2000	-0.2000

Table 7.10: System eigenvalues of leading Pf loading conditions with J_2 settings, single-point tuning, individual design

No Control	PSS	SVC	TCSC	TCPS
$0.2182 \pm 6.6656i$,	$-4.1296 \pm$	$-1.9478 \pm$	$-2.7433 \pm$	$-9.5097 \pm$
-0.0327	$7.6332i, 0.4800$	$4.5965i, 0.3902$	$3.3690i, 0.6314$	$19.368i, 0.4407$
$-10.387 \pm$	$-5.5900 \pm$	$-6.4373 \pm$	$-9.4010 \pm$	$-9.6428 \pm$
$5.6970i$	$7.0000i$	$6.9273i$	$16.2358i$	$2.2443i$
--	-1.9000	-20.5555	-15.9395	-1.7100
--	-0.4000	-4.3917	-0.6316	-0.8111
--	-0.2000	-0.6179	-0.3800	-0.3337
--	--	-0.2000	-0.2000	-0.2000

Damping Torque Coefficient Analysis: To quantitatively measure the effectiveness of the proposed PSS, SVC-, TCSC-, and TCPS-based stabilizers in improving the system damping characteristics, the damping torque coefficient K_d is estimated. The damping torque coefficient is calculated for each stabilizer over a wide range of loading conditions. Specifically, K_d is calculated for a range of 45 operating points specified by $P_e = [0.05 - 1.45]$ pu in steps of 0.10 pu and $Q_e = [-0.40, 0.00, 0.40]$ pu.

For comparison purposes, damping torque coefficient for all stabilizers at $Q = -0.4$, $Q = 0.0$, and $Q = 0.4$ pu are shown in Figures 7.15, 7.16, and 7.17, respectively. From these figures, the following conclusions can be drawn:

- In general, the TCPS-based stabilizer outperforms the other stabilizers. An exception appears with the heavy loading at unity power factor, where the TCSC-based stabilizer becomes more effective.
- The PSS, SVC, and TCSC suffer from low damping characteristics at light loading.

- Generally, the SVC-based controller is the least effective in damping system oscillations.
- The damping torque coefficients K_d associated with the PSS, SVC-, and TCSC-based stabilizers increase almost linearly with loading level. However, the damping torque coefficient of the TCPS-based stabilizer improves only slightly as loading level increases.
- The TCSC and TCPS are less effective at leading power factor conditions, whereas the PSS is more effective at leading power factor conditions. However, The SVC performance is almost unaffected by power factor characteristics.

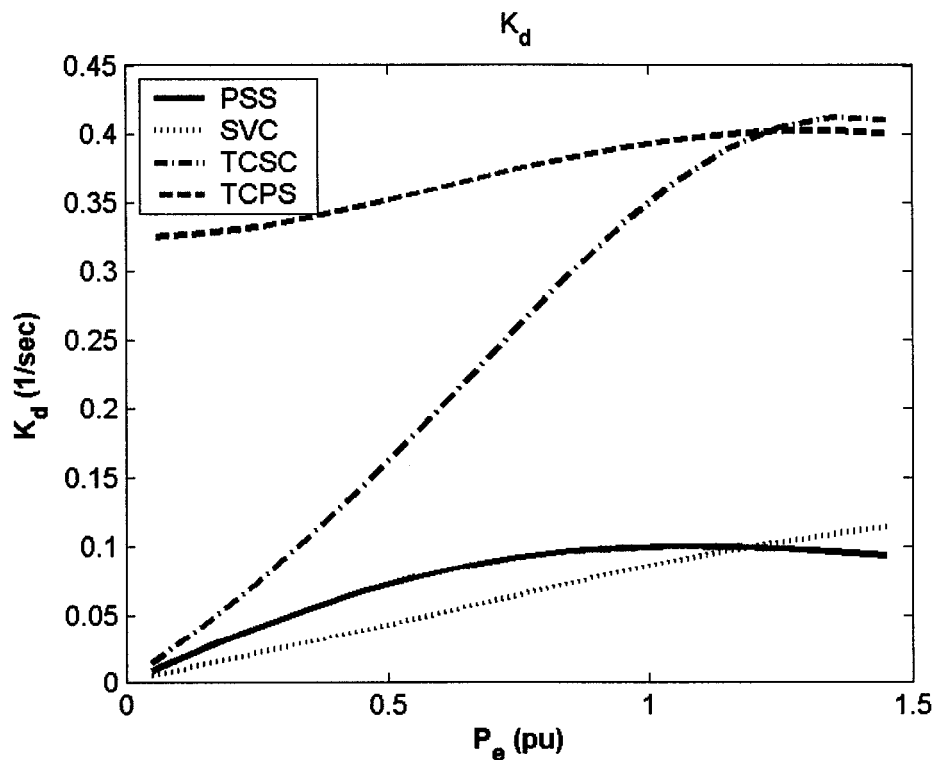


Figure 7.15: Damping torque coefficient with the proposed controllers at $Q = -0.4$ pu, J_2 settings, single-point tuning, individual design

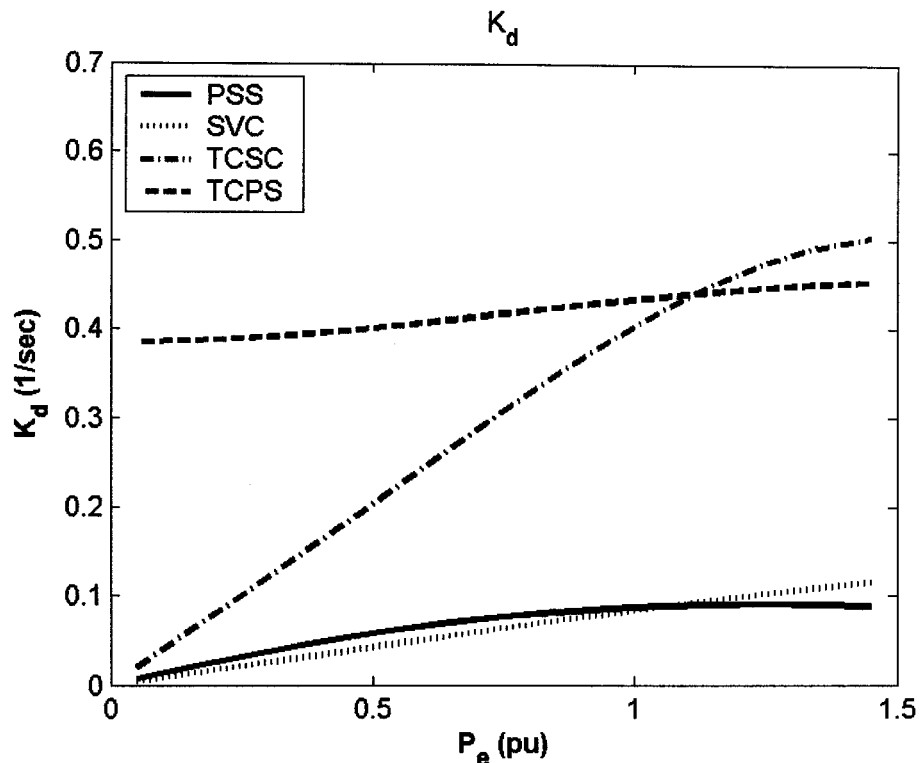


Figure 7.16: Damping torque coefficient with the proposed controllers at $Q = 0.0$ pu, J_2 settings, single-point tuning, individual design

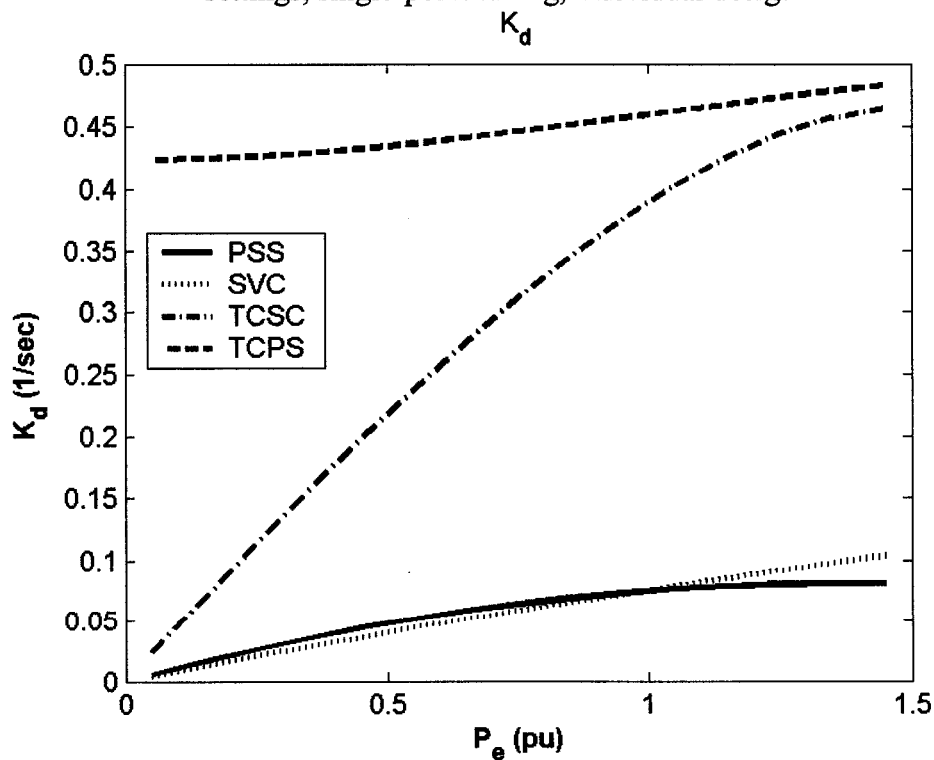


Figure 7.17: Damping torque coefficient with the proposed controllers at $Q = 0.4$ pu, J_2 settings, single-point tuning, individual design

Nonlinear Time-Domain Simulations: Figures 7.18-7.21 show the rotor angle, speed deviation, electrical power, and machine terminal voltage responses, respectively, for a 6-cycle three-phase fault at the nominal loading conditions. Clearly, the TCSC and TCPS outperform the PSS and SVC in terms of reduction of overshoot and settling time. This is consistent with the damping torque coefficient analysis results. However, the damping effort provided by the SVC is not sufficient to keep the system stable. Figures 7.22-7.25 show the control effort provided by the stabilizing signal of PSS, U_{PSS} , the susceptance of SVC, B_{SVC} , the reactance of TCSC, X_{TCSC} , and the angle of TCPS, Φ_{TCPS} , respectively.

An important point to mention in here is that the system responses associated with the stabilizers designed based on optimizing J_2 are generally slower than those associated with the stabilizers designed based on optimizing J_1 . The point behind this is that minimizing the damping factor does not guarantee improving the settling time of system response. However, maximizing the damping ratio guarantees improving the settling time.

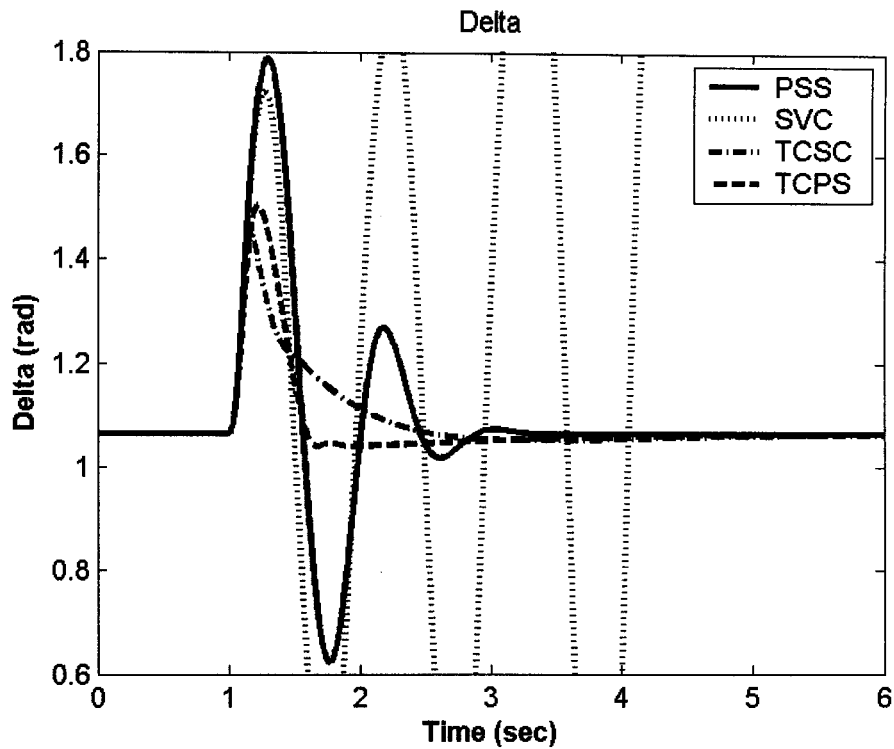


Figure 7.18: Rotor angle response for 6-cycle fault with nominal loading, J_2 settings, single-point tuning, individual design

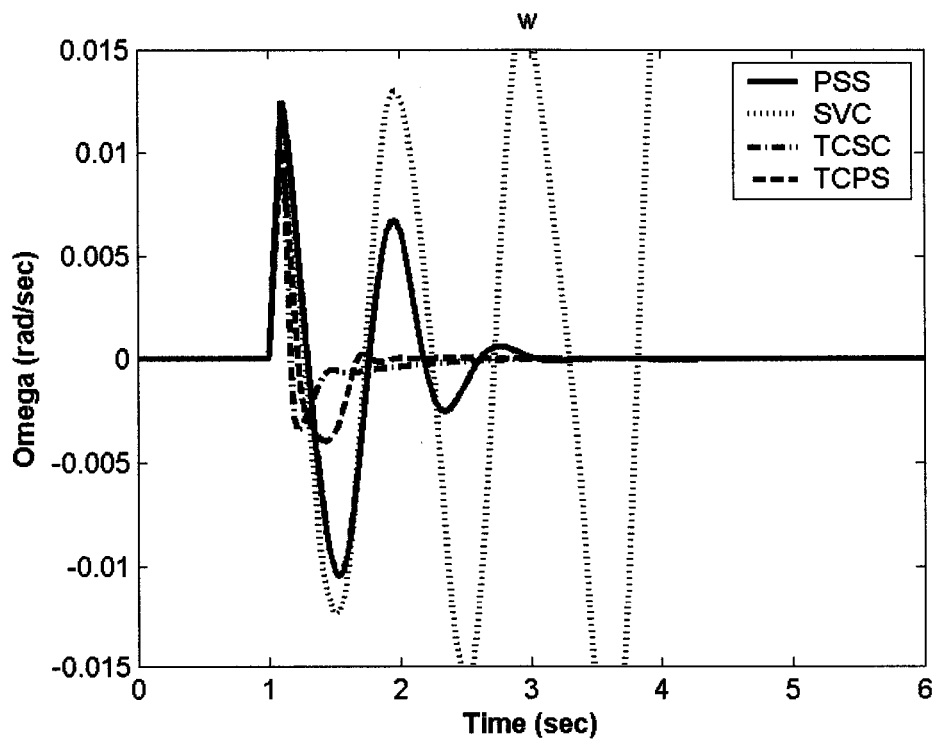


Figure 7.19: Speed response for 6-cycle fault with nominal loading, J_2 settings, single-point tuning, individual design

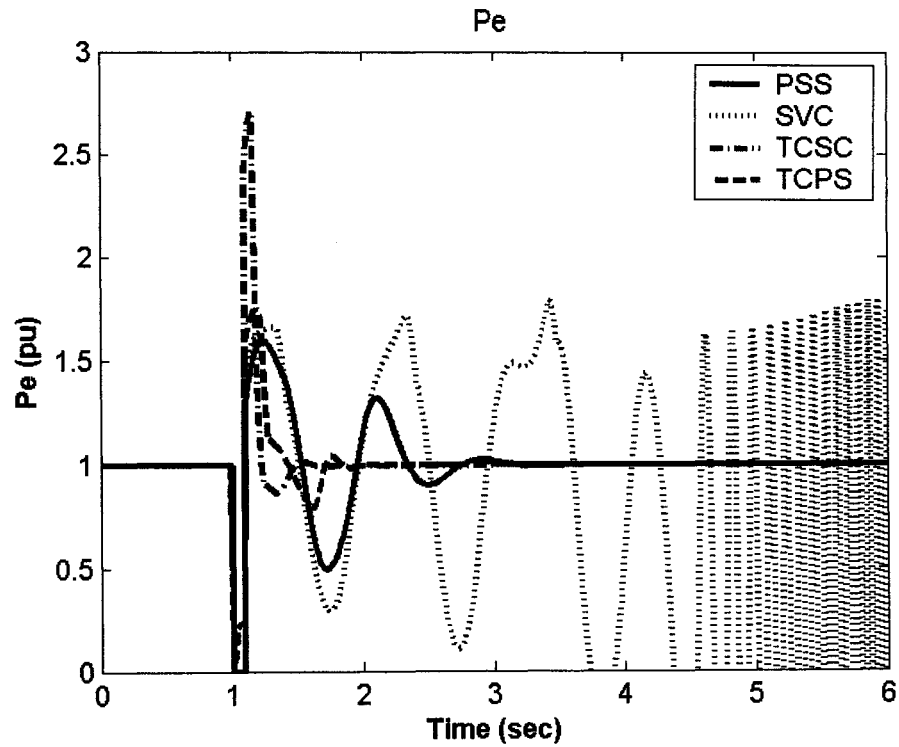


Figure 7.20: Electrical power response for 6-cycle fault with nominal loading, J_2 settings, single-point tuning, individual design

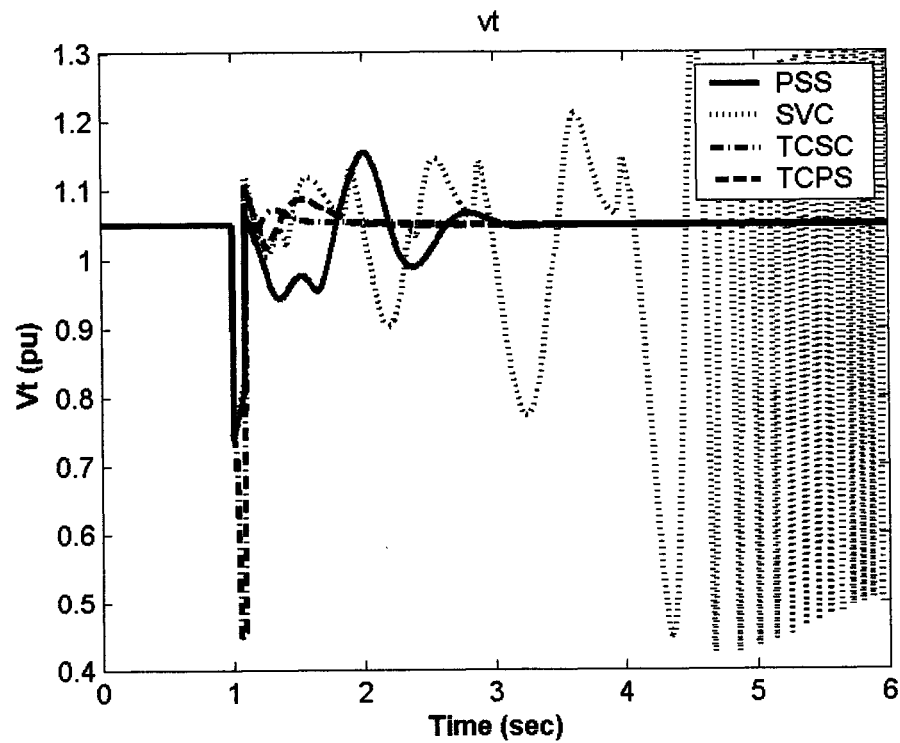


Figure 7.21: Terminal voltage response for 6-cycle fault with nominal loading, J_2 settings, single-point tuning, individual design

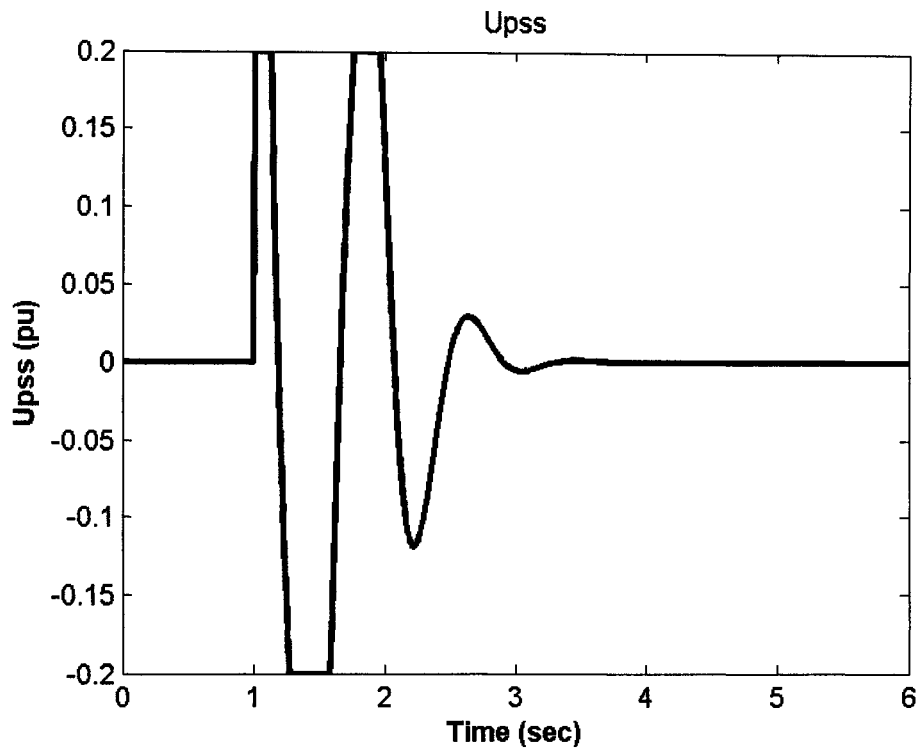


Figure 7.22: PSS stabilizing signal for 6-cycle fault with nominal loading, J_2 settings, single-point tuning, individual design

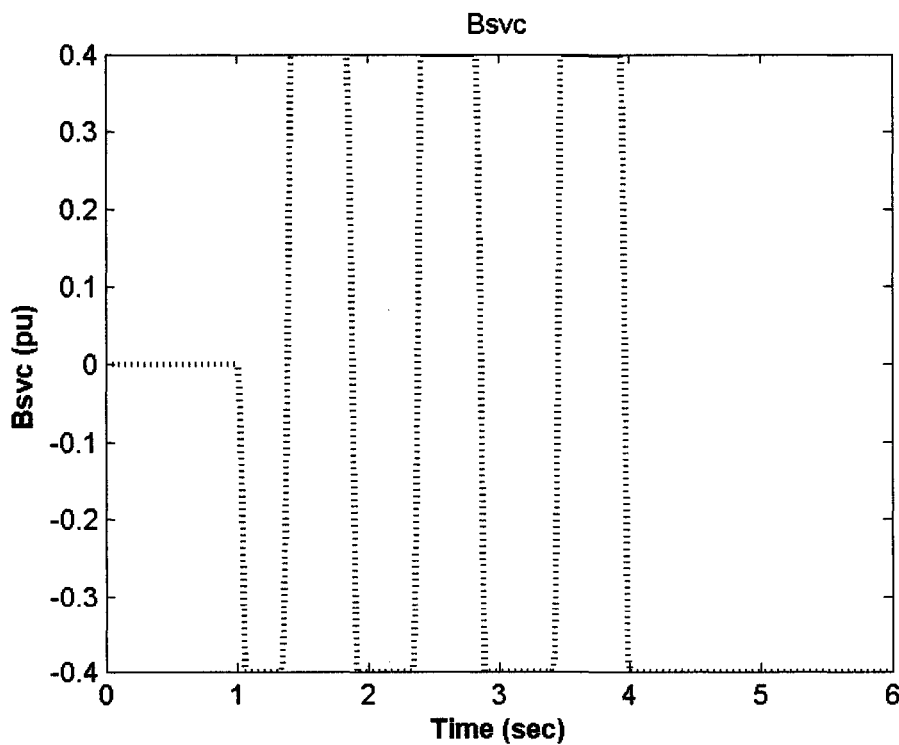


Figure 7.23: B_{svc} response for 6-cycle fault with nominal loading, J_2 settings, single-point tuning, individual design

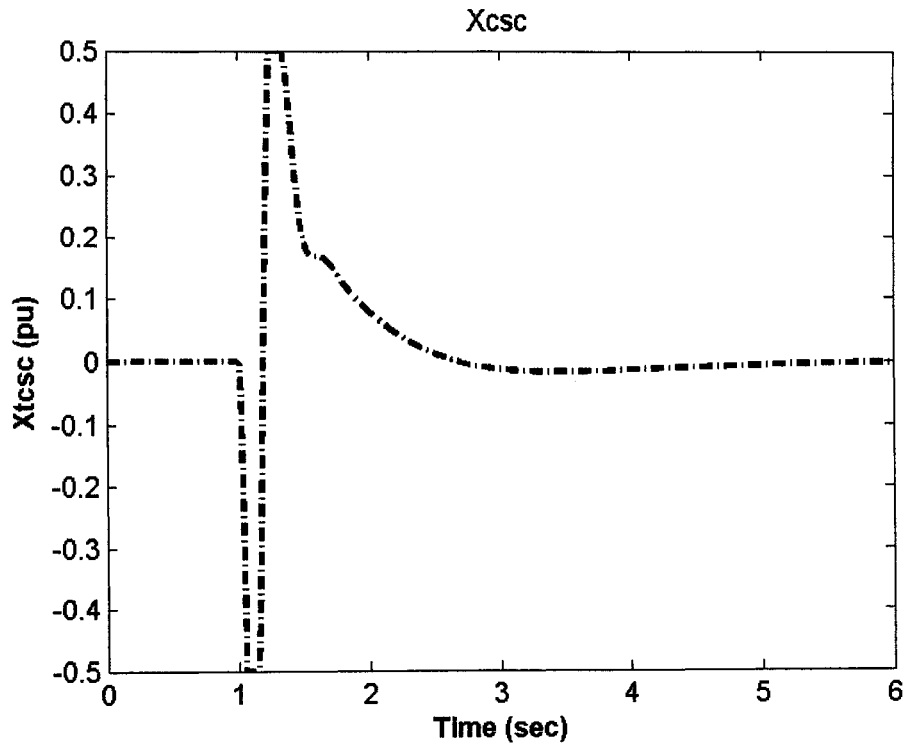


Figure 7.24: X_{tcsc} response 6-cycle fault with nominal loading, J_2 settings, single-point tuning, individual design

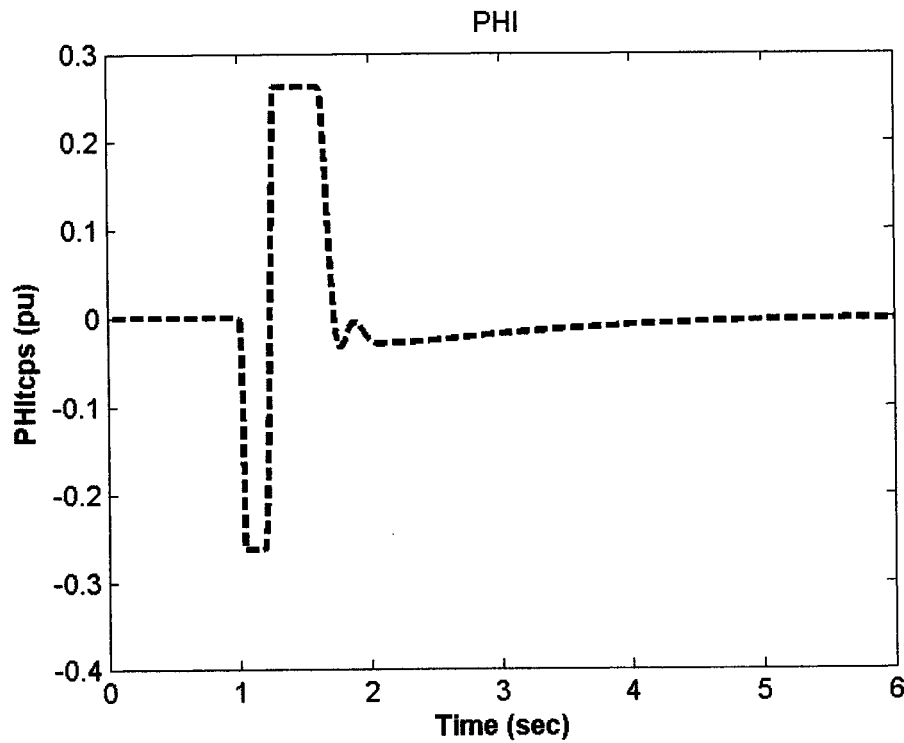


Figure 7.25: Φ_{tcps} response 6-cycle fault with nominal loading, J_2 settings, single-point tuning, individual design

7.2.1.3 Coordinated Design with J_2

The controllability measure analysis based on the singular value decomposition and the damping torque coefficient analyses indicate that the PSS and SVC-based stabilizer do not perform well individually. These two stabilizers have poor capabilities in controlling the EM mode, especially at low loading conditions. The same conclusion can be drawn from nonlinear time-domain simulations illustrated previously. In this section, a coordinated design of PSS and SVC-based stabilizer is considered at the nominal loading condition with J_2 .

Stabilizer Design: PSO is used to simultaneously search for the optimum parameter settings of both controllers that minimize the maximum damping factor of all the system complex eigenvalues at nominal loading condition. The final settings of the optimized parameters for the proposed stabilizers are given in Table 7.11.

Eigenvalue Analysis: The system eigenvalues without and with the proposed PSS and SVC-based controllers when applied individually and through coordinated design at the four loading conditions, nominal, light, heavy, and leading Pf, are given in Tables 7.12-7.15, respectively. The bold rows of these tables represent the EM mode eigenvalue and its damping ratio. It is evident that, using the proposed coordinated stabilizers design, the damping factor of the EM mode eigenvalue is greatly shifted to the left of the s-plane. Hence, it can be concluded that this well enhances the system stability.

Table 7.11: Optimal parameter settings with J_2 , single-point tuning, coordinated design

	Individual		Coordinated	
	PSS	SVC	PSS	SVC
K	28.0087	300.00	58.843	251.77
T₁	0.1204	5.0000	2.7219	4.5530
T₂	2.4795	1.0539	2.6619	1.9899
T₃	2.5447	0.0874	4.9355	5.0000
T₄	0.0100	0.9528	1.5738	1.4737

Table 7.12: System eigenvalues of nominal loading conditions with J_2 settings, single-point tuning, coordinated design

No Control	PSS	SVC	PSS & SVC
0.5255±6.5919i,	-4.8800±	-4.7139±	-7.6143±
-0.0795	7.3600i, 0.5500	6.0035i, 0.6176	31.224i, 0.2369
-10.6940±	-4.7700±	-4.7174±	-21.3625
5.6612i	7.5100i	6.1699i	-1.5361
--	-101.03	-20.223	-1.4023
--	-0.4000	-2.5441	-1.0797
--	-0.2000	-0.7052	-1.0065
--	--	-0.2000	-0.5401
--	--	--	-0.3733
--	--	--	-0.2002
--	--	--	-0.2000

Table 7.13: System eigenvalues of light loading conditions with J_2 settings, single-point tuning, coordinated design

No Control	PSS	SVC	PSS & SVC
0.0382±0.3601i,	-1.0294±	-0.6616±	-2.5985±
-0.0060	6.5799i, 0.1500	6.2866i, 0.1047	2.8011i, 0.6801
-10.2067±	-8.9600±	-9.3697±	-6.9145±16.680i
6.3849i	7.0800i	6.5542i	-0.6903± 0.0775i
--	-100.35	-20.080	-21.2253
--	-0.4000	-1.3933	-0.2001
--	-0.2000	-0.7989	-0.5226
--	--	-0.2000	-0.3746
--	--	--	-0.2000

Table 7.14: System eigenvalues of heavy loading conditions with J_2 settings, single-point tuning, coordinated design

No Control	PSS	SVC	PSS & SVC
0.6384±6.0839i,	-2.7903±	-2.7446±	-0.4313±
-0.1044	6.3723i, 0.4000	7.2369i, 0.3546	0.6933i, 0.5282
-10.8069±	-6.9000±	-7.6138±	-8.1291± 33.440i
5.9347i	8.1100i	6.0957i	-18.4242
--	-100.95	-0.9377±	-5.4793
--	-0.4000	0.3573i	-0.6601
--	-0.2000	-0.2000	-0.2002
--	--	-19.7432	-0.4716
--	--	--	-0.3728
--	--	--	-0.2000

Table 7.15: System eigenvalues of leading Pf loading conditions with J_2 settings, single-point tuning, coordinated design

No Control	PSS	SVC	PSS & SVC
0.2182±6.6656i,	-4.1296±	-1.9478±	-1.2732±
-0.0327	7.6332i, 0.4800	4.5965i, 0.3902	2.5337i, 0.4490
-10.387±	-5.5900±	-6.4373±	-0.5448± 0.2156i
5.6970i	7.0000i	6.9273i	-6.8033± 25.045i
--	-1.9000	-20.5555	-24.3116
--	-0.4000	-4.3917	-0.6012
--	-0.2000	-0.6179	-0.3737
--	--	-0.2000	-0.2002
--	--	--	-0.2000

Damping Torque Coefficient Analysis: To quantitatively measure the effectiveness of the proposed PSS-SVC coordinated design in improving the system damping characteristics and compare it with both individual designs, the damping torque coefficient K_d is estimated. K_d is calculated for a range of 45 operating points specified by $P_e=[0.05 - 1.45]$ pu in steps of 0.10 pu and $Q_e=[-0.40, 0.00, 0.40]$ pu.

For comparison purposes, the damping torque coefficient for the coordinated PSS-SVC stabilizer design and both individual designs at $Q=-0.4$, $Q=0.0$, and $Q=0.4$ pu are shown in Figures 7.26-7.28, respectively. These figures demonstrate the highly effective coordinated design, as compared with PSS and SVC individual designs, over the different loading conditions.

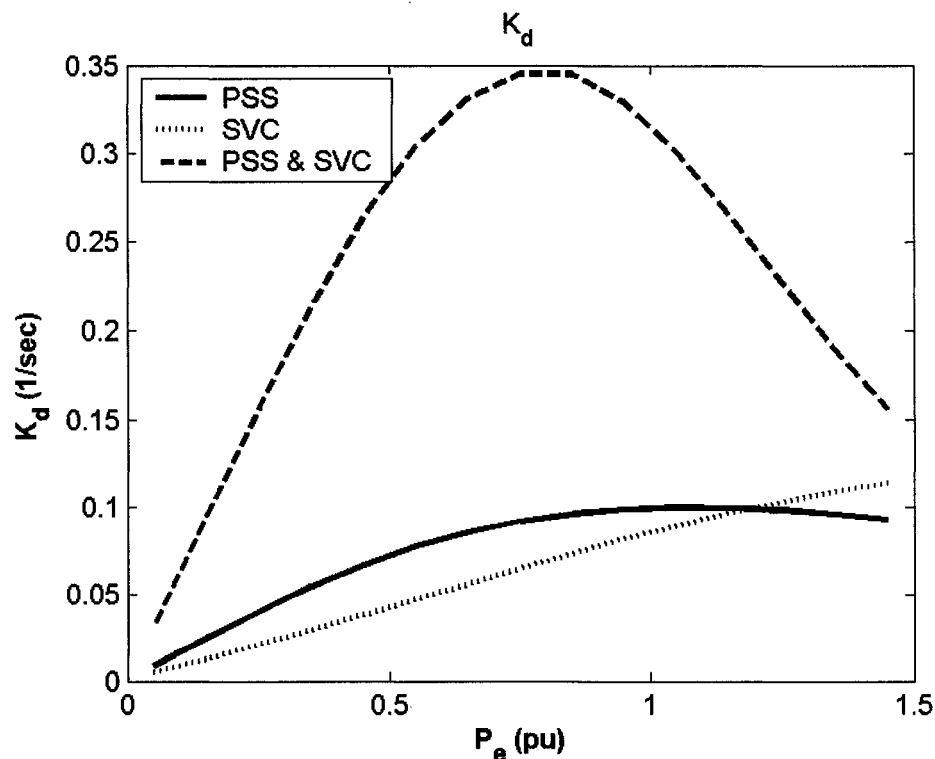


Figure 7.26: Damping torque coefficient with coordinated PSS & SVC-based stabilizer at $Q = -0.4$ pu, J_2 settings, single-point tuning

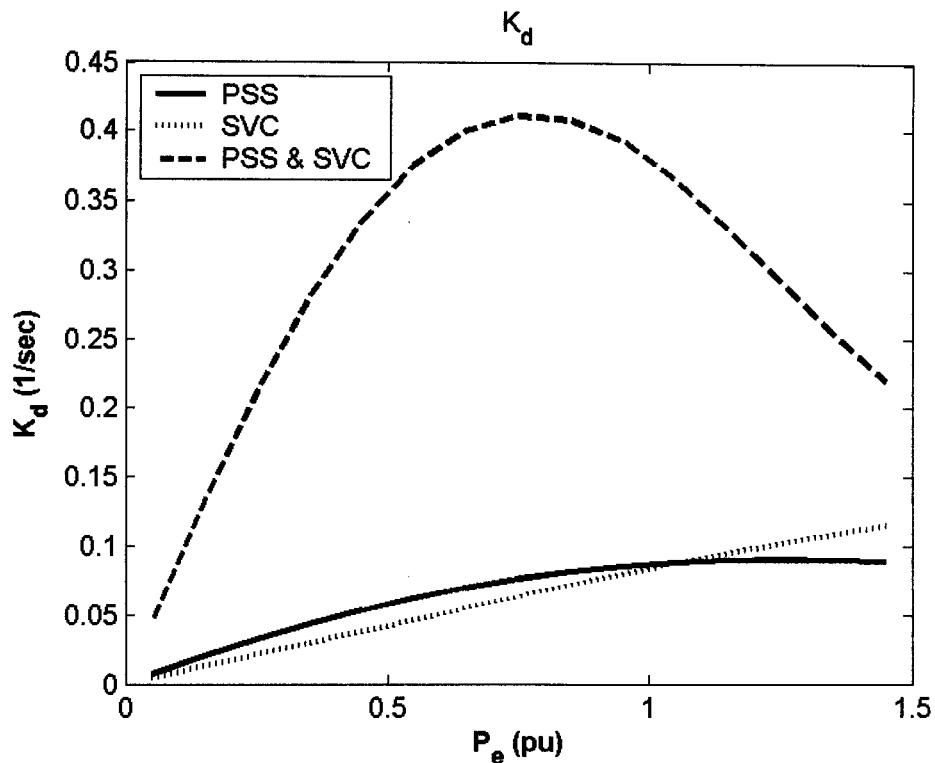


Figure 7.27: Damping torque coefficient with coordinated PSS & SVC-based stabilizer at $Q = 0.0$ pu, J_2 settings, single-point tuning

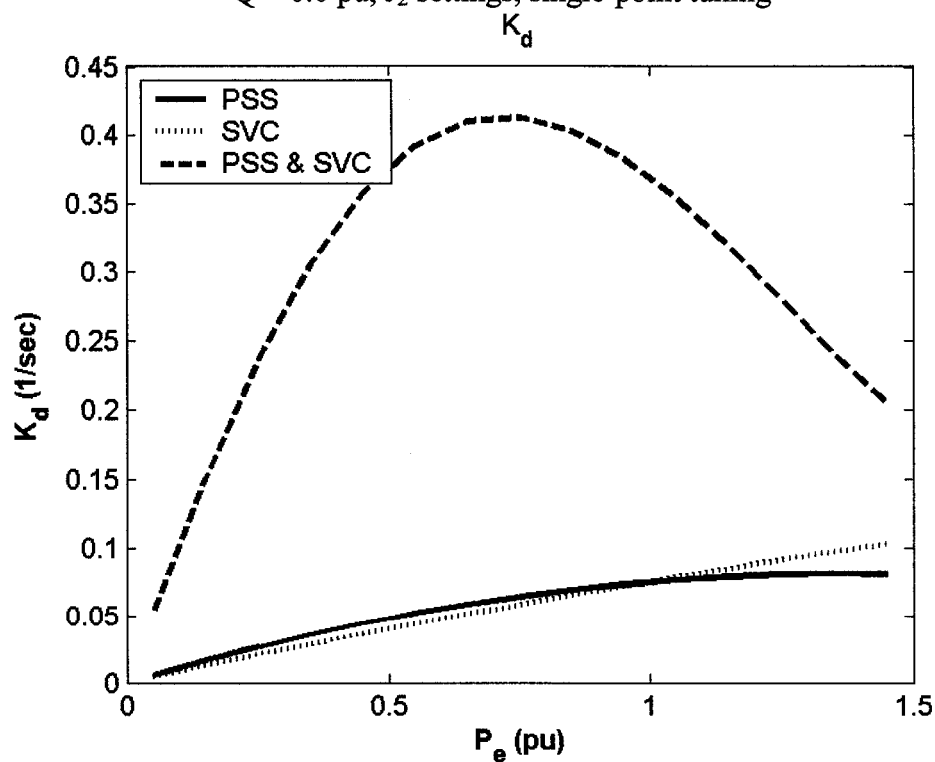


Figure 7.28: Damping torque coefficient with coordinated PSS & SVC-based stabilizer at $Q = 0.4$ pu, J_2 settings, single-point tuning

Nonlinear Time-Domain Simulations: The nonlinear time-domain simulations are carried out at the nominal and light loading conditions specified previously. The rotor angle, speed deviation, electrical power, and machine terminal voltage responses for a 6-cycle three-phase fault at the nominal loading conditions are shown in Figures 7.29-7.32, respectively. Figure 7.33 and Figure 7.34 show the control effort provided by the stabilizing signal of PSS, U_{PSS} , and the susceptance of SVC, B_{SVC} , when applied individually and through coordinated design. A slight improvement can be observed in this case.

In a similar manner, the simulation results with a 6-cycle three-phase fault at light loading condition are shown in Figures 7.35-7.38. The control signals of the two stabilizers are given in Figure 7.39 and Figure 7.40. The simulation results obtained clearly indicate that the proposed coordinated PSS-SVC design outperforms both the individual designs in terms of first swing stability, overshoot, and settling time. These results confirm the conclusions drawn for damping torque coefficient analysis results. This solves the problem of low effectiveness of the individual designs at light loading level.

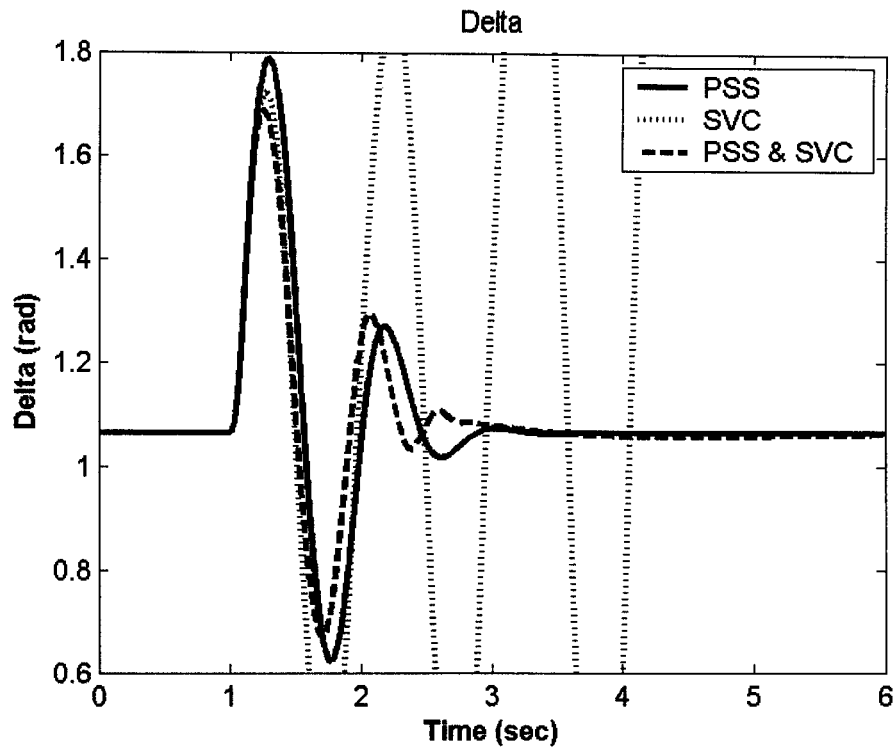


Figure 7.29: Rotor angle response for 6-cycle fault with nominal loading, J_2 settings, single-point tuning, coordinated design

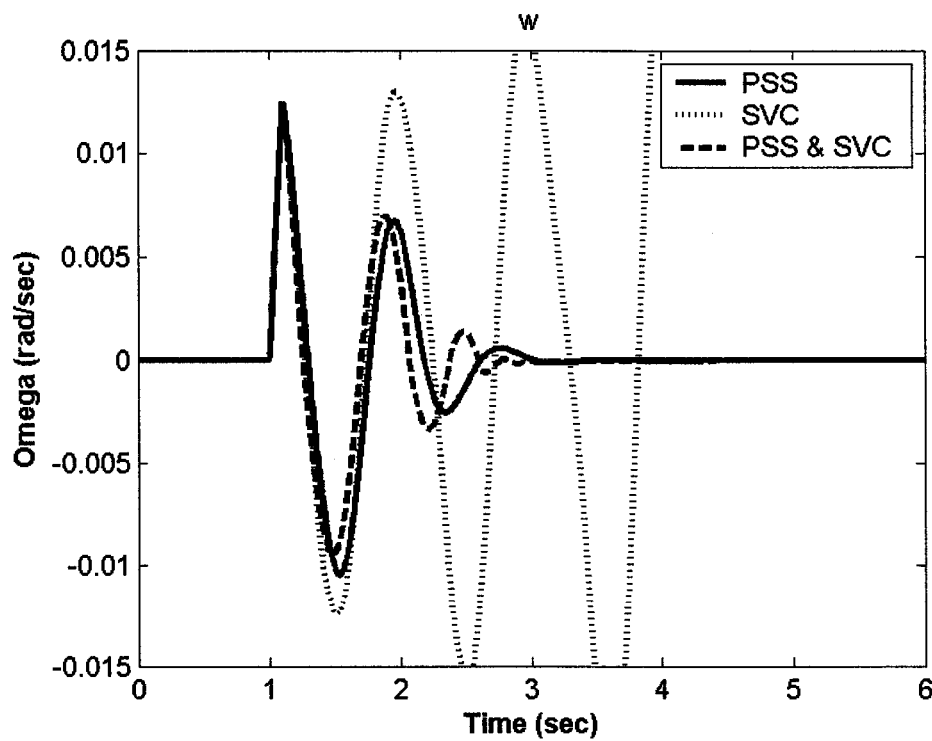


Figure 7.30: Speed response for 6-cycle fault with nominal loading, J_2 settings, single-point tuning, coordinated design

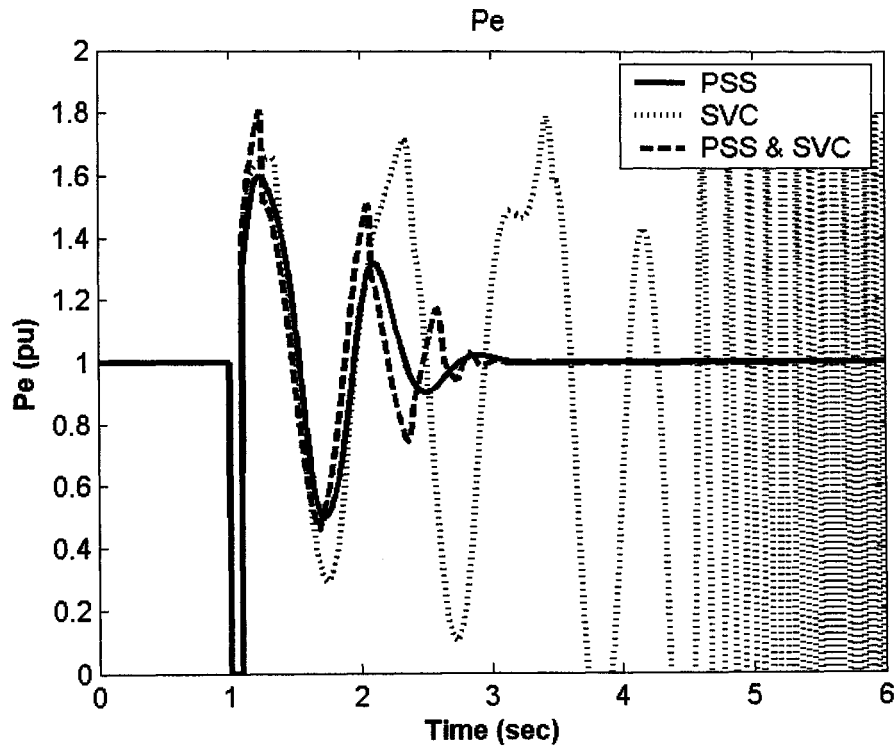


Figure 7.31: Electrical power response for 6-cycle fault with nominal loading, J_2 settings, single-point tuning, coordinated design

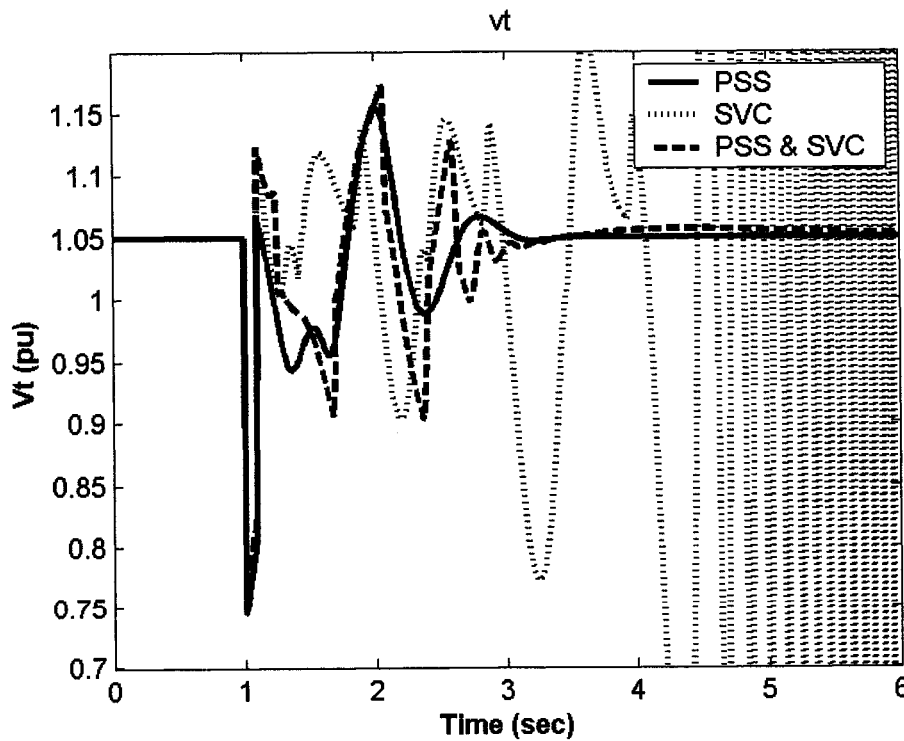


Figure 7.32: Terminal voltage response for 6-cycle fault with nominal loading, J_2 settings, single-point tuning, coordinated design

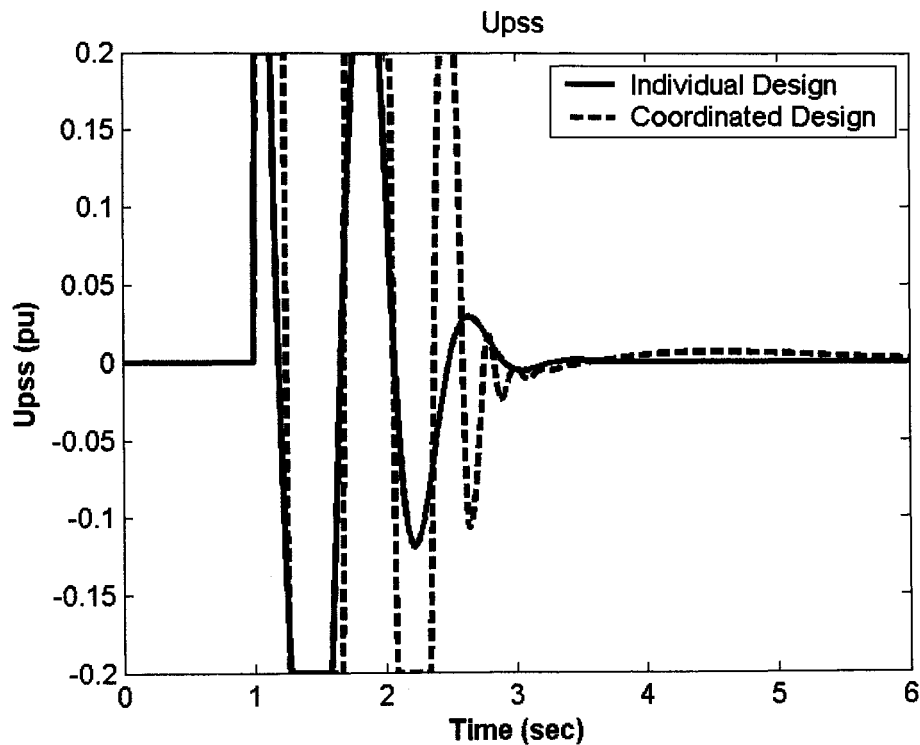


Figure 7.33: PSS stabilizing signal for 6-cycle fault with nominal loading, J_2 settings, single-point tuning, coordinated design

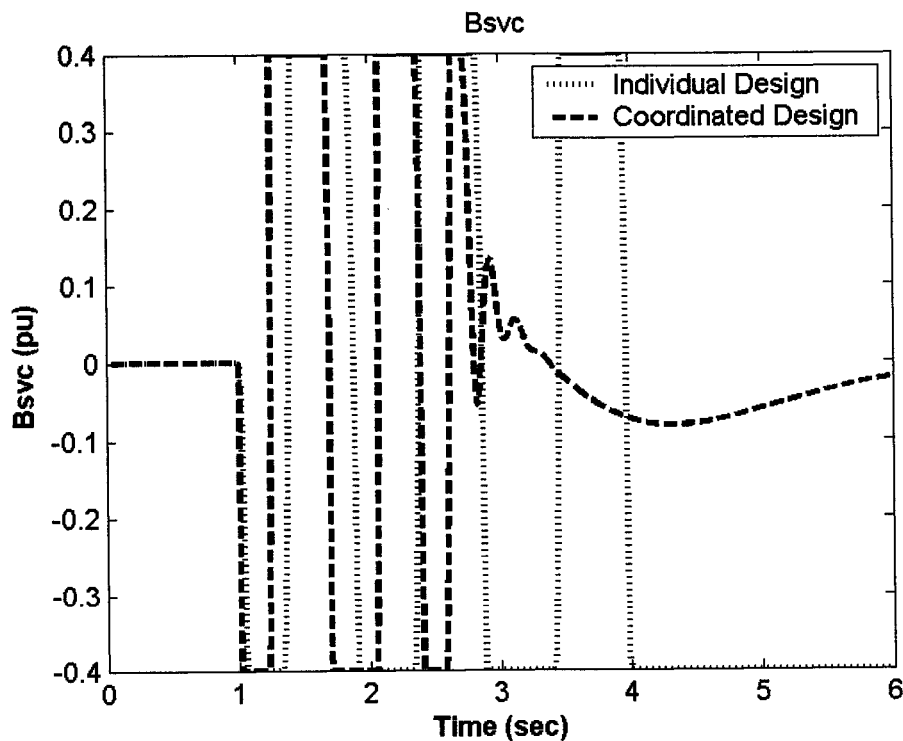


Figure 7.34: B_{svc} response for 6-cycle fault with nominal loading, J_2 settings, single-point tuning, coordinated design

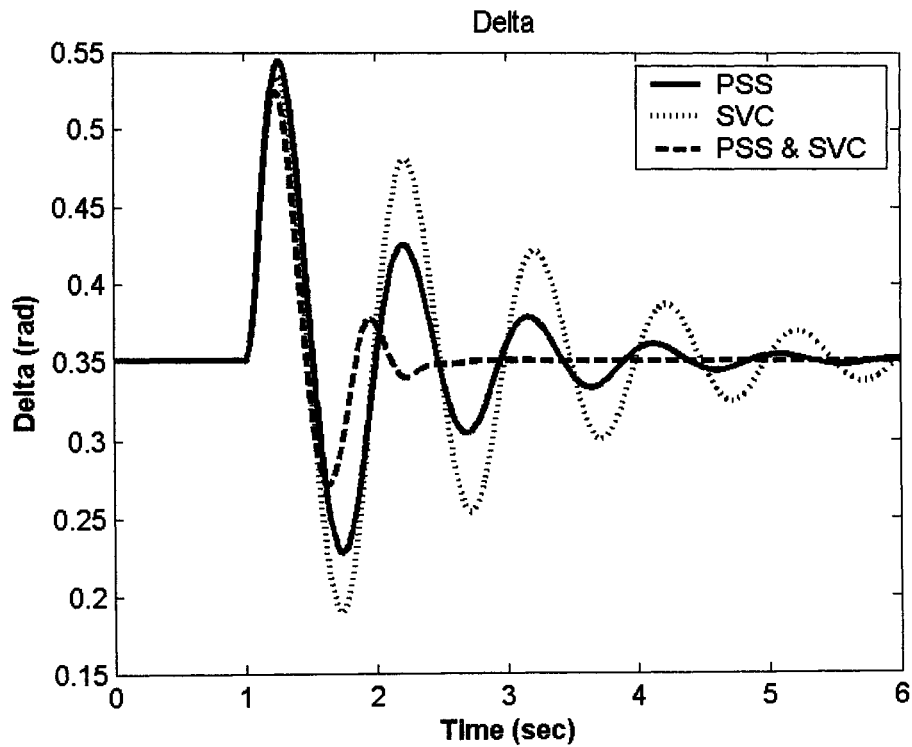


Figure 7.35: Rotor angle response for 6-cycle fault with light loading, J_2 settings, single-point tuning, coordinated design

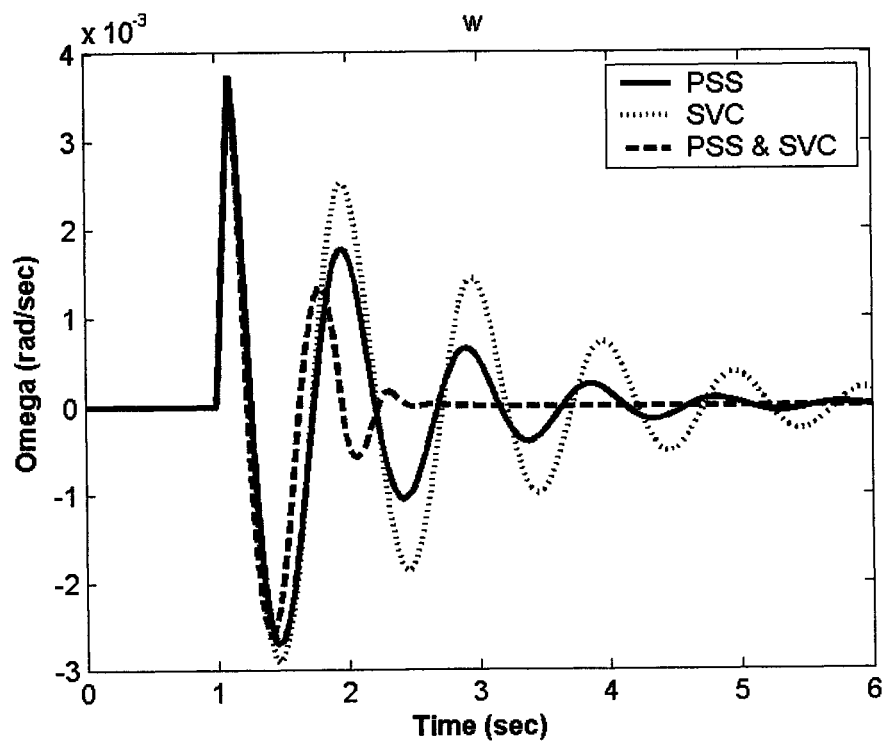


Figure 7.36: Speed response for 6-cycle fault with light loading, J_2 settings, single-point tuning, coordinated design

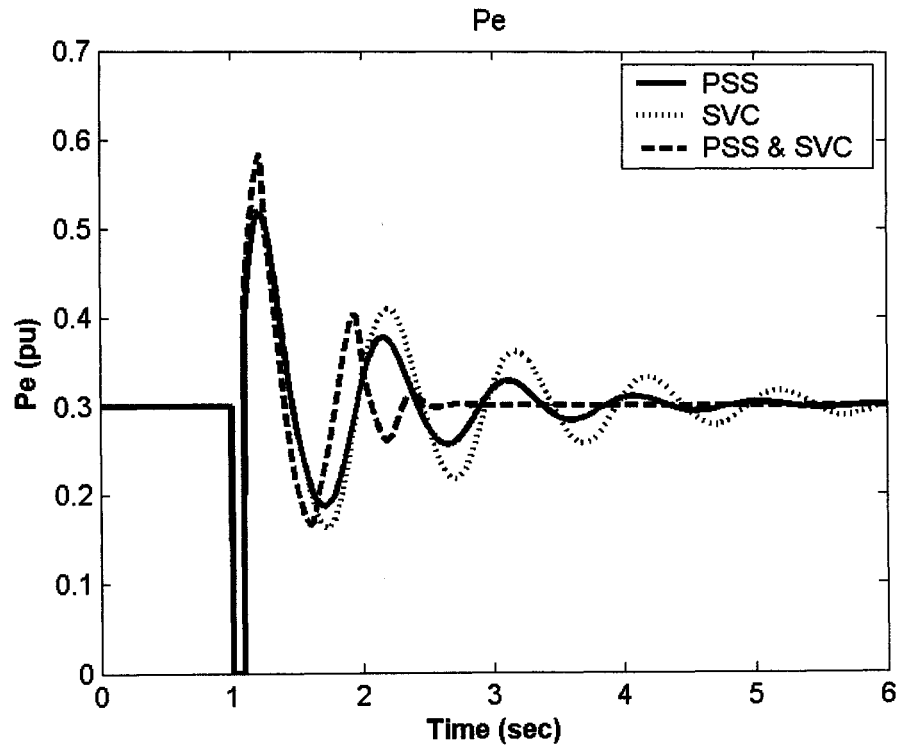


Figure 7.37: Electrical power response for 6-cycle fault with light loading, J_2 settings, single-point tuning, coordinated design

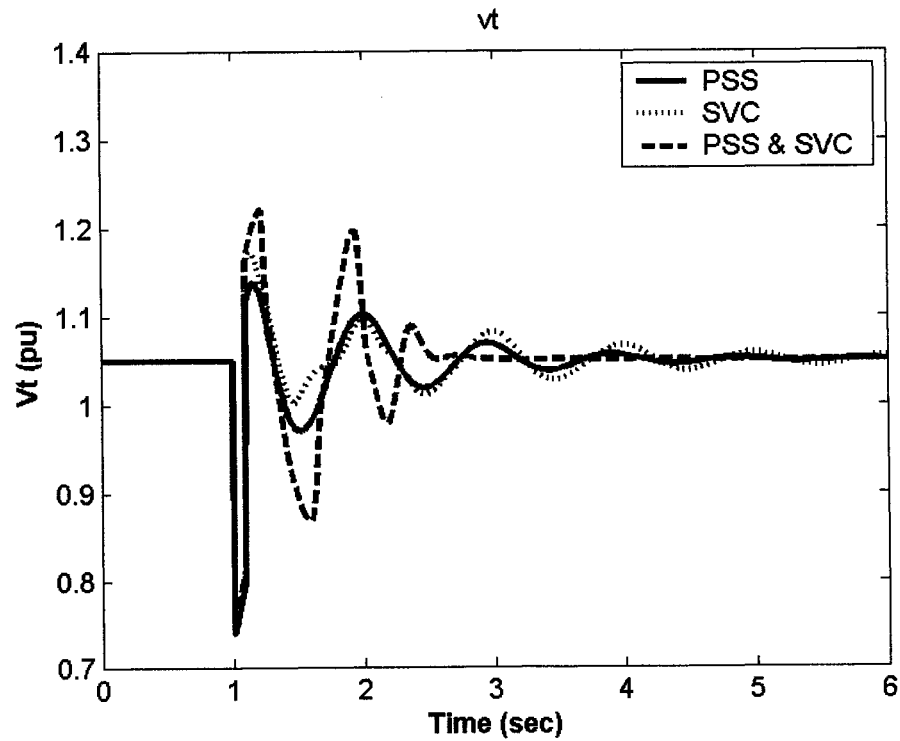


Figure 7.38: Terminal voltage response for 6-cycle fault with light loading, J_2 settings, single-point tuning, coordinated design

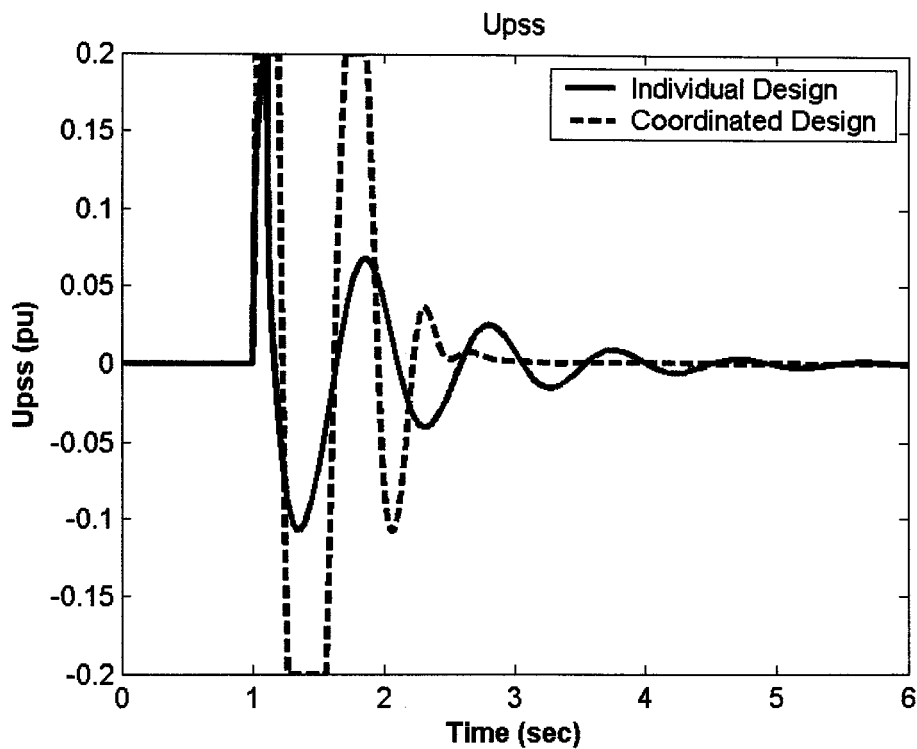


Figure 7.39: PSS stabilizing signal for 6-cycle fault with light loading, J_2 settings, single-point tuning, coordinated design

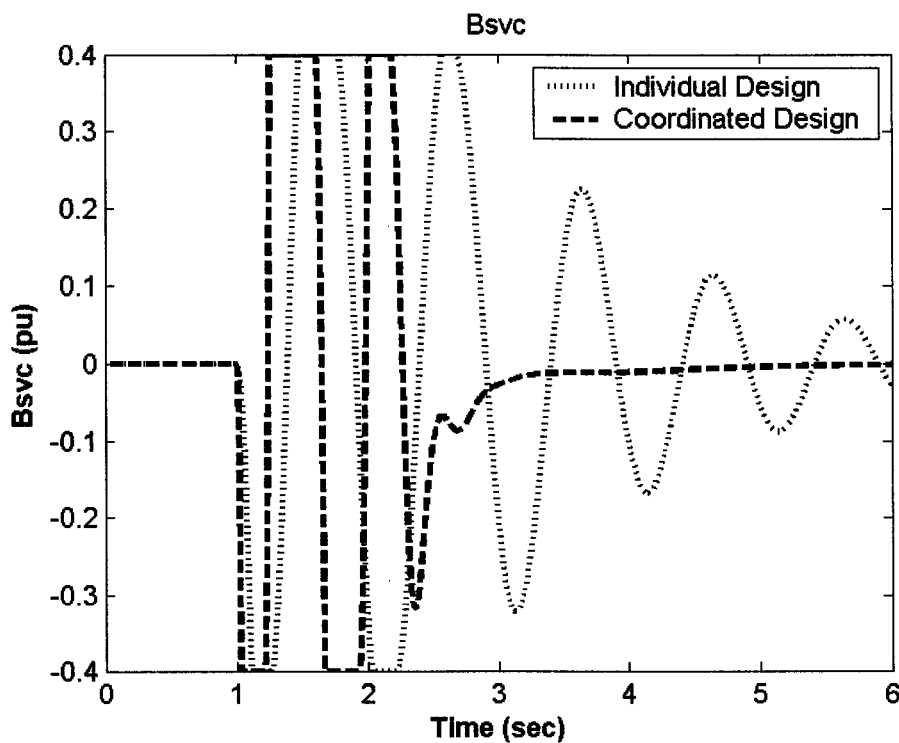


Figure 7.40: B_{svc} response for 6-cycle fault with light loading, J_2 settings, single-point tuning, coordinated design

7.2.2 Multiple-Point Tuning

In this situation, the objective is to design robust stabilizers to ensure their effectiveness over a wide range of operating conditions. The design process takes into account several loading conditions including nominal, light, heavy, and leading Pf conditions. These loading conditions are considered without and with system parameter uncertainties, such as machine inertia, line impedance, and field time constant. The total number of 16 operating conditions is considered during the design process as given in Table 7.16.

Tables 7.17 and 7.18 list the open-loop eigenvalues and corresponding damping ratios associated with the EM modes of all the 16 points considered in the robust design process, respectively. It is evident that all these modes are unstable.

Table 7.16: Loading conditions and parameter uncertainties considered in the design stage

Loading Condition	(P_e, Q_e) pu	Parameter Uncertainties
Nominal	(1.0, 0.015)	No parameter uncertainties
Light	(0.3, 0.100)	30% increase of line reactance X
Heavy	(1.1, 0.100)	25% decrease of machine inertia M
Leading Pf	(0.7, -0.30)	30% decrease of field time constant T' _{do}

Table 7.17: Open-loop eigenvalues associated with the EM modes of all the 16 points considered in the robust design process

	No parameter uncertainties	30% increase of line reactance X	25% decrease of machine inertia M	30% decrease of field time constant T'_{do}
Nominal	0.5255±6.5920i	0.5871±6.0962i	0.6125±7.5151i	0.5140±6.7592i
Light	0.0382±6.3602i	0.0434±5.8924i	0.0457±7.3365i	0.0350±6.3725i
Heavy	0.6384±6.0840i	0.7067±5.3230i	0.7580±6.9144i	0.6011±6.2766i
Leading Pf	0.2182±6.6657i	0.2522±6.3265i	0.2538±7.6535i	0.2131±6.7376i

Table 7.18: Damping ratios of the open-loop eigenvalues associated with the EM modes of all the points considered in the robust design process

	No parameter uncertainties	30% increase of line reactance X	25% decrease of machine inertia M	30% decrease of field time constant T'_{do}
Nominal	-0.0795	-0.0959	-0.0812	-0.0758
Light	-0.0060	-0.0074	-0.0062	-0.0055
Heavy	-0.1044	-0.1316	-0.1090	-0.0953
Leading Pf	-0.0327	-0.0398	-0.0331	-0.0316

Table 7.19: Optimal parameter settings with J_1 , multiple-point tuning, individual design

	PSS	SVC	TCSC	TCPS
K	19.582	300.00	9.7630	54.613
T₁	4.3897	4.5732	3.4177	1.7740
T₂	0.0100	2.2747	0.8224	0.5512
T₃	0.1601	0.0100	3.2050	1.3387
T₄	1.8253	0.2338	0.8392	2.8446

7.2.2.1 Individual Design with J_1

The PSS, SVC-, TCSC-, and TCPS-based controllers are designed individually considering all the operating points mentioned above.

Stabilizer Design: PSO is used to optimize the parameters of each controller that maximize the minimum damping ratio of all the complex eigenvalues associated with the 16 operating points. The final settings of the optimized parameters for the proposed stabilizers are given in Table 7.19.

Eigenvalue Analysis: The system eigenvalues without and with the proposed stabilizers at the four operating points, nominal, light, heavy, and leading Pf, are given in Tables 7.20-7.23, respectively. The bold rows of these tables represent the EM mode eigenvalue and its damping ratio. It is evident that the proposed stabilizers greatly improve the system stability at all the points considered.

Table 7.20: System eigenvalues of nominal loading conditions with J_1 settings, multiple-point tuning, individual design

No Control	PSS	SVC	TCSC	TCPS
0.5255±6.5919i, -0.0795	-3.2124± 3.4158i, 0.6900	-1.4523± 3.5268i, 0.3808	-1.2994± 2.1131i, 0.5238	-3.4310± 4.2613i, 0.6271
-10.6940±	-5.8100±	-18.674±	-10.209±	-9.6650±
5.6612i	14.8000i	1.2999i	17.194i	11.983i
--	-102.23	-2.1862±	-11.0406	-13.5594
--	-0.2000	10.2664i	-7.8146	-2.4027
--	-0.6200	-0.4290	-0.8735	-0.3428
--	--	-0.1999	-0.2001	-0.2062

Table 7.21: System eigenvalues of light loading conditions with J_1 settings, multiple-point tuning, individual design

No Control	PSS	SVC	TCSC	TCPS
0.0382±0.3601i, -0.0060	-2.0575± 5.9049i, 0.3300	-1.0287± 6.3396i, 0.1602	2.7088± 5.7479i, 0.4263	2.9511± 1.2231i, 0.9238
-10.2067±	-7.7100±	-6.0001±	-10.206±	-8.6153±
6.3849i	9.1400i	4.6408i	6.5901i	9.7524i
--	-100.77	-19.7821	-13.803	-9.5109±
--	-0.2000	-10.7784	-2.1523	5.6480i
--	-0.5700	-0.4358	-0.9596	-0.3404
--	--	-0.1999	-0.2000	-0.2078

Table 7.22: System eigenvalues of heavy loading conditions with J_1 settings, multiple-point tuning, individual design

No Control	PSS	SVC	TCSC	TCPS
0.6384±6.0839i, -0.1044	-2.9002± 3.4982i, 0.6400	-2.3894± 2.8871i, 0.6376	-0.7226± 1.7171i, 0.3879	-3.4061± 2.5350i, 0.8022
-10.807±	-6.1900±	-1.7019±	-10.512±	-9.9693
5.9347i	14.1400i	9.9908i	17.774i	±13.045i
--	-102.08	-20.939	-9.7260±	-11.844
--	-0.2000	-15.4751	6.3736i	-3.5602
--	-0.6200	-0.4570	-0.8229	-0.3390
--	--	-0.2003	-0.2002	-0.2089

Table 7.23: System eigenvalues of leading Pf loading conditions with J_1 settings,
multiple-point tuning, individual design

No Control	PSS	SVC	TCSC	TCPS
0.2182±6.6656i, -0.0327	-3.3123± 3.5537i, 0.6800	-0.8192± 3.9456i, 0.2033	-1.8696± 3.8811i, 0.4340	-3.8252± 4.7060i, 0.6307
-10.387±	-5.8500±	-18.345±	-9.8230±	-9.2850±
5.6970i	14.1100i	2.4700i	14.045i	10.375i
--	-101.96	-3.1560±	-16.2547	-13.609
--	-0.2000	9.6010i	-2.1598	-2.3237
--	-0.6100	-0.4140	-0.9448	-0.3438
--	--	-0.1995	-0.2001	-0.2054

Damping Torque Coefficient Analysis: The damping torque coefficient K_d is calculated for the proposed robust stabilizers to quantitatively measure their effectiveness in enhancing the system damping characteristics. The damping torque coefficient is calculated for a range of 45 operating points specified by $P_e=[0.05 - 1.45]$ pu in steps of 0.10 pu and $Q_e=[-0.40, 0.00, 0.40]$ pu.

For comparison purposes, damping torque coefficient for all stabilizers at $Q=-0.4$, $Q=0.0$, and $Q=0.4$ pu are shown in Figures 7.41-7.43, respectively. These figures illustrate that:

- The TCPS-based stabilizer outperforms the other stabilizers at light loading conditions. In contrast, The TCSC is the winner at nominal and heavy loading conditions.
- Among all the stabilizers, the SVC gives the least support to system stability enhancement.
- The PSS, SVC, and TCSC suffer from low damping characteristics at light loading.

- The damping torque coefficients K_d associated with the PSS, SVC-, and TCSC-based stabilizers are directly proportional to system loading. However, the damping torque coefficient of SVC diminishes at heavy loading.
- For low and moderate loading, K_d of the TCPS-based stabilizer is almost constant. However, it starts decreasing at very high loading.
- The TCSC and TCPS are most effective at lagging power factor conditions, whereas the PSS is most effective at leading power factor conditions. On the other hand, The SVC has its best performance at unity power factor.

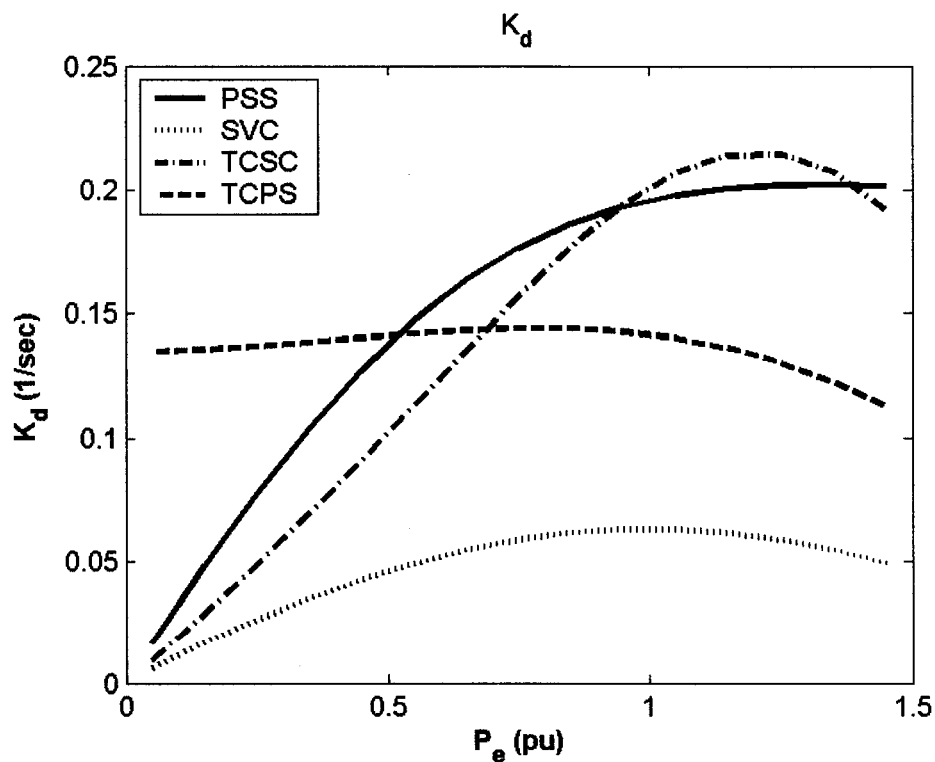


Figure 7.41: Damping torque coefficient with the proposed controllers at $Q = -0.4$ pu, J_1 settings, multiple-point tuning, individual design

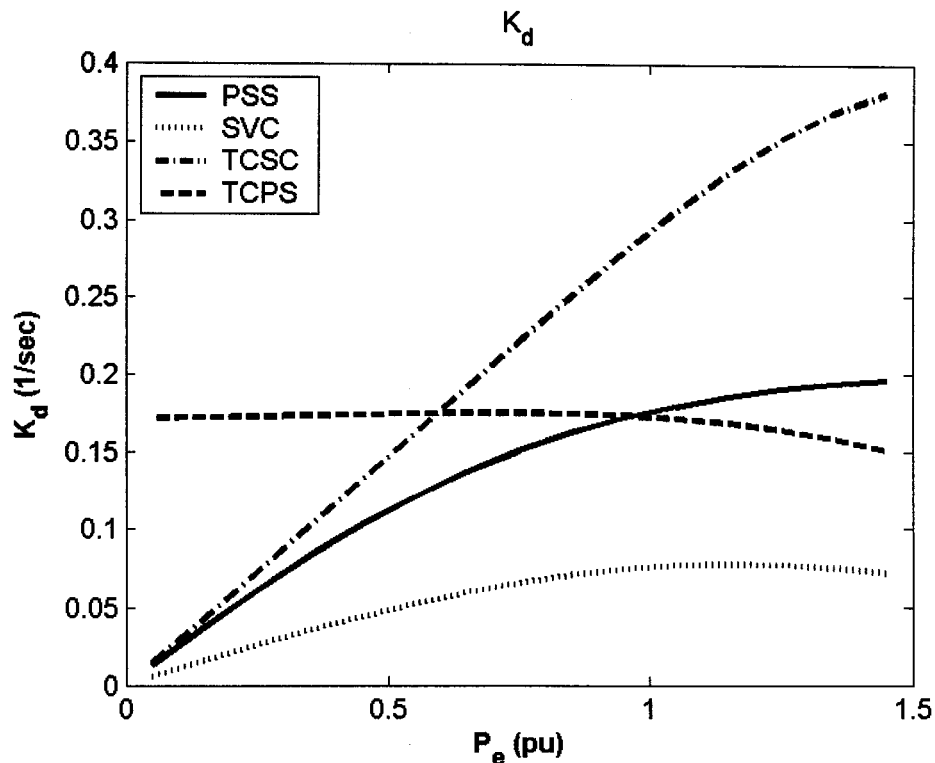


Figure 7.42: Damping torque coefficient with the proposed controllers at $Q = 0.0$ pu, J_1 settings, multiple-point tuning, individual design

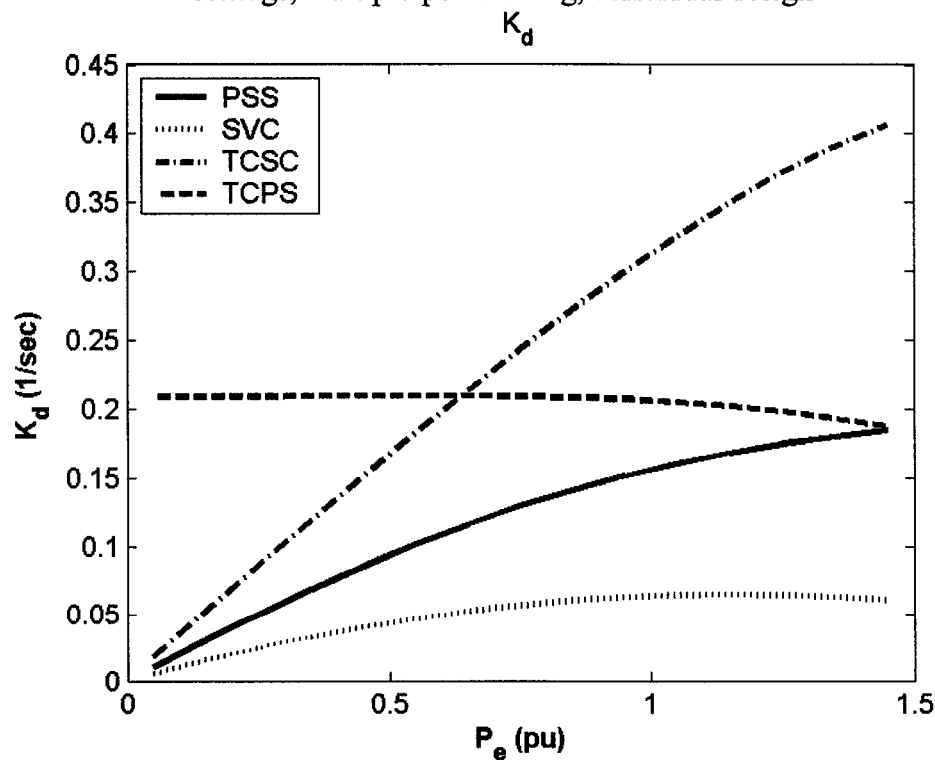


Figure 7.43: Damping torque coefficient with the proposed controllers at $Q = 0.4$ pu, J_1 settings, multiple-point tuning, individual design

Nonlinear Time-Domain Simulations: Figures 7.44-7.47 show the system responses for a 6-cycle three-phase fault at the nominal loading conditions. Figures 7.48-7.51 show the control effort provided by the stabilizing signal of PSS, U_{PSS} , the susceptance of SVC, B_{SVC} , the reactance of TCSC, X_{TCSC} , and the angle of TCPS, Φ_{TCPS} , respectively. Clearly, the TCSC and TCPS outperform the PSS and SVC in terms of reduction of overshoot and settling time. Moreover, The TCSC is relatively more effective than the TCPS. This is consistent with damping torque coefficient analysis results. However, the damping effort provided by the SVC is not sufficient to keep the system stable.

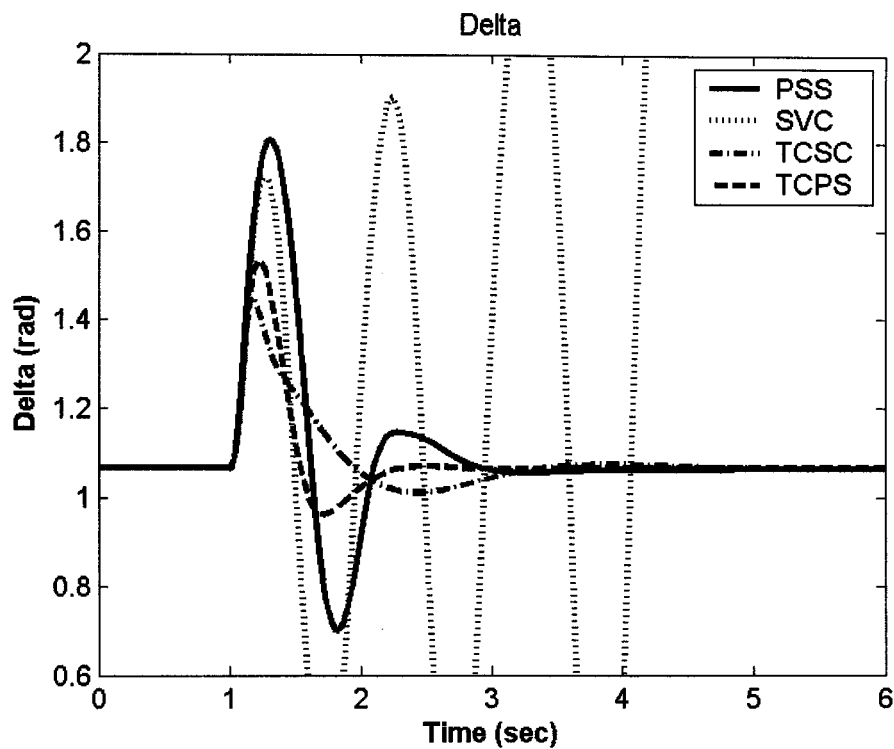


Figure 7.44: Rotor angle response for 6-cycle fault with nominal loading, J_1 settings, multiple-point tuning, individual design

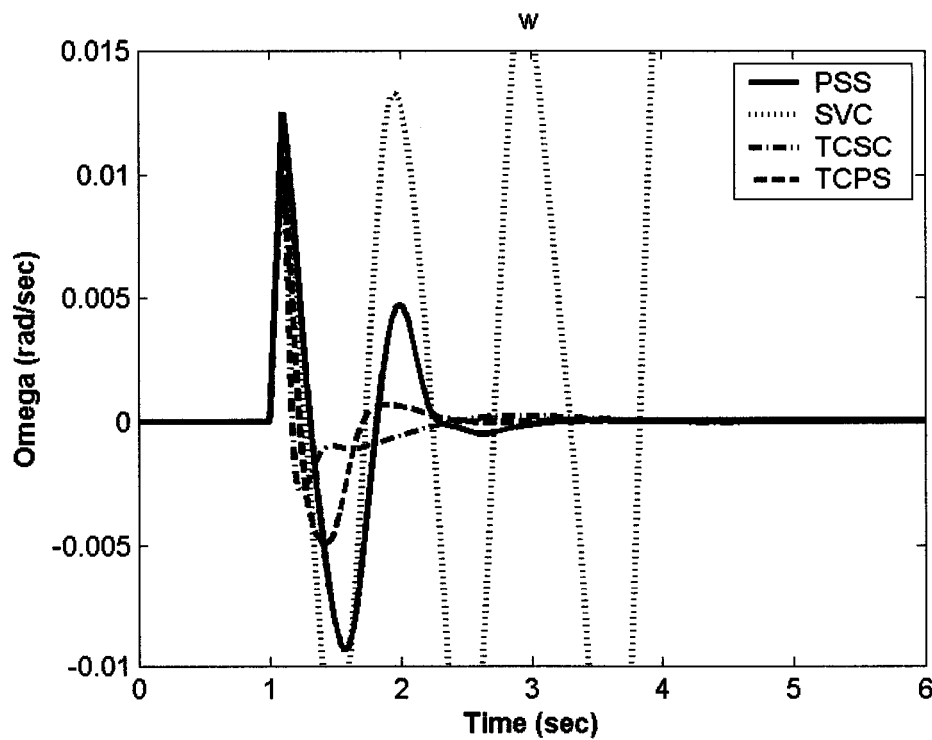


Figure 7.45: Speed response for 6-cycle fault with nominal loading, J_1 settings, multiple-point tuning, individual design

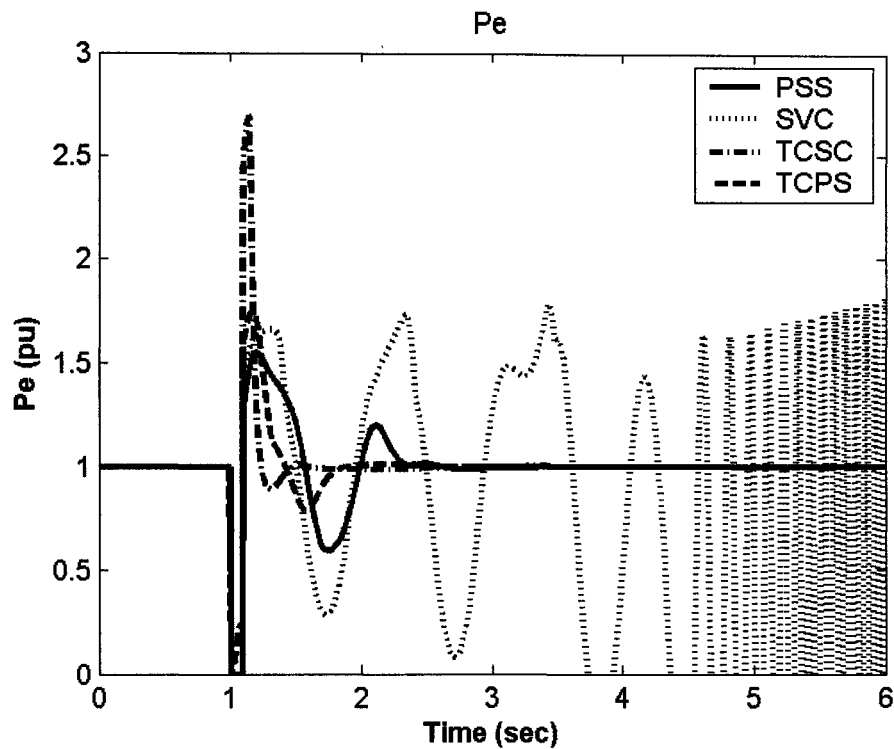


Figure 7.46: Electrical power response for 6-cycle fault with nominal loading, J_1 settings, multiple-point tuning, individual design

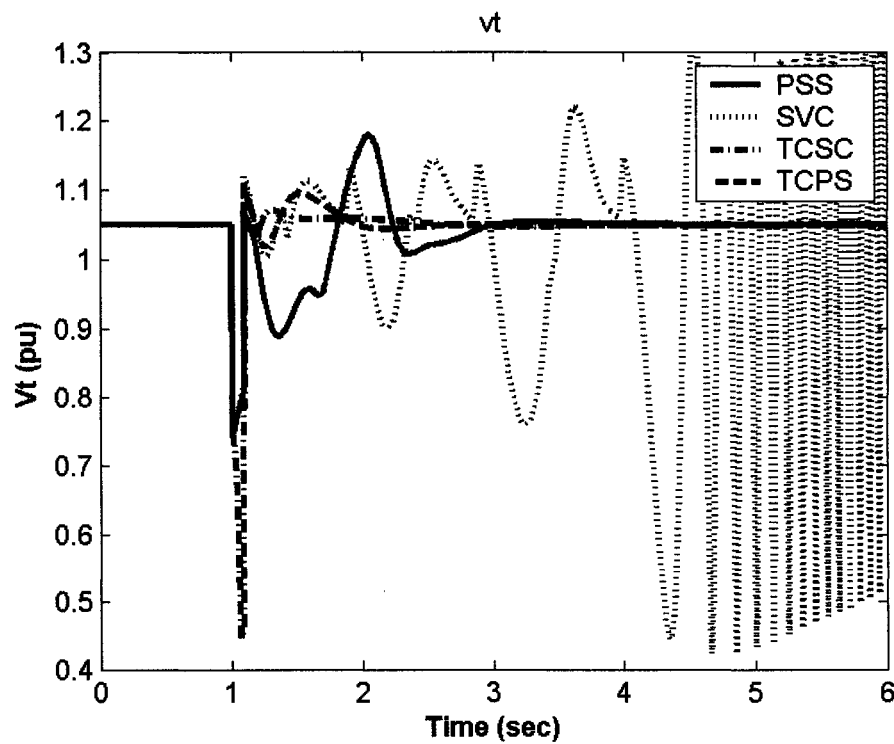


Figure 7.47: Terminal voltage response for 6-cycle fault with nominal loading, J_1 settings, multiple-point tuning, individual design

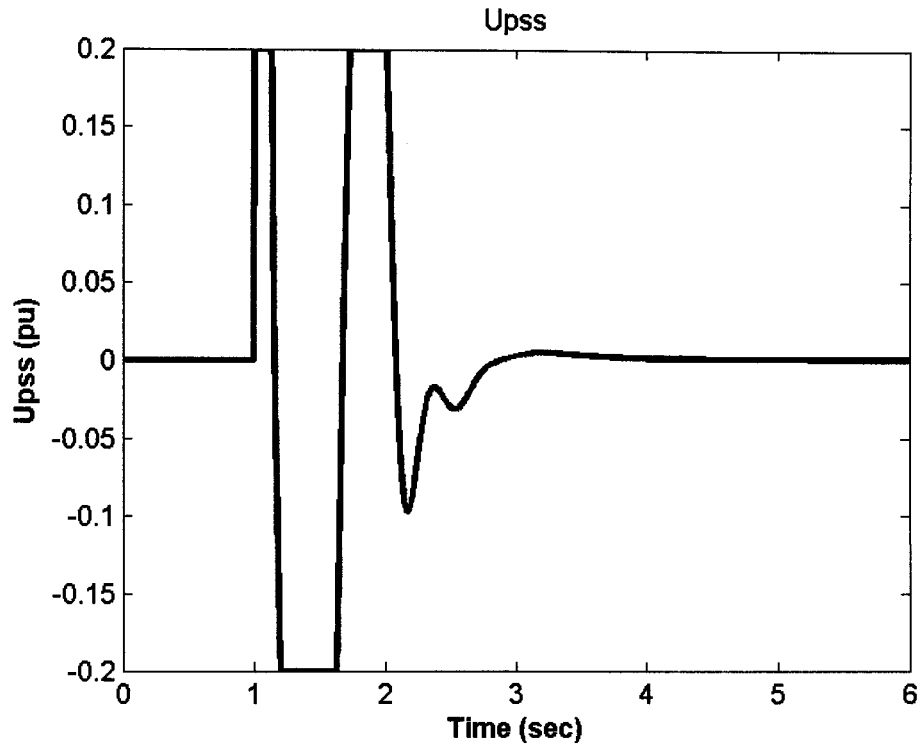


Figure 7.48: PSS stabilizing signal for 6-cycle fault with nominal loading, J_1 settings, multiple-point tuning, individual design

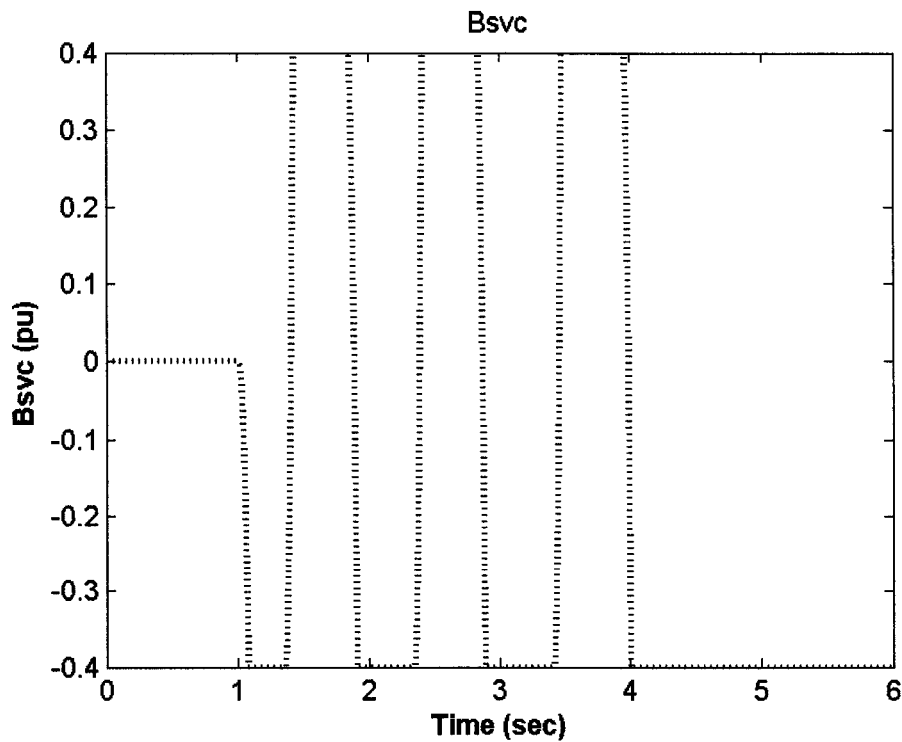


Figure 7.49: B_{svc} response for 6-cycle fault with nominal loading, J_1 settings, multiple-point tuning, individual design

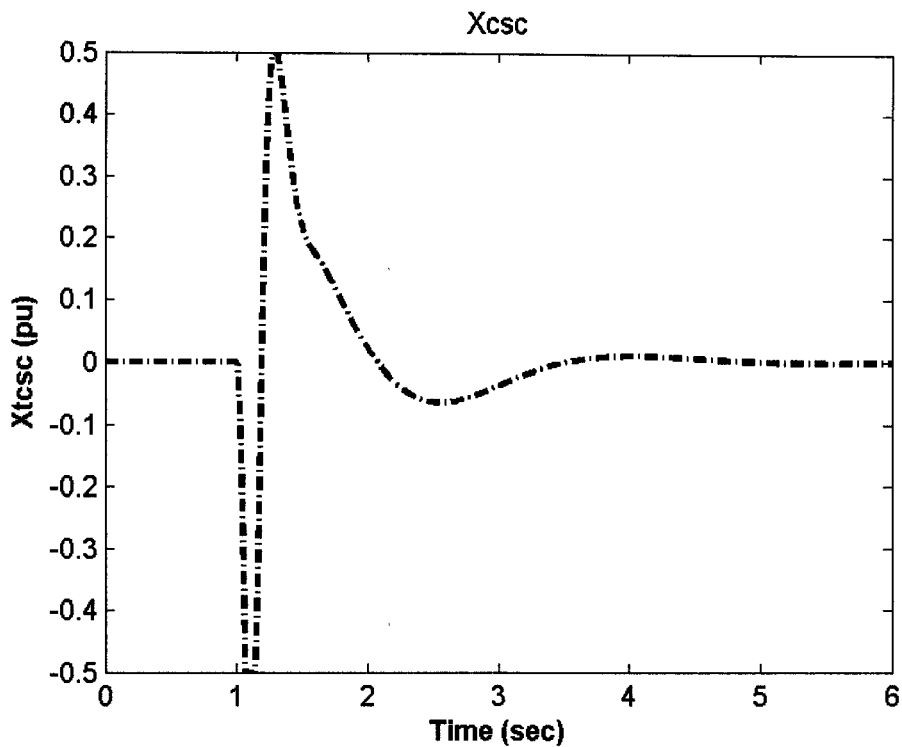


Figure 7.50: X_{tcsc} response 6-cycle fault with nominal loading, J_1 settings, multiple-point tuning, individual design

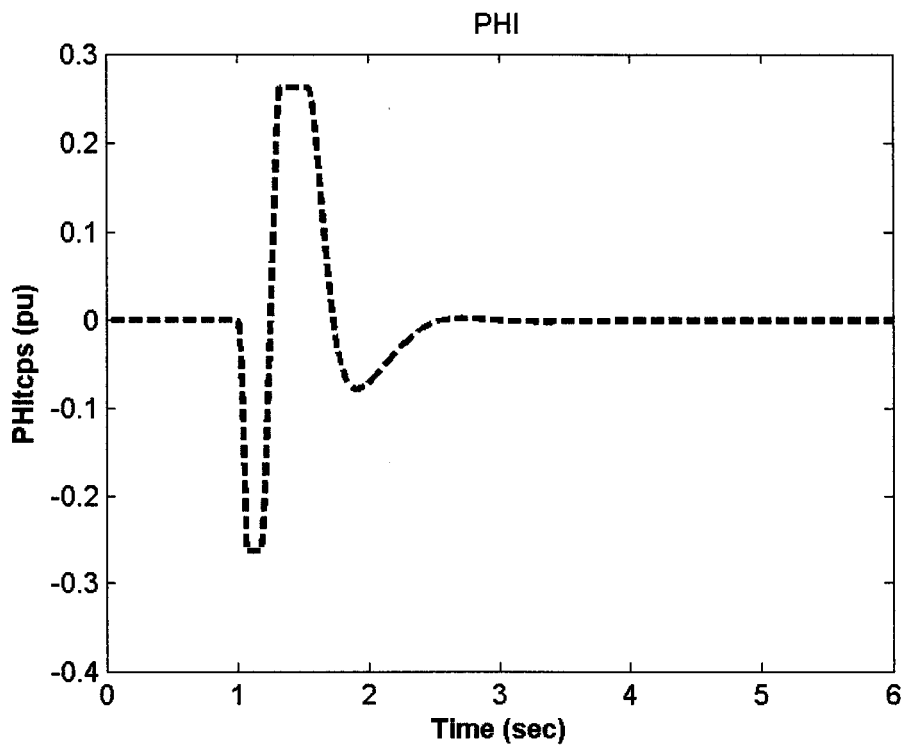


Figure 7.51: Φ_{tcps} response 6-cycle fault with nominal loading, J_1 settings, multiple-point tuning, individual design

7.2.2.2 Individual Design with J_2

The PSS, SVC-, TCSC-, and TCPS-based controllers are designed individually considering all the operating points mentioned above.

Stabilizer Design: PSO is used to optimize the parameters of each controller that minimizes the maximum damping factors of all the complex eigenvalues associated with the 16 operating points. The final settings of the optimized parameters for the proposed stabilizers are given in Table 7.24.

Eigenvalue Analysis: The system eigenvalues without and with the proposed stabilizers at the four operating points, nominal, light, heavy, and leading Pf, are given in Tables 7.25-7.28, respectively. The bold rows of these tables represent the EM mode eigenvalue and its damping ratio. It is evident that the proposed stabilizers greatly improve the system stability at all the points considered.

Table 7.24: Optimal parameter settings with J_2 , multiple-point tuning, individual design

	PSS	SVC	TCSC	TCPS
K	44.529	300.00	100.00	100.00
T₁	5.0000	0.0128	5.0000	5.0000
T₂	2.1339	0.7570	3.2870	3.3272
T₃	0.1059	5.0000	5.0000	5.0000
T₄	0.0100	0.8098	3.2870	3.3218

Table 7.25: System eigenvalues of nominal loading conditions with J_2 settings, multiple-point tuning, individual design

No Control	PSS	SVC	TCSC	TCPS
0.5255±6.5919i, -0.0795	-3.8149± 17.948i, 0.2100	-1.3939 ± 2.3477i, 0.5105	-9.6288± 21.374i, 0.4107	-9.6635± 22.375i, 0.3965
-10.6940±	-103.11	-1.5139±	-9.5067±	-9.5670 ±
5.6612i	-7.7100	10.116i	1.0406i	0.7422i
--	-1.7000	-18.836	-1.9503	-1.7503
--	-0.6600	-17.425	-0.4632	-0.4694
--	-0.2000	-0.8160	-0.2610	-0.2578
--	--	-0.2000	-0.2000	-0.2000

Table 7.26: System eigenvalues of light loading conditions with J_2 settings, multiple-point tuning, individual design

No Control	PSS	SVC	TCSC	TCPS
0.0382±0.3601i, -0.0060	-4.6400 ± 4.020i, 0.7600	-1.0287 ± 6.7605i, 0.1504	-4.9258 ± 6.8650i, 0.5830	-9.4317± 20.578i, 0.4167
-10.2067±	-4.9600±	-8.8244 ±	-9.9694 ±	-10.1130 ±
6.3849i	10.7900i	3.5213i	6.7280i	6.0745i
--	-101.09	-19.838	-10.5163	-0.2000
--	-0.5100	-2.3944	-0.3650	-1.0243
--	-0.2000	-0.9540	-0.2738	-0.5703
--	--	-0.2000	-0.2000	-0.2547

Table 7.27: System eigenvalues of heavy loading conditions with J_2 settings, multiple-point tuning, individual design

No Control	PSS	SVC	TCSC	TCPS
0.6384±6.0839i, -0.1044	-4.0774 ± 17.167i, 0.2300	-0.9824 ± 9.8959i, 0.0988	-0.6539 ± 0.2696i, 0.9245	-0.7540 ± 0.0486i, 0.9979
-10.8069±	-102.90	-1.2193 ±	-9.8154±	-9.8379 ±
5.9347i	-7.4200	0.6424i	22.5010i	24.129i
--	-1.6600	-0.2000	-9.8766 ±	-9.7508 ±
--	-0.6800	-20.6823	6.3352i	3.1363i
--	-0.2000	-14.5161	-0.2537	-0.2531
--	--	-3.2911	-0.2000	-0.2000

Table 7.28: System eigenvalues of leading Pf loading conditions with J_2 settings,
multiple-point tuning, individual design

No Control	PSS	SVC	TCSC	TCPS
0.2182±6.6656i, -0.0327	-3.9652± 17.081i, 0.2300	-0.8200 ± 2.9853i, 0.2649	-2.9140 ± 3.2103i, 0.6721	-9.4451 ± 20.071i, 0.4258
-10.387±	-102.73	-17.814 ±	-9.3213 ±	-9.6669 ±
5.6970i	-7.5600	1.6968i	17.111i	2.3724i
--	-1.9700	-2.4604 ±	-15.8263	-2.0114
--	-0.6200	9.3915i	-0.3777	-0.4439
--	-0.2000	-0.7040	-0.2708	-0.2595
--	--	-0.2000	-0.2000	-0.2000

Damping Torque Coefficient Analysis: The damping torque coefficient K_d is calculated for the proposed robust stabilizers to measure their effectiveness in enhancing the system damping characteristics. The damping torque coefficient is calculated for a range of 45 operating points specified by $P_e=[0.05 - 1.45]$ pu in steps of 0.10 pu and $Q_e=[-0.40, 0.00, 0.40]$ pu.

For comparison purposes, damping torque coefficient for all stabilizers at $Q=-0.4$, $Q=0.0$, and $Q=0.4$ pu are shown in Figures 7.52-7.54, respectively. From these figures, the following conclusions can be drawn:

- In general, the TCPS-based stabilizer outperforms the other stabilizers. An exception appears with the heavy loading at unity and leading power factors, where the TCSC-based stabilizer becomes more effective.
- The PSS, SVC, and TCSC suffer from low damping characteristics at light loading. Special attention must be drawn to the TCSC at very low loading conditions with leading power factor.
- Generally, the SVC-based controller is the least effective in damping system oscillations.

- The damping torque coefficients K_d associated with the PSS, SVC-, and TCSC-based stabilizers increase almost linearly with loading level. However, it starts diminishing at heavy loading in the case of PSS and SVC. On the other hand, the damping torque coefficient of the TCPS-based stabilizer improves only slightly as loading level increases.

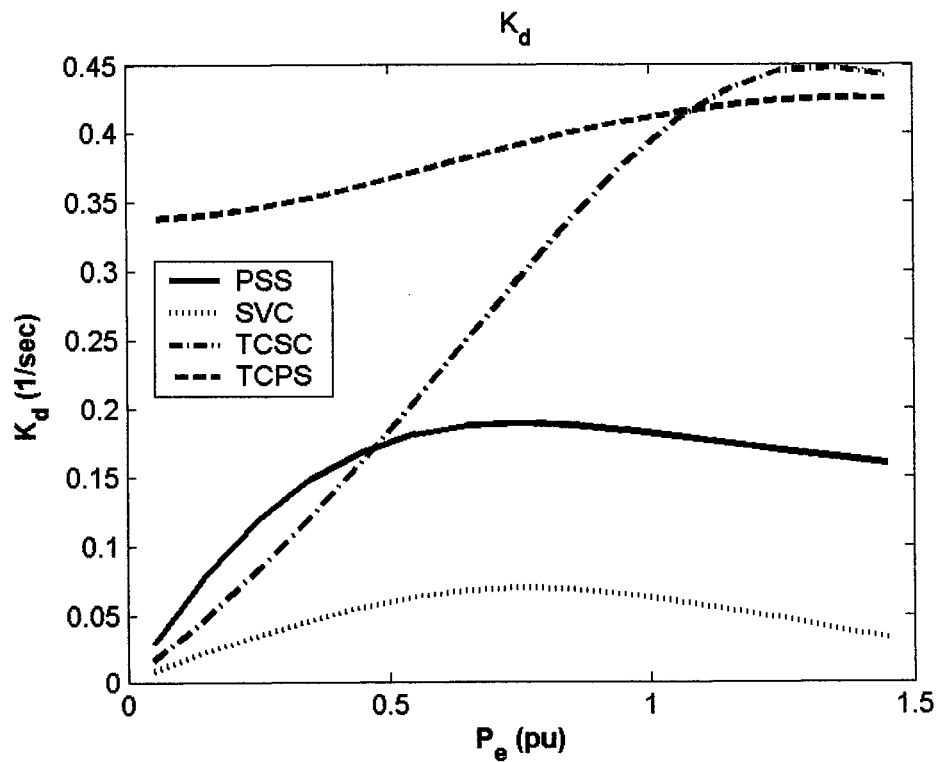


Figure 7.52: Damping torque coefficient with the proposed controllers at $Q = -0.4$ pu, J_2 settings, multiple-point tuning, individual design

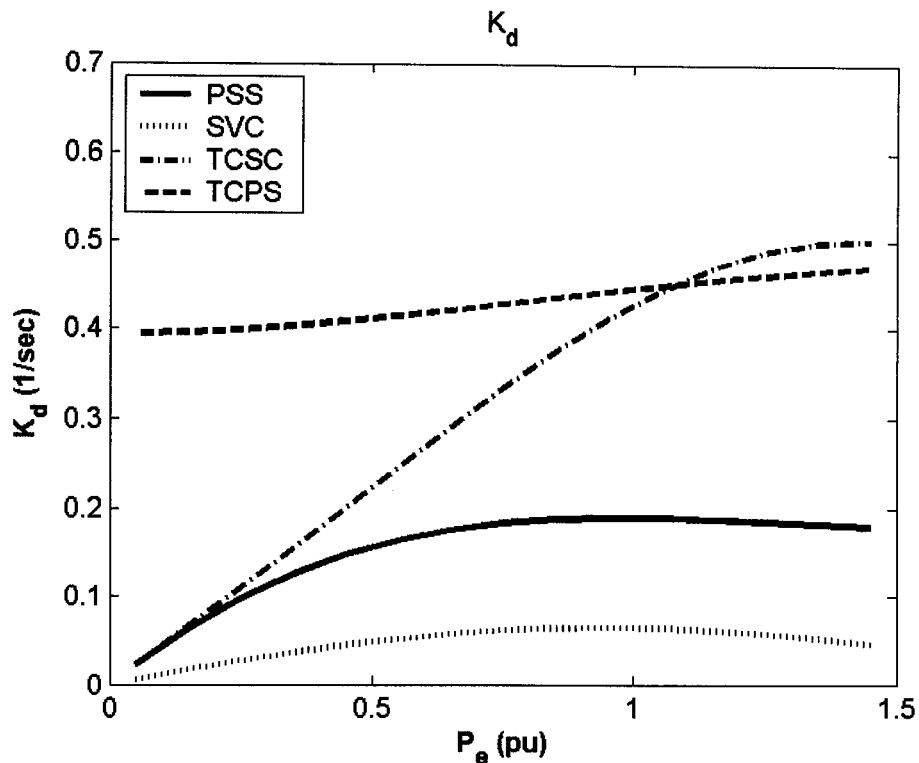


Figure 7.53: Damping torque coefficient with the proposed controllers at $Q = 0.0$ pu, J_2 settings, multiple-point tuning, individual design

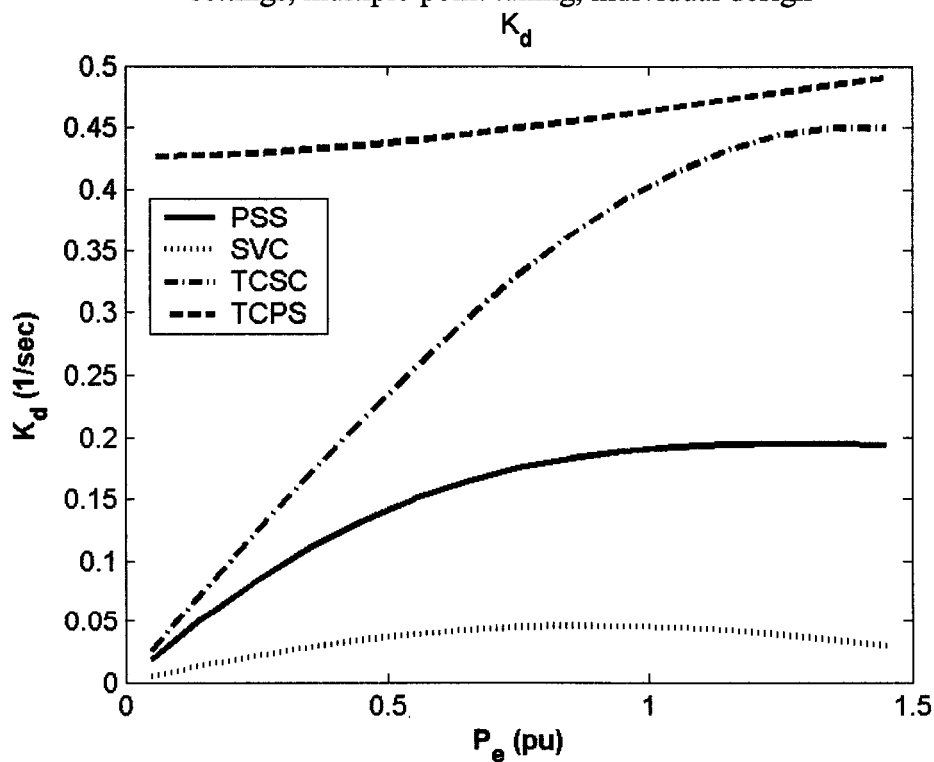


Figure 7.54: Damping torque coefficient with the proposed controllers at $Q = 0.4$ pu, J_2 settings, multiple-point tuning, individual design

Nonlinear Time-Domain Simulations: Figures 7.55-7.62 show system responses and control efforts for a 6-cycle three-phase fault at the nominal loading conditions. Clearly, the TCSC and TCPS outperform the PSS and SVC in terms of reduction of overshoot and settling time. This agrees with the results obtained from damping torque coefficient analysis. However, the damping effort provided by the SVC is not sufficient to keep the system stable.

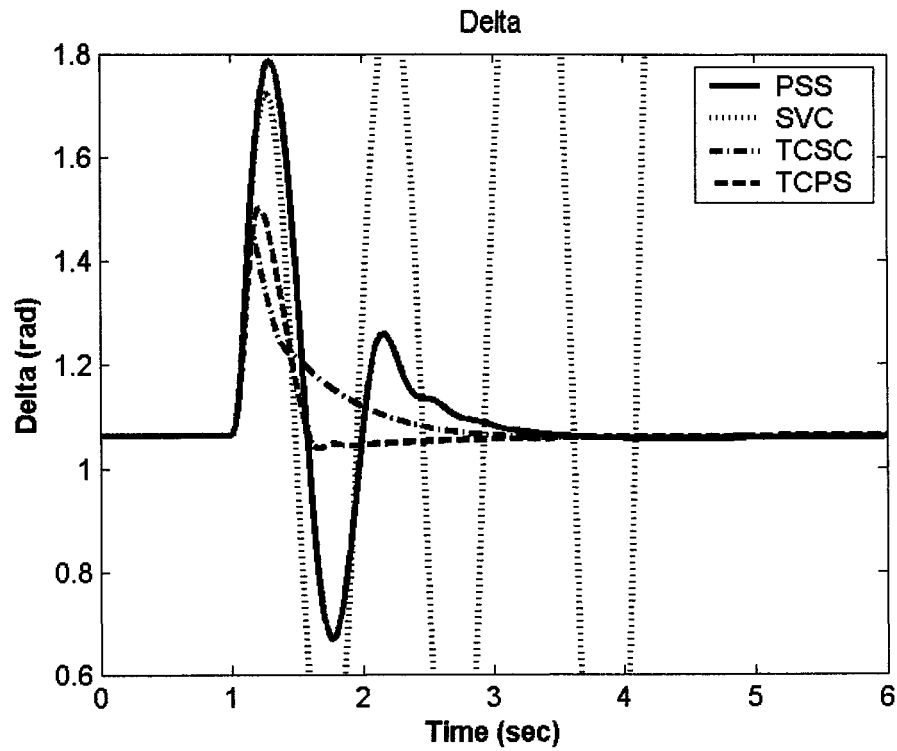


Figure 7.55: Rotor angle response for 6-cycle fault with nominal loading, J_2 settings, multiple-point tuning, individual design

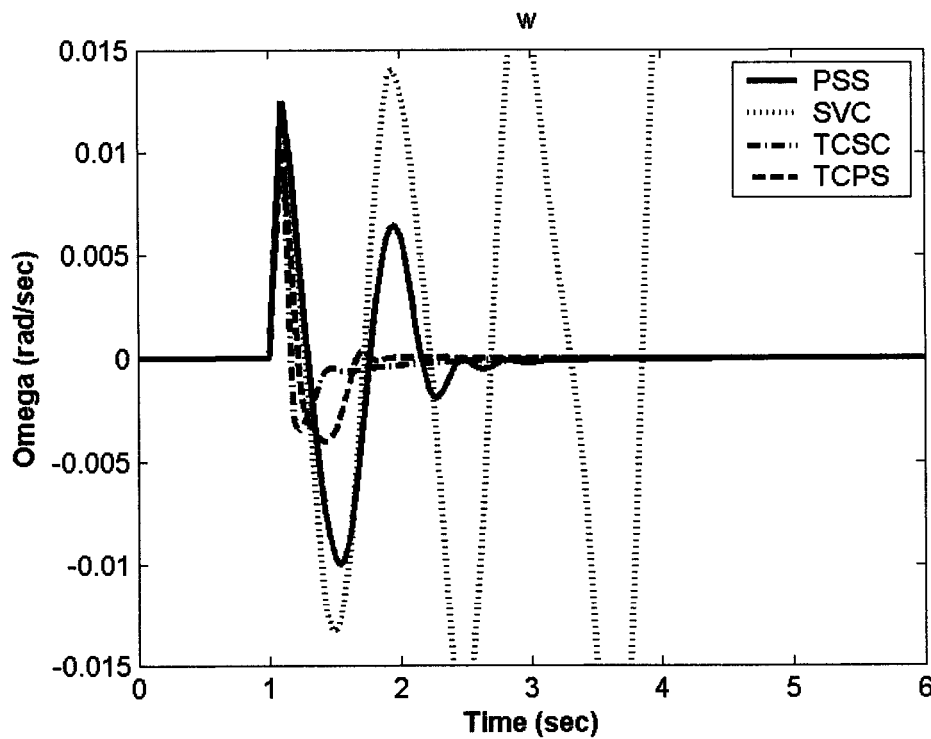


Figure 7.56: Speed response for 6-cycle fault with nominal loading, J_2 settings, multiple-point tuning, individual design

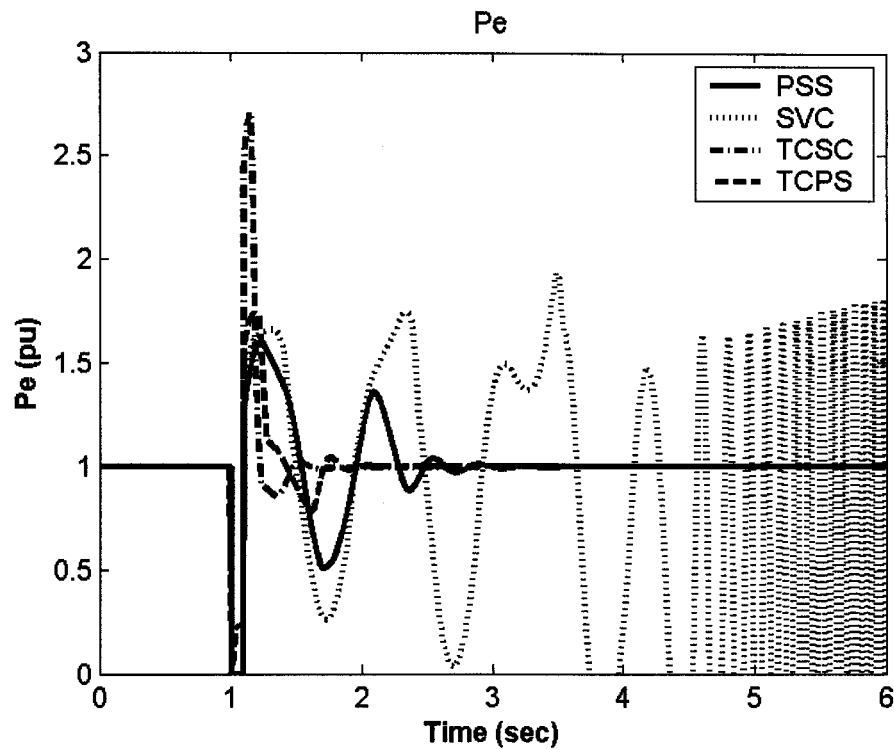


Figure 7.57: Electrical power response for 6-cycle fault with nominal loading, J_2 settings, multiple-point tuning, individual design

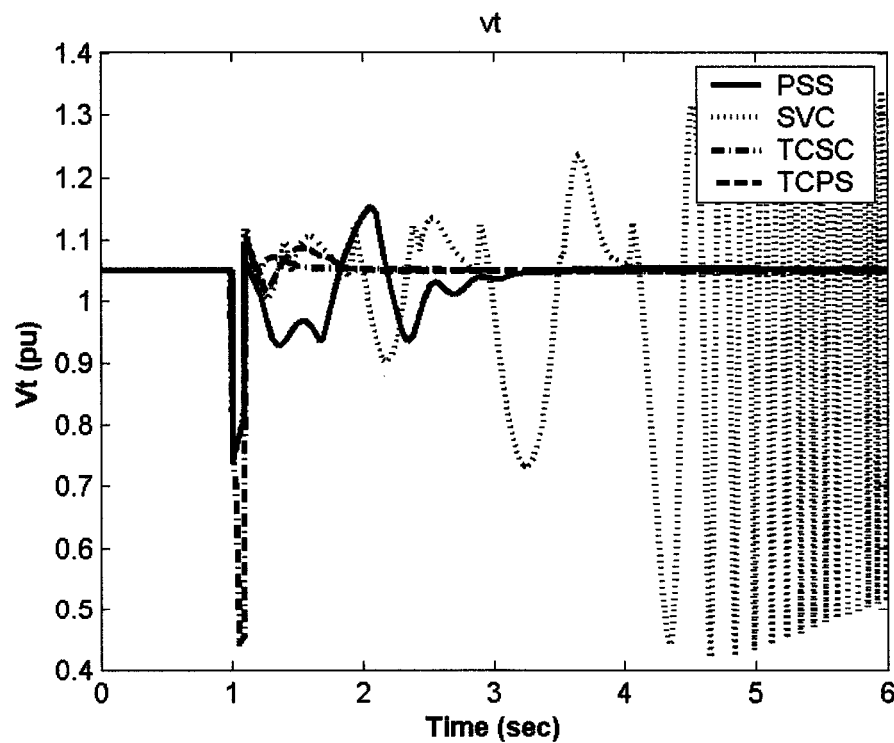


Figure 7.58: Terminal voltage response for 6-cycle fault with nominal loading, J_2 settings, multiple-point tuning, individual design

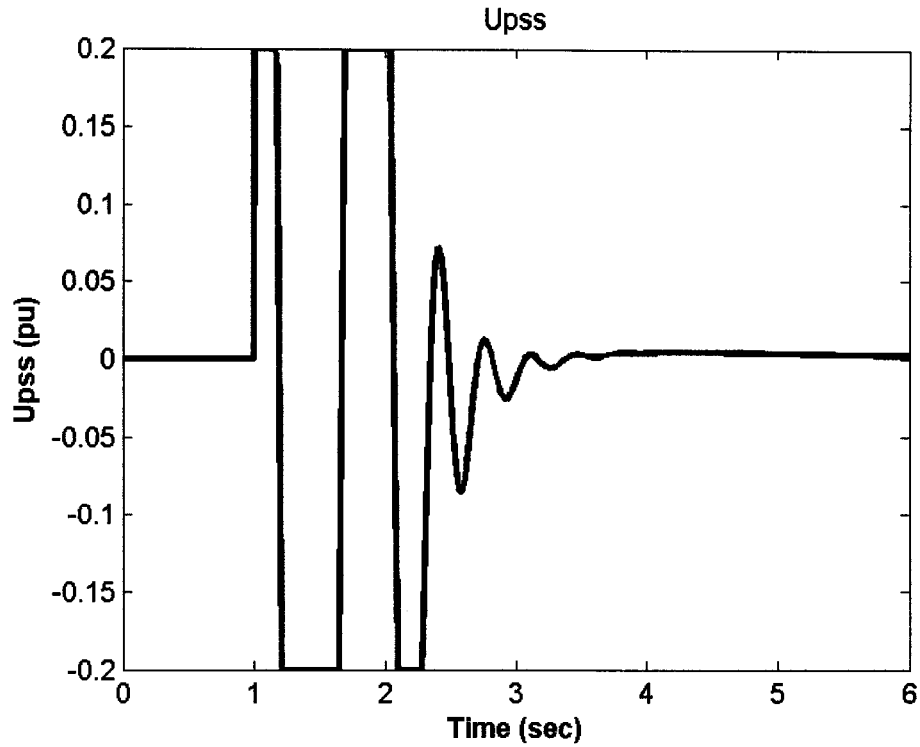


Figure 7.59: PSS stabilizing signal for 6-cycle fault with nominal loading, J_2 settings, multiple-point tuning, individual design

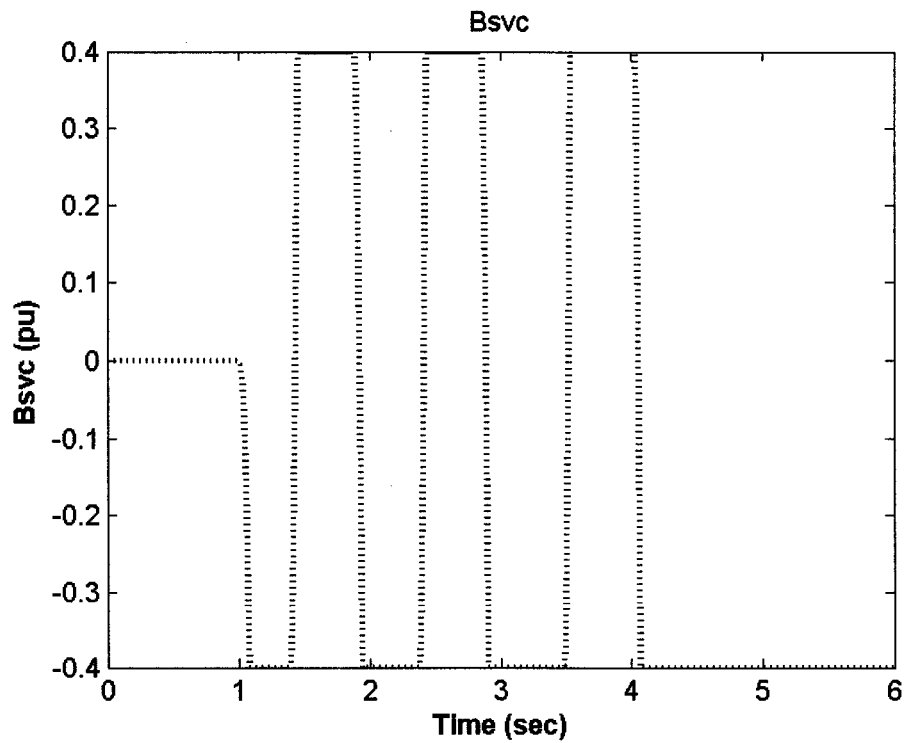


Figure 7.60: B_{svc} response for 6-cycle fault with nominal loading, J_2 settings, multiple-point tuning, individual design

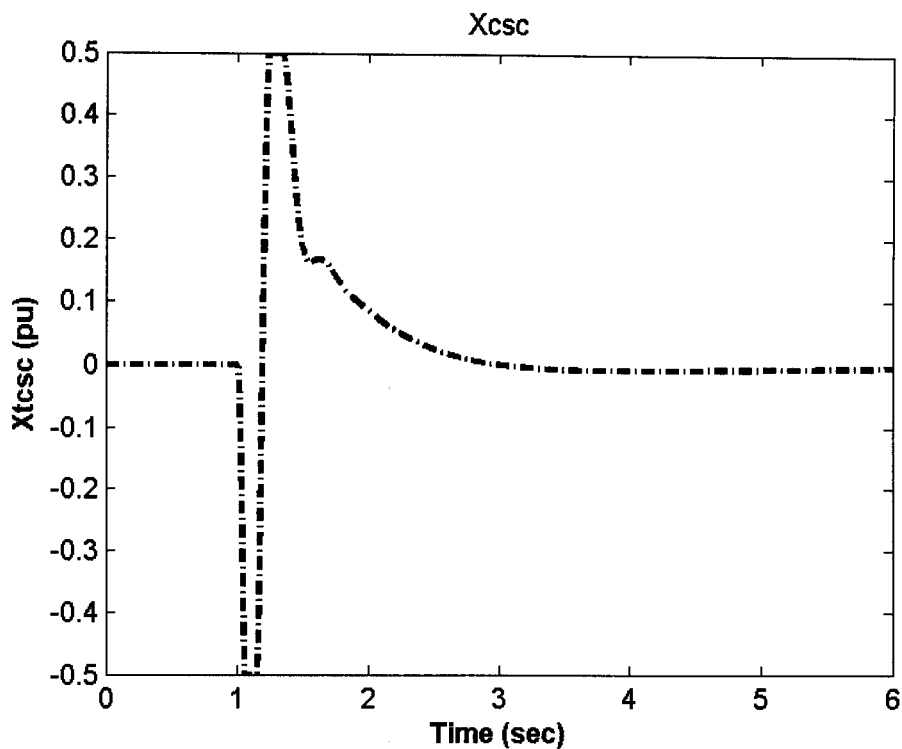


Figure 7.61: X_{tpsc} response 6-cycle fault with nominal loading, J_2 settings, multiple-point tuning, individual design

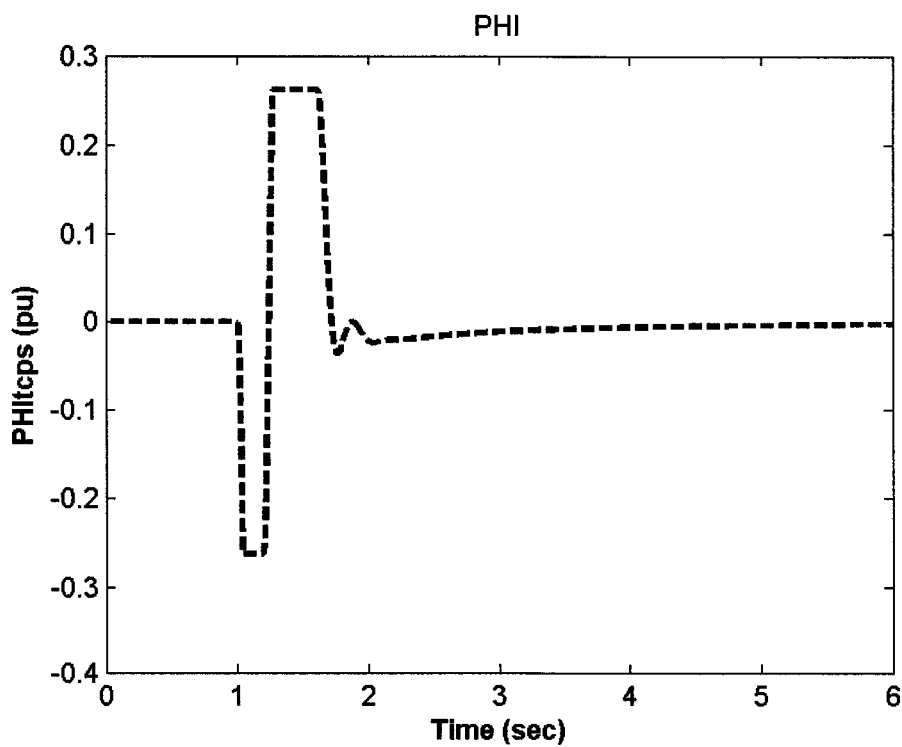


Figure 7.62: Φ_{tpsc} response 6-cycle fault with nominal loading, J_2 settings, multiple-point tuning, individual design

7.2.2.3 Coordinated Design with J_1

The controllability measure analysis based on the singular value decomposition and the damping torque coefficient analyses indicate that the PSS and TCSC-based stabilizer do not perform well individually. These two stabilizers have poor capabilities in controlling the EM mode at light loading. The same conclusion can be drawn from nonlinear time-domain simulations illustrated previously. In this section, the coordinated design of PSS and TCSC-based stabilizer is carried out considering all the 16 operating points mentioned earlier.

Stabilizer Design: PSO is used to simultaneously search for the optimum parameter settings of both controllers that maximizes the minimum damping ratios of all the system complex eigenvalues at all the 16 operating points. The final settings of the optimized parameters for the proposed stabilizers are given in Table 7.29.

Eigenvalue Analysis: The system eigenvalues without and with the proposed PSS and TCSC-based controllers when applied individually and through coordinated design at the four loading conditions, nominal, light, heavy, and leading Pf, are given in Tables 7.30-7.33, respectively. The bold rows of these tables represent the EM mode eigenvalue and its damping ratio.

Table 7.29: Optimal parameter settings with J_1 , multiple-point tuning, coordinated design

	Individual		Coordinated	
	PSS	TCSC	PSS	TCSC
K	19.582	9.7630	57.509	58.015
T₁	4.3897	3.4177	1.7179	1.1088
T₂	0.0100	0.8224	0.9825	0.0813
T₃	0.1601	3.2050	1.4656	0.9778
T₄	1.8253	0.8392	2.2942	3.4338

Table 7.30: System eigenvalues of nominal loading conditions with J_1 settings,
multiple-point tuning, coordinated design

No Control	PSS	TCSC	PSS & TCSC
0.5255±6.5919i,	-3.2124±	-1.2994±	-6.0024±
-0.0795	3.4158i, 0.6900	2.1131i, 0.5238	6.4575i, 0.6808
-10.6940±	-5.8100±	-10.209±	-14.1627±
5.6612i	14.8000i	17.194i	20.627i
--	-102.23	-11.0406	-9.1850
--	-0.2000	-7.8146	-2.9508
--	-0.6200	-0.8735	-1.2001
--	--	-0.2001	-0.2000
--	--	--	-0.2322
--	--	--	-0.2631
--	--	--	-0.4209

Table 7.31: System eigenvalues of light loading conditions with J_1 settings, multiple-point
tuning, coordinated design

No Control	PSS	TCSC	PSS & TCSC
0.0382±0.3601i,	-2.0575±	2.7088±	-3.2414±
-0.0060	5.9049i, 0.3300	5.7479i, 0.4263	6.6229i, 0.4396
-10.2067±	-7.7100±	-10.206±	-16.436± 9.3773i
6.3849i	9.1400i	6.5901i	-6.6224± 5.1904i
--	-100.77	-13.803	-1.0600
--	-0.2000	-2.1523	-0.2846
--	-0.5700	-0.9596	-0.2000
--	--	-0.2000	-0.2082
--	--	--	-0.4305

Table 7.32: System eigenvalues of heavy loading conditions with J_1 settings, multiple-point tuning, coordinated design

No Control	PSS	TCSC	PSS & TCSC
0.6384±6.0839i,	-2.9002±	-0.7226±	-3.1696±
-0.1044	3.4982i, 0.6400	1.7171i, 0.3879	1.5142i, 0.9023
-10.807±	-6.1900±	-10.512±	-14.718±
5.9347i	14.1400i	17.774i	22.154i
--	-102.08	-9.7260±	-8.3436±
--	-0.2000	6.3736i	8.0176i
--	-0.6200	-0.8229	-0.2453±
--	--	-0.2002	0.0253i
--	--	--	-1.2084
--	--	--	-0.2000
--	--	--	-0.4209

Table 7.33: System eigenvalues of leading Pf loading conditions with J_1 settings, multiple-point tuning, coordinated design

No Control	PSS	TCSC	PSS & TCSC
0.2182±6.6656i,	-3.3123±	-1.8696±	-4.1387±
-0.0327	3.5537i, 0.6800	3.8811i, 0.4340	7.6969i, 0.4736
-10.387±	-5.8500±	-9.8230±	-13.685±15.684i
5.6970i	14.1100i	14.045i	-14.0020
--	-101.96	-16.2547	-2.8427
--	-0.2000	-2.1598	-1.1693
--	-0.6100	-0.9448	-0.2807
--	--	-0.2001	-0.2000
--	--	--	-0.2175
--	--	--	-0.4221

Damping Torque Coefficient Analysis: To measure the effectiveness of the proposed PSS-TCSC coordinated design in improving the system damping characteristics and compare it with both individual designs, the damping torque coefficient K_d is estimated. K_d is calculated for a range of 45 operating points specified by $P_e=[0.05 - 1.45]$ pu in steps of 0.10 pu and $Q_e=[-0.40, 0.00, 0.40]$ pu.

For comparison purposes, the damping torque coefficient for the coordinated PSS-TCSC stabilizer design and the both individual designs at $Q=-0.4$, $Q=0.0$, and $Q=0.4$ pu are shown in Figures 7.63-7.65, respectively. These figures point out the effectiveness of the coordinated design, as compared with the PSS and TCSC individual designs, over the different loading conditions.

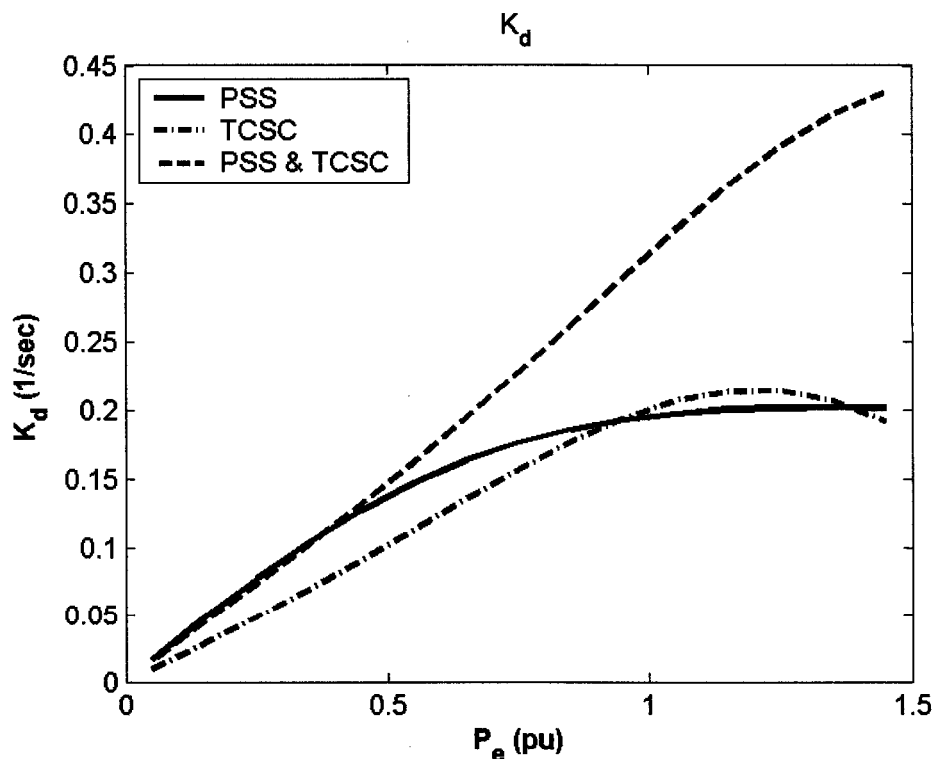


Figure 7.63: Damping torque coefficient with coordinated PSS & TCSC-based controller at $Q = -0.4$ pu, J_1 settings, multiple-point tuning

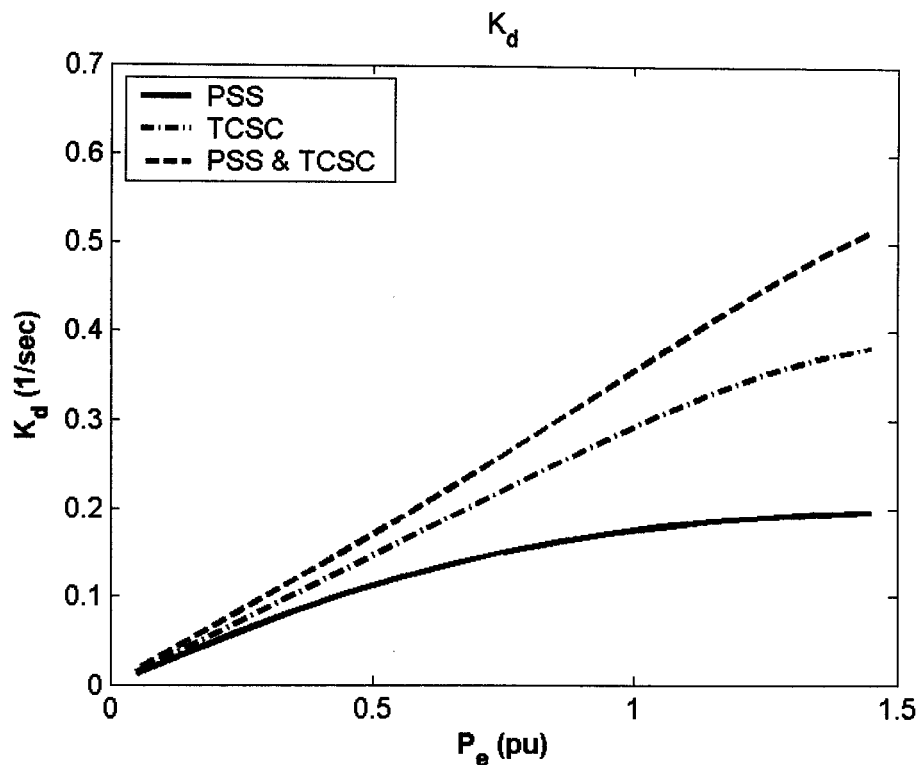


Figure 7.64: Damping torque coefficient with coordinated PSS & TCSC-based controller at $Q = 0.0$ pu, J_1 settings, multiple-point tuning

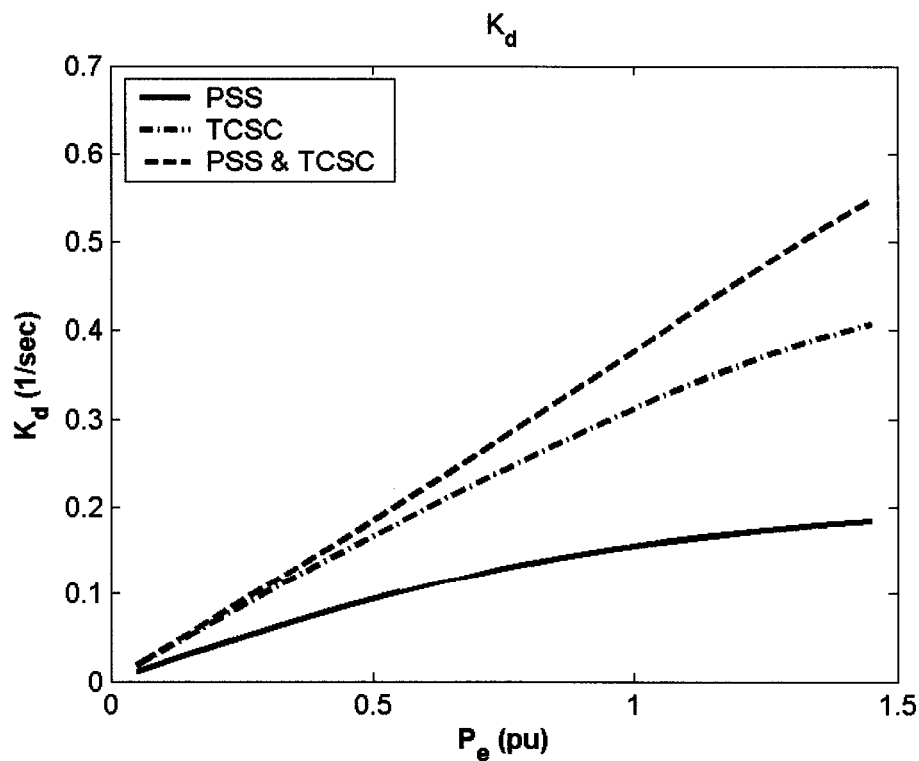


Figure 7.65: Damping torque coefficient with coordinated PSS & TCSC-based controller at $Q = 0.4$ pu, J_1 settings, multiple-point tuning

Nonlinear Time-Domain Simulations: The rotor angle, speed deviation, electrical power, and machine terminal voltage responses for a 6-cycle three-phase fault at the nominal loading conditions are shown in Figures 7.66-7.69, respectively. Figure 7.70 and Figure 7.71 show the control effort provided by the stabilizing signal of PSS, U_{PSS} , the reactance of TCSC, X_{TCSC} , when applied individually and through coordinated design.

In a similar manner, the simulation results with a 6-cycle three-phase fault at light loading condition are shown in Figures 7.72-7.75. The control signals of the two stabilizers are given in Figure 7.76 and Figure 7.77. The simulation results obtained indicate that the proposed coordinated PSS-TCSC design is more effective than both the individual designs.

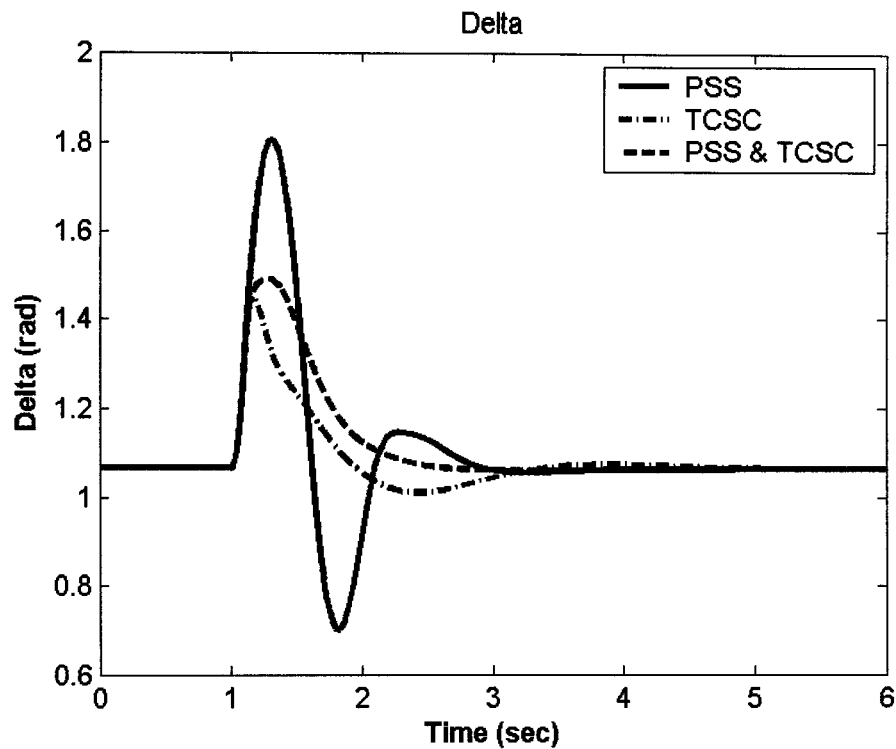


Figure 7.66: Rotor angle response for 6-cycle fault with nominal loading, J_1 settings, multiple-point tuning, coordinated design

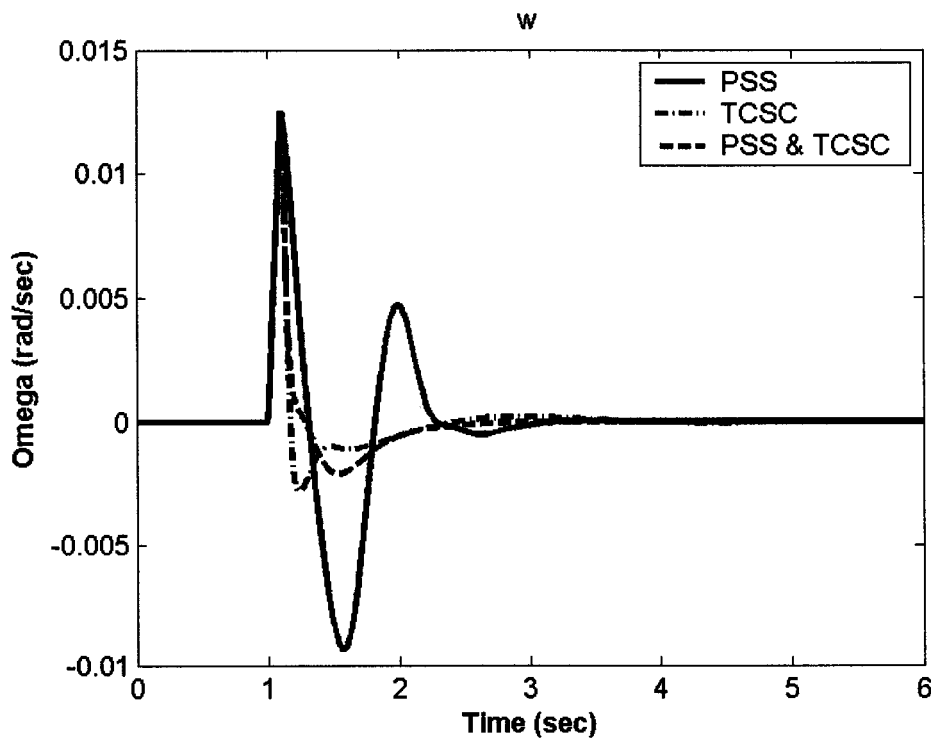


Figure 7.67: Speed response for 6-cycle fault with nominal loading, J_1 settings, multiple-point tuning, coordinated design

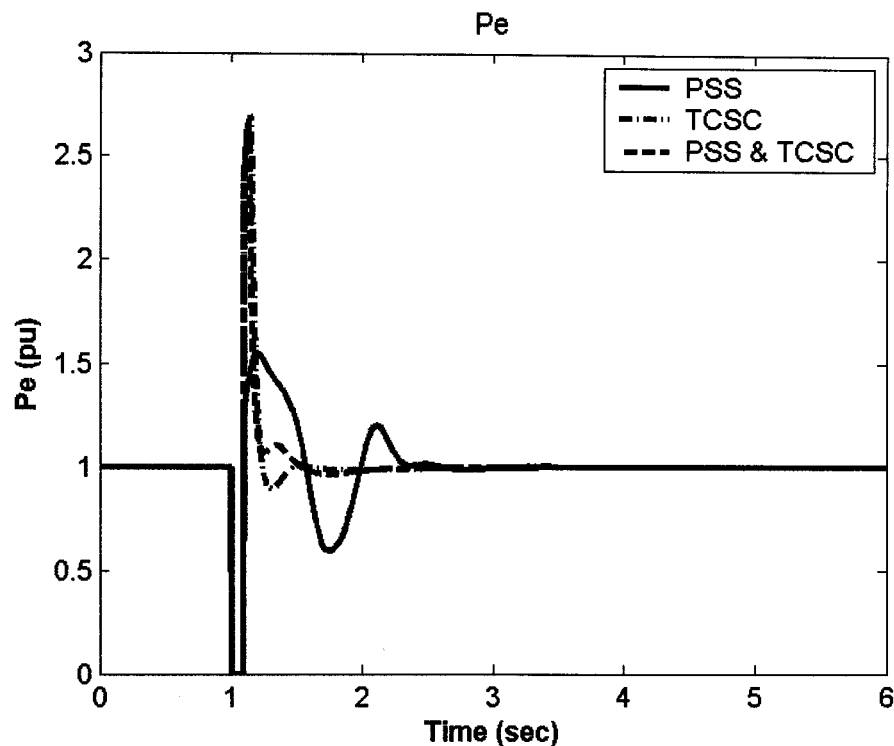


Figure 7.68: Electrical power response for 6-cycle fault with nominal loading, J_1 settings, multiple-point tuning, coordinated design

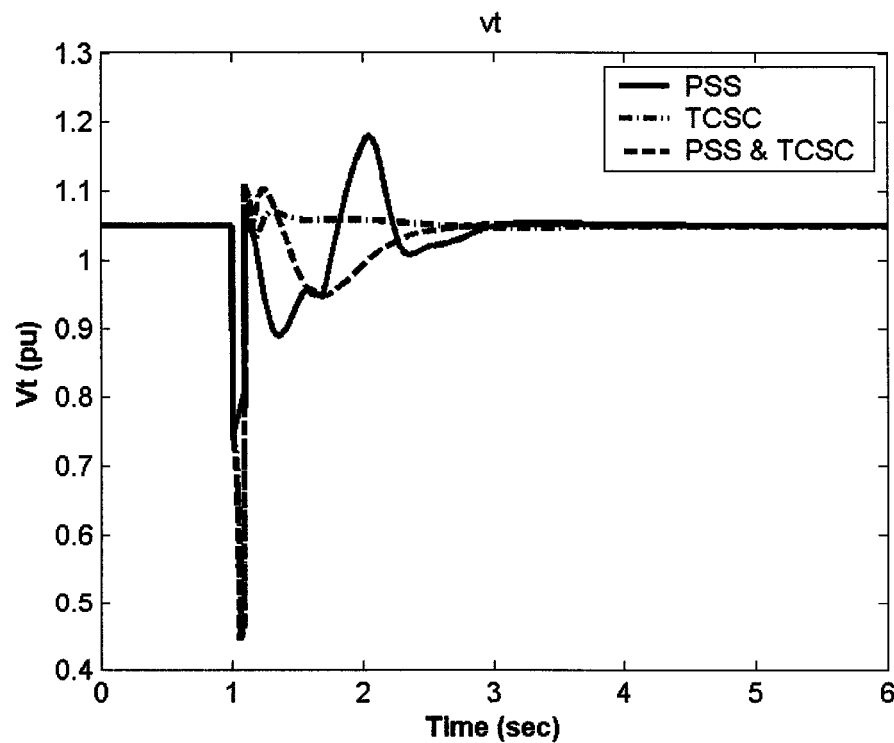


Figure 7.69: Terminal voltage response for 6-cycle fault with nominal loading, J_1 settings, multiple-point tuning, coordinated design

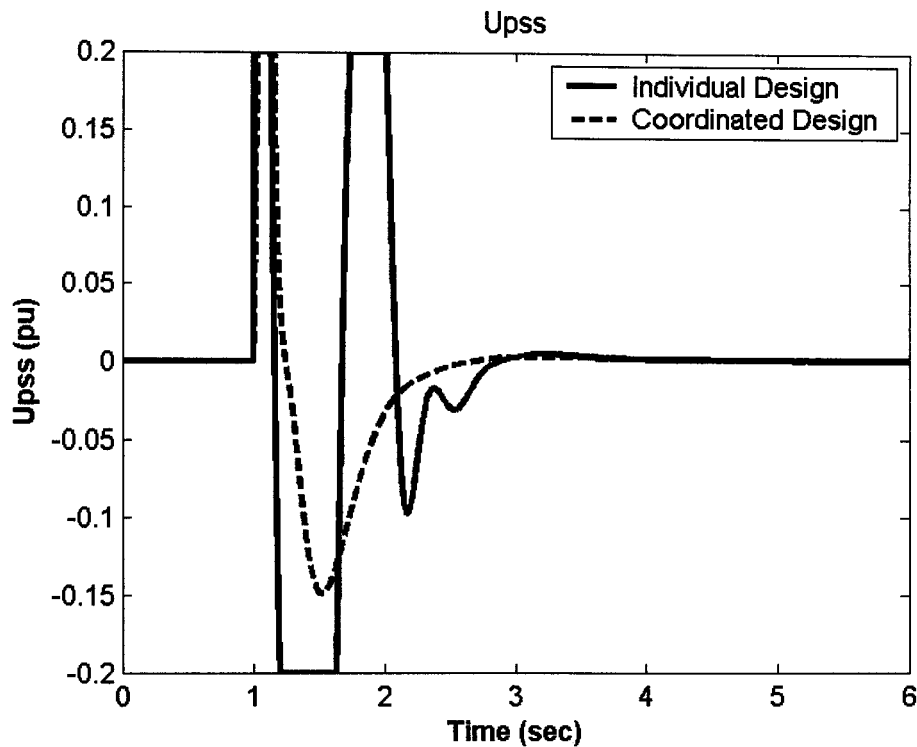


Figure 7.70: PSS stabilizing signal for 6-cycle fault with nominal loading, J_1 settings, multiple-point tuning, coordinated design

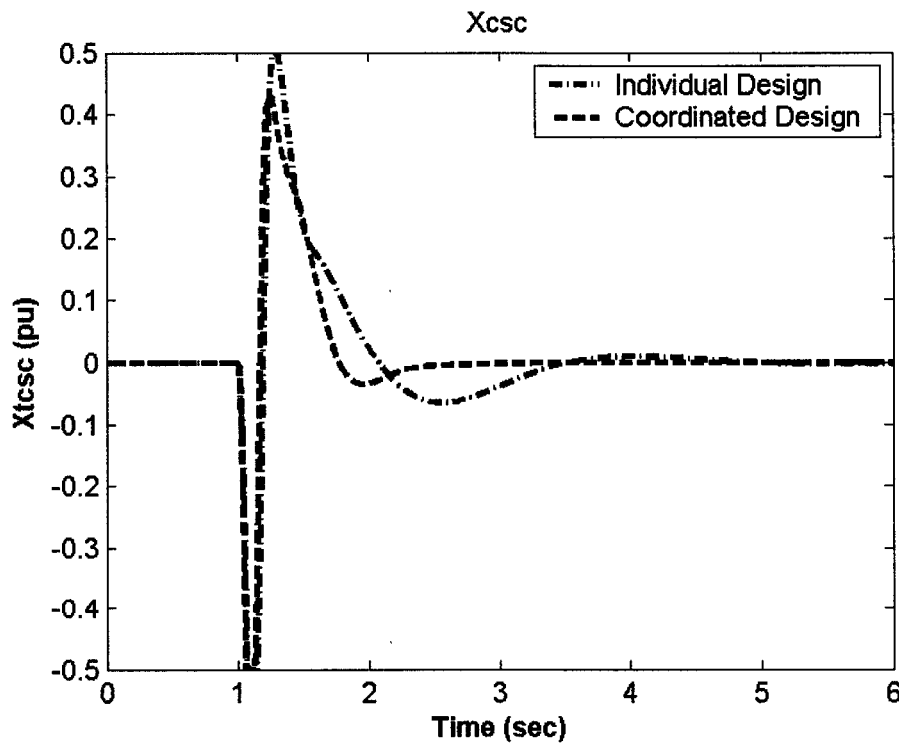


Figure 7.71: X_{tcsc} response 6-cycle fault with nominal loading, J_1 settings, multiple-point tuning, coordinated design

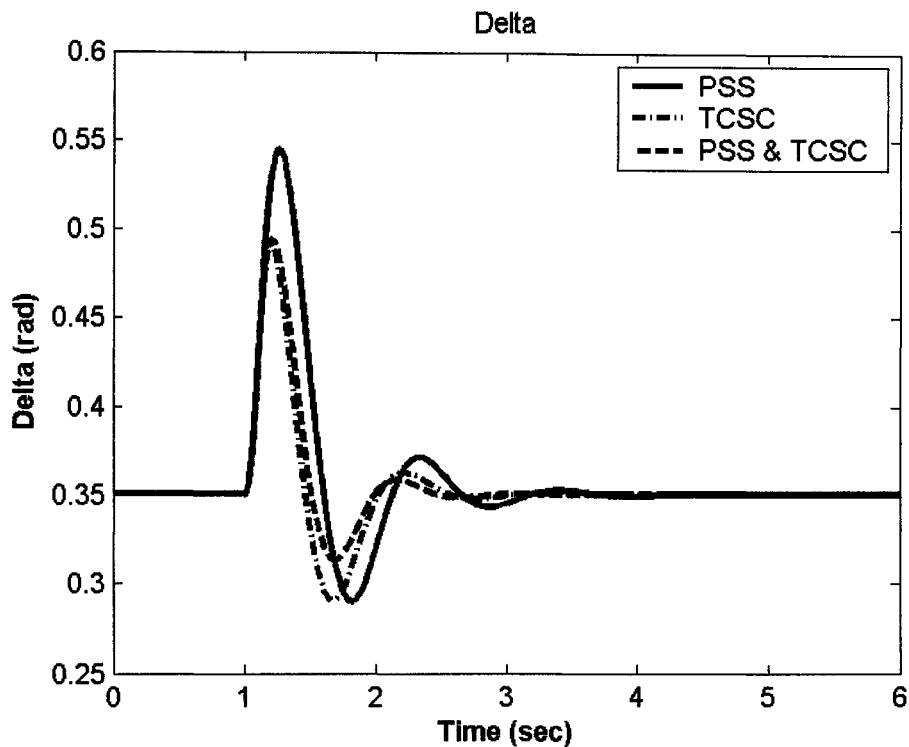


Figure 7.72: Rotor angle response for 6-cycle fault with light loading, J_1 settings, multiple-point tuning, coordinated design

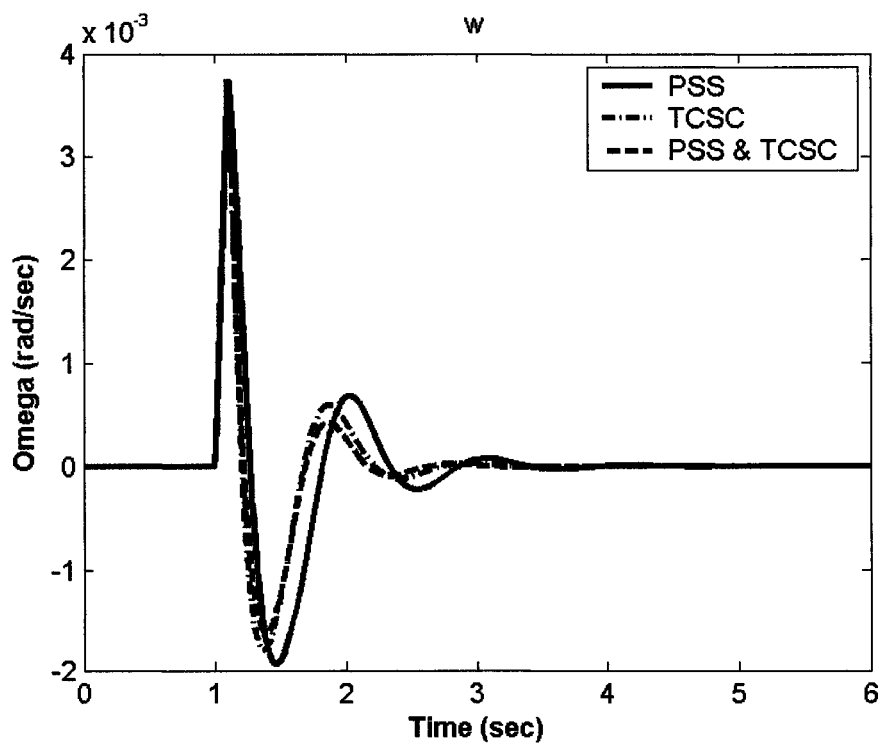


Figure 7.73: Speed response for 6-cycle fault with light loading, J_1 settings, multiple-point tuning, coordinated design

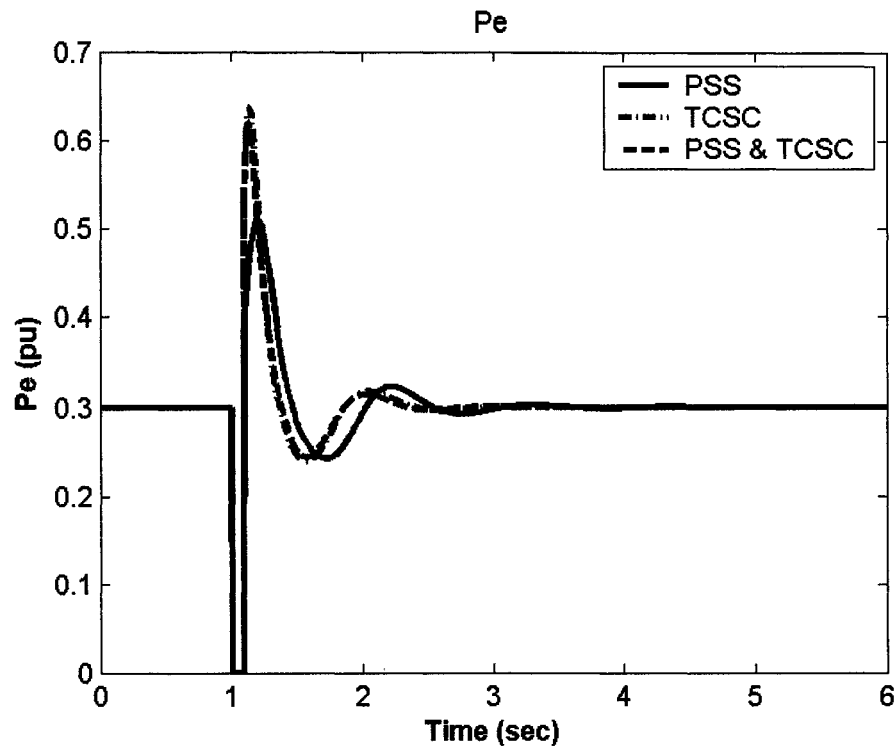


Figure 7.74: Electrical power response for 6-cycle fault with light loading, J_1 settings, multiple-point tuning, coordinated design

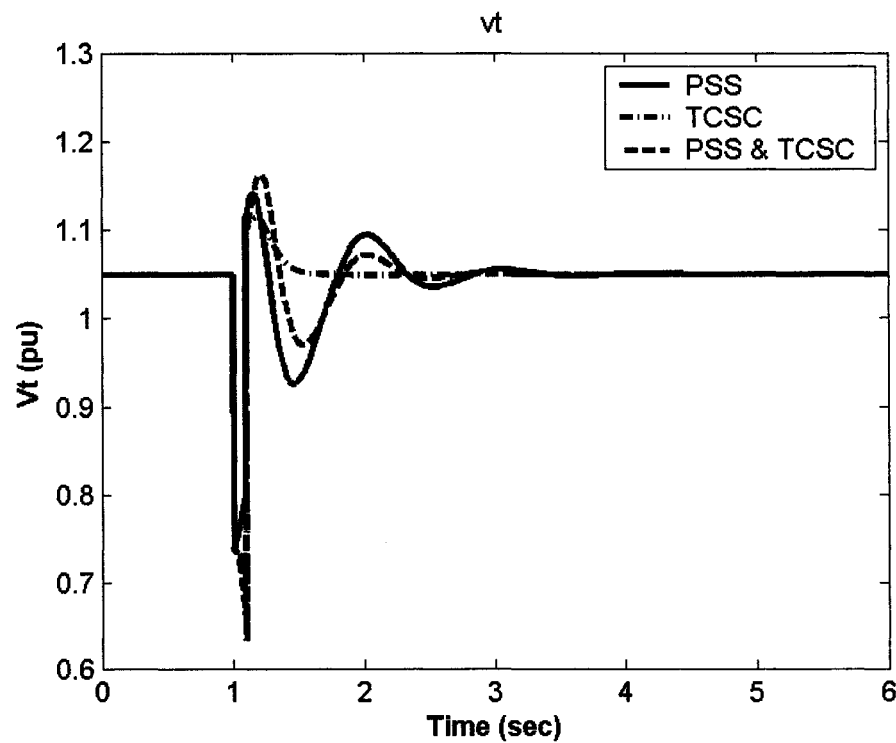


Figure 7.75: Terminal voltage response for 6-cycle fault with light loading, J_1 settings, multiple-point tuning, coordinated design

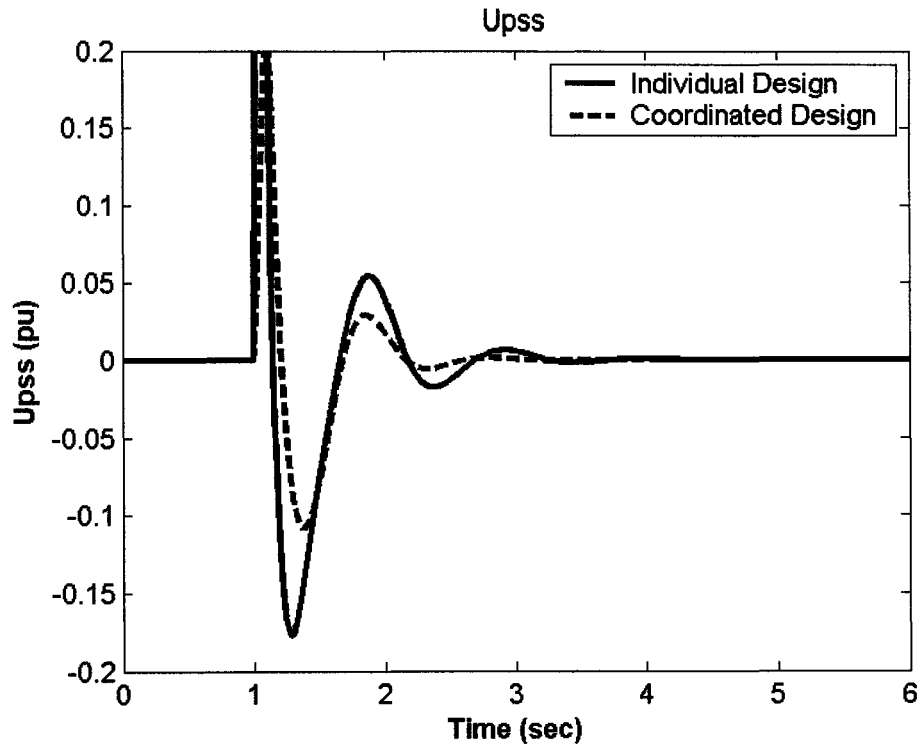


Figure 7.76: PSS stabilizing signal for 6-cycle fault with light loading, J_1 settings, multiple-point tuning, coordinated design

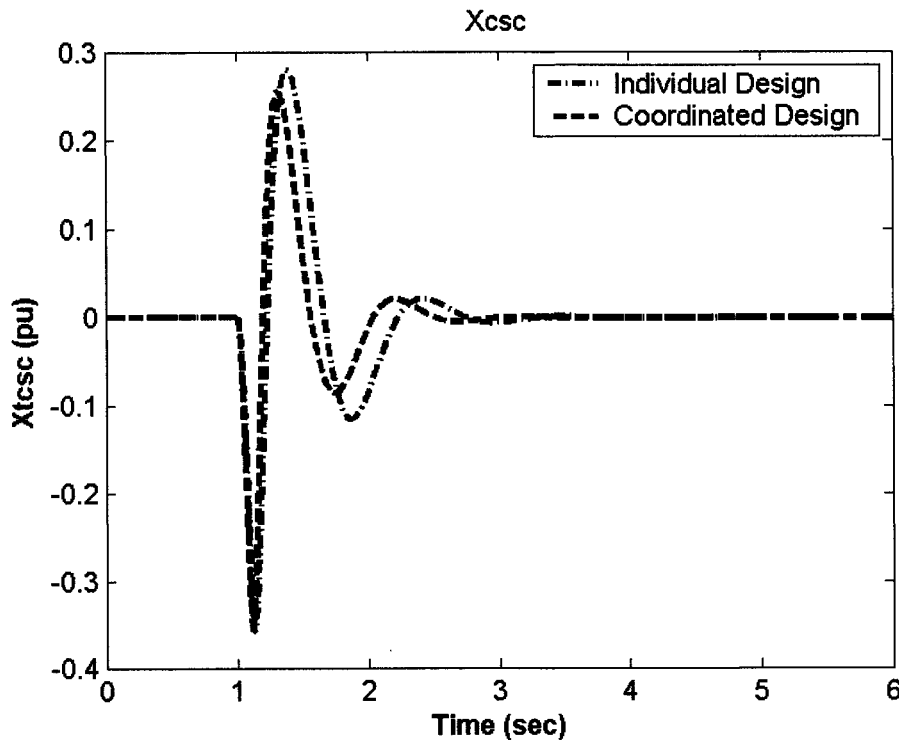


Figure 7.77: X_{tcsc} response 6-cycle fault with light loading, J_1 settings, multiple-point tuning, coordinated design

CHAPTER 8

OPTIMIZATION RESULTS:

UNIFIED POWER FLOW CONTROLLER

8.1 Electromechanical Mode Controllability Measure

SVD is employed to measure the controllability of the electromechanical (EM) mode from the PSS input signal and the four UPFC control signals: m_E , δ_E , m_B , and δ_B . The minimum singular value, σ_{\min} , is estimated over a wide range of operating conditions. For SVD analysis, P_e ranges from 0.05 to 1.4 pu and $Q_e = [-0.4, 0, 0.4]$. At each loading condition, the system model is linearized, the EM mode is identified, and the SVD-based controllability measure is implemented.

For comparison purposes, the minimum singular values for all inputs at $Q_e = -0.4, 0.0$ and 0.4 pu are shown in Figures 8.1-8.3, respectively. From these figures, the following can be noticed:

- The capabilities of the PSS, m_E , m_B , and δ_B to control the EM mode are directly proportional to system loading. However, the δ_E capability of controlling the EM mode is less dependent on loading.
- The controllability of δ_E is generally higher than those of the other stabilizers, especially for low and moderate loading.
- At very low loading, all the stabilizers, except the m_B -based stabilizer at nominal loading and the δ_E -based stabilizer, suffer from poor controllability.
- Both the m_E - and δ_B -based stabilizers have very low control effect on the EM mode

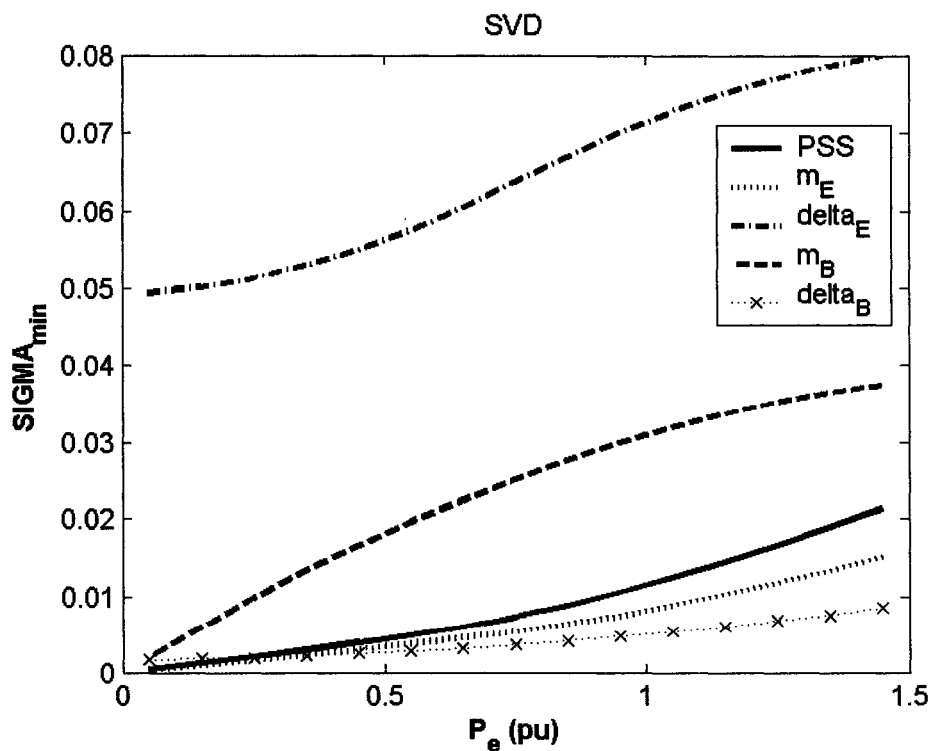


Figure 8.1: Minimum singular value with all controllers at $Q = -0.4$ pu

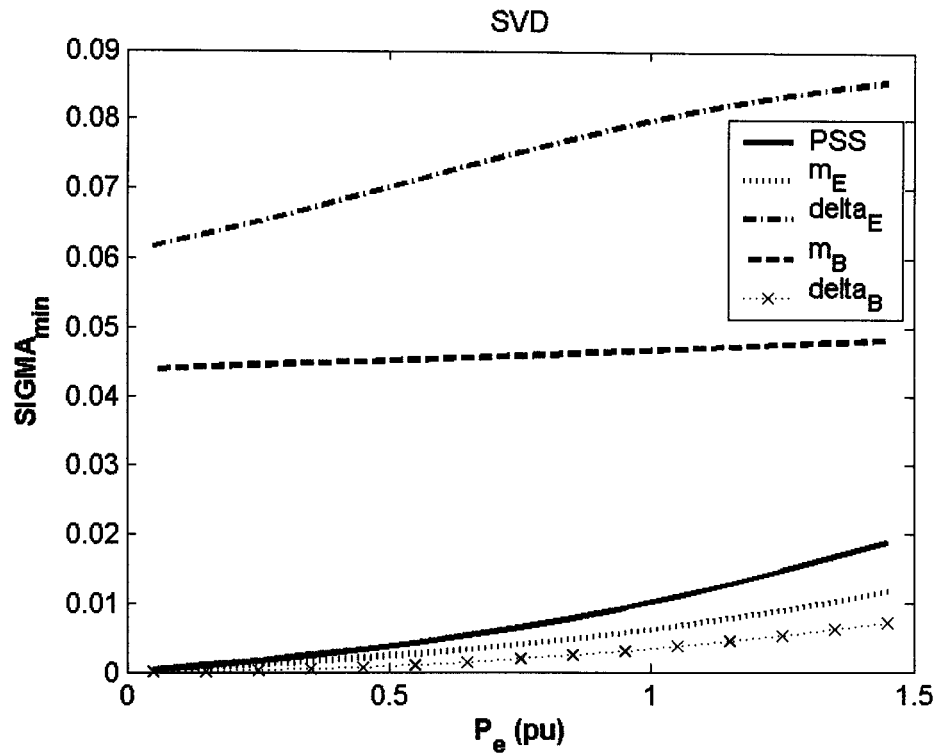


Figure 8.2: Minimum singular value with all controllers at $Q = 0.0$ pu

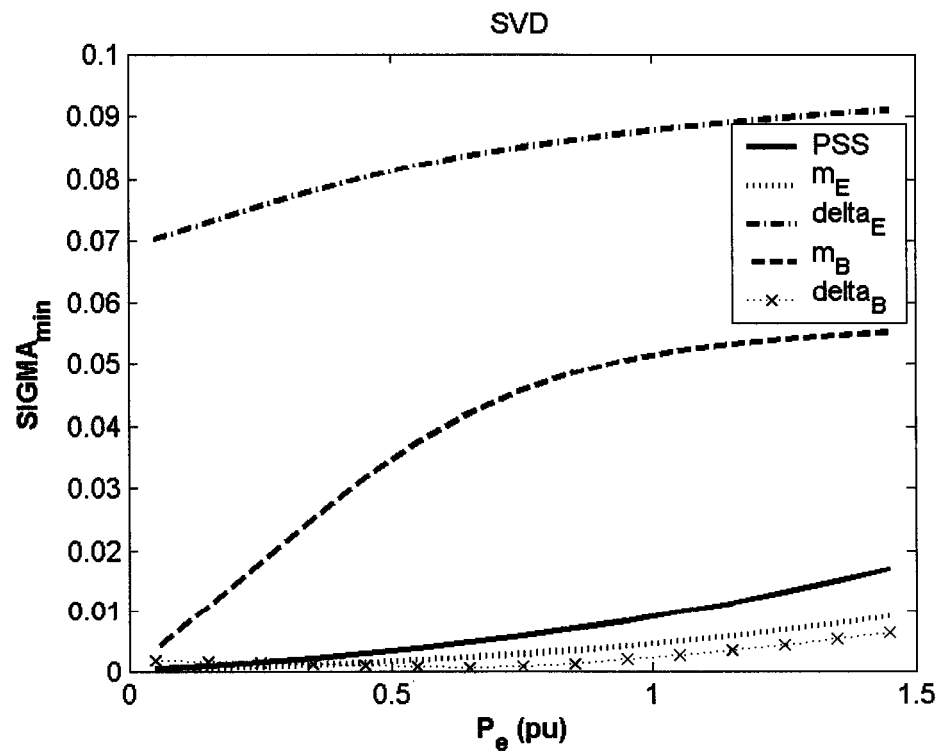


Figure 8.3: Minimum singular value with all controllers at $Q = 0.4$ pu

8.2 Optimization Results for PSS and the UPFC-Based Stabilizers

This chapter presents the optimization results of the two objective functions: J_1 , maximizing the minimum damping ratio, and J_2 , minimizing the maximum damping factor. Both the single-point and multiple-point tuning processes for individual and coordinated designs are considered. The system data is given in Appendix B.

To assess the effectiveness of the proposed controllers, four different loading conditions are considered for eigenvalue analysis. These conditions and disturbances are:

5. Nominal loading (P_e, Q_e)=(1.0,0.015) pu.
6. Light loading (P_e, Q_e)=(0.3,0.015) pu.
7. Heavy loading (P_e, Q_e)=(1.1,0.40) pu.
8. Leading power factor (Pf) loading (P_e, Q_e)=(0.7,-0.3) pu.

Moreover, the nominal and light loading conditions with 6-cycle three-phase fault disturbances are considered for nonlinear time-domain simulations

8.2.1 Single-Point Tuning

In this section, the stabilizers are tuned with only the nominal loading condition, (P_e, Q_e)=(1.0,0.015) pu, taken into account.

8.2.1.1 Individual Design with J_1

The PSS, m_{E^-} , δ_{E^-} , m_{B^-} , and δ_{B^-} -based stabilizers are designed individually considering the nominal loading condition.

Stabilizer Design: PSO is used to search for the optimum parameter settings of each controller that maximizes the minimum damping ratio of all the system complex eigenvalues. The final settings of the optimized parameters for the proposed stabilizers are given in Table 8.1.

Eigenvalue Analysis: The system eigenvalues without and with the proposed stabilizers at the four operating points, nominal, light, heavy, and leading Pf, are given in Tables 8.2-8.5, respectively. The bold rows of these tables represent the EM mode eigenvalue and its damping ratio. These tables clearly demonstrate the effectiveness of the δ_E - and m_B -based stabilizers in enhancing system stability. In addition, It can be observed that, in most cases, the EM mode is either unstable or poorly damped when driven by m_E - or δ_B -based stabilizers. This conclusion is in line with those already drawn from SVD analysis.

Table 8.1: Optimal parameter settings with J_1 , single-point tuning, individual design

	PSS	m_E	δ_E	m_B	δ_B
K	16.9203	-22.706	-100.00	29.062	-42.210
T₁	4.5673	0.2489	0.0637	2.8973	5.0000
T₂	2.0440	0.0100	1.2846	0.9339	3.9351
T₃	0.0835	3.2277	5.0000	0.1039	3.3874
T₄	0.0100	2.0000	1.2242	0.0100	0.1405

Table 8.2: System eigenvalues of nominal loading conditions with J_1 settings,
single-point tuning, individual design

No Control	PSS	m_E	δ_E	m_B	δ_B
1.5033±	-4.7000±	-1.7000±	-4.5833±	-4.1000±	-1.3543±
5.3328i,	6.8700i,	7.6200i,	5.3983i,	6.0700i,	6.0382i,
-0.2713	0.5600	0.2200	0.6472	0.5600	0.2189
-11.4584±	-4.8700±	-1.7300±	-4.7536±	-4.2000±	-1.3999±
6.8596i	7.0400i	8.0000i	5.5795i,	6.2400i	6.2543i
-15.5063	-101.12	-108.67	-15.5062	-93.980	-20.8418±
-5.1052	-15.340	-25.090	-5.1355	-28.950	8.0590i
--	-4.8700	-14.760	-2.2236	-15.530	-15.3214
--	-0.5500	-5.1300	-0.5777	-5.1300	-5.1253
--	--	-0.5100	-20.000	-1.4000	-0.2542

Table 8.3: System eigenvalues of light loading conditions with J_1 settings, single-point
tuning, individual design

No Control	PSS	m_E	δ_E	m_B	δ_B
1.3952±	0.2800±	0.9000±	-3.1531±	-3.2300±	1.3102±
5.0825i,	5.500i,	5.3700i,	5.8779i,	6.4500i,	5.1241i,
-0.2647	-0.0500	-0.1700	0.4727	0.4500	-0.2477
-11.3641±	-9.8300±	-8.1500±	-6.1133±	-5.0400±	-10.1481±
6.1234i,	6.3400i	7.9800i	3.4308i	4.8700i	3.8787i
-14.7072	-100.38	-101.83	-14.7071	-94.860	-18.7125
-5.8534	-14.760	-23.370	-6.0338	-28.180	-14.2614
--	-6.2400	-15.080	-2.2360	-14.710	-11.2363
--	-0.5100	-5.7100	-0.5841	-5.8400	-5.7296
--	--	-0.5000	-20.000	-1.4500	-0.2541

Table 8.4: System eigenvalues of heavy loading conditions with J_1 settings, single-point tuning, individual design

No Control	PSS	m_E	δ_E	m_B	δ_B
1.4138±	-2.6900±	0.0600±	-4.0817±	-4.6500±	-1.7635±
5.0066i,	4.2600i,	7.0300i,	8.2789i,	2.5400i,	5.4534i,
-0.2718	0.5300	-0.0100	0.4422	0.8800	0.3077
-11.4375±	-5.2400±	-2.3900±	-1.8270±	-3.5800±	-21.307±
6.1904i	8.6400i	8.0000i	1.7074i	8.2600i	7.2425i
-15.2584	-101.04	-111.43	-15.258	-93.880	-0.4741±
-5.2121	-15.510	-23.140	-8.6979	-29.570	6.3175i
--	-8.0500	-16.310	-5.7725	-15.280	-15.559
--	-0.5400	-4.9600	-0.5672	-4.6700	-4.9864
--	--	-0.5100	-20.000	-1.7100	-0.2542

Table 8.5: System eigenvalues of leading Pf loading conditions with J_1 settings, single-point tuning, individual design

No Control	PSS	m_E	δ_E	m_B	δ_B
1.4502±	-7.9800±	-0.8200±	-1.9680±	-1.2100±	-0.2416±
5.3584i,	7.2500i,	6.3300i,	5.4901i	5.7900i	5.5654i,
-0.2612	0.7400	0.1300	0.3374	0.2000	0.0434
-11.3963±	-2.2200±	-4.6800±	-7.5894±	-7.3600±	-3.4502±
7.0920i	7.1200i	9.0000i	6.4238i	6.7800i	6.5772i
-15.4566	-100.98	-103.76	-15.456	-95.430	-19.907±
-5.1711	-15.090	-26.720	-5.1500	-26.760	7.9932i
--	-3.9800	-13.610	-1.8127	-15.640	-15.1470
--	-0.5500	-5.4200	-0.5816	-5.3600	-5.2924
--	--	-0.5100	-20.000	-1.2600	-0.2542

Damping Torque Coefficient Analysis: To quantitatively measure the effectiveness of the proposed PSS and the four UPFC-based stabilizers in enhancing the system damping characteristics, the damping torque coefficient K_d is calculated. The damping torque coefficient K_d is estimated for each stabilizer over a wide range of loading conditions. Specifically, K_d is calculated for a range of 45 operating points specified by $P_e=[0.05 - 1.45]$ pu in steps of 0.10 pu and $Q_e=[-0.40, 0.00, 0.40]$ pu.

For comparison purposes, K_d for all stabilizers at $Q=-0.4$, $Q=0.0$, and $Q=0.4$ pu are shown in Figures 8.4, 8.5, and 8.6, respectively. These figures demonstrate the following:

- At low and moderate loading, the δ_E -based stabilizer outperforms the other stabilizers. However, at nominal and high loading the PSS becomes more effective.
- Generally, the damping torques supplied by m_E and δ_B are either negative or very low positive quantities.
- The PSS and m_B suffer from negative damping characteristics at light loading.
- The damping torque coefficients of the m_B -based stabilizer at nominal loading and δ_E -based stabilizer are almost unaffected by loading level.
- The damping torque coefficients K_d associated with the PSS and m_B -based stabilizers are directly proportional to system loading.
- The PSS is more effective at leading power factor conditions, whereas the δ_E and m_B are least effective at this power factor conditions.

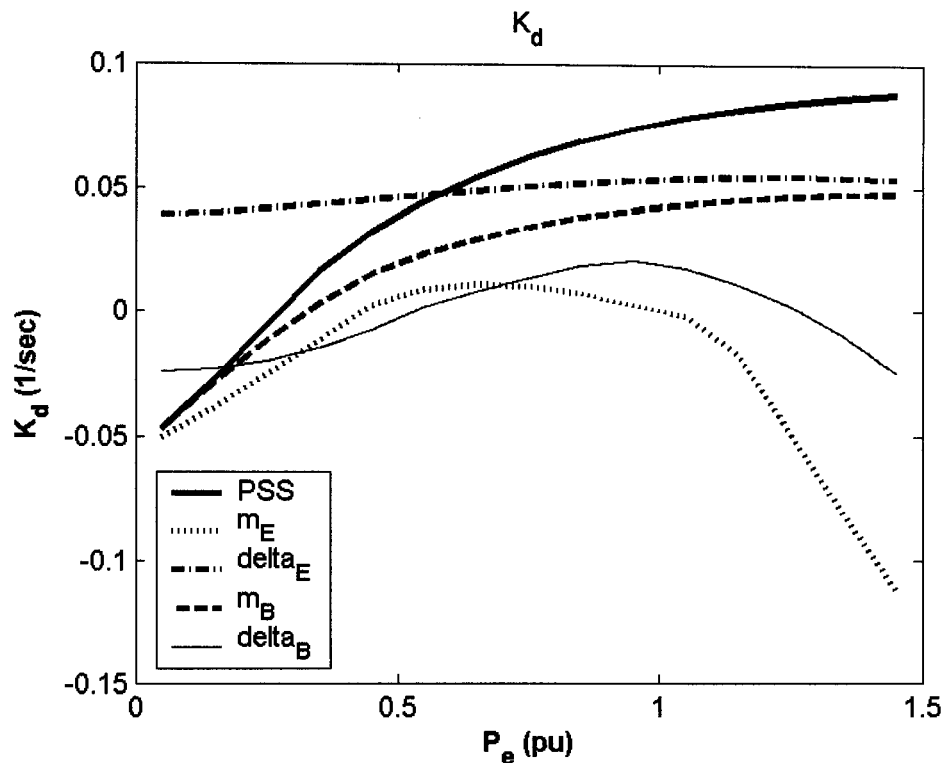


Figure 8.4: Damping torque coefficient with the proposed controllers at $Q = -0.4$ pu, J_1 settings, single-point tuning, individual design

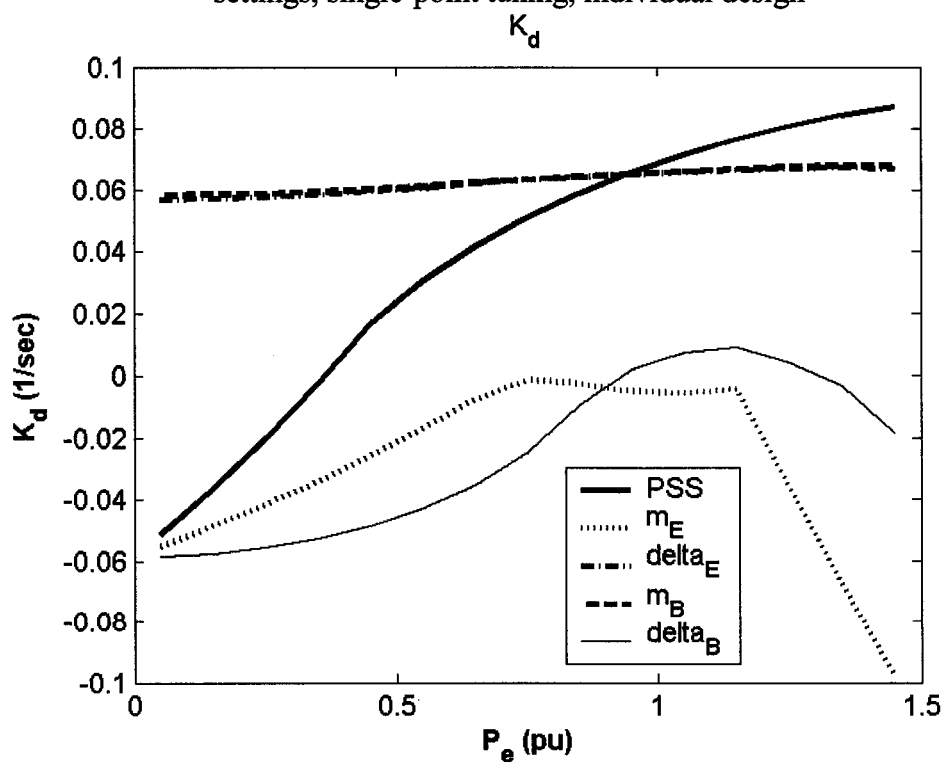


Figure 8.5: Damping torque coefficient with the proposed controllers at $Q = 0.0$ pu, J_1 settings, single-point tuning, individual design

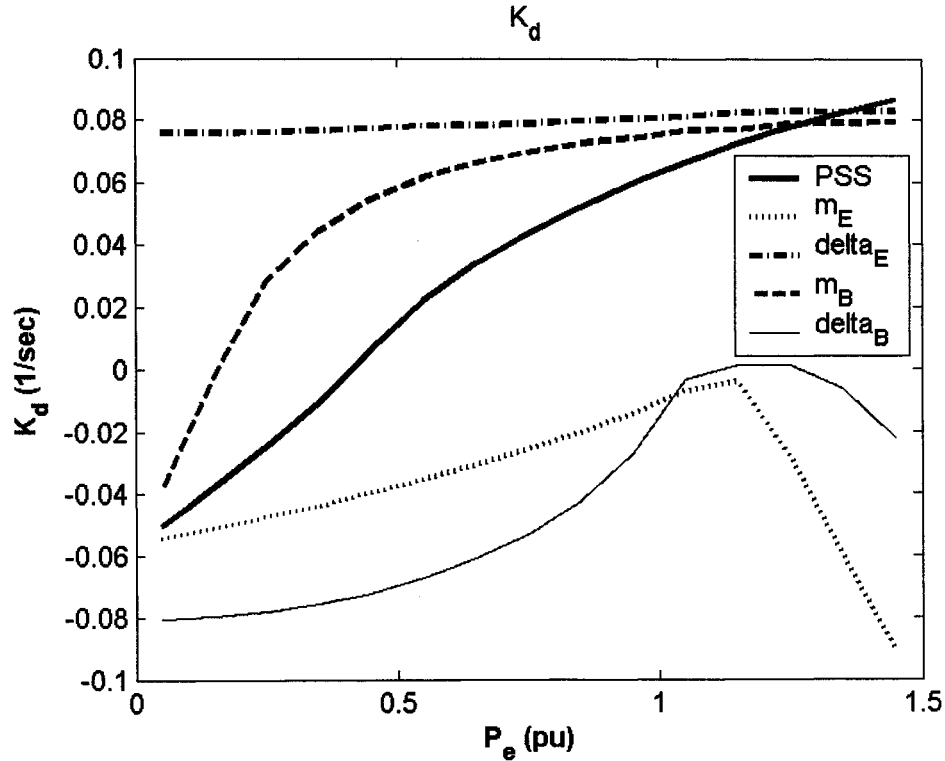


Figure 8.6: Damping torque coefficient with the proposed controllers at $Q = 0.4$ pu, J_1 settings, single-point tuning, individual design

Nonlinear Time-Domain Simulations: Figures 8.7, 8.8, 8.9, 8.10, and 8.11 show the rotor angle, speed deviation, electrical power, machine terminal voltage, and UPFC capacitor DC voltage responses, respectively, for a 6-cycle three-phase fault at the nominal loading conditions. The system responses due to the m_E - and δ_B -based stabilizers are not shown because they result in unstable responses. It can be readily seen that the PSS and δ_E are more effective than the m_B in terms of reduction of overshoot and settling time. This is consistent with damping torque coefficient analysis results. Figures 8.12, 8.13, and 8.14 show the control effort provided by the stabilizing signal of the PSS, the excitation phase angle modulation, δ_E , and the boosting magnitude modulation, m_B , respectively.

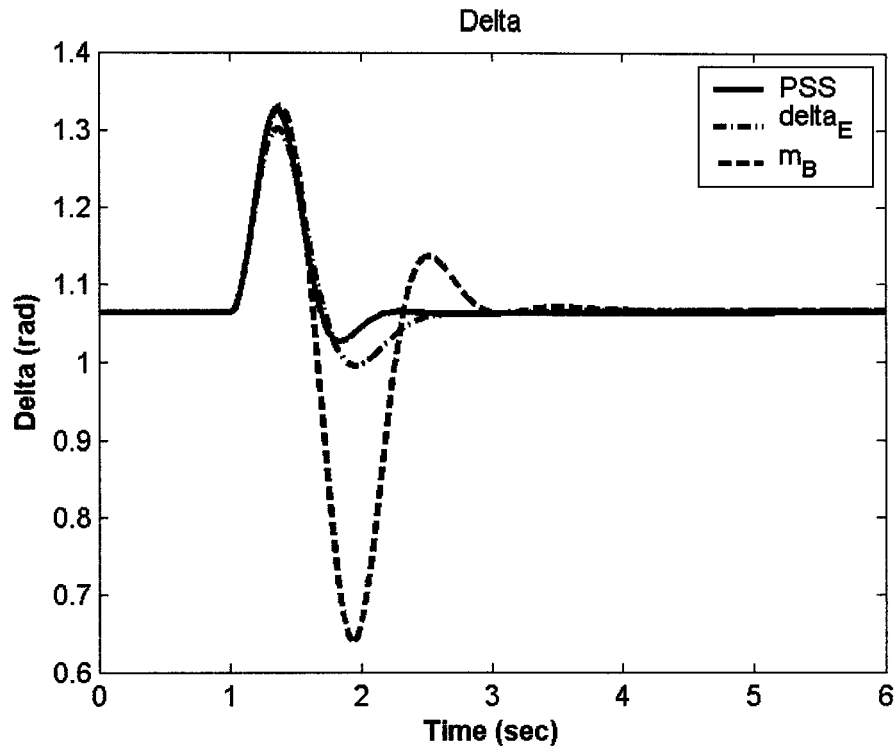


Figure 8.7: Rotor angle response for 6-cycle fault with nominal loading, J_1 settings, single-point tuning, individual design

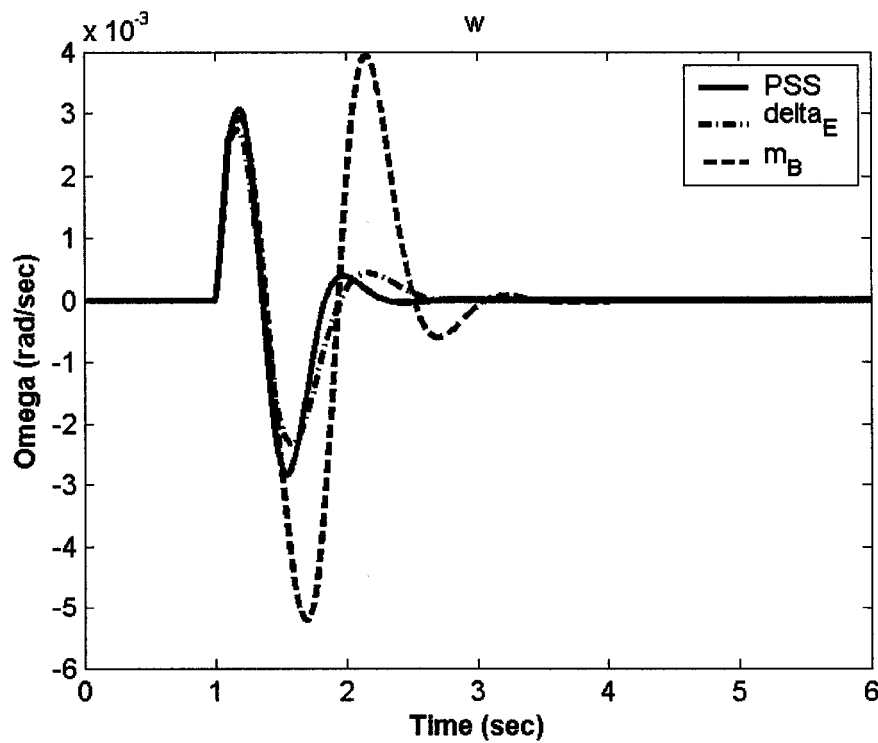


Figure 8.8: Speed response for 6-cycle fault with nominal loading, J_1 settings, single-point tuning, individual design

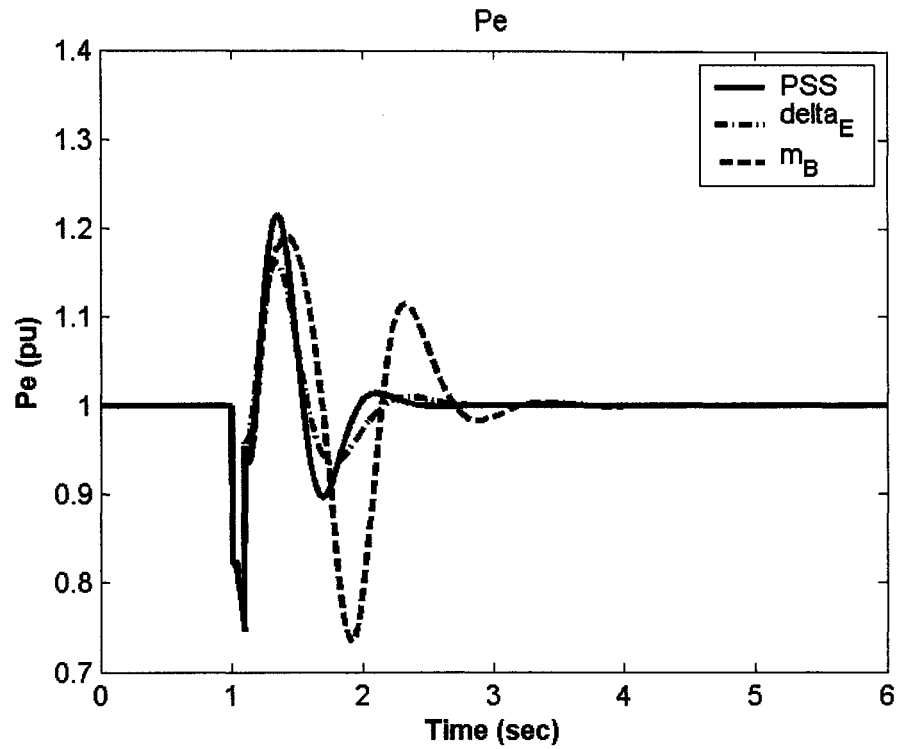


Figure 8.9: Electrical power response for 6-cycle fault with nominal loading, J_1 settings, single-point tuning, individual design

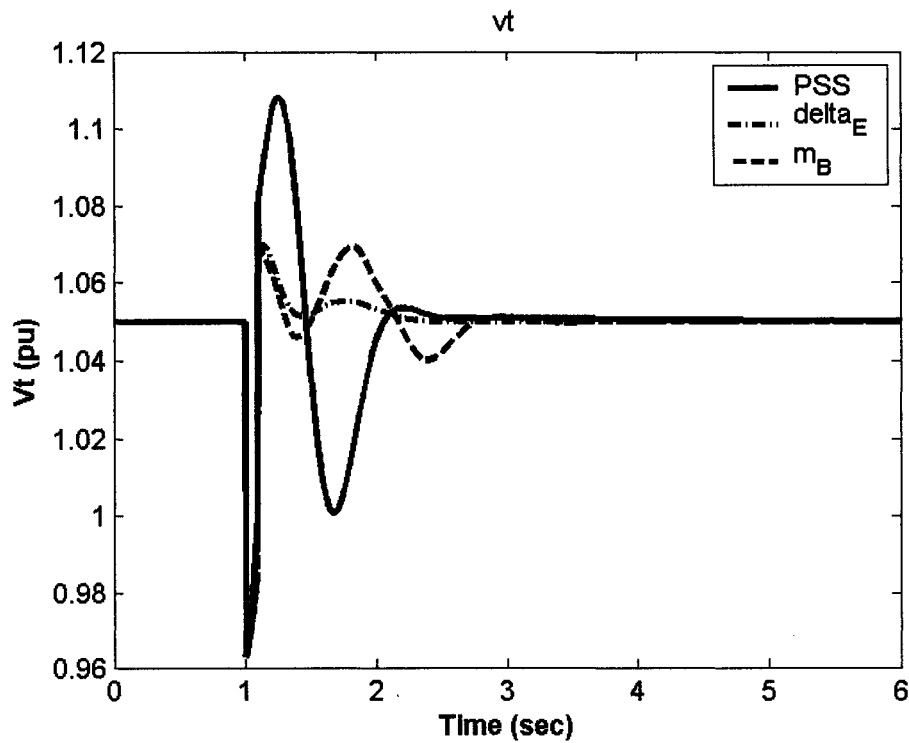


Figure 8.10: Terminal voltage response for 6-cycle fault with nominal loading, J_1 settings, single-point tuning, individual design

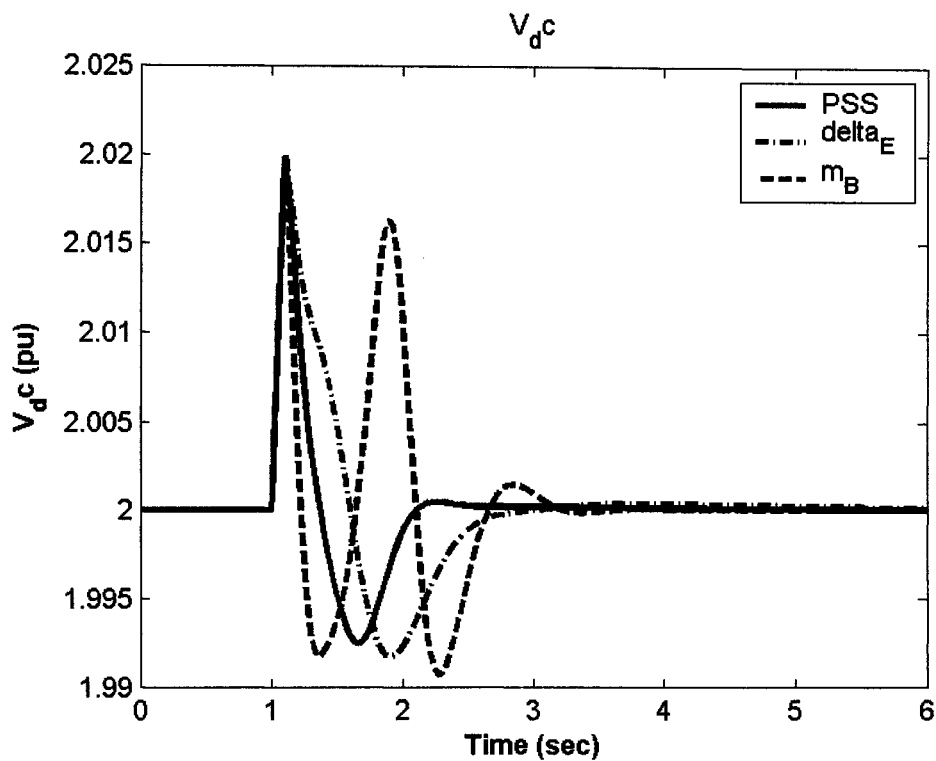


Figure 8.11: DC voltage response for 6-cycle fault with nominal loading, J_1 settings, single-point tuning, individual design

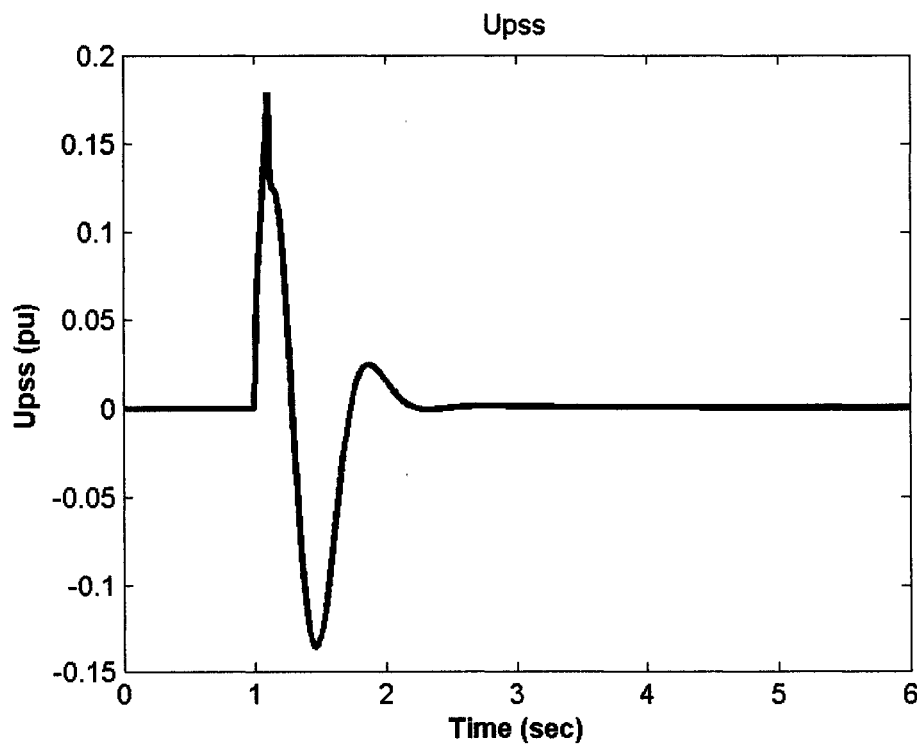


Figure 8.12: PSS stabilizing signal for 6-cycle fault with nominal loading, J_1 settings, single-point tuning, individual design

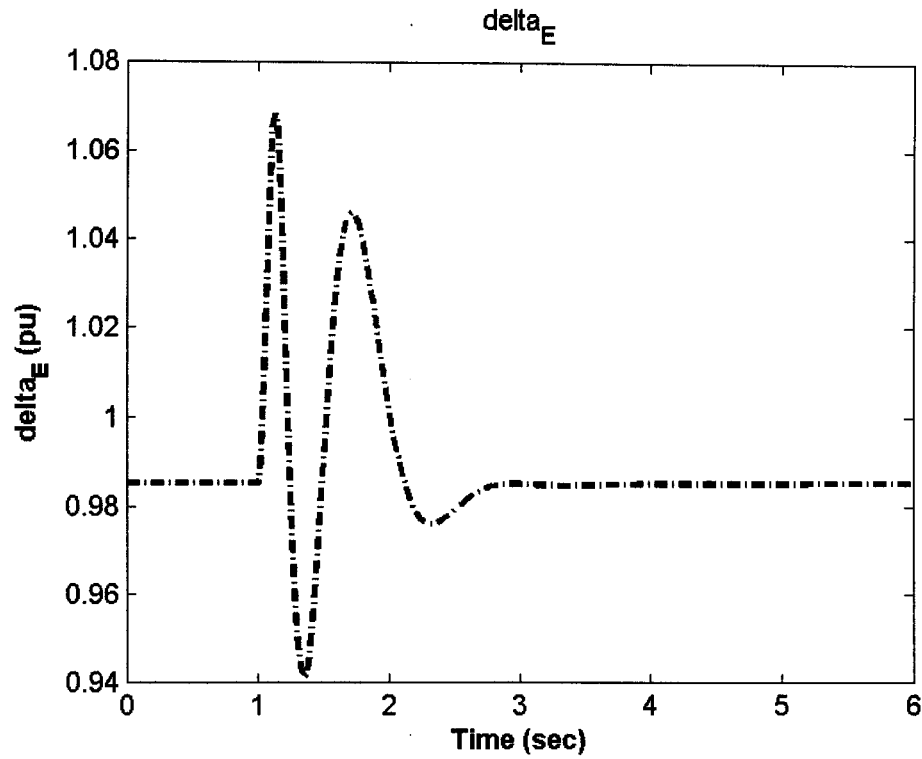


Figure 8.13: δ_E response for 6-cycle fault with nominal loading, J_1 settings, single-point tuning, individual design

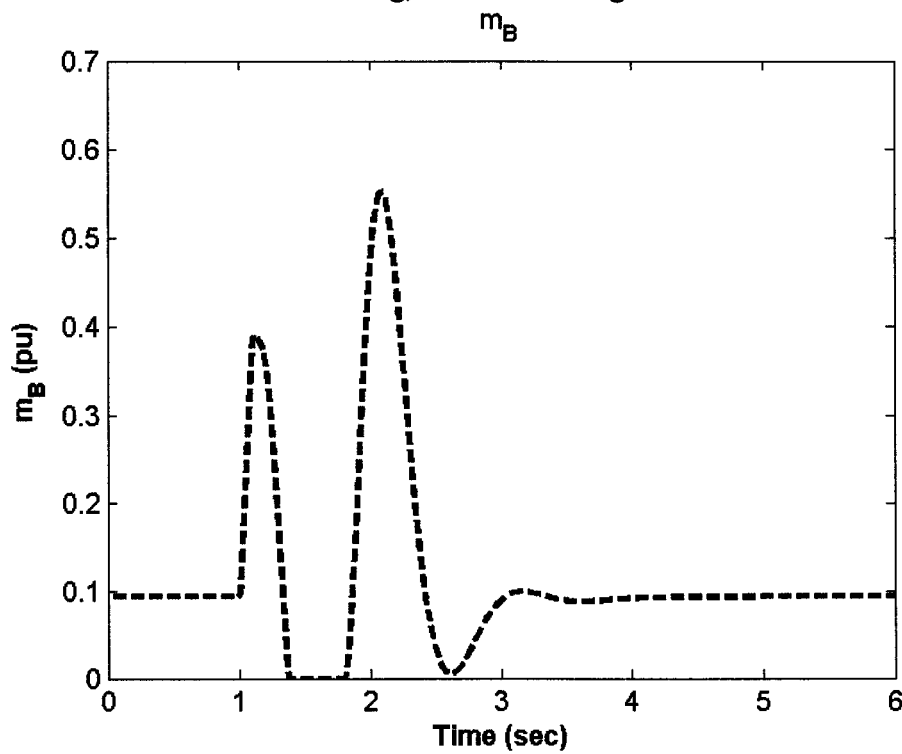


Figure 8.14: m_B response 6-cycle fault with nominal loading, J_1 settings, single-point tuning, individual design

8.2.1.2 Individual Design with J_2

The PSS, m_E , δ_E , m_B , and δ_B -based stabilizers are designed individually considering the nominal loading condition.

Stabilizer Design: PSO is used to search for the optimum parameter settings of each controller that minimizes the maximum damping factor of all the system complex eigenvalues at nominal loading condition. The final settings of the optimized parameters for the proposed stabilizers are given in Table 8.6.

Eigenvalue Analysis: The system eigenvalues without and with the proposed stabilizers at the four operating points, nominal, light, heavy, and leading Pf, are given in Tables 8.7-8.10, respectively. The bold rows of these tables represent the EM mode eigenvalue and its damping ratio. These tables clearly demonstrate the effectiveness of the δ_E - and m_B -based stabilizers in enhancing system stability. Again, It can be observed that, in most cases, the EM mode is either unstable or poorly damped when driven by m_E - or δ_B -based stabilizers. This conclusion is in line with those already drawn from SVD analysis.

Table 8.6: Optimal parameter settings with J_2 , single-point tuning, individual design

	PSS	m_E	δ_E	m_B	δ_B
K	29.2620	-29.8340	-100.00	100.00	-72.891
T₁	2.9290	0.2573	5.0000	0.1154	2.0223
T₂	1.1934	2.4670	1.0884	0.0100	0.1342
T₃	0.1379	2.9524	0.0634	2.1825	2.9499
T₄	0.0100	0.0100	1.4439	2.3575	2.4243

Table 8.7: System eigenvalues of nominal loading conditions with J_1 settings,
single-point tuning, individual design

No Control	PSS	m_E	δ_E	m_B	δ_B
1.5033±	-15.0200,	-1.6900±	-4.6726±	-4.1500±	-1.3943±
5.3328i,	1.0000	7.6200i,	5.0244i	6.0600i,	6.0239i,
-0.2713	-5.4400±	0.2200	0.6810	0.5600	0.2255
-11.4584±	0.1816i	-1.7000±	-4.6271±	-4.1600±	-20.9691±
6.8596i	-103.53	8.0400i	5.8807i	7.2000i	8.1471i
-15.5063	-4.7200	-108.73	-15.5062	-93.020	-1.3992±
-5.1052	-2.7000	-25.110	-5.1378	-30.230	6.3632i
--	-24.600	-14.7600	-2.3247	-15.530	-15.3230
--	-2.0300	-5.1300	-0.5649	-5.1200	-5.1246
--	-0.2000	-0.4100	-20.0000	-0.4200	-0.4126
--	--	-0.2000	-0.2000	-0.2100	-0.2002

Table 8.8: System eigenvalues of light loading conditions with J_1 settings, single-point
tuning, individual design

No Control	PSS	m_E	δ_E	m_B	δ_B
1.3952 ±	-1.1000±	0.9000±	-6.0387±	-3.2400±	1.3095±
5.0825i, -	4.6700i,	5.3700i,	3.3148i,	6.8800i,	5.1260i,
0.2647	0.2300	-0.1700	0.8766	0.4300	-0.2475
-11.3641 ±	-7.9700±	-8.1400±	-3.1753±	-5.0500±	-9.8576±
6.1234i	10.2600i	8.0000i	5.8872i	5.5100i	4.0356i
-14.7072	-101.25	-101.85	-14.7071	-94.060	-18.6090
-5.8534	-14.9400	-23.390	-6.0537	-29.320	-14.0635
--	-6.0700	-15.080	-2.3500	-14.710	-12.4361
--	-0.9300	-5.7100	-0.5708	-5.8500	-5.7451
--	-0.2000	-0.4100	-0.2000	-0.4200	-0.4125
--	--	-0.2000	-20.0000	-0.2100	-0.2000

Table 8.9: System eigenvalues of heavy loading conditions with J_1 settings, single-point tuning, individual design

No Control	PSS	m_E	δ_E	m_B	δ_B
1.4138±	-1.7100±	0.0800±	-1.8131±	-4.6200±	-1.7987±
5.0066i,	2.0000i,	7.0500i,	1.7468i,	3.7500i,	5.4812i,
-0.2718	0.6500	-0.0100	0.7201	0.7800	0.3118
-11.437±	-5.6300±	-2.3800±	-4.0711±	-3.5700±	-21.442±
6.1904i	17.6700i	8.0100i	8.2859i	8.6800i	7.3091i
-15.2584	-103.29	-111.51	-15.2583	-92.900	-0.4684±
-5.2121	-15.9000	-23.150	-8.7998	-30.890	6.3725i
--	-6.2600	-16.320	-5.7472	-15.290	-15.5567
--	-1.2300	-4.9500	-0.5556	-5.0700	-4.9940
--	-0.2000	-0.4100	-0.2000	-0.4100	-0.4126
--	--	-0.2000	-20.0000	-0.2200	-0.2002

Table 8.10: System eigenvalues of leading Pf loading conditions with J_1 settings, single-point tuning, individual design

No Control	PSS	m_E	δ_E	m_B	δ_B
1.4138±	-1.7100±	0.0800±	-1.8131±	-4.6200±	-1.7987±
5.0066i,	2.0000i,	7.0500i,	1.7468i,	3.7500i,	5.4812i,
-0.2718	0.6500	-0.0100	0.7201	0.7800	0.3118
-11.437±	-5.6300±	-2.3800±	-4.0711±	-3.5700±	-21.442±
6.1904i	17.6700i	8.0100i	8.2859i	8.6800i	7.3091i
-15.2584	-103.29	-111.51	-15.2583	-92.900	-0.4684±
-5.2121	-15.9000	-23.150	-8.7998	-30.890	6.3725i
--	-6.2600	-16.320	-5.7472	-15.290	-15.5567
--	-1.2300	-4.9500	-0.5556	-5.0700	-4.9940
--	-0.2000	-0.4100	-0.2000	-0.4100	-0.4126
--	--	-0.2000	-20.0000	-0.2200	-0.2002

Damping Torque Coefficient Analysis: To measure the effectiveness of the proposed PSS and the four UPFC-based stabilizers in improving the system damping characteristics, the damping torque coefficient K_d is calculated. The damping torque coefficient K_d is estimated for each stabilizer over a wide range of loading conditions. Specifically, K_d is calculated for a range of 45 operating points specified by $P_e=[0.05 - 1.45]$ pu in steps of 0.10 pu and $Q_e=[-0.40, 0.00, 0.40]$ pu.

For comparison purposes, K_d for all stabilizers at $Q=-0.4$, $Q=0.0$, and $Q=0.4$ pu are shown in Figures 8.15-8.17, respectively. These figures illustrate the following:

- The PSS is the most effective stabilizer at all loading conditions except at low loading.
- At low loading, the δ_E -based stabilizer becomes more effective.
- In general, the damping torques supplied by m_E and δ_B are either negative or very low positive quantities.
- The PSS and m_B suffer from negative damping characteristics at light loading.
- The damping torque coefficients of the m_B -based stabilizer at nominal loading and δ_E -based stabilizer are almost unaffected by loading level.
- The damping torque coefficients K_d associated with the PSS and m_B -based stabilizers are directly proportional to system loading.
- The PSS is more effective at leading power factor conditions, whereas the δ_E and m_B are least effective at this power factor conditions.

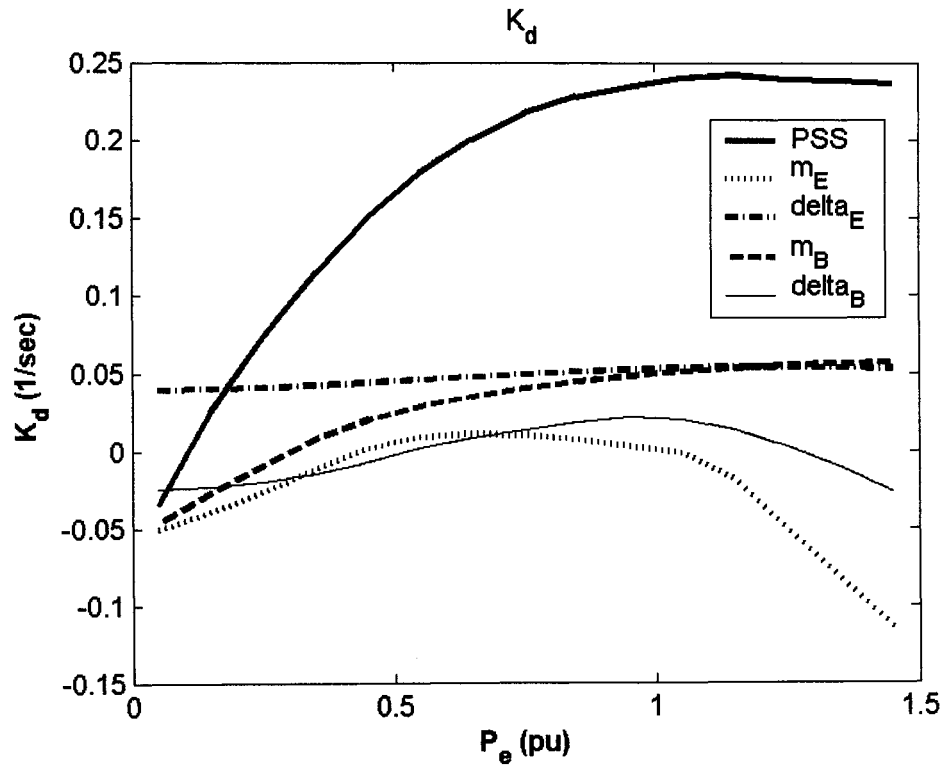


Figure 8.15: Damping torque coefficient with the proposed stabilizers at $Q = -0.4$ pu, J_2 settings, single-point tuning, individual design

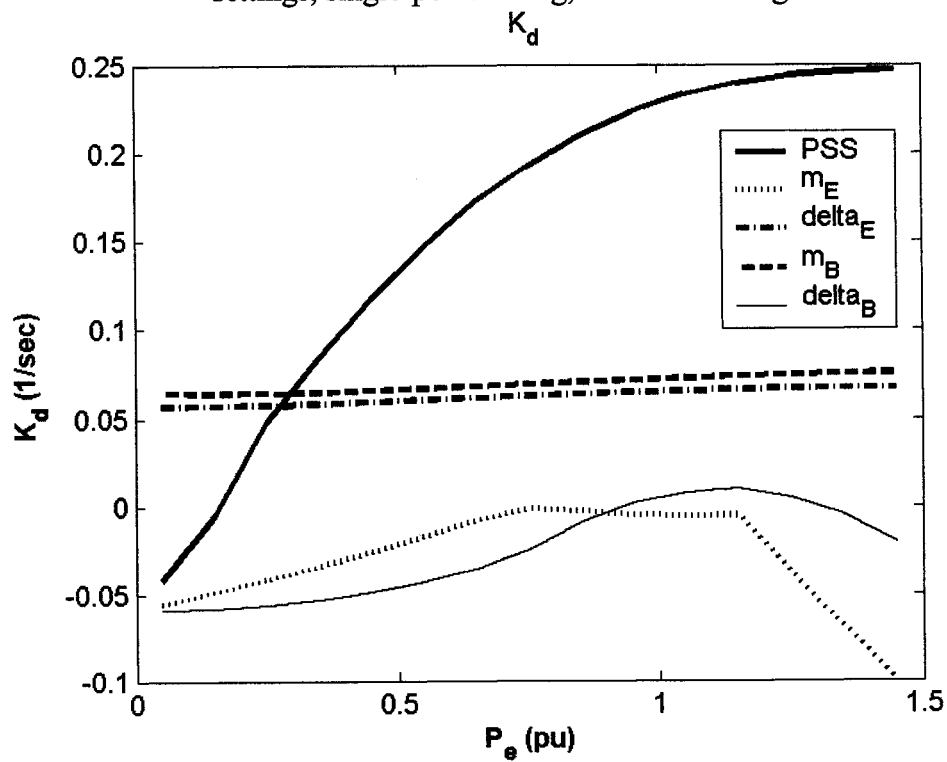


Figure 8.16: Damping torque coefficient with the proposed stabilizers at $Q = 0.0$ pu, J_2 settings, single-point tuning, individual design

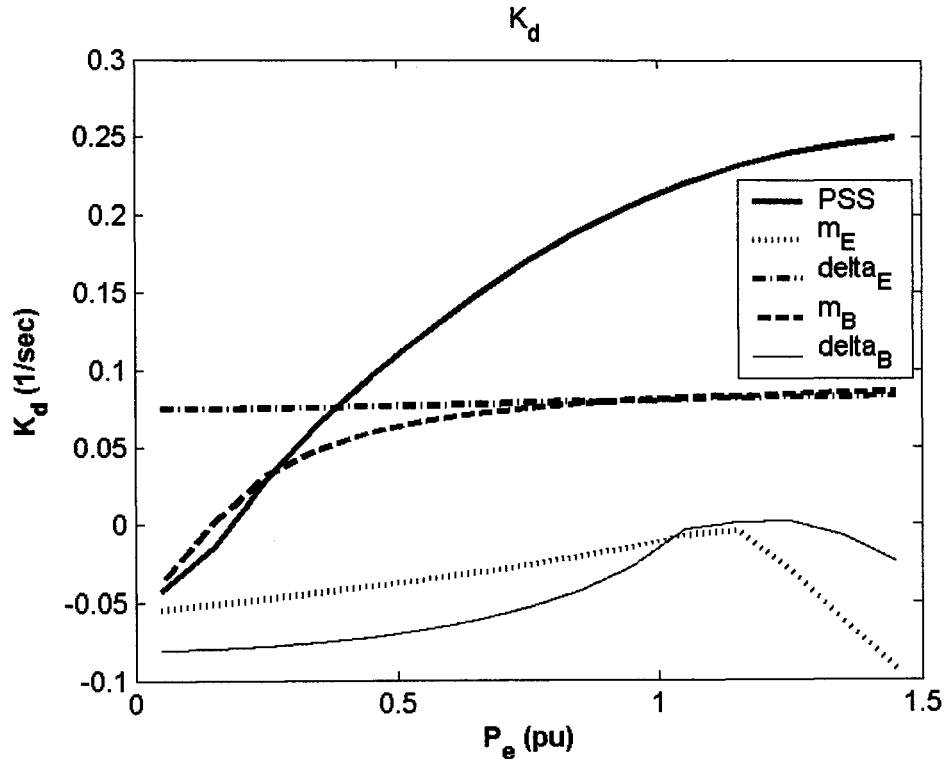


Figure 8.17: Damping torque coefficient with the proposed stabilizers at $Q = 0.4$ pu, J_2 settings, single-point tuning, individual design

Nonlinear Time-Domain Simulations: Figures 8.18-8.22 show the system responses, respectively, due to a 6-cycle three-phase fault at the nominal loading conditions. The system responses due to the m_E - and δ_B -based stabilizers are not shown because they result in unstable responses in almost all cases. It can be readily seen that the PSS is the most effective stabilizer. This agrees with damping torque coefficient analysis results. Figures 8.23-8.25 show the control effort provided by the stabilizing signal of the PSS, the excitation phase angle modulation, δ_E , and the boosting magnitude modulation, m_B , respectively.

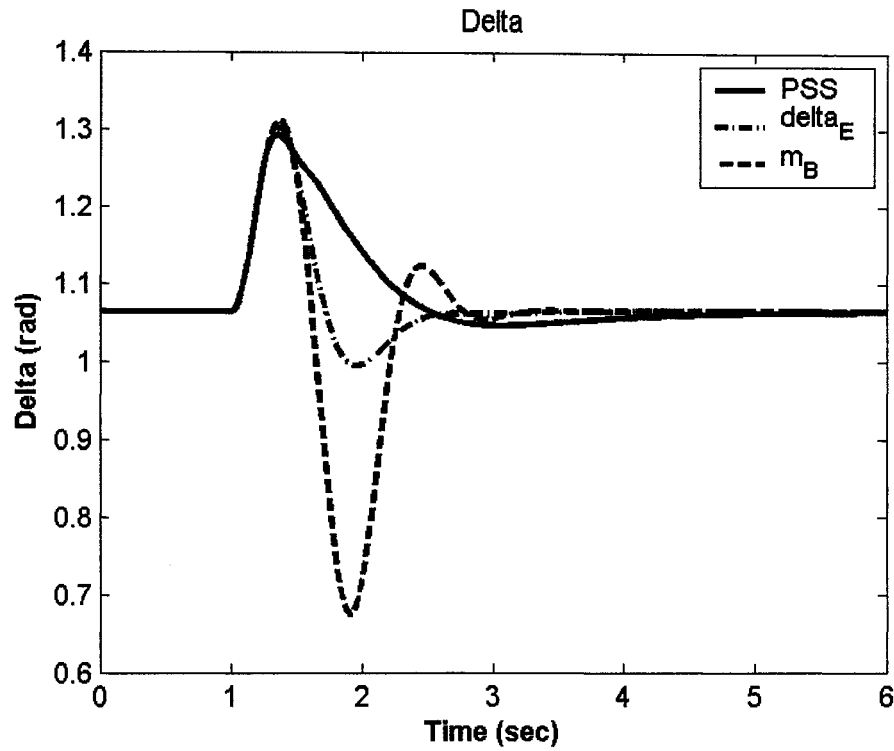


Figure 8.18: Rotor angle response for 6-cycle fault with nominal loading, J_2 settings, single-point tuning, individual design

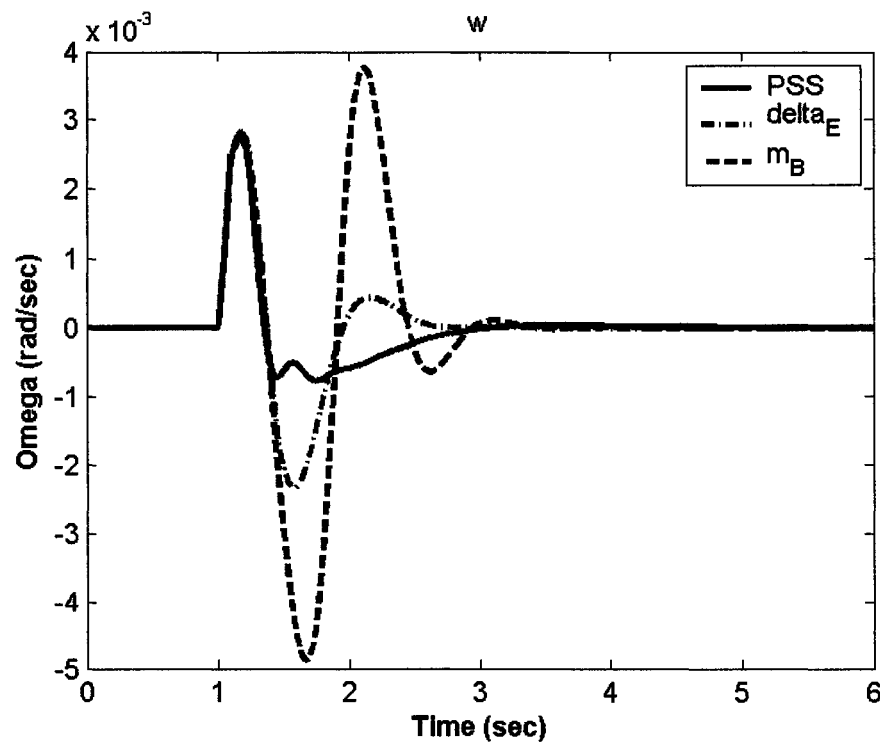


Figure 8.19: Speed response for 6-cycle fault with nominal loading, J_2 settings, single-point tuning, individual design

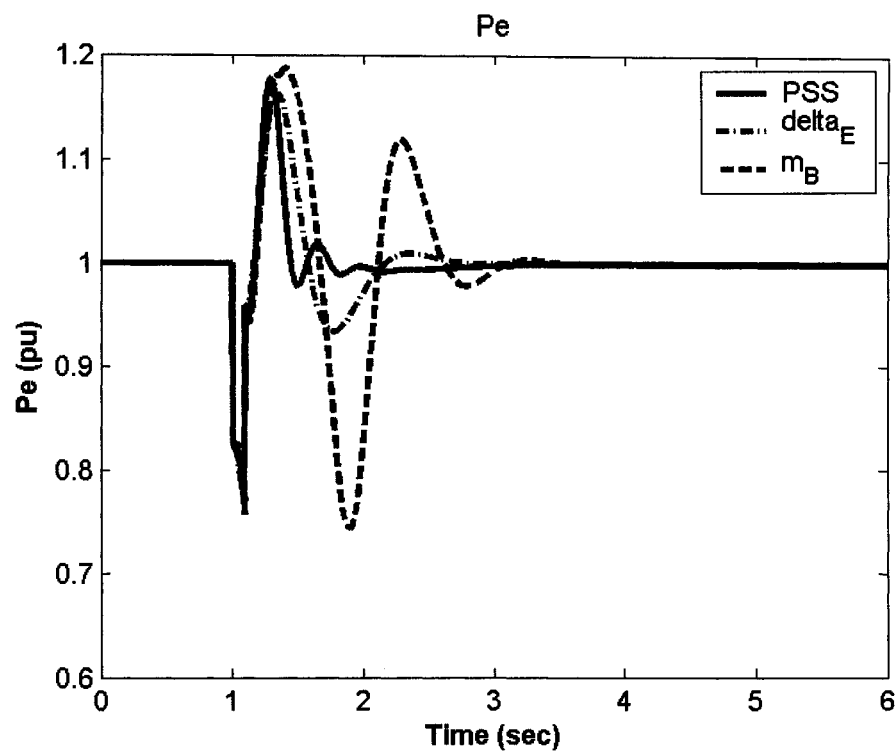


Figure 8.20: Electrical power response for 6-cycle fault with nominal loading, J_2 settings, single-point tuning, individual design

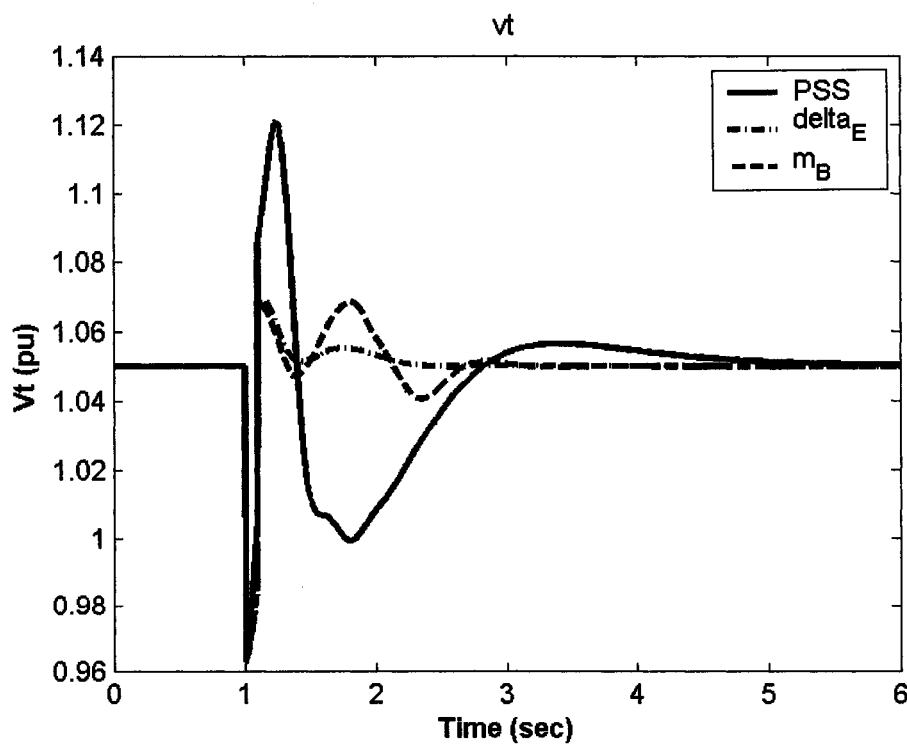


Figure 8.21: Terminal voltage response for 6-cycle fault with nominal loading, J_2 settings, single-point tuning, individual design

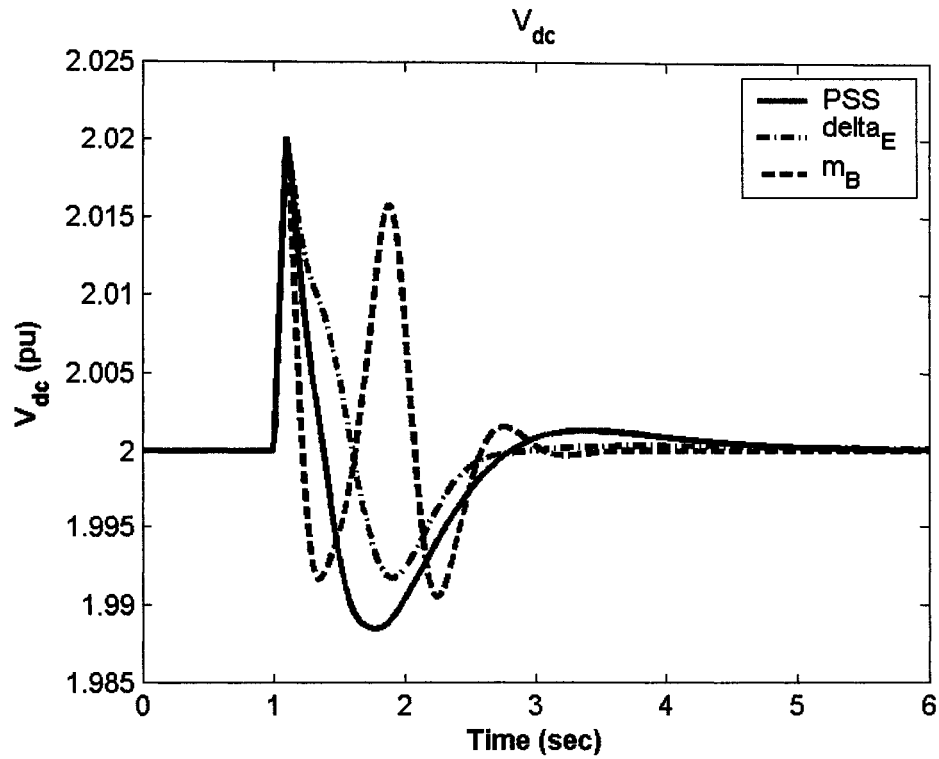


Figure 8.22: DC voltage response for 6-cycle fault with nominal loading, J_2 settings, single-point tuning, individual design

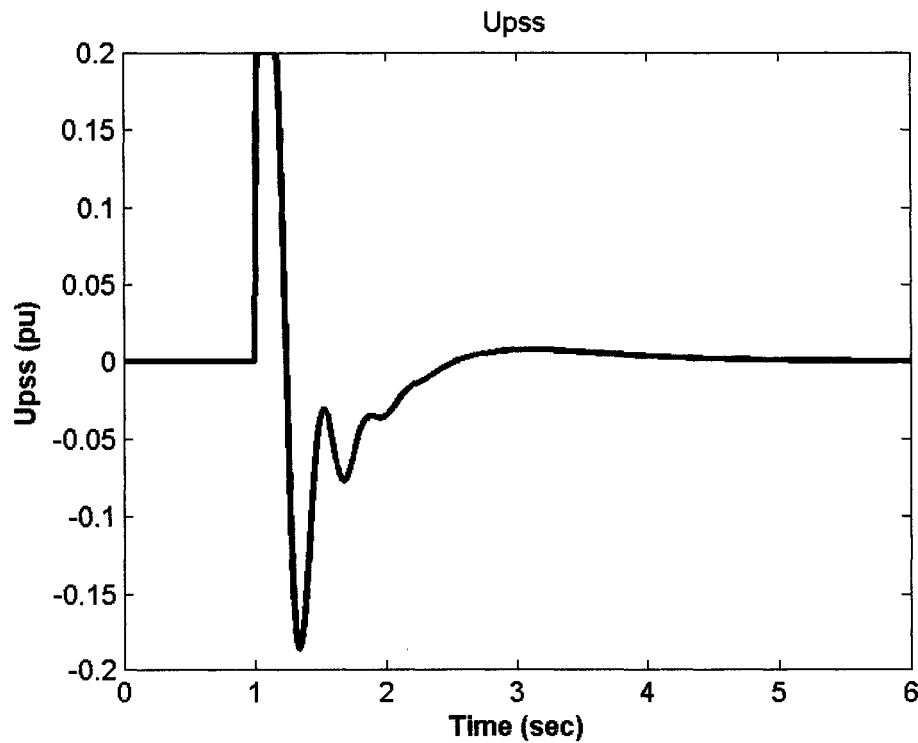


Figure 8.23: PSS stabilizing signal for 6-cycle fault with nominal loading, J_2 settings, single-point tuning, individual design

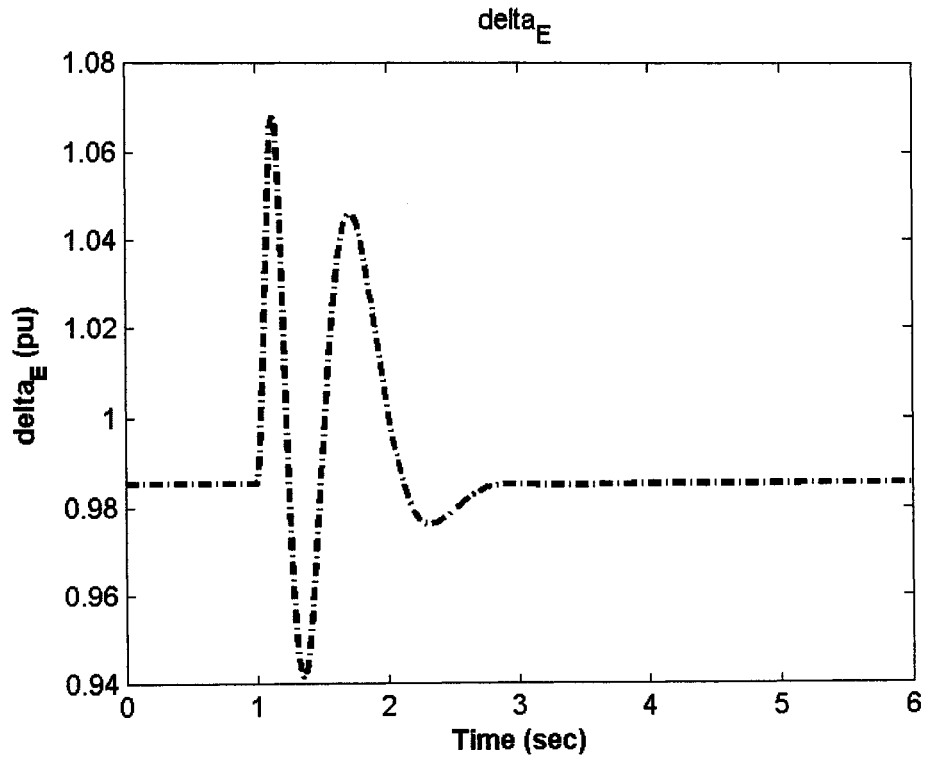


Figure 8.24: δ_E response for 6-cycle fault with nominal loading, J_2 settings, single-point tuning, individual design

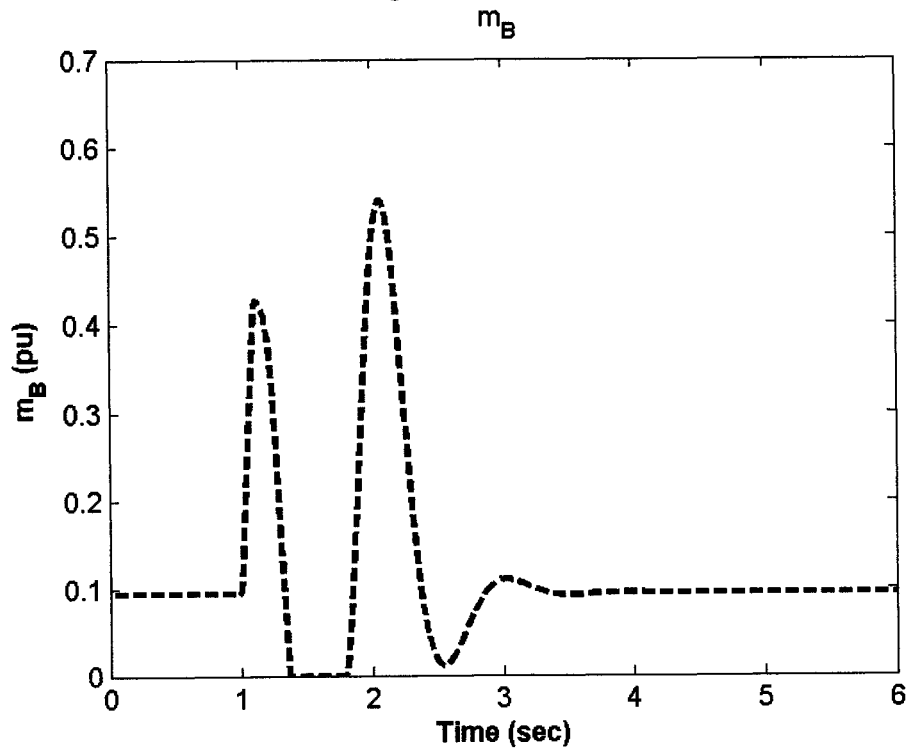


Figure 8.25: m_B response 6-cycle fault with nominal loading, J_2 settings, single-point tuning, individual design

8.2.1.3 Coordinated Design with J_1

The controllability measure analysis based on the singular value decomposition and the damping torque coefficient analyses indicate that the PSS and m_B -based stabilizer do not perform well individually. These two stabilizers have poor capabilities in controlling the EM mode at low loading. The same conclusion can be drawn from nonlinear time-domain simulations illustrated previously. In this section, the coordinated design of PSS and m_B -based stabilizer is considered at the nominal loading condition.

Stabilizer Design: PSO is used to simultaneously search for the optimum parameter settings of both controllers that maximize the minimum damping ratio of all the system complex eigenvalues at nominal loading. The final settings of the optimized parameters for the proposed stabilizers are given in Table 8.11.

Eigenvalue Analysis: The system eigenvalues without and with the proposed PSS and m_B -based controllers when applied individually and through coordinated design at the four loading conditions, nominal, light, heavy, and leading Pf, are given in Tables 8.12-8.15, respectively. The bold rows of these tables represent the EM mode eigenvalue and its damping ratio. It is evident that, using the proposed coordinated stabilizers design, the damping ratio of the EM mode eigenvalue is greatly enhanced. Hence, it can be concluded that this well improves the system stability.

Table 8.11: Optimal parameter settings with J_1 , single-point tuning, coordinated design

	Individual		Coordinated	
	PSS	m_B	PSS	m_B
K	16.9203	29.062	40.336	72.954
T₁	4.5673	2.8973	1.5852	0.1163
T₂	2.0440	0.9339	2.0945	0.0100
T₃	0.0835	0.1039	4.7773	0.1130
T₄	0.0100	0.0100	5.0000	0.0100

Table 8.12: System eigenvalues of nominal loading conditions with J_1 settings, single-point tuning, coordinated design

No Control	PSS	m_B	PSS & m_B
1.5033± 5.3328i, -0.2713	-4.7000± 6.8700i, 0.5600	-4.1000± 6.0700i, 0.5600	-7.1317± 6.8248i, 0.7200
-11.4584± 6.8596i	-4.8700± 7.0400i	-4.2000± 6.2400i	-7.2300± 6.8000i
-15.5063	-101.12	-93.980	-101.83± 69.950i
-5.1052	-15.340	-28.950	-15.290
--	-4.8700	-15.530	-8.4600
--	-0.5500	-5.1300	-4.4100
--	--	-1.4000	-0.4500
--	--	--	-0.2100
--	--	--	-0.2100

Table 8.13: System eigenvalues of light loading conditions with J_1 settings, single-point tuning, coordinated design

No Control	PSS	m_B	PSS & m_B
1.3952± 5.0825i, -0.2647	0.2800± 5.500i, -0.0500	-3.2300± 6.4500i, 0.4500	-2.0487± 4.4154i, 0.4200
-11.3641± 6.1234i,	-9.8300± 6.3400i	-5.0400± 4.8700i	-10.050± 9.8000i
-14.7072	-100.38	-94.860	-101.72± 65.100i
-5.8534	-14.760	-28.180	-14.820
--	-6.2400	-14.710	-11.340
--	-0.5100	-5.8400	-6.6900
--	--	-1.4500	-0.4700
--	--	--	-0.2100
--	--	--	-0.2100

Table 8.14: System eigenvalues of heavy loading conditions with J_1 settings, single-point tuning, coordinated design

No Control	PSS	m_B	PSS & m_B
1.4138± 5.0066i, -0.2718	-2.6900± 4.2600i, 0.5300	-4.6500± 2.5400i, 0.8800	-3.1196± 2.1014i, 0.8300
-11.4375± 6.1904i	-5.2400± 8.6400i	-3.5800± 8.2600i	-101.96± 70.270i
-15.2584	-101.04	-93.880	-10.980± 6.1500i
-5.2121	-15.510	-29.570	-6.4300± 9.3900i
--	-8.0500	-15.280	-15.540
--	-0.5400	-4.6700	-0.4500
--	--	-1.7100	-0.2100
--	--	--	-0.2100

Table 8.15: System eigenvalues of leading Pf loading conditions with J_1 settings, single-point tuning, coordinated design

No Control	PSS	m_B	PSS & m_B
1.4502± 5.3584i, -0.2612	-7.9800± 7.2500i, 0.7400	-1.2100± 5.7900i 0.2000	-2.8332± 6.5861i 0.4000
-11.3963± 7.0920i	-2.2200± 7.1200i	-7.3600± 6.7800i	-101.53± 61.920i
-15.4566	-100.98	-95.430	-14.380± 0.6500i
-5.1711	-15.090	-26.760	-9.6600± 7.7900i
--	-3.9800	-15.640	-0.2100± 0.0100i
--	-0.5500	-5.3600	-3.7200
--	--	-1.2600	-0.4500

Damping Torque Coefficient Analysis: To quantitatively measure the effectiveness of the proposed PSS- m_B coordinated design in improving the system damping characteristics and compare it with both individual designs, the damping torque coefficient K_d is estimated. K_d is calculated for a range of 45 operating points specified by $P_e=[0.05 - 1.45]$ pu in steps of 0.10 pu and $Q_e=[-0.40, 0.00, 0.40]$ pu.

For comparison purposes, the damping torque coefficient for the coordinated PSS- m_B stabilizer design and the both individual designs at $Q=-0.4$, $Q=0.0$, and $Q=0.4$ pu are shown in Figures 8.26-8.28, respectively. These figures address the highly effective coordinated design, as compared with PSS and m_B individual designs, over the different loading conditions.

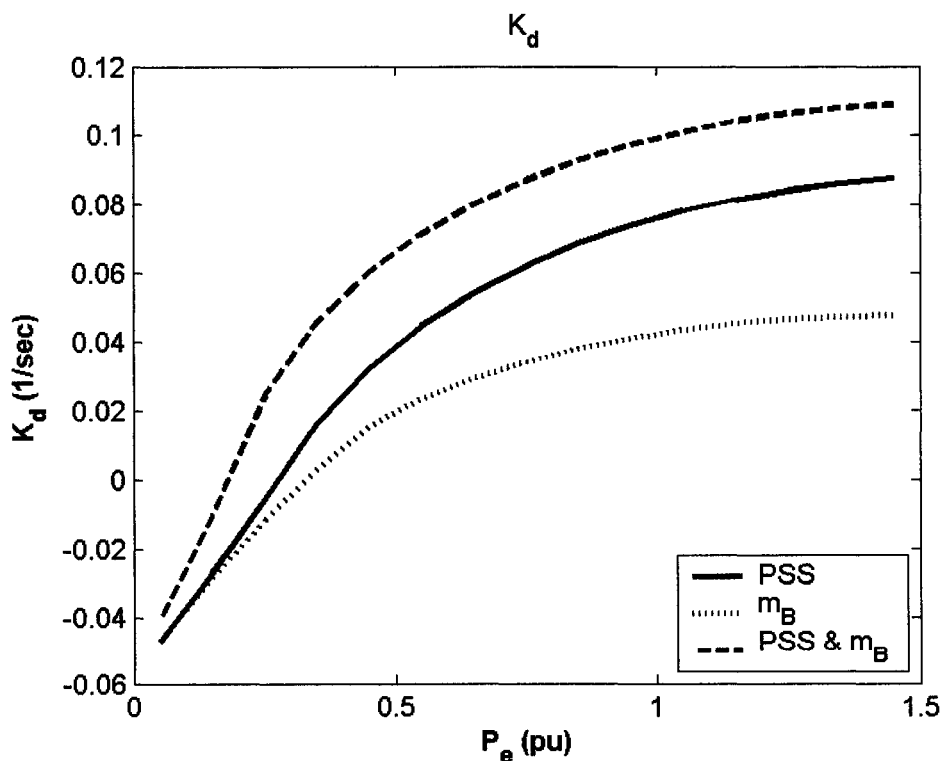


Figure 8.26: Damping torque coefficient with coordinated PSS & m_B -based controller at $Q = -0.4$ pu, J_1 settings, single-point tuning

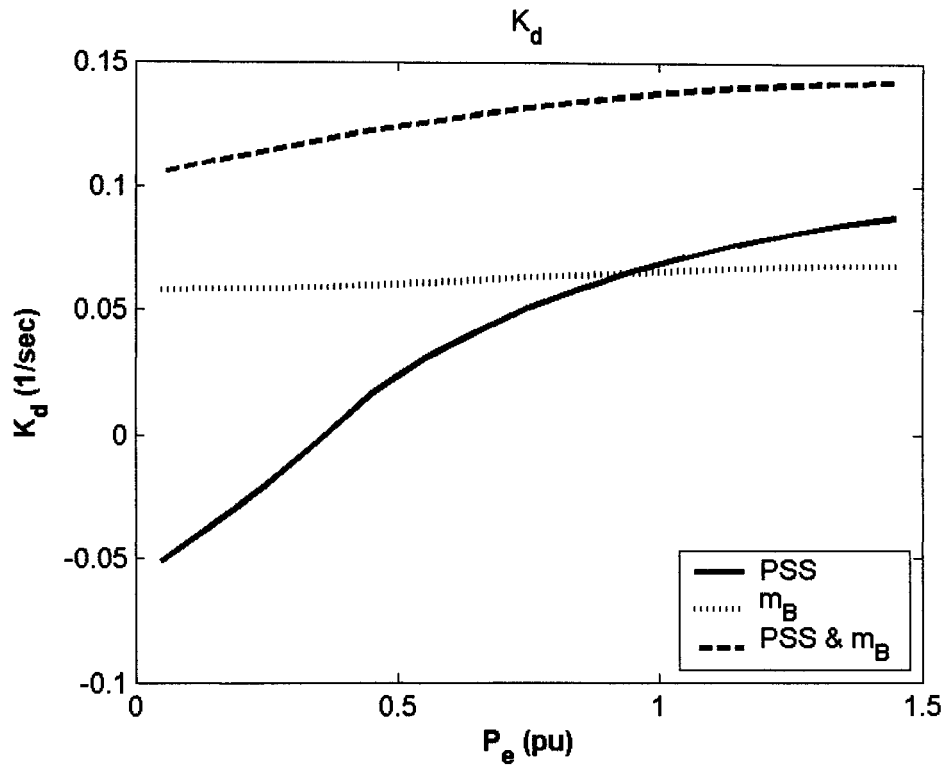


Figure 8.27: Damping torque coefficient with coordinated PSS & m_B -based controller at $Q = 0.0$ pu, J_1 settings, single-point tuning

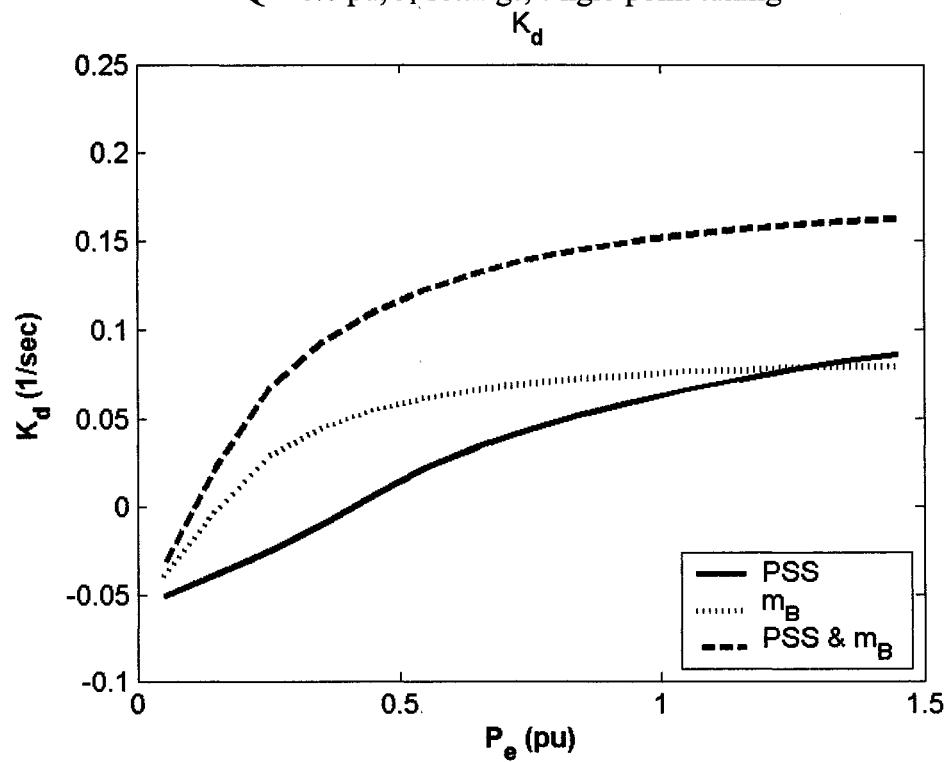


Figure 8.28: Damping torque coefficient with coordinated PSS & m_B -based controller at $Q = 0.4$ pu, J_1 settings, single-point tuning

Nonlinear Time-Domain Simulations: The rotor angle, speed deviation, electrical power, and machine terminal voltage responses for a 6-cycle three-phase fault at the nominal loading conditions are shown in Figures 8.29-8.33, respectively. Figure 8.34 and Figure 8.35 show the control effort provided by the stabilizing signal of PSS and m_B when applied individually and through coordinated design. The improvement on the system responses when using the coordinated design over the m_B responses is evident.

Similarly, the simulation results with a 6-cycle three-phase fault at light loading condition are shown in Figures 8.36-8.40. The control signals of the two stabilizers are given in Figure 8.41 and Figure 8.42. The simulation results obtained clearly indicate that the proposed coordinated PSS- m_B design outperforms both the individual designs in terms of first swing stability, overshoot, and settling time. These results confirm the conclusions drawn for damping torque coefficient analysis results. This solves the problem of low effectiveness of the individual designs at light loading level.

From these results, it can be readily seen that the coordinated PSS- m_B design solves two problems: the poor effectiveness of the PSS at light loading, and the relatively long settling time and high overshoot of the m_B -based stabilizer responses.

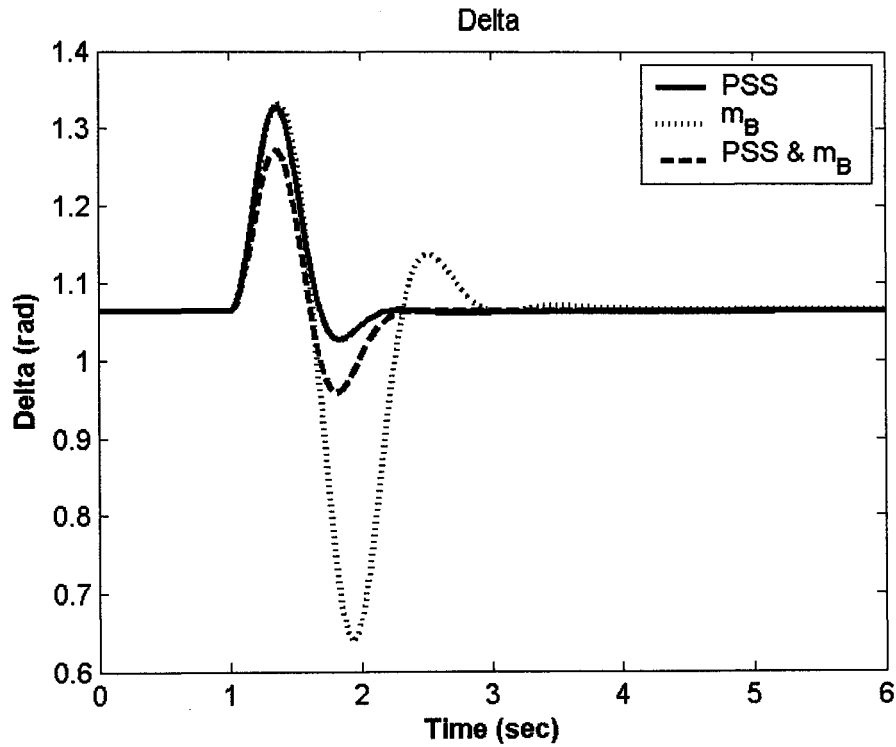


Figure 8.29: Rotor angle response for 6-cycle fault with nominal loading, J_1 settings, single-point tuning, coordinated design

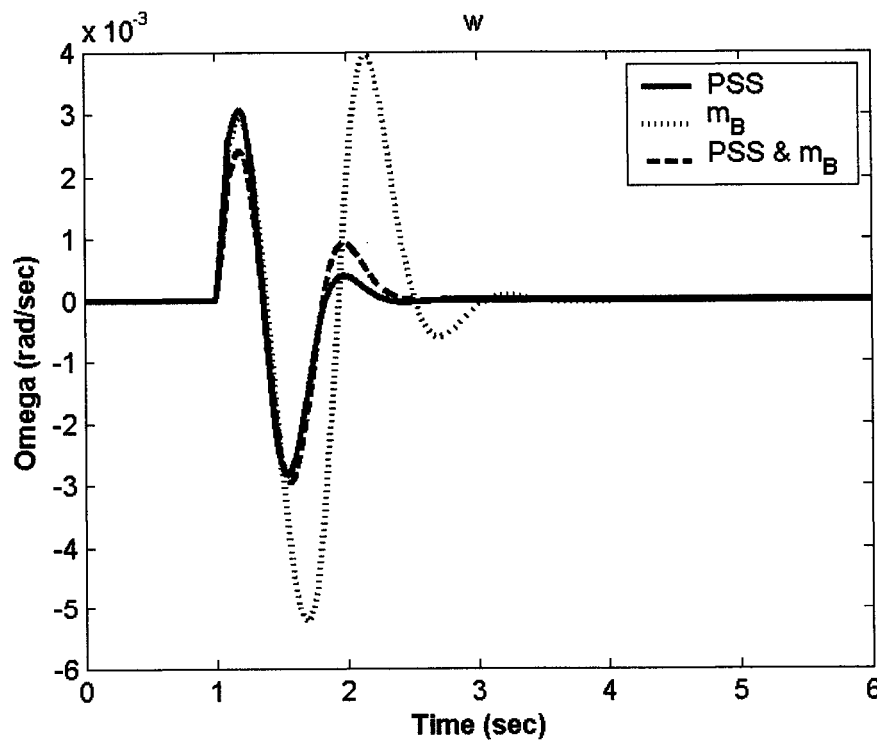


Figure 8.30: Speed response for 6-cycle fault with nominal loading, J_1 settings, single-point tuning, coordinated design

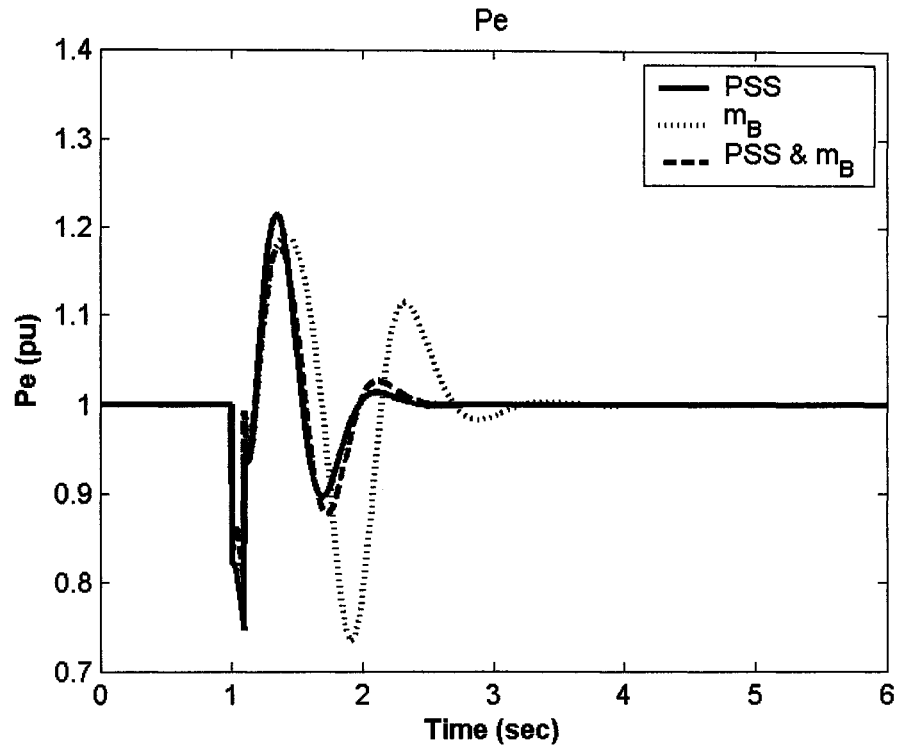


Figure 8.31: Electrical power response for 6-cycle fault with nominal loading, J_1 settings, single-point tuning, coordinated design

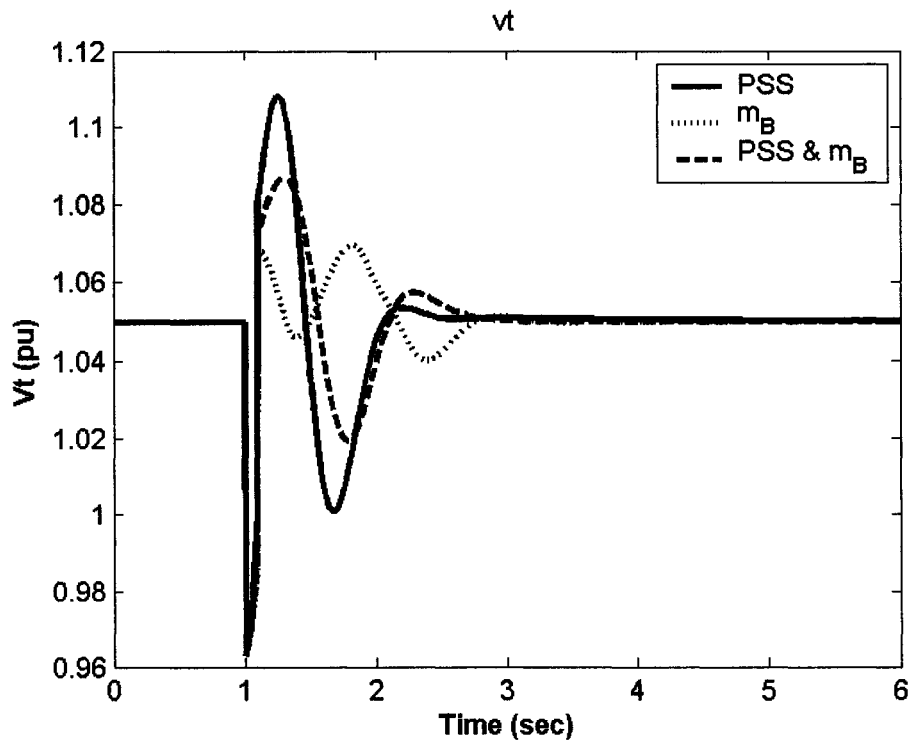


Figure 8.32: Terminal voltage response for 6-cycle fault with nominal loading, J_1 settings, single-point tuning, coordinated design

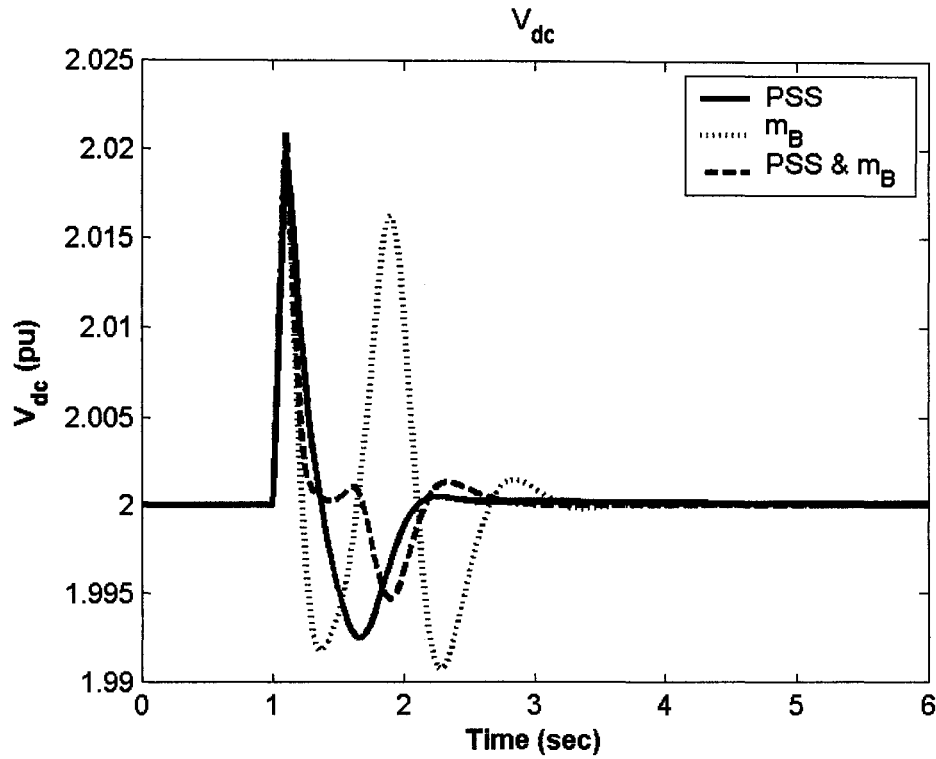


Figure 8.33: DC voltage response for 6-cycle fault with nominal loading, J_1 settings, single-point tuning, coordinated design

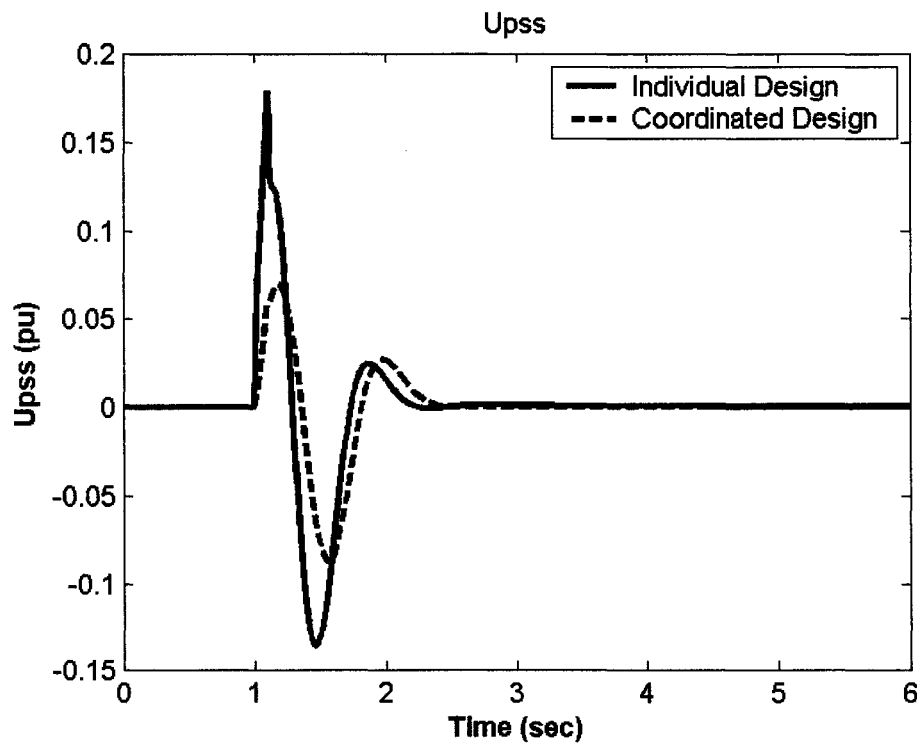


Figure 8.34: PSS stabilizing signal for 6-cycle fault with nominal loading, J_1 settings, single-point tuning, coordinated design

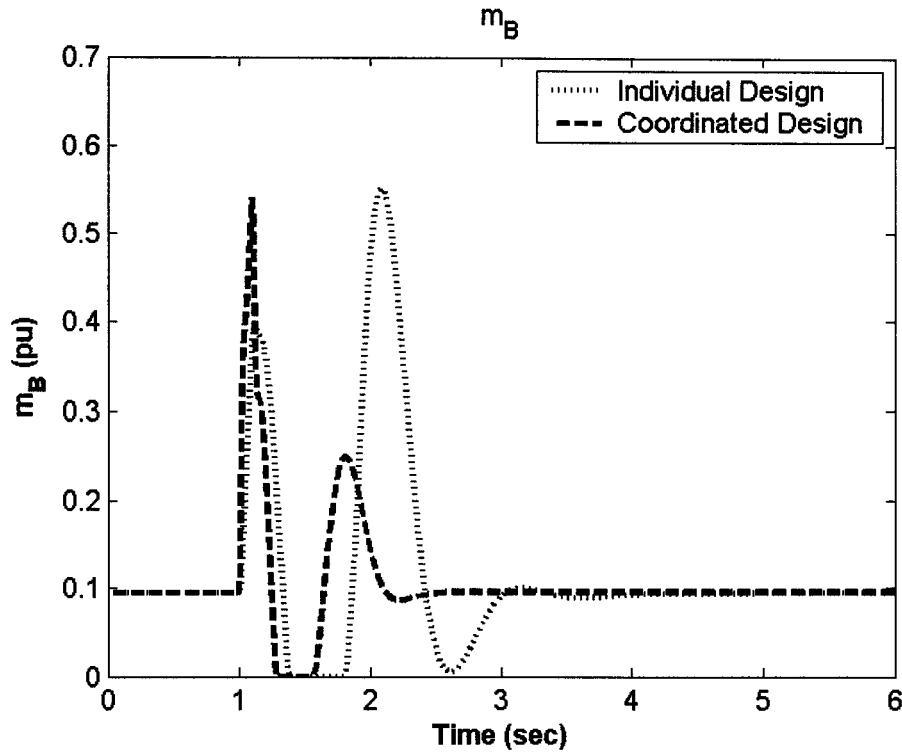


Figure 8.35: m_B response 6-cycle fault with nominal loading, J_1 settings, single-point tuning, coordinated design

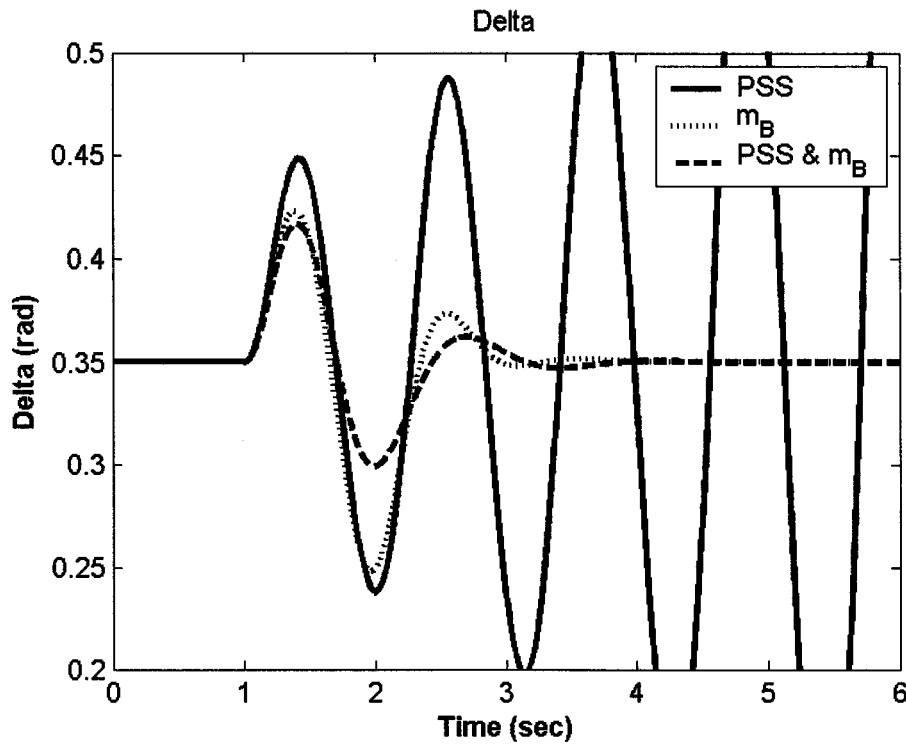


Figure 8.36: Rotor angle response for 6-cycle fault with light loading, J_1 settings, single-point tuning, coordinated design

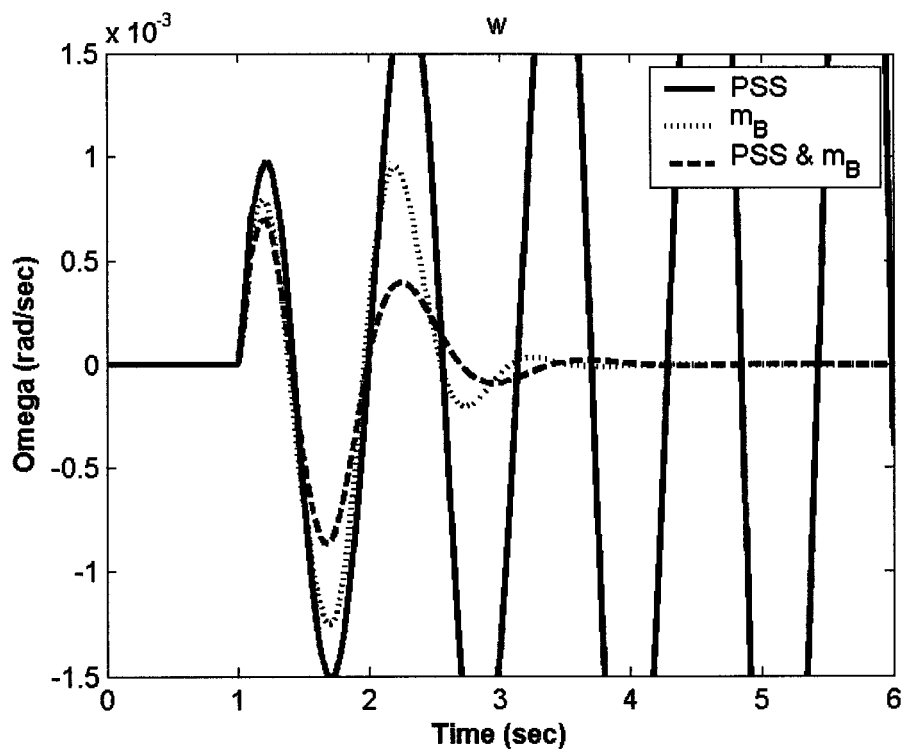


Figure 8.37: Speed response for 6-cycle fault with light loading, J_1 settings, single-point tuning, coordinated design

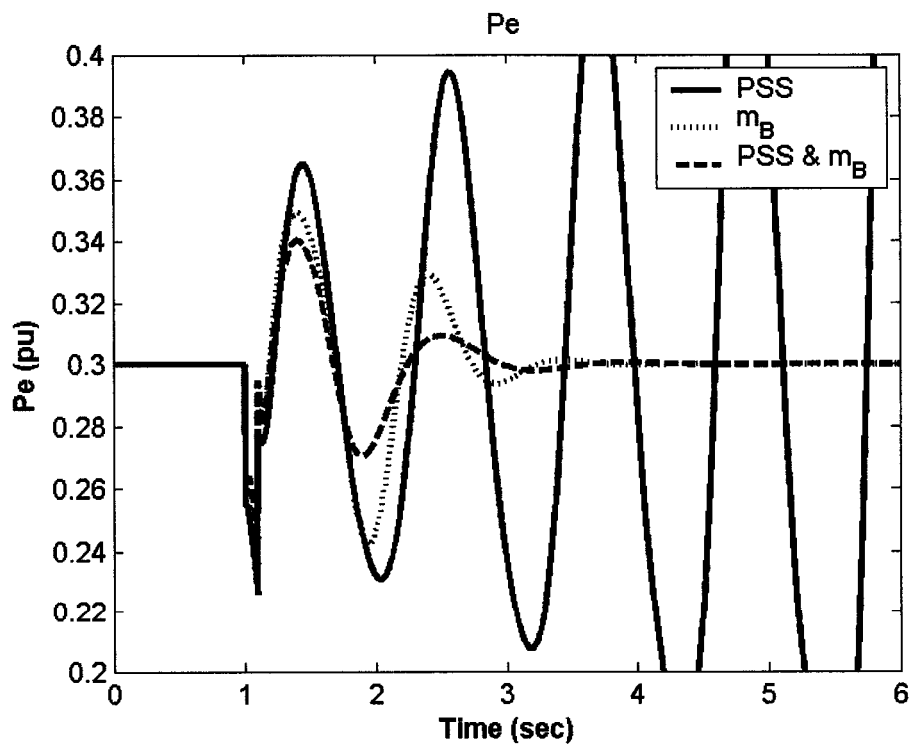


Figure 8.38: Electrical power response for 6-cycle fault with light loading, J_1 settings, single-point tuning, coordinated design

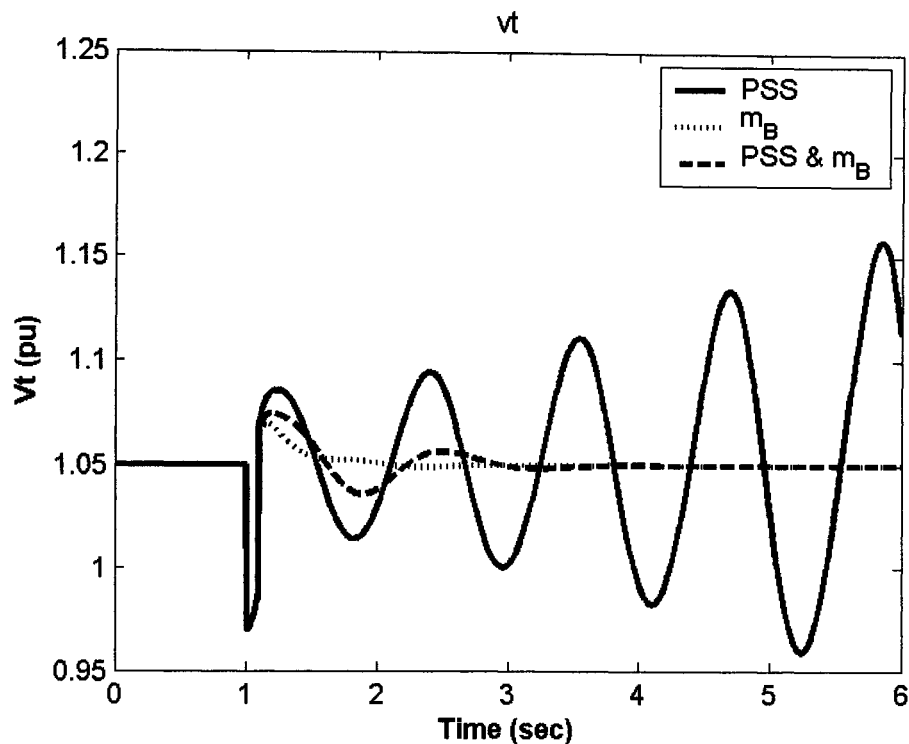


Figure 8.39: Terminal voltage response for 6-cycle fault with light loading, J_1 settings, single-point tuning, coordinated design

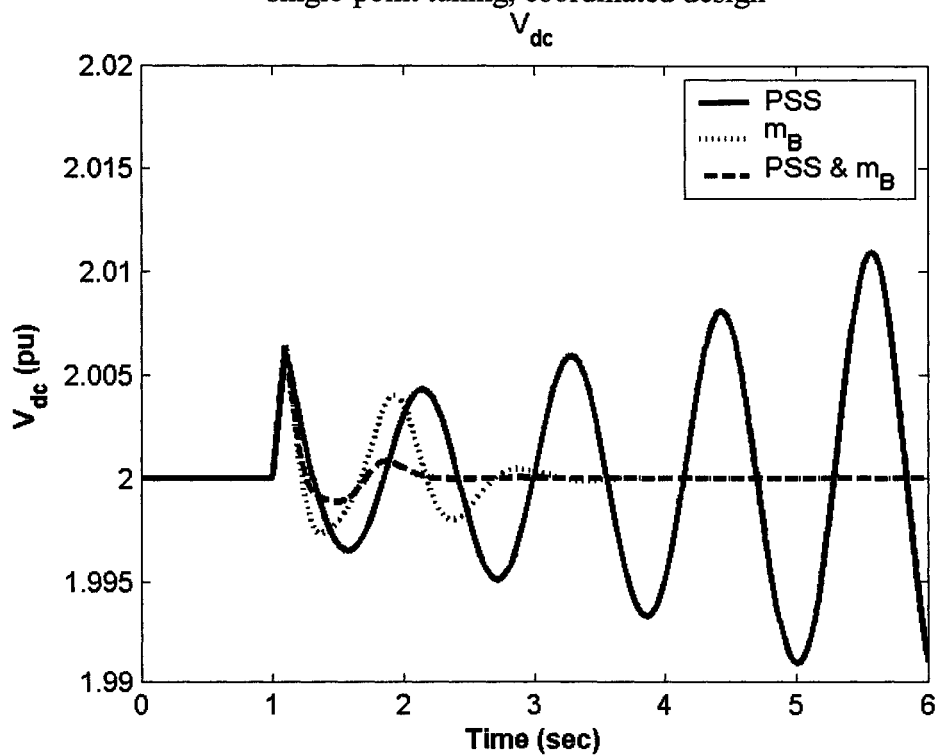


Figure 8.40: DC voltage response for 6-cycle fault with light loading, J_1 settings, single-point tuning, coordinated design

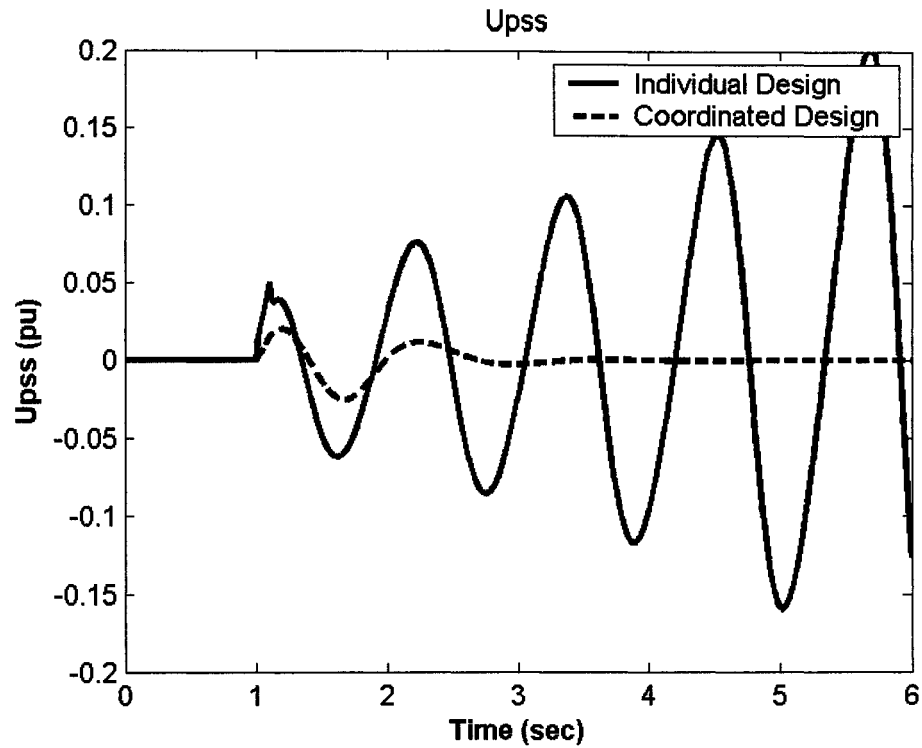


Figure 8.41: PSS stabilizing signal for 6-cycle fault with light loading, J_1 settings, single-point tuning, coordinated design

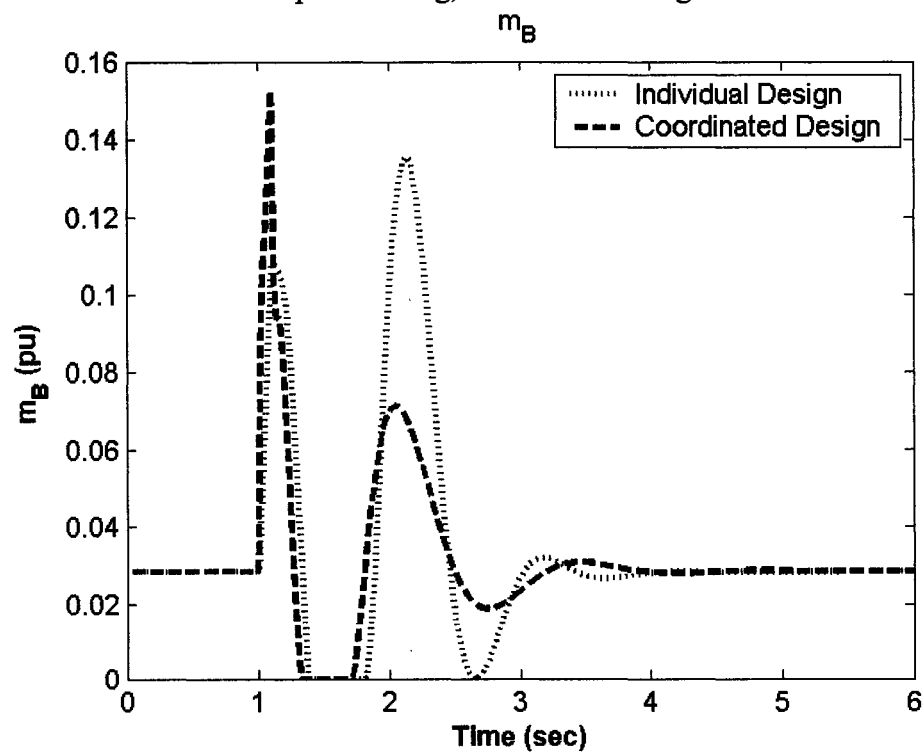


Figure 8.42: m_B response 6-cycle fault with light loading, J_1 settings, single-point tuning, coordinated design

8.2.2 Multiple-Point Tuning

In this situation, the objective is to design robust stabilizers to ensure their effectiveness over a wide range of operating conditions. The design process takes into account several loading conditions including nominal, light, heavy, and leading Pf conditions. These conditions are considered without and with system parameter uncertainties, such as machine inertia, line impedance, and field time constant. The total number of 16 operating conditions is considered during the design process as given in Table 8.16

Tables 8.17 and 8.18 list the open-loop eigenvalues and corresponding damping ratios associated with the EM modes of all the 16 operating points considered in the robust design process, respectively. It is evident that all these modes are unstable.

8.2.2.1 Individual Design with J_1

The PSS, m_E -, δ_E -, m_B -, and δ_B -based stabilizers are designed individually considering all the operating points mentioned above.

Stabilizer Design: PSO is used to optimize the parameters of each controller that maximizes the minimum damping ratio of all the complex eigenvalues associated with the 16 operating points simultaneously. The final settings of the optimized parameters for the proposed stabilizers are given in Table 8.19. It is worth mentioning that the optimization of the m_E - and δ_B -based stabilizers parameter settings gives rise to unstable EM modes. That is, these two stabilizers cannot simultaneously stabilize the EM mode for all the 16 operating conditions. Hence, these stabilizers and their results are excluded from the analysis hereafter.

Table 8.16: Loading conditions and parameter uncertainties considered in the design stage

Loading Condition	(P_e , Q_e) pu	Parameter Uncertainties
Nominal	(1.0, 0.015)	No parameter uncertainties
Light	(0.3, 0.100)	30% increase of line reactance X_{BV}
Heavy	(1.1, 0.100)	25% decrease of machine inertia M
Leading Pf	(0.7, -0.30)	30% decrease of field time constant T'_{do}

Table 8.17: Open-loop eigenvalues associated with the EM modes of all the 16 points considered in the robust design process

	No parameter uncertainties	30% increase of line reactance X	25% decrease of machine inertia M	30% decrease of field time constant T'_{do}
Nominal	1.5033±5.3328i	1.4191±4.9900i	1.8047±5.9408i	1.5034±5.4025i
Light	1.3952±5.0825i	1.3254±4.7414i	1.6730±5.6676i	1.3951±5.0913i
Heavy	1.4138±5.0066i	1.2553±4.5295i	1.7027±5.5775i	1.4038±5.0846i
Leading Pf	1.4502±5.3584i	1.4092±5.0888i	1.7461±5.9774i	1.4498±5.3952i

Table 8.18: Damping ratios of the open-loop eigenvalues associated with the EM modes of all the points considered in the robust design process

	No parameter uncertainties	30% increase of line reactance X_{BV}	25% decrease of machine inertia M	30% decrease of field time constant T'_{do}
Nominal	-0.2713	-0.2735	-0.2907	-0.2681
Light	-0.2647	-0.2692	-0.2831	-0.2643
Heavy	-0.2718	-0.2671	-0.2920	-0.2661
Leading Pf	-0.2612	-0.2669	-0.2804	-0.2595

Table 8.19: Optimal parameter settings with J_1 , multiple-point tuning, individual design

	PSS	δ_E	m_B
K	42.262	-100.00	19.017
T₁	0.1093	0.0868	5.0000
T₂	1.4177	1.2140	0.8077
T₃	2.6284	5.0000	0.1458
T₄	0.0100	1.1200	0.0100

Eigenvalue Analysis: The system eigenvalues without and with the proposed stabilizers at the four operating points, nominal, light, heavy, and leading Pf, are given in Tables 8.20-8.23, respectively. The bold rows of these tables represent the EM mode eigenvalue and its damping ratio.

Table 8.20: System eigenvalues of nominal loading conditions with J_1 settings, multiple-point tuning, individual design

No Control	PSS	δ_E	m_B
$1.5033 \pm 5.3328i,$ -0.2713	$-5.4300 \pm 0.9900i,$ 0.9800	$-6.5930 \pm 10.068i,$ 0.6027	$-2.0800 \pm 2.8100i,$ 0.5900
-11.4584 \pm 6.8596i	-4.6600 \pm 16.7700i	-2.2173 \pm 2.9354i	-5.0400 \pm 11.3500i
-15.5063	-103.02	-3.3733	-87.400
-5.1052	-15.090	-15.508	-37.280
--	-1.7600	-5.1306	-15.530
--	-1.1700	-0.6059	-5.1200
--	-0.2100	-20.0000	-2.2000
--	--	-0.2000	-0.2000

Table 8.21: System eigenvalues of light loading conditions with J_1 settings, multiple-point tuning, individual design

No Control	PSS	δ_E	m_B
$1.3952 \pm 5.0825i,$ -0.2647	$-1.4900 \pm 5.0500i,$ 0.2800	$-2.2726 \pm 2.7631i,$ 0.6352	$-2.0300 \pm 2.5400i,$ 0.6200
-11.364 \pm 6.1234i	-7.5300 \pm 8.8600i	-6.4003 \pm 8.8056i	-4.9200 \pm 10.7900i
-14.707	-101.06	-14.7077	-89.440
-5.8534	-14.890	-5.9360	-35.390
--	-6.4400	-3.6128	-14.710
--	-0.7600	-0.6126	-5.8500
--	-0.2000	-20.000	-2.4400
--	--	-0.2000	-0.2000

Table 8.22: System eigenvalues of heavy loading conditions with J_1 settings, multiple-point tuning, individual design

No Control	PSS	δ_E	m_B
1.4138 ± 5.0066i, -0.2718	-2.0900 ± 1.6600i, 0.7800	-1.2901 ± 1.9892i, 0.5441	-1.5600 ± 1.8600i, 0.6400
-11.437 ± 6.1904i	-4.8600 ± 16.3200i	-5.9589 ± 0.5526i	-4.6100 ± 11.700i
-15.258	-102.81	-5.9418 ± 10.5574i	-87.140
-5.2121	-15.830	-15.2592	-38.150
--	-7.7200	-0.5939	-15.290
--	-0.9600	-0.2000	-5.0600
--	-0.2100	-20.0000	-3.7600
--	--	--	-0.2000

Table 8.23: System eigenvalues of leading Pf loading conditions with J_1 settings, multiple-point tuning, individual design

No Control	PSS	δ_E	m_B
1.4502 ± 5.3584i, -0.2612	-5.8600 ± 2.9600i, 0.8900	-2.0346 ± 3.9874i, 0.4545	-1.7400 ± 4.0600i, 0.3900
-11.396 ± 7.0920i	-4.8600 ± 15.430i	-7.2838 ± 9.3855i	-5.8800 ± 10.020i
-15.457	-102.66	-15.4652	-90.720
-5.1711	-14.420	-5.1518	-33.140
--	-1.4900	-2.3723	-15.690
--	-1.2200	-0.6105	-5.2800
--	-0.2100	-0.2000	-1.6700
--	--	-20.0000	-0.2000

Damping Torque Coefficient Analysis: The damping torque coefficient K_d is calculated for the proposed robust stabilizers to measure their effectiveness in enhancing the system damping characteristics. The damping torque coefficient is calculated for a range of 45 operating points specified by $P_e=[0.05 - 1.45]$ pu in steps of 0.10 pu and $Q_e=[-0.40, 0.00, 0.40]$ pu.

For comparison purposes, K_d for all stabilizers at $Q=-0.4$, $Q=0.0$, and $Q=0.4$ pu are shown in Figures 8.154-8.156, respectively. These figures illustrate the following:

- The PSS is the most effective stabilizer at all loading conditions except at low loading.
- At low loading and unity power factor, the m_B -based stabilizer becomes more effective. Otherwise, the δ_E -based stabilizer is the winner.
- The PSS and m_B suffer from negative damping characteristics at light loading.
- The damping torque coefficients of the m_B -based stabilizer at nominal loading and δ_E -based stabilizer are almost unaffected by loading level.
- The damping torque coefficients K_d associated with the PSS and m_B -based stabilizers are increasing almost linearly with system loading.
- The PSS is more effective at leading power factor conditions, whereas the δ_E and m_B are least effective at this power factor conditions.

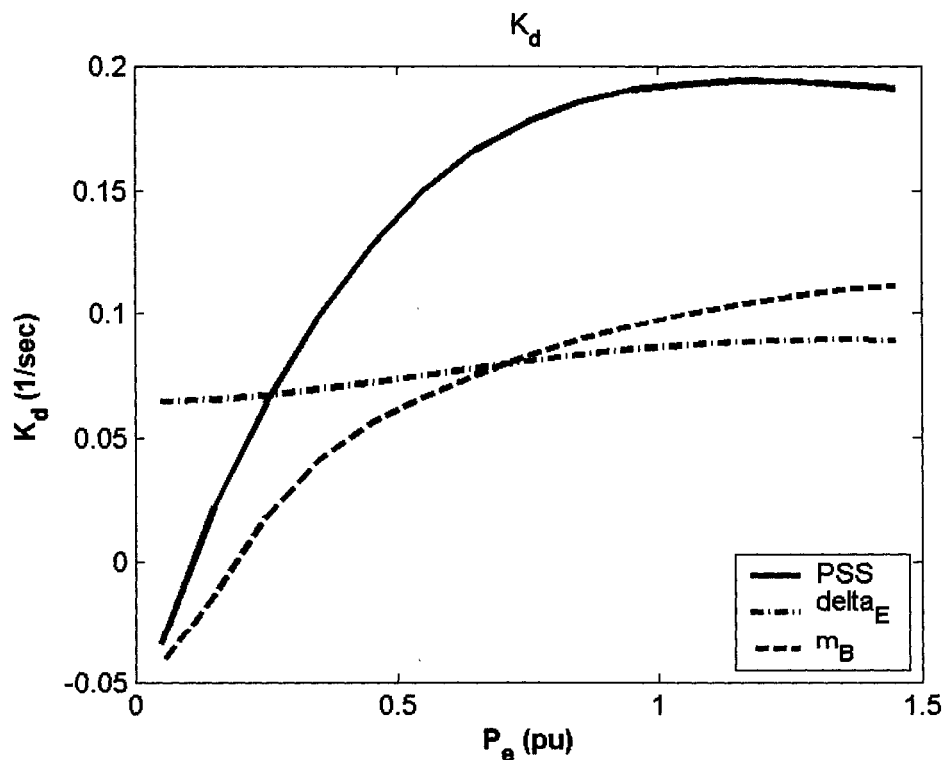


Figure 8.43: Damping torque coefficient with the proposed stabilizers at $Q = -0.4$ pu, J_1 settings, multiple-point tuning, individual design

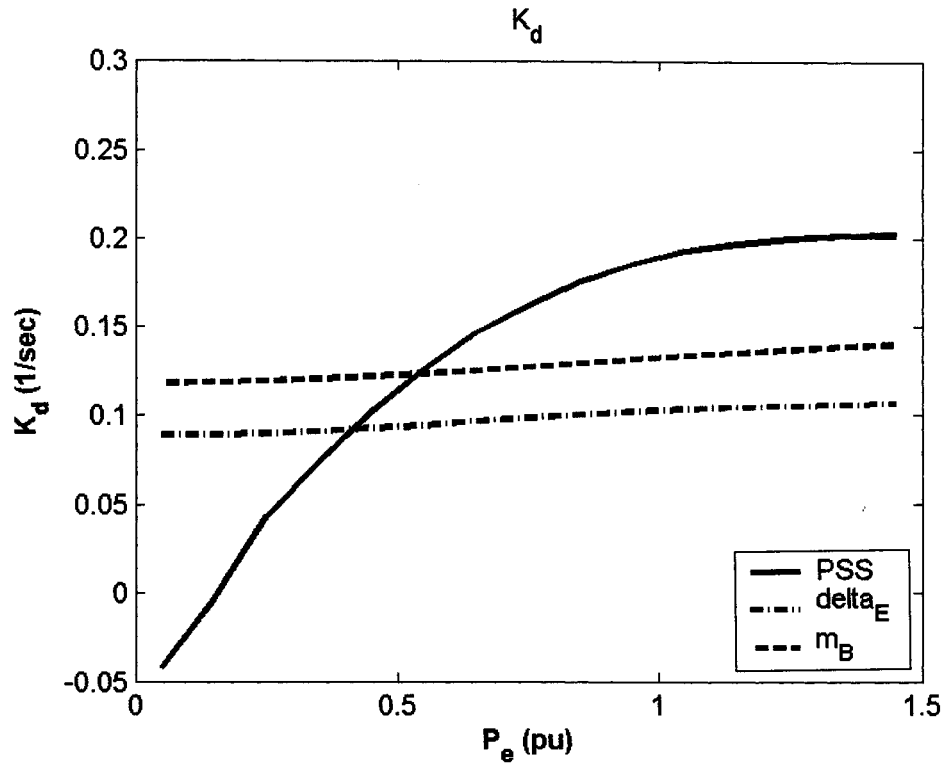


Figure 8.44: Damping torque coefficient with the proposed stabilizers at $Q = 0.0$ pu, J_1 settings, multiple-point tuning, individual design

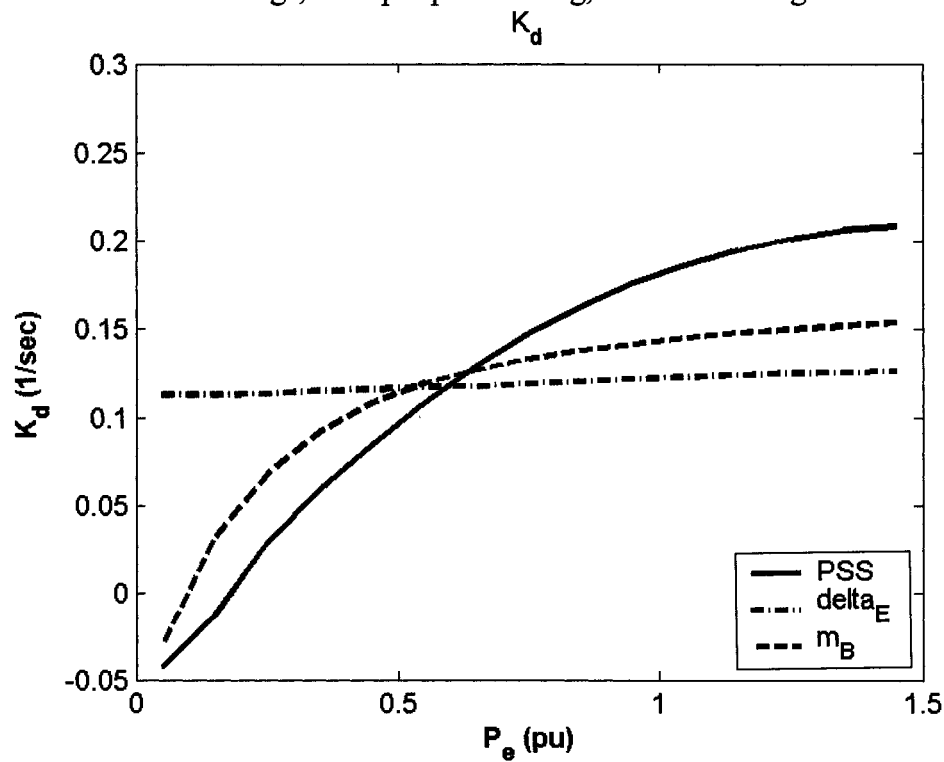


Figure 8.45: Damping torque coefficient with the proposed stabilizers at $Q = 0.4$ pu, J_1 settings, multiple-point tuning, individual design

Nonlinear Time-Domain Simulations: Figures 8.43-8.47 show the system responses, respectively, due to a 6-cycle three-phase fault at the nominal loading conditions. It can be readily seen that the PSS is the most effective stabilizer. This agrees with the damping torque coefficient analysis results. Figures 8.48-8.52 show the control effort provided by the stabilizing signal of the PSS, the excitation phase angle modulation, δ_E , and the boosting magnitude modulation, m_B , respectively.

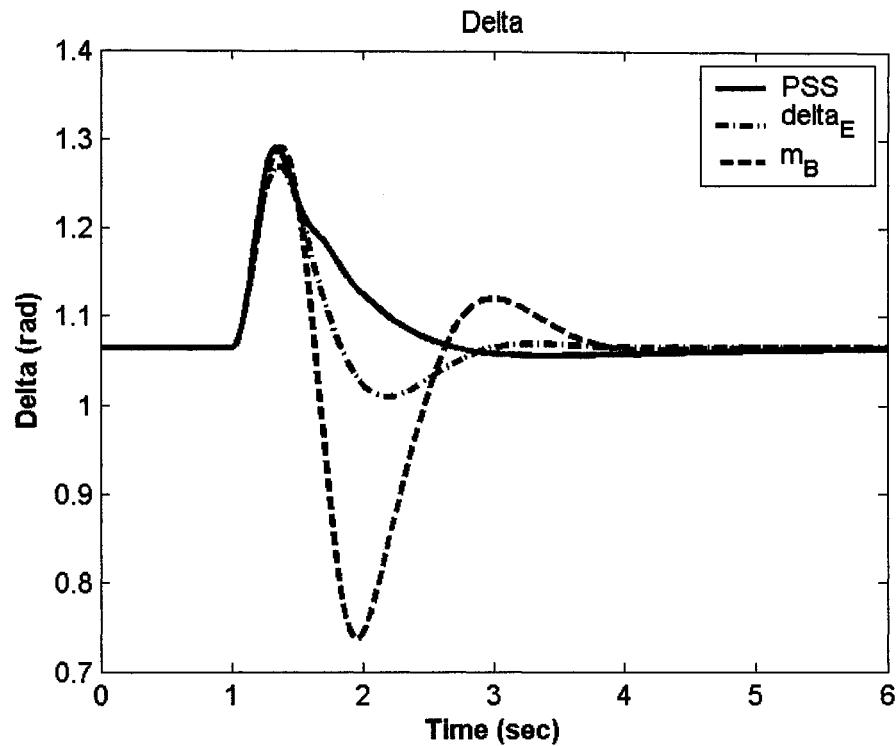


Figure 8.46: Rotor angle response for 6-cycle fault with nominal loading, J_1 settings, multiple-point tuning, individual design

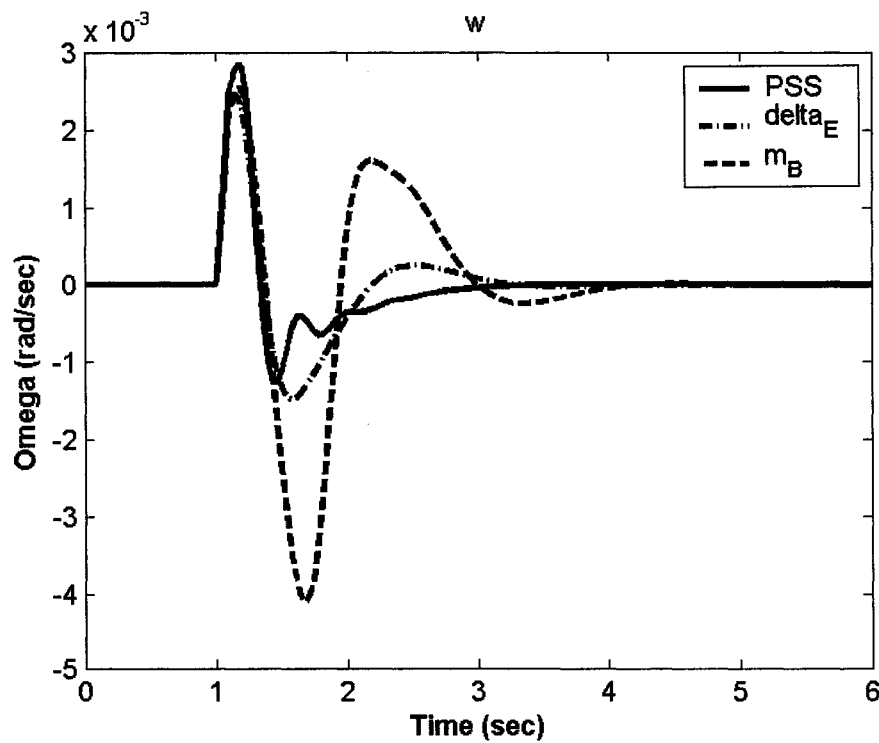


Figure 8.47: Speed response for 6-cycle fault with nominal loading, J_1 settings, multiple-point tuning, individual design

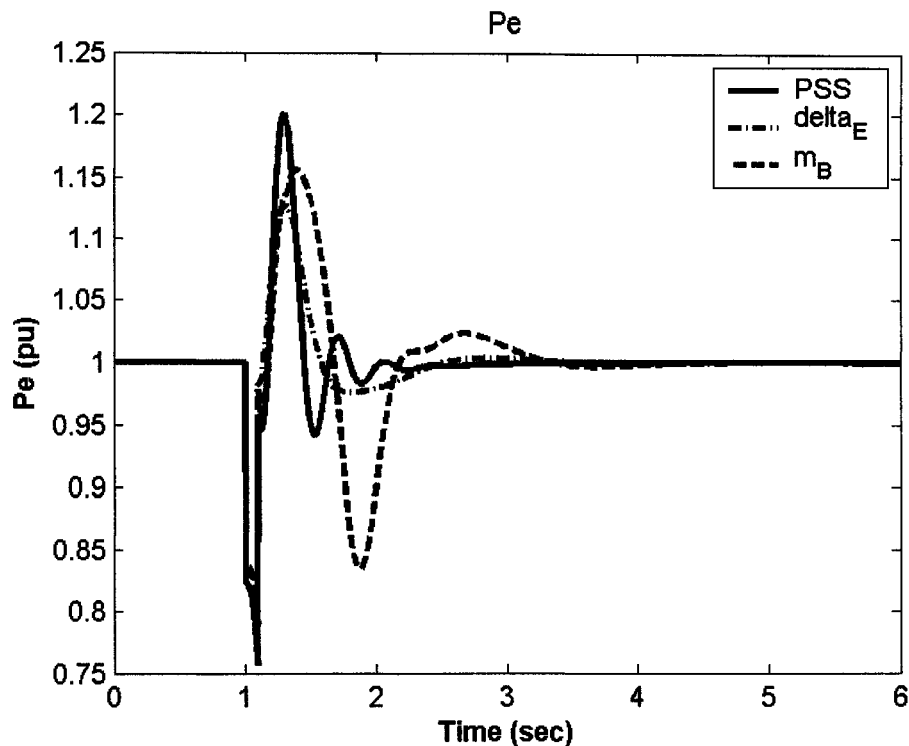


Figure 8.48: Electrical power response for 6-cycle fault with nominal loading, J_1 settings, multiple-point tuning, individual design

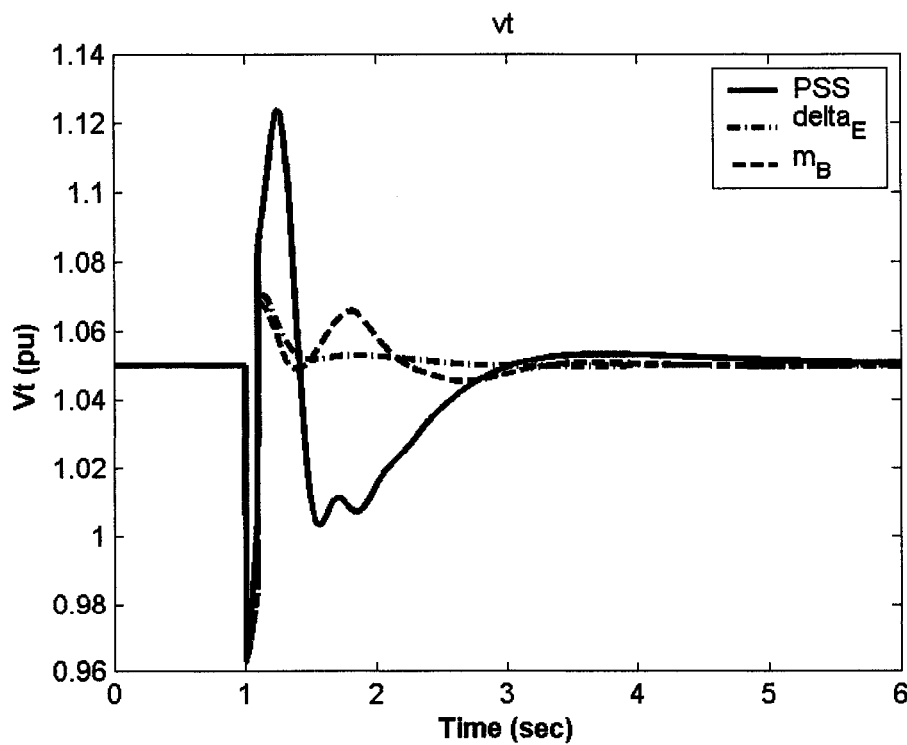


Figure 8.49: Terminal voltage response for 6-cycle fault with nominal loading, J_1 settings, multiple-point tuning, individual design

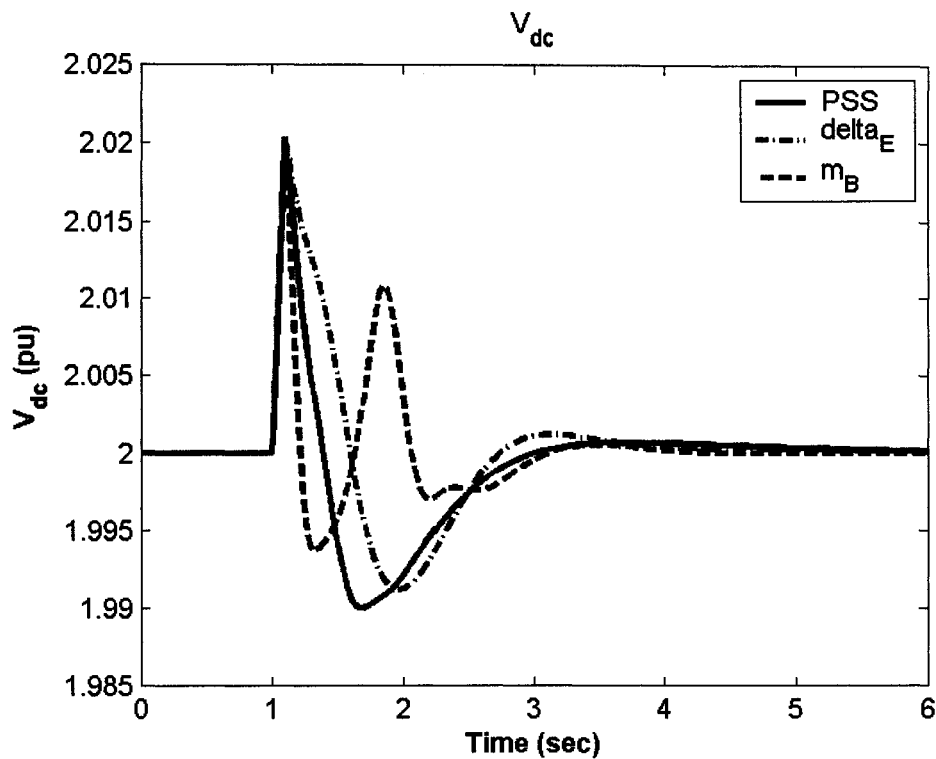


Figure 8.50: DC voltage response for 6-cycle fault with nominal loading, J_1 settings, multiple-point tuning, individual design

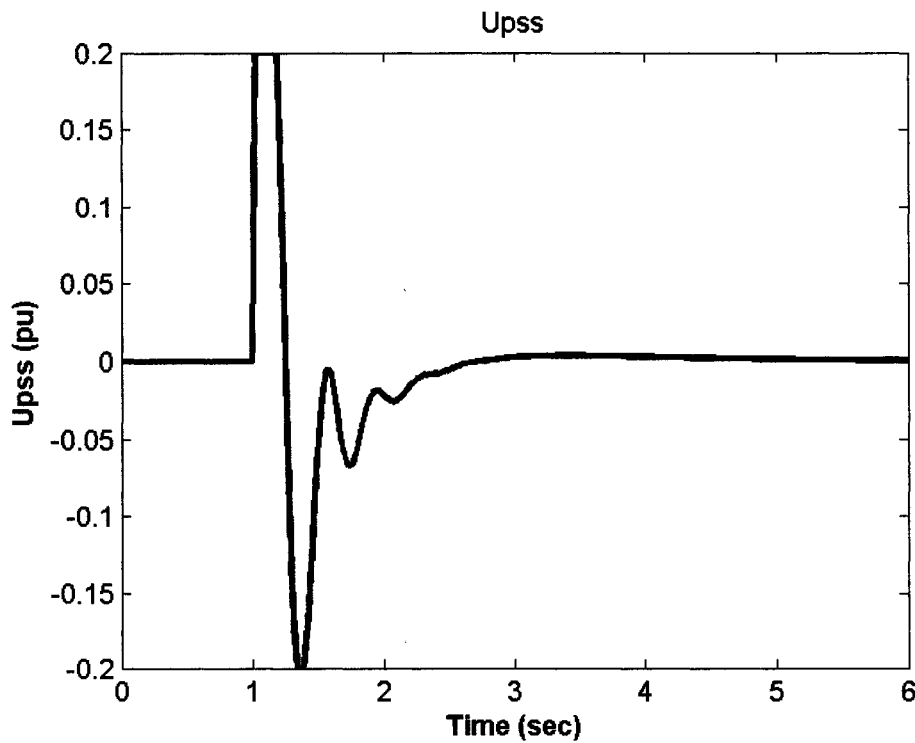


Figure 8.51: PSS stabilizing signal for 6-cycle fault with nominal loading, J_1 settings, multiple-point tuning, individual design

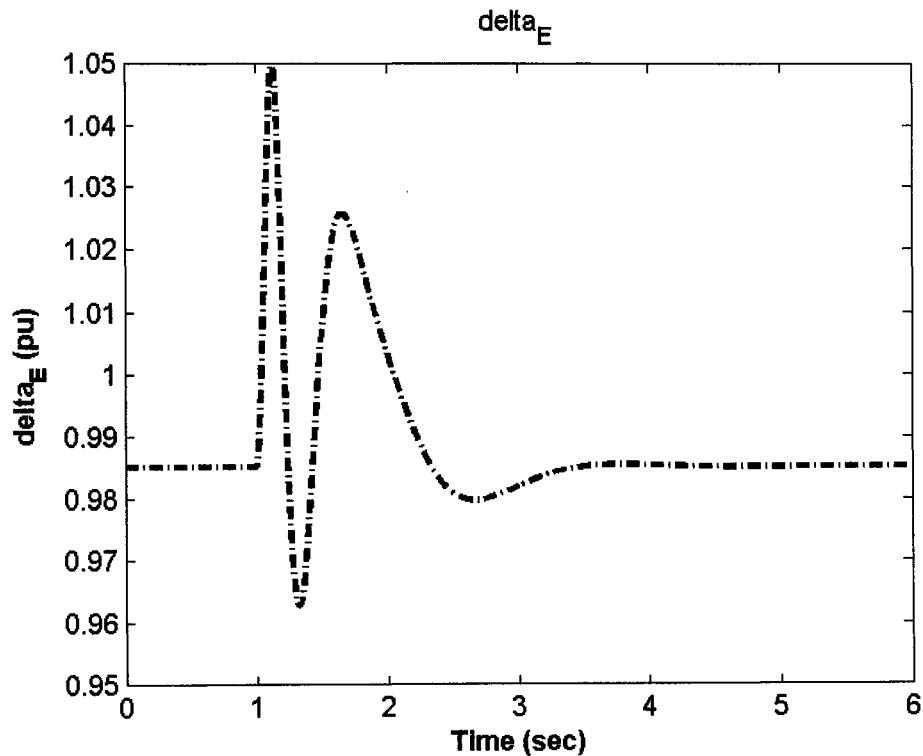


Figure 8.52: δ_E response for 6-cycle fault with nominal loading, J_1 settings, multiple-point tuning, individual design

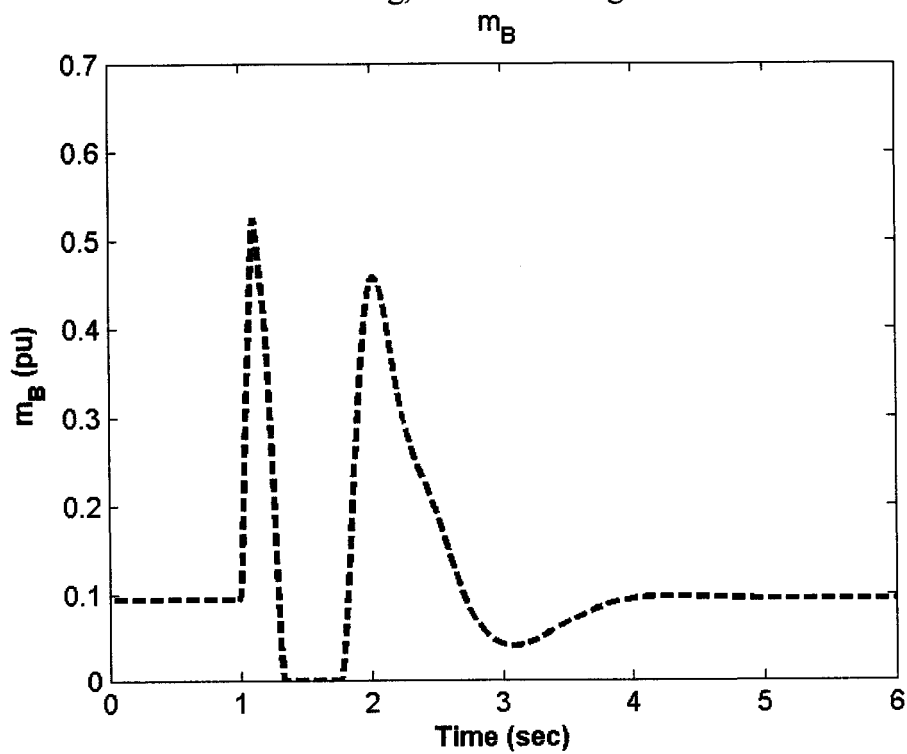


Figure 8.53: m_B response 6-cycle fault with nominal loading, J_1 settings, multiple-point tuning, individual design

8.2.2.2 Individual Design with J_2

The PSS, δ_E , m_B -based stabilizers are designed individually considering all the operating points mentioned above.

Stabilizer Design: PSO is used to optimize the parameters of each controller that minimize the maximum damping factor of all the complex eigenvalues associated with the 16 operating points simultaneously. The final settings of the optimized parameters for the proposed stabilizers are given in Table 8.24.

Eigenvalue Analysis: The system eigenvalues without and with the proposed stabilizers at the four operating points, nominal, light, heavy, and leading Pf, are given in Tables 8.25-8.28, respectively. The bold rows of these tables represent the EM mode eigenvalue and its damping ratio.

Table 8.24: Optimal parameter settings with J_2 , multiple-point tuning, individual design

	PSS	δ_E	m_B
K	95.580	-100.00	96.862
T₁	4.3413	5.0000	4.9980
T₂	0.0100	1.0379	2.5728
T₃	0.0761	0.0643	0.1203
T₄	3.5155	1.5452	0.0100

Table 8.25: System eigenvalues of nominal loading conditions with J_2 settings, multiple-point tuning, individual design

No Control	PSS	δ_E	m_B
$1.5033 \pm 5.3328i,$ -0.2713	-1.2000, 1.0000 -2.5800 \pm 17.550i	$-5.8331 \pm 5.8251i,$ 0.7076	$-3.9100 \pm 12.720i,$ 0.2900
-11.4584 \pm 6.8596i	-103.02	-3.5239 \pm 5.3275i	-82.530
-15.5063	-15.250	-15.5062	-41.500
-5.1052	-10.420	-5.1307	-15.530
--	-5.3800	-2.2327	-5.4900
--	-0.3500	-0.5487	-4.7900
--	-0.2100	-0.2000	-2.7600
--	--	-20.0000	-0.4900
--	--	--	-0.2000

Table 8.26: System eigenvalues of light loading conditions with J_2 settings, multiple-point tuning, individual design

No Control	PSS	δ_E	m_B
$1.3952 \pm 5.0825i,$ - 0.2647	$-3.9100 \pm 3.6200i,$ 0.7300	$-6.3690 \pm 3.9101i,$ 0.8522	-38.6900, 1.0000 -3.7100 \pm 12.190i
-11.3641 \pm 6.1234i	-3.8400 \pm 9.0200i	-2.9370 \pm 5.6541i	-5.8100 \pm 0.1400i
-14.7072	-101.06	-14.7071	-85.640
-5.8534	-14.790	-5.9913	-14.710
--	-9.1300	-2.2444	-2.2900
--	-0.3000	-0.5541	-0.5100
--	-0.2000	-20.000	-0.2000
--	--	-0.2000	--

Table 8.27: System eigenvalues of heavy loading conditions with J_2 settings, multiple-point tuning, individual design

No Control	PSS	δ_E	m_B
$1.4138 \pm 5.0066i$, -0.2718	-1.8900, 1.0000 -2.8000 \pm 17.070i	$-1.9204 \pm 1.7604i$, 0.7372	$-3.5600 \pm 13.120i$, 0.2600
-11.4375 \pm 6.1904i	-102.82	-4.1470 \pm 8.1099i	-1.4500
-15.2584	-15.640	-15.258	-82.100
-5.2121	-11.770	-8.3276	-42.600
--	-2.7200	-5.8671	-15.290
--	-0.3400	-0.5407	-6.1700
--	-0.2100	-0.2000	-5.6200
--	--	-20.000	-0.5700
--	--	--	-0.2000

Table 8.28: System eigenvalues of leading Pf loading conditions with J_2 settings, multiple-point tuning, individual design

No Control	PSS	δ_E	m_B
$1.4502 \pm 5.3584i$, - 0.2612	-8.1200 \pm 1.9900i , 0.97	$-1.8267 \pm 5.4732i$, 0.3166	$-3.5300 \pm 2.6100i$, 0.8000
-11.3963 \pm 7.0920i	-2.7200 \pm 16.280i	-7.7343 \pm 6.5214i	-4.3500 \pm 11.140i
-15.4566	-102.66	-15.4564	-87.520
-5.1711	-14.920	-5.1516	-35.860
--	-1.1800	-1.8490	-15.700
--	-0.3500	-0.5516	-5.6200
--	-0.2100	-0.2000	-0.4500
--	--	-20.000	-0.2000

Damping Torque Coefficient Analysis: The damping torque coefficient K_d is calculated for the proposed robust stabilizers to measure their effectiveness in enhancing the system damping characteristics. The damping torque coefficient is calculated for a range of 45 operating points specified by $P_e=[0.05 - 1.45]$ pu in steps of 0.10 pu and $Q_e=[-0.40, 0.00, 0.40]$ pu.

For comparison purposes, K_d for all stabilizers at $Q=-0.4$, $Q=0.0$, and $Q=0.4$ pu are shown in Figures 8.54-8.56, respectively. From these figures, the following can be noticed:

- At lagging power factor, except for very low loading, and at unity power factor, the m_B -based stabilizer becomes the most effective in damping the EM mode oscillation .
- At leading power factor, δ_E is the most effective at light loading, PSS becomes the best at moderate and nominal loading, and m_B is the strongest at heavy loading.
- The PSS and m_B suffer from negative damping characteristics at light loading.
- The damping torque coefficients of the δ_E -based stabilizer is almost unaffected by loading level.
- The damping torque coefficients K_d associated with the PSS is increasing almost linearly with system loading. At heavy loading, however, the damping torque coefficient starts decreasing.
- The damping torque coefficients K_d associated with the m_B is increasing almost linearly with system loading, except for unity power factor where K_d is almost unaffected by the loading.
- Except for heavy loading, the PSS is more effective at leading power factor conditions, whereas the δ_E and m_B are least effective at this power factor conditions.

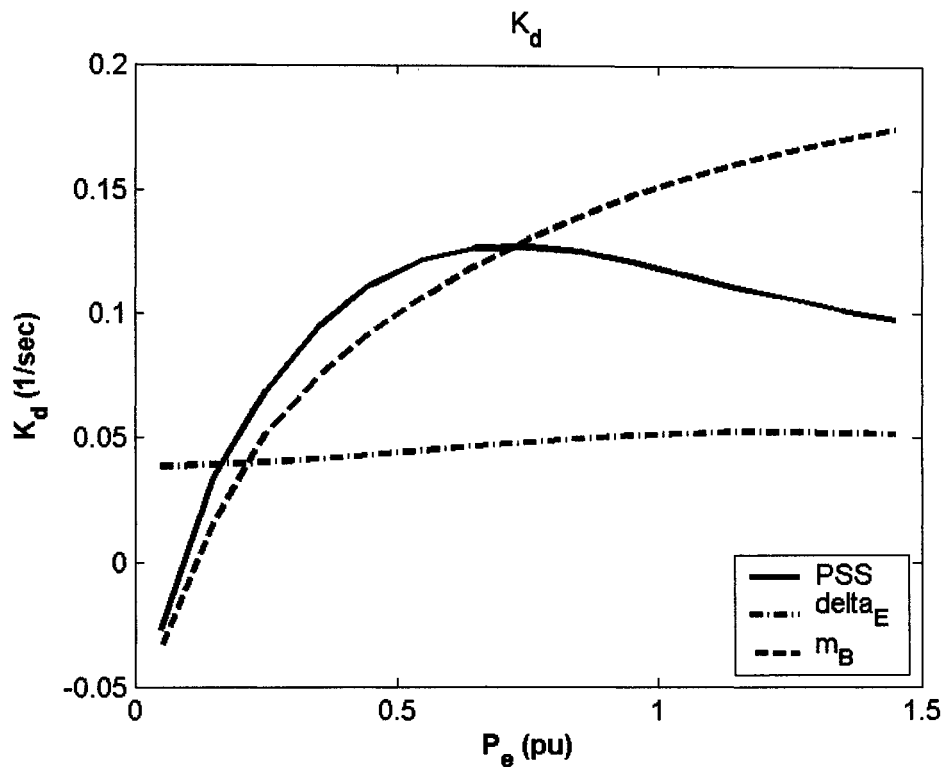


Figure 8.54: Damping torque coefficient with the proposed stabilizers at $Q = -0.4$ pu, J_2 settings, multiple-point tuning, individual design

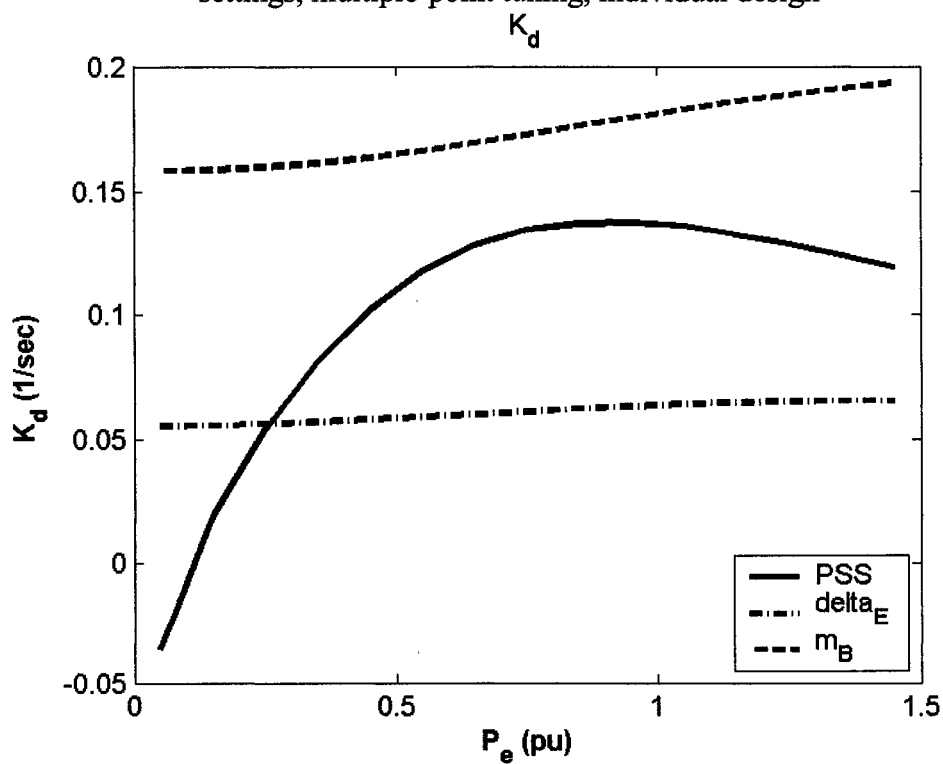


Figure 8.55: Damping torque coefficient with the proposed stabilizers at $Q = 0.0$ pu, J_2 settings, multiple-point tuning, individual design

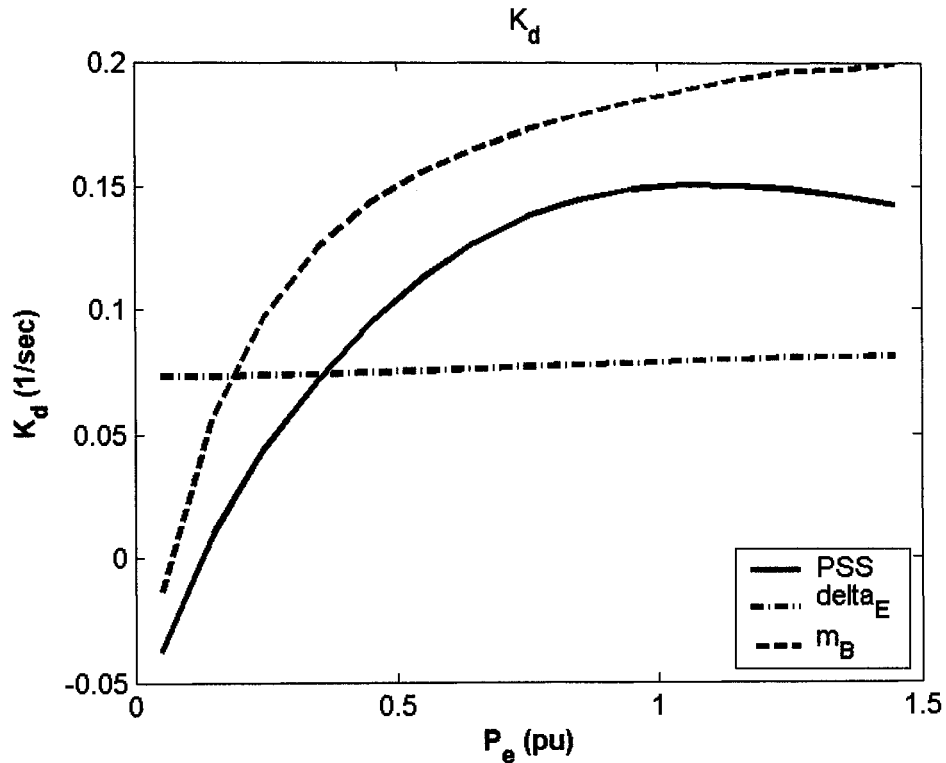


Figure 8.56: Damping torque coefficient with the proposed stabilizers at $Q = 0.4$ pu, J_2 settings, multiple-point tuning, individual design

Nonlinear Time-Domain Simulations: Figures 8.57-8.61 show the system responses, respectively, due to a 6-cycle three-phase fault at the nominal loading conditions. It can be readily seen that the PSS is more effective than δ_E . This agrees with the damping torque coefficient analysis results. Figures 8.62-8.64 show the control effort provided by the stabilizing signal of the PSS, the excitation phase angle modulation, δ_E , and the boosting magnitude modulation, m_B , respectively.

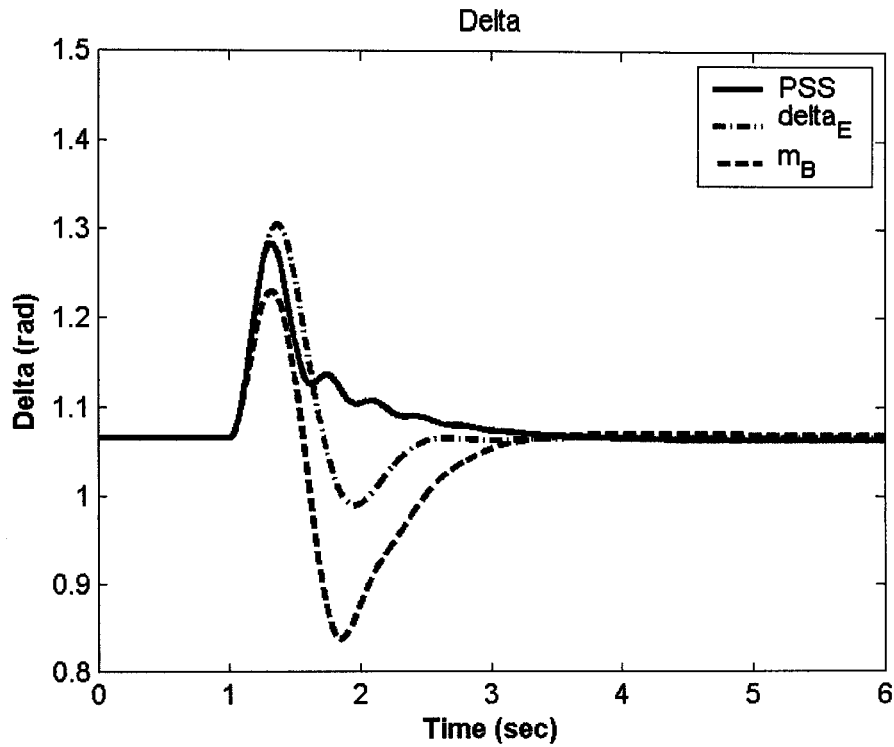


Figure 8.57: Rotor angle response for 6-cycle fault with nominal loading, J_2 settings, multiple-point tuning, individual design

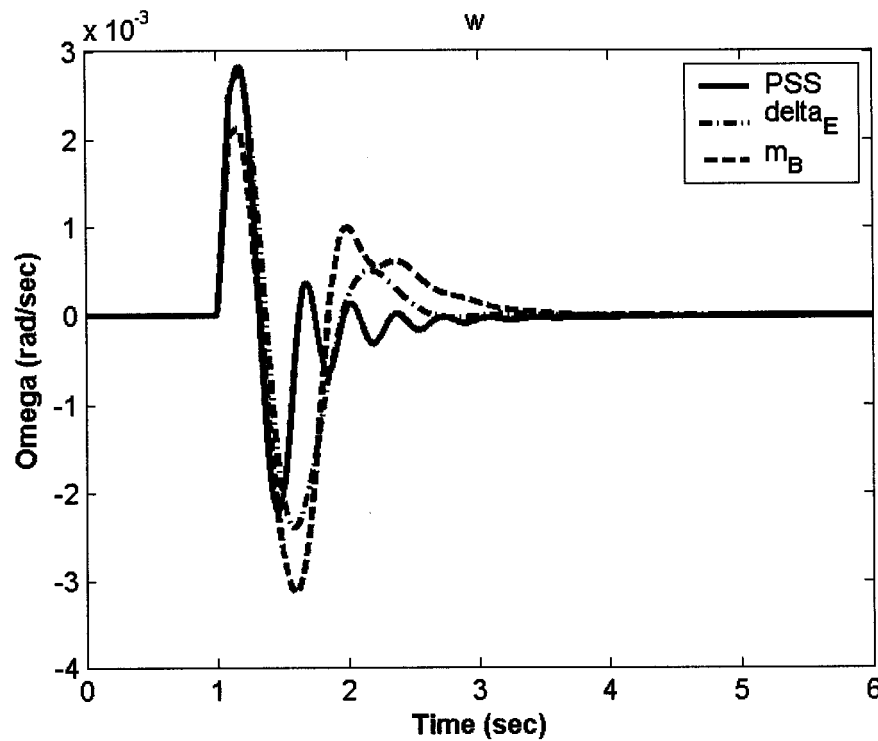


Figure 8.58: Speed response for 6-cycle fault with nominal loading, J_2 settings, multiple-point tuning, individual design

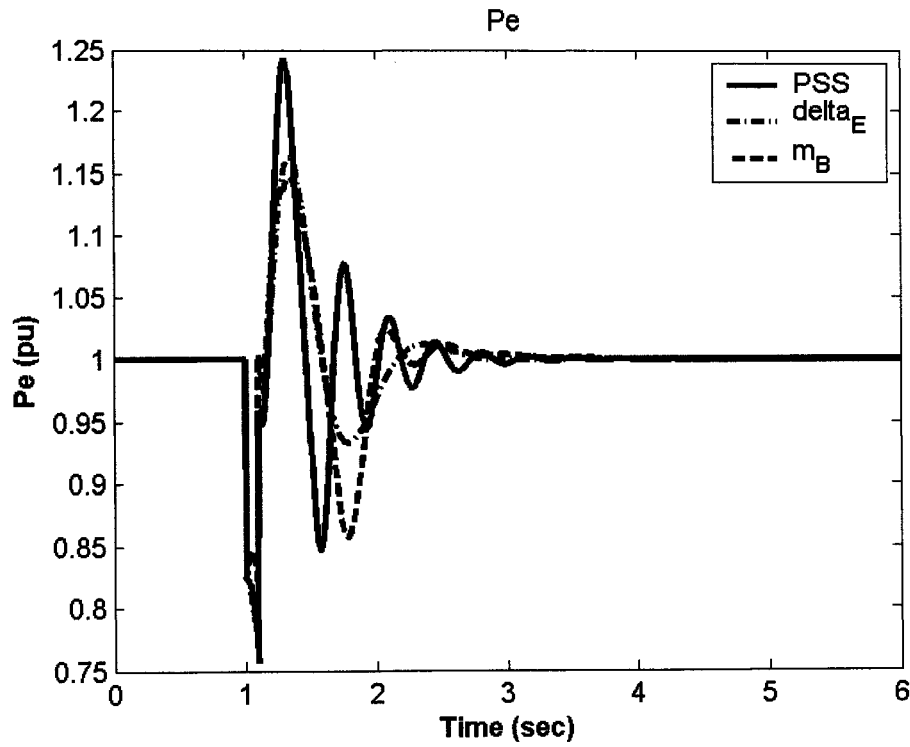


Figure 8.59: Electrical power response for 6-cycle fault with nominal loading, J_2 settings, multiple-point tuning, individual design

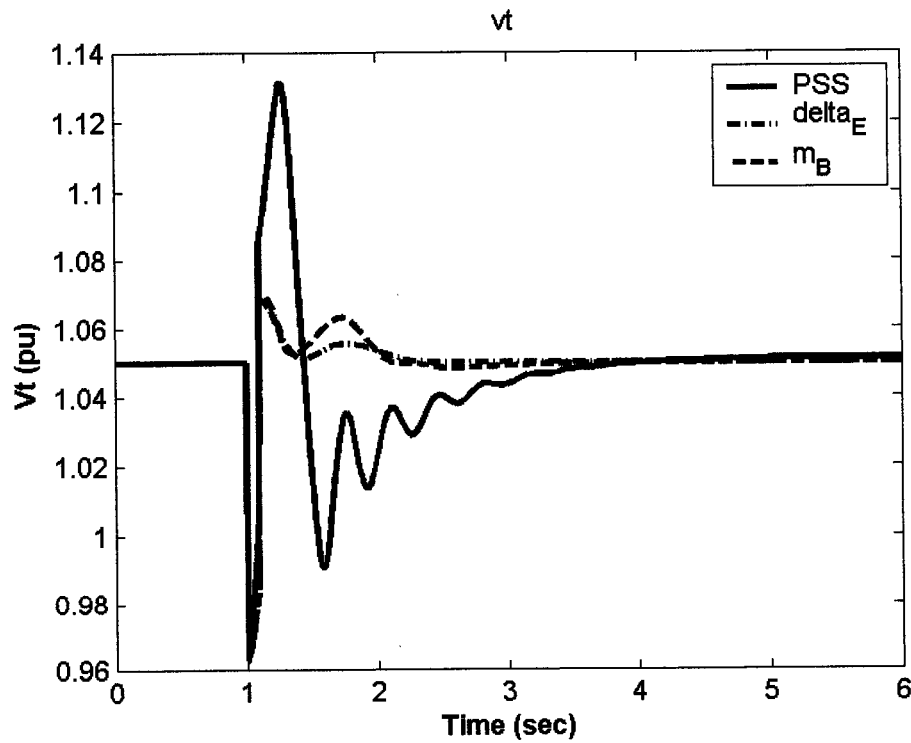


Figure 8.60: Terminal voltage response for 6-cycle fault with nominal loading, J_2 settings, multiple-point tuning, individual design

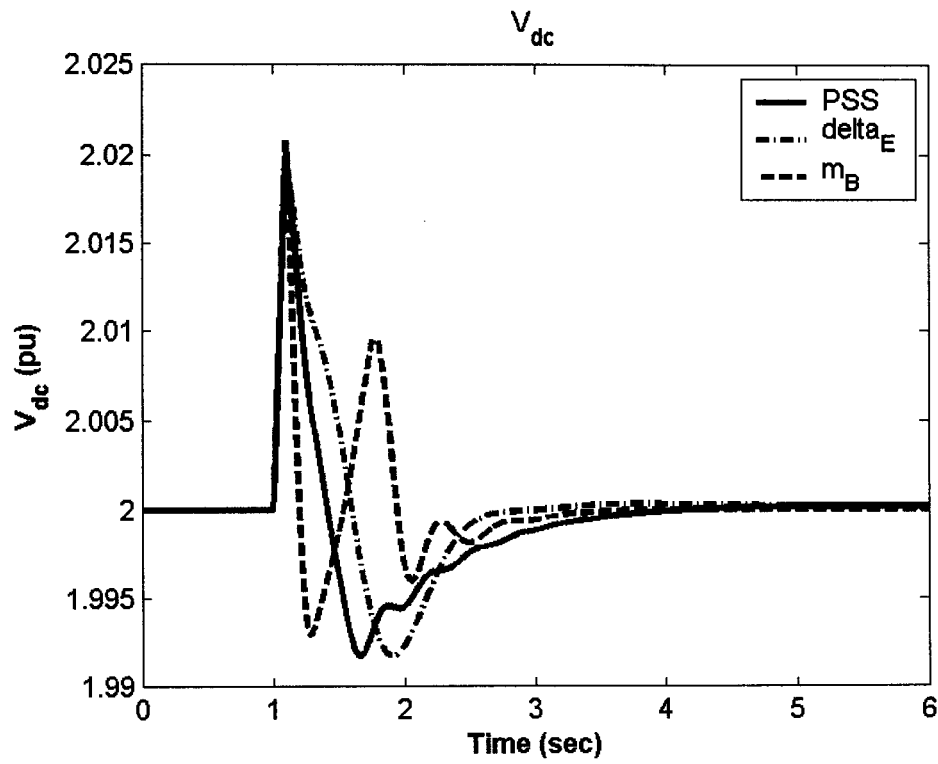


Figure 8.61: DC voltage response for 6-cycle fault with nominal loading, J_2 settings, multiple-point tuning, individual design

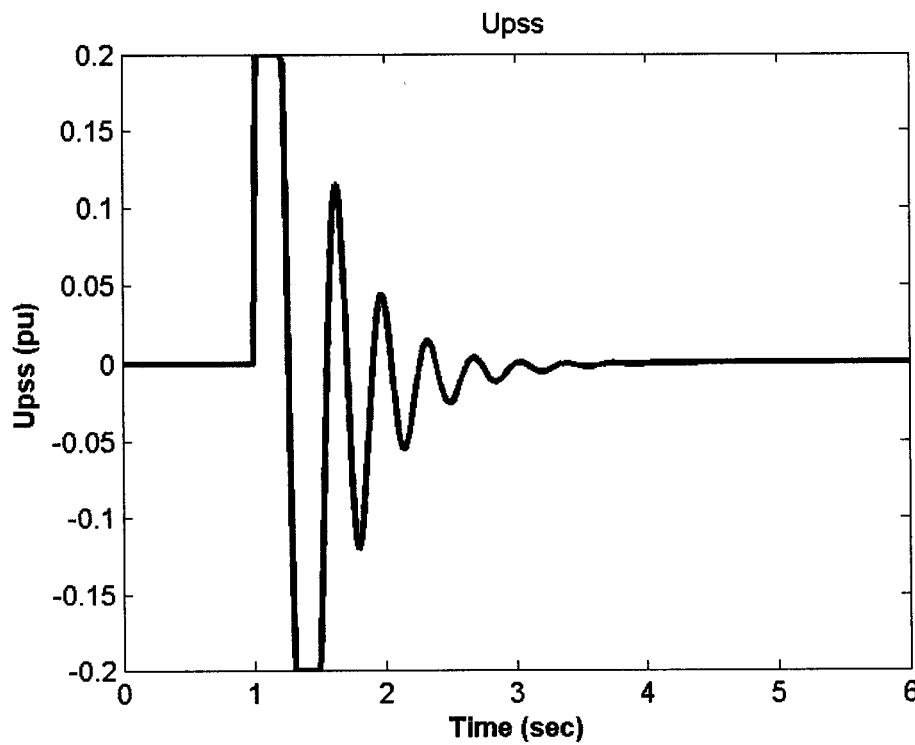


Figure 8.62: PSS stabilizing signal for 6-cycle fault with nominal loading, J_2 settings, multiple-point tuning, individual design

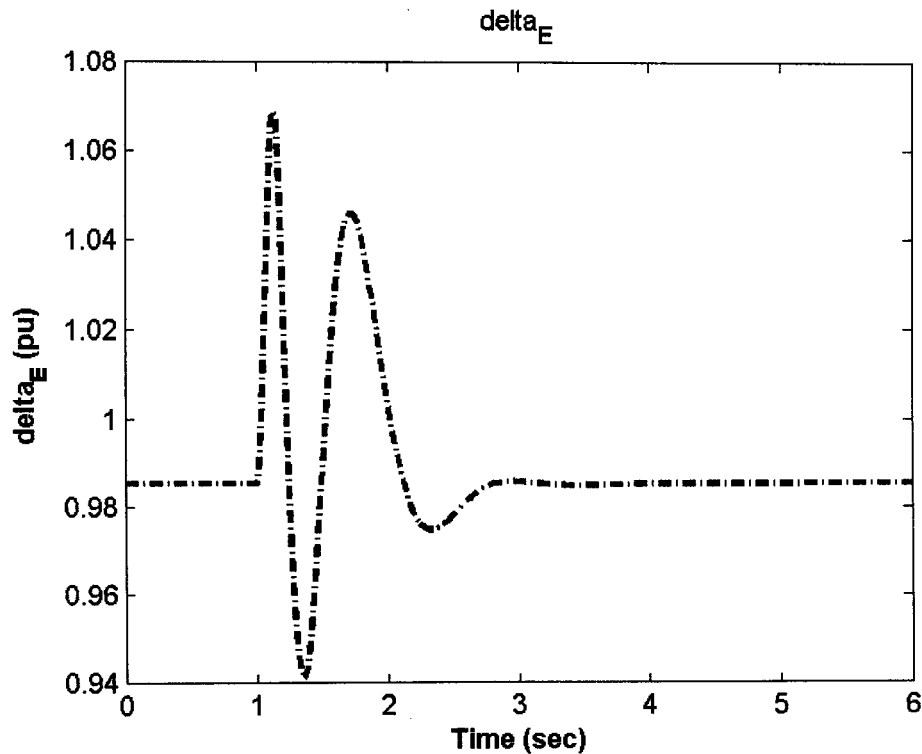


Figure 8.63: δ_E response for 6-cycle fault with nominal loading, J_2 settings, multiple-point tuning, individual design

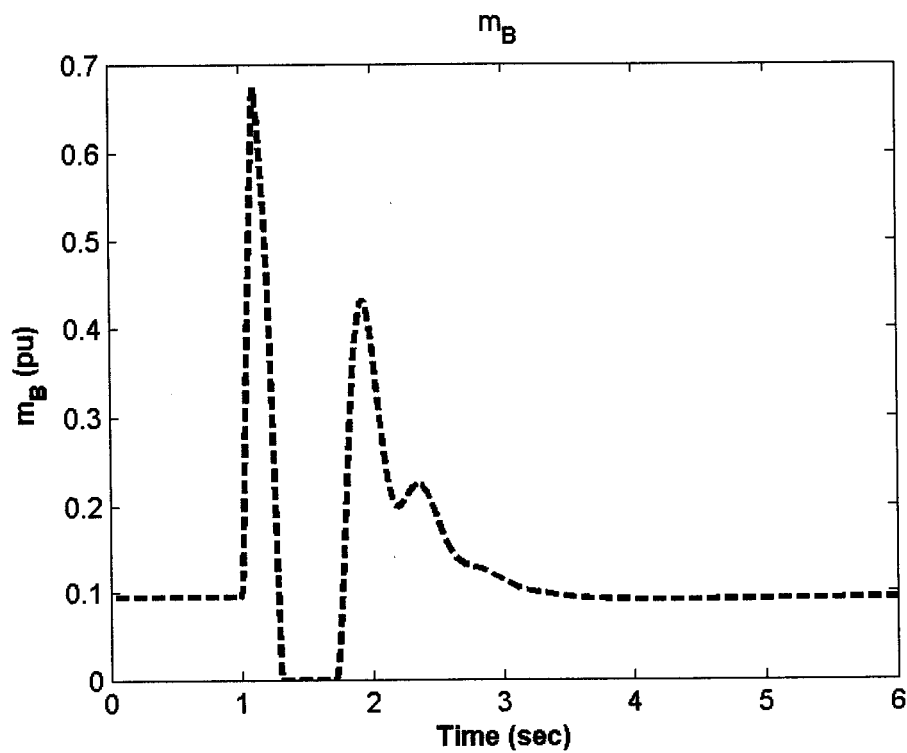


Figure 8.64: m_B response 6-cycle fault with nominal loading, J_2 settings, multiple-point tuning, individual design

8.2.2.3 Coordinated Design with J_2

Although the controllability measure analysis based on the singular value decomposition, the damping torque coefficient analysis, and the nonlinear time-domain simulation show the relative robustness of the δ_E -based stabilizer in damping the EM mode oscillation, still there is room for more improvement through coordination with the m_B -based stabilizer. In this section, the coordinated design of δ_E - and m_B -based stabilizers is considered at all the 16 operating points described earlier.

Stabilizer Design: PSO is used to simultaneously search for the optimum parameter settings of both controllers that minimize the maximum damping factor of all the system complex eigenvalues at all the 16 operating points simultaneously. The final settings of the optimized parameters for the proposed stabilizers are given in Table 8.29.

Eigenvalue Analysis: The system eigenvalues without and with the proposed δ_E - and m_B -based controllers when applied individually and through coordinated design at the four loading conditions; nominal, light, heavy, and leading Pf, are given in Tables 8.30-8.33, respectively. The bold rows of these tables represent the EM mode eigenvalue and its damping ratio. It is evident that the damping factor of the EM mode eigenvalue is greatly enhanced using the proposed coordinated stabilizers design.

Table 8.29: Optimal parameter settings with J_2 , multiple-point tuning, coordinated design

	Individual		Coordinated	
	δ_E	m_B	δ_E	m_B
K	-100.00	96.862	-66.1817	100
T₁	5.0000	4.9980	1.5345	5.0000
T₂	1.0379	2.5728	1.6110	3.0948
T₃	0.0643	0.1203	4.4207	5.0000
T₄	1.5452	0.0100	3.9503	3.3213

Table 8.30: System eigenvalues of nominal loading conditions with J_2 settings, multiple-point tuning, coordinated design

No Control	δ_E	m_B	δ_E & m_B
1.5033± 5.3328i, -0.2713	-5.8331 ± 5.8251i, 0.7076	-3.9100± 12.720i, 0.2900	-10.841± 2.8884i, 0.9663
-11.458± 6.8596i	-3.5239 ± 5.3275i	-82.530	-11.642±14.362i
-15.506	-15.5062	-41.500	-7.1791± 10.060i
-5.1052	-5.1307	-15.530	-1.1594
--	-2.2327	-5.4900	-0.6470
--	-0.5487	-4.7900	-0.5818
--	-0.2000	-2.7600	-0.2625
--	-20.0000	-0.4900	-0.2518
--	--	-0.2000	-0.1997

Table 8.31: System eigenvalues of light loading conditions with J_2 settings, multiple-point tuning, coordinated design

No Control	δ_E	m_B	δ_E & m_B
1.3952± 5.0825i, -0.2647	-6.3690 ± 3.9101i, 0.8522	-38.6900, 1.0000 -3.7100 ± 12.190i	-13.421± 12.312i, 0.7369
-11.364± 6.1234i,	-2.9370 ± 5.6541i	-5.8100 ± 0.1400i	-5.8186± 11.047i
-14.707	-14.7071	-85.640	-10.472± 3.9307i
-5.8534	-5.9913	-14.710	-0.9481
--	-2.2444	-2.2900	-0.7128
--	-0.5541	-0.5100	-0.6049
--	-20.000	-0.2000	-0.2615
--	-0.2000	--	-0.2520
--	--	--	-0.1997

Table 8.32: System eigenvalues of heavy loading conditions with J_2 settings, multiple-point tuning, coordinated design

No Control	δ_E	m_B	δ_E & m_B
1.4138± 5.0066i, -0.2718	-1.9204 ± 1.7604i, 0.7372	-3.5600± 13.120i, 0.2600	-0.6485± 0.3310i, 0.8907
-11.4375± 6.1904i	-4.1470 ± 8.1099i	-1.4500	-12.174± 14.267i
-15.258	-15.258	-82.100	-7.2182± 11.654i
-5.2121	-8.3276	-42.600	-10.507± 1.6998i
--	-5.8671	-15.290	-0.6165
--	-0.5407	-6.1700	-0.2590
--	-0.2000	-5.6200	-0.2512
--	-20.000	-0.5700	-0.1997
--	--	-0.2000	

Table 8.33: System eigenvalues of leading Pf loading conditions with J_2 settings, multiple-point tuning, coordinated design

No Control	δ_E	m_B	δ_E & m_B
1.4502± 5.3584i, -0.2612	-1.8267 ± 5.4732i, 0.3166	-3.5300 ± 2.6100i, 0.8000	-12.325± 3.7890i, 0.9559
-11.3963± 7.0920i	-7.7343 ± 6.5214i	-4.3500 ± 11.140i	-10.914± 14.3290i
-15.456	-15.4564	-87.520	-5.8657± 6.4690i
-5.1711	-5.1516	-35.860	-2.4041
--	-1.8490	-15.700	-0.6239
--	-0.5516	-5.6200	-0.4671
--	-0.2000	-0.4500	-0.2672
--	-20.000	-0.2000	-0.2521
--			-0.1997

Damping Torque Coefficient Analysis: To measure the effectiveness of the proposed δ_E - m_B coordinated design in improving the system damping characteristics and compare it with both individual designs, the damping torque coefficient K_d is estimated. K_d is calculated for a range of 45 operating points specified by $P_e=[0.05 - 1.45]$ pu in steps of 0.10 pu and $Q_e=[-0.40, 0.00, 0.40]$ pu.

For comparison purposes, the damping torque coefficient for the coordinated δ_E - m_B stabilizer design and the both individual designs at $Q=-0.4$, $Q=0.0$, and $Q=0.4$ pu are shown in Figures 8.65-8.67, respectively. These figures address the highly effective coordinated design, as compared with δ_E and m_B individual designs, over the different loading conditions.

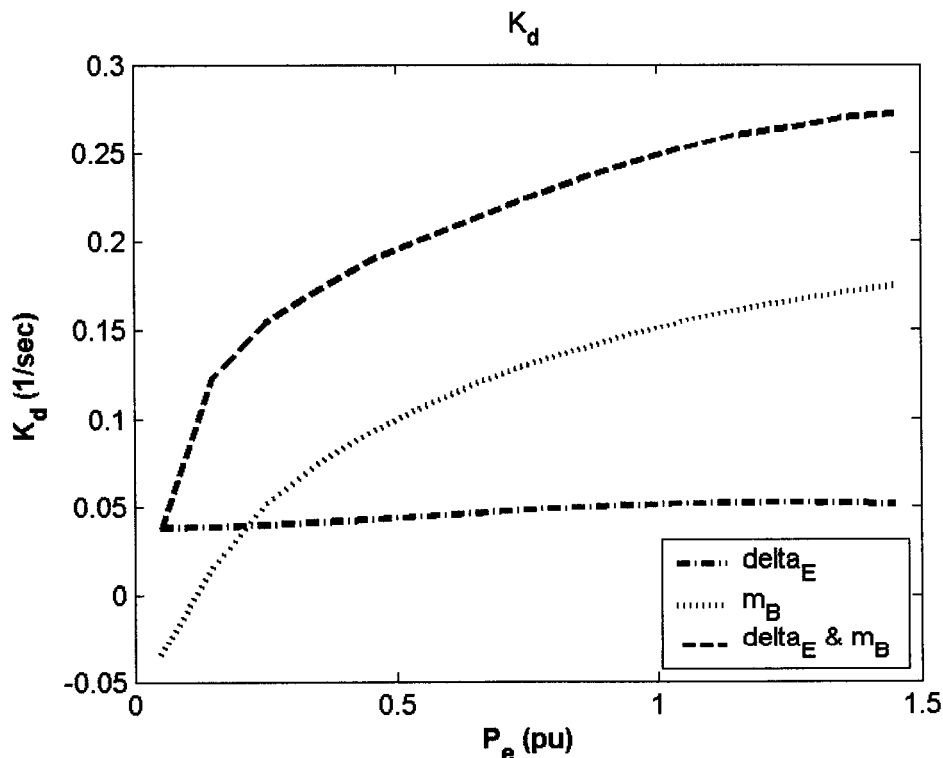


Figure 8.65: Damping torque coefficient with coordinated δ_E and m_B -based controller at $Q = -0.4$ pu, J_2 settings, multiple-point tuning

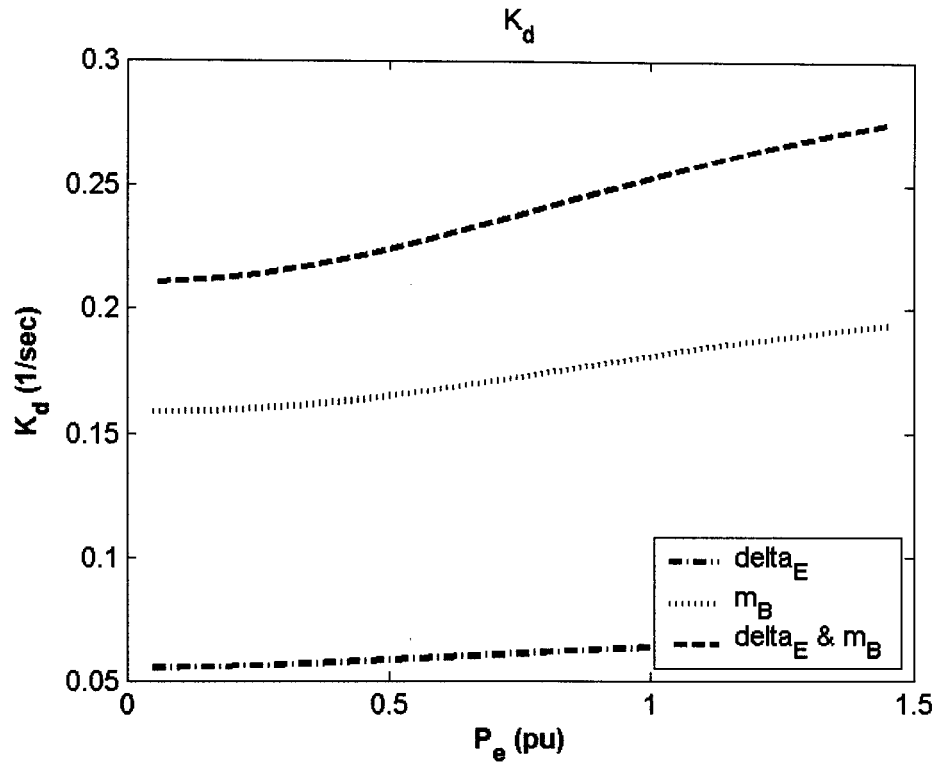


Figure 8.66: Damping torque coefficient with coordinated δ_E and m_B -based controller at $Q = 0.0$ pu, J_2 settings, multiple-point tuning

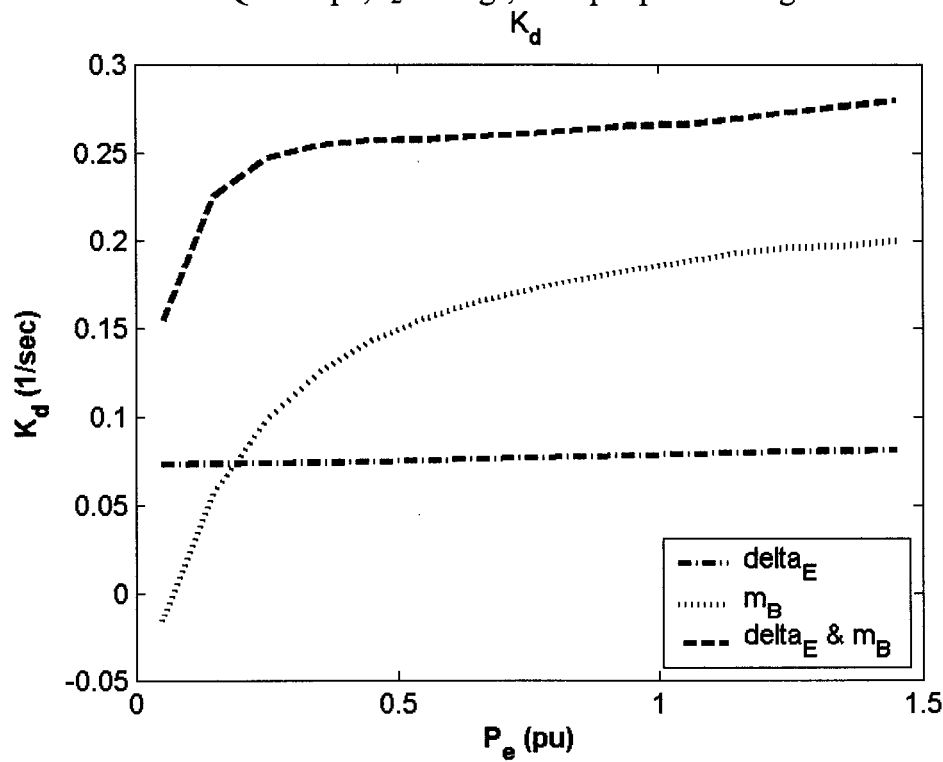


Figure 8.67: Damping torque coefficient with coordinated δ_E and m_B -based controller at $Q = 0.4$ pu, J_2 settings, multiple-point tuning

Nonlinear Time-Domain Simulations: The system responses as well as the control efforts delivered by the stabilizing signals of δ_E and m_B for a 6-cycle three-phase fault at the nominal loading conditions are shown in Figures 8.68-8.74, respectively. The improvement on the system responses when using the coordinated design over the two individual-stabilizer responses is quite evident. This confirms the results obtained from the K_d analysis results.

Likewise, the simulation results and control efforts with a 6-cycle three-phase fault at light loading condition are shown in Figures 8.75-8.81. The simulation results obtained indicate a clear enhancement of the proposed coordinated δ_E - m_B design over both the individual designs. These results agree with the conclusions drawn for damping torque coefficient analysis results. This solves the problem of low effectiveness of the m_B -based stabilizer individual designs at light loading level.

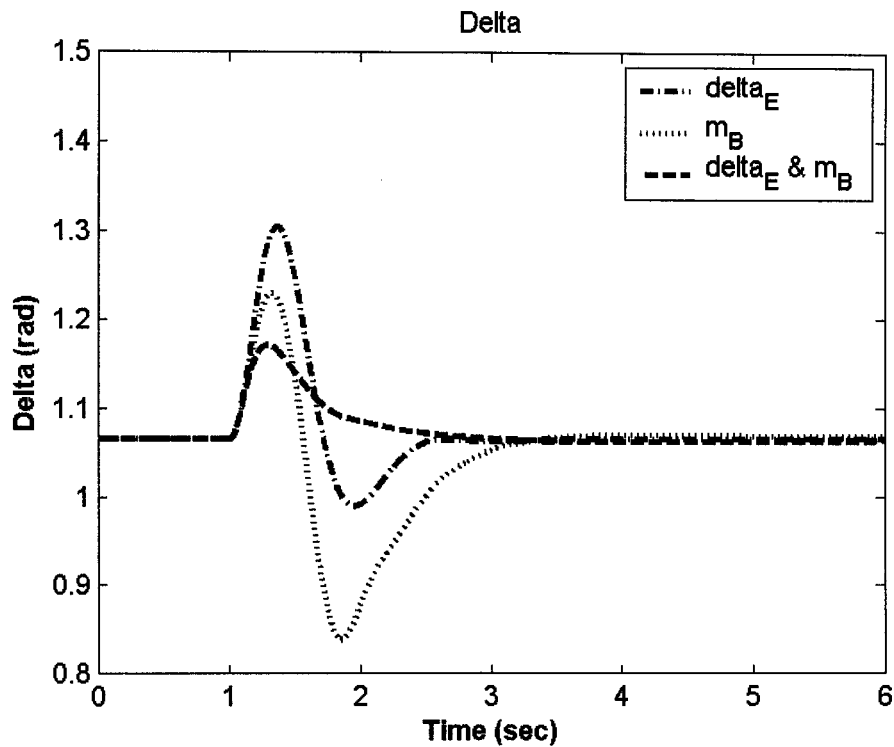


Figure 8.68: Rotor angle response for 6-cycle fault with nominal loading, J_2 settings, multiple-point tuning, coordinated design

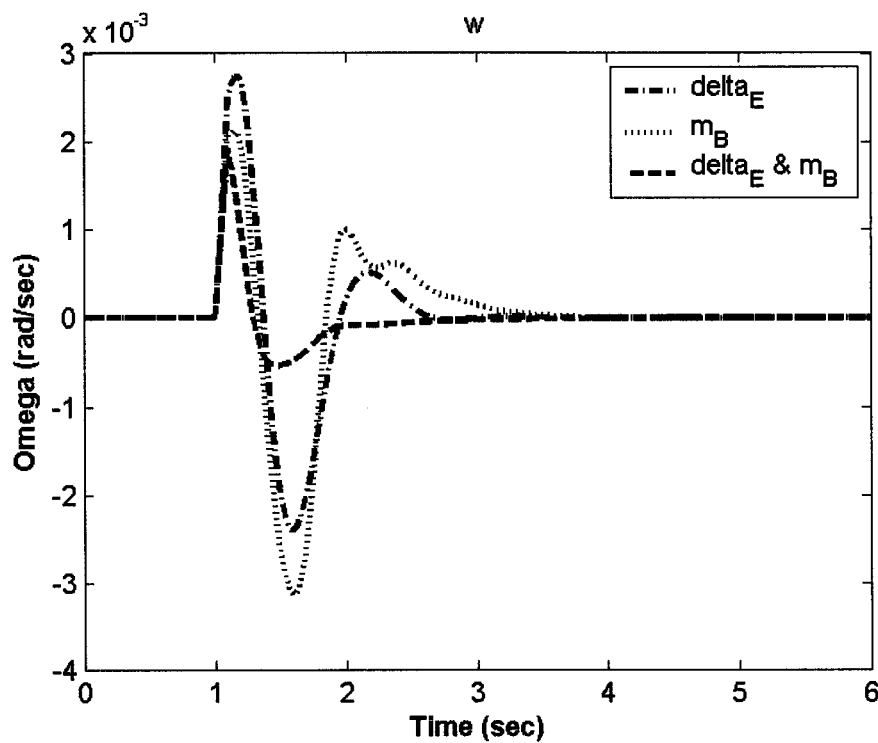


Figure 8.69: Speed response for 6-cycle fault with nominal loading, J_2 settings, multiple-point tuning, coordinated design

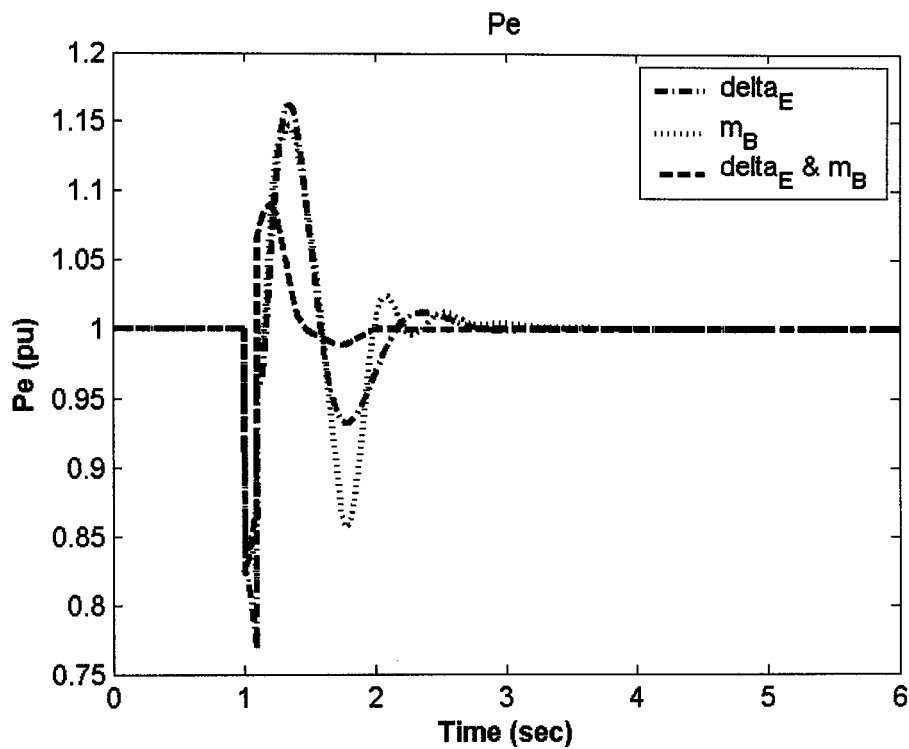


Figure 8.70: Electrical power response for 6-cycle fault with nominal loading, J_2 settings, multiple-point tuning, coordinated design

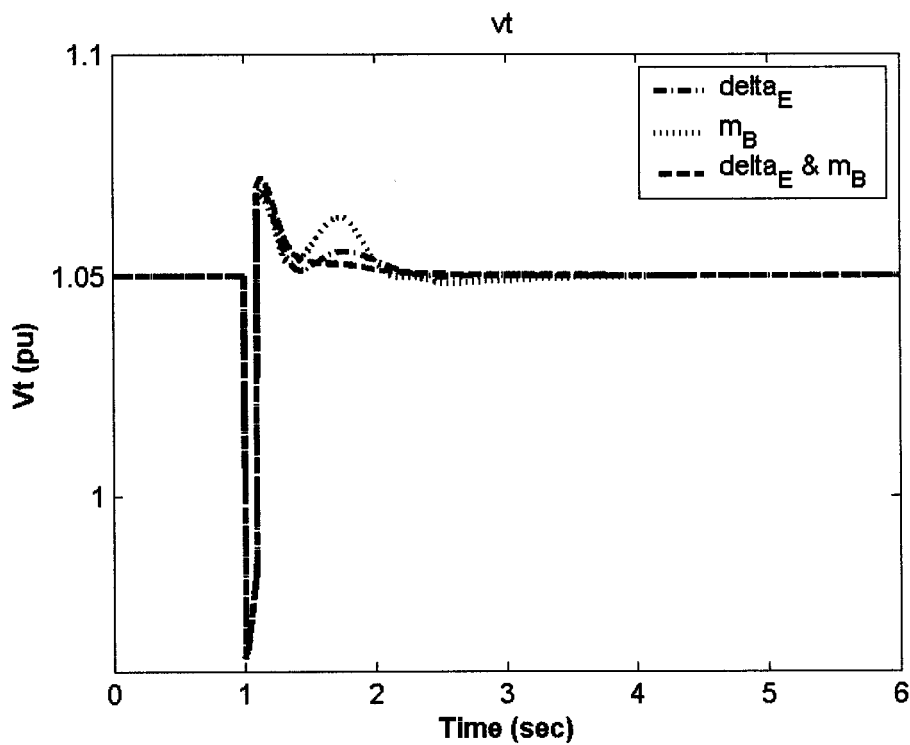


Figure 8.71: Terminal voltage response for 6-cycle fault with nominal loading, J_2 settings, multiple-point tuning, coordinated design

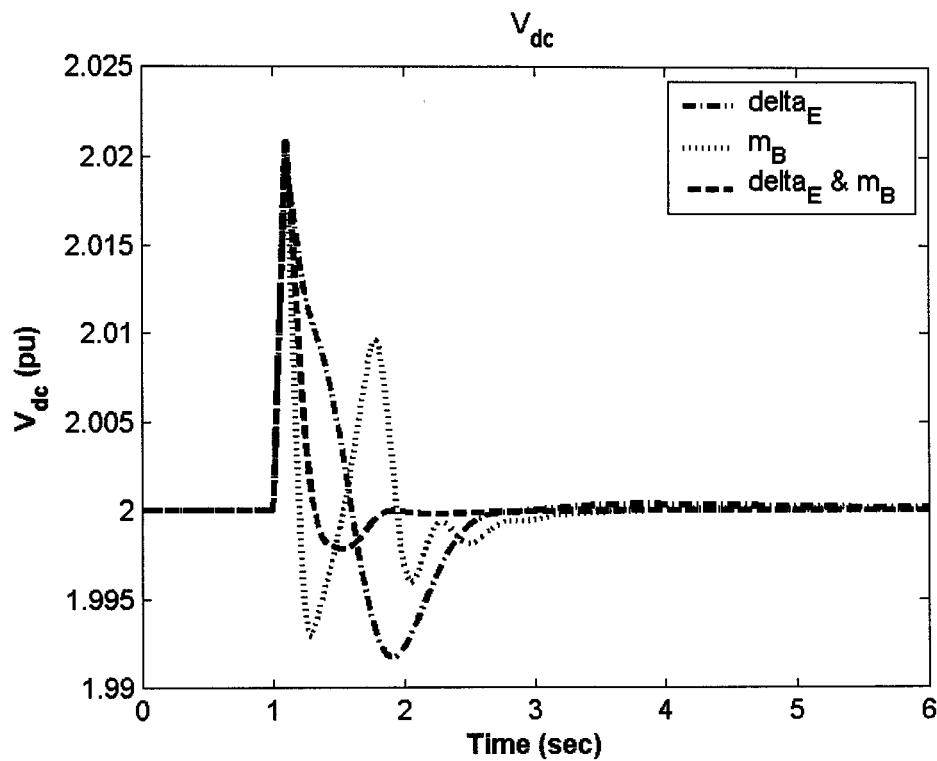


Figure 8.72: DC voltage response for 6-cycle fault with nominal loading, J_2 settings, multiple-point tuning, coordinated design

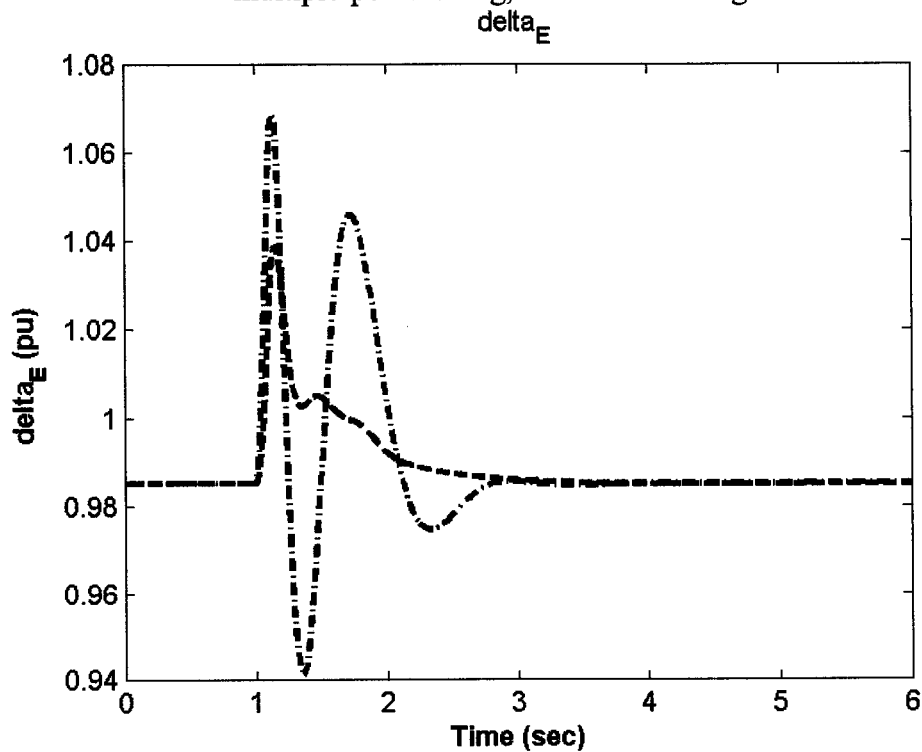


Figure 8.73: δ_E response for 6-cycle fault with nominal loading, J_2 settings, multiple-point tuning, coordinated design

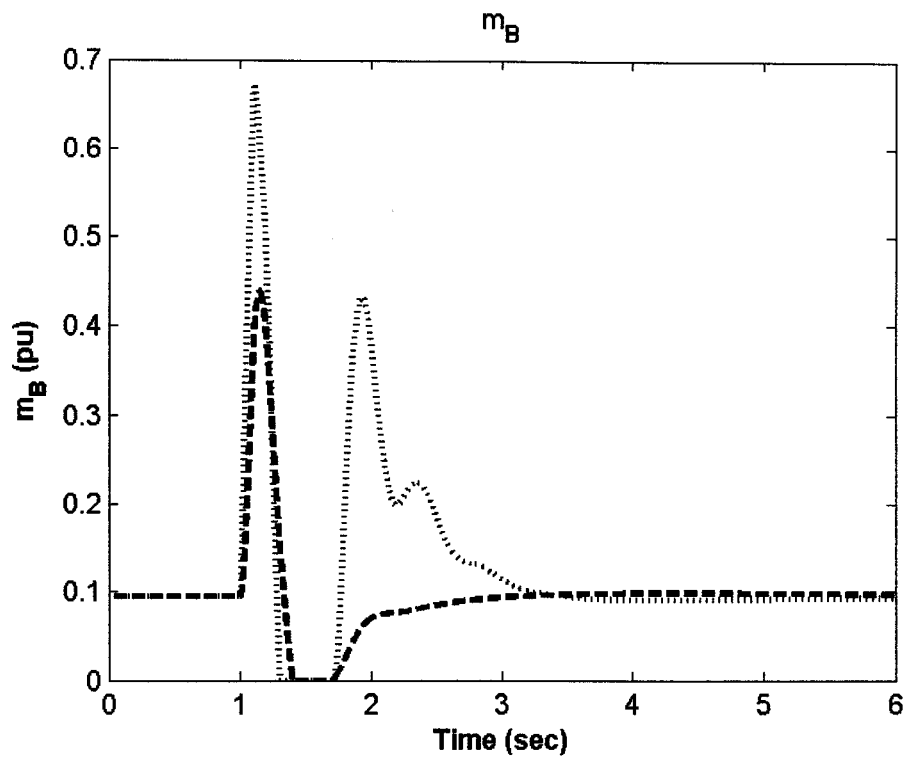


Figure 8.74: m_B response 6-cycle fault with nominal loading, J_2 settings, multiple-point tuning, coordinated design

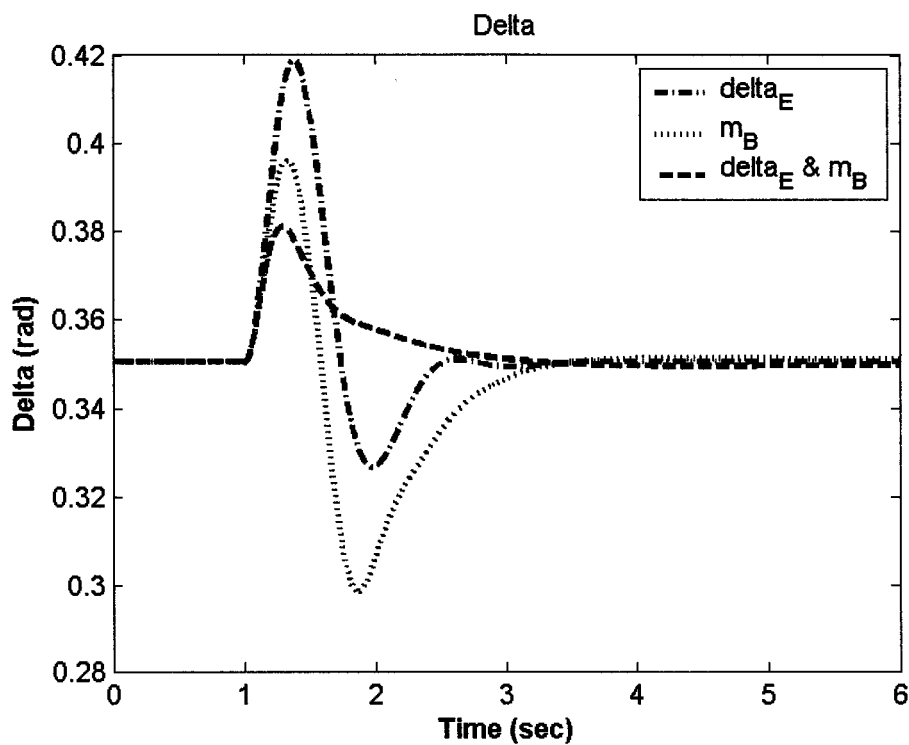


Figure 8.75: Rotor angle response for 6-cycle fault with light loading, J_2 settings, multiple-point tuning, coordinated design

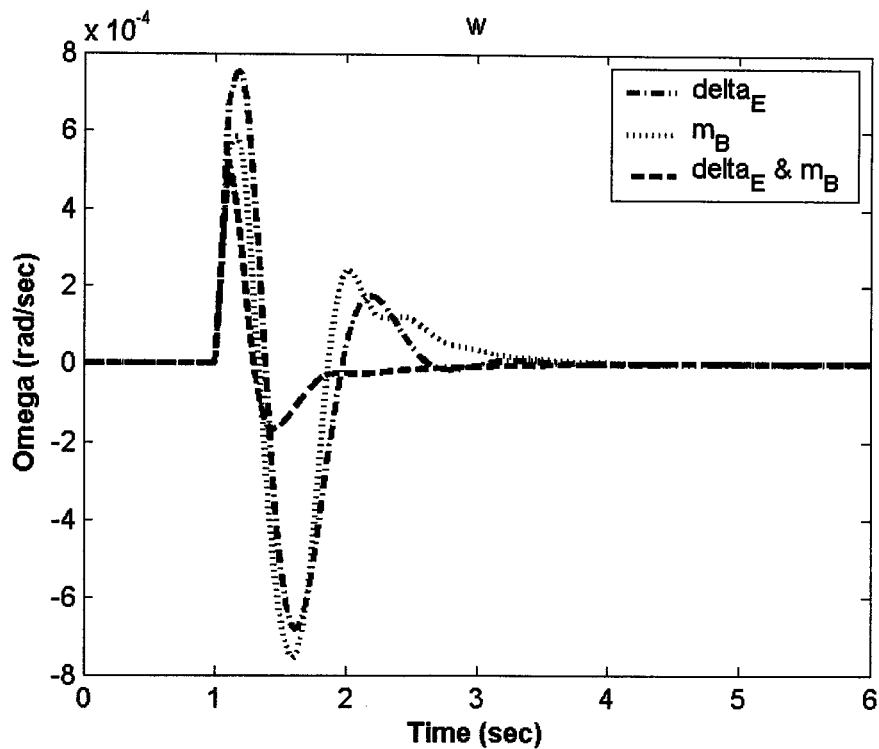


Figure 8.76: Speed response for 6-cycle fault with light loading, J_2 settings, multiple-point tuning, coordinated design

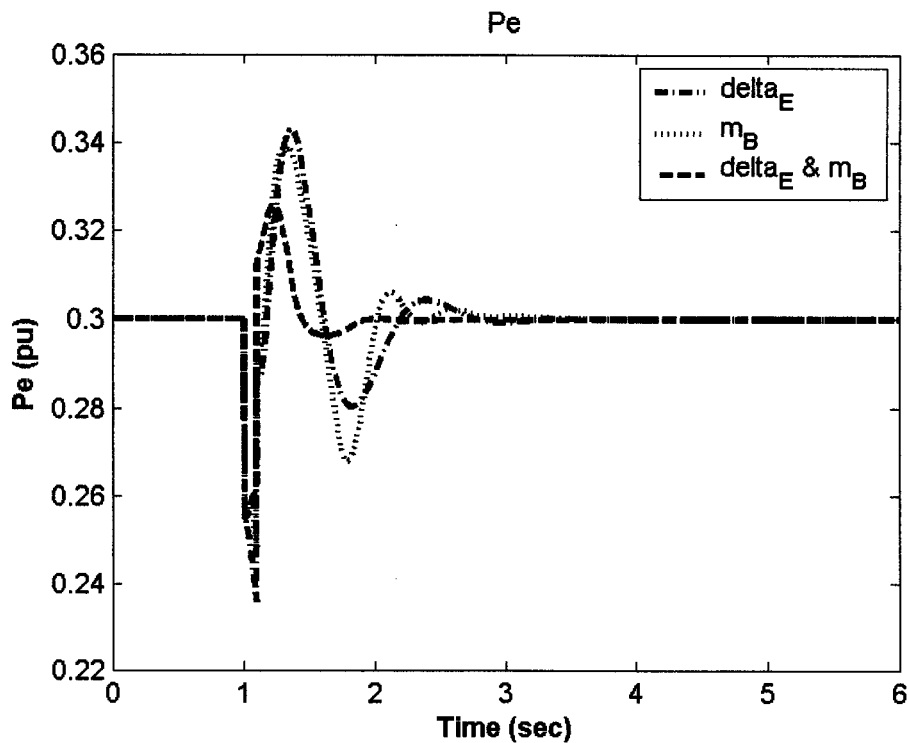


Figure 8.77: Electrical power response for 6-cycle fault with light loading, J_2 settings, multiple-point tuning, coordinated design

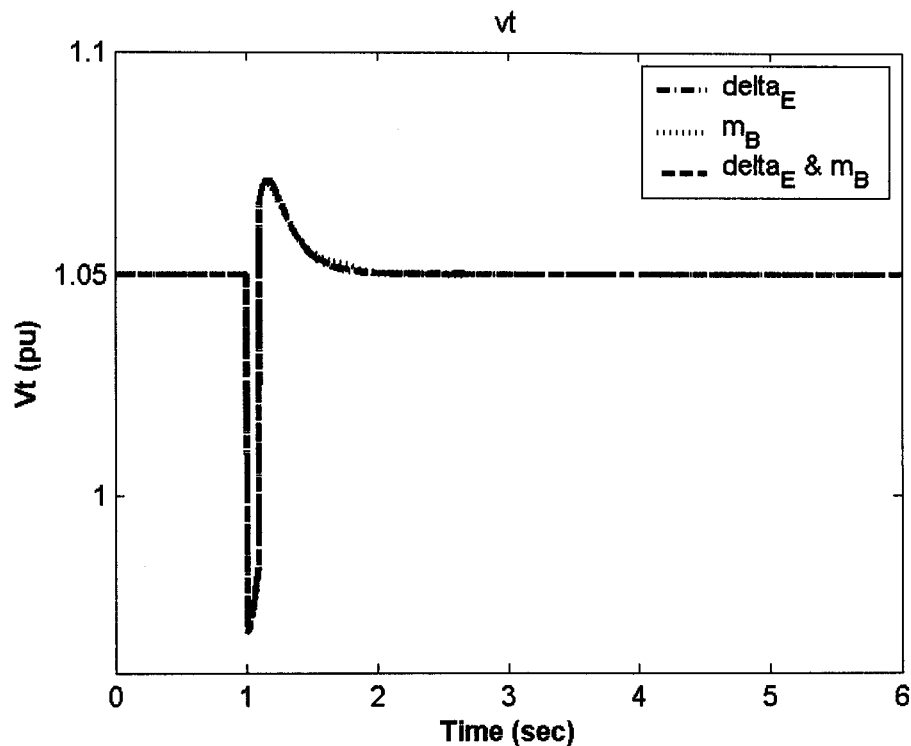


Figure 8.78: Terminal voltage response for 6-cycle fault with light loading, J_2 settings, multiple-point tuning, coordinated design

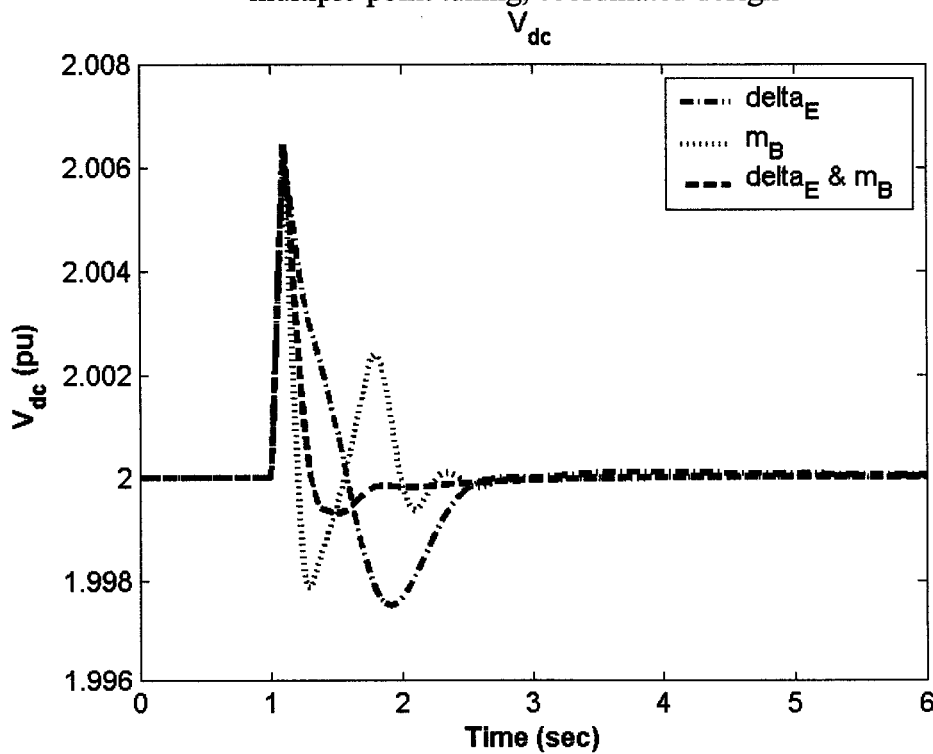


Figure 8.79: DC voltage response for 6-cycle fault with light loading, J_2 settings, multiple-point tuning, coordinated design

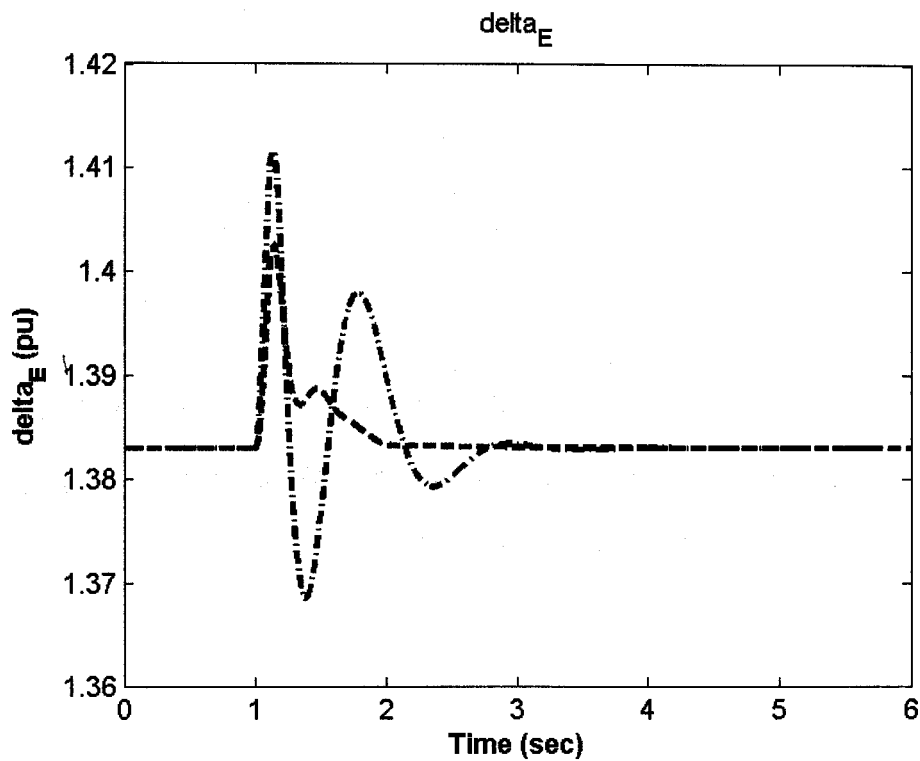


Figure 8.80: δ_E response for 6-cycle fault with light loading, J_2 settings, multiple-point tuning, coordinated design

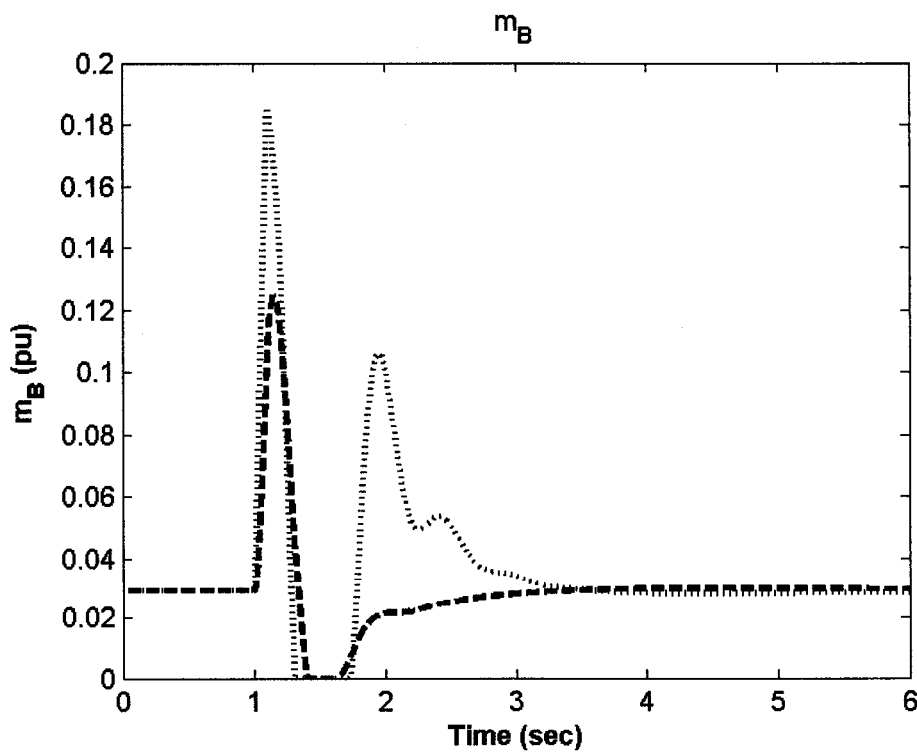


Figure 8.81: m_B response 6-cycle fault with light loading, J_2 settings, multiple-point tuning, coordinated design

CHAPTER 9

ROBUST COORDINATED DESIGN OF PSS AND SVC

FOR MULTIMACHINE POWER SYSTEM

To validate the effectiveness of the proposed technique in enhancing power system stability, the tools of this technique are extended to the multimachine case. The system considered in this study is the three-generator nine-bus system. The system one-line diagram and the details of the system data are given in Appendix C. It is assumed that each generator is equipped with a PSS and each load bus can be equipped with an SVC. This chapter shows the optimization results using J_1 , i.e. maximizing the minimum damping ratio. Both the single-point and multiple-point tuning processes for individual and coordinated designs are considered in designing the PSSs and SVC-based stabilizers.

9.1 Electromechanical Mode Controllability Measure

SVD is employed to measure the controllability of each of two electromechanical (EM) modes from each input signal of the three PSSs and the six SVC-based stabilizers. The minimum singular value, σ_{\min} , is estimated over a wide range of operating conditions. For SVD analysis, the total generated real power that feeds the three loads and the transmission system losses ranges from 0.16 to 5.6 pu and the loads reactive demand is: $Q_A=0.55$ pu, $Q_B=0.35$ pu, and $Q_C=0.25$ pu . At each operating point, the system model is linearized, the EM mode is identified, and the SVD-based controllability measure is implemented.

The capabilities of the three PSSs and the six SVC-based stabilizers to control the two EM modes over the specified range of operating conditions are shown in Figures 9.1 and 9.2. It can be observed that:

- Generally, the capabilities of the different control signals in improving the EM modes damping increases linearly with system loading.
- All the controllers suffer from low controllability to the EM modes at low loading.
- The first EM mode can be best damped by an SVC located at bus 7.
- A PSS installed in generator 3 is the most effective controller to enhance the damping of the second EM mode.
- If it is decided to use an SVC to damp the second EM mode, the SVC should be located at bus 9.

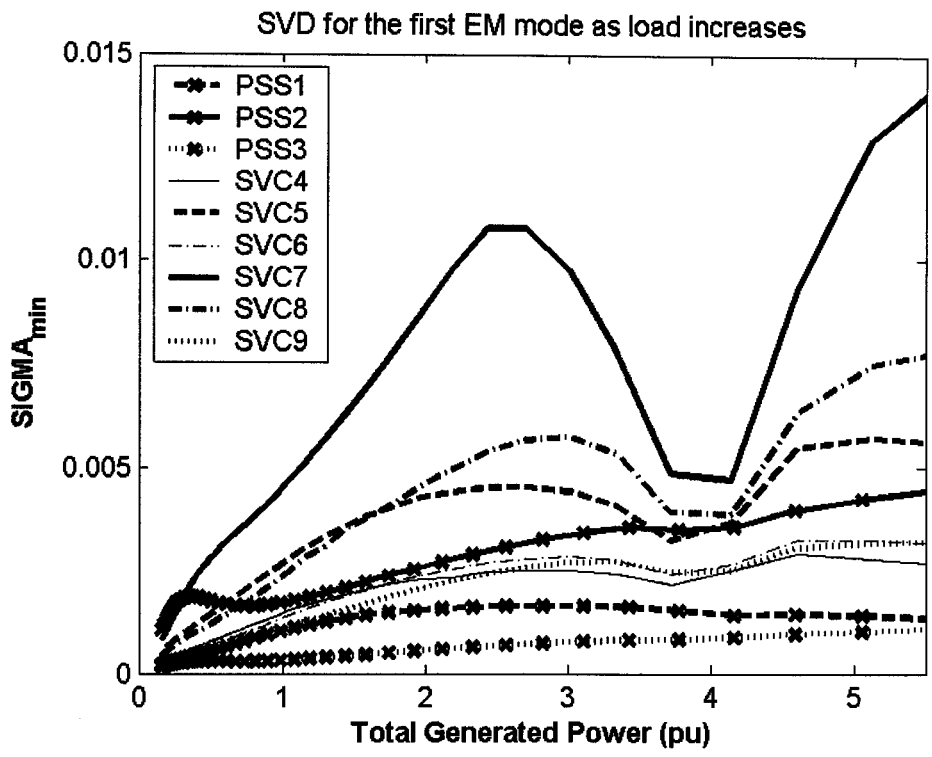


Figure 9.1: Minimum singular values with all controllers with respect to the first EM mode as load increases, $Q_A = 0.55$ pu, $Q_B = 0.35$ pu, and $Q_C = 0.25$ pu

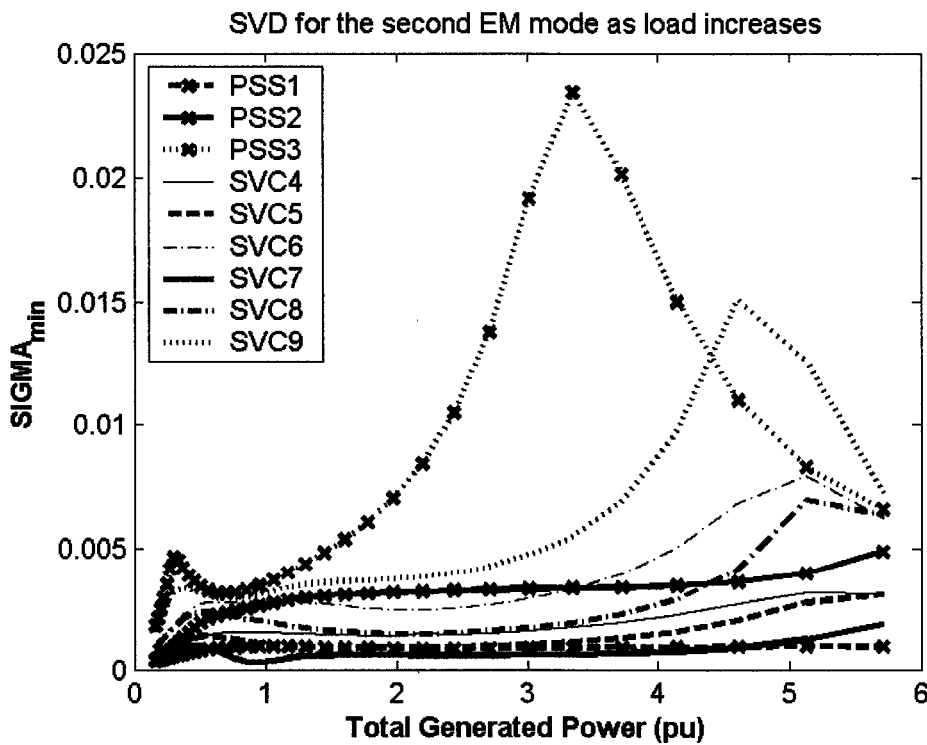


Figure 9.2: Minimum singular values with all controllers with respect to the second EM mode as load increases, $Q_A = 0.55$ pu, $Q_B = 0.35$ pu, and $Q_C = 0.25$ pu

9.2 Optimization Results for PSS and SVC-based Stabilizers

This chapter presents the optimization results obtained using J_1 , maximizing the minimum damping ratio as an objective function. Both the single-point and multiple-point tuning processes for individual and coordinated designs are considered. The system data is given in Appendix C.

To demonstrate the effectiveness of the proposed controllers over a wide range of operating conditions, four operating cases are considered for eigenvalue analysis. The generator operating cases and the loads at these cases are shown in Tables 9.1 and 9.2, respectively. For nonlinear time-domain simulation, a three-phase 6-cycle fault disturbance is applied at bus 7 at the end of line 5-7 with the base case.

Table 9.1: Generator operating conditions

Generator	Base Case		Case 1		Case 2		Case 3	
	P	Q	P	Q	P	Q	P	Q
G_1	0.72	0.27	2.21	1.09	0.36	0.16	0.33	1.12
G_2	1.63	0.07	1.92	0.56	0.80	-0.11	2.00	0.57
G_3	0.85	-0.11	1.28	0.36	0.45	-0.20	1.50	0.38

Table 9.2: System loading conditions

Load	Base Case		Case 1		Case 2		Case 3	
	P	Q	P	Q	P	Q	P	Q
A	1.25	0.50	2.00	0.80	0.65	0.55	1.50	0.90
B	0.90	0.30	1.80	0.60	0.45	0.35	1.20	0.80
C	1.00	0.35	1.50	0.60	0.50	0.25	1.00	0.50

9.2.1 Single-Point Tuning

In this section, the stabilizers are tuned considering only the base case.

9.2.1.1 Individual Design with J_1

The PSSs installed at generators 2 and 3, PSS2 and PSS3, and the SVC-based stabilizers applied to buses 7 and 9, SVC7 and SVC9, are designed individually considering the base case. The reason behind specifying these four stabilizers is that PSS2 is the most effective PSS in controlling the first EM mode, PSS3 is the most effective PSS in damping the second EM mode, SVC7 is the most effective SVC to control the first EM mode, and SVC9 is the most effective SVC to damp the second EM mode.

Stabilizer Design: PSO is used to search for the optimum parameter settings of each controller that maximizes the minimum damping ratio of all the system complex eigenvalues. The final settings of the optimized parameters for the proposed stabilizers are given in Table 9.3.

Eigenvalue Analysis: The system eigenvalues without and with the proposed stabilizers at the four operating points, base case, case 1, case 2, and case 3, are given in Tables 9.4-9.7, respectively. The bold rows of these tables represent the EM modes eigenvalues and their damping ratios. It can be generally observed that, except for the base case considered in the design stage, PSS3 and SVC9 can enhance the second EM mode damping more efficiently than the first EM mode damping. Moreover, SVC7 is more effective in damping the first EM mode than the second EM mode. This agrees with the results obtained from SVD results. PSS2 represents a special case as it can improve the damping of the two EM modes simultaneously.

Table 9.3: Optimal parameter settings with J_1 , single-point tuning, individual design

	PSS2	PSS3	SVC7	SVC9
K	1.3894	0.2693	154.3300	296.90
T₁	1.0000	1.0000	0.4261	0.1138
T₂	0.0500	0.0500	0.7054	0.5550
T₃	0.8301	1.0000	0.8726	0.8567
T₄	0.5000	0.0500	0.1037	0.6579

Table 9.4: System eigenvalues of Base Case loading conditions with J_1 settings, single-point tuning, individual design

No Control	PSS2	PSS3	SVC7	SVC9
-0.3831±	-2.1477±	-0.7796±	-1.7656±	-2.2234±
7.8847i, 0.0485	6.5446i, 0.3118	7.8375i, 0.0990	11.230i, 0.1553	6.8754i, 0.3077
-1.3738±	-5.2482±	-1.5752±	-1.7905±	-3.1636±
11.750i, 0.1161	12.815i, 0.3790	6.7026i, 0.2288	11.382i, 0.1554	9.7678i, 0.3081
-9.8638±	-4.6359±	-5.4966±	-17.0048±	-8.4960±
13.664i	14.156i	24.159i	10.143i	15.423i
-9.9194±	-6.2631±	-9.7168±	-10.8253±	-9.5529±
6.4142i	9.2781i	11.897i	11.459i	6.5212i
-12.7012	-8.0773±	-9.8145±	-4.8217±	-1.5704±
-5.5005	2.7218i	6.1370i	4.9040i	4.8442i
-0.2000	-28.5791	-42.4858	-12.6679	-22.4790
--	-1.9282	-4.0262	-5.5863	-10.4909
--	-0.2304	-0.2047	-1.4512	-0.5373
--	-0.2000	-0.2000	-0.4217	-1.2839
--	--	--	-0.2000	-0.2000

Table 9.5: System eigenvalues of Case 1 loading conditions with J_1 settings, single-point tuning, individual design

No Control	PSS2	PSS3	SVC7	SVC9
-0.2247±	-1.6360±	-1.2241±	-1.2001±	-0.7988±
7.8046i, 0.0288	6.4367i, 0.2463	7.8008i, 0.1550	9.3068i, 0.1279	7.1245i, 0.1114
-0.8657±	-2.4498±	-0.5894±	-0.9021±	-2.8182±
11.798i, 0.0732	11.826i, 0.2028	7.2571i, 0.0810	11.843i, 0.0759	10.107i, 0.2686
-9.8476±	-5.2923±	-5.3452±	-11.7704±	-8.2668±
13.518i	15.749i	24.722i	14.560i	15.433i
-10.150±	-7.9049±	-9.5653±	-15.3209±	-9.9370±
6.8751i	8.8998i	11.327i	7.8140i	6.9120i
-9.5936±	-9.0851±	-10.0653±	-9.7668±	-4.9651±
2.2870i	5.1252i	6.7216i	2.6868i	4.3555i
-0.2000	-28.6614	-42.9090	-6.3539±	-21.7584
--	-0.2474	-4.8684	5.0330i	-7.2932
--	-1.9188	-0.2078	-1.4727	-1.4636
--	-0.2000	-0.2000	-0.5236	-0.7987
--	--	--	-0.2000	-0.2000

Table 9.6: System eigenvalues of Case 2 loading conditions with J_1 settings, single-point tuning, individual design

No Control	PSS2	PSS3	SVC7	SVC9
-0.6770±	-1.8395±	-0.7704±	-2.7045±	-1.8706±
6.5678i, 0.1025	5.5145i, 0.3164	6.3210i, 0.1210	5.4759i, 0.4428	6.2313i, 0.2875
-2.0988±	-3.3784±	-1.4438±	-2.0939±	-5.3919±
9.4216i, 0.2174	7.2113i, 0.4242	5.9728i, 0.2350	9.2988i, 0.2197	8.0321i, 0.5574
-9.7416±	-7.0022±	-6.7942±	-16.4338±	-0.2470±
13.931i	14.401i	22.027i	9.0171i	4.5806i
-9.7880±	-6.6231±	-9.6869±	-9.5302±	-9.1770±
7.0793i	11.492i	12.477i	12.031i	14.811i
-8.3262±	-8.3682±	-9.6939±	-6.1679±	-9.7165±
2.3178i	5.8064i	7.0553i	9.3885i	7.1805i
-0.2000	-26.8831	-40.0838	-8.4474±	-8.1302
--	-1.9418	-4.3985	2.1984i	-22.1853
--	-0.2156	-0.2024	-1.4406	-1.2726
--	-0.2000	-0.2000	-0.3280	-0.3909
--	--	--	-0.2000	-0.2000

Table 9.7: System eigenvalues of Case 3 loading conditions with J_1 settings, single-point tuning, individual design

No Control	PSS2	PSS3	SVC7	SVC9
0.1091±	-1.9410±	-0.1652±	-0.9502±	-0.4226±
8.0287i,	6.7925i, 0.2748	7.6286i, 0.0216	10.066i, 0.0940	7.4534i, 0.0566
-0.0136	-2.2727±	-1.3450±	-0.4359±	-3.0540±
-0.5229±	11.338i, 0.1965	7.7402i, 0.1712	12.207i, 0.0357	10.541i, 0.2783
12.035i, 0.0434	-4.8237±	-5.2673±	-16.6711±	-8.3557±
-10.4209±	14.764i	24.585i	9.6486i	15.098i
13.130i	-8.0766±	-9.8907±	-11.3641±	-9.8556±
-10.0239±	10.077i	11.259i	10.467i	7.0715i
7.0407i	-9.2900±	-9.9711±	-9.9691±	-5.0693±
-9.8009±	5.1527i	6.8921i	2.2098i	3.7994i
1.9872i	-28.5438	-43.0790	-5.9420±	-21.8865
-0.2000	-1.9317	-4.9548	5.5169i	-7.3635
--	-0.2358	-0.2057	-1.4586	-1.4052
--	-0.2000	-0.2000	-0.4563	-0.6713
--	--	--	-0.2000	-0.2000

Nonlinear Time-Domain Simulations: Figures 9.3-9.6 show the rotor angles, speed deviations, electrical power outputs, and machine terminal voltages responses, respectively, for a 6-cycle three-phase fault at bus 7 at the end of line 5-7 at the base case while using the proposed PSS2. Figure 9.7 show the PSS2 control signal in this case. Similarly, Figure 9.8-9.12 show those simulation results while using the proposed PSS3, Figures 9.13-9.17 illustrate the utilization of SVC7, and 9.18-9.22 demonstrate the use of SVC9. It can be readily seen that PSS2 is the most effective stabilizer in damping the EM modes oscillations. However, the system oscillations are relatively poorly damped using PSS3. In addition, SVC7 cannot stabilize the system after applying the disturbance. This is in general consistency with eigenvalue analysis results.

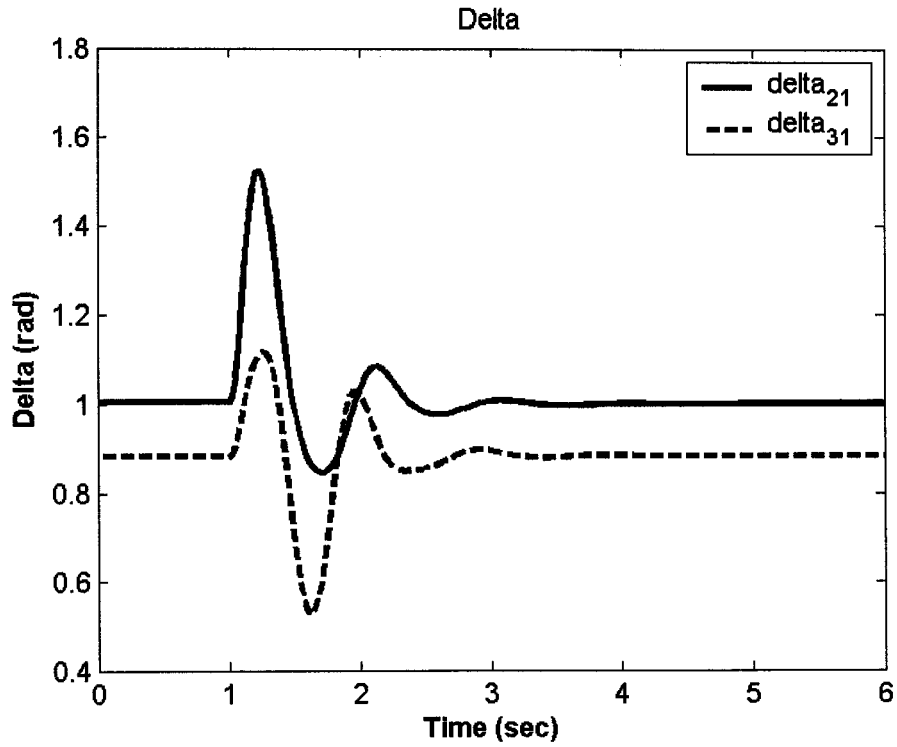


Figure 9.3: Rotor angle response for 6-cycle fault with base case, J_1 settings of PSS2, single-point tuning, individual design

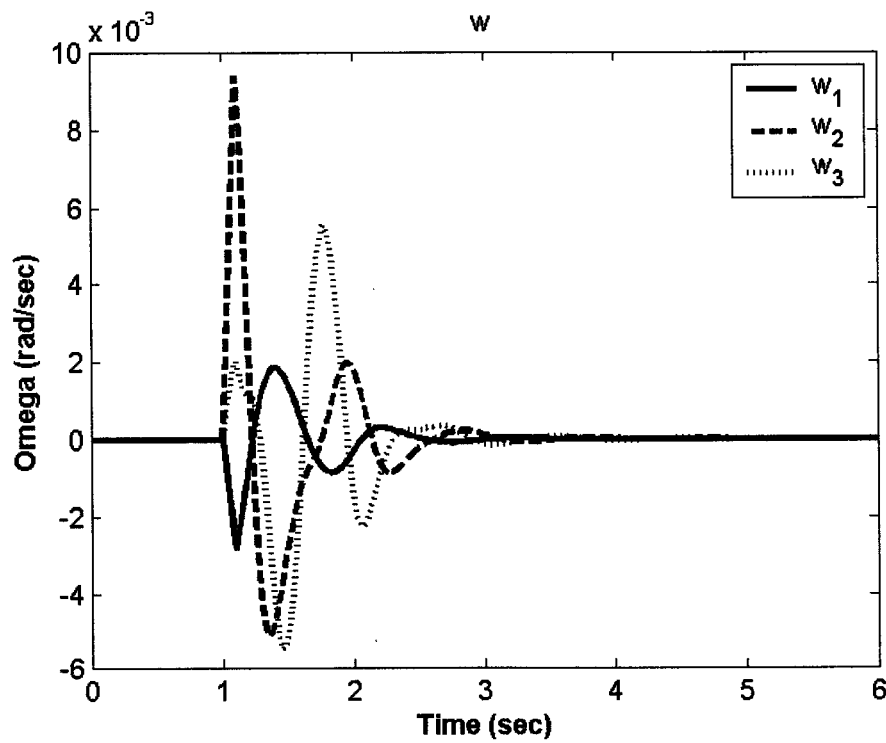


Figure 9.4: Speed response for 6-cycle fault with base case, J_1 settings of PSS2, single-point tuning, individual design

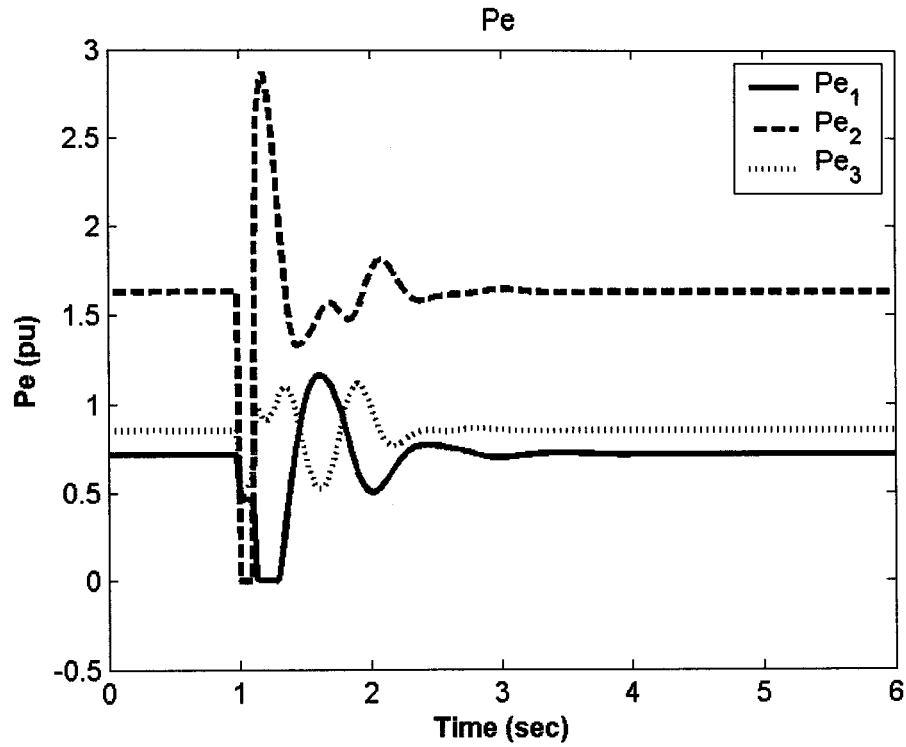


Figure 9.5: Electrical power response for 6-cycle fault with base case, J_1 settings of PSS2, single-point tuning, individual design

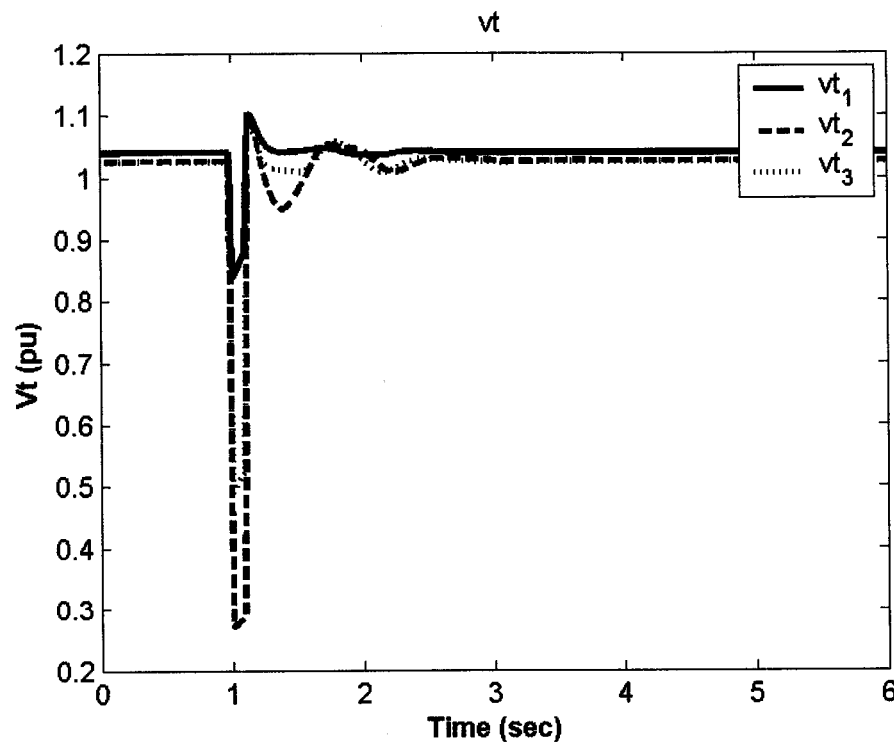


Figure 9.6: Terminal voltage response for 6-cycle fault with base case, J_1 settings of PSS2, single-point tuning, individual design

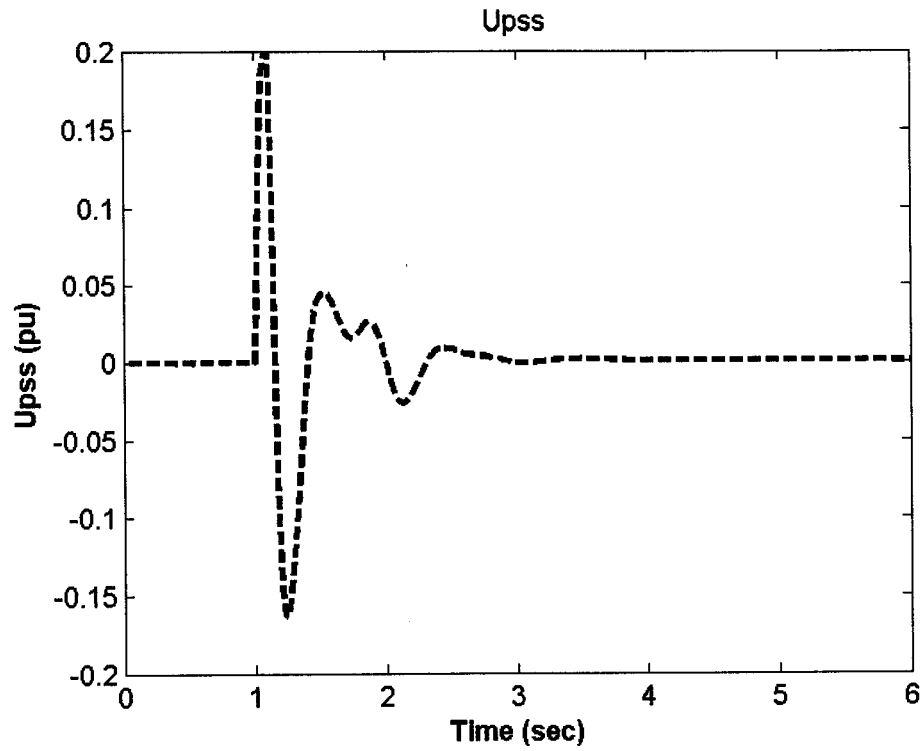


Figure 9.7: PSS stabilizing signal for 6-cycle fault with base case, J_1 settings of PSS2, single-point tuning, individual design

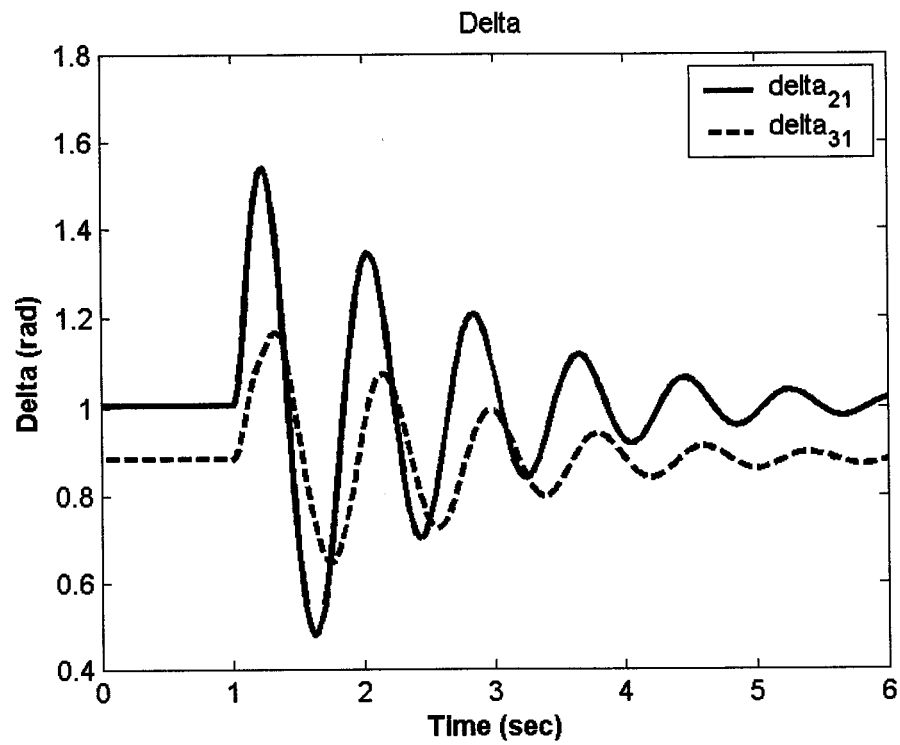


Figure 9.8: Rotor angle response for 6-cycle fault with base case, J_1 settings of PSS3, single-point tuning, individual design

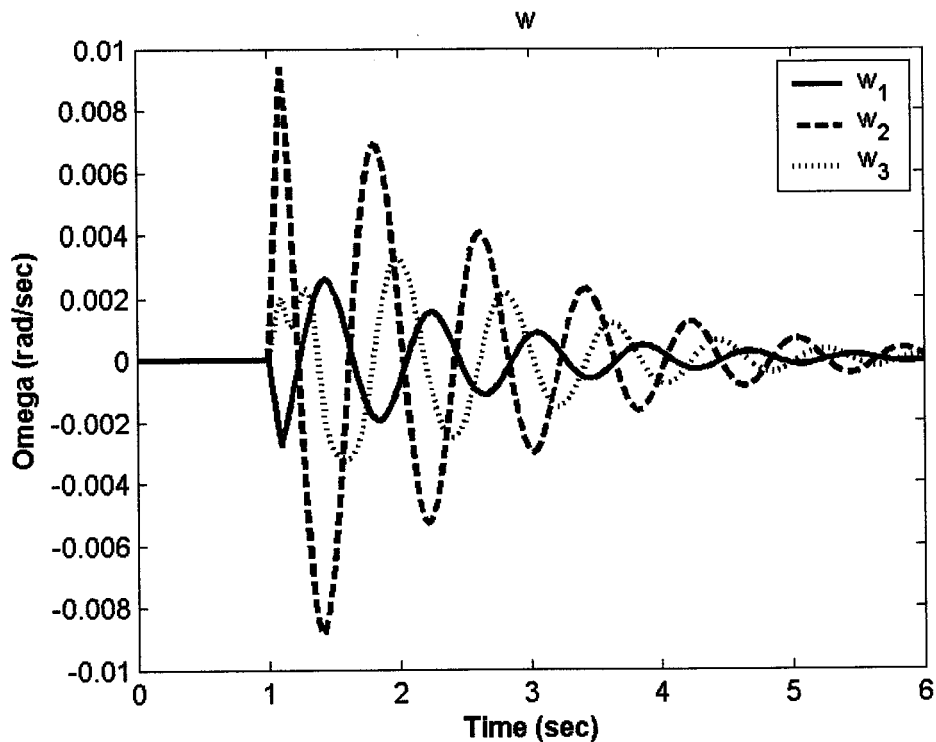


Figure 9.9: Speed response for 6-cycle fault with base case, J_1 settings of PSS3, single-point tuning, individual design

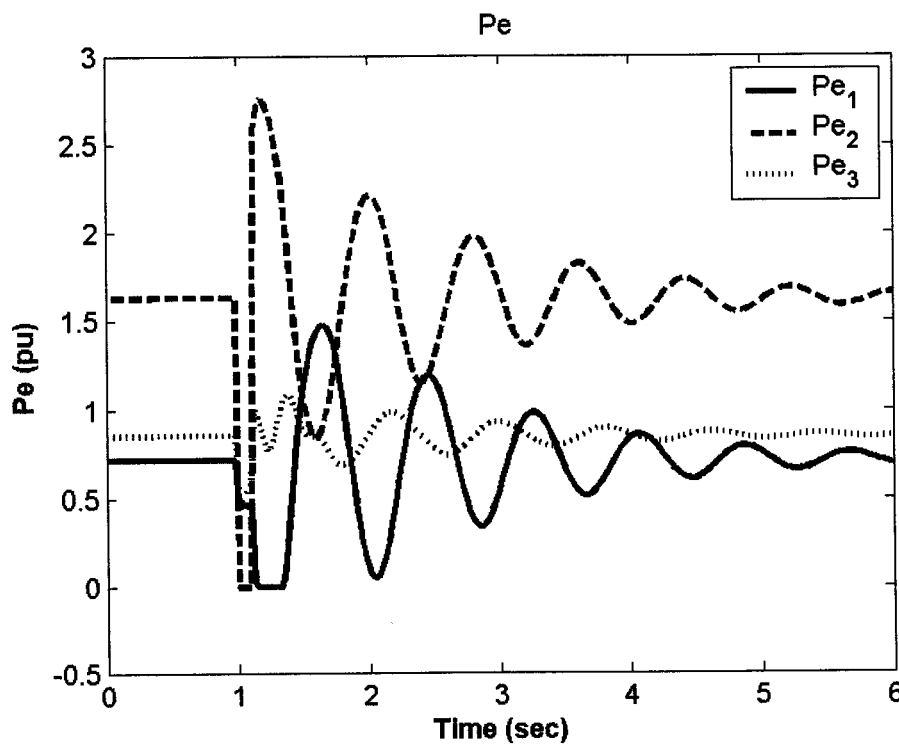


Figure 9.10: Electrical power response for 6-cycle fault with base case, J_1 settings of PSS3, single-point tuning, individual design

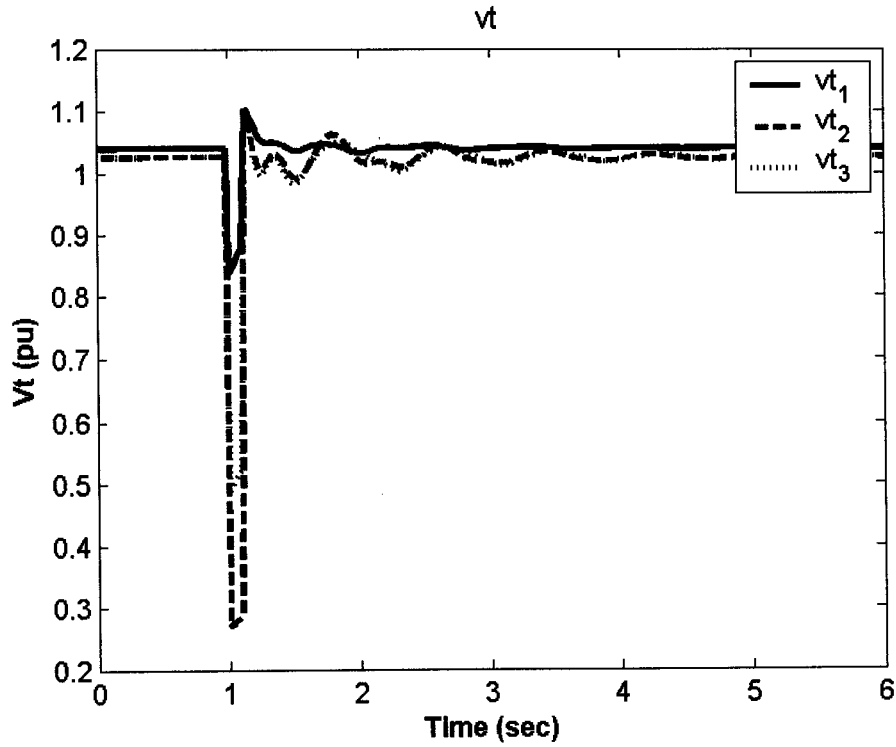


Figure 9.11: Terminal voltage response for 6-cycle fault with base case, J_1 settings of PSS3, single-point tuning, individual design

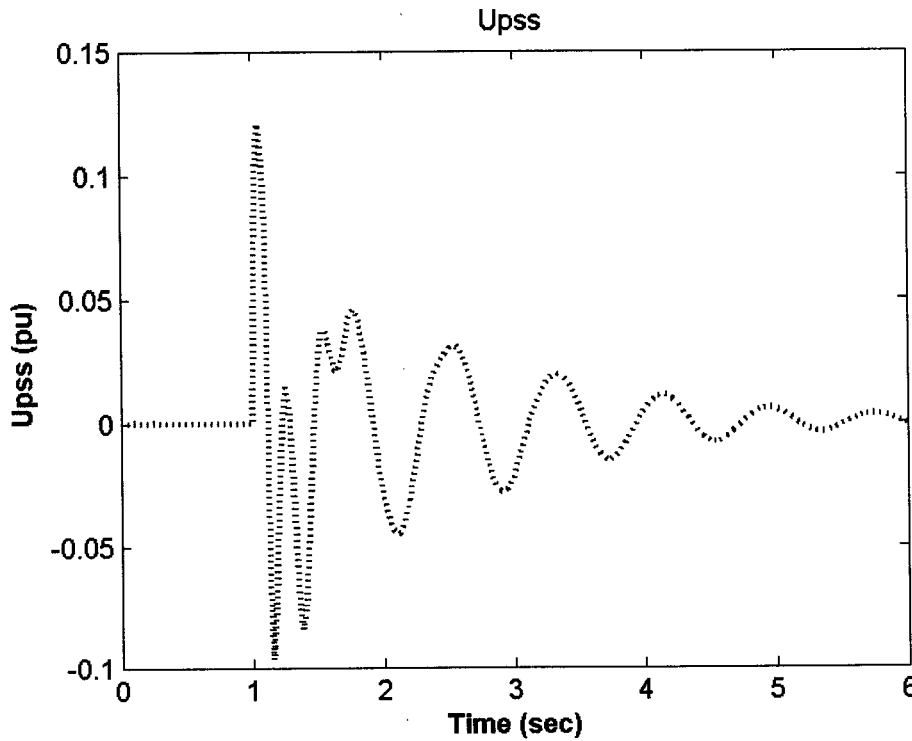


Figure 9.12: PSS stabilizing signal for 6-cycle fault with base case, J_1 settings of PSS3, single-point tuning, individual design

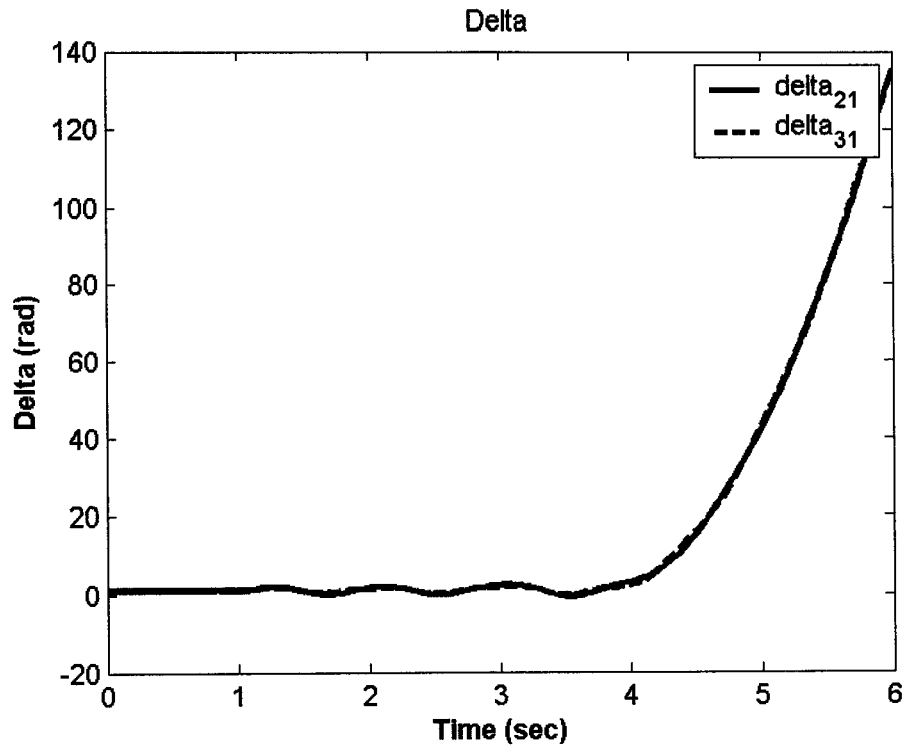


Figure 9.13: Rotor angle response for 6-cycle fault with base case, J_1 settings of SVC7, single-point tuning, individual design

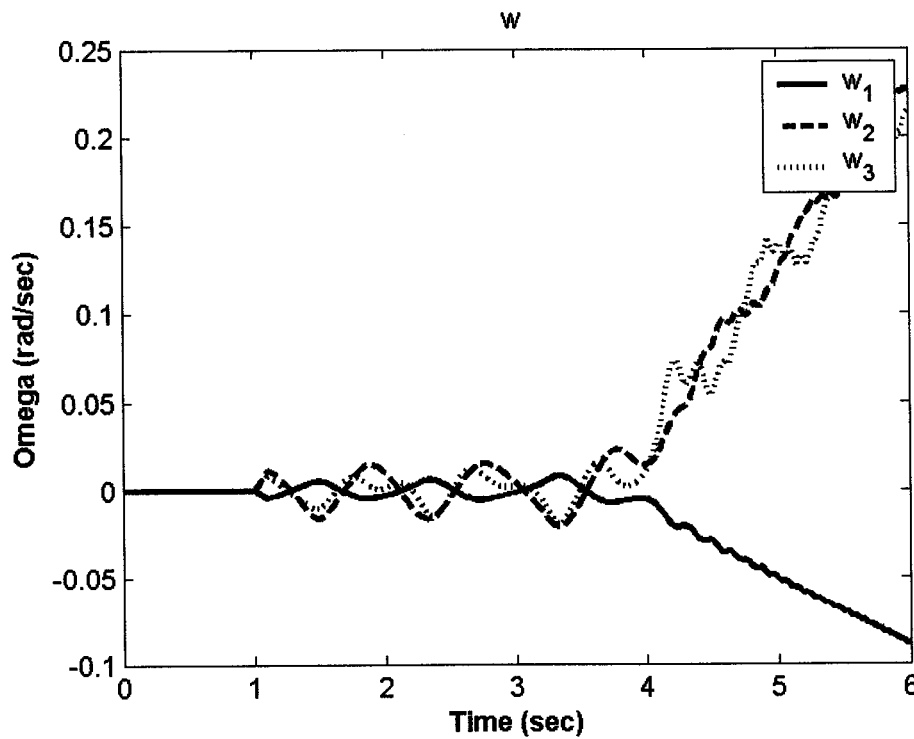


Figure 9.14: Speed response for 6-cycle fault with base case, J_1 settings of SVC7, single-point tuning, individual design

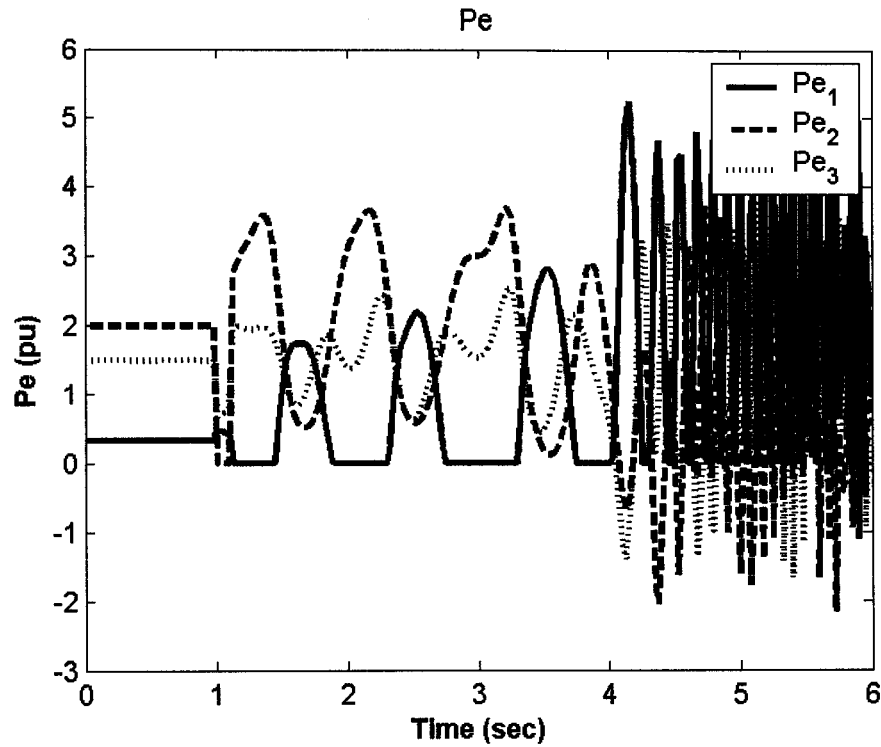


Figure 9.15: Electrical power response for 6-cycle fault with base case, J_1 settings of SVC7, single-point tuning, individual design

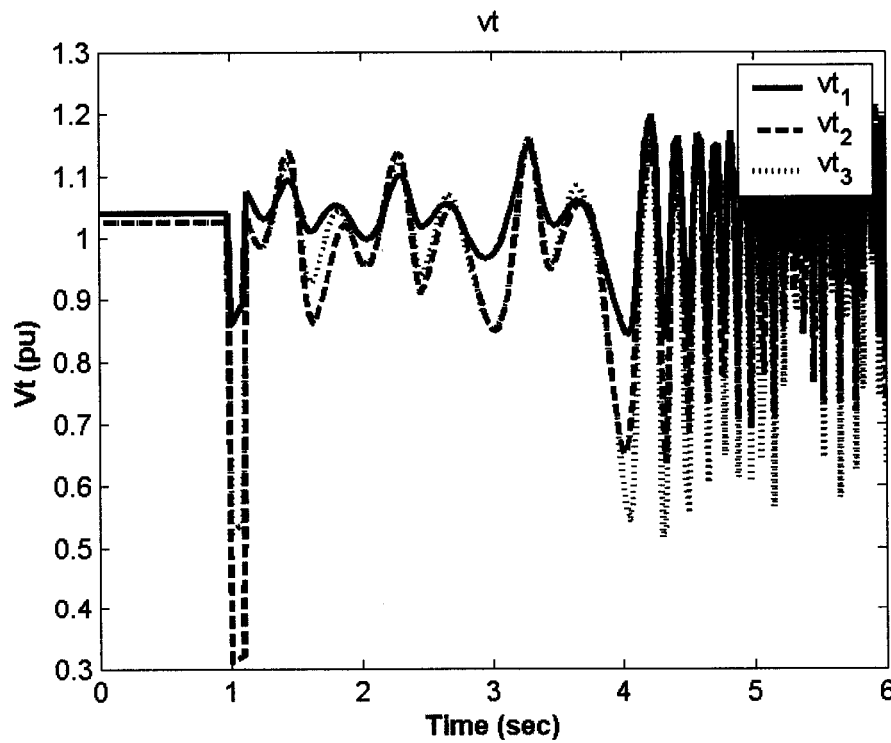


Figure 9.16: Terminal voltage response for 6-cycle fault with base case, J_1 settings of SVC7, single-point tuning, individual design

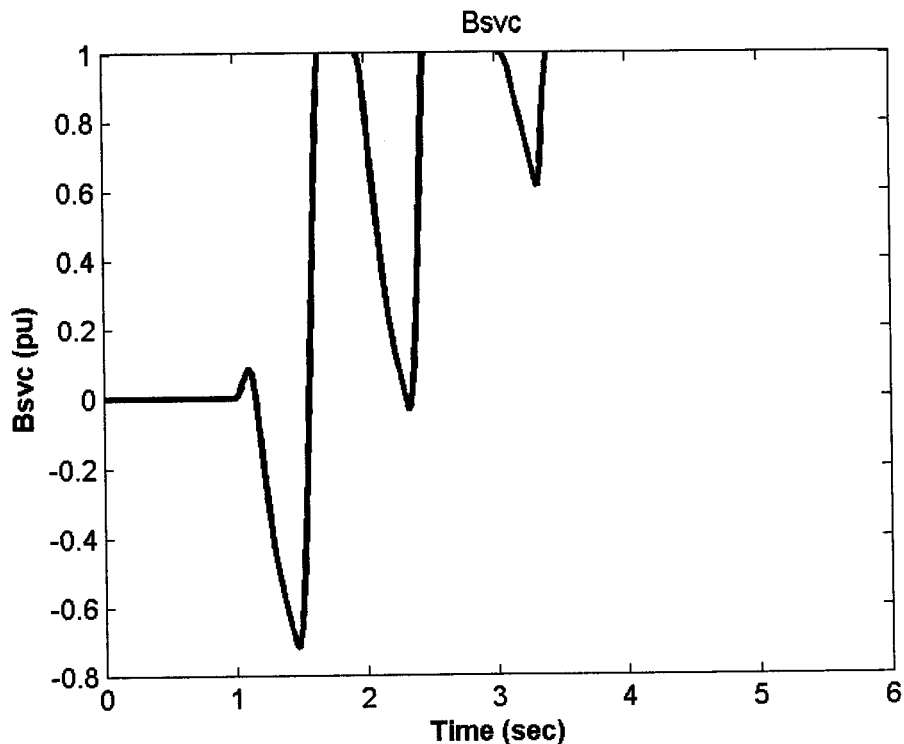


Figure 9.17: B_{svc} response for 6-cycle fault with base case, J_1 settings of SVC7, single-point tuning, individual design

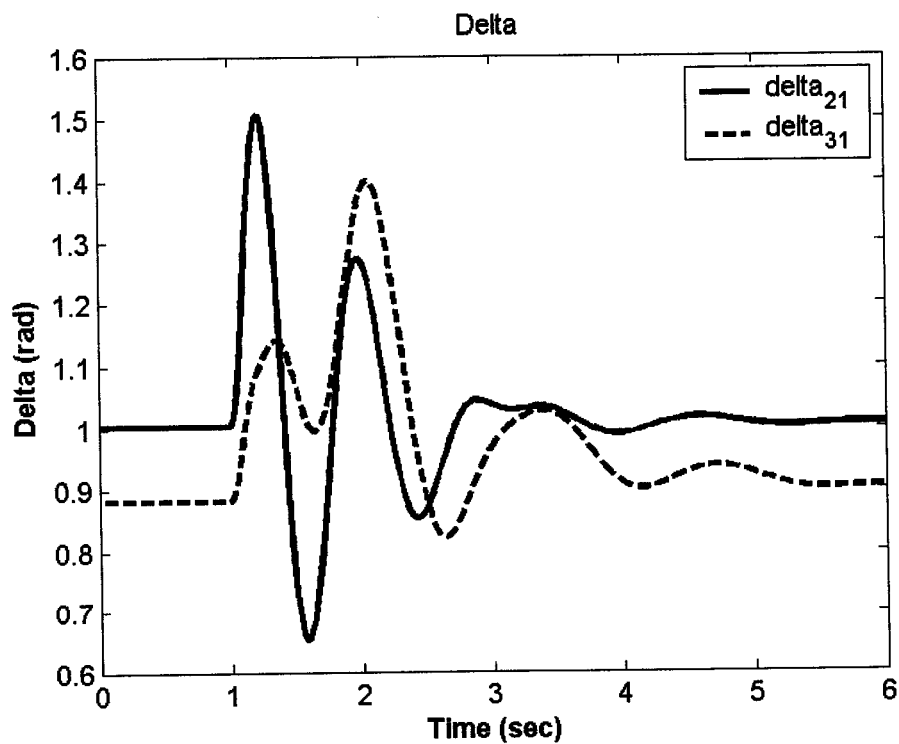


Figure 9.18: Rotor angle response for 6-cycle fault with base case, J_1 settings of SVC9, single-point tuning, individual design

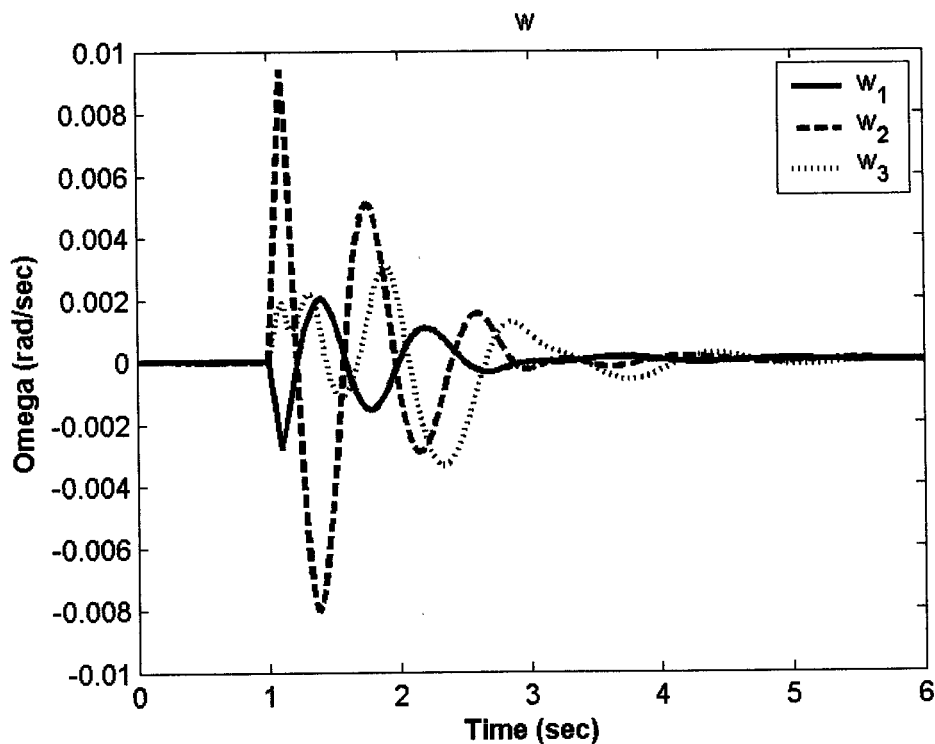


Figure 9.19: Speed response for 6-cycle fault with base case, J_1 settings of SVC9, single-point tuning, individual design

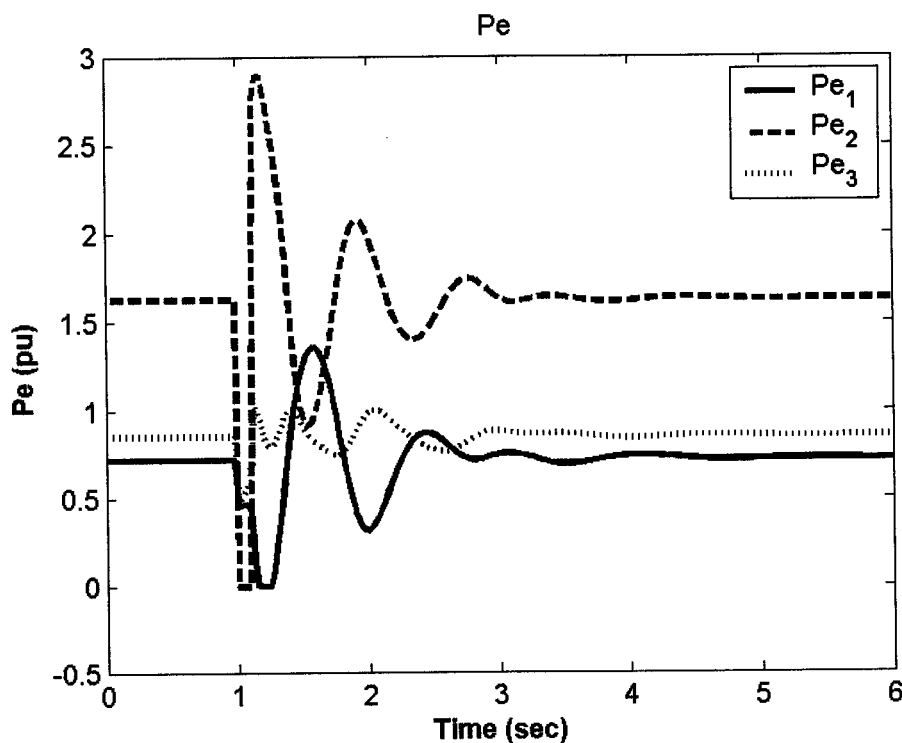


Figure 9.20: Electrical power response for 6-cycle fault with base case, J_1 settings of SVC9, single-point tuning, individual design

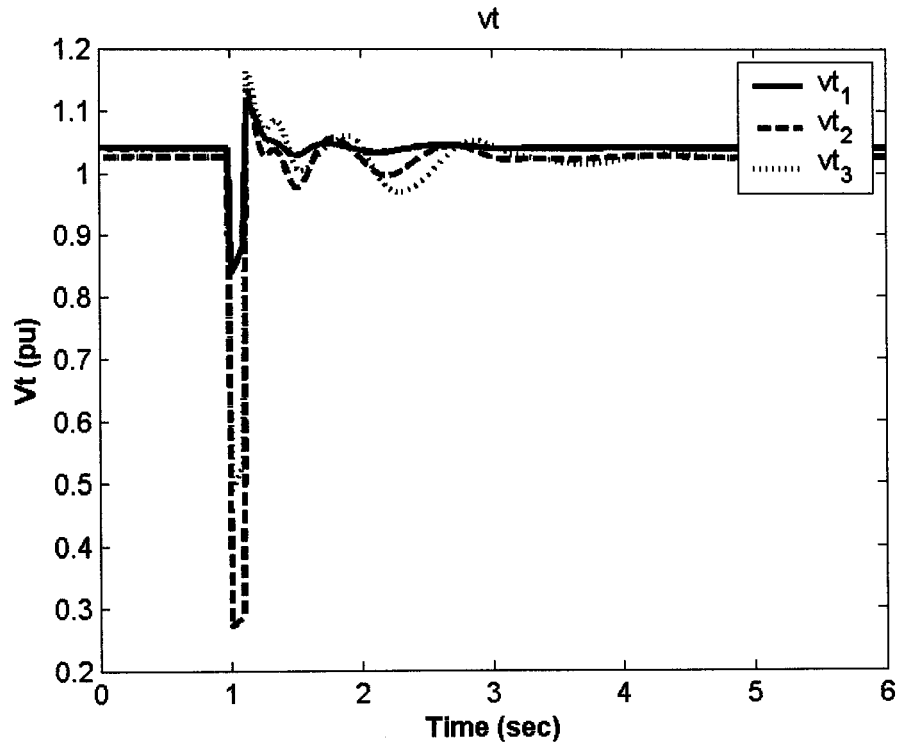


Figure 9.21: Terminal voltage response for 6-cycle fault with base case, J_1 settings of SVC9, single-point tuning, individual design

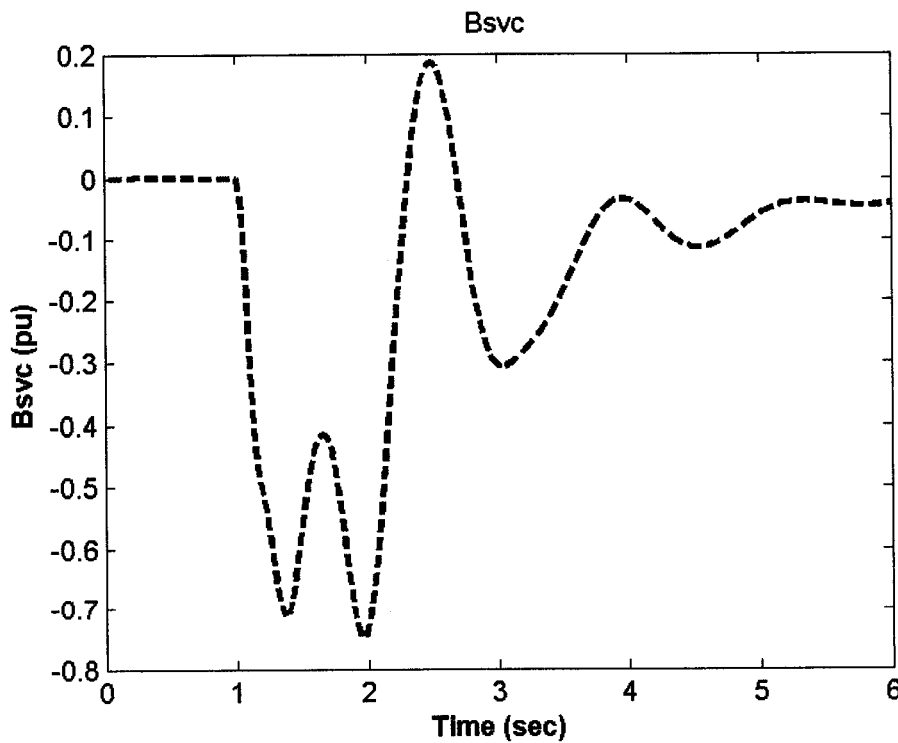


Figure 9.22: B_{svc} response for 6-cycle fault with base case, J_1 settings of SVC9, single-point tuning, individual design

9.2.1.2 Coordinated PSS3-SVC7 Design with J_1

The controllability measure analysis, based on the singular value decomposition, and the eigenvalue analysis indicate that the PSS3 and SVC7-based stabilizer do not perform well individually. This is because SVC7-based stabilizer is the most effective stabilizer in improving the first EM mode damping and PSS3 is the most effective in damping the second EM mode. The same conclusion can be drawn from nonlinear time-domain simulations illustrated in the previous section. In this section, the coordinated design of PSS3 and SVC7-based stabilizer is considered at the base case condition.

Stabilizer Design: PSO is used to simultaneously search for the optimum parameter settings of both controllers that maximize the minimum damping ratio of all the system complex eigenvalues at base case. The final settings of the optimized parameters for the proposed stabilizers are given in Table 9.8.

Eigenvalue Analysis: The system eigenvalues without and with the proposed PSS3 and SVC7-based controllers when applied individually and through coordinated design at the four loading cases are given in Tables 9.9-9.12. The bold rows of these tables represent the EM modes eigenvalues and their damping ratios. It is evident that, using the proposed coordinated stabilizers design, the damping ratio of the EM mode eigenvalue is greatly enhanced. Hence, it can be concluded that this improves the system stability.

Table 9.8: Optimal parameter settings with J_1 , single-point tuning, coordinated PSS3-SVC7 design

	Individual		Coordinated	
	PSS3	SVC7	PSS3	SVC7
K	0.2693	154.330	0.7832	44.3284
T₁	1.0000	0.4261	0.7196	0.9374
T₂	0.0500	0.7054	0.0500	0.0500
T₃	1.0000	0.8726	0.5494	0.9104
T₄	0.0500	0.1037	0.7370	0.6189

Table 9.9: System eigenvalues of Base Case loading conditions with J_1 settings, single-point tuning, coordinated PSS3-SVC7 design

No Control	PSS3	SVC7	PSS3 & SVC7
-0.3831± 7.8847i, 0.0485	-0.7796± 7.8375i, 0.0990	-1.7656± 11.230i, 0.1553	-3.2940± 12.268i, 0.2593
-1.3738± 11.750i, 0.1161	-1.5752± 6.7026i, 0.2288	-1.7905± 11.382i, 0.1554	-3.3341± 12.451i, 0.2586
-9.8638± 13.664i	-5.4966± 24.159i	-17.0048± 10.143i	-22.0557± 13.393i
-9.9194± 6.4142i	-9.7168± 11.897i	-10.8253± 11.459i	-9.7909± 10.021i
-12.7012	-9.8145± 6.1370i	-4.8217± 4.9040i	-3.3181± 6.3525i
-5.5005	-42.4858	-12.6679	-6.8440± 2.0735i
-0.2000	-4.0262	-5.5863	-23.9522
--	-0.2047	-1.4512	-1.5956
--	-0.2000	-0.4217	-1.3565
--	--	-0.2000	-0.2762
--	--	--	-0.2004
--	--	--	-0.2000

Table 9.10: System eigenvalues of Case 1 loading conditions with J_1 settings, single-point tuning, coordinated PSS3-SVC7 design

No Control	PSS3	SVC7	PSS3 & SVC7
-0.2247± 7.8046i, 0.0288	-1.2241± 7.8008i, 0.1550	-1.2001± 9.3068i, 0.1279	-1.9474± 8.5643i 0.2217
-0.8657± 11.798i, 0.0732	-0.5894± 7.2571i, 0.0810	-0.9021± 11.843i, 0.0759	-1.9982± 12.960i 0.1524
-9.8476± 13.518i	-5.3452± 24.722i	-11.7704± 14.560i	-19.2468± 13.860i
-10.150± 6.8751i	-9.5653± 11.327i	-15.3209± 7.8140i	-12.1214± 11.456i
-9.5936± 2.2870i	-10.0653± 6.7216i	-9.7668± 2.6868i	-5.7982± 7.4272i
-0.2000	-42.9090	-6.3539± 5.0330i	-7.5540± 4.4720i
--	-4.8684	-1.4727	-23.9465
--	-0.2078	-0.5236	-1.5852
--	-0.2000	-0.2000	-0.3163
--	--	--	-1.3564
--	--	--	-0.2002
--	--	--	-0.2000

Table 9.11: System eigenvalues of Case 2 loading conditions with J_1 settings, single-point tuning, coordinated PSS3-SVC7 design

No Control	PSS3	SVC7	PSS3 & SVC7
-0.6770± 6.5678i, 0.1025	-0.7704± 6.3210i, 0.1210	-2.7045± 5.4759i, 0.4428	-1.6288± 5.4901i, 0.2844
-2.0988± 9.4216i, 0.2174	-1.4438± 5.9728i, 0.2350	-2.0939± 9.2988i, 0.2197	-3.3524± 10.161i, 0.3133
-9.7416± 13.931i	-6.7942± 22.027i	-16.4338± 9.0171i	-21.502± 12.286i
-9.7880± 7.0793i	-9.6869± 12.477i	-9.5302± 12.031i	-7.4417± 13.469i
-8.3262± 2.3178i	-9.6939± 7.0553i	-6.1679± 9.3885i	-9.1652± 9.0127i
-0.2000	-40.0838	-8.4474± 2.1984i	-5.9979± 4.1119i
--	-4.3985	-1.4406	-23.0595
--	-0.2024	-0.3280	-1.6007
--	-0.2000	-0.2000	-1.3566
--	--	--	-0.2414
--	--	--	-0.2004
--	--	--	-0.2000

Table 9.12: System eigenvalues of Case 3 loading conditions with J₁ settings, single-point tuning, coordinated PSS3-SVC7 design

No Control	PSS3	SVC7	PSS3 & SVC7
0.1091± 8.0287i, -0.0136	-0.1652± 7.6286i, 0.0216	-0.9502± 10.066i, 0.0940	-2.4552± 8.9534i, 0.2645
-0.5229± 12.035i, 0.0434	-1.3450± 7.7402i, 0.1712	-0.4359± 12.207i, 0.0357	-1.5272± 13.472i, 0.1126
-10.4209± 13.130i	-5.2673± 24.585i	-16.6711± 9.6486i	-22.1335± 12.136i
-10.0239± 7.0407i	-9.8907± 11.259i	-11.3641± 10.467i	-10.1097± 9.5557i
-9.8009± 1.9872i	-9.9711± 6.8921i	-9.9691± 2.2098i	-4.7233± 8.8934i
-0.2000	-43.0790	-5.9420± 5.5169i	-7.6185± 4.3342i
--	-4.9548	-1.4586	-24.1192
--	-0.2057	-0.4563	-1.5920
--	-0.2000	-0.2000	-1.3565
--	--	--	-0.2892
--	--	--	-0.2002
--	--	--	-0.2000

Nonlinear Time-Domain Simulations: Figures 9.23-9.28 show the rotor angles, speed deviations, electrical power outputs, and machine terminal voltages responses, as well as PSS3 stabilizing signal and SVC7 response, respectively, for a 6-cycle three-phase fault at bus 7 at the end of line 5-7 at the base case while using the proposed PSS3-SVC7 coordinated design. These figures should be compared with Figures 9.8-9.12, for individual PSS3 design, and 9.13-9.17, for individual SVC7 design. The improvement on the system responses when using the coordinated design is quite evident. This is in agreement with eigenvalue analysis results.

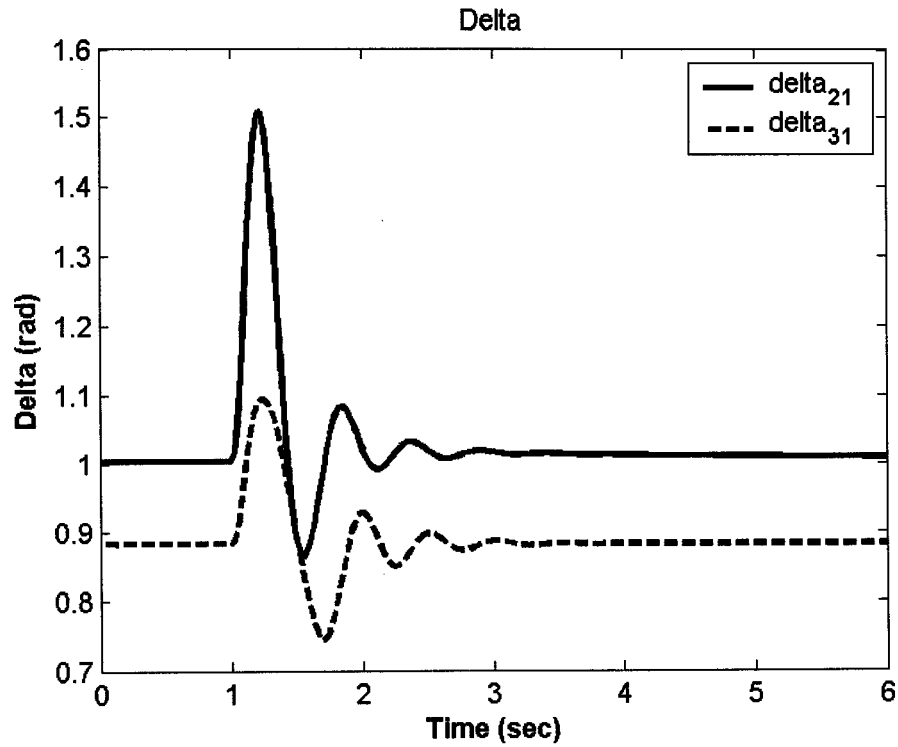


Figure 9.23: Rotor angle response for 6-cycle fault with base case, J_1 settings, single-point tuning, coordinated PSS3-SVC7 design

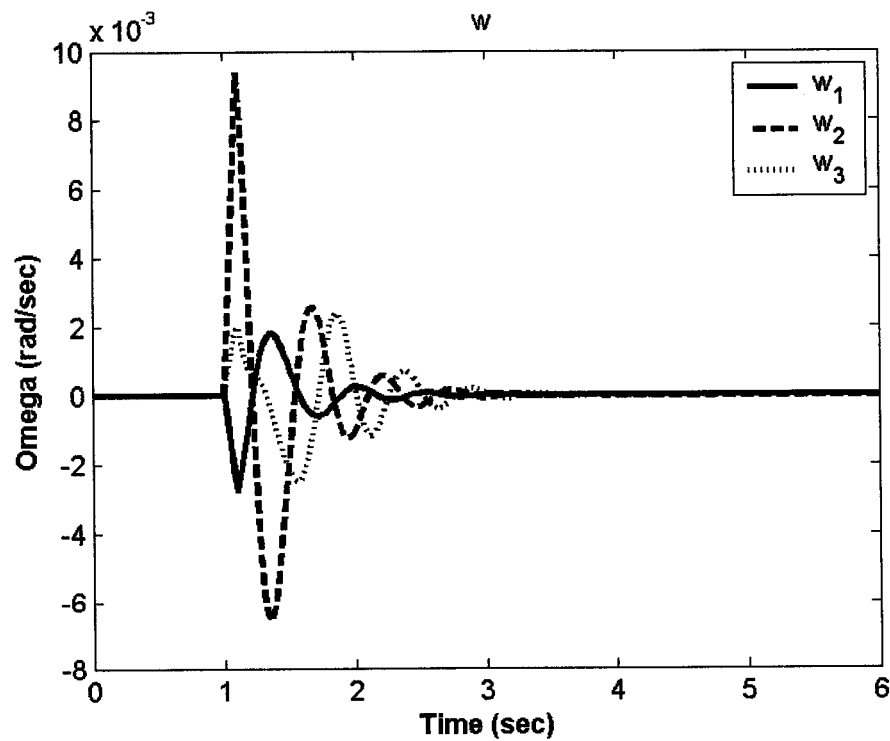


Figure 9.24: Speed response for 6-cycle fault with base case, J_1 settings, single-point tuning, coordinated PSS3-SVC7 design

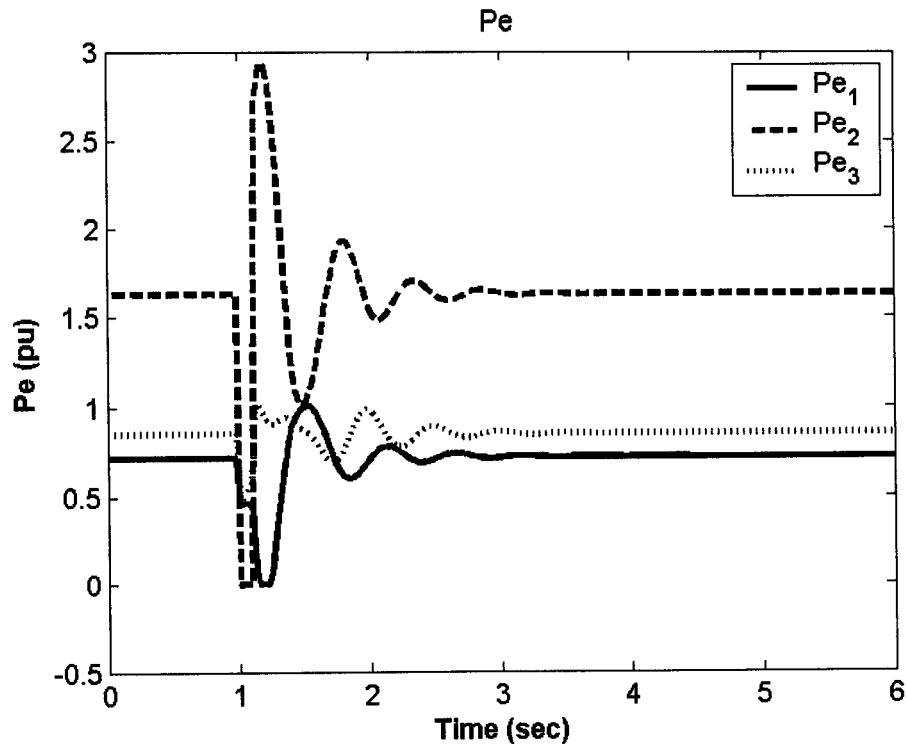


Figure 9.25: Electrical power response for 6-cycle fault with base case, J_1 settings, single-point tuning, coordinated PSS3-SVC7 design

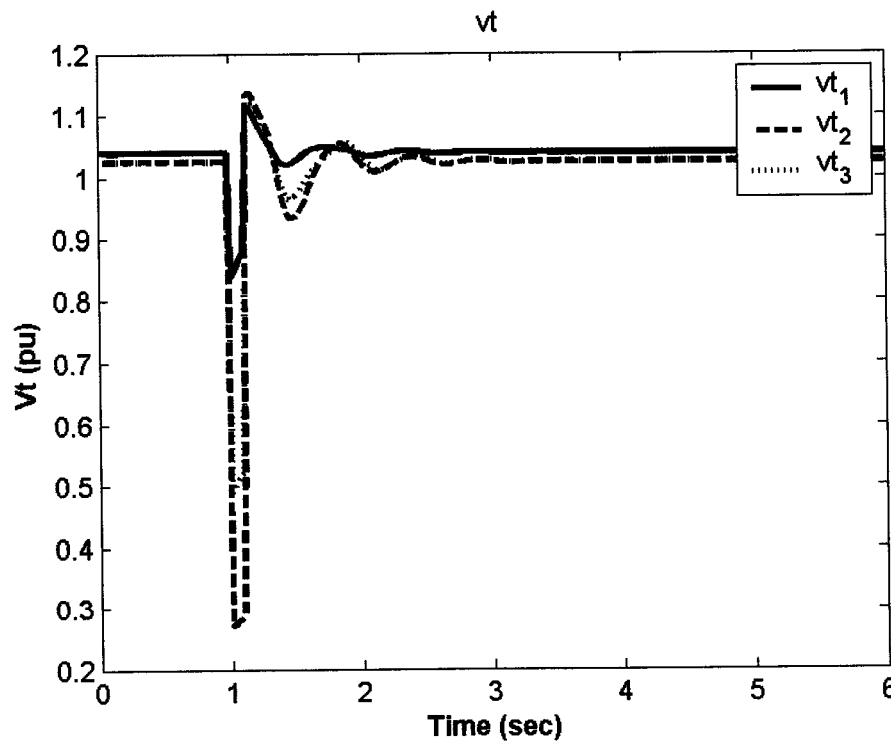


Figure 9.26: Terminal voltage response for 6-cycle fault with base case, J_1 settings, single-point tuning, coordinated PSS3-SVC7 design

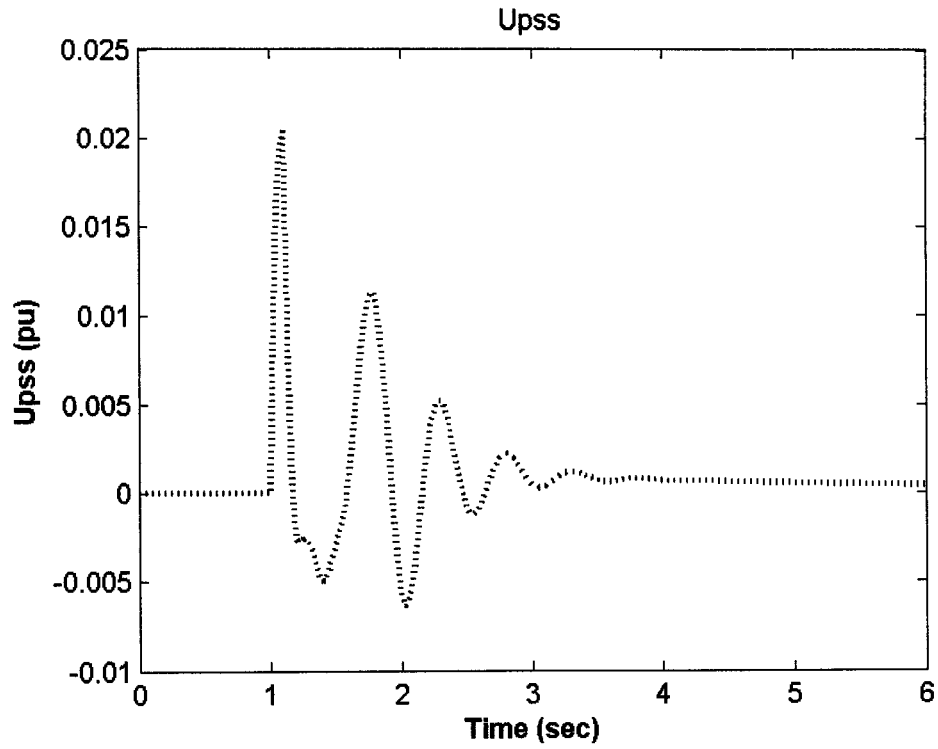


Figure 9.27: PSS stabilizing signal for 6-cycle fault with base case, J_1 settings, single-point tuning, coordinated PSS3-SVC7 design

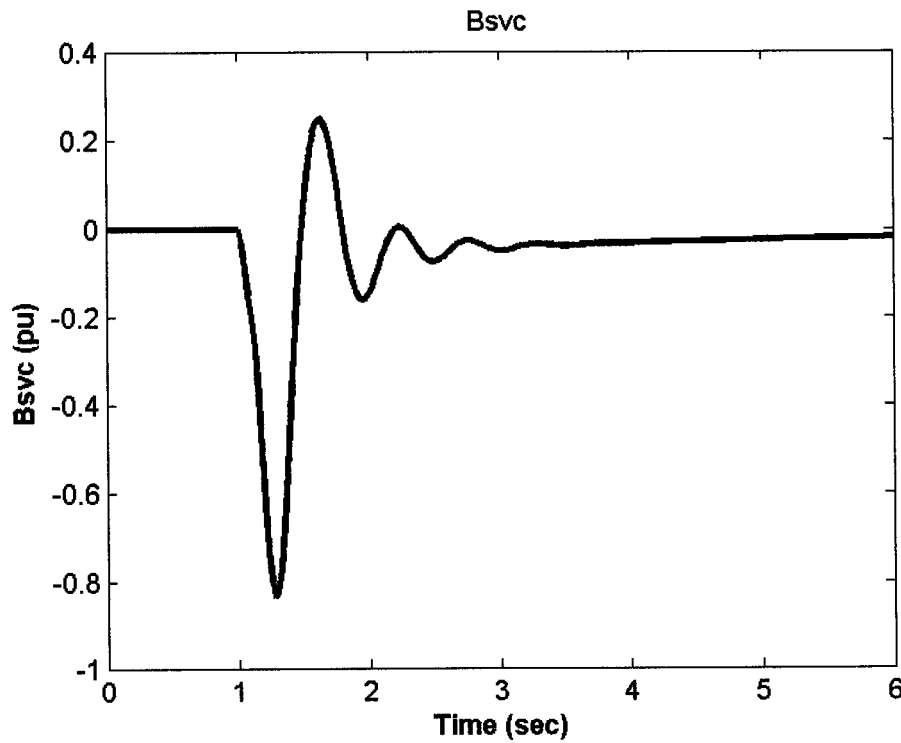


Figure 9.28: B_{svc} response for 6-cycle fault with base case, J_1 settings, single-point tuning, coordinated PSS3-SVC7 design

9.2.1.3 Coordinated SVC7-SVC9 Design with J_1

As an alternative to using the PSS-SVC7 coordinated design, the SVC7-SVC9 coordinated design is considered. The singular value decomposition analysis as well as the eigenvalue analysis show that a single SVC-based stabilizer cannot provide sufficient damping to the two EM modes simultaneously. The same conclusion can be drawn from nonlinear time-domain simulations illustrated earlier. Hence, there is a need for coordination. Since SVC7 is superior in damping the first EM mode and SVC9 is the most effective SVC in damping the second EM mode, the SVC7-SVC9 combination is selected. In this section, the coordinated design of SVC7- and SVC9-based stabilizers is considered at the base case condition.

Stabilizer Design: PSO is used to simultaneously search for the optimum parameter settings of both controllers that maximize the minimum damping ratio of all the system complex eigenvalues at base case. The final settings of the optimized parameters for the proposed stabilizers are given in Table 9.13.

Eigenvalue Analysis: The system eigenvalues without and with the proposed SVC7- and SVC9-based controllers when applied individually and through coordinated design at the four loading cases are given in Tables 9.14-9.17. The bold rows of these tables represent the EM modes eigenvalues and their damping ratios. It is evident that, except for case 2, the damping ratio of the EM mode eigenvalue is greatly enhanced using the proposed coordinated stabilizers design.

Table 9.13: Optimal parameter settings with J_1 , single-point tuning, coordinated SVC7-SVC9 design

	Individual		Coordinated	
	SVC7	SVC9	SVC7	SVC9
K	154.33	296.90	135.75	47.448
T₁	0.4261	0.1138	0.3463	0.7610
T₂	0.7054	0.5550	0.0500	0.6952
T₃	0.8726	0.8567	0.6790	0.5087
T₄	0.1037	0.6579	0.1803	0.2627

Table 9.14: System eigenvalues of Base Case loading conditions with J_1 settings, single-point tuning, coordinated SVC7-SVC9 design

No Control	SVC7	SVC9	SVC7 & SVC9
-0.3831± 7.8847i, 0.0485	-1.7656± 11.230i, 0.1553	-2.2234± 6.8754i, 0.3077	-2.3884± 5.5705i, 0.3941
-1.3738± 11.750i, 0.1161	-1.7905± 11.382i, 0.1554	-3.1636± 9.7678i, 0.3081	-3.4679± 8.0984i, 0.3936
-9.8638± 13.664i	-17.0048± 10.143i	-8.4960± 15.423i	-22.927± 20.991i
-9.9194± 6.4142i	-10.8253± 11.459i	-9.5529± 6.5212i	-6.6085± 15.4580i
-12.7012	-4.8217± 4.9040i	-1.5704± 4.8442i	-9.7724± 9.1377i
-5.5005	-12.6679	-22.4790	-4.4693± 10.465i
-0.2000	-5.5863	-10.4909	-23.8499
--	-1.4512	-0.5373	-4.4299
--	-0.4217	-1.2839	-2.8698
--	-0.2000	-0.2000	-1.4322
--	--	--	-0.4257
--	--	--	-0.1986
--	--	--	-0.2000

Table 9.15: System eigenvalues of Case 1 loading conditions with J_1 settings, single-point tuning, coordinated SVC7-SVC9 design

No Control	SVC7	SVC9	SVC7 & SVC9
-0.2247± 7.8046i, 0.0288	-1.2001± 9.3068i, 0.1279	-0.7988± 7.1245i, 0.1114	-3.1439± 6.4947i, 0.4357
-0.8657± 11.798i, 0.0732	-0.9021± 11.843i, 0.0759	-2.8182± 10.107i, 0.2686	-4.9361± 9.1389i, 0.4752
-9.8476± 13.518i	-11.7704± 14.560i	-8.2668± 15.433i	-1.5108± 9.8584i
-10.150± 6.8751i	-15.3209± 7.8140i	-9.9370± 6.9120i	-19.440± 25.185i
-9.5936± 2.2870i	-9.7668± 2.6868i	-4.9651± 4.3555i	-12.540± 11.028i
-0.2000	-6.3539± 5.0330i	-21.7584	-8.1012± 9.8303i
--	-1.4727	-7.2932	-23.2764
--	-0.5236	-1.4636	-4.5798
--	-0.2000	-0.7987	-3.1854
--	--	-0.2000	-1.4384
--	--	--	-0.5321
--	--	--	-0.1992
--	--	--	-0.2000

Table 9.16: System eigenvalues of Case 2 loading conditions with J_1 settings, single-point tuning, coordinated SVC7-SVC9 design

No Control	SVC7	SVC9	SVC7 & SVC9
-0.6770± 6.5678i, 0.1025	-2.7045± 5.4759i, 0.4428	-1.8706± 6.2313i, 0.2875	-1.4162± 4.9047i, 0.2774
-2.0988± 9.4216i, 0.2174	-2.0939± 9.2988i, 0.2197	-5.3919± 8.0321i, 0.5574	-1.0224± 6.7781i, 0.1492
-9.7416± 13.931i	-16.4338± 9.0171i	-0.2470± 4.5806i	-22.519± 19.553i
-9.7880± 7.0793i	-9.5302± 12.031i	-9.1770± 14.811i	-7.6599± 15.583i
-8.3262± 2.3178i	-6.1679± 9.3885i	-9.7165± 7.1805i	-7.5823± 9.7727i
-0.2000	-8.4474± 2.1984i	-8.1302	-9.6953± 8.6014i
--	-1.4406	-22.1853	-23.3542
--	-0.3280	-1.2726	-4.4144
--	-0.2000	-0.3909	-2.9313
--	--	-0.2000	-1.4316
--	--	--	-0.3329
--	--	--	-0.1985
--	--	--	-0.2000

Table 9.17: System eigenvalues of Case 3 loading conditions with J_1 settings, single-point tuning, coordinated SVC7-SVC9 design

No Control	SVC7	SVC9	SVC7 & SVC9
$0.1091 \pm 8.0287i$, -0.0136	$-0.9502 \pm 10.066i$, 0.0940	$-0.4226 \pm 7.4534i$, 0.0566	$-2.6498 \pm 6.1692i$, 0.3947
$-0.5229 \pm 12.035i$, 0.0434	$-0.4359 \pm 12.207i$, 0.0357	$-3.0540 \pm 10.541i$, 0.2783	$-1.6551 \pm 10.042i$, 0.1626
$-10.4209 \pm 13.130i$	$-16.6711 \pm 9.6486i$	$-8.3557 \pm 15.098i$	$-23.577 \pm 18.515i$
$-10.0239 \pm 7.0407i$	$-11.3641 \pm 10.467i$	$-9.8556 \pm 7.0715i$	$-5.3613 \pm 15.382i$
$-9.8009 \pm 1.9872i$	$-9.9691 \pm 2.2098i$	$-5.0693 \pm 3.7994i$	$-9.8923 \pm 8.7228i$
-0.2000	$-5.9420 \pm 5.5169i$	-21.8865	$-6.5070 \pm 9.7219i$
--	-1.4586	-7.3635	-23.3533
--	-0.4563	-1.4052	-4.5728
--	-0.2000	-0.6713	-3.1971
--	--	-0.2000	-1.4373
--	--	--	-0.4640
--	--	--	-0.1993
--	--	--	-0.2000

Nonlinear Time-Domain Simulations: Figures 9.29-9.33 show the rotor angles, speed deviations, electrical power outputs, and machine terminal voltages responses, as well as the SVC7 and SVC9 responses, respectively, for a 6-cycle three-phase fault at bus 7 at the end of line 5-7 at the base case while using the proposed SVC7-SVC9 coordinated design. These figures should be compared with Figures 9.13-9.17, for individual SVC7 design, and 9.18-9.22, for individual SVC9 design. The improvement on the system responses when using the coordinated design is clear. This is in line with eigenvalue analysis results.

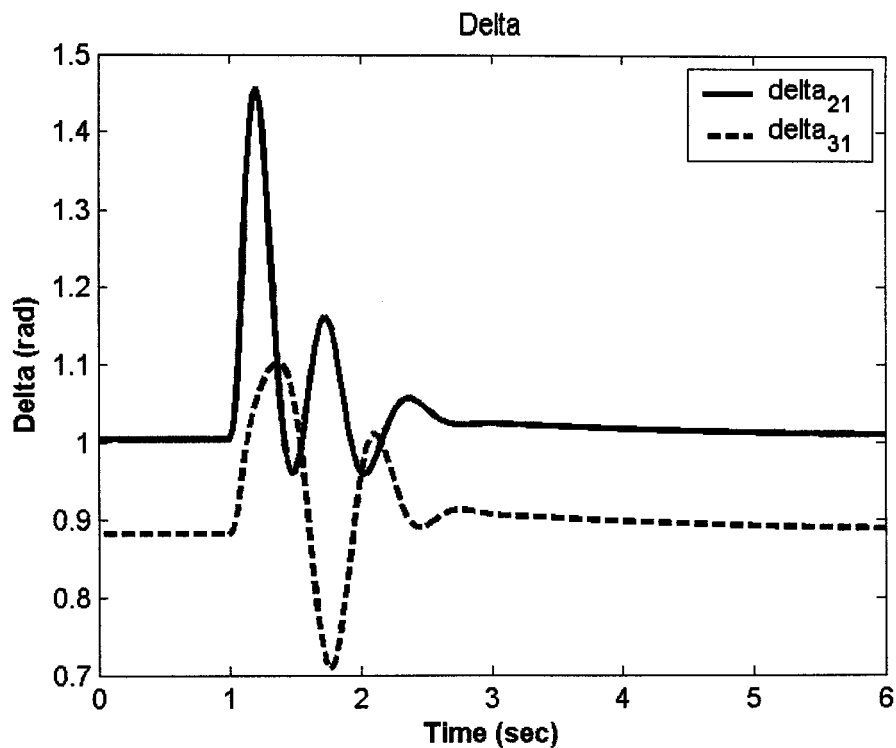


Figure 9.29: Rotor angle response for 6-cycle fault with base case, J_1 settings, single-point tuning, coordinated SVC7-SVC9 design

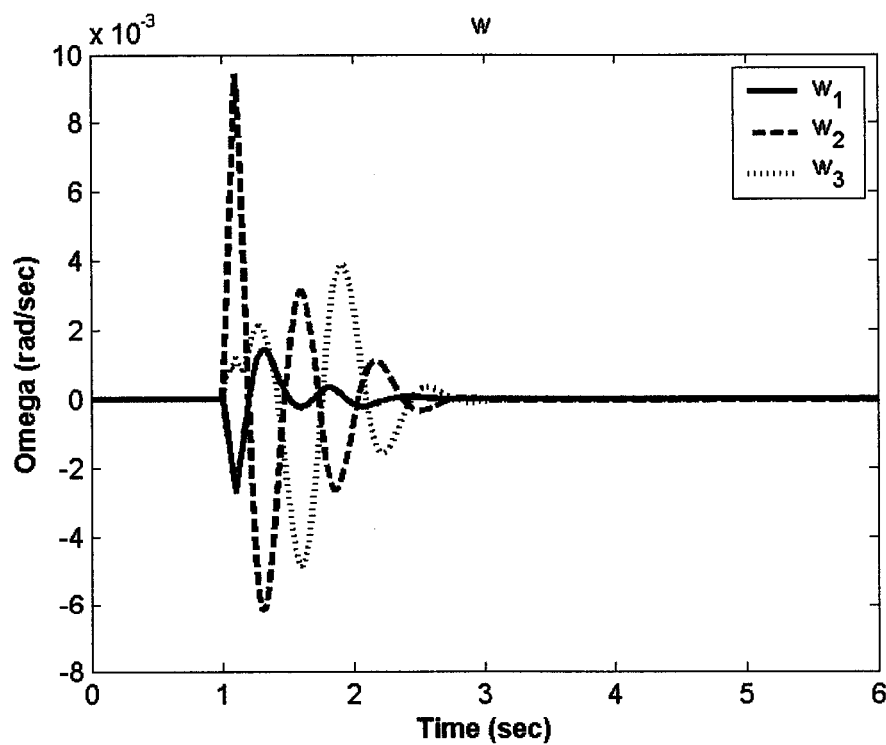


Figure 9.30: Speed response for 6-cycle fault with base case, J_1 settings, single-point tuning, coordinated SVC7-SVC9 design

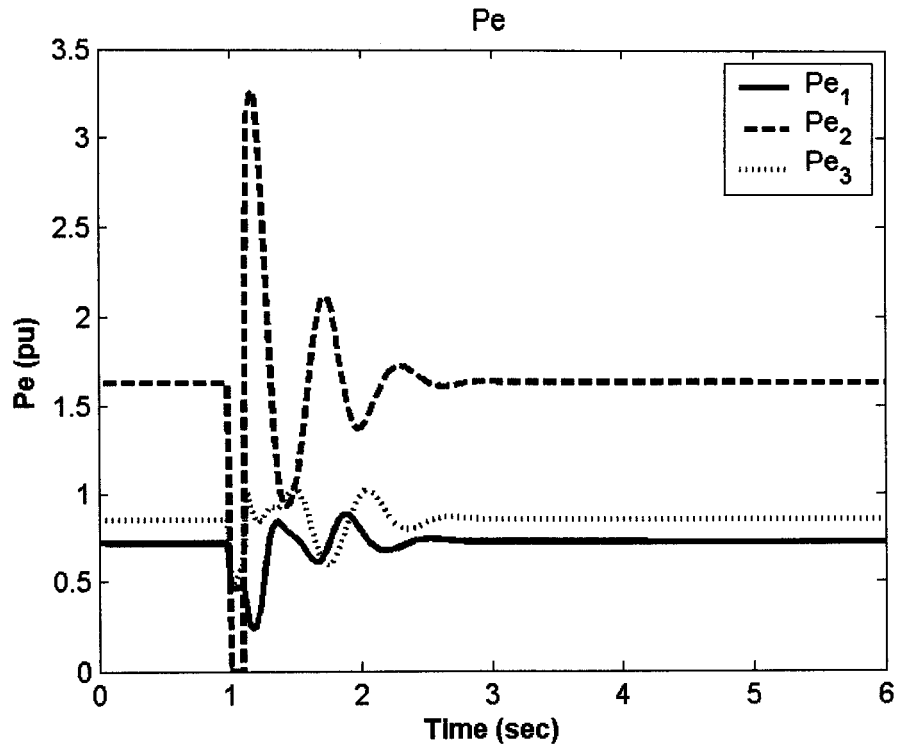


Figure 9.31: Electrical power response for 6-cycle fault with base case, J_1 settings, single-point tuning, coordinated SVC7-SVC9 design

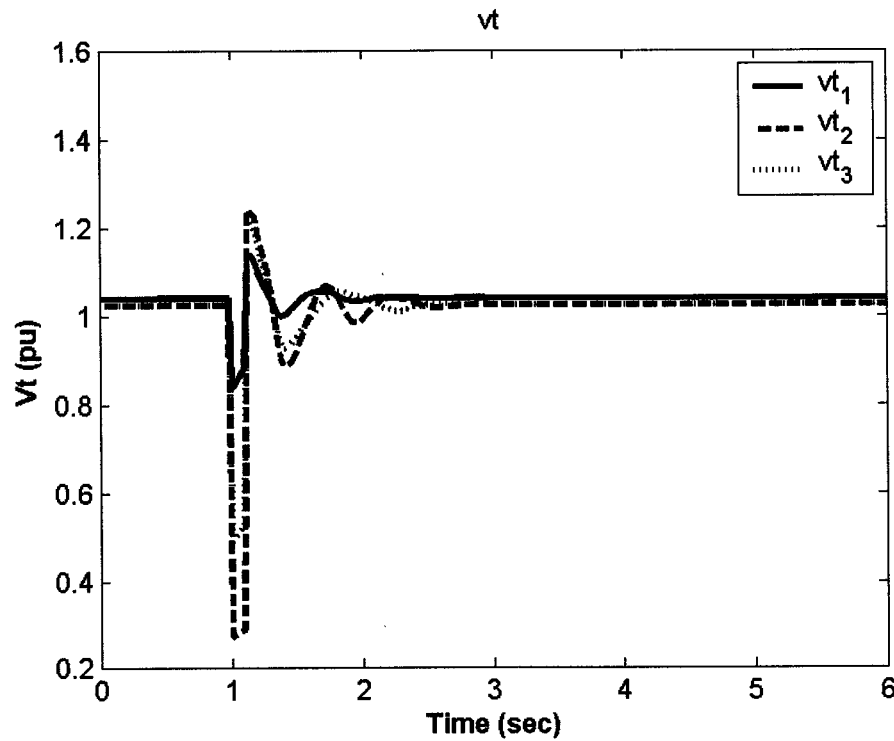


Figure 9.32: Terminal voltage response for 6-cycle fault with base case, J_1 settings, single-point tuning, coordinated SVC7-SVC9 design

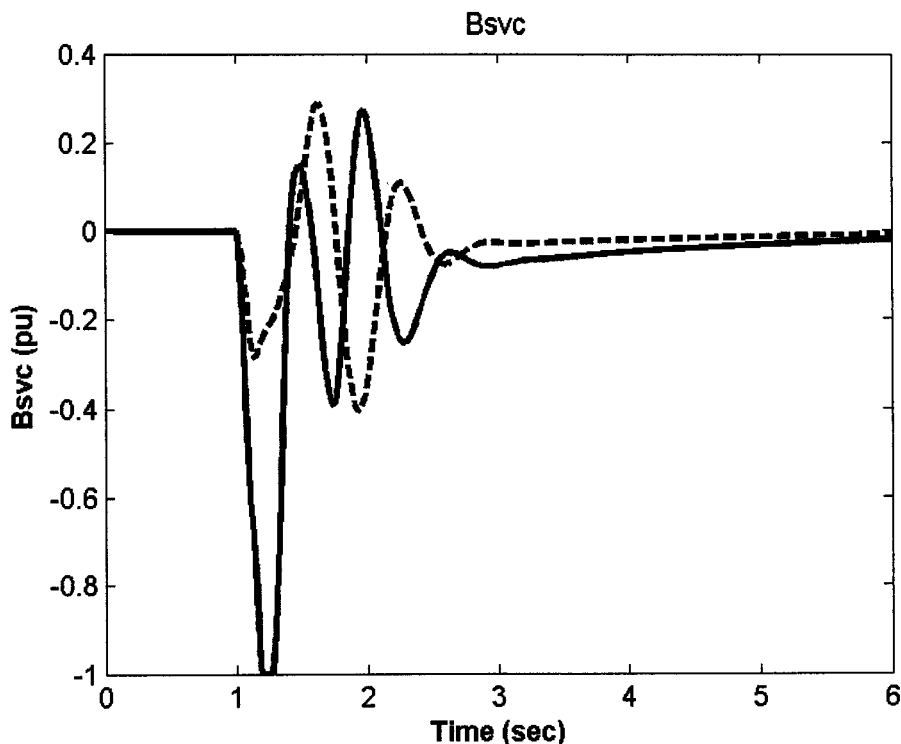


Figure 9.33: B_{svc} response for 6-cycle fault with base case, J_1 settings, single-point tuning, coordinated SVC7-SVC9 design

9.2.2 Multiple-Point Tuning

In this situation, the objective is to design robust stabilizers to ensure their effectiveness over a wide range of operating conditions. The design process takes into account the four loading cases shown in Tables 9.1 and 9.2 simultaneously.

Tables 9.18 and 9.19 list the open-loop eigenvalues and corresponding damping ratios associated with the EM modes of the four operating cases considered in the robust design process, respectively. It can be observed that these modes are either very lightly damped or even unstable.

9.2.2.1 Individual Design with J_1

The PSS2, PSS3, SVC7-, and SVC9-based controllers are designed individually considering the four operating cases mentioned above simultaneously.

Stabilizer Design: PSO is used to optimize the parameters of each controller that maximizes the minimum damping ratio of all the complex eigenvalues associated with the four operating cases simultaneously. The final settings of the optimized parameters for the proposed stabilizers are given in Table 9.20.

Table 9.18: Open-loop eigenvalues associated with the EM modes of the four operating cases considered in the robust design process

	The first EM mode	The second EM mode
Base Case	-0.3831± 7.8847i,	-1.3738± 11.750i,
Case 1	-0.2247± 7.8046i,	-0.8657± 11.798i,
Case 2	-0.6770± 6.5678i,	-2.0988± 9.4216i,
Case 3	0.1091± 8.0287i,	-0.5229± 12.035i,

Table 9.19: Damping ratios of the open-loop eigenvalues associated with the EM modes of the four operating cases considered in the robust design process

	The first EM mode	The second EM mode
Base Case	0.0485	0.1161
Case 1	0.0288	0.0732
Case 2	0.1025	0.2174
Case 3	-0.0136	0.0434

Table 9.20: Optimal parameter settings with J_1 , multiple-point tuning, individual design

	PSS2	PSS3	SVC7	SVC9
K	4.0936	0.3420	155.68	300.00
T₁	0.5870	1.0000	0.4489	0.0500
T₂	0.6617	0.0500	0.3882	0.6000
T₃	0.6677	1.0000	0.8385	0.3752
T₄	0.0500	0.0500	0.0744	0.1955

Eigenvalue Analysis: The system eigenvalues without and with the proposed stabilizers at the four operating points, base case, case 1, case 2, and case 3, are given in Tables 9.21-9.24, respectively. The bold rows of these tables represent the EM mode eigenvalues and their damping ratios. Generally, it can be observed that PSS3 and SVC9 can enhance the second EM mode damping more efficiently than the first EM mode damping. On the other hand, SVC7 is more able to damp the first EM mode than the second EM mode. This agrees with the results obtained from SVD results. PSS2 represents a special case as it can improve the damping of the two EM modes simultaneously.

Table 9.21: System eigenvalues of Base Case loading conditions with J_1 settings, multiple-point tuning, individual design

No Control	PSS2	PSS3	SVC7	SVC9
-0.3831±	-2.8251±	-0.7631±	-3.1597±	-1.7470±
7.8847i, 0.0485	6.9427i, 0.3769	7.9360i, 0.0957	4.4959i, 0.5750	7.7579i, 0.2197
-1.3738±	-5.5498±	-1.3331±	-1.2073±	-4.2055±
11.750i, 0.1161	8.4287i, 0.5499	6.2163i, 0.2097	11.641i, 0.1032	11.089i, 0.3546
-9.8638±	-3.5362±	-4.7843±	-3.1252±	-8.0158±
13.664i	14.653i	25.837i	14.252i	14.112i
-9.9194±	-6.5212±	-9.7337±	-20.1174±	-9.6178±
6.4142i	12.565i	11.970i	16.223i	6.2239i
-12.7012	-7.8780±	-9.8119±	-10.5383±	-1.1636±
-5.5005	2.5128i	6.1435i	9.9125i	4.7050i
-0.2000	-28.5550	-44.5388	-12.6724	-15.8822
--	-0.3061	-3.8850	-5.6173	-2.3128
--	-1.5115	-0.2060	-2.5180	-0.5693
--	-0.2000	-0.2000	-0.3952	-20.0000
--	--	--	-0.2000	-0.2000

Table 9.22: System eigenvalues of Case 1 loading conditions with J_1 settings, multiple-point tuning, individual design

No Control	PSS2	PSS3	SVC7	SVC9
-0.2247±	-2.1542±	-0.8626±	-2.5710±	-0.9845±
7.8046i, 0.0288	6.5236i, 0.3136	7.8604i, 0.1091	10.699i, 0.2337	7.3867i, 0.1321
-0.8657±	-2.8550±	-0.7495±	-0.9977±	-3.7063±
11.798i, 0.0732	11.830i, 0.2346	6.7988i, 0.1096	11.784i, 0.0844	11.436i, 0.3083
-9.8476±	-4.6872±	-4.5981±	-16.2100±	-7.8260±
13.518i	15.455i	26.427i	18.632i	13.855i
-10.150±	-7.5769±	-9.5745±	-13.3093±	-9.9974±
6.8751i	8.8355i	11.404i	10.107i	6.7770i
-9.5936±	-9.0076±	-10.065±	-9.7634±	-2.8678±
2.2870i	5.1442i	6.7249i	2.6012i	5.5533i
-0.2000	-28.6374	-45.0109	-4.4468±	-14.6579
--	-0.3642	-4.6435	5.3437i	-1.9478
--	-1.5116	-0.2099	-2.5056	-0.9764
--	-0.2000	-0.2000	-0.4785	-20.0000
--	--	--	-0.2000	-0.2000

Table 9.23: System eigenvalues of Case 2 loading conditions with J_1 settings, multiple-point tuning, individual design

No Control	PSS2	PSS3	SVC7	SVC9
-0.6770±	-2.5567±	-0.8718±	-1.9222±	-1.6206±
6.5678i, 0.1025	6.2183i, 0.3803	6.3785i, 0.1354	4.3776i, 0.4020	6.2858i, 0.2497
-2.0988±	-3.2332±	-1.1484±	-2.0245±	-5.1918±
9.4216i, 0.2174	5.9904i, 0.4750	5.6265i, 0.2000	9.3458i, 0.2117	9.3646i, 0.4849
-9.7416±	-6.8801±	-6.1500±	-19.2781±	-0.2864±
13.931i	13.751i	23.516i	14.955i	4.4825i
-9.7880±	-6.1775±	-9.6922±	-5.8597±	-8.9581±
7.0793i	12.261i	12.550i	14.030i	14.273i
-8.3262±	-8.3333 -	-9.6954±	-9.8167±	-9.6825±
2.3178i	5.9105i	7.0565i	9.5318i	7.1095i
-0.2000	-26.8467	-41.9369	-8.4213±	-14.0752
--	-1.5115	-4.2075	2.1959i	-2.2870
--	-0.2547	-0.2030	-2.5198	-0.4037
--	-0.2000	-0.2000	-0.3153	-20.0000
--	--	--	-0.2000	-0.2000

Table 9.24: System eigenvalues of Case 3 loading conditions with J_1 settings, multiple-point tuning, individual design

No Control	PSS2	PSS3	SVC7	SVC9
0.1091±	-2.7780±	-0.4453±	-3.7546±	-0.5001±
8.0287i, -0.0136	6.8979i, 0.3736 -2.5905±	7.7443i, 0.0574 -0.8560±	5.3938i, 0.5713 -1.0164±	7.6526i, 0.0652 -3.5012±
-0.5229±	10.732i, 0.2346	7.1971i, 0.1181	11.873i, 0.0853	12.325i, 0.2733
12.035i, 0.0434	-3.8672±	-4.5107±	-1.2088±	-8.2405±
-10.4209±	14.672i	26.332i	13.291i	13.029i
13.130i	-7.8839±	-9.9124±	-20.6823±	-9.9040±
-10.0239±	10.405i	11.324i	14.805i	6.9574i
7.0407i	-9.2180±	-9.9708±	-10.6818±	-3.1405±
-9.8009±	5.1650i	6.8953i	9.3162i	5.2114i
1.9872i	-28.5190	-45.1885	-9.9546±	-14.9865
-0.2000	-0.3246	-4.7330	2.1616i	-1.9794
--	-1.5116	-0.2072	-0.4236	-0.7625
--	-0.2000	-0.2000	-2.5155	-20.0000
--	--	--	-0.2000	-0.2000

Nonlinear Time-Domain Simulations: Figures 9.34-9.38 show the rotor angles, speed deviations, electrical power outputs, and machine terminal voltages responses as well as the PSS2 stabilizing signal, respectively, for a 6-cycle three-phase fault at bus 7 at the end of line 5-7 at the base case while using the proposed PSS2. Similarly, Figure 9.39-9.43 show those simulation results and control signal while using the proposed PSS3, Figures 9.44-9.48 illustrate the utilization of SVC7, and 9.49-9.53 demonstrate the use of SVC9. It can be readily seen that PSS2 is the most effective stabilizer in damping the EM modes oscillations. However, the system oscillations are relatively poorly damped using PSS3 and SVC7. This is consistent with eigenvalue analysis results.

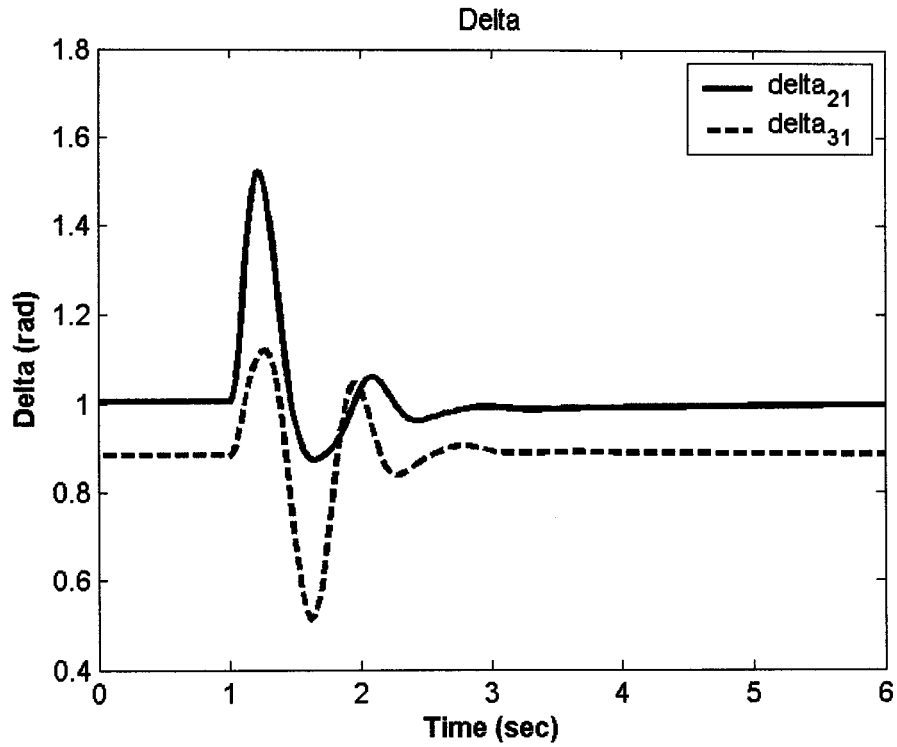


Figure 9.34: Rotor angle response for 6-cycle fault with base case, J_1 settings of PSS2, multiple-point tuning, individual design

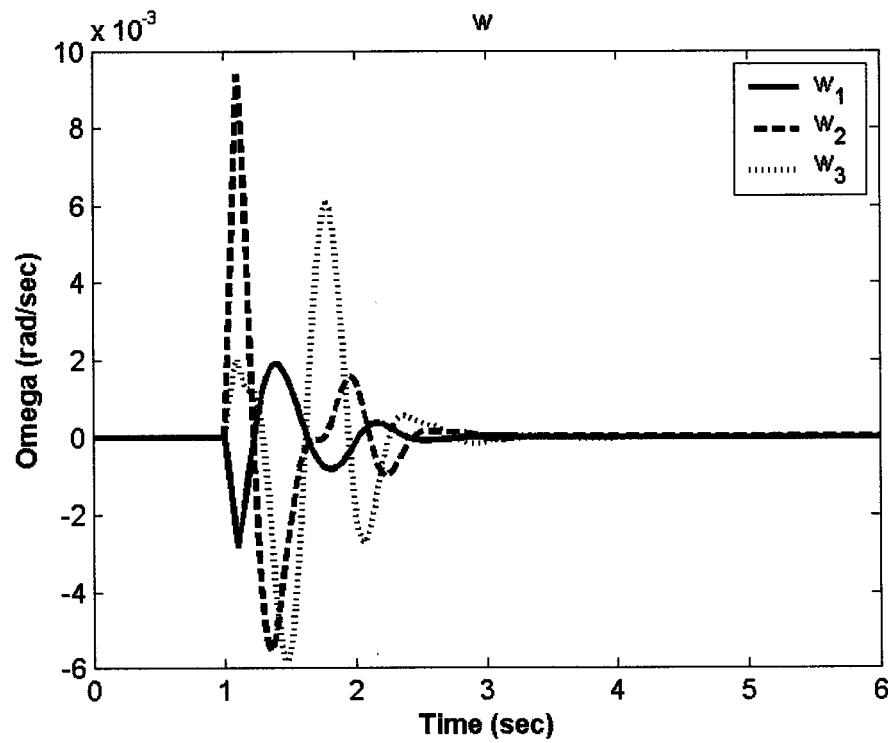


Figure 9.35: Speed response for 6-cycle fault with base case, J_1 settings of PSS2, multiple-point tuning, individual design

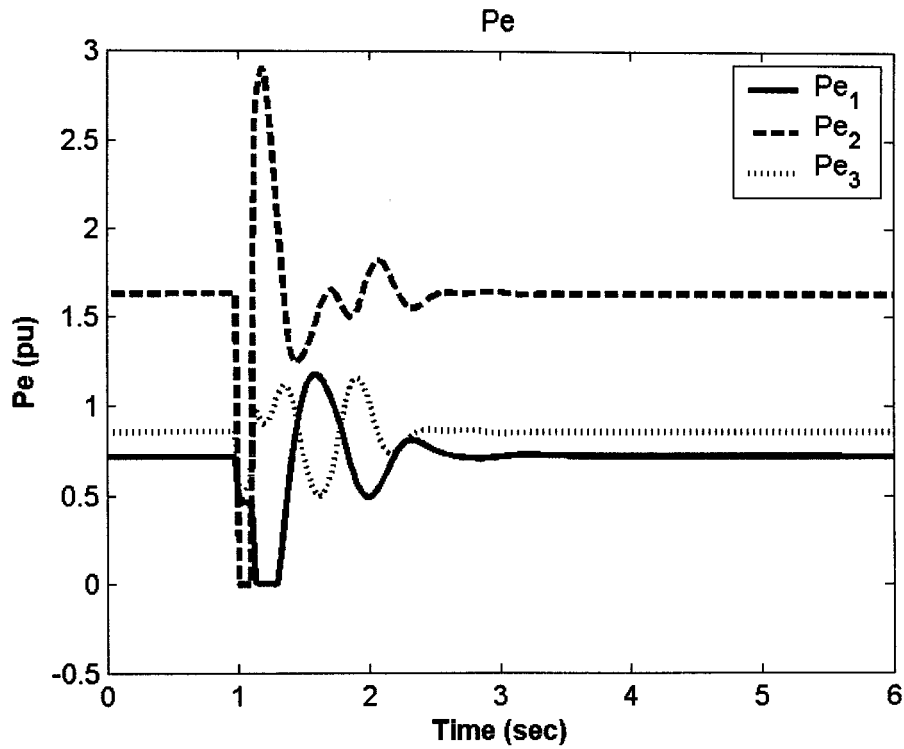


Figure 9.36: Electrical power response for 6-cycle fault with base case, J_1 settings of PSS2, multiple-point tuning, individual design

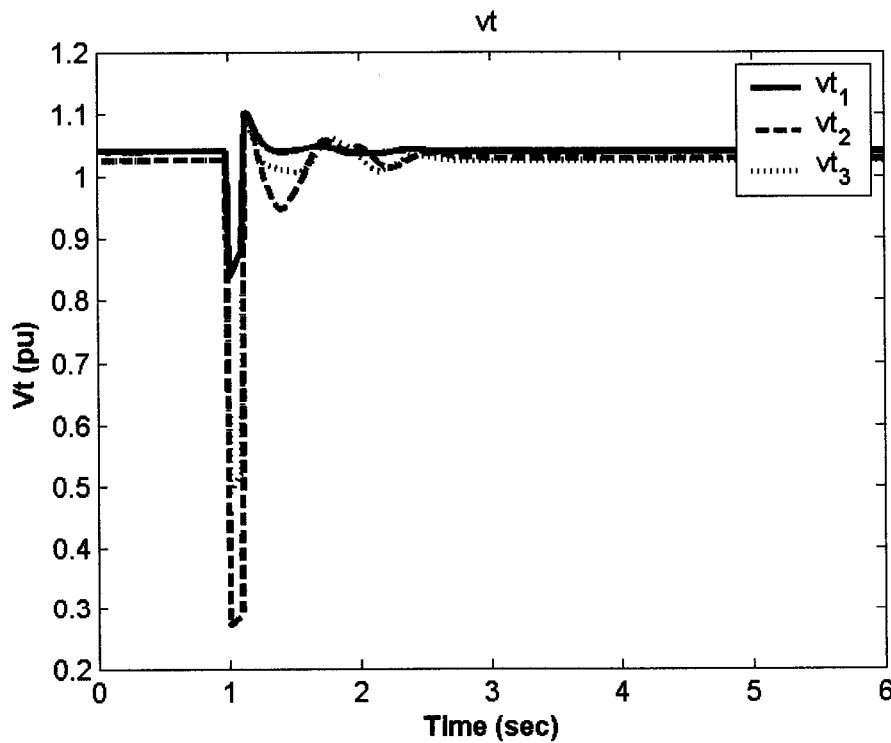


Figure 9.37: Terminal voltage response for 6-cycle fault with base case, J_1 settings of PSS2, multiple-point tuning, individual design

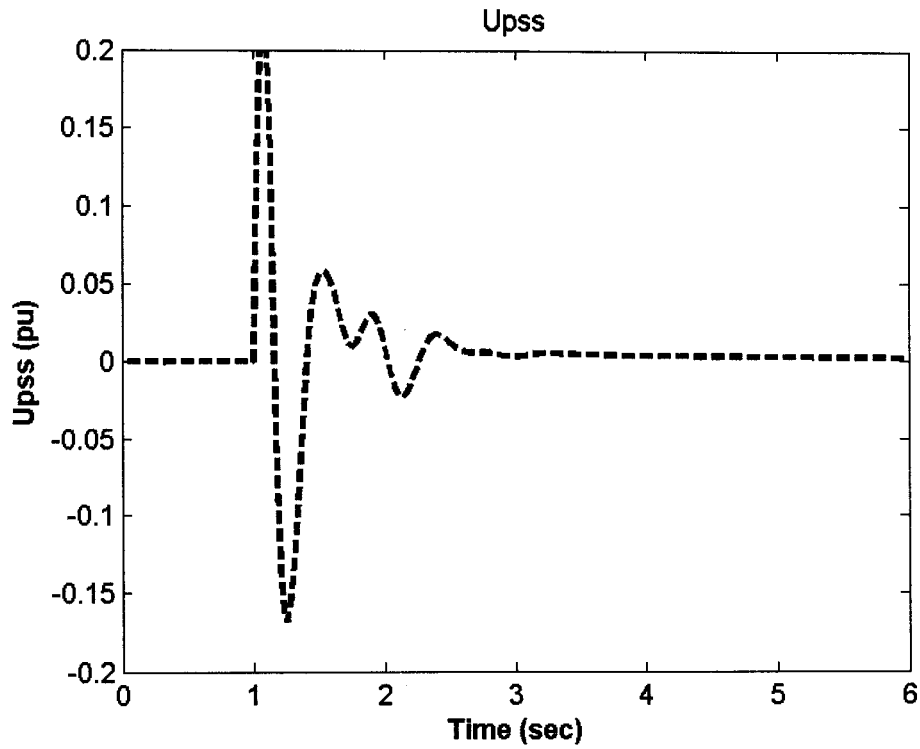


Figure 9.38: PSS stabilizing signal for 6-cycle fault with base case, J_1 settings of PSS2, multiple-point tuning, individual design

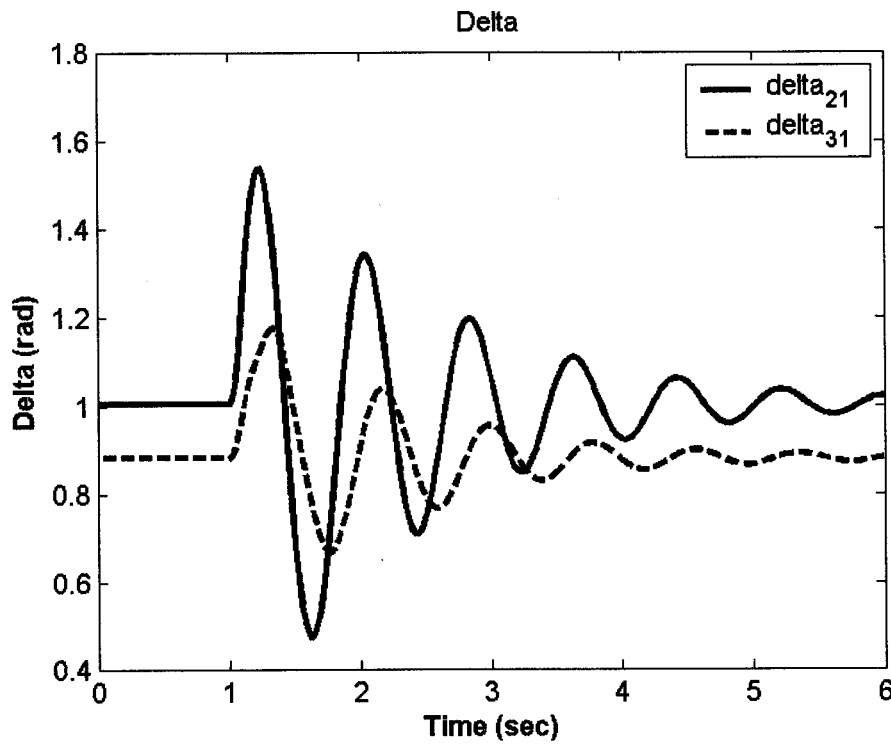


Figure 9.39: Rotor angle response for 6-cycle fault with base case, J_1 settings of PSS3, multiple-point tuning, individual design

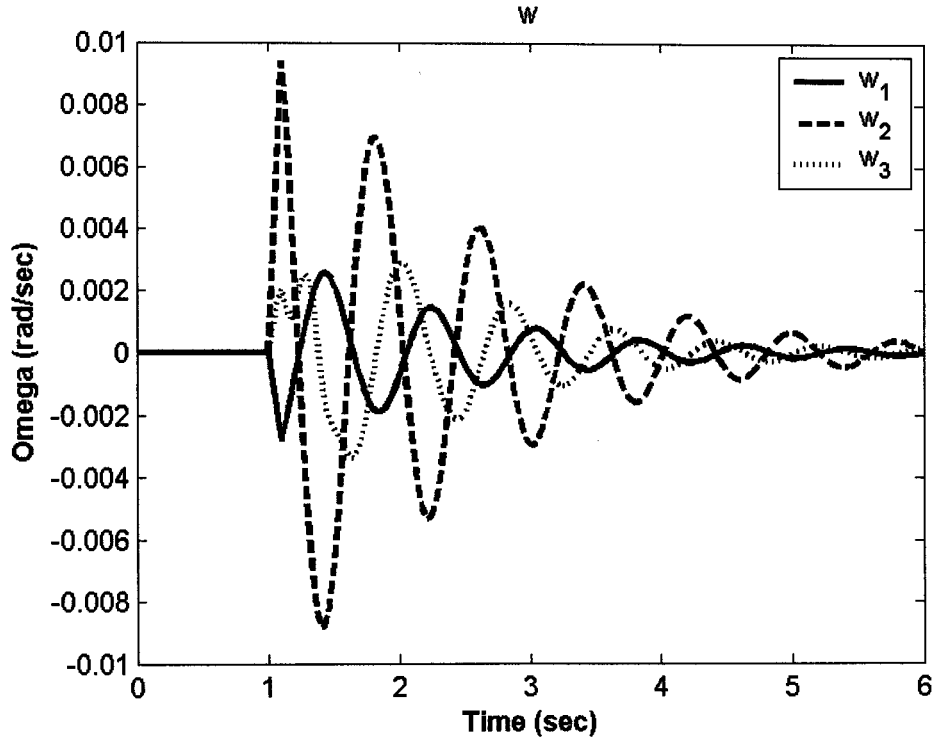


Figure 9.40: Speed response for 6-cycle fault with base case, J_1 settings of PSS3, multiple-point tuning, individual design

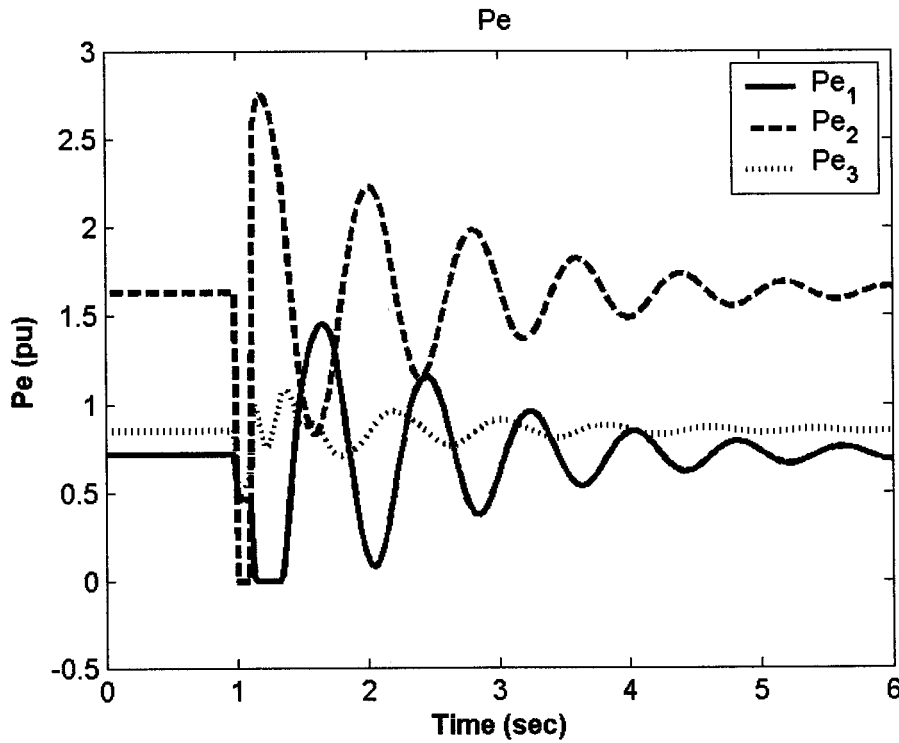


Figure 9.41: Electrical power response for 6-cycle fault with base case, J_1 settings of PSS3, multiple-point tuning, individual design

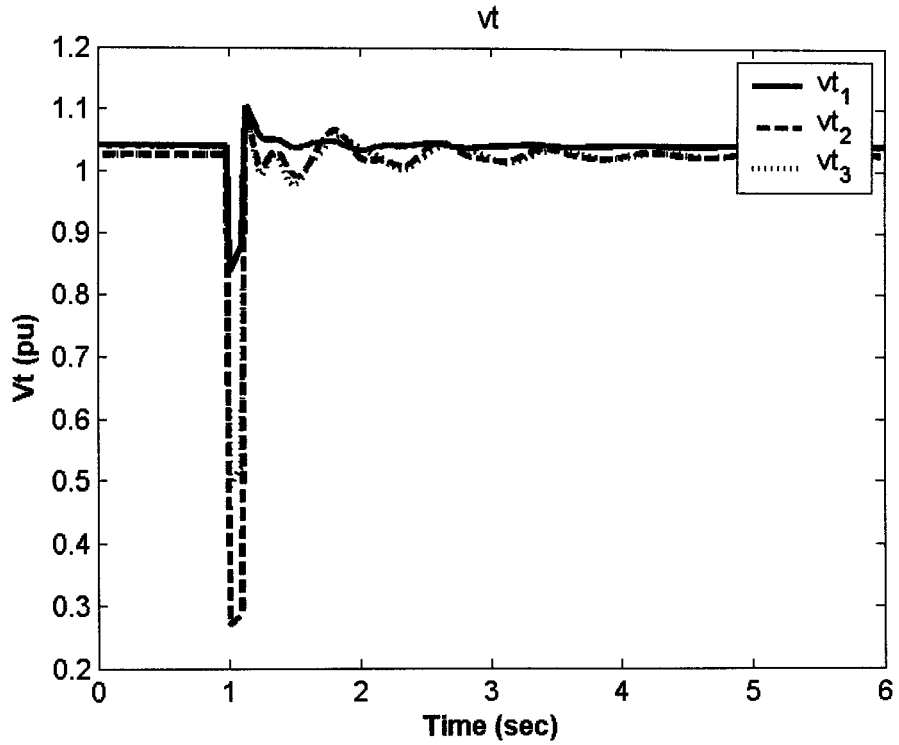


Figure 9.42: Terminal voltage response for 6-cycle fault with base case, J_1 settings of PSS3, multiple-point tuning, individual design

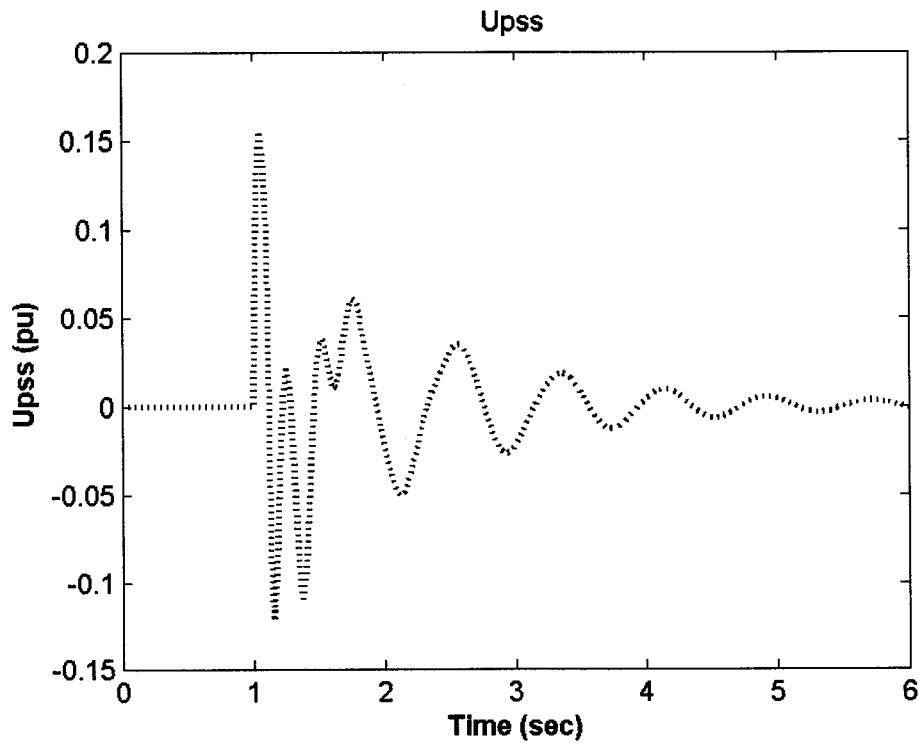


Figure 9.43: PSS stabilizing signal for 6-cycle fault with base case, J_1 settings of PSS3, multiple-point tuning, individual design

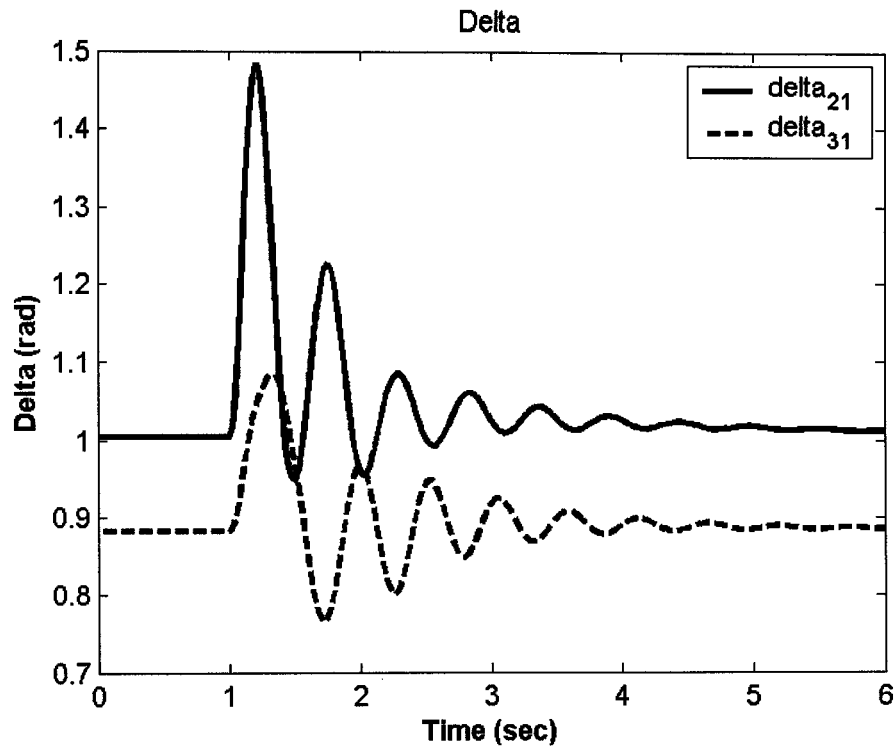


Figure 9.44: Rotor angle response for 6-cycle fault with base case, J_1 settings of SVC7, multiple-point tuning, individual design

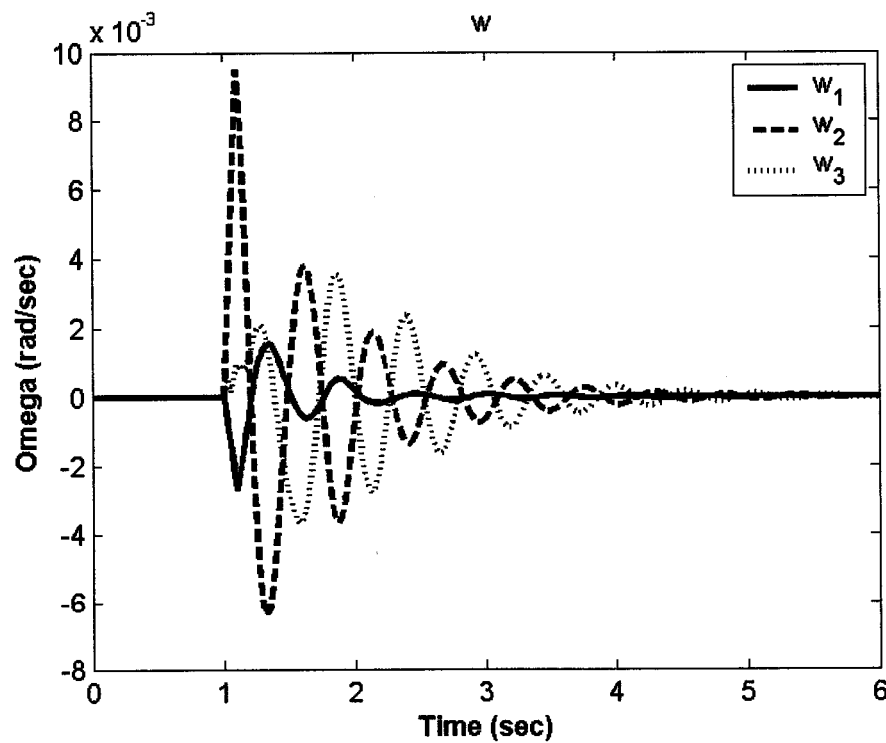


Figure 9.45: Speed response for 6-cycle fault with base case, J_1 settings of SVC7, multiple-point tuning, individual design

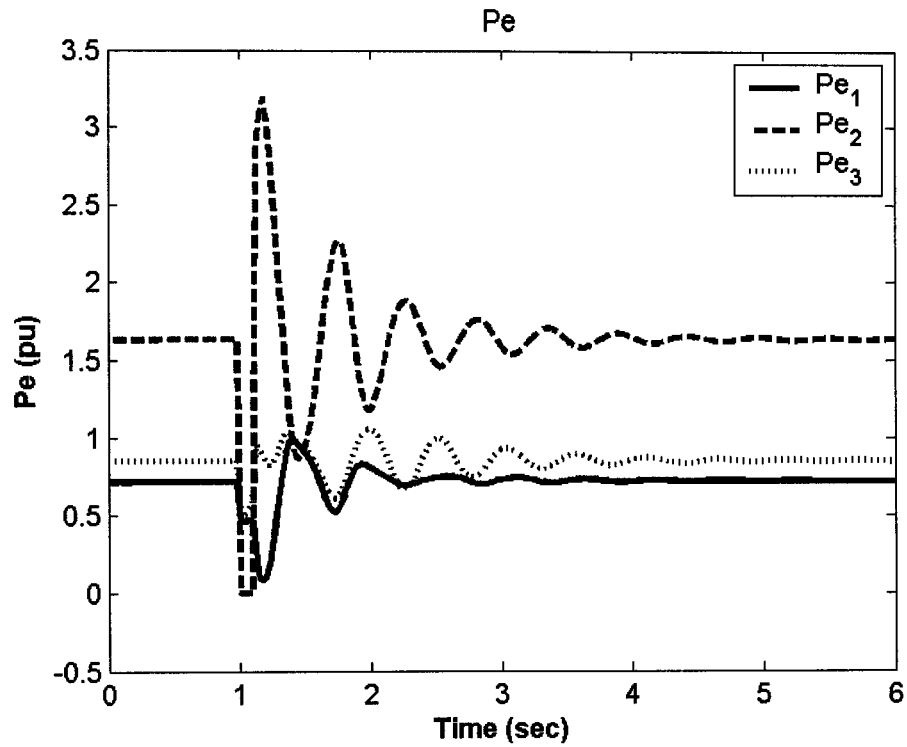


Figure 9.46: Electrical power response for 6-cycle fault with base case, J_1 settings of SVC7, multiple-point tuning, individual design

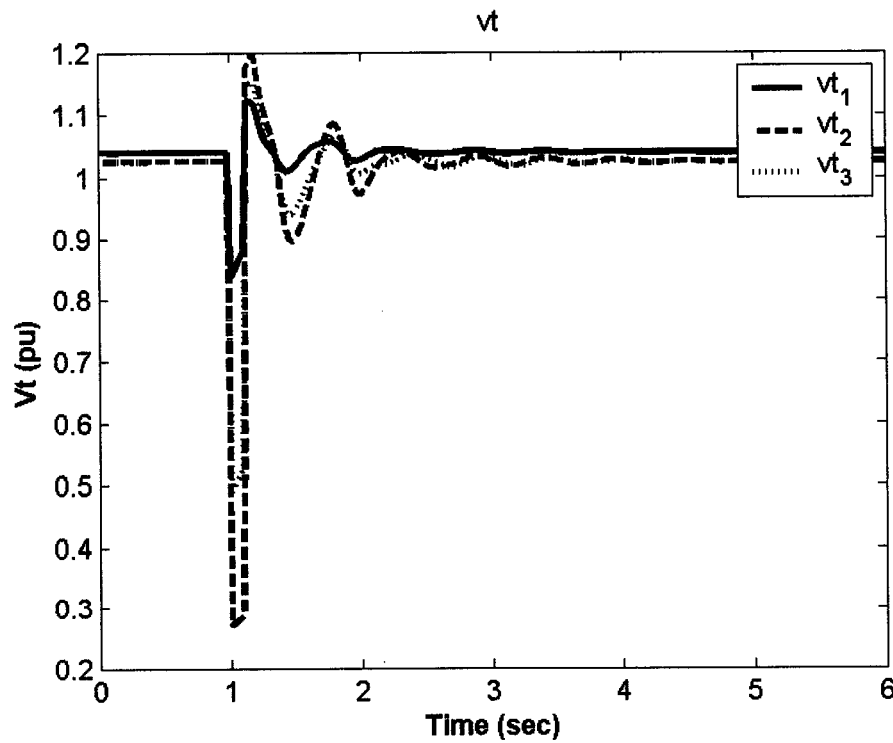


Figure 9.47: Terminal voltage response for 6-cycle fault with base case, J_1 settings of SVC7, multiple-point tuning, individual design

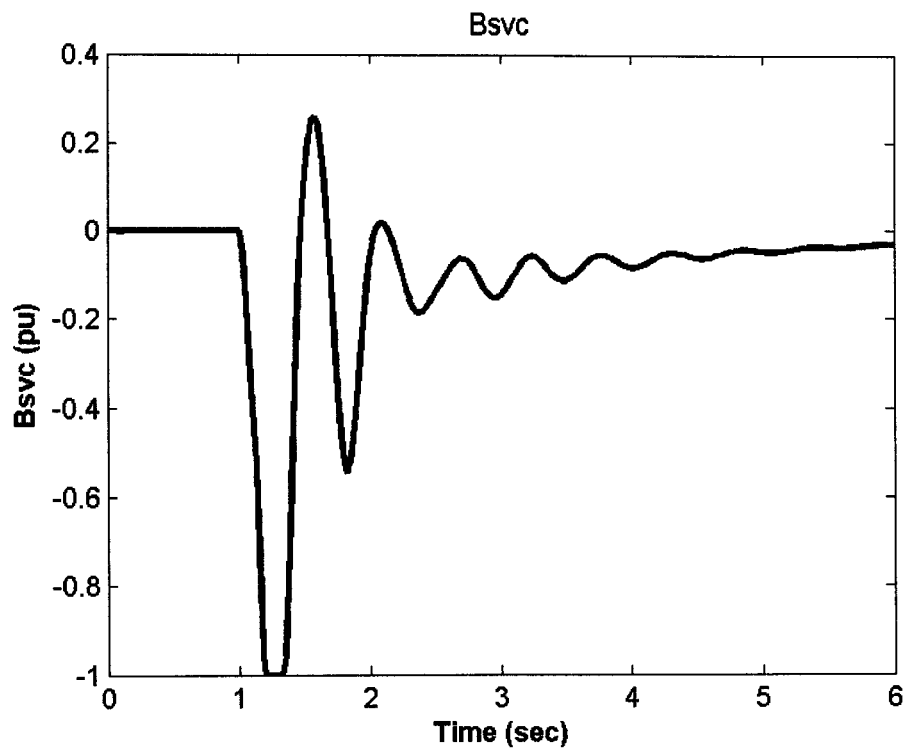


Figure 9.48: B_{svc} response for 6-cycle fault with base case, J_1 settings of SVC7, multiple-point tuning, individual design

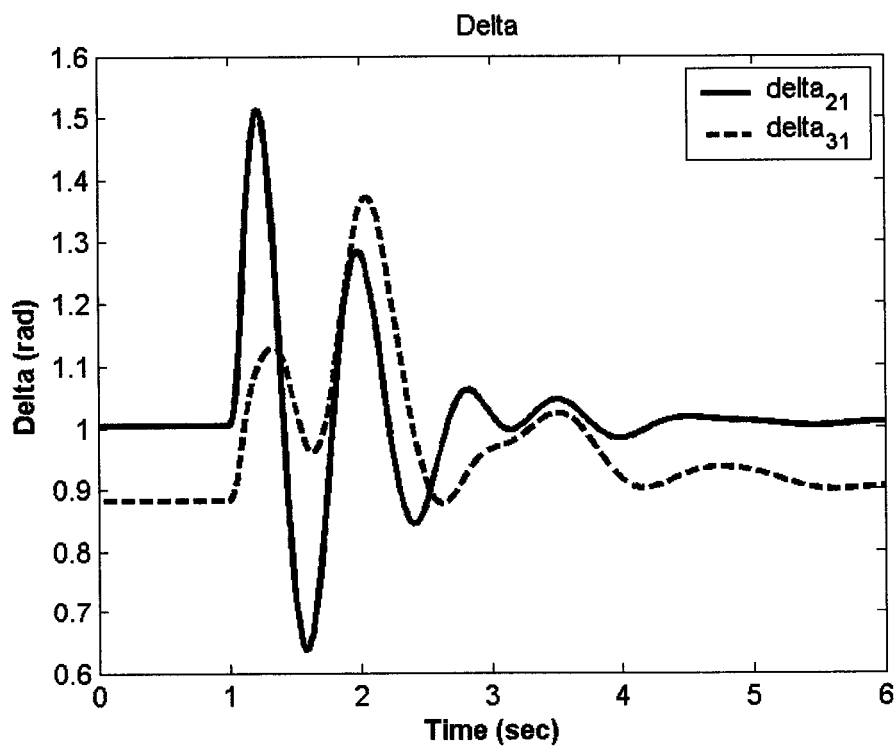


Figure 9.49: Rotor angle response for 6-cycle fault with base case, J_1 settings of SVC9, multiple-point tuning, individual design

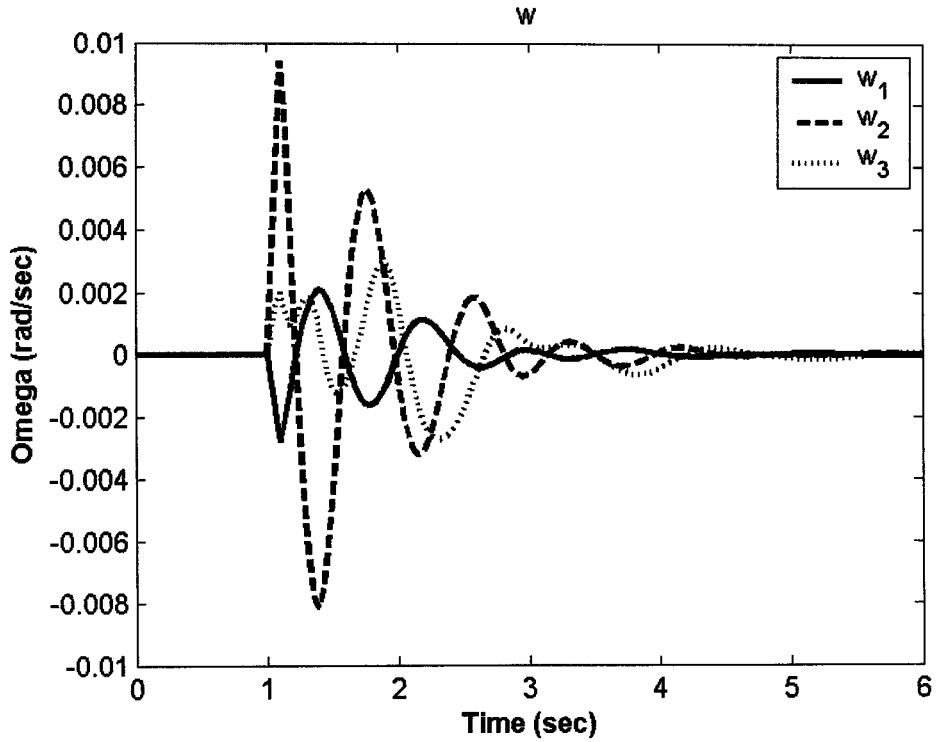


Figure 9.50: Speed response for 6-cycle fault with base case, J_1 settings of SVC9, multiple-point tuning, individual design

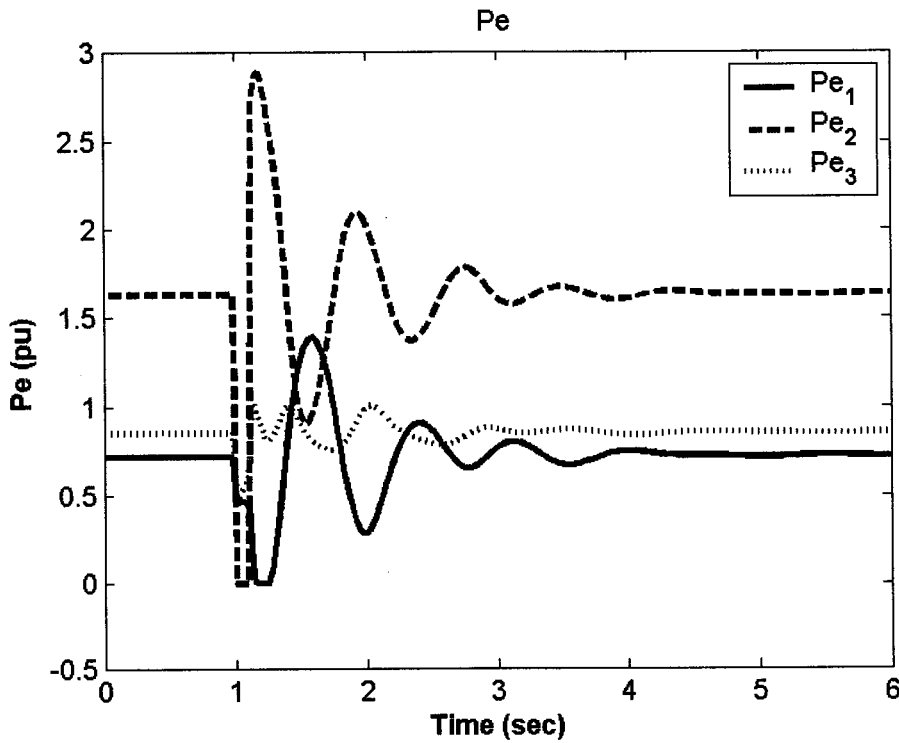


Figure 9.51: Electrical power response for 6-cycle fault with base case, J_1 settings of SVC9, multiple-point tuning, individual design

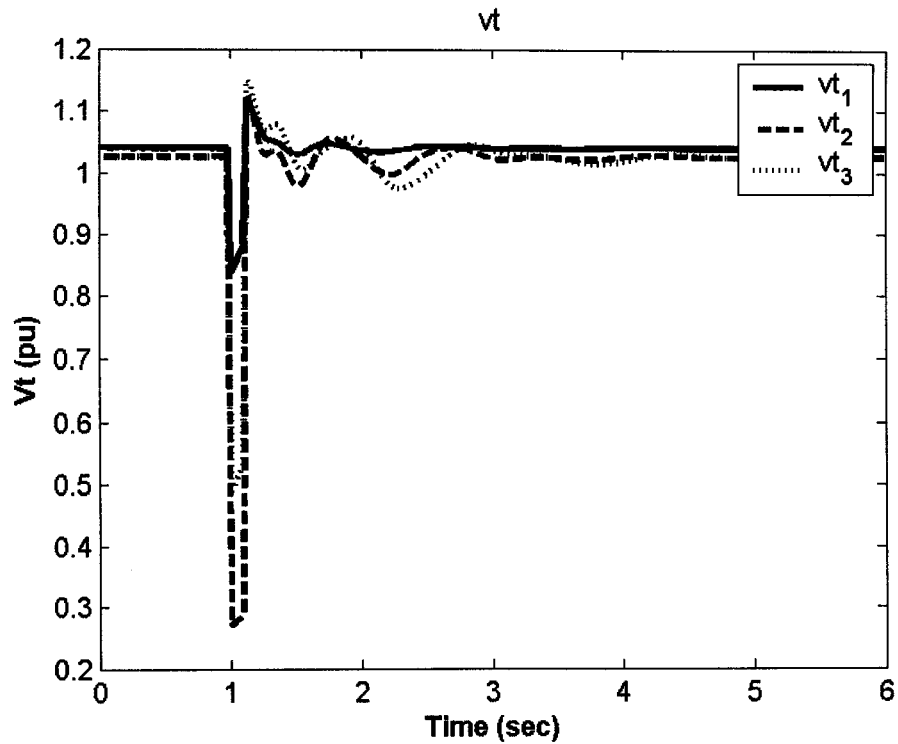


Figure 9.52: Terminal voltage response for 6-cycle fault with base case, J_1 settings of SVC9, multiple-point tuning, individual design

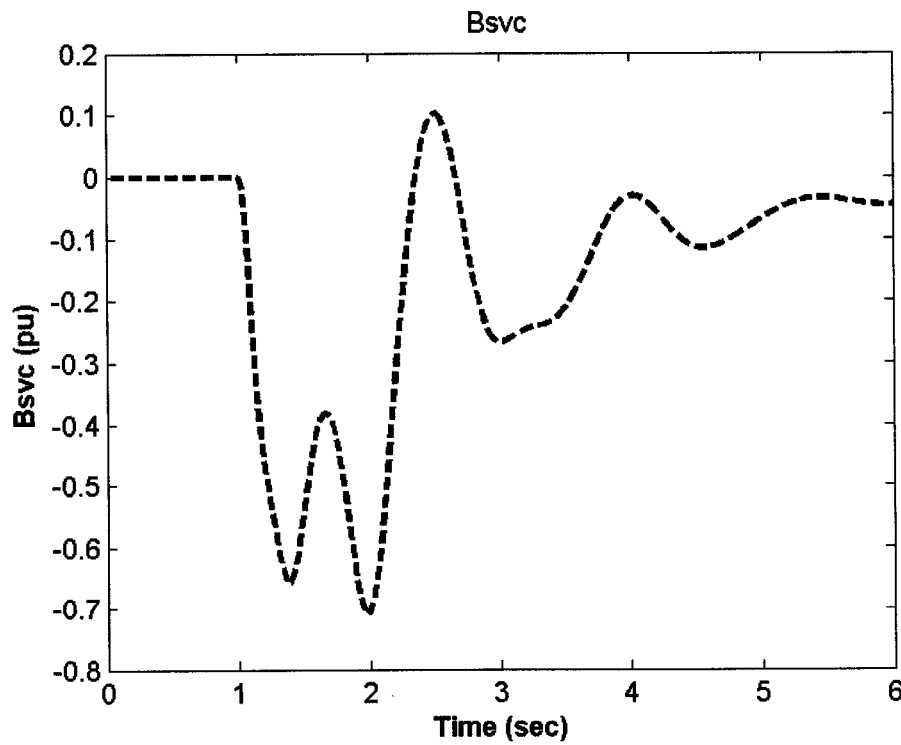


Figure 9.53: B_{svc} response for 6-cycle fault with base case, J_1 settings of SVC9, multiple-point tuning, individual design

9.2.2.2 Coordinated PSS3-SVC7 Design with J_1

The controllability measure analysis, based on the singular value decomposition, and the eigenvalue analysis indicate that the PSS3 and SVC7-based stabilizer do not perform well individually. This is because SVC7-based stabilizer is the most effective stabilizer in improving the first EM mode damping and PSS3 is the most effective in damping the second EM mode. The same conclusion can be drawn from nonlinear time-domain simulations illustrated in the previous section. In this section, the coordinated design of PSS3 and SVC7-based stabilizer is considered at all the four operating cases simultaneously.

Stabilizer Design: PSO is used to simultaneously search for the optimum parameter settings of both controllers that maximize the minimum damping ratio of all the system complex eigenvalues at all the four operating case. The final settings of the optimized parameters for the proposed stabilizers are given in Table 9.25.

Eigenvalue Analysis: The system eigenvalues without and with the proposed PSS3 and SVC7-based controllers when applied individually and through coordinated design at the four loading cases are given in Tables 9.26-9.29. The bold rows of these tables represent the EM modes eigenvalues and their damping ratios. It is evident that, using the proposed coordinated stabilizers design, the damping ratio of the EM mode eigenvalue is greatly enhanced. Hence, it can be concluded that this improves the system stability.

Table 9.25: Optimal parameter settings with J_1 , multiple-point tuning, coordinated PSS3-SVC7 design

	Individual		Coordinated	
	PSS3	SVC7	PSS3	SVC7
K	0.3420	155.68	1.3316	40.4950
T₁	1.0000	0.4489	0.2540	0.8947
T₂	0.0500	0.3882	0.0500	0.0500
T₃	1.0000	0.8385	0.2543	0.7330
T₄	0.0500	0.0744	0.0500	0.4631

Table 9.26: System eigenvalues of Base Case loading conditions with J_1 settings, multiple-point tuning, coordinated PSS3-SVC7 design

No Control	PSS3	SVC7	PSS3 & SVC7
-0.3831± 7.8847i, 0.0485	-0.7631± 7.9360i, 0.0957	-3.1597± 4.4959i, 0.5750	-2.9518± 10.562i, 0.2692
-1.3738± 11.750i, 0.1161	-1.3331± 6.2163i, 0.2097	-1.2073± 11.641i, 0.1032	-2.9059± 6.3870i, 0.4141
-9.8638± 13.664i	-4.7843± 25.837i	-3.1252± 14.252i	-21.835± 13.104i
-9.9194± 6.4142i	-9.7337± 11.970i	-20.1174± 16.223i	-5.3186± 16.797i
-12.7012	-9.8119± 6.1435i	-10.5383± 9.9125i	-10.658± 9.8990i
-5.5005	-44.5388	-12.6724	-7.4051± 6.3836i
-0.2000	-3.8850	-5.6173	-33.7018
--	-0.2060	-2.5180	-5.3871
--	-0.2000	-0.3952	-2.1165
--	--	-0.2000	-0.2855
--	--	--	-0.2006
--	--	--	-0.2000

Table 9.27: System eigenvalues of Case 1 loading conditions with J_1 settings, multiple-point tuning, coordinated PSS3-SVC7 design

No Control	PSS3	SVC7	PSS3 & SVC7
-0.2247± 7.8046i, 0.0288	-0.8626± 7.8604i, 0.1091	-2.5710± 10.699i, 0.2337	-2.3625± 8.4363i, 0.2697
-0.8657± 11.798i, 0.0732	-0.7495± 6.7988i, 0.1096	-0.9977± 11.784i, 0.0844	-2.9136± 8.6507i, 0.3192
-9.8476± 13.518i	-4.5981± 26.427i	-16.2100± 18.632i	-19.341± 13.413i
-10.150± 6.8751i	-9.5745± 11.404i	-13.3093± 10.107i	-6.0116± 16.453i
-9.5936± 2.2870i	-10.065± 6.7249i	-9.7634± 2.6012i	-11.926± 10.426i
-0.2000	-45.0109	-4.4468± 5.3437i	-7.4579± 6.5469i
--	-4.6435	-2.5056	-33.8678
--	-0.2099	-0.4785	-7.3948
--	-0.2000	-0.2000	-2.1000
--	--	--	-0.3321
--	--	--	-0.2004
--	--	--	-0.2000

Table 9.28: System eigenvalues of Case 2 loading conditions with J_1 settings, multiple-point tuning, coordinated PSS3-SVC7 design

No Control	PSS3	SVC7	PSS3 & SVC7
-0.6770± 6.5678i, 0.1025	-0.8718± 6.3785i, 0.1354	-1.9222± 4.3776i, 0.4020	-4.0813± 7.0769i, 0.4996
-2.0988± 9.4216i, 0.2174	-1.1484± 5.6265i, 0.2000	-2.0245± 9.3458i, 0.2117	-1.5365± 5.5232i, 0.2680
-9.7416± 13.931i	-6.1500± 23.516i	-19.2781± 14.955i	-21.362± 11.914i
-9.7880± 7.0793i	-9.6922± 12.550i	-5.8597± 14.030i	-7.1197± 15.750i
-8.3262± 2.3178i	-9.6954± 7.0565i	-9.8167± 9.5318i	-9.7132± 10.035i
-0.2000	-41.9369	-8.4213± 2.1959i	-7.4390± 8.8219i
--	-4.2075	-2.5198	-32.0098
--	-0.2030	-0.3153	-6.7390
--	-0.2000	-0.2000	-2.1217
--	--	--	-0.2460
--	--	--	-0.2006
--	--	--	-0.2000

Table 9.29: System eigenvalues of Case 3 loading conditions with J_1 settings, multiple-point tuning, coordinated PSS3-SVC7 design

No Control	PSS3	SVC7	PSS3 & SVC7
$0.1091 \pm 8.0287i$, -0.0136	$-0.4453 \pm 7.7443i$, 0.0574	$-3.7546 \pm 5.3938i$, 0.5713	$-2.4979 \pm 8.2013i$, 0.2914
$-0.5229 \pm 12.035i$, 0.0434	$-0.8560 \pm 7.1971i$, 0.1181	$-1.0164 \pm 11.873i$, 0.0853	$-2.6963 \pm 9.6050i$, 0.2703
$-10.4209 \pm 13.130i$	$-4.5107 \pm 26.332i$	$-1.2088 \pm 13.291i$	$-21.773 \pm 11.987i$
$-10.0239 \pm 7.0407i$	$-9.9124 \pm 11.324i$	$-20.6823 \pm 14.805i$	$-4.6537 \pm 16.358i$
$-9.8009 \pm 1.9872i$	$-9.9708 \pm 6.8953i$	$-10.6818 \pm 9.3162i$	$-10.700 \pm 9.5588i$
-0.2000	-45.1885	$-9.9546 \pm 2.1616i$	$-7.5258 \pm 7.1379i$
--	-4.7330	-0.4236	-34.2127
--	-0.2072	-2.5155	-7.3588
--	-0.2000	-0.2000	-2.1114
--	--	--	-0.3006
--	--	--	-0.2003
--	--	--	-0.2000

Nonlinear Time-Domain Simulations: Figures 9.54-9.59 show the rotor angles, speed deviations, electrical power outputs, and machine terminal voltages responses, as well as PSS3 stabilizing signal and SVC7 response, respectively, for a 6-cycle three-phase fault at bus 7 at the end of line 5-7 at the base case while using the proposed PSS3-SVC7 coordinated design. These figures should be compared with Figures 9.39-9.43, for individual PSS3 design, and 9.44-9.48, for individual SVC7 design. The improvement on the system responses when using the coordinated design is quite evident. This is in agreement with eigenvalue analysis results.

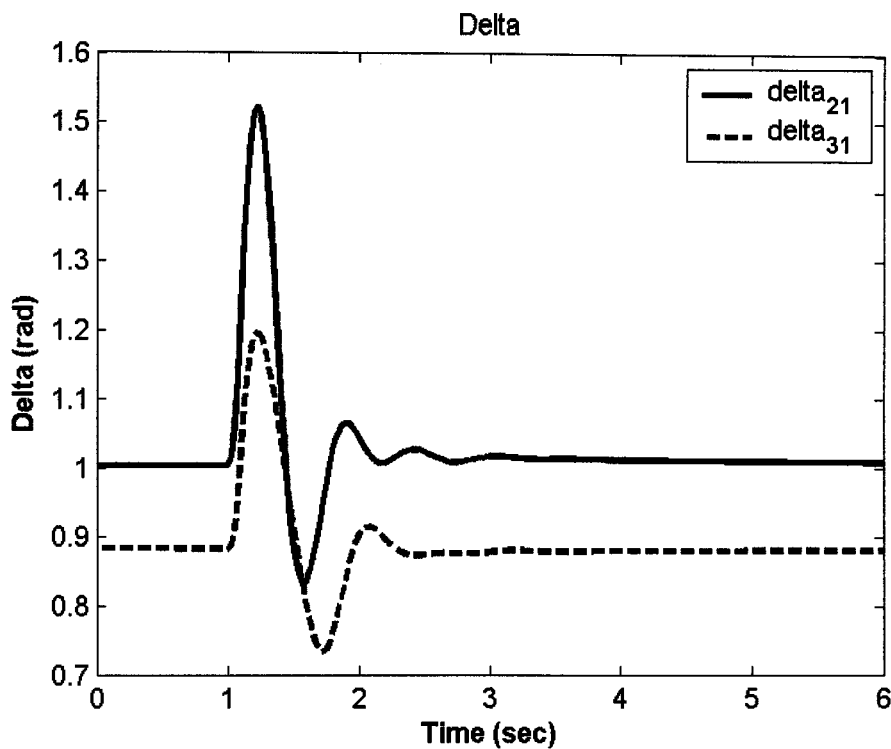


Figure 9.54: Rotor angle response for 6-cycle fault with base case, J_1 settings, multiple-point tuning, coordinated PSS3-SVC7 design

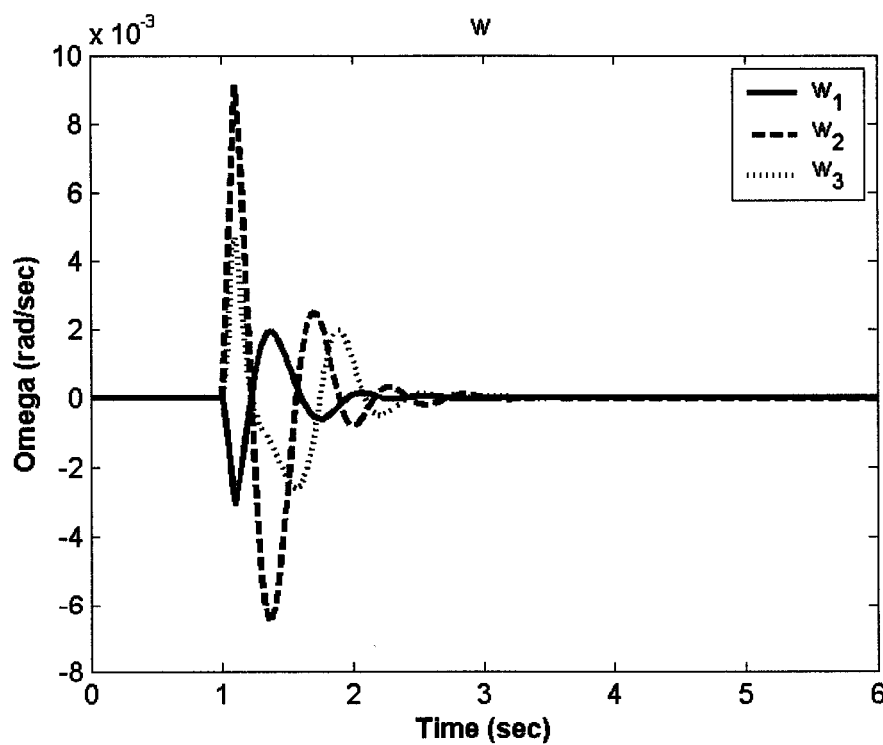


Figure 9.55: Speed response for 6-cycle fault with base case, J_1 settings, multiple-point tuning, coordinated PSS3-SVC7 design

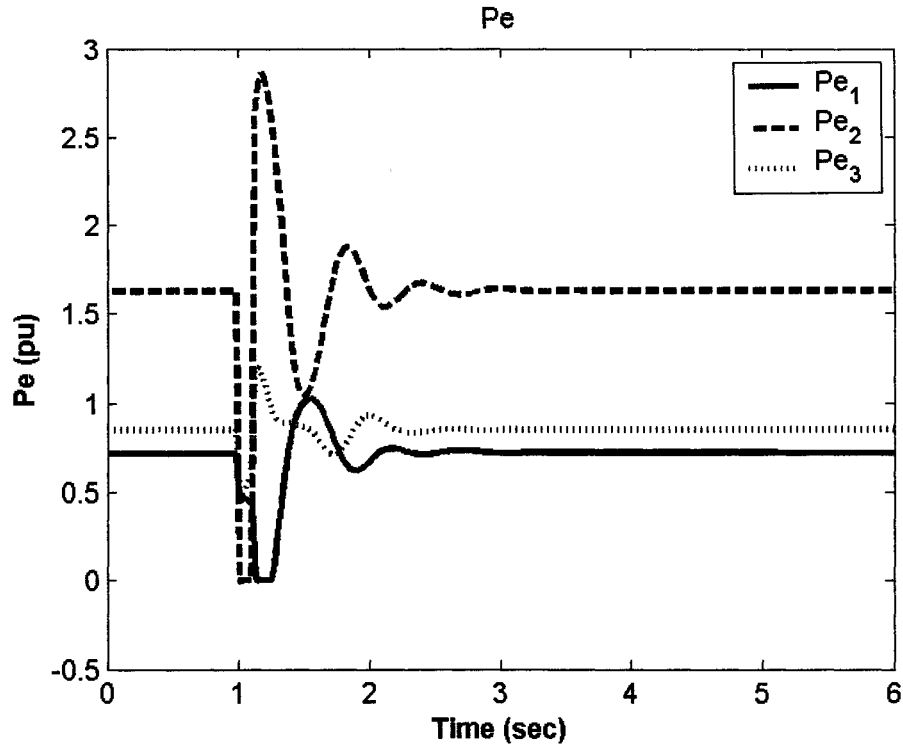


Figure 9.56: Electrical power response for 6-cycle fault with base case, J_1 settings, multiple-point tuning, coordinated PSS3-SVC7 design

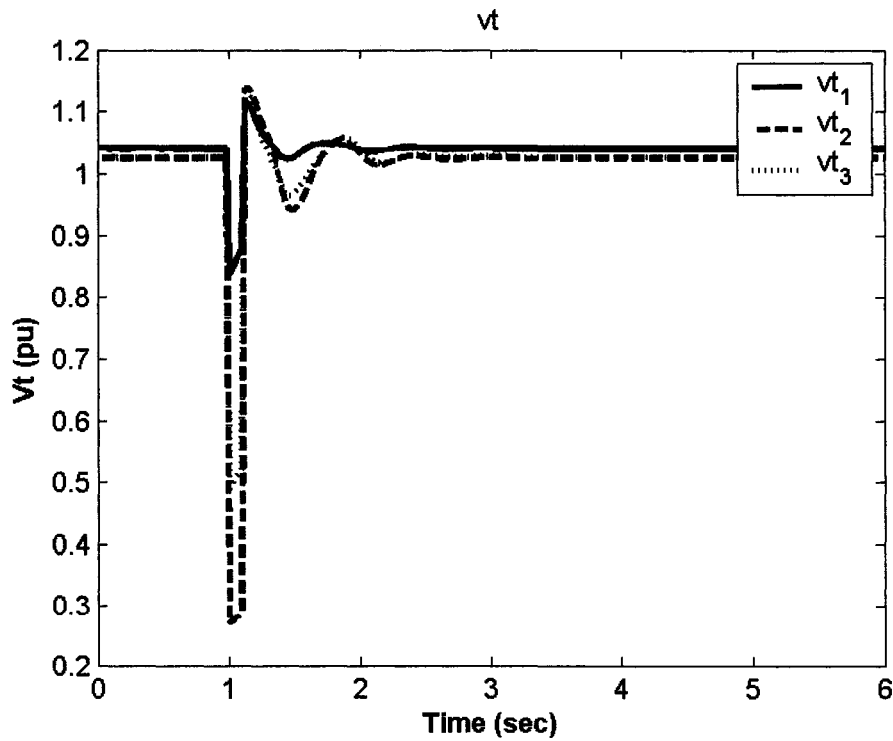


Figure 9.57: Terminal voltage response for 6-cycle fault with base case, J_1 settings, multiple-point tuning, coordinated PSS3-SVC7 design

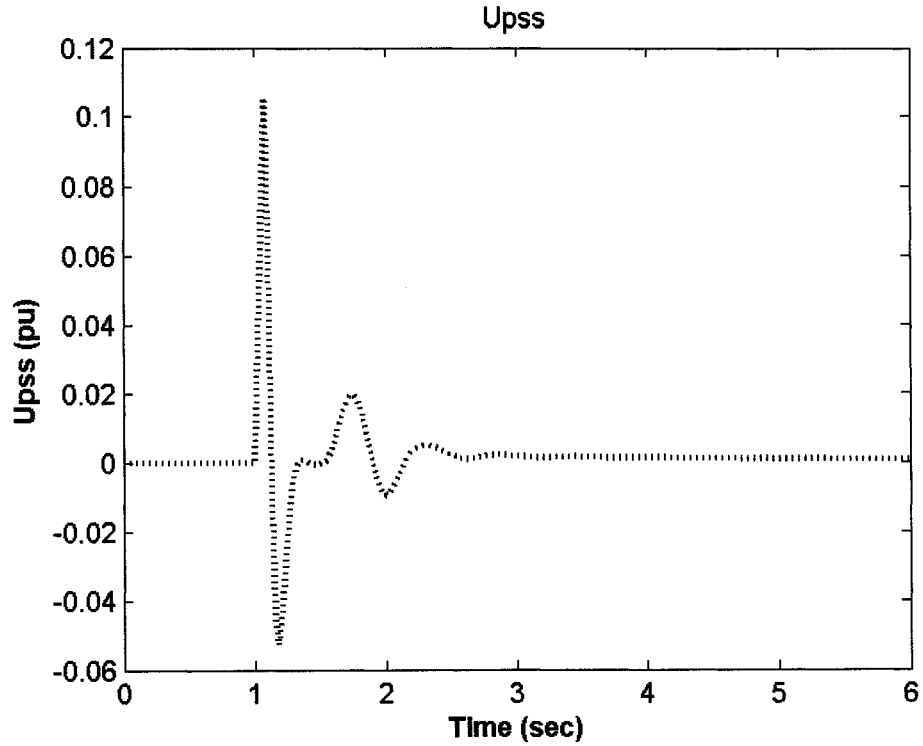


Figure 9.58: PSS stabilizing signal for 6-cycle fault with base case, J_1 settings, multiple-point tuning, coordinated PSS3-SVC7 design

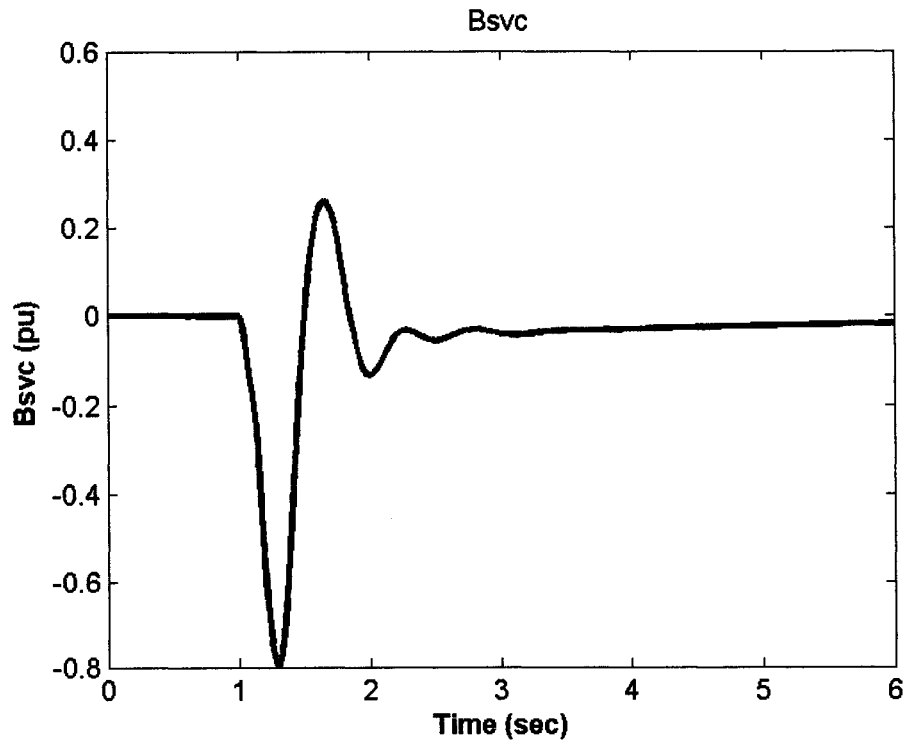


Figure 9.59: B_{svc} response for 6-cycle fault with base case, J_1 settings, multiple-point tuning, coordinated PSS3-SVC7 design

9.2.2.3 Coordinated SVC7-SVC9 Design with J_1

As an alternative to using the PSS-SVC7 coordinated design, the SVC7-SVC9 coordinated design is studied. The singular value decomposition analysis as well as the eigenvalue analysis show that a single SVC-based stabilizer cannot provide sufficient damping to the two EM modes simultaneously. The same conclusion can be drawn from nonlinear time-domain simulations illustrated earlier. Hence, there is a need for coordination. Since SVC7 is superior in damping the first EM mode and SVC9 is the most effective SVC in damping the second EM mode, the SVC7-SVC9 combination is presented. In this section, the coordinated design of SVC7- and SVC9-based stabilizers is considered at the four loading cases simultaneously.

Stabilizer Design: PSO is used to simultaneously search for the optimum parameter settings of both controllers that maximize the minimum damping ratio of all the system complex eigenvalues at all the four loading cases. The final settings of the optimized parameters for the proposed stabilizers are given in Table 9.30.

Eigenvalue Analysis: The system eigenvalues without and with the proposed SVC7- and SVC9-based controllers when applied individually and through coordinated design at the four loading cases are given in Tables 9.31-9.34. The bold rows of these tables represent the EM modes eigenvalues and their damping ratios. It is evident that the damping ratios of the EM modes eigenvalues are greatly enhanced using the proposed coordinated stabilizers design.

Table 9.30: Optimal parameter settings with J_1 , multiple-point tuning, coordinated SVC7-SVC9 design

	Individual		Coordinated	
	SVC7	SVC9	SVC7	SVC9
K	155.68	300.00	201.82	184.42
T₁	0.4489	0.0500	0.5990	0.3737
T₂	0.3882	0.6000	0.0500	0.7055
T₃	0.8385	0.3752	0.5776	0.5851
T₄	0.0744	0.1955	0.2925	0.4883

Table 9.31: System eigenvalues of Base Case loading conditions with J_1 settings, multiple-point tuning, coordinated SVC7-SVC9 design

No Control	SVC7	SVC9	SVC7 & SVC9
-0.3831± 7.8847i, 0.0485	-3.1597± 4.4959i, 0.5750	-1.7470± 7.7579i, 0.2197	-4.3694± 11.780i, 0.3478
-1.3738± 11.750i, 0.1161	-1.2073± 11.641i, 0.1032	-4.2055± 11.089i, 0.3546	-3.7174± 5.4997i, 0.5600
-9.8638± 13.664i	-3.1252± 14.252i	-8.0158± 14.112i	-22.608± 23.606i
-9.9194± 6.4142i	-20.1174± 16.223i	-9.6178± 6.2239i	-6.0009± 16.547i
-12.7012	-10.5383± 9.9125i	-1.1636± 4.7050i	-9.9648± 9.3268i
-5.5005	-12.6724	-15.8822	-1.8727± 4.9516i
-0.2000	-5.6173	-2.3128	-23.8872
--	-2.5180	-0.5693	-3.0229
--	-0.3952	-20.0000	-2.2357
--	-0.2000	-0.2000	-1.5389
--	--	--	-0.6188
--	--	--	-0.1960
--	--	--	-0.2000

Table 9.32: System eigenvalues of Case 1 loading conditions with J_1 settings, multiple-point tuning, coordinated SVC7-SVC9 design

No Control	SVC7	SVC9	SVC7 & SVC9
-0.2247± 7.8046i, 0.0288	-2.5710± 10.699i, 0.2337	-0.9845± 7.3867i, 0.1321	-2.5319± 9.7791i, 0.2506
-0.8657± 11.798i, 0.0732	-0.9977± 11.784i, 0.0844	-3.7063± 11.436i, 0.3083	-3.1069± 5.5365i, 0.4894
-9.8476± 13.518i	-16.2100± 18.632i	-7.8260± 13.855i	-19.217± 28.780i
-10.150± 6.8751i	-13.3093± 10.107i	-9.9974± 6.7770i	-12.516± 10.604i
-9.5936± 2.2870i	-9.7634± 2.6012i	-2.8678± 5.5533i	-6.3763± 11.076i
-0.2000	-4.4468± 5.3437i	-14.6579	-5.1162± 8.4619i
--	-2.5056	-1.9478	-23.3031
--	-0.4785	-0.9764	-2.9996
--	-0.2000	-20.0000	-2.1178
--	--	-0.2000	-1.4116
--	--	--	-0.8867
--	--	--	-0.1978
--	--	--	-0.2000

Table 9.33: System eigenvalues of Case 2 loading conditions with J_1 settings, multiple-point tuning, coordinated SVC7-SVC9 design

No Control	SVC7	SVC9	SVC7 & SVC9
-0.6770± 6.5678i, 0.1025	-1.9222± 4.3776i, 0.4020	-1.6206± 6.2858i, 0.2497	-1.2751± 4.9245i, 0.2507
-2.0988± 9.4216i, 0.2174	-2.0245± 9.3458i, 0.2117	-5.1918± 9.3646i, 0.4849	-1.3002± 4.9985i, 0.2517
-9.7416± 13.931i	-19.2781± 14.955i	-0.2864± 4.4825i	-22.185± 22.037i
-9.7880± 7.0793i	-5.8597± 14.030i	-8.9581± 14.273i	-7.3577± 16.237i
-8.3262± 2.3178i	-9.8167± 9.5318i	-9.6825± 7.1095i	-9.7341± 8.7815i
-0.2000	-8.4213± 2.1959i	-14.0752	-7.0120± 9.9865i
--	-2.5198	-2.2870	-23.3821
--	-0.3153	-0.4037	-3.0155
--	-0.2000	-20.0000	-2.2241
--	--	-0.2000	-1.5440
--	--	--	-0.4565
--	--	--	-0.1957
--	--	--	-0.2000

Table 9.34: System eigenvalues of Case 3 loading conditions with J_1 settings, multiple-point tuning, coordinated SVC7-SVC9 design

No Control	SVC7	SVC9	SVC7 & SVC9
$0.1091 \pm 8.0287i$, -0.0136	$-3.7546 \pm 5.3938i$, 0.5713	$-0.5001 \pm 7.6526i$, 0.0652	$-3.3623 \pm 10.202i$, 0.3130
$-0.5229 \pm 12.035i$, 0.0434	$-1.0164 \pm 11.873i$, 0.0853	$-3.5012 \pm 12.325i$, 0.2733	$-4.8414 \pm 8.5810i$, 0.4914
$-10.4209 \pm 13.130i$	$-1.2088 \pm 13.291i$	$-8.2405 \pm 13.029i$	$-23.6347 \pm 20.558i$
$-10.0239 \pm 7.0407i$	$-20.6823 \pm 14.805i$	$-9.9040 \pm 6.9574i$	$-4.3491 \pm 16.813i$
$-9.8009 \pm 1.9872i$	$-10.6818 \pm 9.3162i$	$-3.1405 \pm 5.2114i$	$-10.024 \pm 8.9083i$
-0.2000	$-9.9546 \pm 2.1616i$	-14.9865	$-2.6322 \pm 5.3742i$
--	-0.4236	-1.9794	-23.3808
--	-2.5155	-0.7625	-3.0348
--	-0.2000	-20.0000	-2.1220
--	--	-0.2000	-1.4436
--	--	--	-0.7351
--	--	--	-0.1978
--	--	--	-0.2000

Nonlinear Time-Domain Simulations: Figures 9.60-9.64 show the rotor angles, speed deviations, electrical power outputs, and machine terminal voltages responses, as well as the SVC7 and SVC9 responses, respectively, for a 6-cycle three-phase fault at bus 7 at the end of line 5-7 at the base case while using the proposed SVC7-SVC9 coordinated design. These figures should be compared with Figures 9.44-9.48, for individual SVC7 design, and 9.49-9.53, for individual SVC9 design. The improvement on the system responses in terms of first swing stability, overshoot, and settling time when using the coordinated design is clear. This is in line with eigenvalue analysis results.

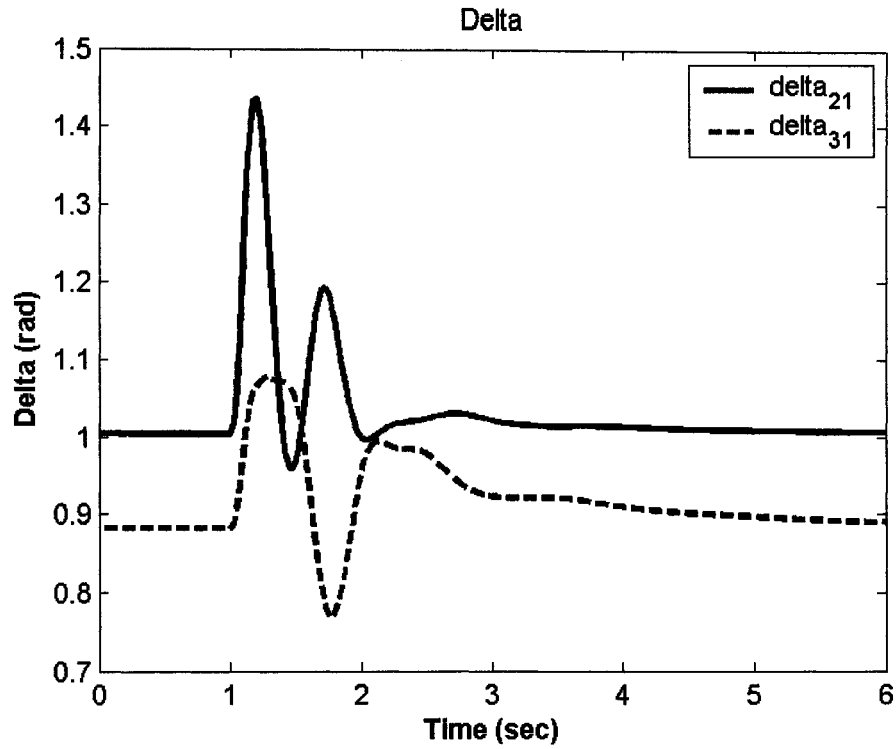


Figure 9.60: Rotor angle response for 6-cycle fault with base case, J_1 settings, multiple-point tuning, coordinated SVC7-SVC9 design

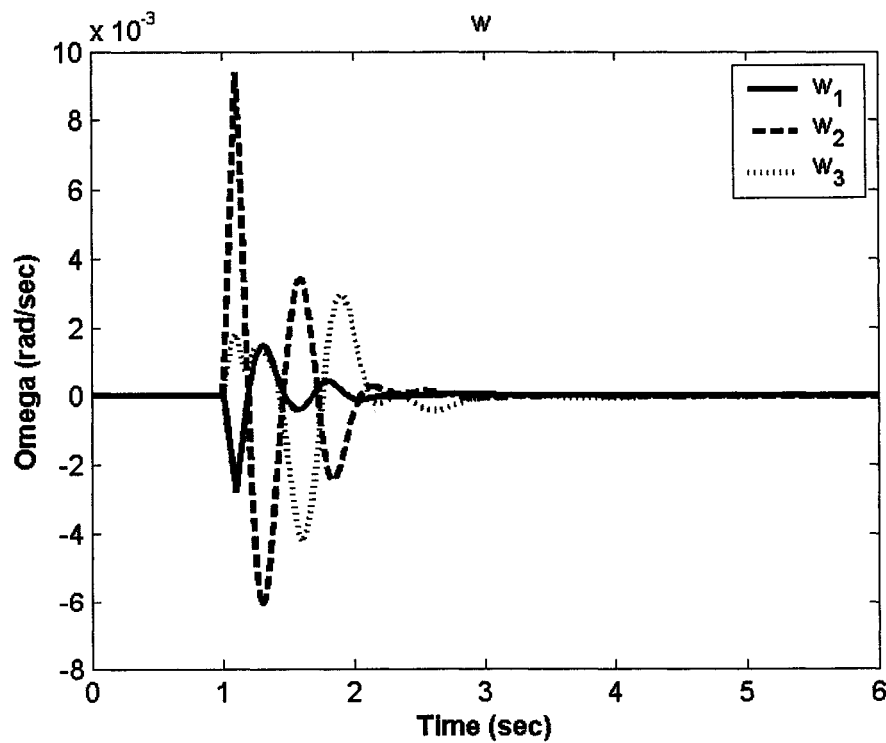


Figure 9.61: Speed response for 6-cycle fault with base case, J_1 settings, multiple-point tuning, coordinated SVC7-SVC9 design

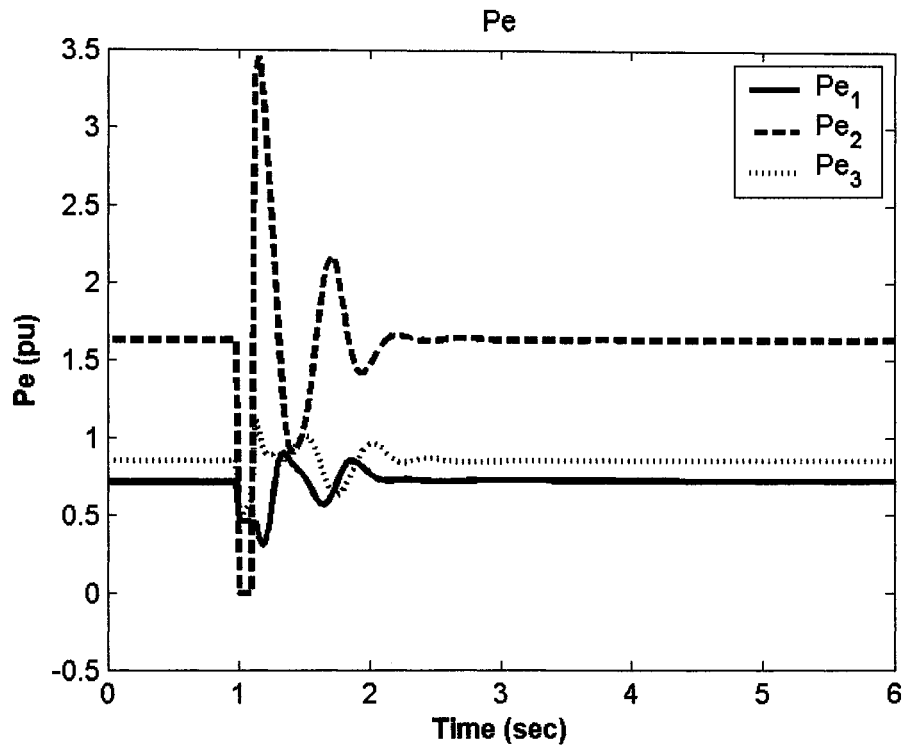


Figure 9.62: Electrical power response for 6-cycle fault with base case, J_1 settings, multiple-point tuning, coordinated SVC7-SVC9 design

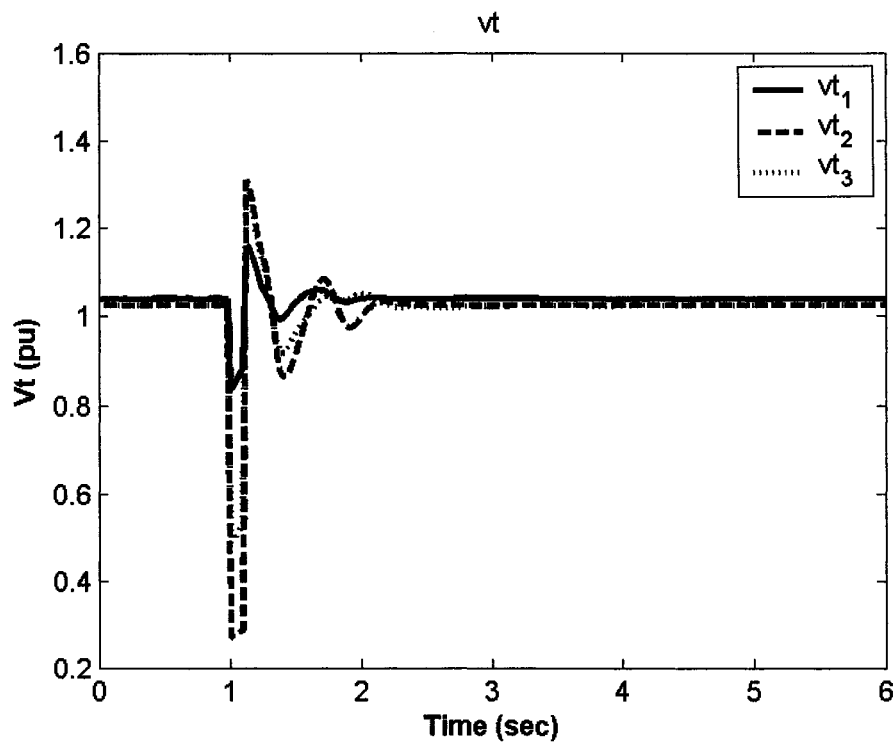


Figure 9.63: Terminal voltage response for 6-cycle fault with base case, J_1 settings, multiple-point tuning, coordinated SVC7-SVC9 design

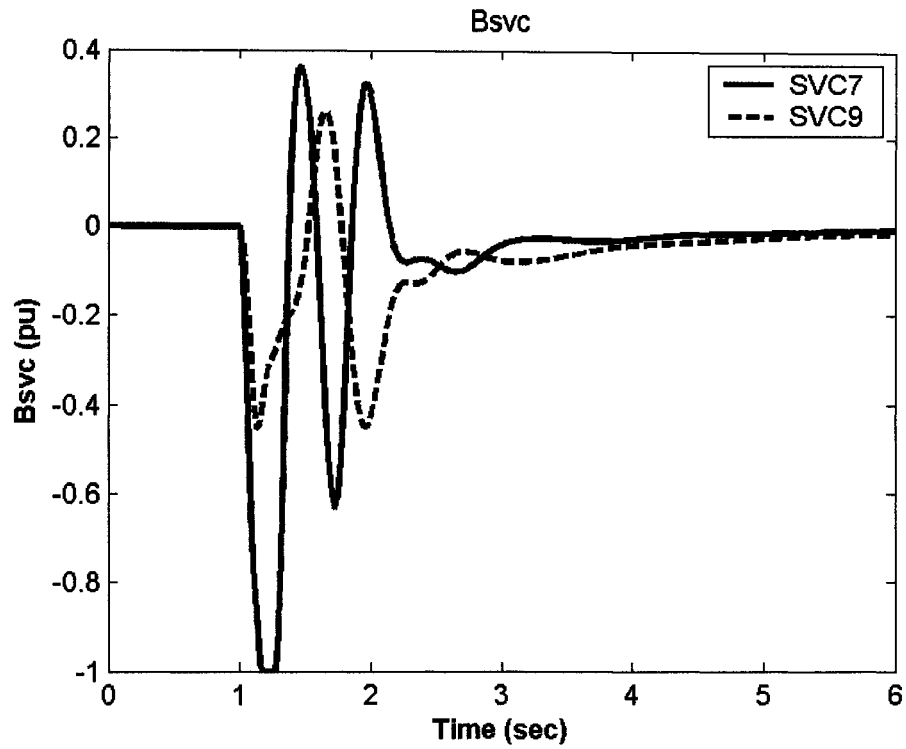


Figure 9.64: B_{svc} response for 6-cycle fault with base case, J_1 settings, multiple-point tuning, coordinated SVC7-SVC9 design

Chapter 10

CONCLUSIONS AND FUTURE WORK

10.1 Conclusions

In this thesis, the effectiveness of the coordinated design of PSSs and FACTS-based stabilizers to enhance power system stability has been investigated. Three different power systems have been considered: a SMIB system with G1 FACTS devices, a SMIB system with a UPFC, and a multimachine power system. Singular value decomposition has been employed to quantitatively measure the capabilities of the various stabilizers control signals in controlling the system EM mode(s). For each system, the stabilizer design problem has been formulated as an optimization problem, with eigenvalue-based objective functions, to be solved using particle swarm optimization algorithm. Two objective functions have been considered. The first objective function is to minimize the maximum damping factor and, hence, to shift the lightly damped EM modes of oscillations to the left-hand side in the complex s -plane. The second objective function is to maximize the minimum damping ratio and, consequently, placing the EM modes of oscillations in a wedge-shape sector in the s -plane.

Individual design and coordinated design of the proposed stabilizers considering a single-operating-point as well as robust multiple-operating-point designs have been discussed. The effectiveness of the proposed control schemes in improving the power system dynamic stability has been verified through damping torque coefficient analysis, eigenvalue analysis, and nonlinear time-domain simulations under different loading conditions and severe fault disturbances. It has been clearly shown that the coordinated design of PSSs and the different FACTS-devices outperforms the individual design of these stabilizers. In addition, it has been observed that in a system equipped with a UPFC, the coordinated design of the UPFC-based stabilizers can improve the system damping more than the individual design of those stabilizers. Furthermore, the study results show that superior stabilizer performance is achieved over a wide range of operating conditions if the robust stabilizers design technique is employed.

10.2 Future Work

During the course of this study, it has been observed that it is worth directing the related future work to the following streams:

- The effect of UPFC-based stabilizers on more complex power systems needs to be studied.
- A methodology of computing the damping torque coefficients in multimachine power systems is an interesting area to investigate.
- Different objective functions, eigenvalue-based or time-domain-based, as well as multi-objective functions need to be considered in the design stage.

- The proposed design techniques can be further explored in some large-scale power system.
- Throughout this work, machine speed has been the only feedback signal considered in all stabilizers. Different local signals, such as electric power may be investigated.

APPENDICES

Appendix A

The parameters of the system used in optimization results of the G1 FACTS devices (Chapter 7) are:

Machine: $x_d=1$; $x_q=0.6$; $x'_d=0.3$; $D=0$; $M=8.0$; $T'_{do}=5.044$; $freq=60$; $v=1.05$;

Exciter : $K_A=50$; $T_A=0.05$; $E_{fd_max}=7.3$; $E_{fd_min}=-7.3$;

PSS: $T_w=5$; $T_{i_min}=0.01$; $T_{i_max}=5$; $i=1,2,3,4$; $upss_max=0.2$; $u_{pss_min}=-0.2$;

Transmission Line: $Z=0.35i$;

Load: $Y_L=0.0$;

FACTS Devices: $K_s=1$; $T_s=0.05$;

Appendix B

The parameters of the system used in optimization results of the UPFC (Chapter 8) are:

Machine: $x_d = 1$; $x_q = 0.6$; $x'_d = 0.3$; $D = 0$; $M = 8.0$; $T'_{do} = 5.044$; $freq = 60$; $v = 1.05$;

Exciter : $K_A = 50$; $T_A = 0.05$; $E_{fd_max} = 7.3$; $E_{fd_min} = -7.3$;

PSS: $T_w = 5$; $T_{i_min} = 0.01$; $T_{i_max} = 5.0$; $i = 1,2,3,4$; $upss_max = 0.2$; $u_{pss_min} = -0.2$;

DC voltage regulator: $k_{dp} = -10$; $k_{di} = 0$;

Transmission Line: $x_{lE} = 0.1$; $x_{BV} = 0.6$;

UPFC: $x_E = 0.1$; $x_B = 0.1$; $K_s = 1$; $T_s = 0.05$; $C_{dc} = 3$; $V_{dc} = 2$; $m_{E_max} = 1$; $m_{E_min} = 0$;

$m_{B_max} = 1$; $m_{B_min} = 0$.

Appendix C

A detailed one-line diagram of the three-machine nine-bus power system (Chapter 9) is shown in Figure C.1. The generator and exciter data is shown in Table C.1:

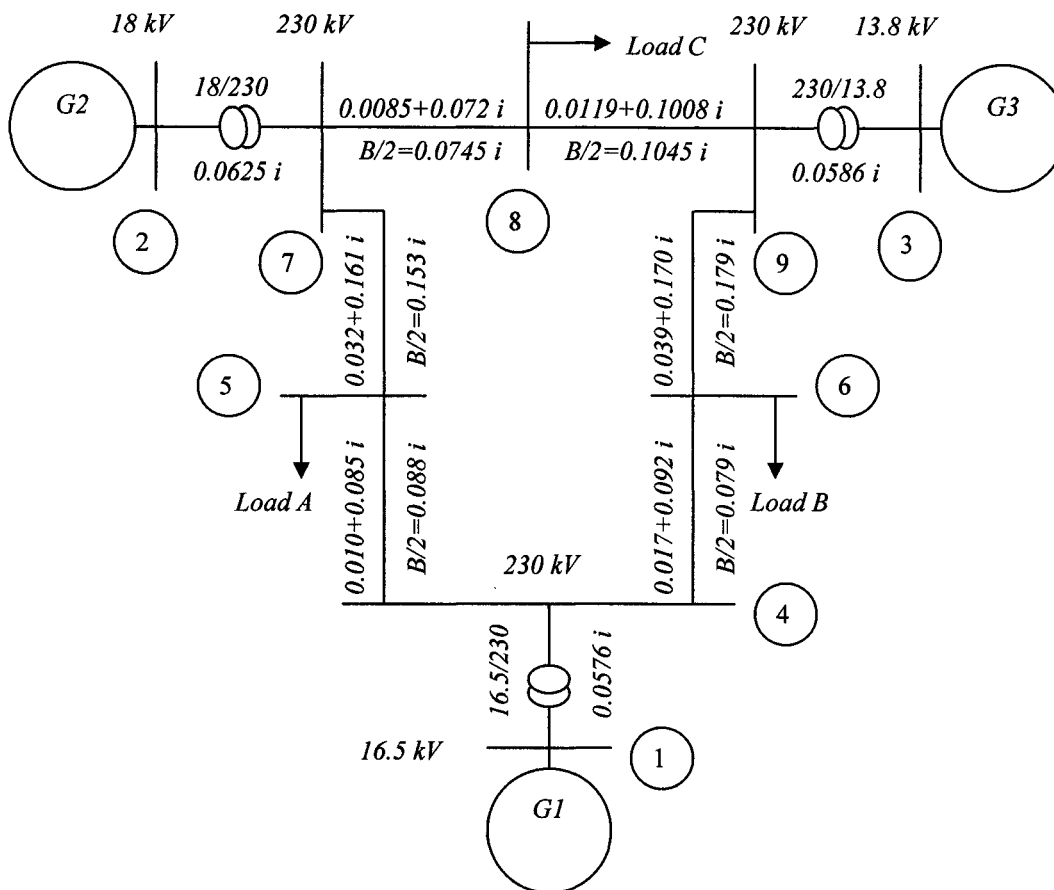


Figure C.1: A detailed three-generator nine-bus system

Table C.1: Generator and exciter data

Generator	1	2	3
H (sec)	23.64	6.40	3.01
D	0.0	0.0	0.0
x_d (pu)	0.146	0.8958	1.3125
x'_d (pu)	0.0608	0.1198	0.1813
x_q (pu)	0.0969	0.1969	0.25
T_{do} (sec)	8.96	6.00	5.89
K_A	100	100	100
T_A (sec)	0.05	0.05	0.05S

NOMENCLATURE

Abbreviations

SMIB	Single-machine infinite bus
PSS	Power system stabilizer
FACTS	Flexible AC transmission systems
G1 FACTS	First generation flexible AC transmission systems
SVC	Static Var compensator
TCSC	Thyristor-controlled series capacitor
TCPS	Thyristor-controlled phase shifter
UPFC	Unified power flow controller
ET, BT	Excitation and boosting transformers
GTO	Gate turn off
VSC	Voltage source converter
EM	Electromechanical mode
DTC	Damping torque coefficient
AVR	Automatic voltage regulator
PSO	Particle swarm optimizer
Pf	Power factor
SVD	Singular value decomposition
pu	Per unit

English Symbols

$P_m, P (P_e)$	Mechanical input power and electrical output power of the generator
M, H	Machine inertia coefficient and inertia constant
D	Machine damping coefficient
i_d, i_q	d- and q-axis armature current
v_d, v_q	d- and q-axis terminal voltage
T_{do}'	Open-circuit field time constant
x_d, x_d'	d-axis reactance and d-axis transient reactances
x_q	Generator q-axis reactance
V or v	Generator terminal voltage
E_q', E_{fd}	Generator internal and field voltages
V_{ref}	Reference voltage
v_b	Infinite bus voltage
K_A, T_A	Gain and time constant of the excitation system
u_{PSS}	PSS control signal
K_s, T_s	FACTS gain and time constant
Z, X, R	Transmission line impedance, reactance, and resistance
Y_L	Load impedance
g, b	Load Inductance and susceptance
i_{SVC}, i_L	SVC and load currents
X_{CSC}	TCSC equivalent reactance
B_{SVC}	SVC equivalent susceptance
m_E, m_B	Excitation and boosting amplitude modulation ratios

v_{Eb}, i_E	Excitation voltage and current
v_{Bb}, i_B	Boosting voltage and current
C_{dc}, v_{dc}	DC link capacitance and voltage
x_E, x_B	ET and BT reactances
K_{syn}, K_d	Synchronizing and damping torques
$pbestx$	Local best solution
$gbestx$	Global best solution
X_i	Vector of particle positions
V_i	Vector of particle velocities
W	Inertia weight
K	Constriction factor
J_1, J_2	First and second objective functions

Greek Symbols

δ	Rotor angle
ω	Rotor speed
ω_b	Synchronous speed
δ_E	Excitation phase angle modulation
δ_B	Boosting phase angle modulation
Φ, Φ_{TCPS}	Phase shift in the voltage phase angle resulting from the TCPS
α	Thyristor firing angle
ζ	Damping ratio
σ	Damping factor

BIBLIOGRAPHY

- [1] Yu Y. N.; **Electric Power System Dynamics**, Academic Press, 1983
- [2] Anderson P. M. and Fouad A. A.; **Power System Control and Stability**, The Iowa State University Press, 1977
- [3] Rogers G.; **Power System Oscillations**, Kluwer Academic Publishers, 2000
- [4] Abido M. A. and Abdel-Magid Y. L.; Power system stability enhancement via coordinated design of PSS and FACTS-based stabilizers, Final Report of a Project Funded by KFUPM, May 2002
- [5] de Mello F. and Concordia C.; Concepts of synchronous machine stability as affected by excitation control, *Power Apparatus and Systems*, IEEE Transactions, Volume: 88, Page(s): 316-329, 1969
- [6] Larsen E. V. and Swann D. A.; Applying power system stabilizers, *Power Apparatus and Systems*, IEEE Transactions, Volume: 100, No. 6, Page(s): 3017-3046, 1981
- [7] Kundur, P.; Klein, M.; Rogers, G.J.; Zywno, M.S.; Application of power system stabilizers for enhancement of overall system stability, *Power Systems*, IEEE Transactions on , Volume: 4 Issue: 2 , May 1989, Page(s): 614 -626
- [8] Klein, M.; Rogers, G.J.; Kundur, P.; A fundamental study of inter-area oscillations in power systems, *Power Systems*, IEEE Transactions on , Volume: 6 Issue: 3 , Aug. 1991, Page(s): 914 -921
- [9] Klein, M.; Rogers, G.J.; Moorty, S.; Kundur, P.; Analytical investigation of factors influencing power system stabilizers performance, *Energy Conversion*, IEEE Transactions on , Volume: 7 Issue: 3 , Sept. 1992, Page(s): 382 -390
- [10] Kundur, P.; Effective use of power system stabilizers for enhancement of power system reliability, *Power Engineering Society Summer Meeting*, 1999. IEEE , Volume: 1 , 18-22 July 1999, Page(s): 96 -103
- [11] de Mello F. P., Nolan P. J., Laskowski T.F., and Undrill J. M.; Coordinated application of stabilizers in multimachine power systems, *Power Apparatus and Systems*, IEEE Transactions, Volume: 99, No. 3, Page(s): 892-901, 1980
- [12] Hsu Y. Y. and Chen C. L.; Identification of optimum location for stabilizer

- applications using participation factors, Pt. C, IEE Proceedings, Volume 134, No. 3, 1987, Page(s): 238-244.
- [13] *Ostojic D. R.*; Identification of optimum site for power system stabiliser applications, Pt. C, IEE Proceedings, Volume 135, No. 5, 1988, Page(s): 416-419.
- [14] *Martins, N.; Lima, L.T.G.*; Determination of suitable locations for power system stabilizers and static VAR compensators for damping electromechanical oscillations in large scale power systems, Power Industry Computer Application Conference, 1989. PICA '89, Conference Papers , 1-5 May 1989, Page(s): 74 -82
- [15] *Xiaoqing Yang; Feliachi, A.*; Stabilization of inter-area oscillation modes through excitation systems, Power Systems, IEEE Transactions on , Volume: 9 Issue: 1 , Feb. 1994, Page(s): 494 -502
- [16] *Lu, J.; Chiang, H.-D.; Thorp, J.S.*; Identification of optimum sites for power system stabilizer applications, Power Systems, IEEE Transactions on , Volume: 5 Issue: 4 , Nov. 1990, Page(s): 1302 -1308
- [17] *Feliachi A.*; Optimum siting of power system stabilisers, Pt. C, IEE Proceedings, Volume 137, No. 2, 1990, Page(s): 101-106.
- [18] *Zhou, E.Z.; Malik, O.P.; Hope, G.S.*; Theory and method for selection of power system stabilizer location, Energy Conversion, IEEE Transactions on , Volume: 6 Issue: 1 , March 1991, Page(s): 170 -176
- [19] *Zhou, E.; Malik, O.P.; Hope, G.S.*; Design of stabilizer for a multimachine power system based on the sensitivity of PSS effect, Energy Conversion, IEEE Transactions on , Volume: 7 Issue: 3 , Sept. 1992, Page(s): 606 -613
- [20] *Fleming R. J., Mohan M. A., and Parvatism K.*; Selection of parameters of stabilizers in multimachine power systems, Power Apparatus and Systems, IEEE Transactions, Volume: 100, No. 5,Page(s): 2329-2333, 1981
- [21] *Abe. S. and Doi A.*; A new power system stabilizer synthesis in multimachine power systems, Power Apparatus and Systems, IEEE Transactions, Volume: 102, No. 12,Page(s): 3910-3918, 1983
- [22] *Gooi H. B., Hill E. F., Mobarak M. A., Throne D. H., and Lee T. H.*; Coordinated multimachine stabilizer settings without eigenvalue drift, IEEE Transactions, Volume: 100, No. 8,Page(s): 3879-3887, 1981
- [23] *Lefebvre S.*; Tuning of stabilizers in multimachine power systems, Power Apparatus and Systems, IEEE Transactions, Volume: 102, No. 2,Page(s): 290-299, 1983
- [24] *Lim C. M., and Elangovan S.*; Design of stabilizers in multimachine power systems, Pt. C, IEE Proceedings, Volume: 132: No. 3,Page(s): 146-153, 1985
- [25] *Chen C. L. and Hsu Y. Y.*; Coordinated synthesis of multimachine power

- system stabilizer using an efficient decentralized modal control (DMC) algorithm, *Power Systems, IEEE Transactions on*, Volume: 9, Issue: 3, 1987, Page(s): 543-551
- [26] *Chen, C.-L.; Hsu, Y.-Y.*; An efficient algorithm for the design of decentralized output feedback power system stabilizer, *Power Systems, IEEE Transactions on*, Volume: 3 Issue: 3, Aug. 1988, Page(s): 999 -1004
- [27] *Yu, Y.-N.; Li, Q.-H.*; Pole-placement power system stabilizers design of an unstable nine-machine system, *Power Systems, IEEE Transactions on*, Volume: 5 Issue: 2, May 1990, Page(s): 353 -358
- [28] *Chandra, A.; Malik, O.P.; Hope, G.S.*; A self-tuning controller for the control of multi-machine power systems, *Power Systems, IEEE Transactions on*, Volume: 3 Issue: 3, Aug. 1988, Page(s): 1065 -1071
- [29] *Hsu Y. Y. and Hsu C. Y.*; Design of a proportional-integral power system stabilizer, *Power Systems, IEEE Transactions on*, Volume: 1 Issue: 2, 1986, Page(s): 46-53
- [30] *Wu Chi-Jui; Hsu Yuan-Yih*; Design of self-tuning PID power system stabilizer for multimachine power systems, *Power Systems, IEEE Transactions on*, Volume: 3 Issue: 3, Aug. 1988, Page(s): 1059 -1064
- [31] *Gibbard M. J.*; Co-ordinated design of multimachine power system stabilisers based on damping torque concepts, Pt. C, *IEE Proceedings*, Volume 135, No. 4, 1988, Page(s): 276-284.
- [32] *Gibbard, M.J.*; Robust design of fixed-parameter power system stabilisers over a wide range of operating conditions, *Power Systems, IEEE Transactions on*, Volume: 6 Issue: 2, May 1991, Page(s): 794 -800
- [33] *Chen, L.; Petroianu, A.*; A new method of tuning power system stabilisers, *Electrical and Computer Engineering, 1996. Canadian Conference on*, Volume: 1, 26-29 May 1996, Page(s): 454 -457 vol.1
- [34] *Klein, M.; Le, L.X.; Rogers, G.J.; Farrokhpay, S.; Balu, N.J.*; H_{∞} damping controller design in large power systems, *Power Systems, IEEE Transactions on*, Volume: 10 Issue: 1, Feb. 1995, Page(s): 158 -166
- [35] *Radman, G.*; Design of power system stabilizer based on LQG/LTR formulations, *Industry Applications Society Annual Meeting, conference Record of the 1992 IEEE*, 4-9 Oct. 1992, Page(s): 1787 -1792 vol.2
- [36] *Lu, Q.; Sun, Y.Z.*; Nonlinear stabilizing control of multimachine systems, *Power Systems, IEEE Transactions on*, Volume: 4 Issue: 1, Feb. 1989, Page(s): 236 -241
- [37] *He, F.; Gibbard, M.J.*; Performance of a nonlinear controller in power system stabilisation, *American Control Conference, 1995. Proceedings of the*, Volume: 3, 21-23 June 1995, Page(s): 1556 -1560
- [38] *Samarasinghe V. G. D. C. and Pahalawaththa N. C.*; Damping of multimodal

- oscillations in power systems using variable structure control techniques, *Generation Transmission and Distribution*, IEE Proceedings, Volume 144, No. 3, 1997, Page(s): 323-331.
- [39] *Urdaneta, A.J.; Bacalao, N.J.; Feijoo, B.; Flores, L.; Diaz, R.*; Tuning of power system stabilizers using optimization techniques, *Power Systems*, IEEE Transactions on , Volume: 6 Issue: 1 , Feb. 1991, Page(s): 127 -134
- [40] *Ostojic, D.R.*; Stabilization of multimodal electromechanical oscillations by coordinated application of power system stabilizers, *Power Systems*, IEEE Transactions on , Volume: 6 Issue: 4 , Nov. 1991, Page(s): 1439 -1445
- [41] *Khaldi, M.R.; Sarkar, A.K.; Lee, K.Y.; Park, Y.M.*; The modal performance measure for parameter optimization of power system stabilizers, *Energy Conversion*, IEEE Transactions on , Volume: 8 Issue: 4 , Dec. 1993, Page(s): 660 -666
- [42] *Xu, L.; Ahmed-Zaid, S.*; Tuning of power system controllers using symbolic eigensensitivity analysis and linear programming, *Power Systems*, IEEE Transactions on , Volume: 10 Issue: 1 , Feb. 1995, Page(s): 314 -322
- [43] *Abdel-Magid, Y. L.; Bettayeb, Maamar; and Dawoud, M. M.*; Simultaneous stabilization of Power System Genetic Algorithms, *Generation, Transmission and Distribution*, IEE Proceedings, Volume 145, No. 1, 1997, Page(s): 39-44.
- [44] *Abdel-Magid, Y.L.; Abido, M.A.; Al-Baiyat, S.; and Mantawy, A. H.*; Simultaneous Stabilization of Multimachine Power Systems via Genetic Algorithms, *Power Systems*, IEEE Transaction on , Volume 14, No. 4, November 1999, pp. 1428-1439.
- [45] *Abdel-Magid, Y.L.; Abido, M. A.; and Mantawy, A. H.*; Robust Tuning of Power System Stabilizers in Multimachine Power Systems, *Power Systems*, IEEE Transactions on , Volume 15, No. 2, May 2000, pp. 735-740.
- [46] *Abdel-Magid, Y.L.; and Abido, M. A.*; Optimal Multiobjective Design of Robust Power system Stabilizers Using Genetic Algorithms, *Power Systems*, IEEE Transactions on , Volume 18, No. 3, August 2003, pp. 11254-1132
- [47] *Yamaguchi, H.; Mizutani, Y.; Magatani, K.; Leelajindakrairerk, M.; Okabe, T.; Kinoshita, Y.; Aoki, H.*; A design method of multi-input PSS by using auto-variable search space type high speed genetic algorithm, *Power Tech Proceedings, 2001 IEEE Porto* , Volume: 2 , 10-13 Sept. 2001, Page(s): 6
- [48] *Abido, M.A.*; Robust design of multimachine power system stabilizers using simulated annealing, *Energy Conversion*, IEEE Transactions on , Volume: 15 Issue: 3 , Sept. 2000, Page(s): 297 -304
- [49] *Kennedy, J.; Eberhart, R.*; Particle swarm optimization, *Neural Networks, 1995. Proceedings.*, IEEE International Conference on , Volume: 4 , 27 Nov.-1 Dec. 1995, Page(s): 1942 -1948
- [50] *El-Gallad, A.I.; El-Hawary, M.; Sallam, A.A.; Kalas, A.*; Swarm intelligence

- or hybrid cost dispatch problem, *Electrical and Computer Engineering, 2001. Canadian Conference on*, Volume: 2, 13-16 May 2001, Page(s): 753 -757
- [51] *Abido, A.A.*; Particle swarm optimization for multimachine power system stabilizer design, *Power Engineering Society Summer Meeting, 2001. IEEE*, Volume: 3, 15-19 July 2001, Page(s): 1346 -1351
- [52] *Abido, M.A.; Abdel-Magid, Y.L.*; Robust design of electrical power-based stabilizers using tabu search, *Power Engineering Society Summer Meeting, 2001. IEEE*, Volume: 3, 15-19 July 2001, Page(s): 1573 -1578
- [53] *Dechanupaprittha, S.; Ngamroo, I.*; Design of robust power system stabilizers in a multimachine power system using tabu search algorithm, *Industrial Technology, 2002. IEEE ICIT '02. 2002 IEEE International Conference on*, Volume: 1, 11-14 Dec. 2002, Page(s): 291 -296
- [54] *Abido, M.A.; Abdel-Magid, Y.L.*; Optimal design of power system stabilizers using evolutionary programming, *Energy Conversion, IEEE Transactions on*, Volume: 17 Issue: 4, Dec. 2002, Page(s): 429 -436
- [55] *Zhang, Y.; Chen, G.P.; Malik, O.P.; Hope, G.S.*; An artificial neural network based adaptive power system stabilizer, *Energy Conversion, IEEE Transactions on*, Volume: 8 Issue: 1, March 1993, Page(s): 71 -77
- [56] *Abido, M.A.; Abdel-Magid, Y.L.*; Radial basis function network based power system stabilizers for multimachine power systems, *Neural Networks, 1997., International Conference on*, Volume: 2, 9-12 June 1997, Page(s): 622 -626
- [57] *El-Metwally, K.A.; Hancock, G.C.; Malik, O.P.*; Implementation of a fuzzy logic PSS using a micro-controller and experimental test results, *Energy Conversion, IEEE Transactions on*, Volume: 11 Issue: 1, March 1996, Page(s): 91 -96
- [58] *Abido, M.A.; Abdel-Magid, Y.L.*; A hybrid neuro-fuzzy power system stabilizer for multimachine power systems, *Power Systems, IEEE Transactions on*, Volume: 13 Issue: 4, Nov. 1998, Page(s): 1323 -1330
- [59] *Hariri, A.; Malik, O.P.*; A fuzzy logic based power system stabilizer with learning ability, *Energy Conversion, IEEE Transactions on*, Volume: 11 Issue: 4, Dec. 1996, Page(s): 721 -727
- [60] *Abido, M.A.; Abdel-Magid, Y.L.*; A fuzzy basis function network for generator excitation control, *Fuzzy Systems, 1997., Proceedings of the Sixth IEEE International Conference on*, Volume: 3, 1-5 July 1997, Page(s): 1445 -1450
- [61] *Ruhua You; Eghbali, H.J.; Nehrir, M.H.*; An online adaptive neuro-fuzzy power system stabilizer for multimachine systems, *Power Systems, IEEE Transactions on*, Volume: 18 Issue: 1, Feb. 2003, Page(s): 128 -135
- [62] *You, R.; Nehrir, M.H.; Eghbali, H.J.*; A neuro-fuzzy power system stabilizer with self-organizing map for multi-machine systems, *Power Engineering*

- Society Winter Meeting, 2002. IEEE , Volume: 2 , 27-31 Jan. 2002, Page(s): 1219 -1224
- [63] *Abido, M.A.; Abdel-Magid, Y.L.*; Tuning of a fuzzy logic power system stabilizer using genetic algorithms, *Evolutionary Computation, 1997.*, IEEE International Conference on , 13-16 April 1997, Page(s): 595 -599
- [64] *Abido, M.A.; Abdel-Magid, Y.L.*; A genetic-based fuzzy logic power system stabilizer for multimachine power systems, *Systems, Man, and Cybernetics, 1997. 'Computational Cybernetics and Simulation'*, 1997 IEEE International Conference on , Volume: 1 , 12-15 Oct. 1997, Page(s): 329 -334
- [65] *Abido, M.A.; Abdel-Magid, Y.L.*; Hybridizing rule-based power system stabilizers with genetic algorithms, *Power Systems, IEEE Transactions on* , Volume: 14 Issue: 2 , May 1999, Page(s): 600 -607
- [66] *Wang, Y.; Hill, D.J.; Middleton, R.H.; Gao, L.*; Transient stability enhancement and voltage regulation of power systems, *Power Systems, IEEE Transactions on* , Volume: 8 Issue: 2 , May 1993, Page(s): 620 -627
- [67] *Hingorani, N.G.*; High Power Electronics and flexible AC Transmission System, *Power Engineering Review, IEEE* , Volume: 8 Issue: 7 , July 1988, Page(s): 3 -4
- [68] *Hingorani, N.G.*; FACTS-flexible AC transmission system, *AC and DC Power Transmission, 1991.*, International Conference on , 17-20 Sep 1991 Page(s): 1 -7
- [69] *Hingorani, N.G.*; Flexible AC transmission, *Spectrum, IEEE* , Volume: 30 Issue: 4 , April 1993, Page(s): 40 -45
- [70] *Hingorani, N.G.*; FACTS technology and opportunities, *Flexible AC Transmission Systems (FACTS) - The Key to Increased Utilisation of Power Systems, IEE Colloquium on (Digest No.1994/005)* , 12 Jan 1994, Page(s): 4/1 -410
- [71] *Hingorani, N.G.*; Future role of power electronics in power systems, *Power Semiconductor Devices and ICs, 1995. ISPSD '95. Proceedings of the 7th International Symposium on* , 23-25 May 1995, Page(s): 13 -15
- [72] *Iravani, M.R.; Maratukulam, D.*; Review of semiconductor-controlled (static) phase shifters for power systems applications, *Power Systems, IEEE Transactions on* , Volume: 9 Issue: 4 , Nov. 1994, Page(s): 1833 -1839
- [73] *Iravani, M.R.; Dandeno, P.L.; Nguyen, K.H.; Zhu, D.; Maratukulam, D.*; Applications of static phase shifters in power systems, *Power Delivery, IEEE Transactions on* , Volume: 9 Issue: 3 , July 1994, Page(s): 1600 -1608
- [74] *Ise, T.; Hayashi, T.; Ishii, J.; Kumagai, S.*; Power system stabilizing control using high speed phase shifter (HSPS), *Power Conversion Conference - Nagaoka 1997.*, Proceedings of the , Volume: 2 , 3-6 Aug. 1997, Page(s): 735 -740

- [75] *Edris, A.-A.*; Enhancement of first-swing stability using a high-speed phase shifter, *Power Systems, IEEE Transactions on* , Volume: 6 Issue: 3 , Aug. 1991, Page(s): 1113 -1118
- [76] *So, P.L.; MacDonald, D.C.*; Stabilization of inter-area modes by controllable phase shifter, *AFRICON, 1996.*, IEEE AFRICON 4th , Volume: 1 , 24-27 Sept. 1996, Page(s): 419 -424
- [77] *Abido, M.A.*; Thyristor controlled phase shifter based stabilizer design using simulated annealing algorithm, *Electric Power Engineering, 1999. PowerTech Budapest 99. International Conference on* , 29 Aug.-2 Sept. 1999, Page(s): 307
- [78] *Yoke Lin Tan; Youyi Wang*; Transient stability improvement of power systems using nonlinear excitation, phase shifter and adaptive control law, *Energy Management and Power Delivery, 1995. Proceedings of EMPD '95.*, 1995 International Conference on , Volume: 2 , 21-23 Nov. 1995, Page(s): 468 -473
- [79] *Hashmani, A.A.; Youyi Wang; Lie, T.*; Design and application of a nonlinear coordinated excitation and TCPS controller in power systems, *American Control Conference, 2001. Proceedings of the 2001* , Volume: 2 , 25-27 June 2001, Page(s): 811 -816
- [80] *Jiang, F.; Choi, S.S.; Shrestha, G.*; Power system stability enhancement using static phase shifter, *Power Systems, IEEE Transactions on* , Volume: 12 Issue: 1 , Feb. 1997, Page(s): 207 -214
- [81] *Ishigane A., Zhao J., and Taniguchi T.*; Representation and control of high speed phase shifter for an electric power system, *Generation Transmission and Distribution, IEE Proceedings*, Volume 145, No. 3, 1998, Page(s): 308-314.
- [82] *Ngan, H.W.*; Modelling static phase shifters in multi-machine power systems, *Advances in Power System Control, Operation and Management, 1997. APSCOM-97. Fourth International Conference on (Conf. Publ. No. 450)* , Volume: 2 , 11-14 Nov. 1997, Page(s): 785 -790
- [83] *Chen X. R., Pahalawaththa N. C., Annakkage U. D., and Kumble C.*; Power system stability enhancement by using controlled series compensation, *International Journal of Power and Energy Systems*, 16, (2), 1996, Page(s) 67-72.
- [84] *Chen X. R., Pahalawaththa N. C., Annakkage U. D., and Kumble C.*; Controlled series compensation for improving stability of multi-machine power systems, *Generation Transmission and Distribution, IEE Proceedings*, Volume 142, No. 4, 1995, Page(s): 361-366.
- [85] *Chen X. R., Pahalawaththa N. C., Annakkage U. D., and Kumble C.*; Output feedback TCSC controllers to improve damping of meshed multi-machine power systems, *Generation Transmission and Distribution, IEE Proceedings*, Volume 144, No. 3, 1997, Page(s): 243-248.

- [86] *Larsen, E.V.; Sanchez-Gasca, J.J.; Chow, J.H.*; Concepts for design of FACTS controllers to damp power swings, Power Systems, IEEE Transactions on , Volume: 10 Issue: 2 , May 1995, Page(s): 948 -956
- [87] *de Mello, F.P.*; Exploratory concepts on control of variable series compensation in transmission systems to improve damping of intermachine/system oscillations, Power Systems, IEEE Transactions on , Volume: 9 Issue: 1 , Feb. 1994, Page(s): 102 -108
- [88] *Lingling Fan; Feliachi, A.*; Robust TCSC control design for damping inter-area oscillations, Power Engineering Society Summer Meeting, 2001. IEEE , Volume: 2 , 15-19 July 2001, Page(s): 784 -789
- [89] *Jaewon Chang; Chow, J.H.*; Time-optimal series capacitor control for damping interarea modes in interconnected power systems, Power Systems, IEEE Transactions on , Volume: 12 Issue: 1 , Feb. 1997 Page(s): 215 -221
- [90] *Jaewon Chang; Chow, J.H.*; Time-optimal control of power systems requiring multiple switchings of series capacitors, Power Systems, IEEE Transactions on , Volume: 13 Issue: 2 , May 1998, Page(s): 367 -373
- [91] *Fujita G., Yokoyama R., Makita D., Takeuchi S., and Shirai G.*; Stabilization of multi-machine power system using variable series capacitor with H_{∞} control theory, Intelligent System Application to Power Systems (ISAP'97), July 6-10 1996, Seoul, Korea, Page(s): 84-88
- [92] *Zhao Q. and Jiang J.*; A TCSC damping controller design using robust control theory, International Journal of Power and Energy Systems, 20, (1), 1998, Page(s) 25-33.
- [93] *Wang, Y.; Mohler, R.R.; Spee, R.; Mittelstadt, W.*; Variable-structure facts controllers for power system transient stability, Power Systems, IEEE Transactions on , Volume: 7 Issue: 1 , Feb. 1992, Page(s): 307 -313
- [94] *Luor T. S. and Hsu. Y. Y.*; Design of an output feedback variable structure thyristor-controlled series compensator for improving power system stability, Electric Power System Research, 47, 1998, Page(s) 71-77.
- [95] *Rajkumar, V.; Mohler, R.R.*; Bilinear generalized predictive control using the thyristor-controlled series-capacitor, Power Systems, IEEE Transactions on , Volume: 9 Issue: 4 , Nov. 1994, Page(s): 1987 -1993
- [96] *Lie T. T., Shrestha G. B., and Ghosh A.*; Design and application of a fuzzy logic control scheme for transient stability enhancement in power systems, Electric Power System Research, 33, 1995, Page(s) 17-23.
- [97] *Dai X., Liu J., Tang Y. Li N., and Chen H.*; Neural network ath-order inverse control of thyristor controlled series compensator, Electric Power System Research, 45, 1998, Page(s) 19-27.
- [98] *Hsu Y.-Y. and Luor T.-S.* Damping of power system oscillations using adaptive thyristor-controlled series compensators tuned by artificial neural

- networks, Generation Transmission and Distribution, IEE Proceedings, Volume 146, No. 2, 1999, Page(s): 137-142.
- [99] *Abido, M.A.*; Genetic-based TCSC damping controller design for power system stability enhancement, Electric Power Engineering, 1999. PowerTech Budapest 99. International Conference on , 29 Aug.-2 Sept. 1999, Page(s): 165
- [100] *Abido M. A.*; Pole placement technique for PSS and TTCSC-based stabilier design using simulated annealing, Electric Power System Research, 22, 2000, Page(s) 543-554.
- [101] *Hammad, A. E.*; Analysis of power system stability enhancement by static VAR compensators, Trans. PWRs, IEEE, Volume 1, No. 4, 1986, Page(s): 222-227
- [102] *Padiyar, K.R.; Varma, R.K.*; Damping torque analysis of static VAR system controllers, Power Systems, IEEE Transactions on , Volume: 6 Issue: 2 , May 1991, Page(s): 458 -465
- [103] *Zhou, E.-Z.*; Application of static VAr compensators to increase power system damping, Power Systems, IEEE Transactions on , Volume: 8 Issue: 2 , May 1993, Page(s): 655 -661
- [104] *De Oliveira, S.E.M.*; Synchronizing and damping torque coefficients and power system steady-state stability as affected by static VAr compensators, Power Systems, IEEE Transactions on , Volume: 9 Issue: 1 , Feb. 1994, Page(s): 109 -119
- [105] *Wang H. F. and Swift F. J.*; Capability of the statis VAR compensator in damping power system oscillations, Generation Transmission and Distribution, IEE Proceedings, Volume 143, No. 4, 1996, Page(s): 353-358.
- [106] *Lee S. and Liu C. C.*; An output feedback static VAR controller for the damping of generator oscillations, Electric Power System Research, 29, 1994, Page(s) 9-16.
- [107] *Li Wang; Ming-Hsin Tsai*; Design of a H^∞ static VAr controller for the damping of generator oscillations, Power System Technology, 1998. Proceedings. POWERCON '98. 1998 International Conference on , Volume: 2, 18-21 Aug. 1998, Page(s): 785 -789 vol.2
- [108] *Parviani M. and Iravani M. R.*; Optimal robust control design of static VAR compensators, Generation Transmission and Distribution, IEE Proceedings, Volume 145, No. 3, 1998, Page(s): 301-307.
- [109] *Rao P. S. and Sen I.*; A QTF-based robust SVC controller for improving the dynamic stability of power systems, Electric Power System Research, 46, 1998, Page(s) 213-219.
- [110] *Dash P. K.; Sahoo N. C., and Doraiswami R.*; A variable structure VAR stabilizer for power system control, Electric Power System Research, 26, 1993, Page(s) 127-136.

- [111] *Hsu Y. Y. and Cheng C. H.*; Design of static VAR compensator using model reference adaptive control, *Electric Power System Research*, 13, 1987, Page(s) 129-138.
- [112] *Dash P. K., Mishra S., and Liew A. C.*; Fuzzy-logic based VAR stabilizer for power system control, *Generation Transmission and Distribution, IEE Proceedings*, Volume 142, No. 6, 1995, Page(s): 618-624.
- [113] *EL-Saady G., El-Sadek M. Z., and Abo-El-Saud M.*; Fuzzy adaptive model reference approach-based power system static VAR stabilizer, *Electric Power System Research*, 45, 1998, Page(s) 1-11.
- [114] *Chang C. S. and Qizhi Y.*; Fuzzy bang-bang control os static VAR compensators for damping system-wide low-frequency oscillations, *Electric Power System Research*, 49, 1999, Page(s) 45-54.
- [115] *Changaroon B., Srivastava S. C., Thukaram D., and Chirarattananon S.*; Neural network based power system damping controller for SVC, *Generation Transmission and Distribution, IEE Proceedings*, Volume 146, No. 4, 1999, Page(s): 370-376.
- [116] *Hongesombut, K.; Mitani, Y.; Tsuji, K.*; An adaptive static VAR compensator using genetic algorithm and radial basis function network for enhancing power system stability, *Power Tech Proceedings, 2001 IEEE Porto* , Volume: 2 , 10-13 Sept. 2001, Page(s): 6 pp. vol.2
- [117] *Lerch, E.N.; Povh, D.; Xu, L.*; Advanced SVC control for damping power system oscillations, *Power Systems, IEEE Transactions on* , Volume: 6 Issue: 2 , May 1991, Page(s): 524 -535
- [118] *Ju P., Handschin E., and Reyer F.*; Genetic algorithm aided controller design with application to SVC, *Generation Transmission and Distribution, IEE Proceedings*, Volume 143, No. 3, 1996, Page(s): 258-262.
- [119] *Hasanovic, A.; Feliachi, A.*; Genetic algorithm based inter-area oscillation damping controller design using MATLAB, *Power Engineering Society Summer Meeting, 2002 IEEE* , Volume: 3 , 21-25 July 2002, Page(s): 1136 - 1141 vol.3
- [120] *Makombe T. and Jenkins N.*;Investigation of a unified power flow controller, *Generation Transmission and Distribution, IEE Proceedings*, Volume 146, No. 4, 1999, Page(s): 400-408.
- [121] *Limyingcharoen S., Annakkage, U. D., and Pahalawaththa N. C.*; Effects of unified power flow controllers on transient stability, *Generation Transmission and Distribution, IEE Proceedings*, Volume 145, No. 2, 1998, Page(s): 182-188.
- [122] *Fujita, H.; Watanabe, Y.; Akagi, H.*; Control and analysis of a unified power flow controller, *Power Electronics, IEEE Transactions on* , Volume: 14 Issue: 6 , Nov. 1999, Page(s): 1021 -1027

- [123] *Nabavi-Niaki, A.; Iravani, M.R.*; Steady-state and dynamic models of unified power flow controller (UPFC) for power system studies, *Power Systems, IEEE Transactions on*, Volume: 11 Issue: 4, Nov. 1996, Page(s): 1937-1943
- [124] *Wang H. F.*; Damping function of unified power flow controller, *Generation Transmission and Distribution, IEE Proceedings*, Volume 146, No. 1, 1999, Page(s): 81-87.
- [125] *Wang H. F.*; Application of modeling UPFC into multi-machine power systems, *Generation Transmission and Distribution, IEE Proceedings*, Volume 146, No. 3, 1999, Page(s): 306-312.
- [126] *Zhengyu Huang; Yinxin Ni; Shen, C.M.; Wu, F.F.; Shousun Chen; Baolin Zhang*; Application of unified power flow controller in interconnected power systems-modeling, interface, control strategy, and case study, *Power Systems, IEEE Transactions on*, Volume: 15 Issue: 2, May 2000, Page(s): 817 -824
- [127] *Meng, Z.J.; So, P.L.*; A current injection UPFC model for enhancing power system dynamic performance, *Power Engineering Society Winter Meeting, 2000. IEEE*, Volume: 2, 23-27 Jan. 2000, Page(s): 1544 -1549 vol.2
- [128] *Schoder, K.; Hasanovic, A.; Feliachi, A.*; Load-flow and dynamic model of the unified power flow controller (UPFC) within the Power System Toolbox (PST), *Circuits and Systems, 2000. Proceedings of the 43rd IEEE Midwest Symposium on*, Volume: 2, 8-11 Aug. 2000, Page(s): 634 -637 vol.2
- [129] *Mishra S., Dash P. K., and Panda G.*; TS-fuzzy controller for UPFC in a multi-machine system, *Generation Transmission and Distribution, IEE Proceedings*, Volume 147, No. 1, 2000, Page(s): 15-22.
- [130] *Schoder, K.; Hasanovic, A.; Feliachi, A.*; Power system damping using fuzzy controlled unified power flow controller, *Power Engineering Society Winter Meeting, 2001. IEEE*, Volume: 2, 28 Jan.-1 Feb. 2001, Page(s): 617-622
- [131] *Dash, P.K.; Mishra, S.; Panda, G.*; A radial basis function neural network controller for UPFC, *Power Systems, IEEE Transactions on*, Volume: 15 Issue: 4, Nov. 2000, Page(s): 1293 -1299
- [132] *Vilathgamuwa M., Zhu X., and Choi S. S.*; A robust control method to improve the performance of a unified power flow controller, *Electric Power System Research*, 55, 2000, Page(s) 103-111.
- [133] *Pal B. C.*; Robust damping of interarea oscillations with unified power flow controller, *Generation Transmission and Distribution, IEE Proceedings*, Volume 149, No. 6, 2002, Page(s): 733-738.
- [134] *Jang-Cheol Seo; Seung-Il Moon; Jong-Keun Park; Jong-Woong Choe*; Design of a robust UPFC controller for enhancing the small signal stability in the multi-machine power systems, *Power Engineering Society Winter Meeting, 2001. IEEE*, Volume: 3, 28 Jan.-1 Feb. 2001, Page(s): 1197 -1202
- [135] *Wang, H.F.; Wu, Q.H.*; Multivariable design of a multiple-functional unified

- power flow controller, Power Engineering Society Summer Meeting, 2000. IEEE, Volume: 3, 16-20 July 2000, Page(s): 1895 -1900
- [136] *Wang H. F.*; Interactions and multivariable design of multiple control functions of a unified power flow controller, Electric Power System Research, 24, 2002, Page(s) 591-600.
- [137] *Xie H., Xu Z., Lu Q., Song Y. H., Yokoyama A., and Goto M.*; Integrated linear and nonlinear control of unified power flow controllers for enhancing power system stability, Electric Power Components and Systems, 31, Page(s) 335-347, 2003
- [138] *Noroozian, M.; Andersson, G.*; Damping of power system oscillations by use of controllable components, Power Delivery, IEEE Transactions on, Volume: 9 Issue: 4, Oct. 1994, Page(s): 2046 -2054
- [139] *Mithulananthan, N.; Canizares, C.A.; Reeve, J.*; Tuning, performance and interactions of PSS and FACTS controllers, Power Engineering Society Summer Meeting, 2002 IEEE, Volume: 2, 21-25 July 2002, Page(s): 981 - 987
- [140] *Pourbeik, P.; Gibbard, M.J.*; Damping and synchronizing torques induced on generators by FACTS stabilizers in multimachine power systems, Power Systems, IEEE Transactions on, Volume: 11 Issue: 4, Nov. 1996, Page(s): 1920 -1925
- [141] *Gibbard, M.J.; Vowles, D.J.; Pourbeik, P.*; Interactions between, and effectiveness of, power system stabilizers and FACTS device stabilizers in multimachine systems, Power Systems, IEEE Transactions on, Volume: 15 Issue: 2, May 2000, Page(s): 748 -755
- [142] *Wang, H.F.; Swift, F.J.*; A unified model for the analysis of FACTS devices in damping power system oscillations. I. Single-machine infinite-bus power systems, Power Delivery, IEEE Transactions on, Volume: 12 Issue: 2, April 1997, Page(s): 941 -946
- [143] *Wang, H.F.; Swift, F.J.; Li, M.*; A unified model for the analysis of FACTS devices in damping power system oscillations. II. Multi-machine power systems, Power Delivery, IEEE Transactions on, Volume: 13 Issue: 4, Oct. 1998, Page(s): 1355 -1362
- [144] *Mahran, A.R.; Hogg, B.W.; El-Sayed, M.L.*; Co-ordinated control of synchronous generator excitation and static VAR compensator, Energy Conversion, IEEE Transactions on, Volume: 7 Issue: 4, Dec. 1992, Page(s): 615 -622
- [145] *Rahim A. H. M. A. and Nassimi S. G. A.*; Synchronous generator damping enhancement through coordinated control of exciter and SVC, Generation Transmission and Distribution, IEE Proceedings, Volume 143, No. 2, 1996, Page(s): 211-218.
- [146] *Hashmani A. A., Wang Y., and Lie T. T.*; Enhancement of power system transient stability using a nonlinear coordinated excitation and TCPS

- controller, *Electric Power System Research*, 24, 2002, Page(s) 201-214.
- [147] *Chen H., Wang Y., and Zhou R.*; Transient and voltage stability enhancement via coordinated excitation and UPFC control, *Generation Transmission and Distribution*, IEE Proceedings, Volume 148, No. 3, 2001, Page(s): 201-208.
- [148] *Chen H., Wang Y., and Zhou R.*; Transient stability enhancement via coordinated excitation and UPFC control, *Electric Power System Research*, 24, 2002, Page(s) 19-29.
- [149] *Seung-Cheol Lee; Seung-Il Moon; Jang-Cheol Seo; Jong-Keun Park*; Observer-based decentralized optimal controller design of PSS and TCSC for enhancement of power system dynamic stability, *Power Engineering Society Summer Meeting, 2000. IEEE*, Volume: 3, 16-20 July 2000, Page(s): 1942-1945
- [150] *Li G., Lie T. T., Shrestha G. B., and Lo K. L.*; Real-time coordinated optimal FACTS controllers, *Electric Power System Research*, 52, 1999, Page(s) 273-286.
- [151] *Li G., Lie T. T., Shrestha G. B., and Lo K. L.*; Design and application of coordinated multiple FACTS controllers, *Generation Transmission and Distribution*, IEE Proceedings, Volume 147, No. 2, 2000, Page(s): 112-120.
- [152] *Cheng C. H. and Hsu Y. Y.*; Application of power system stabiliser and a static VAR controller to a multimachine power system, Pt. C, *IEE Proceedings*, Volume 137, No. 1, 1990, Page(s): 8-12.
- [153] *Hiyama, T.; Mishiro, M.; Kihara, H.; Ortmeyer, T.H.*; Coordinated fuzzy logic control for series capacitor modules and PSS to enhance stability of power system, *Power Delivery*, *IEEE Transactions on*, Volume: 10 Issue: 2, April 1995, Page(s): 1098-1104
- [154] *Wang, H.F.*; Co-ordination of fixed-parameter robust damping controllers in multi-machine power systems, *Control '98. UKACC International Conference on (Conf. Publ. No. 455)*, 1-4 Sept. 1998, Page(s): 1140-1145 vol.2
- [155] *Taranto G. N., Shiau J.-K., Chow J. H., and Othmai H. A.*; Robust decentralized design for multiple FACTS dampinf controllers, *Generation Transmission and Distribution*, IEE Proceedings, Volume 144, No. 1, 1997, Page(s): 61-67.
- [156] *Sanchez-Gasca, J.J.*; Coordinated control of two FACTS devices for damping interarea oscillations, *Power Systems*, *IEEE Transactions on*, Volume: 13 Issue: 2, May 1998, Page(s): 428-434
- [157] *So, P.L.; Yu, T.*; Coordination of TCSC and SVC for inter-area stability enhancement, *Power System Technology, 2000. Proceedings. PowerCon 2000. International Conference on*, Volume: 1, 4-7 Dec. 2000, Page(s): 553-558
- [158] *Pourbeik, P.; Gibbard, M.J.*; Simultaneous coordination of power system

- stabilizers and FACTS device stabilizers in a multimachine power system for enhancing dynamic performance, *Power Systems, IEEE Transactions on* , Volume: 13 Issue: 2 , May 1998, Page(s): 473 -479
- [159] *Fang W. and Ngan H. W.*; Enhancing small signal power system stability by coordinating unified power flow controller with power system stabilizer, *Electric Power System Research*, 65, 2003, Page(s) 91-99.
- [160] *Ramirez, J.M.; Davalos, R.J.; Valenzuela, V., A.*; Coordination of FACTS-based stabilizers for damping oscillations, *Power Engineering Review, IEEE* , Volume: 20 Issue: 12 , Dec. 2000, Page(s): 46 -49
- [161] *Xianzhang Lei; Lerch, E.N.; Povh, D.*; Optimization and coordination of damping controls for improving system dynamic performance, *Power Systems, IEEE Transactions on* , Volume: 16 Issue: 3 , Aug. 2001, Page(s): 473 -480
- [162] *Eberhart, R.C.; Shi, Y.*; Comparing inertia weights and constriction factors in particle swarm optimization, *Evolutionary Computation, 2000. Proceedings of the 2000 Congress on* , Volume: 1 , 16-19 July 2000, Page(s): 84 -88
- [163] *Mathur, R.M.; Varma R.K.*; **Thyristor-Based FACTS Controllers for Electrical Transmission Systems**, IEEE Press, 2002
- [164] *Hamdan A. M. A.*; An investigation of the significance of singular value decomposition in power system dynamics, *Int. Journal of Electrical Power and Energy Systems*, 21, Page(s) 417-424, 1999
- [165] *Abdel-Magid Y. L.; Abido M. A.*; Robust coordinated design of excitation and TCSC-based stabilizers using genetic algorithm, *Electric Power System Research*, 69, 2004, Page(s) 129-141.
- [166] *Failat E.A., Battayeb M.; Al-Duwaish H.; Abido M.A.; Mantawy A.*; A neural network based approach for on-line dynamic stability assessment using synchronizing and damping torque coefficients, *Electric Power System Research*, 39, No. 2, 1996, Page(s) 103-110.

Vita

- Ali Sayed Taleb Al-Awami
- Born in Qatif, Saudi Arabia on March 31, 1978.
- Received Bachelor of Science (B.S.) degree in Electrical Engineering from King Fahd University of Petroleum & Minerals (KFUPM), Dhahran, Saudi Arabia in 2000.
- Joined King Fahd University of Petroleum & Minerals in April 2002.
- E-mail: aliawami@kfupm.edu.sa